Dissertation zur Erlangung des Doktorgrades

der Fakultät für Chemie und Pharmazie

der Ludwig-Maximilians-Universität München

Precise aminoethylene-based nanocarriers for dynamic nucleic acid delivery: A balancing act between polyplex stability and cargo release

Simone Berger (geb. Hager)

aus Burghausen, Deutschland

2023

Erklärung

Diese Dissertation wurde im Sinne von § 7 der Promotionsordnung vom 28. November 2011 von Herrn Prof. Dr. Ernst Wagner betreut.

Eidesstattliche Versicherung

Diese Dissertation wurde eigenständig und ohne unerlaubte Hilfe erarbeitet.

München, 27.04.2023

.....

Simone Berger

Dissertation eingereicht am: 04.05.2023

1. Gutachter: **Prof. Dr. Ernst Wagner**
2. Gutachter: **Prof. Dr. Olivia Merkel**

Mündliche Prüfung am: 06.07.2023

Meiner Familie und insbesondere
meinem geliebten Ehemann Martin

“The important thing is to never stop questioning.”

Albert Einstein

Table of contents

1. Introduction

This chapter is intended to shortly introduce into the topic and is not considered to cover the complete scientific area. More details are described in chapters **2.** (ref. [1]) and **4.** (ref. [2]).

1.1 Therapeutic nucleic acids and their application fields

Therapeutic intervention at the genomic level offers various options for the preventive or causal treatment of severe and life-threatening diseases such as viral infections, cancer, or genetic defects/disorders.[3-9] The classical way is to substitute defective genes or introduce new genes by gene expression constructs such as viral vectors, plasmid DNA (pDNA), or messenger RNA (mRNA).[3] However, gene expression can also be modulated at the stage of mRNA biosynthesis and translation *via* RNA interference, alternative splicing, or single-stranded antisense oligodeoxynucleotides (ODNs).[3] Another strategy is genome editing mediated *e.g.,* by the RNA-guided CRISPR/Cas9 system.[10-12] Recently, an increasing number of such therapeutic approaches is evaluated in clinical trials and even achieves market authorization.[6, 13-19] In view of translation into the clinical setting, sufficient stability, high transfection efficiency, and good biocompatibility of the drug product are important. So far, the majority of clinical gene therapy trials has been carried out with viral vectors,[6] and only few have been conducted with non-viral formulations, with most simple and unsophisticated systems such as naked and chemically modified nucleic acids.[18, 20-22] Nevertheless, also some more complex formulations like lipid nanoparticles (LNPs) have been successfully implemented in the past few years. Currently, mRNA vaccines emerged as the big hope in the SARS-CoV-2 pandemic,[23] small-interfering RNA (siRNA) LNPs reached the medical market,[17] and Cas9 mRNA LNPs have been applied for the first successful *in vivo* genetic correction by CRISPR Cas9/single guide RNA in patients.[24]

1.2 The challenges in efficient nucleic acid delivery

Despite the enormous potential of therapeutic synthetic nucleic acid formulations, translation into the clinics has been rather slow due to many reasons. A major bottleneck is the challenging delivery process with many restrictions due to the big size, in most cases negative charge, and limited biological stability of naked nucleic acids.[3] Thus, efficient

and appropriate delivery systems for stabilization and protection of the cargo are required for successful therapeutic application. One option is the use of synthetic, cationic polymer- or lipid-based nanocarriers (polyplexes, lipoplexes, lipopolyplexes).[25] However, the production of such nanotherapeutics in pharmaceutical grade and scale is demanding.[13] Moreover, different cargos place different requirements on their carriers.[3, 13, 26] It is particularly important that the delivery system comprises extracellular stability and intracellular release of the cargo in its active form at the site of action. Various extra- and intracellular barriers have to be overcome dependent on the different application routes of these nanocarriers (*ex vivo* vs*. in vivo*, local vs. systemic).[3] Bio-/stimuli-responsiveness can be a helpful tool for creating delivery systems, which change their properties in a dynamic mode upon specific endogenous or exogenous stimuli (*e.g.*, changes in pH, redox-potential, or temperature).[1] Furthermore, one lately emerged obstacle is an observed weak correlation between the *in vitro* and *in vivo* performance. This problem was not that clear in early stages, when cellular delivery of nanocarriers was primarily tested in standard cell culture. With advanced pharmacological *in vivo* studies in mice or even human patients, however, the low reliability and validity of cell culture testing for therapeutic application became apparent.[27-33] Formulations with good *in vitro* activity may or may not perform *in vivo*. Even worse, a selection process of nanocarriers based on only *in vitro* assays might eliminate very potent *in vivo* candidates.

After intravenous administration (*i.e.,* the probably most challenging application route), the nanoparticles have to face several obstacles that differ from *in vitro*. Firstly, they get in contact with blood components. Usually, the nanoparticles are then covered by a biomolecular multi-layer (so-called protein corona or biomolecular corona),[34, 35] which creates a biological identity,[35, 36] thereby altering the physico-chemical properties, the pharmacokinetics, and toxicity profile of the nanoparticles.[37] Interaction with electrolytes, plasma proteins, and blood cells (*e.g.*, erythrocytes and thrombocytes) can cause nanoparticle dissociation, self-aggregation, or aggregation with *e.g.*, erythrocytes.[3, 38] Cationic nanoparticles, for instance, are known to bind and activate complement proteins, thereby inducing innate immune responses with serious side effects.[39, 40] In addition, destabilizing shear forces within the blood stream act on the nanoparticles.[41, 42] Functionalization of the nanoparticle surface with shielding agents such as polyethylene glycol (PEG) can reduce, but not completely prevent the protein corona formation and

creates a “stealth” character, by this hindering dissociation or aggregation.[36, 43-45] Secondly, the nanoparticles have to extravasate, penetrate and accumulate in the right tissue, followed by uptake in the target cells.[3] Endothelial targeting and tumor homing (*e.g., via* integrins and the so-called CendR pathway,[46] or CD44[28]), as well as passive (*via* the so-called enhanced permeation and retention (EPR) effect)[47] and/or active targeting (*via* receptor-mediated endocytosis)[48, 49] can be helpful for efficient delivery *in vivo.*[3] However, it has to be considered that the biomolecular corona can mask targeting ligands, thereby reducing the targeting capability.[37, 44, 50] Thirdly, endosomal escape and cargo release are necessary.[3, 51-53] Also here, masked nanoparticles may be blocked *e.g.*, in their lytic activity, resulting in reduced release from the endosomes and thus reduced transfection efficiency.[29]

Also, for other application routes than intravenous (*e.g.*, inhalative, intravitreal, or transdermal), several biological barriers have to be overcome and the delivery system has to fulfill certain requirements.[54-56] Moreover, there can be difficulties to reach the target organ. The most prominent example is the systemic delivery to the brain, where the blood-brain-barrier (BBB) is a major hurdle.[57]

1.3 Chemical evolution strategy for carrier optimization

“Look at nature, learn from viruses and biological evolution”

Viruses have developed various strategies to meet the above mentioned requirements, as they are optimized by biological evolution for the purpose of nucleic acid transfer into host cells.[58] Thus, they represent very potent delivery vehicles and can serve as models for virus-like synthetic carriers (**Figure 1.1**).[59, 60] With the use of *i)* precise synthetic strategies (*e.g.*, solid-phase assisted peptide synthesis (SPPS),[61-64] or reversible addition fragmentation chain transfer (RAFT) polymerization[65]), *ii)* formulation methods (*e.g.*, microfluidics[66-73]), and *iii)* combinatorial chemistry,[74] libraries of sequence-defined carriers can be generated in a systematic way by modular design, enabling the identification of clear structure-activity relationships by high-throughput library screening. This opens the way for a “chemical and molecular evolution” process,[3, 13, 58] facilitating the development from first generation polycations to multifunctional, bio-inspired sequence-defined delivery systems. Combination with *in silico* simulations,[75] computational/statistical predictions (*e.g.*, “DOE”, design-of-experiments [76-79]), and machine learning approaches[74, 80] may make this whole optimization process more

efficient and faster. The “synthetic artificial viruses” mimic the efficient process of viral transfection. Therefore, they should be dynamic and react to changes in microenvironment. In this manner, pinpointed, spatiotemporal controlled release as well as reduced cytotoxicity of the carrier can be obtained, resulting in improved specific nucleic acid delivery as well as in increased biocompatibility. Combined responsiveness may be very advantageous and can enhance availability of the nucleic acid at its site of action.

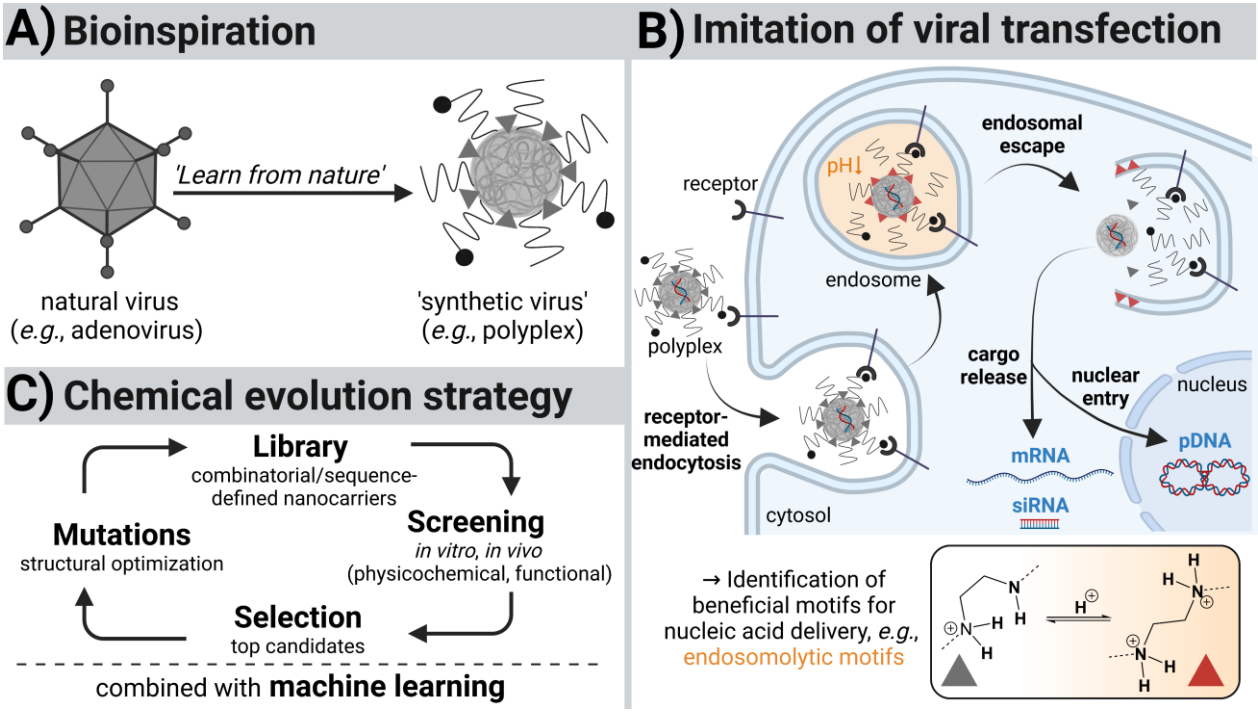

Figure 1.1. Bioinspired chemical evolution strategy for the optimization of non-viral nucleic acid carriers. (**A**) Viruses optimized by biological evolution for efficient nucleic acid transfer into host cells can serve as models for virus-like synthetic delivery systems. (**B**) These ‘synthetic viruses’ (*e.g.*, polyplexes) imitate the highly effective viral transfection process. Chemical motifs that are beneficial for the single delivery steps have to be identified. For example, aminoethylene units (*right bottom*) turned out to be potent endosomolytic motifs. (**C**) Chemical evolution is done by creating libraries of combinatorial/sequence-defined nanocarriers with different motifs and topologies, followed by cycles of high-throughput screening, rational selections, and systematic structural mutations/optimization. Combination with machine learning approaches may make this whole optimization process more efficient and faster. Created with BioRender.com.

1.4 Aims of the thesis

In the last few decades, the growing field of non-viral delivery vectors gained more and more importance as safer alternatives to viral vectors. The latter exhibit some disadvantages like immunogenicity, limited cargo capacity, rather sophisticated production, difficult production upscale, and high production costs.[58, 81] The history of polymeric gene delivery systems goes more than 50 years back.[3, 81] Optimization of cationic polymers during this time led to increasingly improved nucleic acid transfer efficiency. Concrete starting points were given by the gained understanding of the single delivery steps and how nature deals with these different barriers as well as by the increased knowledge about the demands of the different nucleic acids on their carriers. Optimization of such non-viral carriers can be done by a so-called "chemical evolution strategy"[13] – this means look at nature, and learn from viruses and natural evolution (**Figure 1.1**). First, one has to identify chemical motifs (*e.g.,* natural or artificial amino acids, suitable building blocks) that are beneficial for the single delivery steps. Second, libraries of potential carrier structures can be designed by assembling the different motifs into defined sequences with various topologies, followed by cycles of high-throughput screening, rational selections, and systematic structural variations. Hereby, SPPS is a smart way to generate peptide-based carrier libraries in a precise, sequence-defined way by modular design (**Figure 1.2**).[64]

Nevertheless, transfection efficiency of synthetic nanocarriers is still quite low – especially in comparison with viral vectors – and further improvement is necessary.

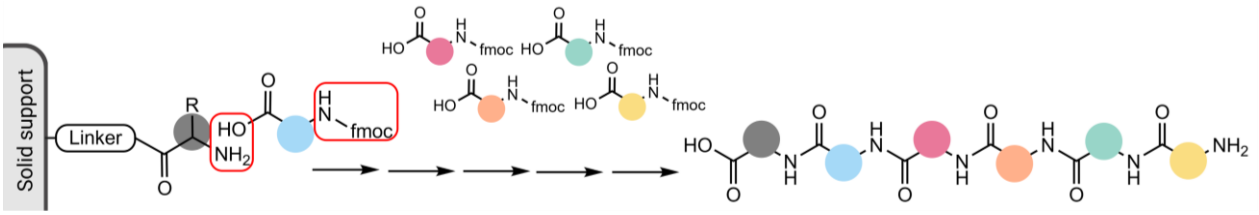

Figure 1.2. Solid-phase assisted peptide synthesis enables the systematic generation of peptide-based carrier libraries in a precise, sequence-defined way by modular design. Created with BioRender.com.

The first aim of the thesis was to develop safe and efficient peptide-based nanocarriers for the complexation of nucleic acids cargos, in particular of pDNA and mRNA, into polyplexes. Hereto, SPPS was to be utilized to generate a library of sequence-defined T-shaped lipo-oligoaminoamides (OAA) with different functional moieties. All lipo-OAAs should have a polycationic backbone with four units of succinoyl tetraethylene pentamine (Stp) and tyrosine tripeptides at each end of the linear backbone. Structure variations should comprise *i*) histidines in alternating or block-wise sequence with Stp, *ii*) cysteines, or disulfide blocks, and *iii*) a hydrophobic diacyl domain in the side-chain, consisting of two lysine-connected fatty acids. Various saturated fatty acids of different chain lengths in comparison to unsaturated oleic acid as well as modified fatty acids (namely, hydroxy-stearic acid, and 8-nonanamido-octanoic acid) should be tested. With screening of this library and systematic structure-activity relationship studies (physicochemical, functional, and biological evaluation), the most appropriate carriers, beneficial structural motifs, and critical bottlenecks in pDNA and mRNA delivery *in vitro* and *in vivo* were to be identified. A balance was to be figured out between polyplex stability and efficient cargo release at its site of action in bioactive form. Additionally, new assays investigating the impact of 90% full serum on the properties and behavior of lipo-OAAs and corresponding lipo-polyplexes were to be established in order to find explanations for the observed weak correlation between *in vitro* and *in vivo* gene-transfer and to provide a better basis for the prediction of the *in vivo* performance in the future.

The second aim of the thesis was to investigate transcriptional targeting to dendritic cells *in vitro* and *in vivo* as a potential DNA-based vaccination approach. Deeper knowledge about the role of the tumor microenvironment in cancer development and progression has resulted in new strategies such as gene-based cancer immunotherapy. DNA-based vaccines are intended to be expressed in antigen-presenting cells (*e.g.*, dendritic cells, DCs), inducing anti-tumor responses of the adaptive immune system (**Figure 1.3**). Besides effective delivery systems (*e.g.*, polyplexes) and the use of appropriate adjuvants, an optimized cargo is important for successful DNA vaccines. The concept of DC-focused transcriptional targeting was to be tested by using a plasmid encoding for the firefly luciferase reporter gene under the control of an optimized derivative of the human fascin1 (Fscn1) gene promoter (pFscnLuc), comprising an upstream DC-specific enhancer region

fused with the proximal core promoter. Linear polyethylenimine 22 kDa (LPEI) as well as succinylated branched PEI 25 kDa (succPEI, 10% succinylation) should be used as effective pDNA carriers. The activity of pFscnLuc was to be analyzed *in vitro* in Fscn1 positive cell lines (DC-like cell line DC2.4; tumor cell lines N2a and Hepa1-6), in comparison to the standard plasmid pCMVLuc encoding for luciferase under the control of the strong ubiquitously active cytomegalovirus promoter and enhancer. The two plasmids should also be compared *in vivo* by intravenous administration in BALB/c mice. The organ-specific expression profile of pFscnLuc versus pCMVLuc as well as the expression on single cell level (more precisely, in DCs and macrophages of according organs) were to be evaluated.

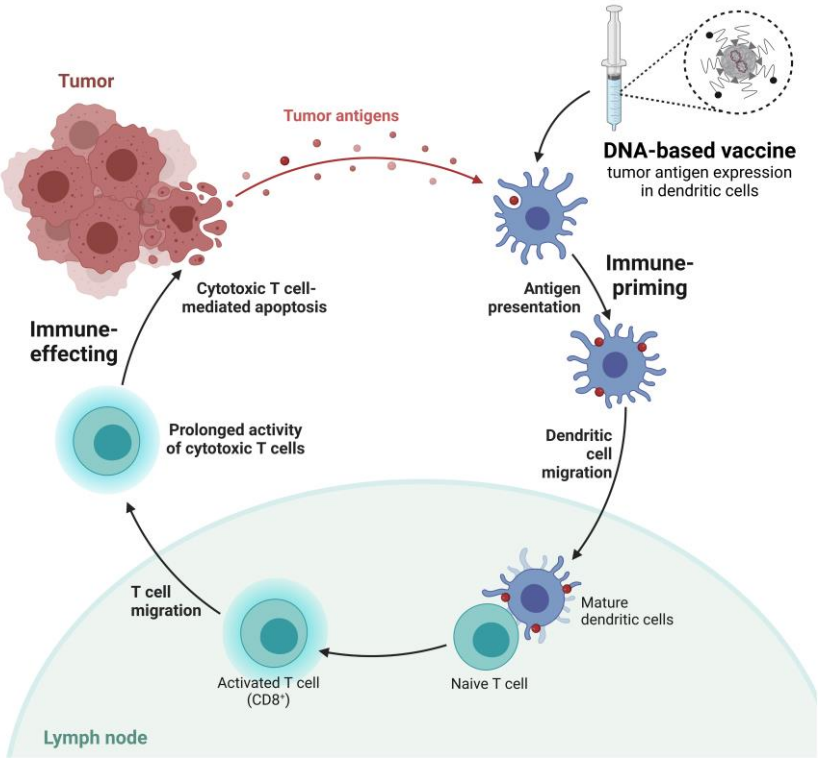

Figure 1.3. Dendritic cells are the most potent immune stimulatory cells and thus an ideal target for vaccine approaches. DNA-based vaccines are intended to be expressed in dendritic cells and other antigen-presenting cells, resulting in an activation of the adaptive immune system, which then can effectively fight, for example, cancer cells. Created with BioRender.com.

2. Bioresponsive polyplexes – chemically programmed for nucleic acid delivery

*Simone Hager and Ernst Wagner**

Pharmaceutical Biotechnology, Department of Pharmacy, and Center for NanoScience (CeNS), Ludwig-Maximilians-Universität (LMU) Munich, Butenandtstr. 5-13, D-81377 Munich, Germany

* Corresponding author: E. Wagner

This chapter is adapted from a pre-copy-edited version of a peer-reviewed review article published in ***Expert Opin. Drug Delivery*** **2018, 15, (11), 1067-1083 (ref. [1]).**

Author contributions

Both authors have substantially contributed to drafting this review. S. Hager, and E. Wagner conceptualized the review topic, wrote, edited, and revised the manuscript draft incl. illustrations. E. Wagner was responsible for funding acquisition. All authors have read and agreed to the published version of the manuscript.

Abstract

Introduction. The whole delivery process of nucleic acids is very challenging. Appropriate carrier systems are needed, which show extracellular stability and intracellular disassembly. Viruses have developed various strategies to meet these requirements, as they are optimized by biological evolution to transfer genetic information into host cells. Taking viruses as models, smart synthetic carriers can be designed, mimicking the efficient delivery process of viral infection. These 'synthetic viruses' are pre-programmed and respond to little differences in their microenvironment, caused by either exogenous or endogenous stimuli.

Areas covered. This review deals with polymer-based, bioresponsive nanosystems (polyplexes) for the delivery of nucleic acids. Strategies utilizing pH-responsiveness, redox-responsiveness as well as sensitivity towards enzymes will be described more in detail. Systems, which respond to other endogenous triggers (*i.e.*, reactive oxygen species (ROS), adenosine triphosphate (ATP), hypoxia), will be briefly illustrated. Moreover, some examples for combined bioresponsiveness will be presented.

Expert opinion. Bioresponsive polyplexes are a smart way to facilitate programmed, timely delivery of nucleic acids to desired, specific sites. Nevertheless, further optimization is necessary to improve the still moderate transfection efficiency and specificity – also in regard to medical translation. For this purpose, precise carrier structures are desirable and stability issues of bioresponsive systems have to be considered.

Keywords

Adenosine triphosphate (ATP), bioreducible, bioresponsive, endogenous trigger, hypoxia, non-viral nucleic acid delivery systems, pH, polyplexes, reactive oxygen species (ROS), redox potential.

Article highlights box

- Just like their natural counterparts, ‘artificial, synthetic viruses’ should be responsive to changes in microenvironment, caused by either exogenous or endogenous stimuli (physical or biochemical targeting).
- Bioresponsive triggers include changes in pH value, redox-potential, enzyme-sensitivity, varying levels of ROS or ATP or hypoxia.
- Triggered conformational changes or bond cleavages lead to activation or exposure of functional domains or to breakdown of the nanocarrier.
- Bioresponsiveness enables programmed, timely delivery of nucleic acids to specific sites, as well as reduced cytotoxicity of the carrier, and thus can enhance both transfer efficiency and biocompatibility.
- By combining two and more (bio)responsive moieties in one nanocarrier, even better mimicking of the dynamic, stepwise process of viral infection can be achieved.
- Further optimization of non-viral carriers including their precise manufacture and storage in stable form is required, also in regard to medical translation.

This box summarizes key points of the article.

2.1 Introduction: Challenges for the delivery of nucleic acids

Gene therapy gained importance over the last few decades. The number of clinical gene therapy trails is continuously increasing. At the moment, nearly 2600 trials are recorded worldwide. In addition, more and more gene therapies achieve medicinal market authorization. In the year 2017 alone, three gene therapies have been approved by the U.S. Food and Drug Administration (FDA).[6]

Therapeutic intervention at the genomic level is an interesting approach due to the fact that severe and life-threatening diseases such as cancer or genetic defects can be treated in a causal way. The increasing knowledge about natural nucleic acids and their biological functions offers various opportunities for diverse gene therapy concepts. Thereby, different steps of the gene expression process can be addressed.[3] The classical way is to substitute defective genes or introduce new genes by gene expression constructs like plasmid DNA (pDNA) or messenger RNA (mRNA). However, gene expression can also be modulated at the stage of mRNA biosynthesis and translation *via* alternative splicing, RNA interference or single-stranded antisense oligodeoxynucleotides (ODNs). Recently, genome editing systems such as the combination of CRISPR/Cas9 mRNA, guide RNA and repair template DNA have been found to be a promising new method.[6, 11]

All therapeutic nucleic acids are polar macromolecules and far larger than conventional chemical drugs. Additionally, in most cases they are negatively charged. Thus, they are not able to diffuse across lipid membranes. Biological stability in general is also very limited. Naked nucleic acids are degraded rapidly in blood by nucleases and cleared by the kidneys.[3] Efficient and appropriate delivery systems to stabilize and protect nucleic acids are required for successful therapeutic application. One option is the use of synthetic, cationic polymer- or lipid-based nanocarriers (polyplexes, lipoplexes, lipopolyplexes).[25]

Various extra- and intracellular barriers have to be overcome dependent on the different application ways of these nanocarriers (*ex vivo* vs. *in vivo*, local vs. systemic)[3] (**Figure 2.1**). Among them, systemic application is most challenging. After intravenous administration, polyplexes have to firstly withstand extracellular barriers. Polyplex stability is usually low in blood and other biological fluids. Unspecific interactions with electrolytes, serum proteins or cellular surfaces lead to dissociation of the nanoparticles, and thus to a loss of transfection efficiency. Moreover, serum complement proteins can be activated,

inducing immune response by the innate immune system. Self-aggregation into larger microstructures or aggregation with erythrocytes and other blood cells are further adverse events.

The next critical steps of the delivery process are specific cell binding and efficient cellular uptake. Passive targeting into tumor tissue can be achieved to some extent due to the enhanced permeability and retention (EPR) effect.[47, 82] In this context, polyplex size plays an important role. However, a more effective and faster accumulation in the tumor tissue is possible by active tumor homing *via* peptides with tissue- and cell-penetrating function that are, for example, peptides with RGD (arginine-glycine-aspartate) or NGR (asparagine-glycine-arginine) sequence motif.[46, 83] These peptides recognize specific markers on tumor vasculature (*e.g.*, integrins), which are usually expressed on parenchymal cells of the tumor tissue as well. After initial binding and proteolytic cleavage, interaction with a second receptor (neurophilin-1 or -2) activates an active bulk trans-tissue pathway (the so-called CendR pathway), resulting in effective extravasation and deep tumor penetration of the peptide and its co-administrated payload (by-stander effect). The entry across cell surface membranes happens mostly *via* endocytosis, as passive diffusion is not possible for nanoparticles such as polyplexes.[51] Internalization can be enhanced by cell-penetrating peptides (CPPs) such as TAT (transactivator of transcription) peptide,[84] but this is no cell-type specific process. To increase specificity, CPPs can be combined with targeting ligands or homing peptides, or they can be masked in a bio-reversible manner.[46, 83] After uptake, endosomal escape is necessary to avoid lysosomal degradation of the nucleic acids.

Once released into the cytosol, the polyplexes have to cope with intracellular hurdles.[3] Polyplex disassembly is essential for the liberation of its cargo in bioactive form. Free nucleic acids are relatively fast degraded by cytosolic enzymes. Furthermore, the nucleic acids have to reach their respective sites of action. This can be the cytosol in case of, for example, mRNA and small-interfering RNA (siRNA), whereas pDNA has to be introduced into the nucleus. Nuclear entry is one of the main bottlenecks in pDNA delivery.[3, 85, 86] For this step, microtubules-mediated endosomal trafficking of the pDNA polyplexes to the perinuclear space, followed by endosomal escape would be advantageous. Nuclear import takes place by size-dependent active mechanisms through the nuclear pore complex or during cell division. The latter is only possible in proliferating cells. Conjugation

of short cationic nuclear localization signal (NLS) peptides has been reported to enhance nuclear transport. Other options can be chromatin-targeting, incorporation of histone H3 tails or cell division-responsive peptides. Altogether, the success is very variable, so that further research is requested.

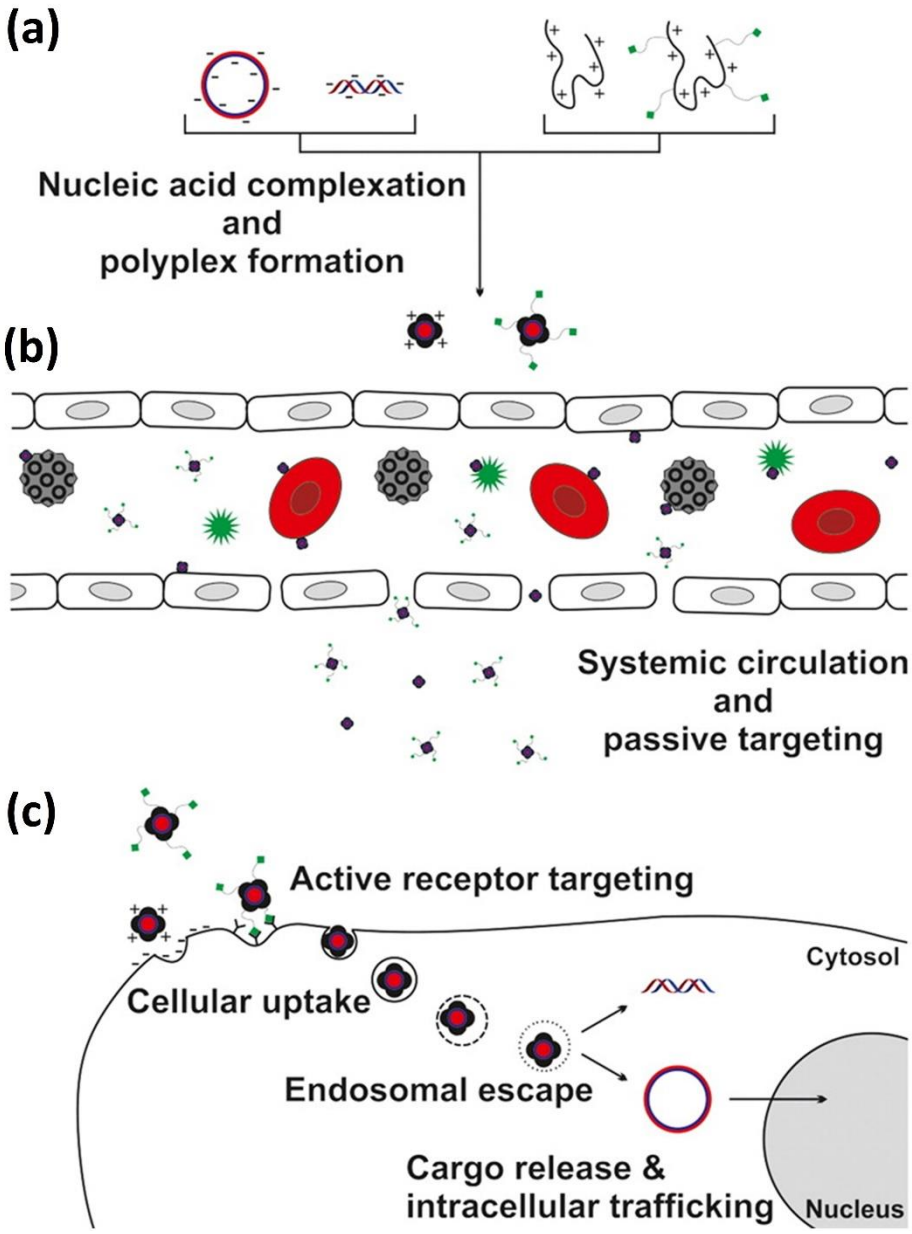

Figure 2.1. Barriers in the nucleic acid delivery pathway of polyplexes. (**a**) Formation of stable polyplexes, (**b**) avoidance of rapid clearance and unspecific interactions with blood components, and (**c**) cellular barriers. Reprinted with permission from [3]. Copyright © 2018; American Chemical Society.

Finally, it has to be considered that polycationic polymers like polyethylenimine (PEI) may exhibit significant toxicity by non-specific interactions with negatively charged biomolecules such as cytoplasmic, mitochondrial and nuclear membranes.[3, 87, 88] Therefore, final degradation of the polymers into non-toxic fragments is preferable in order to reduce cytotoxicity and to improve biocompatibility.

To sum up, the whole nucleic acid delivery process is very challenging. In general, extracellular stability and intracellular lability of the delivery system are required.[3] The cargo should be protected during the whole extra- and intracellular delivery process but released at its site of action. The delivery system should be inert to biological surfaces and molecules but interact with its target cell. Moreover, membrane activity, which is required for endosomal release, should be limited to acidic endosomal vesicles, and must not destroy other membranes.

Viruses have developed various strategies to meet these requirements, as they are optimized by biological evolution for the purpose of nucleic acid transfer into host cells.[58] They represent very potent delivery vehicles. Therefore, they can serve as models for virus-like synthetic carriers,[59, 60] which contain different domains for mimicking the efficient, dynamic delivery process of viral infection.

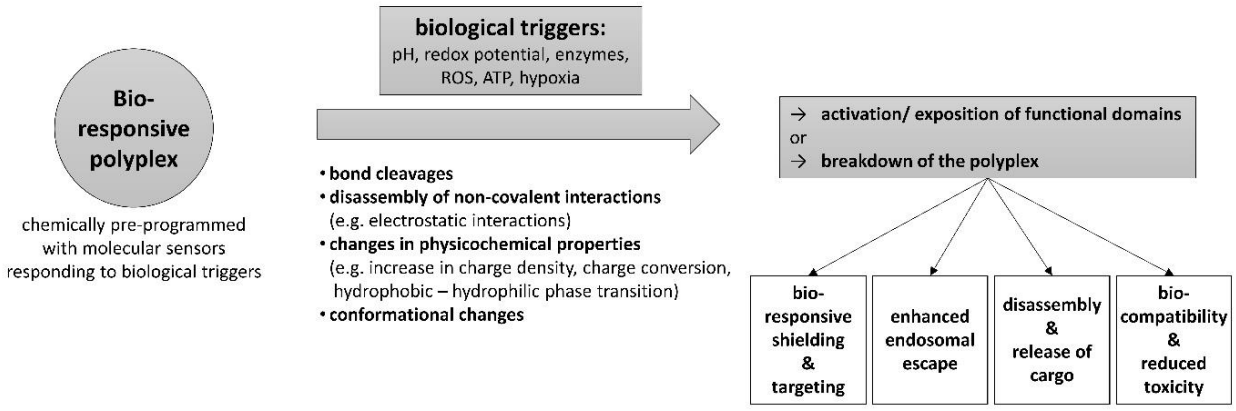

Figure 2.2. Different mechanisms of bioresponsiveness.

2.2 Strategies to meet the challenges: Bioresponsive nanosystems

In order to ensure ‘programmed’ controlled delivery in a dynamic way, ‘smart’ virus-inspired delivery systems should be responsive – like their natural templates. For this purpose, exogenous or endogenous stimuli should trigger either bond cleavages, disassembly of non-covalent interactions, or changes in physicochemical properties or conformation, leading to activation or exposition of functional domains or to the breakdown of the nanoparticle. The result is a selective and timed release of cargo at specific, desired sites, which can be regarded as some kind of ‘physical targeting’ (in case of external triggers) or ‘biochemical targeting’ (in case of internal triggers).[89] Exogenous stimuli can be physical forces like heat, light, ultrasound, electric or magnetic fields.[89, 90] Delivery systems can also be bioresponsive and react to endogenous stimuli. These are little changes in microenvironment, as they appear at physiological (special compartments, types of cells, tissues, organs) or pathological conditions (such as cancer, infection, inflammation). Thereby, differences in pH value, redox potential, enzyme activity, reactive oxygen species (ROS) or adenosine triphosphate (ATP) levels as well as hypoxia can be sensed by the chemically pre-programmed nanocarriers (**Figure 2.2;Table 2.1**).

Table 2.1. Examples of chemical bonds that are cleavable in response to biological triggers.

Bioresponsive chemical bonds		References
Enzyme-sensitive moieties		
MMP2-sensitive peptide linker	-PLG*LAG-	[91-93]
	-GPL*GIAGQ-	[94]
	-GPL*GVRG-	[95]
esterase-sensitive linker	*N*-propionic 4-acetoxybenzyl ester	[96]
	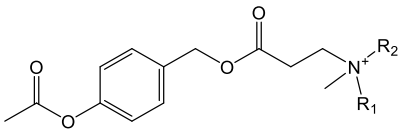	
Cathepsin B-sensitive peptide linker	-FK*FL-	[97]
pH-labile bonds		
vinyl-ether	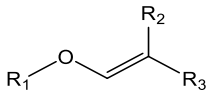	
acetal; ketal	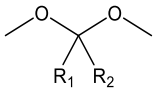	
pyridyl-hydrazone	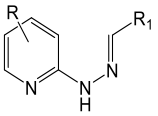	
β-thiopropionate	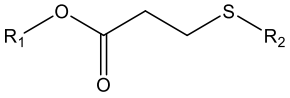	Reviews [3, 89, 98]
phosphoramidate	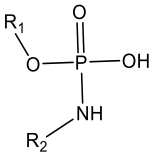	
orthoester	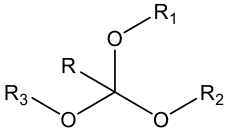	
imine	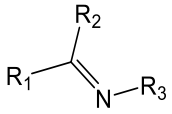	[99-101]
phenylboronate ester	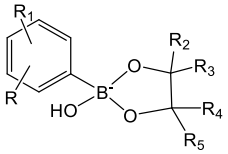	[102, 103]
maleic acid amide derivatives	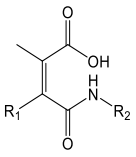	[104-111]

Table 2.1 ***continued.***

Redox-responsive bonds		
disulfide bond	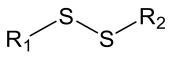	[104, 105, 109, 112-128]
diselenide bond	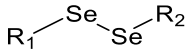	[125]
ROS-responsive bonds		
thioketal	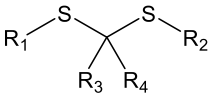	[129]
boronic esters	phenylboronic ester	[130]
	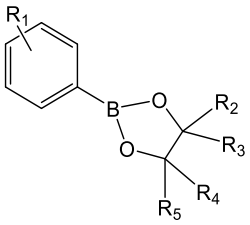	
	polysulfonium with boronic ester motif	[131]
	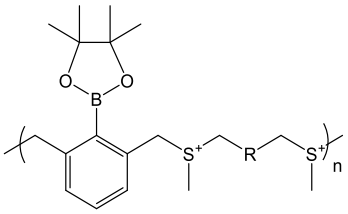	
ROS degradable peptide	-CP_5K-	[132]
ATP-responsive bonds		
phenylboronate ester	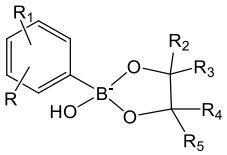	[102, 133, 134]
Hypoxia-sensitive moieties		
azobenzene	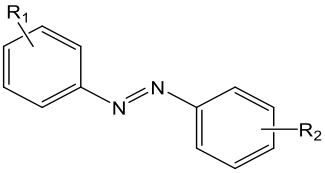	[135]

For even better mimicking of the dynamic and bioresponsive behavior of viruses and for improved specificity, several stimuli-responsive domains can be incorporated into combined responsive, multifunctional delivery systems, paving the way towards ‘synthetic, artificial viruses’. Such ‘artificial viruses’ include several functional units like nucleic acid

binding moieties, stabilizing and protecting units, shielding domains, targeting ligands, endosomolytic or membrane-active moieties and nuclear localization signals.[3, 58]

Stabilizing units include hydrophobic domains (*e.g.*, fatty acids[64, 136] or tyrosines[137]) as well as covalent crosslinks within the particle core (*e.g.*, disulfide bonds[112-114], twin disulfide forming cysteine-arginine-cysteine (CRC) motif[138]). In case of siRNA, polyplex stability might be more important, because with 21–23 base pairs (bps) it is much smaller than, for example, pDNA (several kilo bps) and therefore, entropy-driven electrostatic interactions of siRNA with cationic polymers are less pronounced.[86] Besides stabilizing units within the nanoparticle core, there exist further strategies to stabilize siRNA polyplexes.[58, 86, 139] For example, by reversible multimerization of siRNA into larger polyanions through disulfide-crosslinking, enhanced electrostatic interactions with the polycationic carrier and thus improved polyplex stability can be obtained. Another option is the direct covalent conjugation of siRNA to the polycationic carrier, for example, *via* disulfide bonds[104, 105, 115, 116] or acid-labile bonds such as maleic acid amide.[140] The reversible characteristics of these linkers are advantageous, as siRNA can be released in a timely bioresponsive manner.

Furthermore, shielding by neutral, hydrophilic molecules like polyethylene glycol (PEG)[141] or poly(*N*-(2-hydroxypropyl)-methacrylamide) (pHPMA)[106] avoids side effects, undesired interactions with blood components and biological surfaces as well as self-aggregation of the nanoparticles. This ‘stealth effect’ may lead to increased polyplex stability, a prolonged blood circulation time and a higher biocompatibility.

One obstacle coming along with shielding is the decreased transfection efficiency due to reduced interactions with biological membranes. In case of PEG as shielding agent, this is called ‘PEG-dilemma’.[87] Incorporation of targeting ligands can enhance both, specificity and efficiency of cellular uptake.[142] Therefore, active targeting can help to at least partially solve this shielding dilemma. Targeting ligands comprise small chemical compounds such as vitamins or drugs, carbohydrates, peptides, proteins (*e.g.*, growth factors or antibodies) or artificial nucleic acids like aptamers.[3]

Moreover, shielding may hinder efficient endosomal escape by masking of membrane-active domains. Bioresponsive shielding strategies can be an option to solve this problem. Beneficial moieties for enhanced endosomal escape are, for example, the aminoethane-motif in ‘proton-sponge polymers’ (like polyethylenimine (PEI)[88, 143]) or endosomal pH-

sensitive amines with buffering capacity (*e.g.*, imidazole group of histidine[144]). Moreover, endosomolytic domains within the polyplexes (*e.g.*, fatty acids[136]) or incorporation of fusogenic or cell-penetrating peptides (CPPs)[84, 145, 146] can increase endosomal release. However, it should be noted in regard to reduced cytotoxicity that any membrane activity should be restricted to acidic endosomal vesicles and have no effect on other membranes.[58] This can be achieved to some extent by bioresponsive shielding strategies or bioresponsive masking of membrane-active domains.

In the following, polymer-based nanosystems for the delivery of nucleic acids utilizing bioresponsiveness – enzyme-, redox- and pH-responsiveness in particular – will be presented. **Table 2.2** gives an overview of examples for bioresponsive nucleic acid delivery systems.

Table 2.2. Examples for bioresponsive nucleic acid delivery systems.

	Mechanism(s) of bioresponsiveness	Bioresponsive unit(s)	Carrier system	Cargo	Type of study (*in vitro/in vivo*)	Reference
Bioresponsive shielding	***Enzyme-sensitive shielding***					
	MMP-cleavable linker	peptide sequence -PLG*LAG-	core: cell penetrating peptide PepFect14; shell: polyethylene glycol (PEG)	pDNA	*in vitro &in vivo* (mice)	[91]
	MMP-cleavable linker	peptide sequence -GPL*GIAGQ-	core: polyethylenimine – 1,2-dioleoyl-*sn*-glycero-3-phosphoethanolamine (PEI-DOPE); shell: PEG	siRNA & hydrophobic drug paclitaxel	*in vitro & in vivo* (mice)	[94]
	pH-responsive shielding					
	acid-labile bond	imine	core: polyethylenimine (PEI); shell: dextran derivatives	pDNA	*in vitro & in vivo* (mice)	[100]
	electrostatic coating with a charge-switchable shell	2,3-dimethylmaleamate unit	core: folate incorporated cell penetrating peptide CR_8C, cross-linked with triphenyl phosphonium incorporated proapoptotic peptide $KK(KLAKLAK)_2C$; shell: PEG -*block*- 2,3-dimethylmaleic anhydride modified poly-(*L*)-lysine (PLL)	pDNA	*in vitro & in vivo* (mice)	[109]
	Redox-responsive shielding					
	reducible bonds	disulfide bond & diselenide bond	core: diselenide-conjugated oligoethylenimine (OEI); shell: disulfide-modified hyaluronic acid	pDNA	*in vitro & in vivo* (mice)	[125]
	reducible bonds	disulfide bond	*host-guest supramolecular complex:* host segment: β-cyclodextrin-crosslinked PEI, conjugated with a targeting ligand; guest segment: adamantyl group, linked with PEG *via* disulfide bond	pDNA	*in vitro & in vivo* (mice)	[120]
	Hypoxia-sensitive shielding					
	hypoxic-sensitive bioreductive linker	azobenzene	core: PEI-DOPE; shell: PEG	siRNA	*in vitro & in vivo* (mice)	[135]

Table 2.2 *continued.*

Enhanced endosomal escape	***Beneficial moieties for endosomal escape***					
	proton-sponge effect & direct lytic effects	aminoethane-motif; imidazole group of histidine	sequence-defined library of oligo(ethanamino)amides, containing an alternating motif of selected oligoethanamino acids and histidines	pDNA	*in vitro & in vivo* (mice)	[144]
	Membrane-active peptides					
	pH-specific conformational changes	endosomolytic peptide INF7	cationic T-shaped lipo-oligoamino amide, sequentially surface-modified with PEG-linked targeting ligand transferrin and endosomolytic peptide INF7	siRNA	*in vitro & in vivo* (mice)	[147]
	acid-driven removal of masking groups	2,3-dimethylmaleamate bond	hepatocyte-targeted *N*-aceytlgalactosamine (GalNAc)-conjugated melittin-like peptide	cholesterol-conjugated siRNA	*in vitro & in vivo* (rodents, nonhuman primates)	[110]
					in vivo (chimpanzees ; humans [phase 2 clinical trial)]	[111]
	reversible conjugation *via* acid-labile bond	hydrazone	PEG – 1,2-distearoyl-phosphatidylethanolamine (DSPE) lipids with conjugated melittin	–	– (analytical study: calcein leakage assay)	[148]
	exposure due to pH-specific hydrophobic-hydrophilic phase transition	diisopropylaminoethyl (DPA) motif	*VIPER (virus-inspired polymer for endosomal release):* block copolymer with a hydrophilic polycationic dimethylaminoethyl block, and a pH-sensitive DPA block that hides melittin at physiological pH	pDNA	*in vitro & in vivo* (mice)	[149]
	redox-responsive activation	disulfide bond	PEI (25kDa), conjugated with endosomolytic protein listeriolysin O *via* disulfide bond, and disulfide-crosslinked PEI (1.8kDa)	pDNA	*in vitro*	[117]
	redox-responsive activation	disulfide bond	disulfide polymerized melittin/ pDNA condensate	pDNA	*in vitro*	[119]
Disassembly & release of cargo	**Enzyme-mediated disassembly**					
	charge conversion due to esterase-mediated hydrolysis	N-propionic 4-acetoxybenzyl ester	quaternized PEI with *N*-propionic 4-acetoxybenzyl ester substituents, and lipid coating	pDNA	*in vitro & in vivo* (mice)	[96]
	Cathepsin B-mediated polymer degradation	peptide sequence -FK*FL-	copolymer, consisting of *N*-(2-hydroxypropyl)methacrylamide (HPMA), a Cathepsin B-cleavable peptide and oligo-(*L*)-lysine	pDNA	*in vitro*	[97]
	pH-responsive disassembly					
	hydrophobic-hydrophilic phase transition	diisopropylamino-ethyl (DPA) motif	hybrid micelles, composed of a pH-responsive diblock PEG-methacrylate copolymer with DPA motif and covalently conjugated photosensitizer, and 1,2-epoxytetradecane alkylated OEI	siRNA	*in vitro & in vivo* (mice)	[150]
	hydrophobic-hydrophilic phase transition	benzoic imine	methacrylate block copolymer with dimethylaminoethyl, oligo(ethylene glycol) and benzoic imine groups	pDNA	*in vitro & in vivo* (mice)	[101]
	Redox-responsive disassembly					
	reducible disulfide linker	disulfide building block (ssbb): succinoyl-cystamine	sequence-defined lipo-oligoamino amides with ssbb between a lipophilic diacyl domain and an ionizable oligocationic unit	siRNA	*in vitro*	[123]

Table 2.2 *continued.*

	Reduction-triggered reversal of hydrophobicity	lipoic acid	PEI (1.8kDa), modified with hydrophobic lipoic acid	pDNA	*in vitro*	[124]
	ROS-responsive disassembly					
	ROS-mediated biodegradation	phenylboronic ester	branched PEI (1.2kDa), crosslinked with phenylboronic esters	pDNA, siRNA	*in vitro & in vivo* (mice)	[130]
	ROS-mediated biodegradation	phenylboronic ester	polysulfonium with phenylboronic ester moieties	pDNA	*in vitro & in vivo* (mice)	[131]
	ATP-responsive release of cargo					
	competitive displacement	single-stranded DNA aptamer	ternary nanocomplex, composed of PEI, doxorubicin/ DNA-duplex (DNA aptamer & its complementary DNA) and siRNA	siRNA & doxorubicin	*in vitro*	[151]
	competitive displacement	phenylboronate	PEG-PLL with 4-carboxy-3-fluorophenylboronic acid moiety in the PLL side chains	cholesterol-conjugated siRNA	*in vitro*	[134]
Combined responsiveness	**pH & redox responsiveness**					
	pH-triggered cascading charge-conversion; redox-mediated nanoparticle degradation	maleic amide derivatives: 2,3-dimethylmaleic anhydride (DMMA) and citraconic anhydride (CIT); disulfide bond	lipids, modified with dendritic lysine and with DMMA or CIT & disulfide bond containing dendronized polylysine	pDNA	*in vitro & in vivo* (mice)	[128]
	acid-driven removal of masking groups; redox-triggered release of cargo	2,3-dimethyl maleamate (DMM) bond; disulfide bond	siRNA conjugate, consisting of PLL, PEG, the lytic peptide melittin masked with DMM, and siRNA attached at the 5′-end of the sense strand *via* a bioreducible disulfide bond	siRNA	*in vitro & in vivo* (mice)	[104]
	acid-driven removal of masking groups; redox-triggered release of cargo	2,3-dimethyl maleamate (DMM) bond; disulfide bond	siRNA Dynamic Poly-conjugate, consisting of endosomolytic poly(butyl and amino vinyl ether) (pBAVE) with bioreducibly attached siRNA as well as acid-labile attached GalNAc and PEG	siRNA	*in vitro & in vivo* (mice)	[105]
	pH & hypoxia responsiveness					
	hydrophobic-hydrophilic phase transition due to hypoxia-induced reduction; increase of cationic charge in acidic tumor tissue	nitro-imidazole; amino groups	liposomes, composed of DSPE-PEG, cholesterol and lipids, which contain nitroimidazole groups in the hydrophobic tail and a tertiary amine head group	siRNA	*in vitro & in vivo* (mice)	[152]
	pH & enzyme responsiveness					
	pH- & MMP2-sensitive exposure of cell penetrating peptide	pH-responsive masking peptide E_4K_4; MMP2-cleavable peptide sequence -PLG*LAG-	dendrigraft poly-(*L*)-lysines, conjugated with dual-masked cell penetrating peptide R_9	pDNA	*in vitro & in vivo* (mice)	[92]
	pH & ATP responsiveness					
	pH- or/and ATP-mediated bond cleavage	phenylboronate	cationic polymer composed of phenylboronic acid, galactose-installed PEI, and PEG	pDNA	*in vitro & in vivo* (mice)	[102]
	pH & ROS responsiveness					
	increase of cationic charge at endosomal pH; ROS-responsive shielding	2-propylacrylic acid (PAA); ROS-cleavable peptide sequence -CP_5K-	methacrylate block copolymer with dimethylaminoethyl, butyl and free carboxyl groups; PEG attached *via* ROS degradable peptide linker	pDNA	*in vitro*	[132]

2.3 Sensitivity to enzymes

Tumors often overexpress certain enzymes. One prominent class are matrix metalloproteinases (MMPs), especially types 2 and 9, which degrade extracellular matrix of tumor tissue and therefore, play an important role in tumor growth, angiogenesis, and metastasis.[153] MMPs cleave their substrates between glycine and leucine. Incorporation of shielding agents into polyplexes *via* MMP-sensitive peptide linkers (*e.g.*, peptide sequence PLG*LAG[91-93]) leads to targeting with at least partial tumor specificity, because the polyplexes are deshielded by the up-regulated MMPs of the tumor tissue and can be then internalized into tumor cells.[91-95]

Zhu *et al.*, for example, designed a MMP2-sensitive co-polymer for siRNA and drug co-delivery, where PEG was attached in a MMP-reversible way (peptide sequence GPL*GIAGQ).[94] MMP2-triggered removal of PEG led to the exposure of previously hidden PEI, resulting in enhanced cell internalization. Another approach was carried out by Veiman *et al.*[91] They formed nanoparticles, where condensed cell-penetrating peptide PepFect14 and pDNA were shielded by PEG in a MMP2-responsive fashion (peptide sequence PLG*LAG), demonstrating efficient transfection as well as tumor specificity to some extent. Wang *et al.* developed a block copolymer for siRNA delivery, containing PEG, MMP2-sensitive peptide-linker (peptide sequence PLG*LAG), cationic cell-penetrating peptide nona-arginine (R9) and poly(ε-caprolactone).[93] The resulting micelles showed prolonged blood circulation time, accumulation in tumor and enhanced cellular uptake, mediated by exposed R9 after MMP2-triggered deshielding.

Furthermore, tumor cells often exhibit much higher intracellular esterase activity than normal cells. Qiu *et al.* created an esterase-responsive polymer containing quaternary amines carrying *N*-propionic 4-acetoxybenzyl ester substituents.[96] The ester groups were hydrolyzed rapidly by cytosolic esterases, resulting in charge conversion from cationic to zwitterionic state. Thereupon, the lipid-coated polyplexes disassembled and released their cargo (pDNA).

Enzyme-sensitive units can also be introduced to generate less toxic polymers. Pun and co-workers synthesized such an enzymatically degradable polymer by incorporation of a cathepsin B-sensitive peptide sequence (FK*FL).[97] Cathepsin B is an endo-lysosomal endopeptidase with acidic dependent proteolytic activity. By addressing this enzyme,

compartment-specific degradation, the release of cargo and reduced toxicity could be obtained.

2.4 pH-responsiveness

pH-responsive delivery systems are able to sense the differences in pH values of different biological compartments. Endosomes and lysosomes have acidic milieu with pH values of 4.5–6.5, whereas the cytosolic pH is around 7.2.[139, 154] Moreover, diseases like cancer can have an influence on the extra- and intracellular pH-profile. The extracellular pH is neutral (7.4) at physiological conditions. In solid tumors, for instance, it tends to be slightly acidic (~6.5) due to the so-called 'Warburg Effect'.[155, 156] Both endosomal acidification as well as acidic tumor tissue can trigger bond cleavages, charge conversions or conformational changes of pH-sensitive moieties within the polyplexes. This can be utilized for shielding strategies, endosomal escape as well as for degradation of polymers. Acid-triggered removal of shielding can be achieved by either breaking covalent bonds or reversal of charge-charge interactions of electrostatic coating, resulting in exposure of the underlying cationic polymer or other endosomolytic, membrane-active units. There exist several reviews on the topic of pH-responsive shielding strategies.[3, 89, 98] Acid-labile chemical bonds include vinylethers, acetals, ketals, pyridyl-hydrazones, β-thiopropionates, phosphoramidates, ortho-esters, esters,[157] imines,[99, 100] phenylboronates,[102, 103] and maleic acid amide linkers like dimethyl-, 2-propionic-3-methyl-[105, 107, 108] or azidomethyl-methyl-maleic acid amide.[106]

Another deshielding strategy, for example, was pursued by Chen *et al.* They designed a delivery system, where the PEG shield was attached *via* electrostatic interaction.[109] At acidic conditions in tumor tissue, 2,3-dimethylmaleic unit was split off, resulting in charge switch and detachment of the PEG shell. Thereby exposed folate and cationic charge led to enhanced cellular uptake.

pH-response also plays an important role in view of endosomal release, which is necessary to avoid lysosomal nucleic acid degradation. In this context, the so-called 'proton-sponge effect', firstly described for polyethylenimine (PEI) polyplexes,[143] together with endosomal buffering and direct lytic effects, provide an efficient escape mechanism.[3, 81, 88] This is based on inhibition of endosomal maturation and rupture of endosomal membranes, caused by osmotic vesicle swelling through chloride and water influx as well

as direct, destabilizing interactions with endosomal phospholipid-membranes (so-called 'needle-effect'). The latter can be observed for high-density polycationic polymers like PEI.[88] The aminoethane-motifs of, for example, PEI or artificial building blocks like succinoyl tetraethylene pentamine (Stp)[158] exhibit strong proton-sponge characteristics with sufficient protonation at neutral pH for nucleic acid binding and high endosomal cationization, which is responsible for buffering and lytic effects. Incorporation of histidines can further enhance endosomal escape due to the imidazole groups with pK_a values in the endosomal pH range, showing an advantageous cationization profile and high endosomal buffer capacity.[144]

Improvement of endosomal escape can be also obtained by incorporation of membrane-active peptides, inter alia, synthetic peptides like INF peptides (derived from influenza virus hemagglutinin HA2),[115, 147] melittin (derived from bee venom apitoxin),[104, 148, 159] or amphipathic artificial peptides such as GALA (glutamic acid-alanine-leucine-alanine motif).[160] Endosomal acidic milieu is exploited to activate acidic fusogenic peptides by pH-specific conformational changes (*e.g.*, in case of INF peptides),[115, 147] or to remove masking groups and thus restore lytic activity (*e.g.*, acid-labile 2,3-dimethyl maleamate protection group for melittin[104] and melittin-like peptides, respectively,[110, 111] or reversible conjugation of melittin to a carrier by an acid-labile hydrazone bond[148]).[89] Another approach for efficient endosomal release has been implemented by Cheng *et al.* (**Figure 2.3**).[149] The research group developed a so-called 'virus-inspired polymer for endosomal release' (VIPER), consisting of a cationic hydrophilic block for nucleic acid compaction and a pH-sensitive diisopropylaminoethyl (DPA) block, which shows a sharp phase transition around pH 6.3.[161, 162] At physiological pH, DPA is unprotonated, enabling self-assembly of VIPER into nanoparticles. Upon endocytosis it gets protonated in the endosomal acidic milieu. This switch from hydrophobic to hydrophilic leads to destabilization of the self-assembled nanostructures and to exposure of formerly hidden membrane-active melittin, resulting in enhanced endosomal release. Wang *et al.* also made use of the DPA building block to generate acid-activable micelleplexes for combined siRNA delivery and photodynamic therapy.[150] Cheng *et al.* further applied this concept of hydrophobic-hydrophilic phase transition to create a polymer, which underwent a hydrophilic shift in endosomes through the cleavage of acid-labile benzoic imines.[101] This loss of hydrophobicity led to a quick release of the nucleic acid.

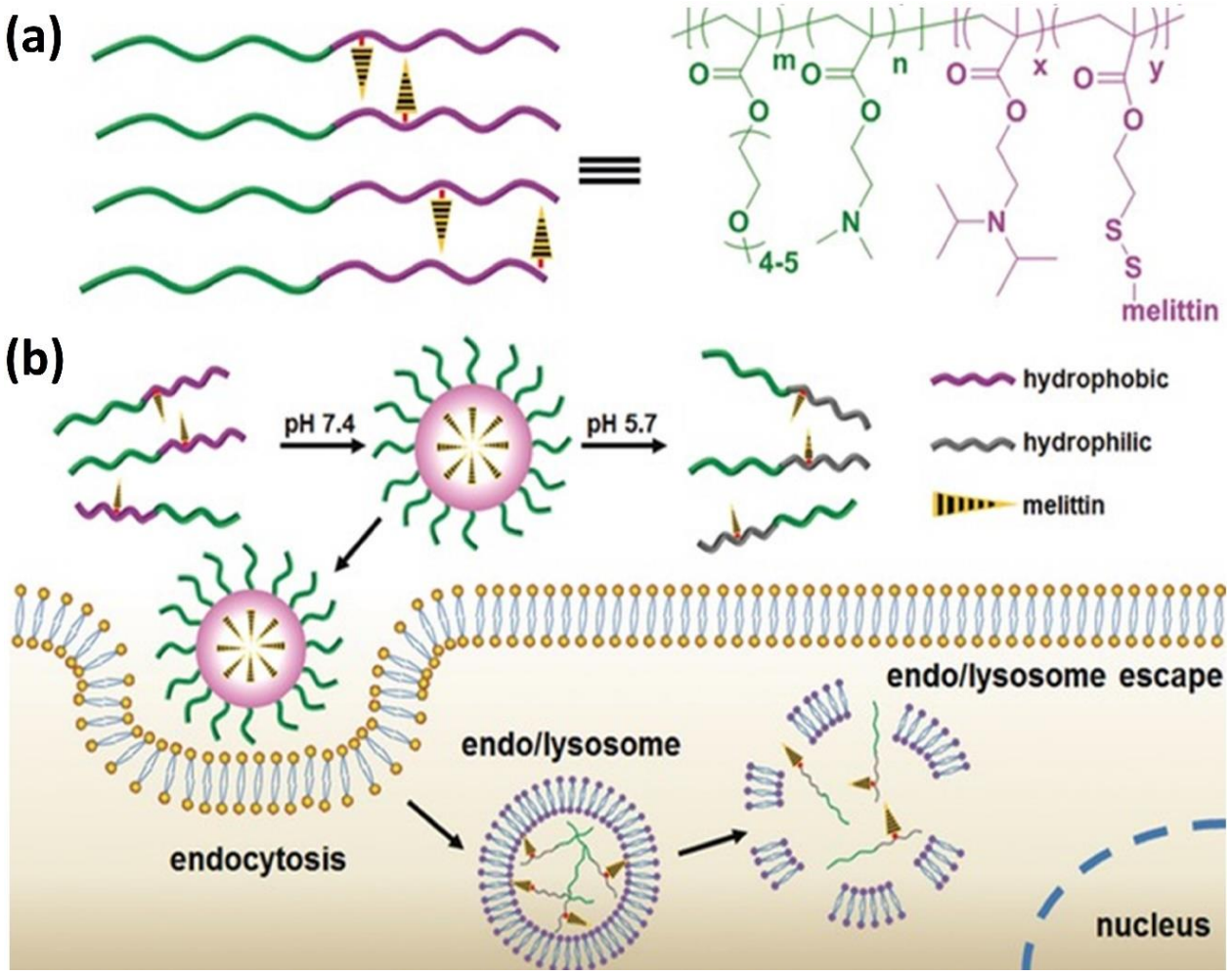

Figure 2.3. (**a**) Chemical structure of VIPER (virus-inspired polymer for endosomal release). (**b**) Illustration of VIPER-induced endo/lysosomal escape. At neutral pH, VIPER self-assembles into nanoparticles with melittin restricted to the pH-sensitive domain. After endocytosis by cells, the acidic endo/lysosome environment induces the hydrophilic phase transition of poly(2-diisopropylaminoethyl methacrylate) (pDIPAMA), enabling melittin exposure, disruption of the endo/lysosomal membrane, and endo/lysosomal escape. Reprinted with permission from [149]. Copyright © 2018; John Wiley and Sons.

Furthermore, pH-responsiveness can be also utilized to reduce cytotoxicity of cationic polymers like PEI. Smaller oligoamine subunits were linked through pH-sensitive bonds, resulting in larger polyamines.[3, 81, 88] Using this approach, advantages of both reduced toxicity of low molecular weight (LMW) oligomers and high transfection efficiency of high molecular weight (HMW) polymers can be exploited. Acid-labile linkages applied for this strategy include, amongst other things, esters, acetals, ketals, imines, hydrazones, and carbamates.

2.5 Redox-responsiveness

Bioreducible disulfide crosslinks can be used for extracellular stabilization of polyplexes, for attaching of shielding agents or targeting ligands, for masking of endosomolytic agents, as well as to enable biodegradation, resulting in release of cargo and improved biocompatibility.[3, 89, 114]

Intracellular glutathione (GSH) concentrations are 100- to 1000-fold higher than extracellular levels. Together with enzymes from the thioredoxin family, this creates a reductive cytosolic microenvironment, where disulfide bonds are cleaved by thiol-disulfide-exchange reactions.[114, 139] Moreover, endosomes and lysosomes possess reduction potential as well, mediated by enzymes like gamma-interferon-inducible lysosomal thiol reductase (GILT), which is optimally active at low pH around 4–5.[163] However, there exist also oxidoreductases such as protein disulfide isomerases (PDIs) in the extracellular space, especially at the cell surface, mediating cleavage of disulfides already outside the cell.[114]

Altogether, it is not that clear-cut where exactly bioreduction of disulfides takes place. Leroux and co-workers could show in a mechanistic study that easily accessible surface disulfide bonds of cationic dendrimers are reduced to a large or even total extent extracellularly, whereas, internal, sterically hindered disulfide bonds exhibit less bioreduction at the cell surface.[164] Moreover, they found that endosomal bioreduction is often incomplete and dependent on the target cell line and the carrier system itself.

For some carrier systems, the location of disulfide cleavage is less important anyway, but for others, it might be of greater interest.[114] For example, if the bioreducible nanocarrier should just provide extracellular stability of its cargo, the main cleavage process of the numerous disulfide bonds can be expected for the cytosol due to its higher redox capacity, resulting in intracellular dissociation, release of cargo and fragmentation of the carrier into less toxic units. In this context, it plays no important role, whether some fewer disulfide bonds are already cleaved in the extracellular space or in endosomes. Whereas, endosomal reduction would be preferable for redox-responsive masked endosomolytic agents (*e.g.*, inactive disulfide precursor listeriolysin O (LLO),[117, 118] or disulfide-crosslinked polymeric forms of melittin[119]). In this case, disulfide cleavage should lead to unmasking and activation of these fusogenic peptides, resulting in enhanced endosomal

escape. In case of redox-responsive shielding strategies, cleavage of the disulfide bonds already at the cell surface or within endosomes might be favorable.

Ping *et al.* developed a redox-responsive shielded gene carrier by host-guest supramolecular complexation.[120] The host segment consisted of β-cyclodextrin-crosslinked low molecular polyethylenimine (PEI), conjugated with a targeting ligand, analogous with previous work by Davis and colleagues.[165, 166] The guest segment consisted of an adamantyl group, linked with PEG by a disulfide bond. The PEG chains stabilized the DNA polyplexes extracellularly but could be cleaved intracellularly. This resulted in far higher transfection efficiency compared to corresponding stable shielded vectors. A quite similar approach was carried out by Liu *et al.*, forming multifunctional polymer conjugates for complexation of pDNA or siRNA.[121] As shielding component, mono-adamantane terminated disulfide bonded PEG was used.

Besides generation of HMW polymers by pH-sensitive linkage of LMW subunits, as described in section **2.4**, also disulfide bonds can be incorporated to create polymeric systems from smaller subunits. For example, LMW PEI can be bioreducibly crosslinked, resulting in reduced cytotoxicity but retained transfection potency.[3, 88] Oupický and colleagues synthesized polycations by direct Michael addition polymerization of chemokine receptor type 4 (CXCR4)-inhibitor AMD3100 with a disulfide-containing bisacrylamide.[122] The resulting bioreducible polymers were dual-functional and could serve as potent pDNA delivery vectors with additional antimetastatic efficacy.

However, disulfide bonds can also be integrated in side-chains. Klein *et al.* designed a disulfide-building block (ssbb) as precise cleavage site between a lipophilic diacyl-domain and a hydrophilic oligocationic siRNA binding unit.[123] These bioreducible lipopolyplexes exhibited extracellular stability, but were destabilized at reductive cytosolic conditions. They showed higher gene silencing efficiency and lower cytotoxicity compared to their stable analogs due to glutathione-triggered siRNA liberation and abolished lytic activity in cytosol. Another concept using redox-responsiveness was followed by Zheng *et al.*[124] They modified LMW PEI with hydrophobic lipoic acid, a reduction-sensitive natural compound. These biocompatible vectors showed high pDNA complexation and extracellular stability. After cellular uptake, reduction-triggered reversal of the hydrophobic modification led to release of pDNA.

Furthermore, differences in redox potential appear not only between different compartments at physiological conditions, but also between normal and tumor tissue. In particular, tumor tissue exhibits up to four times higher GSH levels,[167] enabling tumor targeting to some extent. Taking advantage of the GSH concentration gradient between tumor tissue and inside tumor cells, He *et al.* adopted a strategy for reduction-controlled hierarchical unpacking of carriers, mimicking the dynamic, step-by-step transfection of viruses (**Figure 2.4**).[125] They formed polyplexes of diselenide (SeSe)-conjugated oligoethylenimine (OEI) and pDNA, and coated them afterwards with disulfide bond (SS)-modified hyaluronic acid (HA). HA acted both as shielding agent and targeting ligand (CD44 receptor). This dual-responsive delivery system reacted in a stepwise fashion; firstly, disulfide bonds were cleaved at tumor site during cellular attachment or just after cellular uptake, resulting in deshielding and exhibition of the core particle, which then could mediate endosomal escape. Once reached the cytosol, the diselenide bonds were reduced at intracellular high GSH levels, leading to dissociation of the polyplexes and liberation of pDNA.

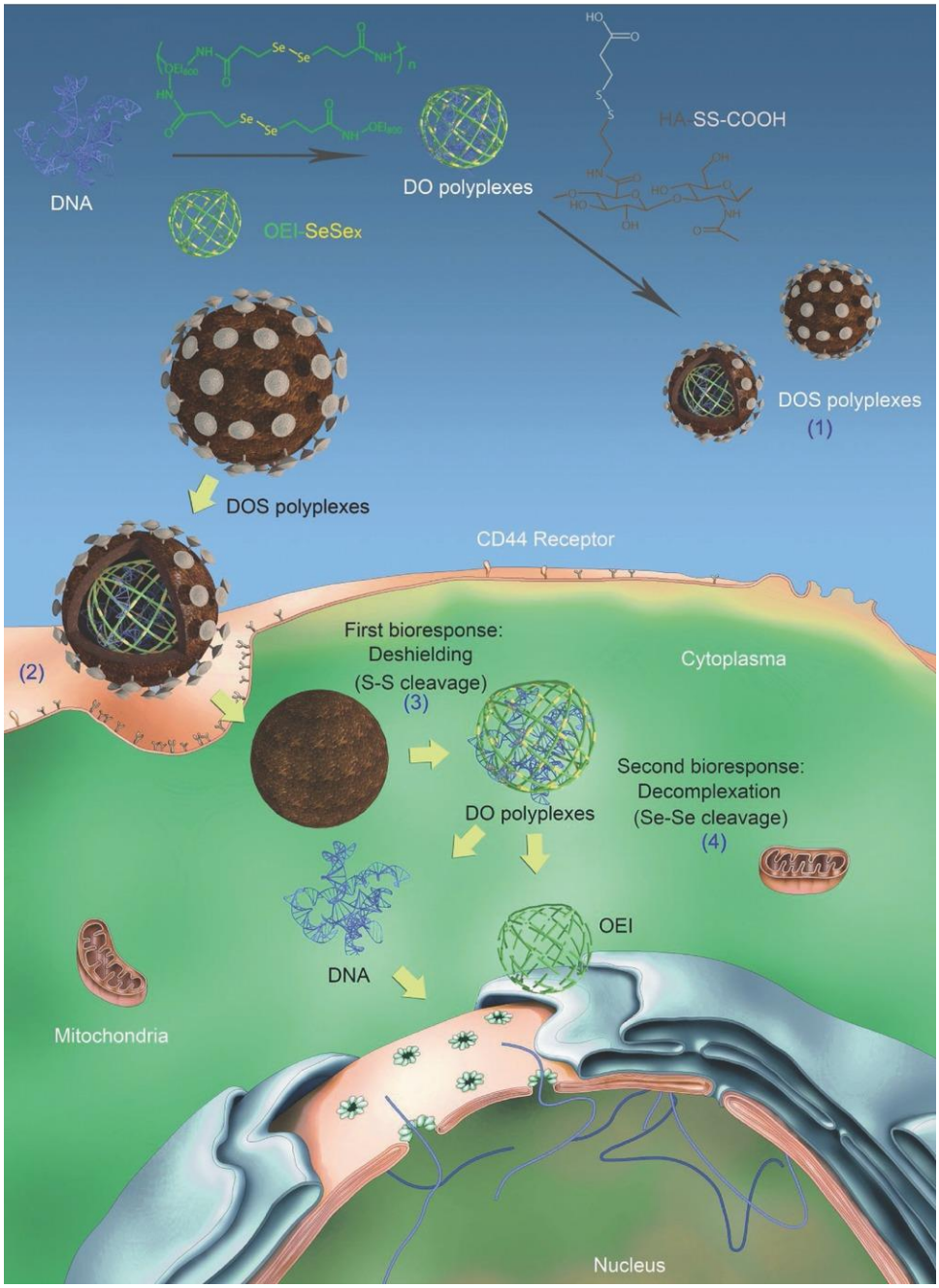

Figure 2.4. Reduction-controlled hierarchical unpacking of ternary polyplexes (DOS) for gene delivery. (**1**) ternary polyplexes formation by introduction of HA-SS-COOH to OEI-SeSe$_x$/DNA binary polyplexes (DO); (**2**) hyaluronic acid (HA)-receptor (CD44 receptor) mediated endocytosis; (**3**) reduction-triggered deshielding of HA-SS-COOH; (**4**) diselenide (Se–Se) cleavage and DNA release in reductive conditions. Reprinted with permission from [125]. Copyright © 2018; John Wiley and Sons.

2.6 Other endogenous triggers: ROS, ATP, hypoxia

Besides differences in enzyme activity, pH values and redox potential, varying ROS or ATP levels as well as hypoxia can be used as endogenous stimuli for bioresponsive delivery systems.[90] In the following, some strategies will be briefly illustrated.

Many serious diseases like cancer, diabetes, atherosclerosis, Alzheimer's disease or Parkinson's disease are related to oxidative stress and ROS overproduction.[168] High ROS levels can appear intra- and extracellularly. This can be exploited by incorporation of ROS-sensitive functional groups (*e.g.*, thioketals,[129] boronates,[130, 131] or ROS degradable peptides[132]) into nucleic acid carriers, achieving some kind of targeting effect. Ruan *et al.*, for example, designed a ROS-biodegradable positively charged polymer for pDNA or siRNA delivery into breast cancer cells by crosslinking of LMW branched polyethylenimine (b-PEI) *via* ROS-responsive phenylboronates.[130] This crosslinked b-PEI polymer was further modified with PEG and a targeting ligand. After receptor-mediated endocytosis and endosomal escape, the boronic ester linkers can be cleaved by intracellular elevated ROS levels, resulting in release of the cargo. The developed nanoparticles exhibited high transfection efficiency as well as biocompatibility.

Zhu *et al.* synthesized polysulfonium polymers with ROS-responsive boronic ester moieties (**Figure 2.5a**).[131] Triggered by intracellular ROS, the polymers degraded into neutral thioether fragments, efficiently releasing pDNA. The vectors showed strong serum resistance, low cytotoxicity, and high gene transfection. Gupta *et al.* created a ROS-responsive carrier, which addressed increased extracellular ROS.[132] This will be described more in detail in section **2.6**.

Cytosolic ATP concentrations are up to tenfold higher than those in the extracellular space.[169] This ATP gradient can be utilized as endogenous trigger. There exist different strategies to achieve ATP-responsiveness.

Zhang *et al.* made use of a single-stranded DNA aptamer, which can specifically bind ATP.[151] They prepared a ternary nanocomplex, composed of cationic polymer PEI, Bcl-2 (B-cell lymphoma 2) siRNA and a DNA duplex, constructed through hybridization of an ATP-responsive aptamer and its complementary DNA. Doxorubicin was stably loaded into this DNA duplex, but rapidly released in the cytosol due to ATP-response, which led to disassembly of the whole nanocomplex. The co-delivery of doxorubicin and Bcl-2 siRNA

had a synergistic, anti-proliferative effect on the tested tumor cell line. This could be helpful for opposing multidrug resistance of tumors.

Another way to create ATP-responsive delivery systems, is the incorporation of phenylboronic acid (PBA) units, which are able to form boronic esters with diol-containing molecules like ATP.[102, 133, 134] Kataoka and co-workers, for example, designed phenylboronate-functionalized polyion complex (PIC) micelles for siRNA or cholesterol-modified siRNA (Chol-siRNA) delivery (**Figure 2.5b**).[133, 134] Phenylboronate can bind 3'-ribose of the siRNA. This stabilizes the complex at conditions comparable with the extracellular environment, but results in rapid dissociation when the complex is exposed to ATP at concentrations associated with the intracellular milieu. In this manner, siRNA is exchanged by ATP and thus released into the cytosol.

Hypoxia is a common phenomenon of fast-growing solid tumors.[170] Rapid proliferation leads to an inadequate intratumoral blood circulation, and even angiogenesis cannot overcome the insufficient blood flow. This results in hypoxic regions and areas of necrosis. By developing hypoxia-sensitive delivery systems, passive tumor targeting is possible to some extent. Perche *et al.* synthesized a nanocarrier for hypoxia-induced siRNA delivery, where azobenzene served as hypoxia-sensitive, bioreductive linker between a PEG shell and the nanoparticle core.[135] After accumulation in the hypoxic tumor tissue, the azo-bond would be cleaved, resulting in deshielding, exposure of cationic core, and thus efficient uptake.

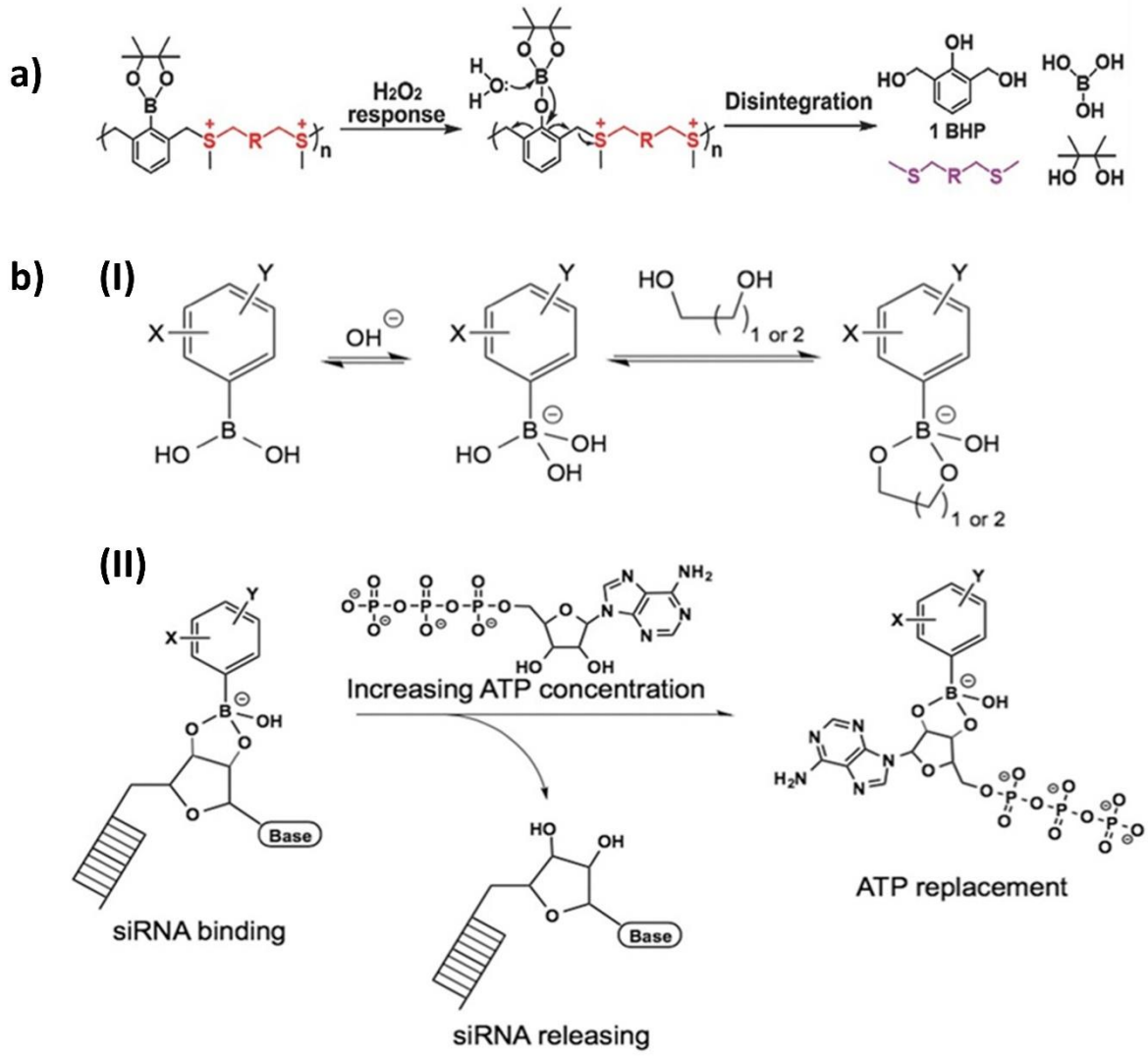

Figure 2.5. (**a**) ROS-responsive disintegrable polysulfonium: ROS-triggered degradation into uncharged thioether fragments. Reprinted with permission from [131]. Copyright © 2018; John Wiley and Sons. (**b, I**) Equilibrium between phenylboronic acid (PBA) derivatives and *cis*-diols in aqueous solution. (**b, II**) Binding of PBA derivatives with 3′ end of siRNA and replacement with ATP. Reprinted with permission from [134]. Copyright © 2018; John Wiley and Sons.

2.7 Examples for combined bioresponsiveness

The incorporation of two and more responsive units into one synthetic carrier formulation allows a better imitation of the stepwise, dynamic viral transfection process, resulting in higher efficiency and specificity. Several approaches exist for dual- and multi-responsive delivery systems, responding to endogenous or exogenous triggers or to both – and the number of approaches is steadily increasing. In the following, some examples for combined bioresponsiveness will be described.

The combination of pH- and redox-responsiveness has been applied by several working groups. Zhu *et al.*, for example, developed a pH- and redox-responsive nanocarrier for siRNA delivery, composed of a pH-responsive copolymer of methoxy-poly(ethylene glycol)-polylactide-polyhistidine (mPEG-b-PLA-pHis) and branched PEI (Mw1.8 k), linked with a redox cleavable disulfide bond.[126] Polyplex disassembly was located in endosomes, triggered by acidic milieu and reducing enzyme GILT. The subsequent efficient endosomal escape of siRNA was facilitated *via* endosomal membrane destabilization of detached PEI as well as 'proton-sponge effects' of pHis and PEI. Polyplexes with low nitrogen-to-phosphate (N/P) ratio (N/P 6) exhibited more efficient gene silencing *in vitro* and *in vivo* compared to those with higher N/P ratios (N/P 10 and 15) due to enhanced disassembly and endosomal release, which seemed to be a potential way to tackle the intracellular delivery bottleneck for siRNA delivery.

Parmar *et al.* developed endosomolytic poly(amido amine disulfide) polymers with a bioreducible backbone and bioreducibly conjugated siRNA.[116] The lytic potential of the polymer was masked at physiological pH in order to reduce cytotoxicity, but it could be restored in the acidic milieu of endosomes, resulting in efficient endosomal escape. In the cytosol, redox-triggered disassembly and release of siRNA led to efficient gene silencing *in vitro* and *in vivo*.

Yang *et al.* created octa-arginine (R8) peptides-conjugated polyamino acid derivatives, which comprised surface charge-switching, pH-responsiveness, intracellular redox-responsiveness and enhanced nuclear import of pDNA.[127] Imidazole and polyaspartate groups within the polymer backbone were responsible for pH-sensitivity. A decreased pH value (*e.g.*, as it occurs in tumor tissue) led to conversion of the polyplex surface charge from negative to positive, promoting enhanced cell membrane binding and cellular uptake. Moreover, these pH-responsive units exhibited enhanced endosomal buffering capacity after endocytosis. After endosomal escape, the disulfide bonds between R8 peptides and polymer side chains were cleaved rapidly under the reductive cytosolic conditions, leading to polyplex dissociation. R8 peptides could then facilitate nuclear import of the released DNA. Yang *et al.* were able to show that their carrier had great potential for both dividing and non-dividing cell transfection as well as for *in vivo* gene delivery.

A similar approach was applied by Jiang *et al.*[128] They constructed multistage-responsive pDNA-nanoparticles for pH-triggered pinpointed cascading charge-conversion and redox-

controlled pDNA release into the cytosol. These nanoparticles were composed of *i*) lipids modified with two different maleic amide derivatives, *ii*) disulfide bond containing dendronized polylysine, and *iii*) an arginine-rich lipid. The incorporated maleic amide derivatives (2,3-dimethylmaleic anhydride (DMMA) and citraconic anhydride (CIT)) served as charge-conversional moieties. Whereby, DMMA and CIT switched charge at different pH values. The first stage of charge reversal, caused by DMMA in the extracellular slightly acidic pH of tumor tissue (pH 6.8), promoted endocytosis. The second stage of charge conversion, caused by CIT, taking place in endosomes (pH 5.5), was supposed to enhance endosomal escape. After reaching the cytosol, redox degradation of the nanoparticles due to disulfide cleavage in the reductive cytosolic environment should lead to controlled pDNA release. The integrated arginines improve membrane penetration and possibly nuclear entry. Significantly enhanced transfection efficiency of these designed multistage-responsive nanoparticles compared to standard PEI were demonstrated *in vitro* as well as *in vivo*.

The combination of pH- and hypoxia-responsiveness was carried out by Liu *et al.*[152] The authors developed lipid molecules that became positively charged at low pH and hypoxia in tumor environment. These lipids consisted of hydrophobic tails conjugated with hypoxia-sensitive nitro-imidazoles, linkers, and tertiary amine head groups. They were integrated into liposomes for siRNA delivery into glioma cells. Thereby, siRNA was encapsulated by electrostatic interactions with the positive charged tertiary amines. Tumor accumulation was achieved to some extent due to enhanced internalization in hypoxic and low pH tumor environment. The hydrophobic nitro-imidazoles can be reduced to hydrophilic amino-imidazoles under hypoxic conditions. Additionally, the positive charge of the liposomes may increase due to protonation of the amino groups in the slightly acidic tumor tissue. This triggers an enhanced cellular uptake into tumor cells because of higher interaction with negatively charged cell surface membranes. Moreover, efficient siRNA delivery could be confirmed *in vitro* and *in vivo*.

Combined pH- and enzyme-responsiveness was utilized by Huang and colleagues.[92] The researchers generated nanoparticles, modified with a masked cell-penetrating peptide (CPP). Its activation was dual-triggered by lowered pH of tumor tissue as well as matrix metalloproteinase 2 (MMP2), up-regulated in many tumors. The internalization domain of CPP was quenched by a pH-responsive masking peptide, which was linked to CPP *via*

MMP2 substrate. After reaching the tumor environment, the masking peptide was cleaved off due to lowered pH, accompanied by enzymatic cleavage of the linker. The exposed CPP could then promote cellular uptake of the nanoparticle.

An example for combined pH- and ATP-responsiveness is the cationic polymer for pDNA delivery, which was developed by Kim *et al.*[102] It consisted of PBA, PEI with attached sugar galactose, and PEG. PBA formed chemical bonds with the diol groups of galactose, by this facilitating crosslinking of LMW PEI. These bonds were disrupted inside the cell by either acidic endosomal pH, intracellular ATP, or both, resulting in dissociation of the polymer and liberation of the payload. Moreover, PBA mediated some kind of tumor targeting because of high affinity to sialylated glycoproteins, often overexpressed on tumor cell surface.

Another dual-responsive nanocarrier was designed by Gupta and colleagues for pDNA delivery into vascular smooth muscle cells, which are overproducing ROS due to inflammation in context with atherosclerosis.[132] This PEGylated, oligoproline-derived block-copolymer was programmed to react first to extracellular high ROS levels, and then to endosomal pH. Extracellular ROS-sensitive de-PEGylation was obtained by incorporation of cysteine-(proline)$_5$-lysine peptide (CP$_5$K) as a ROS degradable linker between PEG and a cationic, pDNA condensing polymer block. Furthermore, a hydrophobic polymer block was included for core-stabilization. This block was ampholytic under physiological pH (pH 7.4), consisting of hydrophobic butyl methacrylate (BMA) as well as nearly equimolar ratios of positively charged *N,N*-dimethylaminoethyl methacrylate (DMAEMA) and negatively charged 2-propylacrylic acid (PAA). Under low endosomal pH, PAA gets protonated with simultaneous increasing positive charge of DMAEMA. This destabilizes the polyplex core and leads to membrane disruption, promoting endosomal release of the nanocarrier.

2.8 Conclusion

Many different extra- and intracellular steps and barriers exist in the systemic delivery of nucleic acids, making the whole delivery process very challenging. Furthermore, the different types of therapeutic nucleic acids have different demands on their carriers. Appropriate, efficient, and safe carrier systems are needed. In this context, non-viral, synthetic nano formulations such as lipo- and polyplexes have come into focus. Imitation

of the efficient, dynamic behavior of viruses can be achieved by incorporation of responsive, pre-programmed units into these non-viral delivery systems, which react to exogenous or endogenous triggers. Bioresponsive polyplexes sense changes in, for example, pH value, redox potential, or enzyme activity, resulting in activation or exposure of functional domains within or in collapse of the nanoparticle. This facilitates programmed, timely delivery of nucleic acids to the desired, specific sites. Besides this biochemical targeting, bioresponsiveness can help to reduce cytotoxicity and improve biocompatibility of cationic polymers. Combination of two and more responsive elements can help to increase both efficiency and specificity of the transfection process.

2.9 Expert opinion

In the last few decades, the growing field of non-viral delivery vectors gained more and more importance. The various examples for bioresponsive polymeric nucleic acid delivery systems, described in this review, underline the increasing interest in ‘artificial, synthetic viruses’ as alternatives to viral vectors. The latter represent very potent delivery systems and the majority of clinical gene therapy trials has been carried out with viral vectors so far.[6] Nevertheless, there are some disadvantages like immunogenicity, limited cargo capacity, rather sophisticated production, difficult production upscale and high production costs.[58, 81] In order to overcome these drawbacks and to create safer alternatives, non-viral, synthetic nanocarriers have come into focus.

The history of polymeric gene delivery systems goes more than 50 years back.[3, 81] Optimization of cationic polymers during this time led to increasingly improved nucleic acid transfer efficiency. Concrete starting points were given by the gained understanding of the single delivery steps and how nature deals with these different barriers as well as by the increased knowledge about the demands of the different nucleic acids on their carriers. By using precise synthetic strategies (like solid-phase assisted peptide synthesis, reversible addition fragmentation chain transfer (RAFT) polymerization or microfluidics) and combinatorial chemistry, libraries of well-defined carriers could be synthesized, enabling the identification of clear structure-activity relationships by high-throughput library screening. This opened the way for a ‘chemical and molecular evolution’ process,[3, 58, 81] facilitating the development from first generation polycations to multifunctional, bio-inspired sequence-defined delivery systems. These ‘synthetic artificial viruses’ mimic the

efficient process of viral transfection. Therefore, they should be dynamic and react to changes in microenvironment. In this manner, pinpointed, spatiotemporal controlled release as well as reduced cytotoxicity of the carrier can be obtained, resulting in improved specific nucleic acid delivery as well as in increased biocompatibility. Combined responsiveness is very advantageous and can enhance availability of the nucleic acid at its site of action. Nevertheless, transfection efficiency is still quite low – especially in comparison with viral vectors – and further improvement is necessary.

Moreover, stability issues of bioresponsive systems have to be considered in manufacture. Bioresponsive linkers are rather labile, as they are pre-programmed to sense marginal differences in microenvironment such as little changes in pH value or redox potential. This lability can cause problems, concerning production and storage of the nanoparticles. Furthermore, it might be difficult to ensure specificity and selectivity of the response. Altogether, high requirements are placed on the properties of the linker chemistry. Non-covalent responsive linkers can be an alternative to covalent ones. In such cases, stimuli-triggered charge conversion or changes in conformation or physicochemical properties lead to reversible disassembly of the nanocarrier. Thus, such non-covalent linkers might be more robust, as the disassembly is reversed in absence of the stimulus. In contrast, covalent bonds once cleaved cannot easily rebuild.

In view of translation into clinical settings, sufficient stability, high transfection efficiency as well as biocompatibility are desirable. At the moment, there are only few human clinical gene therapy trials with non-viral delivery formulations,[6] with most simple and stable systems such as naked DNA for vaccination[20] prevailing. It is noteworthy that already several synthetic oligonucleotides reached market approval[18] with chemical modifications, but without sophisticated formulation. Nevertheless, also some more complex formulations like lipid nanoparticles, cyclodextrin polyplexes, and N-aceytlgalactosamine (GalNAc) conjugates got in clinical studies.[21, 22] First examples of virus-mimetic nanosystems for siRNA delivery have entered clinical evaluation, such as transferrin receptor-targeted siRNA polyplexes for cancer therapy,[166] liver-tropic cholesterol-conjugated siRNA with GalNAc-conjugated masked endosomolytic melittin-like peptide,[111] or asialoglyco protein receptor targeted, stabilized siRNA conjugates, which are in advanced clinical trials for liver diseases.[111, 171-173] In August 2018, a major breakthrough has been achieved, with the FDA approving Patisiran (Onpattro™, a

bioresponsive shielded liposomal TTR (transthyretin) siRNA formulation) as first siRNA drug for treatment of hereditary transthyretin-mediated (hATTR) amyloidosis.[174] With further focusing on the optimization of precise synthetic viral mimetics, this trend will go on, and it is very likely that there will be more and more clinical trials and even market authorizations in the field of bioresponsive polyplexes in future.

2.10 Abbreviations

ATP, adenosine triphosphate; Bcl-2, B-cell lymphoma 2; BMA, butyl methacrylate; bp, base pair; b-PEI, branched polyethylenimine; CendR, C-end Rule; Chol-siRNA, Cholesterol-modified siRNA; CIT, citraconic anhydride; CP_5K, cysteine-(proline)5-lysine; CPP, cell-penetrating peptide; CRC, cysteine-arginine-cysteine; CXCR4, chemokine receptor type 4; DMAEMA, *N,N*-dimethylaminoethyl methacrylate; DMM, 2,3-dimethyl maleamate; DMMA, 2,3-dimethylmaleic anhydride; DOPE, 1,2-dioleoyl-*sn*-glycero-3-phosphoethanolamine; DPA, diisopropylaminoethyl; DSPE, 1,2-distearoyl-phosphatidylethanolamine; E_4K_4, $(glutamate)_4$-$(lysine)_4$; EPR, enhanced permeation and retention; FDA, Food and Drug Administration; FK*FL, phenylalanine-lysine-phenylalanine-leucine; GALA, synthetic fusogenic protein with glutamic acid-alanine-leucine-alanine motif; GalNAc, *N*-aceytlgalactosamine; GILT, gamma-interferon-inducible lysosomal thiol reductase; GPL*GIAGQ, glycine-proline-leucine*glycine-isoleucine-alanine-glycine-glutamine; GSH, glutathione; HA, hyaluronic acid; hATTR amyloidosis, hereditary transthyretin-mediated amyloidosis; HMW, high molecular weight; HPMA, *N*-(2-hydroxypropyl)methacrylamide; LLO, listeriolysin O; LMW, low molecular weight; MMP, matrix metalloproteinase; Mw, molecular weight; mPEG-b-PLA-pHis, methoxy-poly(ethylene glycol)-polylactide-polyhistidine; mRNA, messenger RNA; N/P ratio, nitrogen-to-phosphate ratio; NGR, asparagine-glycine-arginine; ODN, oligodeoxynucleotides; OEI, oligoethylenimine; PAA, 2-propylacrylic acid; PBA, phenylboronic acid; pBAVE, poly(butyl and amino vinyl ether); PDI, protein disulfide isomerase; p(DIPAMA), poly(2 -diisopropylaminoethyl methacrylate); pDNA, plasmid DNA; PEG, polyethylene glycol; PEI, polyethylenimine; pHPMA, poly(*N*-(2-hydroxypropyl)-methacrylamide); PIC, polyion complex; PLG*LAG, proline-leucine-glycine*leucine-alanine-glycine; PLL, poly-(*L*)-lysine; R8, octa-arginine; R9, nona-arginine; RGD, arginine-glycine-aspartate; ROS, reactive oxygen species; SeSe,

diselenide; siRNA, small-interfering RNA; SS, disulfide; ssbb, disulfide-building block; Stp, succinoyl tetraethylene pentamine; TAT, transactivator of transcription; TTR, transthyretin; VIPER, virus-inspired polymer for endosomal release.

2.11 Acknowledgements

We are greatly thankful for support of our work by German Research Foundation (DFG) DFG SFB1032 B4 and SFB1066 B5 as well as the DFG Excellence Cluster ‘Nanosystems Initiative Munich (NIM)’.

3. Optimizing pDNA lipo-polyplexes: A balancing act between stability and cargo release

Simone Berger, Ana Krhač Levačić, Elisa Hörterer, Ulrich Wilk, Teoman Benli-Hoppe, Yanfang Wang, Özgür Öztürk, Jie Luo, and Ernst Wagner*

Pharmaceutical Biotechnology, Department of Pharmacy, and Center for NanoScience (CeNS), Ludwig-Maximilians-Universität (LMU) Munich, Butenandtstr. 5-13, D-81377 Munich, Germany

* Corresponding author: S. Berger

This chapter is adapted from a pre-copy-edited version of a peer-reviewed research article published in ***Biomacromolecules*** **2021, 22, (3), 1282-1296 (ref. [29]).**

Author contributions

The manuscript was written through contributions of all authors. S. Berger: Conceptualization, writing and illustrations – original draft, review, and editing; synthesis of the histidine and histidine-free library; pDNA polyplexes – preparation, physicochemical characterization, and transfections; establishment of in vitro serum assays. A. Krhač Levačić: pDNA polyplex transfections; writing – review. E. Hörterer and U. Wilk: In vivo experiments. T. Benli-Hoppe: Synthesis of mono- and bisDBCO-PEG24 as well as of the oligo-cysteine library; Y. Wang: siRNA polyplexes – preparation, physicochemical characterization, and transfections. Ö. Öztürk: TEM measurements and analysis; J. Luo: synthesis of the histidine-free library; E. Wagner: Supervision, conceptualization, writing – review and editing; funding acquisition. All authors gave approval to the final version of the manuscript.

Table of contents (TOC) figure

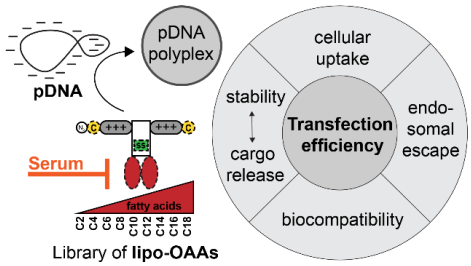

Abstract

When optimizing nanocarriers, the structural motifs that are beneficial for the respective type of cargo need to be identified. Here, succinoyl tetraethylene pentamine (Stp)-based lipo-oligoaminoamides (OAAs) were optimized for delivery of plasmid DNA (pDNA). Structure variations comprised saturated fatty acids with chain lengths between C2 and C18 and terminal cysteines as units promoting nanoparticle stabilization, histidines for endosomal buffering, and disulfide building blocks for redox-sensitive release. Biophysical and tumor cell culture screening established clear-cut relationships between lipo-OAAs and characteristics of formed pDNA complexes. Based on optimized alternating Stp-histidine backbones, lipo-OAAs containing fatty acids around C6 to C10 displayed maximum gene transfer with around 500-fold higher gene expression than C18 lipo-OAA analogs. Promising lipo-OAAs, however, showed only modest *in vivo* efficiency. *In vitro* testing in 90% full serum, revealing considerable inhibition of lytic and gene transfer activity, was found as new screening model predictive for intravenous application *in vivo*.

Keywords

Lipo-polyplexes, saturated fatty acids, bioreducible disulfides, nucleic acids, plasmid DNA.

3.1 Introduction

Gene therapy is a potent field of modern, personalized medicine for tumor and genetic diseases, and its impact is continuously growing.[6] However, there are still a lot of hurdles

to deal with, especially in the case of synthetic therapeutic nucleic acid carriers.[175-180] Cellular internalization of nucleic acids across lipid membranes is hindered due to their big size and, in most cases, negative charge. Therefore, appropriate carrier systems are required for efficient delivery of nucleic acids, comprising extracellular stabilization and protection, efficient cellular uptake, and intracellular cargo release.[3] In addition, these shuttles should be biocompatible and ideally non-toxic. One option is the use of polymer complexes (polyplexes)[3, 25, 181] formed by electrostatic interactions between cationic polymers and anionic nucleic acids like plasmid DNA (pDNA) or small-interfering RNA (siRNA). As alternative to classical synthesis of cationic polymers and dendrimers, solid-phase assisted peptide synthesis (SPPS) presents a feasible way to create oligoaminoamide (OAA) carriers in a sequence-defined manner.[62-64] Thereby, functional moieties and their position within such artificial peptide-like structures can be altered *via* modular design. By doing so, relationships between OAA sequence and polyplex properties can be derived. From this, carriers can be optimized for each type of nucleic acid, as each nucleic acid places different demands on its delivery system.[13, 26, 86, 182] Functional units of interest are inter alia structural motifs for nucleic acid binding, endosomal escape, nanoparticle stabilization, and carrier biodegradability. Succinoyl tetraethylene pentamine (Stp)[158] and homologues such as succinoyl pentaethylene hexamine (Sph)[106, 144, 183, 184] have the ability to bind nucleic acids because of their cationizable aminoethylene motif, and offer together with additionally incorporated histidines an endosomal buffering effect, thereby improving endosomal escape.[144, 184, 185] Based on the pioneer works on polyhistidines[186, 187] as well as on a histidine-containing peptide H5WYG,[188] several working groups incorporated histidines in their carrier structures in order to enhance the buffering capacity at endosomal pH, thereby increasing the osmotic swelling and lysis of endosomes.[3, 189, 190] For example, introducing histidines in polymers like poly-*L*-lysine (PLL)[191-194] or linear polyethylenimine (L-PEI),[195, 196] or histidine-lysine peptides[27, 197, 198] could strongly improve gene transfection. In our own research, lipid-free OAAs with 3-arm and 4-arm topologies, containing three (to four) units of Stp/Sph and histidines in alternating sequence per arm, were found as favorable carrier structures for *in vitro* and *in vivo* gene transfer.[106, 144, 184] Polyplex stability can be increased by bioreversible disulfide-forming cysteines.[64, 114, 199, 200] For siRNA delivery, incorporation of further stabilization domains, in particular tyrosine

tripeptides[137] and fatty acids,[64, 136, 200] into OAAs resulted in siRNA lipo-polyplexes with favorable activities. Fatty acids may show acyl length-dependent membranolytic activity, promoting endosomal release. However, they may also cause cytotoxicity. Redox-sensitive disulfide blocks (ssbb) separating the lipid domain from the cationic backbone can be included to handle the toxicity issue, but they also may display destabilizing effects by premature bioreduction.[123] Systematic studies evaluating the length of fatty acids, the role of the disulfide units and incorporated histidines in lipo-OAA pDNA polyplexes were not available at the start of this study.

As reported in the current work, the design of a novel library of T-shaped lipo-OAAs with different structure variations enables a systematic and comprehensive investigation of the impact of single structural motifs on physicochemical properties such as stability as well as on gene-transfer performance of resulting pDNA lipo-polyplexes in three different tumor cell lines. Structure variations comprised *i)* histidines in alternating sequence with Stp, *ii)* cysteines, or disulfide blocks, and *iii)* a hydrophobic diacyl domain in the side-chain, consisting of two lysine-connected saturated fatty acids. With the screening of this library, the influence of cysteines and disulfide blocks as well as the impact of the chain length of saturated fatty acids on lipo-polyplex stability was investigated. The positive effect of histidines on transfection efficiency, as previously observed for lipid-free structures, was verified. Altogether, the relationship between polyplex stability and transfection efficiency was figured out.

The most promising pDNA carrier structures of the *in vitro* screening were chosen for further evaluation of systemic *in vivo* application in a tumor mouse model. For this purpose, introduction of polyethylene glycol (PEG) was considered as beneficial measure preventing polyplex aggregation and interaction with blood components, thereby improving gene-transfer performance.[3, 201] As recently reported by Klein and colleagues, azido-lysines can be incorporated into lipo-OAAs, enabling post-functionalization of formed siRNA lipo-polyplexes *via* strain-promoted alkyne-azide cycloaddition (SPAAC) with ligand-PEG conjugates bearing one or two dibenzocyclooctyne (DBCO) units as attachment groups.[202, 203] The current work investigated the shielding agents monoDBCO-PEG_{24} and bisDBCO-PEG_{24} for the modification of azido-lipo-OAA pDNA polyplexes. Both have already been used previously in siRNA delivery and siRNA co-delivery with chemotherapeutic drugs.[204, 205] Here, they were tested for pDNA delivery.

Moreover, new assays investigating the impact of serum on the behavior of lipo-OAAs and their resulting pDNA lipo-polyplexes were established, in order to provide a better basis for predictions of *in vivo* properties.

3.2 Experimental section

Further information regarding materials and methods is provided in section **3.5** "**Supporting information**".

3.2.1 Materials

Plasmid pCMVLuc (encoding *Photinus pyralis* firefly luciferase under control of the cytomegalovirus promotor and enhancer)[60] was obtained from Plasmid Factory GmbH (Bielefeld, Germany). Linear polyethylenimine (L-PEI) 22kDa was synthesized and analyzed as described before.[206, 207] The starting product poly(2-ethyl-2-oxazoline) was purchased from Sigma Aldrich (Munich, Germany). Mono- and bivalent DBCO-PEG_{24} agents were synthesized and analyzed as described in previous works.[204, 205] In short, monoDBCO-PEG_{24} and bisDBCO-PEG_{24} were synthesized *via* SPPS. In the case of the latter, a symmetrical branching point was introduced by Fmoc-*L*-Lys(Fmoc)-OH. *N*-Fmoc-*N''*-succinyl-4,7,10-trioxa-1,13-tridecanediamine (Fmoc-STOTDA-OH) was used as a short hydrophilic spacer between the DBCO units and the branching lysine. Cleavage was performed according to an improved protocol with a mixture of 90% (v/v) dichloromethane (DCM), 5% (v/v) trifluoroacetic acid (TFA), 2.5% (v/v) H_2O, and 2.5% (v/v) triisopropylsilane (TIS).[202] Both DBCO agents were purified by preparative HPLC (high performance liquid chromatography), lyophilized and mass was confirmed by MALDI-TOF (matrix-assisted laser desorption/ionization time-of-flight) mass spectrometry (MS). Oleic acid-containing lipo-OAAs ***1214*** ((H-Stp)$_2$-cys-C18:1) and ***1218*** ((H-Stp)$_2$-ssbb-C18:1) were synthesized and analyzed as published previously.[28, 208] An important point to be noted here is that an optimized cleavage protocol was used comprised of an ice-cooled cleavage cocktail and a reduced incubation time of 30 min instead of 90 min in order to avoid TFA adducts and hydroxylation at the double bond.[209]

3.2.2 Synthesis of lipo-oligoaminoamides *via* solid-phase assisted peptide synthesis

Lipo-OAAs were synthesized under standard Fmoc-based SPPS with a 2-chlorotrityl chloride resin as a solid support, which was preloaded with the first C-terminal amino acid (for resin loading, *see* section *3.5.1.3*). Coupling steps were carried out using a Syro

Wave synthesizer (Biotage, Uppsala, Sweden). The artificial Fmoc-/Boc-protected oligoamino acid Fmoc-Stp(Boc)$_3$-OH as well as the solid-phase-compatible redox-sensitive disulfide building block (ssbb) were synthesized as described before.[123, 158] Reagents were prepared in separate bottles as follows: 4 equiv of Fmoc-α-*L*-amino acid were dissolved together with 4 equiv of 1-hydroxybenzotriazole (HOBt) in *N,N*-dimethylformamide (DMF), 4 equiv of 2-(1H-benzotriazol-1-yl)-1,1,3,3-tetramethyluronium-hexafluorophosphate (HBTU) in DMF, and 8 equiv of *N,N*-diisopropylethylamine (DIPEA) in *N*-methyl-2-pyrrolidone (NMP). Each coupling was conducted twice in 10 mL/g resin for 90 min at room temperature (RT) (double couplings). Deprotection was done four times for 10 min with 20% (v/v) piperidine in DMF (10 mL/g resin). After each coupling or deprotection step, the resin was washed with DMF (10 mL/g resin) five times for 1 min each. Symmetrical branching points were introduced using Fmoc-*L*-Lys(Fmoc)-OH, and asymmetric branching points were introduced using Fmoc-*L*-Lys(Dde)-OH. Removal of the *N*-(1-(4,4-dimethyl-2,6-dioxocyclohexylidene)ethyl) (Dde) protection group was performed with 2% (v/v) hydrazine in DMF for 15 cycles of 2 min each. Then, the resin was washed with DMF for five cycles of 1 min each, with 10% (v/v) DIPEA in DMF for five cycles of 2 min each, and finally with DMF for six cycles of 1 min each. With the whole sequence completed, the resin was dried *in vacuo* prior to cleavage. The lipo-OAAs were cleaved off the resin by incubation with a mixture (10 mL/g resin) of 95% (v/v) TFA, 2.5% (v/v) H_2O, and 2.5% (v/v) TIS for 90 min at RT. In the case of cysteine-containing structures, a cleavage cocktail (10 mL/g resin) consisting of 94% (v/v) TFA, 2.5% (v/v) H_2O, 2.5% (v/v) 1,2-ethanedithiol (EDT), and 1% (v/v) TIS was used. The lipo-OAAs were immediately precipitated in 40 mL methyl *tert*-butyl ether (MTBE)/*n*-hexane 1:1 at –20 °C. After centrifugation (4000 rpm, 4 °C, 10 min), the pellets were dried *in vacuo* and then resolved in H_2O. Purification took place by dialysis against 10 mM hydrochloric acid (HCl) overnight (~16 h) at 4 °C. Pre-wetted dialysis membranes made of regenerated cellulose with a molecular weight cut-off (MWCO) of 2 kDa or 3.5 kDa were used (Spectra/Por 7, Carl Roth, Karlsruhe, Germany). Finally, acetonitrile (AcN) was added to the dialyzed samples, reaching a final concentration of 70% (v/v) 10 mM HCl and 30% (v/v) AcN. OAAs used in the *in vivo* study were purified by size exclusion chromatography using an Äkta system (GE Healthcare Bio-Sciences AB, Uppsala, Sweden) based on a P-900 solvent pump module, a UV-900 spectrophotometrical detector,

a pH/C-900 conductivity module, a Frac-950 automated fractionator, and a Sephadex G-10 column. As solvent, 10 mM HCl/AcN in a ratio of 7:3 was used. In the end, the purified OAA solutions were lyophilized using a Christ Alpha 2-4 Ldplus laboratory freeze-drier (Martin Christ Gefriertrocknungsanlagen, Osterode am Harz, Germany). OAA identities were validated by MALDI-TOF MS and ^{1}H NMR (nuclear magnetic resonance) spectroscopy (both methods are described in detail in the *supporting information* – sections *3.5.1.4* and *3.5.1.5*).

3.2.3 Erythrocyte leakage assay

Fresh human blood, buffered with 25 mM citrate, was washed with phosphate-buffered saline (PBS) until a clear supernatant was obtained. After centrifugation (2000 rpm, 4 °C, 10 min), the cell pellet was diluted to 5×10^{7} erythrocytes per mL with different PBS buffers (pH 7.4, 6.5, and 5.5). A volume of 75 µL of OAA solution, previously diluted with PBS of the respective pH value, was pipetted to each well of a V-bottom 96-well plate (NUNC, Denmark). The same volume of erythrocyte suspension at the same pH value was added to each well. The final concentration of lipo-OAA per well was 2.5, 5, or 7.5 µM. The plates were incubated at 37 °C under constant shaking for 60 min. After centrifugation, 100 µL of the supernatant was analyzed for hemoglobin release at the wavelength λ = 405 nm using a microplate reader (Spectrafluor Plus, Tecan, Männedorf, Switzerland). PBS at the indicated pH values served as negative control (0% value), whereas Triton X-100 at the indicated pH values was used as positive control (100% value). Data are presented as mean value (± SD) out of quadruplicate.

The erythrocyte leakage assay was also performed with OAAs pre-incubated in 90% (v/v) fetal bovine serum (FBS) for 2 h at 37 °C under constant shaking (250 rpm). These serum-incubated OAAs were then diluted with PBS of different pH values (pH 5.5, 6.5, and 7.4), and the experiment was performed as described above with a final OAA concentration of 5 µM.

3.2.4 Formation of pDNA lipo-polyplexes and post-functionalization *via* orthogonal click-chemistry

pDNA and lipo-OAAs at an indicated N/P (nitrogen to phosphate) ratio of 12 were diluted separately with HBG (20 mM HEPES buffered with 5% (w/v) glucose; pH 7.4) to equal volumes. The pDNA solution was added to the lipo-OAA solution, mixed by 10× rapid pipetting and incubated for 40 min at RT. The N/P ratio was calculated under

consideration of the cationic secondary amines of the building block Stp as well as the amino group of the N-terminal amino acid, and the anionic phosphate groups of the pDNA backbone. In the case of shielded polyplexes, the pDNA lipo-polyplexes were modified with 0.25 equiv of different DBCO agents (monoDBCO-PEG_{24}, bisDBCO-PEG_{24}) in the second step. Here, equivalents are defined as molar ratios of DBCO agent to OAA in the polyplex solution.[202] The concentrations of DBCO agents were calculated according to the desired 0.25 equiv. The DBCO agents were diluted in one-fourth of the volume of the polyplex solutions. After addition and mixing by 5× rapid pipetting, the polyplexes were incubated for 4 h at RT. For comparison, unmodified polyplexes were prepared in the same manner, but HBG was added instead of DBCO agent.

3.2.5 Luciferase gene-transfer in cell culture

24 h prior to transfection, cells were seeded in 96-well plates at the desired density (10,000 cells per well in the case of Huh7 and N2a cells; 8000 cells per well in the case of KB cells). Transfection efficiency of the lipo-OAAs was evaluated using 200 ng pCMVLuc per well. HBG served as negative control and L-PEI polyplexes at the non-toxic optimum N/P ratio of 6 as positive control.[144, 210] All experiments were performed in triplicate. The medium was replaced with 75 µL of fresh medium containing 10% (v/v) FBS, and polyplexes formed at an N/P ratio of 12 in 25 µL HBG as described above (section 3.2.4) were added to each well. The plates were incubated at 37 °C without change of the medium. For all experiments, at 24 h after transfection, the cells were treated with 100 µL luciferase cell culture lysis reagent 0.5× [12.5 mM tris(hydroxymethyl)aminomethane buffer (pH 7.8) with phosphoric acid, 1 mM dithiothreitol (DTT), 1 mM 1,2-diaminocyclohexane-*N,N,N',N'*-tetraacetic acid (CDTA), 5% glycerol, 0.5% Triton X-100; Promega, Mannheim, Germany] for 45 min at RT. Luciferase activity in 35 µL cell lysate was measured for 10 sec in a Centro LB 960 plate reader luminometer (Berthold Technologies, Bad Wildbad, Germany), using 100 µL/well of a LAR buffer solution (20 mM glycylglycine, 1.0 mM $MgCl_2$, 0.10 mM EDTA (ethylenediaminetetraacetic acid), 3.3 mM DTT, 0.55 mM ATP (adenosine 5′-triphosphate), 0.28 mM Coenzyme A stock solution; pH 8-8.5) supplemented with 5% (v/v) of a mixture of 10 mM luciferin and 29 mM glycylglycine. The transfection efficiency is presented as relative light units (RLU) per well.

3.2.6 Transfection experiments with serum-incubated pDNA lipo-polyplexes

Transfection experiments (luciferase gene expression assay; CellTiter-Glo assay) were also performed with serum-incubated pCMVLuc lipo-polyplexes in different settings. Therefore, polyplexes (N/P = 12; HBG) were prepared at higher pDNA concentration (30-times higher than used in normal *in vitro* transfections, better resembling the *in vivo* conditions). These concentrated polyplexes were diluted 1:10 with 100% FBS, 50% FBS/50% HBG, or 100% HBG, respectively, and were instantly put on the cells (0 min time point) or incubated for 2 h under constant slight shaking (250 rpm) at 37 °C (serum) or RT (HBG). Transfection took place under normal conditions (25 µL polyplex per well, containing 600 ng pCMVLuc; 75 µL medium supplemented with 10% FBS). Incubation of polyplexes on cells was for 24 h at 37 °C. Finally, the read-out was at 24 h after transfection according to the protocols described in section 3.2.5 (luciferase gene expression assay) as well as in section *3.5.1.12* (CellTiter-Glo assay), respectively.

3.2.7 Luciferase gene-transfer *in vivo*

In vivo experiments were performed according to the guidelines of the German Animal Welfare Act and were approved by the animal experiments ethical committee of the Government of Upper Bavaria (accreditation number Gz. ROB-55.2-2532.Vet_02-19-20). N2a cells (1×10^6 cells in 150 µL PBS) were inoculated subcutaneously into the left flank of 6-week-old female mice, Rj:NMRI-nu (nu/nu) (Janvier, Le Genest-St-Isle, France), and the animals were randomly divided into groups of three. Mice were housed in isolated ventilated cages under specific pathogen-free conditions with a 12 h day/night interval, and food and water were provided *ad libitum*. The weight and general well-being were monitored continuously. Tumor size was measured with a caliper and determined by using the formula: $\frac{a\times b^2}{2}$ (*a* = longest side of the tumor; *b* = widest side vertical to *a*). When tumors reached a size of approximately 500 mm^3, the experiments started by intravenous injection of lipo-polyplexes formed at an N/P ratio of 12 as described above (section 3.2.4), containing 60 µg of pCMVLuc in 250 µL HBG. As positive control, L-PEI polyplexes (N/P = 6, HBG) were used. Mice were euthanized 24 h after injection. The tumors were dissected and washed carefully with PBS, followed by analysis *via* an *ex vivo* luciferase gene expression assay. For this purpose, tumor tissues were homogenized *via* grinding in a mortar under liquid nitrogen cooling and incubated in

luciferase cell culture lysis reagent 1× (for composition *see* section 3.2.5; Promega, Mannheim, Germany) for 20 min at RT. Then, the samples were frozen overnight at –80 °C to ensure full lysis. In a next step, the samples were thawed and centrifuged for 10 min at maximum speed (~ 13 000 rpm) and 4 °C. Luciferase activity was measured in 50 µL of the supernatant at the same conditions as described in section 3.2.5. The transfection efficiency is presented as RLU per gram (g) tumor.

3.2.8 Statistical analysis

Results are presented as arithmetic mean ± standard deviation (SD) out of at least triplicates. Unpaired Student's two-tailed *t*-test was performed using GraphPad Prism in order to analyze the statistical significance. Significance levels are indicated with symbols: ns $p > 0.05$; * $p \leq 0.05$; ** $p \leq 0.01$; *** $p \leq 0.001$; **** $p \leq 0.0001$.

3.3 Results and discussion

3.3.1 Design of the lipo-oligoaminoamides library

A library of novel sequence-defined lipo-OAAs was synthesized *via* standard Fmoc SPPS (**Scheme 3.1**). The library is based on a previously reported T-shaped lipo-OAA structure, ID ***454***.[137] This carrier has favorable efficacy for siRNA delivery. All sequences of the library have following motifs in common: four Stp units, two tyrosine tripeptides (Y_3), central branching lysines (K) for attachment of the diacyl side chain, and an additionally incorporated azido-lysine [K(N_3)] for optional click modification of formed lipo-polyplexes with DBCO-containing targeting and shielding agents (**Scheme 3.2** in section 3.3.3).

Scheme 3.1. Structures of the histidine library (*left*) and the histidine-free library (*right*).

Structures:		**Residue X:**
Histidine library **(H-Stp)$_2$**	Histidine-free library **Stp$_2$**	Acetic acid (**C2**)
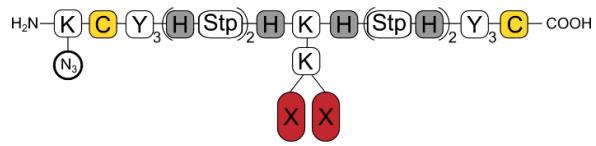 with cysteines (**cys**)	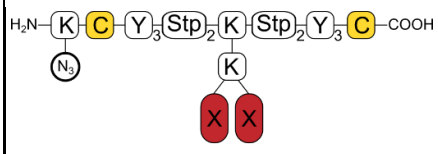 with cysteines (**cys**)	Butyric acid (**C4**)
		Hexanoic acid (**C6**)
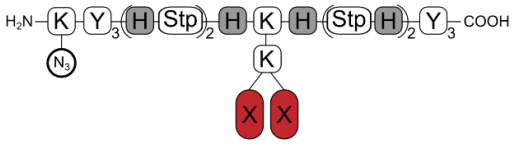 without cysteines (**0**)	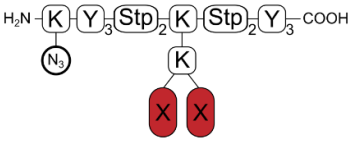 without cysteines (**0**)	Octanoic acid (**C8**)
		Decanoic acid (**C10**)
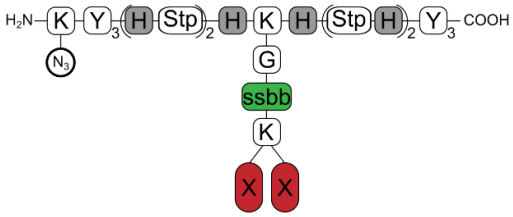 with disulfide block (**ssbb**)	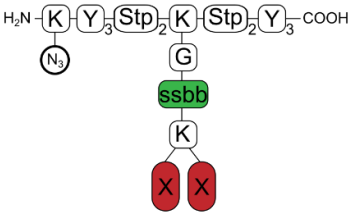 with disulfide block (**ssbb**)	Lauric acid (**C12**)
		Myristic acid (**C14**)
		Palmitic acid (**C16**)
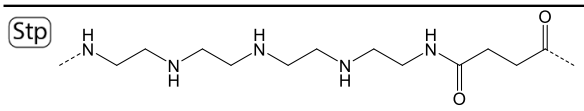	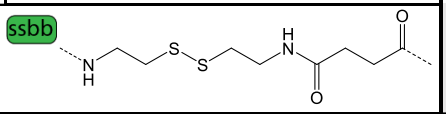	Stearic acid (**C18**)

K(N_3): azido-lysine; C: cysteine; Y: tyrosine; H: histidine; K: lysine; G: glycine; ssbb: cystamine disulfide building block; Stp: succinoyl tetraethylene pentamine; X: residue with saturated fatty acids of different chain lengths, as presented on the very right. The individual compound IDs are listed in **Table 3.1** and **Table 3.2**.

In the preferred (and subsequently also verified as most potent) form, the Stp units are combined with histidines (H) in alternating sequence, presenting the “histidine library” (**Scheme 3.1** *left*; **Table 3.1**). Structure variations include cysteines (C) and disulfide blocks (ssbb), so that the histidine library can be divided into three sub-groups, namely structures with cysteines [(H-Stp)$_2$-cys], structures without cysteines [(H-Stp)$_2$-0] and structures with disulfide block [(H-Stp)$_2$-ssbb]. Cysteines may increase the stability of the lipo-polyplexes by forming disulfide crosslinks,[64, 114, 199, 200] whereas the incorporated disulfide blocks rather destabilize but may increase biocompatibility due to redox-

sensitivity and bioreducible degradation.[114, 123] Each of these three groups consists of nine OAAs with the same backbone but modified with different saturated fatty acids (from C2 to C18) in the side chain. Depending on their chain length, fatty acids can exhibit *i)* stabilizing effects by hydrophobic interaction and /or *ii)* membranolytic activity.[64, 136, 200] With the systematic investigation of the entire library, the impact of stabilizing units within the lipo-polyplexes regarding biophysical and gene-transfer properties was evaluated. By doing so, beneficial structure motifs could be identified.

In addition to the histidine library [$(H\text{-}Stp)_2$–library], corresponding structures without histidines were synthesized and named as histidine-free library (Stp_2–library) (**Scheme 3.1** *right*; **Table 3.2**). The *in vitro* screening in three different cell lines (Huh7, N2a, and KB) showed that this histidine-free library has no advantages over the $(H\text{-}Stp)_2$–library (**Figure 3.7**). This is also in accordance with previous findings for lipid-free polyplexes.[144, 184] Histidines exhibit buffering properties at endosomal pH and thus enhance endosomal escape.[3, 190]

Furthermore, for selected histidine library structures, a block-wise motif of Stp and histidines (H_3Stp_2) instead of the alternating sequence was tested **(Figure 3.8a**). The resulting lipo-polyplexes showed good pDNA compaction ability with hydrodynamic diameters around 75 nm (**Figure 3.8b**) and good stability even in 90% (v/v) serum (FBS) (**Figure 3.8c**). However, the transfection efficiency in the Huh7 cell line was low (**Figure 3.8d**). As these H_3Stp_2**-**structures form much more stable polyplexes compared to the corresponding $(H\text{-}Stp)_2$–structures (**Figure 3.8c**), while being less efficient (**Figure 3.8d**), one can assume that the balance between stability and cargo release is important in view of transfection performance. Another example confirming this hypothesis is a small T-Shape lipo-OAA library (referred to as oligo-cysteine library) that was designed based on the $(H\text{-}Stp)_2$–library (**Figure 3.9a, Table 3.3**). The structures of these library contain two times three cysteines in the backbone, either in alternating sequence with tyrosines or in a block-wise motif. By this, multiple disulfide crosslinking may lead to increased stability of the formed polyplexes. Nevertheless, all these oligo-cysteine OAAs turned out to be ineffective in terms of pDNA transfection in two different cell lines (Huh7 and N2a cells; **Figure 3.9b**). These findings are in line with the conclusion drawn before that too stable polyplexes are less efficient.

Considering all the results of the preliminary screening, the main focus of further evaluation was on the most promising (H-Stp)$_2$–library.

The identity of each single OAA was proved by MALDI-TOF MS and ^{1}H NMR spectroscopy. The found masses are listed in **Table 3.4 – Table 3.6**; **Figure 3.10** shows the mass spectra and **Figure 3.11** shows the ^{1}H NMR spectra of representative effective lipo-OAAs used in the *in vivo* study later on.

The main screening presented in this work was performed for pDNA lipo-polyplexes, but the library was also tested for siRNA delivery, as briefly discussed in section *3.3.2.3* and in section *3.5.2.1*.

3.3.2 Characterization of lipo-polyplexes

3.3.2.1 Investigation of physicochemical properties of pDNA polyplexes

The screening of the (H-Stp)$_2$-library started with the evaluation of physicochemical properties of pDNA polyplexes formed at an N/P ratio of 12. For this purpose, size and polydispersity as well as pDNA compaction, also under polyanionic stress, were determined. The aim was to draw conclusions on stabilizing and destabilizing motifs and on the impact of the chain length of incorporated fatty acids on the stability of the lipo-polyplexes. The N/P ratio of 12 was chosen based on previous stability data with similar carriers, revealing this N/P ratio as necessary for efficient pDNA binding and formation of defined lipo-polyplexes.[137, 211] At higher N/P ratios, toxicity might be an issue.[123, 200] As a consequence, all experiments of the current study were conducted with lipo-polyplexes at the most reasonable and suitable N/P ratio of 12. By selecting the same N/P ratio for all lipo-OAAs, the obtained results were better comparable, and structure-activity relationships could be derived.

In the case of shorter fatty acids (C2–C8), DLS (dynamic light scattering) measurements revealed formation of larger particles (**Figure 3.1a**). This was especially the case for the two groups without disulfide-forming cysteines. The biggest polyplexes with z-averages around 250–350 nm were obtained for lipo-OAAs of the (H-Stp)$_2$-ssbb group, followed by lipo-polyplexes of the (H-Stp)$_2$-0 group with sizes around 110–180 nm. Increasing chain length of the incorporated fatty acids led to smaller particles in these two groups, so that z-averages around 75–95 nm were obtained for fatty acids of chain length ≥C10. In the case of the cysteine group, the incorporated fatty acids had no influence on the particle

size, being around 70–105 nm for all lipo-polyplexes of this group. TEM (transmission electron microscopy) measurements of cysteine-containing pDNA lipo-polyplexes revealed the formation of homogenous, globular nanoparticles (**Figure 3.12**), which are very consistent with previous findings for similar pDNA lipo-polyplexes.[211] The chain length of the incorporated fatty acids (C10, C14, and C18) did not significantly affect the mean diameter of the nanoparticles, which was around 40 nm in each case (**Figure 3.12**). The discrepancy in smaller size of the dehydrated fixed polyplex samples as compared with their native larger hydrodynamic diameters is exaggerated by DLS, where minor fractions of aggregates might contribute to an apparent large size.[211] Nevertheless, polydispersity indices (PdIs) of polyplexes were moderate (<0.2), which is in accordance with the finding of largely non-aggregated particles (**Figure 3.13b**). The results of the DLS measurements suggest that the incorporated fatty acids have a strong impact on the stability of the corresponding lipo-polyplexes: the shorter the chain length (<C10), the less stable and larger the resulting nanoparticles. In addition, cysteines have a stabilizing effect on lipo-polyplexes, resulting in small particles even in the case of shorter fatty acids. Moreover, polyplexes seem to be less stable when the disulfide-block ssbb is incorporated, forming the biggest particles in the case of shorter fatty acids.

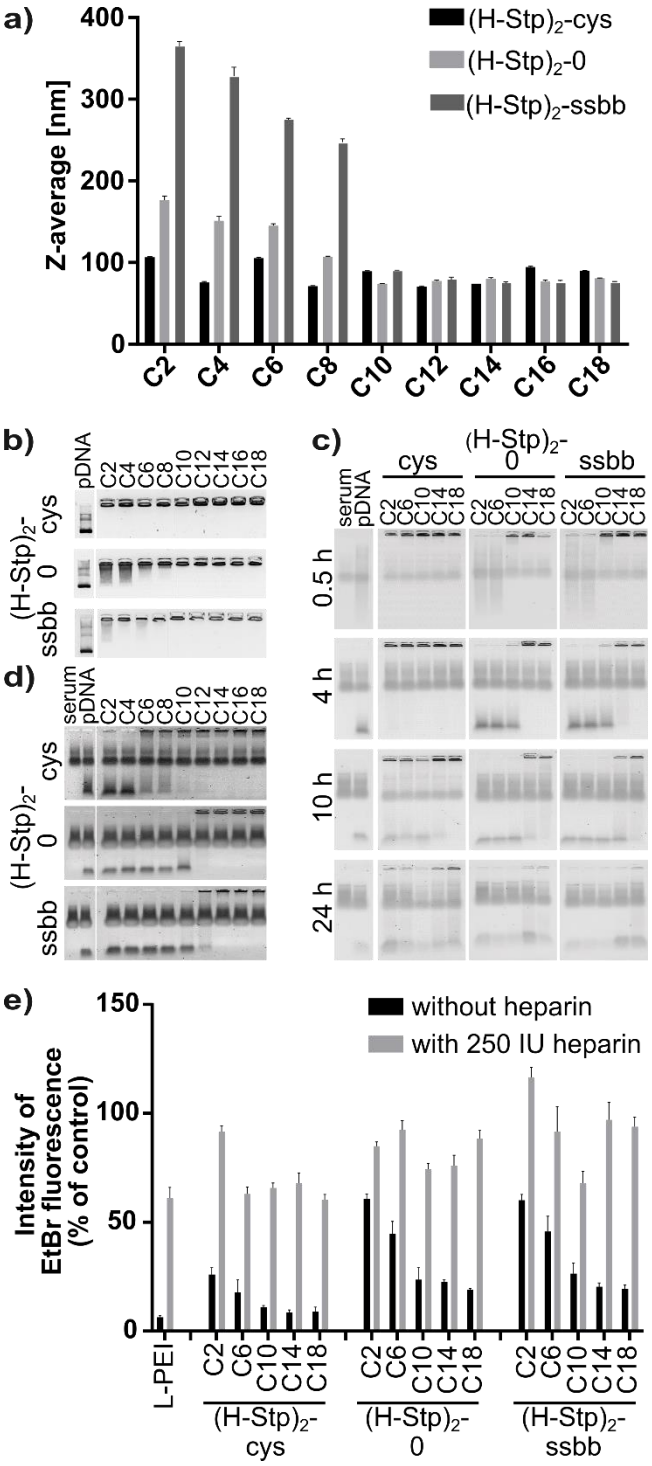

Figure 3.1. Physicochemical characterization of pDNA polyplexes (N/P = 12, HBG) of the (H-Stp)$_2$-library. (**a**) Sizes (z-average diameters in nm) measured *via* DLS (mean + SD; *n* = 3). (**b**) Standard agarose gel shift assay. (**c**) Serum agarose gel shift assay after incubation of polyplexes for 0.5, 4, 10, and 24 h in 90% (v/v) serum (FBS) at 37 °C, and (**d**) after incubation for 48 h in 90% (v/v) serum (FBS) at 25 °C. (**e**) Ethidium bromide (EtBr) exclusion assay and polyanionic stress test (mean + SD; *n* = 3). Intensity of EtBr fluorescence is presented as percentage relative to free pDNA.

In order to confirm these first findings on stability, gel shift assays were performed in the next step. The standard gel shift assay showed that all lipo-polyplexes of the $(H\text{-}Stp)_2$-cys group were stable without detectable release of pDNA (**Figure 3.1b**). In the case of the other two groups, polyplexes formed with lipo-OAAs containing shorter fatty acids (C2–C8) exhibited less stability, and free pDNA was visible in the associated gel bands. The lowest stability could be recognized for the shortest fatty acids. With increasing acyl chain length, the stability of the corresponding lipo-polyplexes increased. In order to get a better understanding of polyplex stability in a more relevant setting, namely under *in vivo* conditions, polyplexes were incubated in 90% (v/v) serum (FBS) at 37 °C (**Figure 3.1c**). Aliquots were taken at certain time points, and electrophoresis was performed. Free pDNA showed fast degradation in 90% (v/v) serum that can be seen at the tailed gel lane after incubation for 30 min in serum. Lipo-polyplexes of the $(H\text{-}Stp)_2$-cys group were stable in serum up to 4 h. At that time point, a slight release of pDNA was detectable in the case of polyplexes formed with lipo-OAA $(H\text{-}Stp)_2$-cys-C2. After 10 h, pDNA release was found in almost all polyplexes of this group, except those with the longest fatty acid (C18). Here, free pDNA was visible in the gel after 24 h. It should be mentioned, however, that for the whole cysteine group pDNA was present in the gel pockets even after 24 h, indicating still intact polyplexes. In the case of the other two groups, lipo-polyplexes were far less stable in serum. Already after 30 min, pDNA release was recorded for polyplexes containing shorter fatty acids (C2, C6, and C10 to small extent). After 10 h, free pDNA could be detected in all cases, and after 24 h almost no pDNA was remained in the pockets. Polyplex formation with lipo-OAAs of the $(H\text{-}Stp)_2$-ssbb group led to particles with the lowest stability. Even polyplexes formed with lipo-OAA $(H\text{-}Stp)_2$-ssbb-C14 slightly released pDNA after only 4 h. The serum gel shift assay was also performed with polyplexes incubated in 90% (v/v) serum (FBS) at 25 °C, slowing down the kinetics of pDNA release and degradation (**Figure 3.1d**; the whole time course is shown in **Figure 3.14**). In this way, pDNA release and thus polyplex stability in dependence on the chain length of the included fatty acids could be illustrated more clearly. The polyplexes released pDNA in accordance with their stability: free pDNA was first detected in the case of polyplexes with shorter fatty acids, followed by those with fatty acids of middle chain lengths. Longer fatty acids promote higher stability, so that polyplexes containing C14, C16, or C18 fatty acids showed little to no pDNA release even after an incubation time of

96 h. Again, cysteine-containing polyplexes exhibited highest stability, followed by polyplexes of the (H-Stp)$_2$-0 group. Less stability was noted in the case of ssbb-containing polyplexes.

The pDNA compaction ability of the single lipo-OAAs is another indicator for polyplex stability and was therefore determined by an ethidium bromide (EtBr) exclusion assay (**Figure 3.1e**). EtBr only shows a fluorescent signal when intercalated in DNA. This is possible for freely accessible, that is, little to not compacted DNA. Therefore, polyplexes formed with lipo-OAAs with high pDNA compaction ability show only low EtBr fluorescence. The findings of this assay underline the results of the other physicochemical experiments. In each group, longer fatty acids led to better pDNA compaction of the corresponding lipo-polyplexes, whereas pDNA was less compacted in the case of lipo-polyplexes with shorter fatty acids. The best pDNA compaction was found for cysteine-containing polyplexes, showing the lowest intensity of EtBr fluorescence. In the case of fatty acids with chain lengths ≥C10, pDNA compaction of the cysteine-containing polyplexes was comparable to that of L-PEI polyplexes, known as the gold standard for pDNA delivery with good pDNA binding abilities.[88, 143] Polyplexes of the other two groups showed lower and quite similar tendency in pDNA compaction ability in dependence on the fatty acid chain length. In a next step, the response of the single polyplexes to polyanionic stress was examined by adding heparin and measuring the EtBr fluorescence intensity in the samples again. Higher resistance to polyanionic stress can be interpreted as higher pDNA binding ability and in the end as better stabilized nanoparticles. Again, polyplexes of the (H-Stp)$_2$-cys group showed the highest stability, followed by polyplexes of the (H-Stp)$_2$-0 group. Less stability was again recognized for ssbb-containing polyplexes.

Summing up the results of the stability studies of pDNA lipo-polyplexes formed with lipo-OAAs of the (H-Stp)$_2$-library, the following conclusions can be made. Cysteines have a stabilizing effect on the resulting lipo-polyplexes, most likely due to disulfide crosslink formation. On the contrary, incorporation of bioreductive disulfide blocks into the carrier leads to destabilization. Furthermore, fatty acids have a great impact on the stability: the longer the chain lengths of the incorporated fatty acids, the more stable the corresponding polyplexes due to hydrophobic interactions.

3.3.2.2 Investigation of gene-transfer activity of pDNA lipo-polyplexes

In a next step, the pDNA polyplexes were tested *in vitro* regarding transfection efficiency as well as cytotoxicity in three different cell lines (Huh7, N2a, and KB; **Figure 3.2** and **Figure 3.7**). The screening in the Huh7 cell line revealed that cysteine-containing polyplexes mediated the highest luciferase marker gene transfer, followed by ssbb-containing polyplexes (**Figure 3.2a**). Polyplexes of the $(H\text{-}Stp)_2$-0 group showed almost no transfection. Within the cysteine group, shorter fatty acids with chain lengths of C2–C12 mediated more effective gene transfer than longer ones, with a maximum of transfection efficiency for polyplexes with fatty acids C6–C10. OAAs containing these fatty acids even outperformed the gold standard L-PEI. In the case of ssbb-containing polyplexes, transfection efficiency increased with increasing acyl chain length with a maximum at C10, and then decreased again. OAA $(H\text{-}Stp)_2$-ssbb-C10 showed similar transfection results as its cysteine analog and was even better than L-PEI. All in all, especially in the $(H\text{-}Stp)_2$-cys group, lower stability appears to be beneficial for transfection efficiency, and shorter fatty acids show better results than longer ones. However, a certain threshold stability seems to be required; altogether, a maximum transfection efficiency for acyl chain lengths of C6–C10 was found. When comparing the three sub-groups of the histidine library, it is worth noting that in the absence of stabilizing cysteines, the maximum transfection efficiency is shifted toward longer fatty acids, namely, from C6 to C10. This underlines the assumption that polyplexes should display optimum but not maximum stability for good gene-transfer performance.

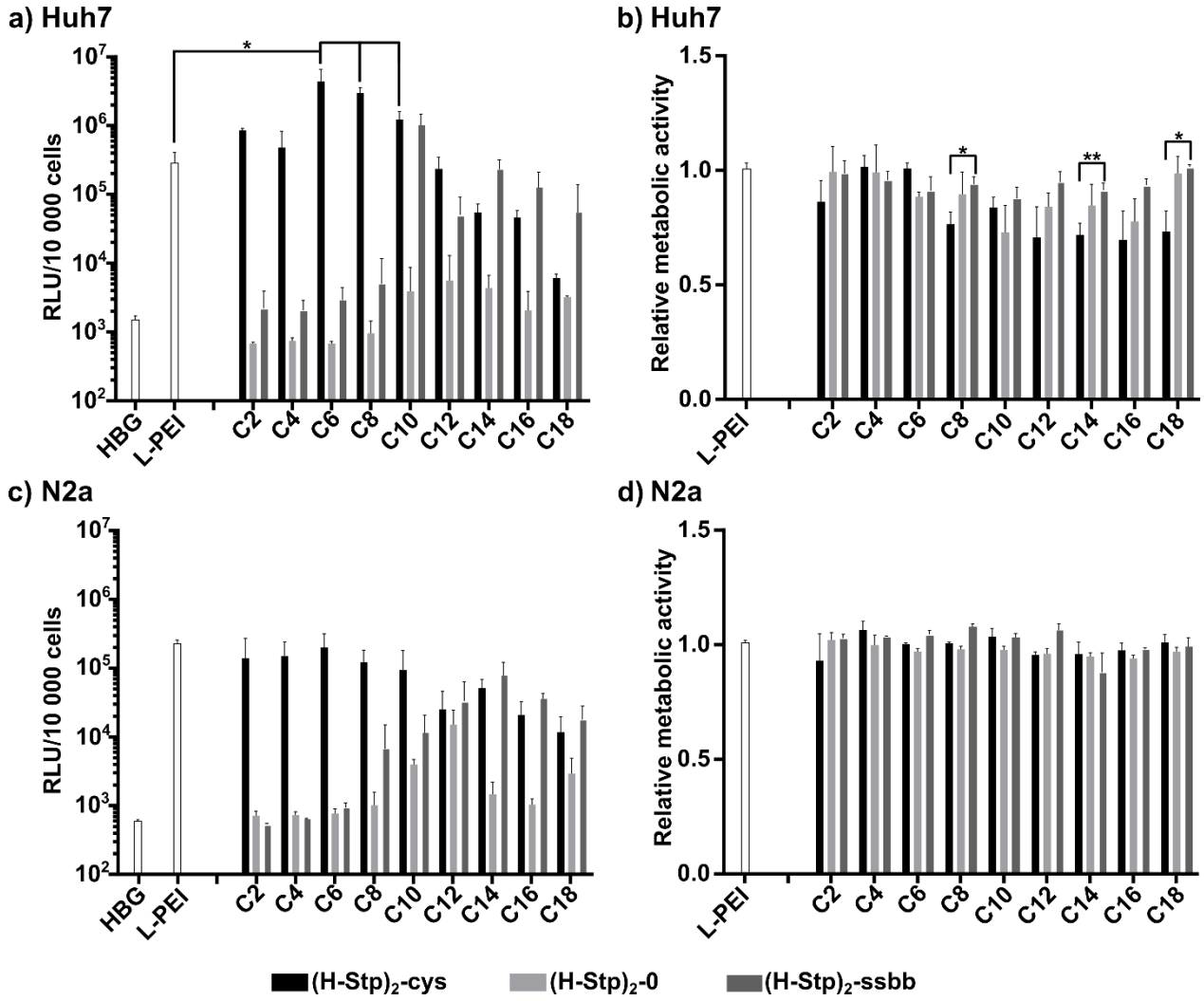

Figure 3.2. Gene-transfer performance of pCMVLuc polyplexes (N/P = 12, HBG) of the (H-Stp)$_2$-library. Both the luciferase gene expression assay (*left*; **a, c**) and the CellTiter-Glo assay (*right*; **b, d**) were performed in Huh7 cells (*above*; **a, b**) as well as in N2a cells (*below*, **c, d**) 24 h after transfection (mean + SD; *n* = 3). Metabolic activities, determined *via* CellTiter-Glo, are presented relative to HBG buffer-treated control cells. L-PEI pDNA polyplexes (N/P = 6, HBG) served as positive control. Transfections were performed by Dr. Ana Krhač Levačić (Pharmaceutical Biotechnology, LMU Munich).

In N2a cells, the trend was the same as observed in Huh7 cells (**Figure 3.2c**). Cysteine-containing polyplexes worked best, followed by those containing ssbb, and polyplexes lacking both motifs were inferior. (H-Stp)$_2$-cys OAAs with acyl chain lengths of C2–C10 exhibited similar transfection efficiency as L-PEI. For longer fatty acids, the transfection efficiency decreased. In the case of the other two groups, the gene expression levels improved with increasing acyl chain length and decreased again after reaching a

maximum at an acyl chain length of C14 in the case of the $(H\text{-}Stp)_2$-ssbb group and of C12 in the case of the $(H\text{-}Stp)_2$-0 group. The screening in KB cells showed again that cysteine-structures exhibited better transfection results than the other two groups, especially in the case of shorter fatty acids (C2–C6) (**Figure 3.7e**). However, in this cell line, polyplexes of the $(H\text{-}Stp)_2$-ssbb group exhibited almost no transfection efficiency. This phenomenon was also observed in earlier works.[123, 212] The reason for this could be a high redox potential of KB cells even on the cell surface, leading to notable premature polyplex degradation *via* carrier cleavage. This assumption is supported by findings of the working group of Leroux.[164] They reported high reducing potential of HeLa cells, of which KB cells are a derivative.

Cytotoxicity of polyplexes was also evaluated *via* the CellTiter-Glo assay. The determined metabolic activity of the treated cells indicates their viability and is therefore a measure of the cytotoxicity of the single polyplexes. Polyplexes of the $(H\text{-}Stp)_2$-cys group with fatty acids of middle to long chain lengths (C8–C18) were quite toxic to Huh7 cells (**Figure 3.2b**). The metabolic activity of cells was less than 80% of the control. Polyplexes of the $(H\text{-}Stp)_2$-0 group were less harmful. And by further incorporation of the redox-sensitive disulfide block ssbb, cytotoxicity could be reduced by 20–25%, resulting in cell metabolic rates greater than 90–95%. In the case of the other two cell lines (N2a and KB cells), this toxicity phenomenon was not observed (**Figure 3.2d, Figure 3.7f**). These cell lines seem to be less sensitive to the lipo-polyplexes compared to the Huh7 cells.

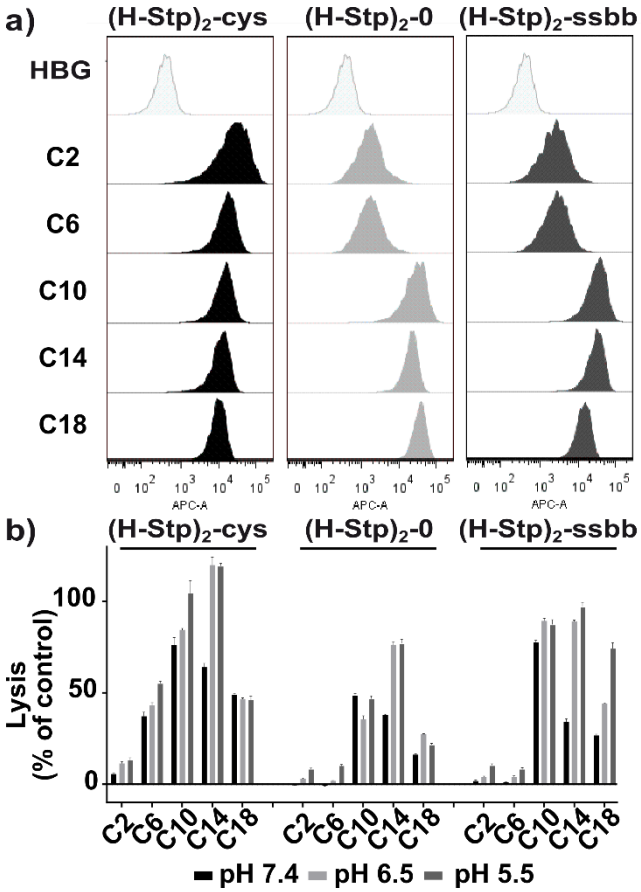

Figure 3.3 (**a**) Cellular uptake of pDNA polyplexes (N/P = 12, HBG) of the (H-Stp)$_2$-library in Huh7 cells after 4 h, in comparison to HBG buffer-treated control cells. (**b**) Lytic potential of the single OAAs of the (H-Stp)$_2$-library at a concentration of 5 µM, measured in an erythrocyte leakage assay at different pH values (pH 5.5, 6.5, and 7.4). Data are presented as mean + SD out of quadruplicates. The experiments were performed together with Dr. Ana Krhač Levačić (Pharmaceutical Biotechnology, LMU Munich).

As the histidine library is not effective in KB cells and shows much better and comparable results in case of the other two cell lines, further screening was continued in Huh7 and N2a cells.

The differences in gene-transfer mediated by the various OAAs cannot be fully explained by the different polyplex stabilities. In order to find further reasons for the different behavior, degrees of cellular internalization and lytic activities were investigated. Both the cellular uptake and the subsequent endosomal escape are necessary steps in the delivery process of polyplexes.[3] As the cellular uptake of polyplexes happens mostly *via* endocytosis, it is necessary that the polyplexes are released from endosomes.[3, 51] Lytic activity of carriers can be helpful for endosomal escape. However, high lytic activity,

especially at physiological pH (pH 7.4), may cause toxicity due to unspecific interactions with biologicals membranes. Therefore, pH dependent lytic activity is desirable, showing only lytic effects in acidic milieu of endosomes/lysosomes (pH 5.5–6.5), but not at physiological pH.

Cellular uptake studies were performed *via* flow cytometry. Internalization into Huh7 cells after 4 h was observed for all polyplexes (**Figure 3.3a**). Within both groups lacking cysteines, however, lower uptake rates were recorded for the polyplexes with shorter fatty acids (C2–C6). In contrast, cysteine-containing polyplexes were internalized efficiently even when based on lipo-OAAs with short acyl lengths. Similar data were obtained in the case of N2a cells (**Figure 3.15**). These findings may explain the low transfection efficiency in the case of shorter fatty acids in the $(H\text{-}Stp)_2$-0 and in the $(H\text{-}Stp)_2$-ssbb group. Nevertheless, decreasing transfection efficiency in the case of longer fatty acids cannot be explained by these results.

The lytic activity of the single OAAs of the $(H\text{-}Stp)_2$-library was examined in an erythrocyte leakage assay at three different pH values (pH 5.5, 6.5, and 7.4). In all three groups, the OAAs showed different lytic potential depending on their incorporated fatty acids (**Figure 3.3b**). The trend was similar in each group. Structures with shortest fatty acids (C2 in the cysteine group; C2 and C6 in the other two groups) displayed lysis less than 10%. At pH 7.4, the lytic potential increased with increasing acyl chain lengths, and decreased again after reaching a maximum at C10. At both other pH values, the tendency was the same, but the maximum was shifted to C14. The reason for this is that within each group, structures with fatty acid C14 showed the highest pH-dependent lytic activity. Comparing the values at pH 7.4 with those at pH 6.5, the lytic potential raised here by more than 40–50%. However, there was no notable difference between pH 6.5 and pH 5.5. OAA $(H\text{-}Stp)_2$-ssbb-C18 showed also high pH-dependent lytic activity with an increase from 25% (pH 7.4) to 70% (pH 5.5). Moreover, a difference in lytic activity between the three $(H\text{-}Stp)_2$-groups was detected. Overall, the lytic activity was highest in the case of cysteine-containing structures, followed by ssbb-containing ones. The lowest lytic activity was detected in the case of the $(H\text{-}Stp)_2$-0 group. These findings might be surprising at the first glance, since all structures comprise analogous amphiphilic characteristics with a hydrophilic cationic backbone and a hydrophobic side chain. Therefore, it was expected that only the different fatty acids would tune the differences in lytic potential. However, it

appears that the backbone structure also has an impact. The cysteine-containing structures may form disulfide-based oligomers and thus exhibit higher lytic potential due to a higher fatty acid amount per molecule. This could be an explanation for the difference in lytic potential between the $(H\text{-}Stp)_2$-cys and the $(H\text{-}Stp)_2$-0 groups, supported by the fact that the lytic activity of the cysteine structures is almost twice as high as that of the $(H\text{-}Stp)_2$-0 structures. The slightly different results for the $(H\text{-}Stp)_2$-ssbb group might be due to the glycine–disulfide block linker in the side chain, which increases the spacing between hydrophobic and hydrophilic part and thus alters the amphiphilic characteristics.[123] In addition, three different OAA concentrations were tested, showing a concentration-dependent lytic activity (**Figure 3.16**). Regarding the transfection data, the findings of the erythrocyte leakage assay can be interpreted as follows. When comparing the three groups, the ranking in lytic potential is the same as the order found for transfection efficiency: first, the $(H\text{-}Stp)_2$-cys group, followed by the $(H\text{-}Stp)_2$-ssbb group, and finally the $(H\text{-}Stp)_2$-0 group. Therefore, on the one hand higher lytic potential seems to be beneficial for transfection efficiency. On the other hand, structures with less lytic activity might be less toxic. The $(H\text{-}Stp)_2$-0 group with the lowest lytic activity showed reduced toxicity compared to the cysteine group in Huh7 cells (**Figure 3.2b**). Although the $(H\text{-}Stp)_2$-ssbb group exhibits higher lytic potential than the $(H\text{-}Stp)_2$-0 group, the toxicity might be lower because of the incorporated redox-sensitive unit.[123] This toxicity phenomenon was only observed in Huh7 cells, suggesting that the other tested cell lines might be less sensitive to membranolytic activity.

To sum up the findings of the cell culture experiments, the following can be stated. Among the three groups, cysteine-containing structures worked best in transfection of Huh7 as well as of N2a cells, followed by ssbb-containing structures, and finally structures of the $(H\text{-}Stp)_2$-0 group showed almost no transfection efficiency. A lower stability seems to be advantageous. However, a certain threshold stability is necessary, thus in sum resulting in an optimum for structures containing fatty acids of middle chain length (C6–C10). Too stable nanoparticles might not liberate OAA molecules in the endosome, which mediate endosomal release into the cytosol.[213] Furthermore, too stable polyplexes may not sufficiently release the pDNA in the nucleus in well transcribable form.[214-216] Polyplexes formed with C2–C6 structures of both groups lacking cysteines were internalized to a smaller amount than all other polyplexes. The lytic potential of fatty acids of middle chain

length (C10–C14) can be beneficial for endosomal release but might also cause toxicity. This was observed for the cysteine group in Huh7 cells. Incorporation of a bioreducible disulfide-block can reduce toxicity. Both other cell lines (N2a and KB) were less sensitive towards membranolytic activity. All in all, a balance must be found between stability, lytic potential, and cytotoxicity in order to optimize the transfection efficiency. This was handled best so far in pDNA polyplexes formed with OAAs $(H\text{-}Stp)_2$-cys-C6 to -C10 and $(H\text{-}Stp)_2$-ssbb-C10 to -C14.

3.3.2.3 Investigation of siRNA lipo-polyplexes

Different nucleic acids require different properties from their carrier systems.[13, 26, 86] It is important to know which structural elements are valuable for each nucleic acid. Therefore, in addition to the screening of the $(H\text{-}Stp)_2$-library for pDNA delivery, these structures were also tested for the delivery of siRNA. By this, beneficial structure motifs as well as differences in comparison to pDNA polyplexes should be found. The results are presented and discussed in detail in the *supporting information* (section *3.5.2.1* as well as **Figure 3.17 – Figure 3.20** and **Table 3.7**). In short, cysteines and longer fatty acids improved stability of siRNA polyplexes. Overall, however, the siRNA polyplexes were less stable than the analogous pDNA polyplexes, and their gene silencing efficacies were low as compared with previously established lipo-polyplexes.[28, 64, 137, 147, 200, 205, 208, 209, 217]

3.3.3 Characterization of pDNA core-shell polyplexes

Based on incorporation of azido-lysines into the carrier sequence, pDNA polyplexes display azide units on their surface, which can be post-functionalized *via* orthogonal click chemistry in a next step (**Scheme 3.2**). By doing so, shielding and targeting agents can be introduced as shell around the pre-formed nanoparticle core. This is especially of interest when considering systemic application *in vivo.* In the current study, 0.25 equiv of mono- and bivalent DBCO-PEG agents for shielding purposes were evaluated for pDNA core-shell polyplexes (N/P = 12, HBG), namely, monoDBCO-PEG_{24} and bisDBCO-PEG_{24} (**Figure 3.21**). The detailed results and discussion can be found in the *supporting information* – section *3.5.2.2* and are shortly summarized in the following. Zetasizer data (**Figure 3.13**) revealed more effective shielding in the case of bisDBCO-PEG_{24}, as indicated by a notable drop in surface charge, which was not detected for monoDBCO-PEG_{24}. Thus, the bivalent DBCO agent was selected for further experiments. At

0.25 equiv, defined nanoparticles with sizes below 200 nm could be generated based on lipo-OAAs containing middle to longer fatty acids.

Scheme 3.2. Preparation of pDNA core-shell lipo-polyplexes in a two-step process.

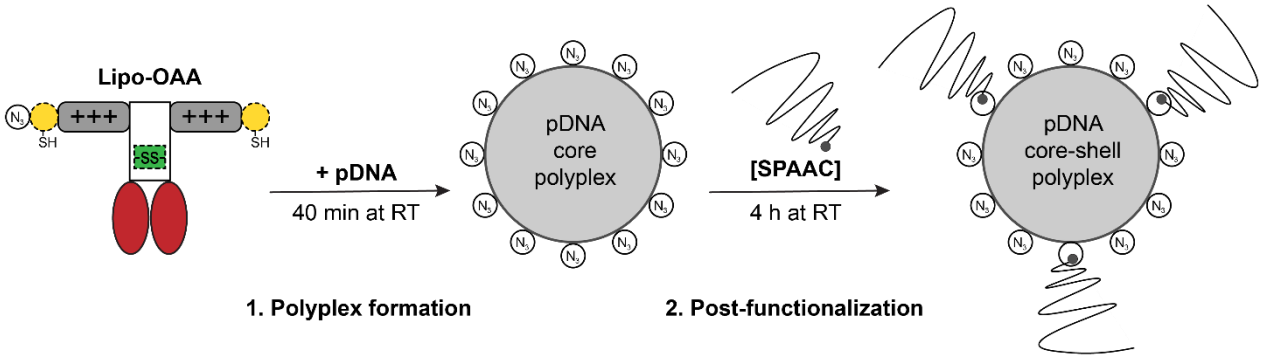

Formation of core lipo-polyplexes out of lipo-oligoaminoamides (lipo-OAAs) and pDNA for 40 min at room temperature (RT), followed by post-functionalization of surface-exposed azide units with mono- or bivalent DBCO-PEG agents *via* strain-promoted alkyne-azide cycloaddition (SPAAC) for 4 h at RT. Here, illustrated with monoDBCO-PEG$_{24}$.

3.3.4 Characteristics of pDNA lipo-polyplexes in serum and in a tumor model *in vivo*

3.3.4.1 Selecting the most promising candidates for in vivo testing

Taking all the findings so far together, the most promising candidates for evaluation *in vivo* are (H-Stp)$_2$-cys-C14 and (H-Stp)$_2$-ssbb-C14. By choosing structures of both groups with the same fatty acid, a direct comparison between the functional units – cysteine *versus* disulfide building block – can be drawn. Both structures form well-defined pDNA nanoparticles, also when post-functionalized with bisDBCO-PEG$_{24}$ (**Figure 3.13a)**. This is especially important in regard of systemic application *in vivo*, where instable particles tending towards aggregation are inacceptable. Moreover, for these two structures within their groups, stability, lytic activity, and transfection efficiency are balanced well. Although this balancing act was even better handled in the case of the C10-structures, the more stable C14-structures have been selected. Higher stability may be beneficial in the *in vivo* situation. Polyplexes of the C14-structures are stable in 90% (v/v) serum at 37 °C up to 4 (in the case of the ssbb-containing OAA) or 10 h (in the case of the cysteine-containing OAA), respectively (**Figure 3.1c**). This should be sufficient for *in vivo* application. In previous works on siRNA biodistribution, it could be shown that similar carrier systems as

used in the current pDNA study exhibited only short-time circulation and entered the tumor and other organs within only minutes to a few hours.[28, 137, 202] Since polyplexes of the $(H\text{-}Stp)_2$-0 group had shown almost no transfection activity, this group was completely excluded from the further screening. Prior to *in vivo* evaluation, the PEG-shielded polyplexes were tested in Huh7 and N2a cells (**Figure 3.22**). Small but, in most cases, no significant decrease in transfection efficiency could be noticed after 24 h incubation of the nanoparticles on the cells (**Figure 3.22a+b**), indicating that the transfection at least was not or only minor hampered by the PEG shield. Moreover, no toxicity was caused by the PEG agent and the toxicity profile was even significantly improved as shown exemplarily in Huh7 cells (**Figure 3.22c**). Unmodified pDNA polyplexes with fatty acids of middle to longer chain lengths were quite toxic in this cell line (**Figure 3.2b**); PEGylation is here advantageous. This is in line with the observed reduction of the surface charge of the PEG-shielded polyplexes (**Figure 3.13c**). Nanoparticles with high cationic surface charge are known to be potentially toxic due to interaction with cell membranes (*e.g.*, of erythrocytes), which can be inter alia avoided by PEGylation and decationization.[3, 88, 201, 218] Moreover, the lytic fatty acids may be masked by the PEG shield and therefore may be less harmful to cell membranes.[201]

3.3.4.2 Selecting oleic acid analogs of the two best performers for in vivo testing

As the library presented in this work is built on saturated fatty acids, the best performers should be compared upon the *in vivo* situation with corresponding structures containing oleic acid, an unsaturated fatty acid with one double bond (C18:1). This fatty acid has proven previously to be particularly beneficial for delivery of siRNA,[28, 64, 137, 147, 200, 205, 208, 209, 217] but displayed carrier activity for pDNA as well.[64, 136] The oleic acid analogs of the two best performers, $(H\text{-}Stp)_2$-cys-C18:1 and $(H\text{-}Stp)_2$-ssbb-C18:1 (**Figure 3.23a**), have been already intensively tested as potent and well-tolerated siRNA carriers,[28, 208] but their potential in pDNA delivery was unknown at begin of the current study and thus had to be determined. Both structures compacted pDNA well (**Figure 3.23c**) and formed well-defined spheric pDNA polyplexes (**Figure 3.23b)** with hydrodynamic diameters around 80 nm and PdI values below 0.2, as determined *via* DLS (**Figure 3.23e, f**). The polyplexes were stable in 90% (v/v) serum (FBS) at 37 °C up to 10 h (ssbb structure) or 24 h (cysteine structure), respectively, with only slight pDNA release at these time points **(Figure 3.23d)**. This fits well to the data presented in **Figure 3.1c**; cysteines and longer fatty acids

promote stabilization. Post-functionalization with 0.25 equiv of bisDBCO-PEG_{24} had no influence on the particle size (**Figure 3.23e**), but a decrease in the zeta-potential indicated effective shielding (**Figure 3.23g**). In Huh7 cells as well as in N2a cells, both structures showed good transfection abilities, which were not diminished in the case of post-functionalization with the PEG shield (**Figure 3.23h, i**). On the sidelines, there is a huge discrepancy in gene-transfer efficiency between the same structures bearing C18 fatty acids without and with a double bond, respectively (**Figure 3.2a, c; Figure 3.23h, i**). The incorporated oleic acid (C18:1) appears to be superior to stearic acid (C18), most probably because of better interaction with membranes due to the natural bend (*cis* configuration) in the carbon chain.[209, 219, 220] However, a direct comparison of the transfection efficiency of the C14 and the C18:1 structures does not reveal big differences (**Figure 3.22a, b; Figure 3.23h, i**). Only within the ssbb group, it seems that the C18:1 structure is more effective, at least in Huh7 cells.

3.3.4.3 Establishing of new in vitro assays in high serum and translation to the in vivo situation

In the next step, these four structures (*i.e.*, $(H\text{-}Stp)_2$-cys-C14, $(H\text{-}Stp)_2$-ssbb-C14 and their C18:1 analogs) should be compared in a neuroblastoma (N2a) tumor model upon intravenous injection. Preliminary *in vivo* studies in two different tumor models (Huh7 and N2a), however, revealed a disappointing gene-transfer efficiency without or with PEGylation (*data not shown*), which was far lower than the efficiencies of previously tested lipid-free OAA and related oligoethylenimine polyplexes.[113, 144, 184, 210, 221] The encouraging *in vitro* data of the new lipo-OAA polyplexes would predict a far better *in vivo* performance. One major difference between cell culture experiments and systemic administration in a tumor mouse model is the presence of blood in the case of the latter. Interaction with blood components and rapid attachment of plasma proteins on the nanoparticle surface forming a so-called “protein corona” change the physicochemical properties of the nanoparticle such as hydrodynamic size, surface charge, and aggregation behavior.[37, 38, 222-224] This in turn influences biodistribution, interaction with cell membranes and cellular uptake *via* endocytosis, as well as toxicity of nanoparticles. PEGylation may reduce but not completely avoid adsorption of plasma proteins.[38, 224-227]

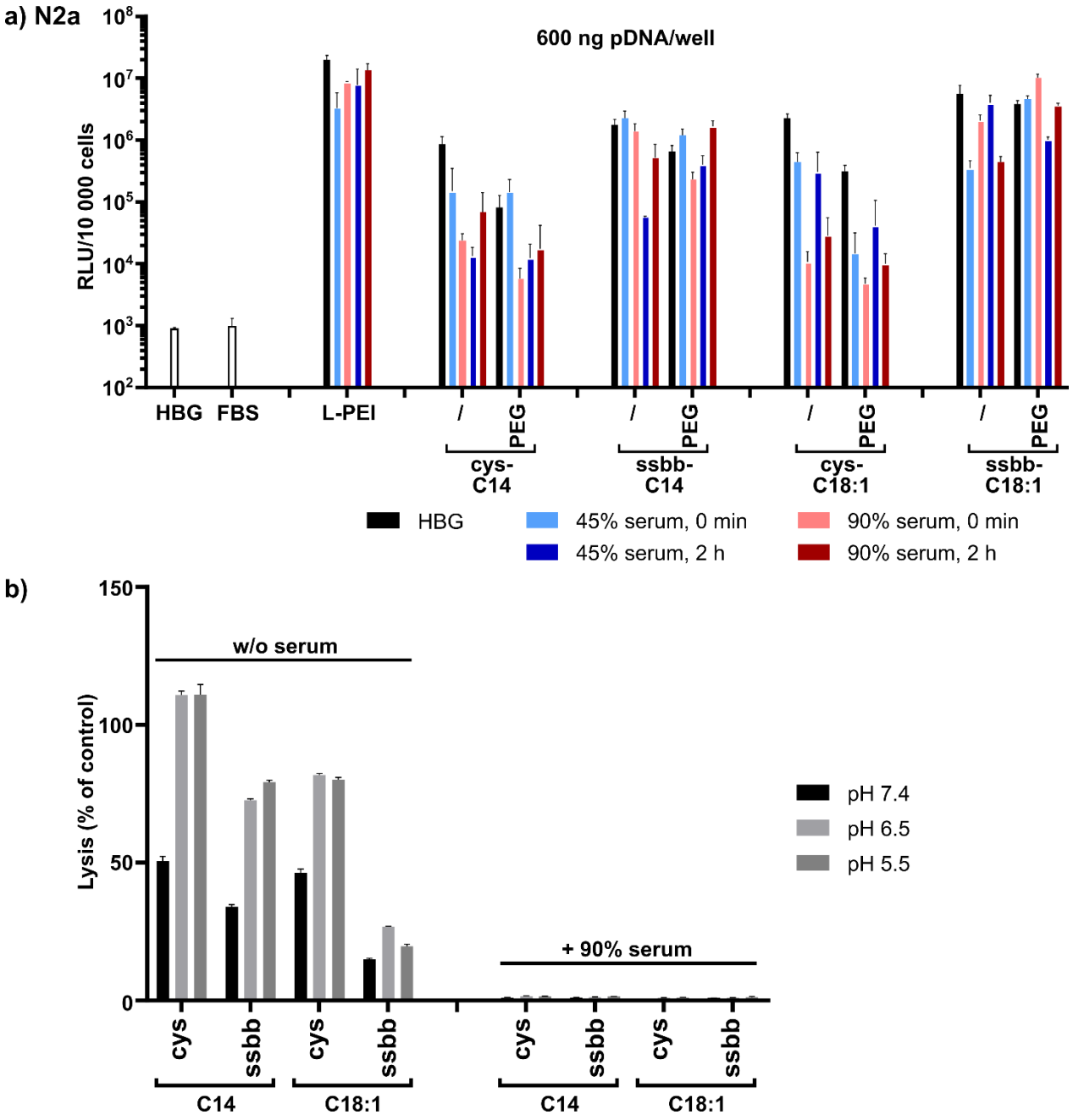

Figure 3.4. Effect of full serum on gene-transfer and lytic activity. (**a**) Gene-transfer performance in N2a cells in the presence of serum (FBS). Unmodified (/) and PEGylated (PEG; 0.25 equiv of bisDBCO-PEG_{24}) pCMVLuc polyplexes (N/P = 12, HBG, 600 ng of pCMVLuc per well) formed with selected $(H\text{-}Stp)_2$-OAAs as well as L-PEI pDNA polyplexes (N/P = 6, HBG) were incubated in 45% (v/v) FBS, 90% (v/v) FBS, or HBG, respectively, for 0 min or 2 h at 37 °C (FBS) or RT (HBG) prior to transfection. The luciferase gene expression assay was performed 24 h after transfection (mean + SD; *n* = 3). (**b**) Lytic potential in the presence of serum (FBS) of selected $(H\text{-}Stp)_2$-OAAs at a concentration of 5 µM, measured in an erythrocyte leakage assay at different pH values (pH 7.4, 6.5, and 5.5). Untreated OAAs (*i.e.*, without pre-incubation in FBS) were compared with OAAs pre-incubated in 90% (v/v) FBS for 2 h at 37 °C. Data are presented as mean + SD out of quadruplicates.

In order to find possible explanations for the observed discrepancy between the *in vitro* and the *in vivo* situation, new *in vitro* assays in high serum (FBS) were established. At first, transfections in N2a and Huh7 cells were performed with pCMVLuc polyplexes mixed with serum to reach 45% or 90% (v/v) FBS, and optionally pre-incubated for 2 h at 37 °C. For *in vivo* experiments, polyplexes are injected into mice with a total blood volume of around 2 mL, which represents approximately a 1:10 dilution of polyplex assuming a complete blood mixing. Therefore, polyplex formation was done at a pDNA concentration that is used *in vivo* (*i.e.*, 30-times higher than used *in vitro*), and after 1:10 dilution with 100% FBS, 50% (v/v) FBS in HBG, or 100% HBG, respectively, the final amount of pDNA per well was 600 ng. The negative impact of serum on the transfection efficiency was quite high for most lipo-polyplexes (**Figure 3.4a, Figure 3.24**). It was more pronounced for the cysteine-containing formulations as well as for the transfection in N2a cells. PEGylation did not improve the performance of lipo-OAA polyplexes. In contrast, L-PEI polyplexes as well as ssbb-containing polyplexes were far less or not affected by serum. This was particular the case for the transfection in Huh7 cells (**Figure 3.24**). A performed toxicity assay showed that neither of the conditions (high pDNA amount and increased serum content per well) was notably harmful to the cells (**Figure 3.25**).

As already described in section *3.3.2.1*, high serum [90% (v/v) FBS] did affect pDNA polyplex stability only for lipo-OAAs with short FA modification (C2–C10; **Figure 3.1c**); thus, polyplex dissociation can be ruled out as dominating mechanism for this observed serum effect. In the new *in vitro* serum assays, lipo-OAAs with longer fatty acids (C14, C18:1) were tested. Therefore, reduced stability in presence of serum is not likely the main reason for the strong inhibition of transfection by full serum. To obtain a better understanding of the mechanism of inhibition, in a second assay, the lytic potential of polyplexes in presence of serum was investigated. All four structures are inactive in lysis when pre-incubated in 90% (v/v) FBS for 2 h at 37 °C (**Figure 3.4b**). This could be a possible explanation for the observed great reduction in transfection potential. The lytic activity of free lipo-OAAs as one of the main promoters of endosomal escape was found as essential for good transfection (**Figure 3.3b**). However, free lipo-OAAs are blocked in their lytic potential by serum (**Figure 3.4b**). As ssbb-containing polyplexes are less stable than the cysteine counterparts (**Figure 3.1; Figure 3.14, Figure 3.23d**), the lytic lipo-OAAs may be released from the polyplex bit by bit within the endosomes, leading to better

transfection results in the presence of serum. Whereas, in case of the cysteine-containing polyplexes, the lytic lipo-OAAs are more bound in the nanoparticle most probably due to crosslinking, resulting in a lower transfection efficiency in the presence of serum. The release of L-PEI polyplexes (which do not contain any lipidic domain) from endosomes obviously works according to another mechanism.[88, 228-230] Therefore, performance of L-PEI polyplexes is less influenced by serum.

A small experiment in neuroblastoma-bearing mice was conducted to see if the findings of the *in vitro* serum assays can be translated to the *in vivo* situation. Therefore, unmodified polyplexes (N/P = 12; HBG) were applied systemically, containing 60 µg of pCMVLuc in 250 µL injection volume. As PEGylation did not exhibit any beneficial effects in the *in vitro* serum assays as well as in the preliminary *in vivo* studies (data not shown), only unmodified polyplexes were used for the *in vivo* examination. The overall gene expression in the tumor determined *via* an *ex vivo* luciferase gene expression assay was only moderate, and none of the tested formulations outperformed the positive control L-PEI (**Figure 3.5**). This is in line with the results obtained in the *in vitro* serum studies; serum reduces but not completely inhibits transfection efficiency. Moreover, the polyplexes formed with oleic acid structures seem to be more robust carrier systems. Tumor signals could be detected for each group, which was not the case for the C14 formulations. Here, the luciferase expression in the tumor was even below background threshold for the ssbb formulation (n.d., not detectable). In addition, cysteine formulations seem to work better than their ssbb counterparts. A possible explanation for this could be the different stabilities of cysteine- and ssbb-containing polyplexes as well as of the different acyl chain lengths of the incorporated fatty acids (**Figure 3.1, Figure 3.14, Figure 3.23d**). Polyplexes formed with $(H\text{-}Stp)_2$-ssbb-C14 were less stable than the other tested formulations and probably too instable for an *in vivo* application. Certain polyplex stability is necessary to avoid rapid polyplex disintegration and renal clearance.[3, 137]

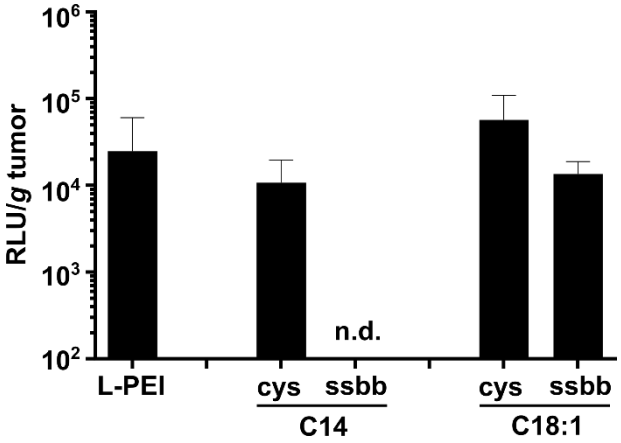

Figure 3.5. *In vivo* study in a subcutaneous neuroblastoma (N2a) mouse model. Four $(H\text{-}Stp)_2$-structures containing cysteines (cys) or disulfide building block (ssbb) as well as myristic acid (C14) or oleic acid (C18:1) were tested for their gene-transfer efficiency *in vivo.* For this purpose, polyplexes containing 60 µg of pCMVLuc and indicated lipo-OAAs (N/P = 12) in 250 µL HBG were applied systemically *via* tail vein injection, and an *ex vivo* luciferase gene expression assay of the N2a tumors was performed at 24 h after polyplex injection (mean + SD; *n* = 3). L-PEI pDNA polyplexes (N/P = 6, HBG) served as positive control. n.d., not detectable. The *in vivo* study was conducted by Elisa Hörterer and Ulrich Wilk (both Pharmaceutical Biotechnology, LMU Munich).

To conclude, the findings of the various *in vitro* serum assays investigating polyplex stability (**Figure 3.1c+d, Figure 3.14, Figure 3.23d**), lytic potential (**Figure 3.4b**) as well as gene-transfer performance (**Figure 3.4a, Figure 3.24**) in the presence of serum fit well to the results obtained *in vivo*. As all the conditions used in these new *in vitro* serum assays are just model conceptions, the findings are only approximations. The conditions chosen in the *in vitro* serum assays were quite harsh with a high serum content compared to the pDNA amount and long incubation times. Not the whole blood volume of a mouse is circulating, and polyplexes may reach their target organ already within seconds to minutes after injection and not after 2 h circulation with the complete blood volume. Moreover, instead of serum, polyplexes will face whole blood impacting on their biological identity.[224] Furthermore, the shear forces occurring during polyplex injection and also in the blood stream can have an influence on the nanoparticle stability and its protein corona.[41] Nevertheless, these *in vitro* serum assays can be valuable for better predictions how carrier systems may work *in vivo*.

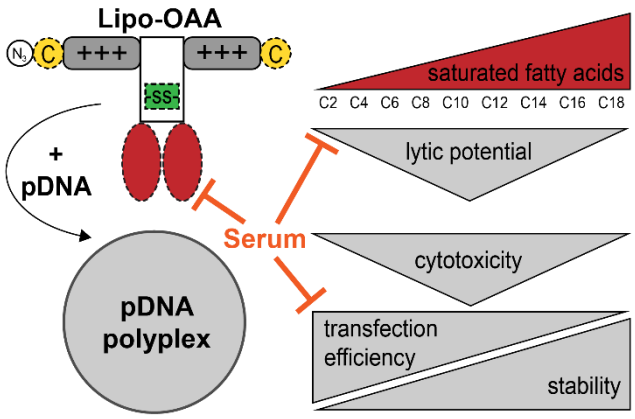

Figure 3.6. Schematic illustration of the key findings of the pDNA screening.

3.4 Conclusion

SPPS is a feasible way to create libraries of oligoaminoamides (OAAs) as nanocarriers in a sequence-defined manner. In the present study, structural variations of a T-shaped artificial lipo-peptide based on four Stp units and two terminal tyrosine tripeptide units comprised histidines, cysteines, disulfide blocks, and saturated fatty acids of different lengths. A thorough investigation of the synthesized OAAs figured out the structural motifs that are advantageous for pDNA polyplexes in terms of physicochemical properties and gene-transfer performance. The key findings are outlined in **Figure 3.6**. A balancing act between extracellular polyplex stability, efficient uptake, endosomal escape, and cargo release into the cytosol is necessary for successful pDNA delivery. Moreover, biocompatibility is desirable. Histidines, in alternating sequence with Stp, prove to be beneficial in terms of endosomal release due to endosomal buffering. Cysteines as well as longer fatty acids improve polyplex stability. Terminal tyrosine tripeptides may substitute for cysteines as polyplex-stabilizing domains.[137] Too stable polyplexes, however, might release their pDNA cargo insufficiently, resulting in a low transfection efficiency.[213-216] Therefore, balancing the stability is of great importance. Independent of their stabilizing effects, fatty acids can also display lytic activity depending on their chain length. Maximum lytic activity was observed for fatty acids of middle chain lengths (C8–C14). On the one hand, endosomolytic activity can be beneficial for endosomal escape into the cytosol. On the other hand, high lytic potential can cause toxicity due to unspecific interactions with cell surfaces and other biological membranes (*e.g.*, of erythrocytes). Therefore, pH-dependent lytic activity is desirable, showing preferred lytic activity at pH

values of the endosome/lysosome, but not at physiological pH. In the case of fatty acid C14, the profile of lytic potential seems to fit best. In addition, incorporation of bioresponsive elements such as redox-sensitive disulfide blocks can reduce cytotoxicity by subsequent carrier degradation.[123, 231]

For siRNA delivery, however, the novel lipo-OAAs seem not to be suitable. A balance between sufficient stability, lytic potential, transfection efficiency, and cytotoxicity could not be reached. Saturated fatty acids are not advantageous here; unsaturated fatty acids like oleic acid or linoleic acid, or larger cholanic acid derivatives have previously proven to be preferable motifs for the delivery of siRNA,[28, 64, 137, 147, 200, 202, 205, 208, 209, 217] or small nucleic acid analogs.[232] Fine-tuning of the required properties is necessary to optimize the carriers for every single nucleic acid type.

Finally, new *in vitro* assays were established that investigate the influence of serum on the behavior of lipo-OAAs and corresponding pDNA polyplexes. By this, hopefully better predictions as well as correlations between *in vitro* and *in vivo* can be drawn in the future. In the current study, pDNA lipo-polyplexes showed only moderate gene-transfer efficiency in a neuroblastoma mouse model, which confirmed the obtained results of the *in vitro* serum assays. Serum exerts a great impact on the lytic activity of the T-shaped lipo-OAAs, thereby lowering the transfection efficiency of corresponding pDNA polyplexes *in vitro* and *in vivo*. For efficient *in vivo* gene-transfer performance of such carrier systems, better protection from serum is required. For example, coating of the polyplexes with hyaluronic acid[28] or anionic lipids[233] might be possible options. Alternatively, lipid-free OAAs and related oligoethylenimine structures, which have already displayed favorable *in vivo* gene-transfer properties,[106, 113, 144, 184, 210, 221] could be the starting points of further optimization. Nevertheless, the current lipo-OAA formulations are highly potent pDNA carrier systems *in vitro* and might be beneficial for *ex vivo* or localized gene therapy approaches like nucleic acid-based vaccines.[234]

3.5 Supporting information

3.5.1 Supporting experimental section

3.5.1.1 Additional materials

Protected Fmoc-α-*L*-amino acids, 2-chlorotrityl chloride resin, DMF, NMP, DIPEA, and TFA were purchased from Iris Biotech (Marktredwitz, Germany). TIS, EDT, HOBt, all used fatty acids, dimethyl sulfoxide (DMSO), 3-(4,5-dimethylthiazol-2-yl)-2,5-diphenyiltetrazolium bromide (MTT), super-DHB (sDHB), and Triton X-100 were purchased from Sigma-Aldrich (Munich, Germany). DCM was purchased from Bernd Kraft (Duisburg, Germany). *N*-hexane and MTBE were obtained from Brenntag (Mühlheim an der Ruhr, Germany). HBTU and micro reactors were obtained from Multi-SynTech (Witten, Germany). All cell culture consumables were obtained from Faust Lab Science (Klettgau, Germany). Cell culture media as well as FBS were purchased from Sigma Aldrich. Antibiotics were purchased from Invitrogen (Karlsruhe, Germany), HEPES from Biomol GmbH (Hamburg, Germany), and glucose from Merck (Darmstadt, Germany). Agarose BioReagent – low EEO was purchased from Sigma Aldrich (Munich, Germany), and GelRed 10,000× from VWR (Darmstadt, Germany). Citrate-buffered human blood was provided by the hospital of the Ludwig-Maximilians-Universität (Munich, Germany). Heparin sodium (5000 IU/mL) was purchased from Ratiopharm (Ulm, Germany). Luciferase Cell Culture Lysis Reagent 5×, D-luciferin sodium salt, and CellTiter-Glo Reagent were obtained from Promega (Mannheim, Germany). All further solvents and other reagents were purchased from Sigma-Aldrich (Munich, Germany), Iris Biotech (Marktredwitz, Germany), Merck (Darmstadt, Germany), or AppliChem (Darmstadt, Germany).

siRNA duplexes[64, 200] were obtained from Axolabs GmbH (Kulmbach, Germany). eGFP-targeting siRNA (siGFP) (sense: 5′-AuAucAuGGccGAcAAGcAdTsdT-3′; antisense: 5′-UGCUUGUCGGCcAUGAuAUdTsdT-3′; small letters: 2’methoxy-RNA; s: phosphorothioate) for silencing of eGFPLuc protein; EG5-targeting siRNA (siEG5) (sense: 5′-ucGAGAAucuAAAcuAAcudTsdT-3′; antisense: 5′-AGUuAGUUuAGAUUCUCGAdTsdT-3′) for silencing EG5 motor protein; control siRNA (siCtrl) (sense: 5′-AuGuAuuGGccu-GuAuuAGdTsdT-3′; antisense: 5′-CuAAuAcAGGCcAAuAcAUdTsdT-3′).

3.5.1.2 Cell lines

The human hepatocellular carcinoma cell line Huh7 (JCRB0403) was purchased from the Japanese Collection of Research Bioresources Cell Bank (Osaka, Japan). The murine neuroblastoma cell line Neuro2a (N2a) was purchased from the American Type Culture Collection (Manassas, Virginia, USA). The human cervical cancer cell line KB (ACC-136) was purchased from the German Collection of Microorganisms and Cell Cultures (Braunschweig, Germany).

3.5.1.3 Loading of 2-chlorotrityl chloride resin with Fmoc protected amino acids

After swelling of 1 g of 2-chlorotrityl chloride resin (1.6 mmol chloride) in water-free DCM for 20 min, the first Fmoc-protected α-*L*-amino acid (0.3 equiv Fmoc-*L*-Tyr(*t*Bu)-OH or Fmoc-*L*-Cys(trt)-OH) dissolved in water-free DCM and DIPEA (0.9 equiv) were added to the resin for 1 h. The reaction solvent was drained, and a mixture of DCM/methanol/DIPEA (80:15:5) was added for at least 30 min. After removal of the reaction mixture, the resin was washed three times with DMF and DCM each. About 30 mg of the resin were collected and dried to determine the loading of the resin. For this purpose, an exact amount of resin was treated with 1 mL deprotection solution (20% (v/v) piperidine in DMF) for 1 h under constant shaking. After centrifugation, the supernatant was diluted with DMF, and absorption was measured at wavelength λ = 301 nm. Deprotection solution diluted in DMF served as blank. The loading was then calculated according to the equation: $resin\ load\ [mmol/g] = \frac{A \times 1000}{m\ [mg] \times 7800 \times f}$ with *f* as dilution factor. Next, the resin was treated four times with 20% (v/v) piperidine in DMF. The resin was washed three times with DMF, three times with DCM, and finally two times with *n*-hexane and dried *in vacuo*.

3.5.1.4 MALDI-TOF MS

1 µL matrix solution (10 mg/mL sDHB (super-DHB: 9:1 (w/w) mixture of 2,5-dihydroxybenzoic acid and 2-hydroxy-5-methoxybenzoic acid) in TA30 (AcN/H_2O (3:7) with 0.1% (v/v) TFA)) and 1 µL of sample solution (concentration: 1 mg/mL) were spotted together on a MTP AnchorChip (Bruker Daltonics, Bremen, Germany). After co-crystallization, the spots were analyzed in positive or negative reflector mode using an Autoflex II mass spectrometer (Bruker Daltonics, Bremen, Germany).

3.5.1.5 ^{1}H NMR spectroscopy

^{1}H NMR spectroscopy was carried out using an AVANCE III HD 500 (500 MHz) by Bruker at room temperature (RT). All chemical shifts were calibrated to the residual proton signal of the solvent (deuterium oxide (D_2O); δ = 4.79 ppm) and reported in ppm. The spectra were analyzed using the software MestreNova (Ver.11.0.4; Mestrelab Research, Santiago de Compostela, Spain). Integrals were set manually and normalized to the singlet peak of the methyl group of the corresponding fatty acid (6 H, -CH_3).

Experiments with pDNA lipo-polyplexes

3.5.1.6 Characterization of pDNA lipo-polyplexes via dynamic and electrophoretic light scattering (DLS, ELS)

Measurements were performed in a folded capillary cell (DTS1070) using a Zetasizer Nano ZS with backscatter detection (Malvern Instruments, Worcestershire, U.K.). Lipo-polyplexes (N/P = 12, HBG) without and with post-functionalization (0.25 equiv of DBCO agents) were prepared as described in section 3.2.4, containing 1 µg pDNA in a total volume of 125 µL HBG. For measurements of size (z-average) and polydispersity index (PdI), the following parameters were chosen; equilibration time 0 min, temperature 25 °C, refractive index 1.330, viscosity 0.8872 mPa*s. Each sample was measured three times with six sub runs each. For zeta-potential measurements, the sample was diluted to 800 µL with HBG. Three measurements with 15 sub runs lasting 10 sec each at 25 °C were performed. Zeta-potentials were calculated by the Smoluchowski equation.

3.5.1.7 Transmission electron microscopy (TEM)

Lipo-polyplexes were formed at an N/P ratio of 12 as described section 3.2.4, containing 200 ng pDNA in 20 µL H_2O. Mild plasma cleaning was used to activate the formvar/carbon-coated 300 mesh copper grids (Ted Pella Inc., Redding, CA, USA). Thereafter, 20 µL of the polyplex solution was placed on the grids. After an incubation of 2.5 min, excess liquid was blotted off using filter paper. The grids were then washed with 5 µL of staining solution for 5 sec and incubated with 5 µL of a 2% (w/v) aqueous uranylformate solution for 5 sec. Excess liquid was again blotted off, followed by air-drying for 30 min. Samples were then characterized at 80 kV using a JEM-1011 electron microscope (Jeol, Freising, Germany). Average nanoparticle sizes of the different samples were analyzed using an image processing software (ImageJ, U. S. National

Institutes of Health, Bethesda, Maryland, USA, https://imagej.nih.gov/ij/, 1997-2020) and are presented as diameters in nm (mean ± SD; n>25).

3.5.1.8 Standard agarose gel shift assay for pDNA lipo-polyplexes

A 1% (w/v) agarose gel was prepared by boiling of agarose in TBE buffer (18.0 g of tris(hydroxymethyl)aminomethane, 5.5 g of boric acid, 0.002 M EDTA at pH 8, in 1 L of water). After cooling down to about 50 °C, 1× GelRed (Biotium, Hayward, CA, USA) was added, and the solution was casted in an electrophoresis unit. Lipo-polyplexes at an N/P ratio of 12, containing 200 ng of pDNA in 20 µL HBG, were prepared as described section 3.2.4. Then, 4 µL of loading buffer (6×; prepared from 6 mL of glycerol, 1.2 mL of 0.5 M EDTA, 2.8 mL of H_2O, 0.02 g of bromophenol blue) were added to each sample and the samples were placed into the gel pockets. Electrophoresis was performed at 120 Volt for 70 min in TBE buffer.

3.5.1.9 Agarose gel shift assay for serum-incubated pDNA lipo-polyplexes

Regarding the gel preparation and the electrophoresis parameters, the same conditions were applied as used in the standard gel shift assay. Only the sample preparation was different. Lipo-polyplexes were formed at an N/P ratio of 12, containing 10-fold higher pDNA concentrations as it was the case in the standard gel shift assay (section *3.5.1.8*). After incubation for 40 min at RT, 90% (v/v) FBS was added to each polyplex solution. The samples were incubated under constant shaking at 25 °C and 37 °C, respectively. At certain time points, aliquots were taken and 4 µL of loading buffer (composition as described in section *3.5.1.8*) were added each. Electrophoresis was performed under standard conditions as mentioned above (section *3.5.1.8*).

3.5.1.10 Ethidium bromide (EtBr) exclusion assay & polyanionic stress test

Lipo-polyplexes at an N/P ratio of 12 were prepared as described in section 3.2.4, containing 2 µg pDNA in a total volume of 200 µL HBG. L-PEI polyplexes (N/P = 6, HBG) served as reference, HBG as blank, and free pDNA (2 µg in 200 µL HBG) was used to determine the 100% value. Next, 700 µL of an EtBr solution (concentration: 0.5 µg/mL) were added to each sample. After an incubation of 3 min, the fluorescence intensity of EtBr was measured using a Cary Eclipse Fluorescence Spectrophotometer (Varian – now part of Agilent Technologies, Germany) at the excitation wavelength λ_{ex} = 510 nm and emission wavelength λ_{em} = 590 nm. In a further step, 250 IU of heparin (Ratiopharm, Ulm,

Germany) were added each, and the samples were re-measured using the same conditions as before. The data are presented as fluorescence intensity of EtBr related to free pDNA.

3.5.1.11 Cell culture

Huh7 cells and N2a cells were grown in Dulbecco's Modified Eagle Medium (DMEM)-low glucose (1 g/L glucose). RPMI-1640 was used as medium for KB cells. All media were supplemented with 10% (v/v) FBS, 4 mM of stable glutamine, 100 U/mL penicillin and 100 µg/mL streptomycin. In addition, non-essential amino acids (NEA-100×; Biochrom, Berlin, Germany) were added to RPMI-1640 medium in a ratio of 1:100. The cell lines were cultured at 37 °C and 5% CO_2 in an incubator with a relative humidity of 95%. At 80–90% confluency, the cells were harvested using 0.05%/0.02% (w/v) trypsin-EDTA, followed by resuspension in the required culture media. For cell culture experiments with KB cells, wells were coated with collagen A (0.1% collagen Type I in HCl, 1:10 diluted with water; Biochrom, Berlin, Germany) for 30 min at 37 °C prior to seeding.

3.5.1.12 Cell viability (CellTiter-Glo assay)

Transfections were performed as described in section 3.2.5. The supernatant was removed 24 h after transfection, and 25 µL of medium as well as 25 µL of CellTiter-Glo reagent (Promega, Mannheim, Germany) were added to each well. After incubation on an orbital shaker for 30 min at RT, the luminescence was recorded using a Centro LB 960 plate reader luminometer (Berthold Technologies, Bad Wildbad, Germany). The luminescent signals (in relative light units, RLU) of the samples were set in relation to the luminescent signal of negative control (HBG-treated cells). Results are presented as relative metabolic activity related to negative control. Experiments were performed in triplicate.

3.5.1.13 Cell viability (MTT assay)

This assay was applied for the evaluation of the block-wise motif of Stp (succinoyl tetraethylene pentamine) and histidines. Transfections were performed as described in section 3.2.5. At 24 h after transfection, 10 µL MTT (5 mg/mL) was added to each well, reaching a final concentration of 0.5 mg/mL. After incubation at 37 °C for 2 h, the supernatant was removed. The plates were stored at -80°C for at least 1 h. Afterwards, the purple formazan product was dissolved in 100 µL DMSO. After incubation for 30 min

at 37 °C under constant shaking, quantification was done photometrically using a Tecan microplate reader (Spectrafluor Plus, Tecan, Männedorf, Switzerland). Absorbance was measured at wavelength λ = 590 nm with background correction at λ = 630 nm. The experiments were carried out in triplicate. The relative metabolic activity related to control wells (HBG-treated cells) was calculated by the equation: $\frac{[\mathrm{A}]_{\mathrm{test}}}{[\mathrm{A}]_{\mathrm{control}}}$.

3.5.1.14 Cellular uptake studies

Huh7 cells or N2a cells were seeded in 24-well plates with a density of 50,000 cells per well. Experiments were performed in triplicate. The cellular uptake was evaluated using 1 µg pDNA (20% Cy5-labeled) per well. After 24 h, the medium was replaced by 400 µL fresh medium containing 10% (v/v) FBS. Next, pDNA lipo-polyplexes formed at an N/P ratio of 12 in 100 µL HBG (as described in section 3.2.4) were added to each well. Cells were incubated at 37 °C for 4 h, and then treated with 500 µL PBS containing 1000 IU heparin (Ratiopharm, Ulm, Germany) for 15 min on ice. By this, polyplexes non-specifically bound to the cell surface were removed. After an additional washing step with 500 µL PBS, cells were detached with trypsin/EDTA, centrifuged and the cell pellets were taken up in 600 µL PBS with 10% (v/v) FBS. A volume of 0.6 µL of DAPI (4',6-diamino-2-phenylindole) was added to each sample. Cellular uptake was assayed by excitation of Cy5 at 635 nm and detection of emission at 665 nm. Cells were appropriately gated by forward/sideward scatter and pulse width for exclusion of doublets. Data were recorded by collection of 10,000 events per sample *via* a BD-LSR Fortessa flow cytometer (BD Biosciences, Heidelberg, Germany) using BD FACS Diva software and analyzed by FlowJo 7.6.5 flow cytometric analysis software (FlowJo, Ashland, OR, USA).

Experiments with siRNA lipo-polyplexes

3.5.1.15 Formation of siRNA lipo-polyplexes

siRNA and the calculated amount of lipo-OAA at an N/P ratio of 12 were separately diluted in 10 µL HBG each. The two solutions with the same volume were mixed by rapid pipetting. The mixture was incubated for 45 min at RT, obtaining 20 µL of siRNA polyplexes with a final siRNA concentration of 25 ng/µL.

3.5.1.16 Characterization of siRNA lipo-polyplexes by dynamic and electrophoretic light scattering (DLS, ELS)

Particle size and zeta-potential of siRNA lipo-polyplexes were measured using a Zetasizer Nano ZS with backscatter detection (Malvern Instruments, Worcestershire, U.K.). Same parameters and standard operating procedures as for measurements of pDNA lipo-polyplexes were used (*see* section *3.5.1.6*). siRNA polyplexes were prepared in 20 µL of HBG buffer with a final siRNA concentration of 200 ng/µL, and further diluted with 20 mM HEPES buffer (pH 7.4) to 800 µL prior to measurement.

3.5.1.17 Agarose gel shift assay for siRNA lipo-polyplexes

2.5% (w/v) agarose was dissolved in TBE buffer (for composition see section *3.5.1.8*). The solution was boiled, and then 1:10,000 (v/v) of GelRed (10,000×; Biotium; Hayward, CA, USA) was added. Polyplexes containing 500 ng siRNA were prepared at N/P 12 in 20 µL HBG and subsequently mixed with 4 µL of loading buffer (for composition see section *3.5.1.8*). Then the samples were loaded in the gel pockets, and electrophoresis was performed at 100 Volt for 60 min. The gel shift assay was also performed under standard conditions with siRNA polyplexes pre-incubated in 90% (v/v) serum (FBS) at 37 °C for 4 and 24 h, respectively.

3.5.1.18 Cell culture

Huh7 cells, Neuro2a (N2a) cells and KB cells were cultured in DMEM-low glucose (1 g/L glucose). Huh7 cells and N2a cells, both stably transfected with the eGFPLuc (enhanced green fluorescent protein/luciferase) fusion gene (Huh7/eGFPLuc[235]; N2a/eGFPLuc[64]) were cultured in DMEM/Nutrient Mixture F-12 Ham or DMEM-low glucose, respectively. KB cells stably transfected with the eGFPLuc fusion gene (KB/eGFPLuc[115]) were cultured in RPMI-1640 medium. All media were supplemented with 10% (v/v) FBS, 4 mM of stable glutamine, 100 U/mL penicillin and 100 µg/mL streptomycin. The cells were maintained in ventilated flasks in the cell incubator at 37 °C with 5% CO_2 in a humidified atmosphere. At 80 – 90% confluency, the cells were harvested using 0.05% / 0.02% (w/v) trypsin/EDTA, followed by resuspension in the required culture media. For cell culture experiments with KB cells, wells were coated with collagen A (0.1% collagen Type I in HCl, 1:10 diluted with water; Biochrom, Berlin, Germany) for 30 min at 37 °C prior to seeding.

3.5.1.19 eGFPLuc gene silencing measured via luciferase assay

KB/eGFPLuc cells, N2a/eGFPLuc cells or Huh7/eGFPLuc cells were seeded in 96-well plates in a volume of 100 µL medium per well containing 5000 cells and incubated for 24 h, with the medium replaced with 80 µL fresh serum-containing medium (10% (v/v) FBS) 2 h prior to transfection. Cells were incubated with 20 µL of polyplexes containing 500 ng of control-siRNA or GFP-siRNA (N/P 12, HBG) for 4 h. Thereafter, the medium was replaced with 100 µL of fresh medium and incubated for additional 44 h. The medium was removed, and 100 µL of luciferase cell culture lysis reagent 0.5× (for composition *see* section 3.2.5; Promega, Mannheim, Germany) was added to each well. Luciferase activity of the cell lysates was determined in a Centro LB 960 plate reader luminometer (Berthold Technologies, Bad Wildbad, Germany), using a LAR buffer solution (for composition *see* section 3.2.5, pH 8-8.5) supplemented with 5% (v/v) of a mixture of 10 mM luciferin and 29 mM glycylglycine. Transfection efficiency was evaluated as relative light units (RLU) per well, which were presented as percentage of the luciferase gene expression obtained in HBG-treated control cells. Experiments were performed in triplicate.

3.5.1.20 Antitumoral activity mediated by EG5 gene silencing (MTT assay)

KB cells (4000 cells per well), N2a cells (5000 cells per well), or Huh7 cells (8000 cells per well) were seeded in 100 µL medium per well using a 96-well plate and incubated for 24 h, with the medium replaced with 80 µL fresh medium 2 h prior to transfection. Cells were incubated with 20 µL of polyplexes containing 500 ng of control-siRNA or EG5-siRNA (N/P 12, HBG) for 4 h. Then, the medium was replaced with 100 µL of fresh medium and incubated for additional 44 h. 10 µL of MTT with a final concentration of 0.5 mg/mL was added into each well and incubated for 2 h at 37°C. After the medium was removed, the plate was stored at -80°C for at least 1 h. Afterwards, 100 µL of DMSO was added to each well to dissolve the formazan crystals, which were produced by living cells. The absorbance of the dye was measured using a Tecan microplate reader (Spectrafluor Plus, Tecan, Männedorf, Switzerland) at wavelength λ = 590 nm with background correction at λ = 630 nm. The experiments were carried out in triplicate. Metabolic activities were evaluated as percentage relative to HBG buffer-treated control cells.

3.5.2 Supporting results and discussion

3.5.2.1 Detailed information to section 3.3.2.3 "Investigation of siRNA lipo-polyplexes"

Different nucleic acids require different properties from their carrier systems.[13, 26, 86] It is important to know, which structure elements are valuable for each nucleic acid. Therefore, in addition to the screening of the $(H\text{-}Stp)_2$-library for pDNA delivery, these structures were also tested for siRNA delivery. By this, beneficial structure motifs as well as differences to pDNA polyplexes should be found.

First, the siRNA polyplexes (N/P = 12, HBG) were characterized *via* DLS. Defined particles with sizes around 150–250 nm were obtained in all cases (**Table 3.7**). Stability of the single siRNA polyplexes was determined by agarose gel shift assays at different conditions (**Figure 3.17** and **Figure 3.18**). The standard gel shift assay showed that the incorporated fatty acids have a great impact on the stability: the longer the fatty acid chain lengths, the more stable the corresponding polyplexes (**Figure 3.17**). Moreover, cysteine-containing polyplexes were more stable than polyplexes of the other two groups. These findings were also confirmed by a gel shift assay after incubation of the polyplexes in 90% (v/v) serum (FBS) for 4 and 24 h (**Figure 3.18**). Additionally, the block-wise motif of Stp and histidines (H_3Stp_2) led to more stable particles compared to the corresponding structures with alternating motif. All these stability tendencies are consistent with the stability data obtained for pDNA polyplexes. There, cysteines, and longer fatty acids also improved polyplex stability. Overall, however, the siRNA polyplexes were far less stable than the analogous pDNA polyplexes, showing in all cases at least slight release already after incubation for 4 h at 37 °C in 90% (v/v) serum (**Figure 3.18a**).

Furthermore, gene silencing and metabolic activity of the siRNA polyplexes (N/P = 12, HBG) were investigated *via* luciferase assay and MTT assay in the same three different cell lines used in the pDNA screening (Huh7, N2a, and KB; **Figure 3.19** and **Figure 3.20**). Gene silencing efficacy was in total rather low, and almost completely absent in Huh7/eGFPLuc cells. Best results were obtained in N2a/eGFPLuc cells for cysteine-containing OAAs with middle to longer fatty acid chain lengths (C6–C12) (**Figure 3.19b**). In case of the two cysteine-free groups, longer fatty acids (C12–C18) worked better on N2a/eGFPLuc cells, which goes along with findings for pDNA transfection efficiency. Again, ssbb-containing polyplexes did not work in KB/eGFPLuc cells (**Figure 3.19c**), as already observed in the pDNA screening. In addition, polyplexes with block-wise motif of

Stp and histidines (H_3Stp_2) showed again moderate to no effectiveness in all three cell lines compared to the alternating motif. Overall, polyplexes containing fatty acids of middle chain lengths caused toxicity in all three tested cell lines (Huh7, N2a, and KB; **Figure 3.20**). Lipo-OAAs with these fatty acids exhibit high lytic activity even at physiological pH (**Figure 3.3b**), and thus can be harmful because of unspecific membranolytic activity not only to endosomal membranes. The much higher toxicity of siRNA polyplexes compared to pDNA polyplexes might be due to lower stability of the siRNA complexes and therefore greater amount of free lytic lipo-OAAs.

All in all, stability, lytic activity as well as cytotoxicity are of great importance for successful siRNA delivery. Unfortunately, the balancing act between these three properties could not be accomplished with the histidine library; the performance of siRNA polyplexes of the $(H\text{-}Stp)_2$-library was unsatisfactory. Saturated fatty acids seem to be not suitable. In previous work, it has been shown that unsaturated C18 fatty acids with one or more double bonds (oleic acid, linoleic acid) are more beneficial for siRNA polyplexes.[28, 64, 137, 147, 200, 205, 208, 209, 217]

3.5.2.2 Detailed information to section 3.3.3 “Characterization of pDNA core-shell polyplexes”

In the current study, mono-and bivalent DBCO-PEG agents for shielding purposes were evaluated for pDNA core-shell polyplexes, namely monoDBCO-PEG24 and bisDBCO-PEG24 (**Figure 3.21**). The core polyplexes at an N/P ratio of 12 in HBG were modified with 0.25 equiv of DBCO-PEG agent. The post-functionalization aims at modification of surface-exposed azido-OAAs only. Therefore, intentionally only a fraction of lipo-OAA azides should be modified. The equivalent of 0.25 was used for the DBCO agents because at higher equivalents (*e.g.*, 0.5 equiv), aggregation occurred for many of the shielded lipopolyplexes, probably due to destabilizing effects.

Investigation of Physicochemical Properties of pDNA Core-Shell Polyplexes

In a first step, the post-functionalized polyplexes were characterized regarding size, polydispersity, and zeta-potential (**Figure 3.13**). The findings go along with the results obtained in the stability experiments with the pDNA core-polyplexes (**Figure 3.1**): cysteines as well as longer fatty acids provide nanoparticle stability. In all three groups of the histidine library, post-functionalization led to aggregation in case of carriers containing shorter fatty acids, with particle sizes of more than 1000 nm. OAAs of the cysteine-containing group showed aggregate formation for fatty acids C2 and C4 only, whereas in the other two groups big particles were observed up to fatty acid C10.

Better post-functionalization seems to be achieved in case of the bivalent attachment sites, as indicated by a notable drop in surface charge (**Figure 3.13c**). This strong decrease in zeta-potential was measured only in case of the bivalent PEG agent but not for the monovalent agent. Therefore, it is also not surprising that the polyplexes modified with the bivalent DBCO agent showed higher tendency towards aggregation due to less repulsion at almost neutral surface charge. Nevertheless, also here core-shell polyplexes presenting defined, well-formed nanoparticles with sizes below 200 nm could be generated; these were based on lipo-OAAs containing middle to longer fatty acids C6–C18 in the cysteine group, C12–C18 in the $(H\text{-}Stp)_2$-0 group and C14–C18 in the ssbb group. Further research was conducted with bisDBCO-PEG_{24} based on these first encouraging shielding effects. By the way, similar findings of bivalent attachment sites being superior and resulting in better post-functionalization were already made previously for targeted pDNA[211] and siRNA delivery.[202, 205]

3.5.3 Supporting figures

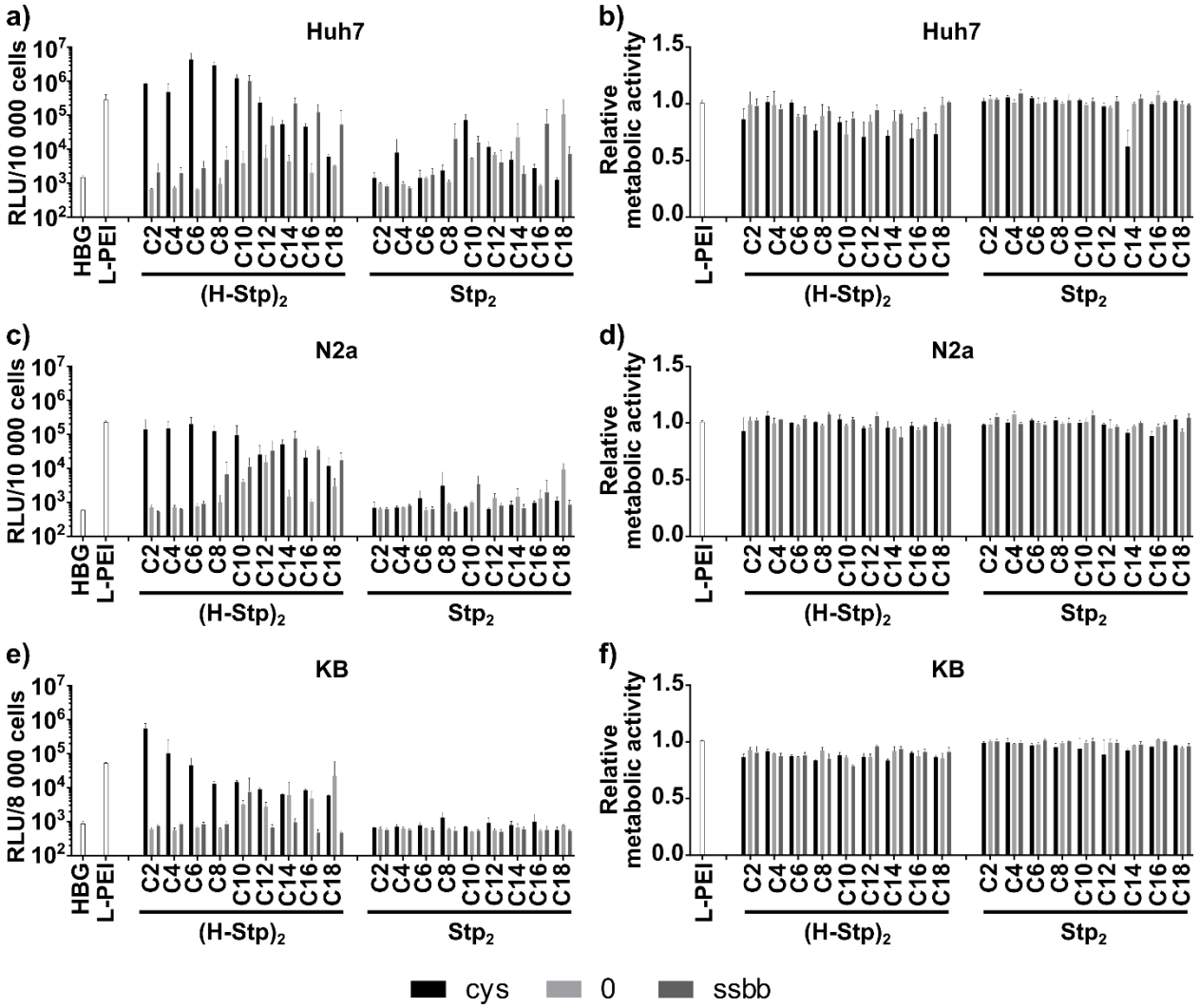

Figure 3.7. Gene-transfer performance of pCMVLuc polyplexes (N/P = 12, HBG) of the $(H\text{-}Stp)_2$- and of the Stp_2-library. Screening in three different cell lines, namely Huh7 (*above*), N2a (*middle*), and KB cells (*below*). Luciferase gene expression assay (mean + SD; *n* = 3) (*le*ft; **a, c, e**), and CellTiter-Glo assay (*right*; **b, d, f**), both performed 24 h after transfection (mean + SD; *n* = 3). Metabolic activities, determined *via* CellTiter-Glo assay, are presented relative to HBG buffer-treated control cells. L-PEI pDNA polyplexes (N/P = 6, HBG) served as positive control. Transfections were performed by Dr. Ana Krhač Levačić (Pharmaceutical Biotechnology, LMU Munich). The histidine-free library was synthesized in cooperation with Jie Luo (Pharmaceutical Biotechnology, LMU Munich).

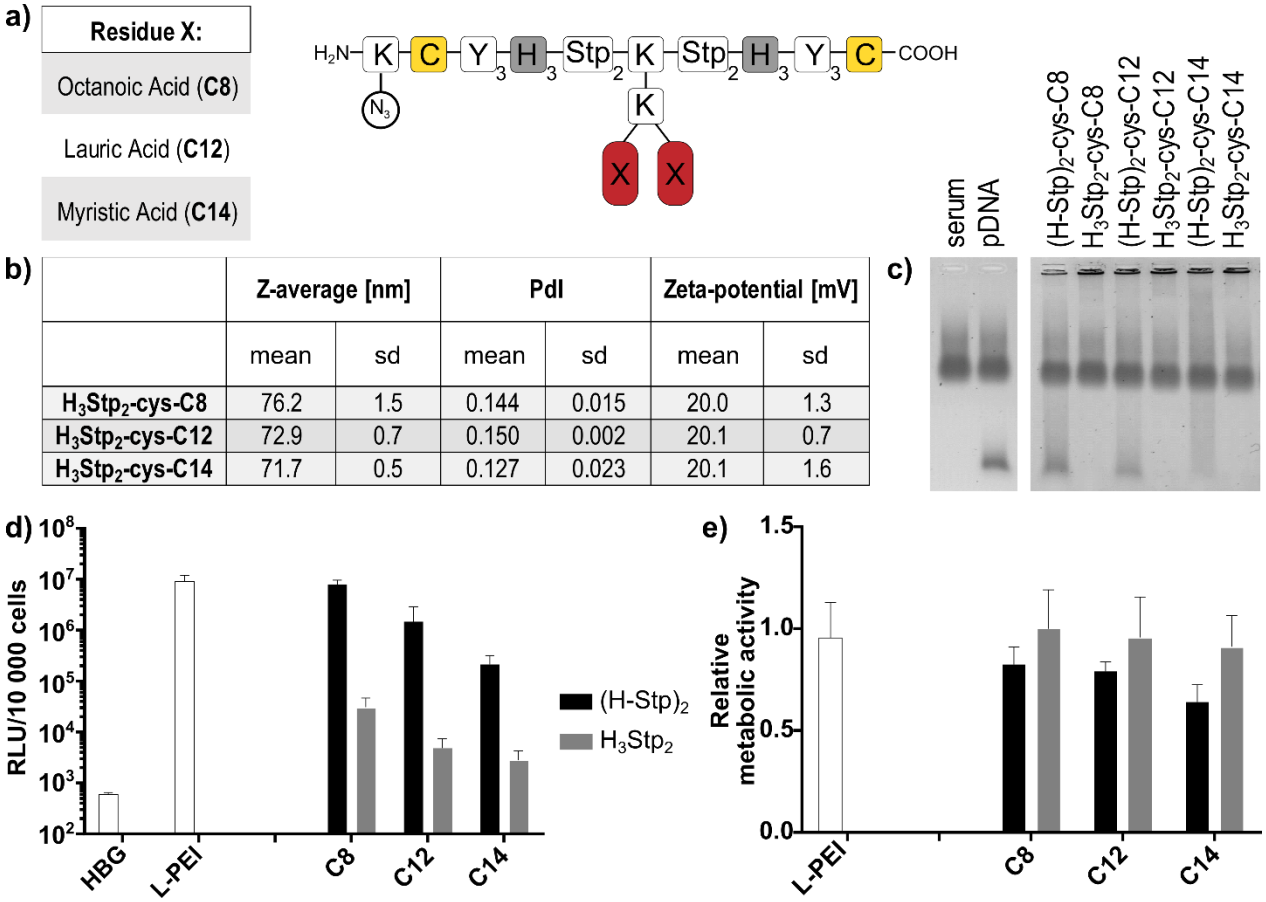

	Z-average [nm]		PdI		Zeta-potential [mV]	
	mean	sd	mean	sd	mean	sd
H_3Stp_2-cys-C8	76.2	1.5	0.144	0.015	20.0	1.3
H_3Stp_2-cys-C12	72.9	0.7	0.150	0.002	20.1	0.7
H_3Stp_2-cys-C14	71.7	0.5	0.127	0.023	20.1	1.6

Figure 3.8. (**a**) Cysteine-containing T-Shape lipo-OAA structures with Stp and histidine in block-wise motif (H_3Stp_2). K(N_3): azido-lysine; K: lysine; C: cysteine; Y: tyrosine; H: histidine; Stp: succinoyl tetraethylene pentamine; X: residue with different saturated fatty acids (octanoic acid, lauric acid and myristic acid). (**b**) DLS and ELS results of corresponding pDNA polyplexes (N/P = 12, HBG) (mean ± SD; *n* = 3). (**c**) Comparison of the stability of polyplexes containing block-wise (H_3Stp_2) or alternating motif ($(H\text{-}Stp)_2$) of Stp and histidines *via* serum agarose gel shift after incubation for 120 h in 90% (v/v) serum (FBS) at 25 °C. Comparison of gene-transfer performance in Huh7 cells of pCMVLuc polyplexes containing block-wise (H_3Stp_2) or alternating motif ($(H\text{-}Stp)_2$) of Stp and histidines *via* luciferase gene expression assay (**d**) and MTT assay (**e**), both performed 24 h after transfection (mean + SD; *n* = 3). Metabolic activities, determined *via* MTT assay, are presented relative to HBG buffer-treated control cells. L-PEI pDNA polyplexes (N/P = 6, HBG) served as positive control.

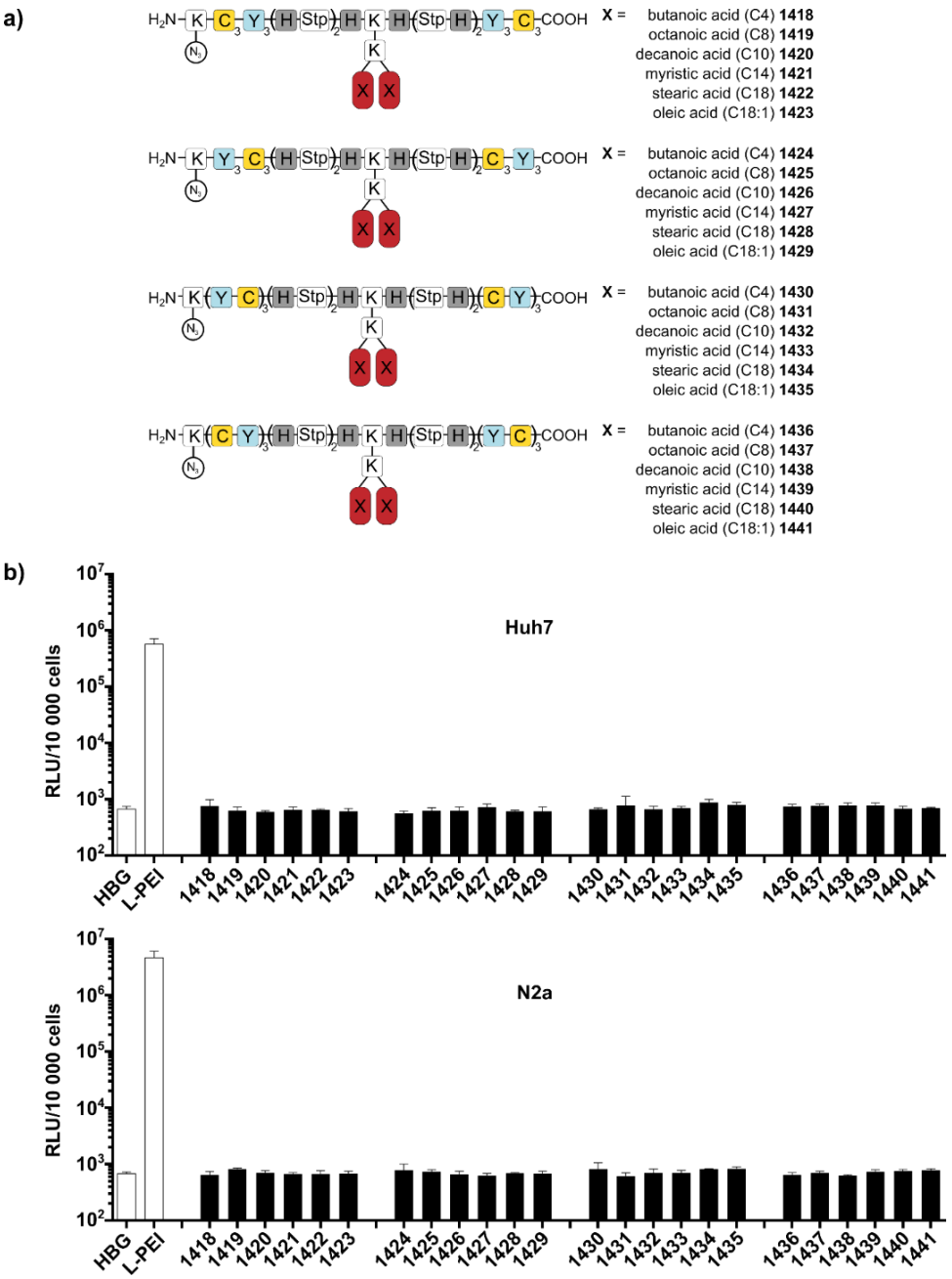

Figure 3.9. (**a**) T-Shape lipo-OAA structures containing two times three cysteines in the backbone, either in alternating sequence with tyrosines or in block-wise motif (referred to as oligo-cysteine library). K(N_3): azido-lysine; C: cysteine; Y: tyrosine; H: histidine; K: lysine; Stp: succinoyl tetraethylene pentamine; X: residue with different fatty acids (butanoic acid, octanoic acid, decanoic acid, myristic acid, stearic acid, oleic acid). (**b**) Gene-transfer performance in Huh7 cells (*above*) and N2a cells (*below*) of corresponding pCMVLuc polyplexes (N/P = 12, HBG), determined *via* luciferase gene expression assay 24 h after transfection (mean + SD; *n* = 3). L-PEI pDNA polyplexes (N/P = 6, HBG) served as positive control. Synthesis of the oligo-cysteine library was done by Teoman Benli-Hoppe (Pharmaceutical Biotechnology, LMU Munich).

a) $(H\text{-}Stp)_2$-cys-C14

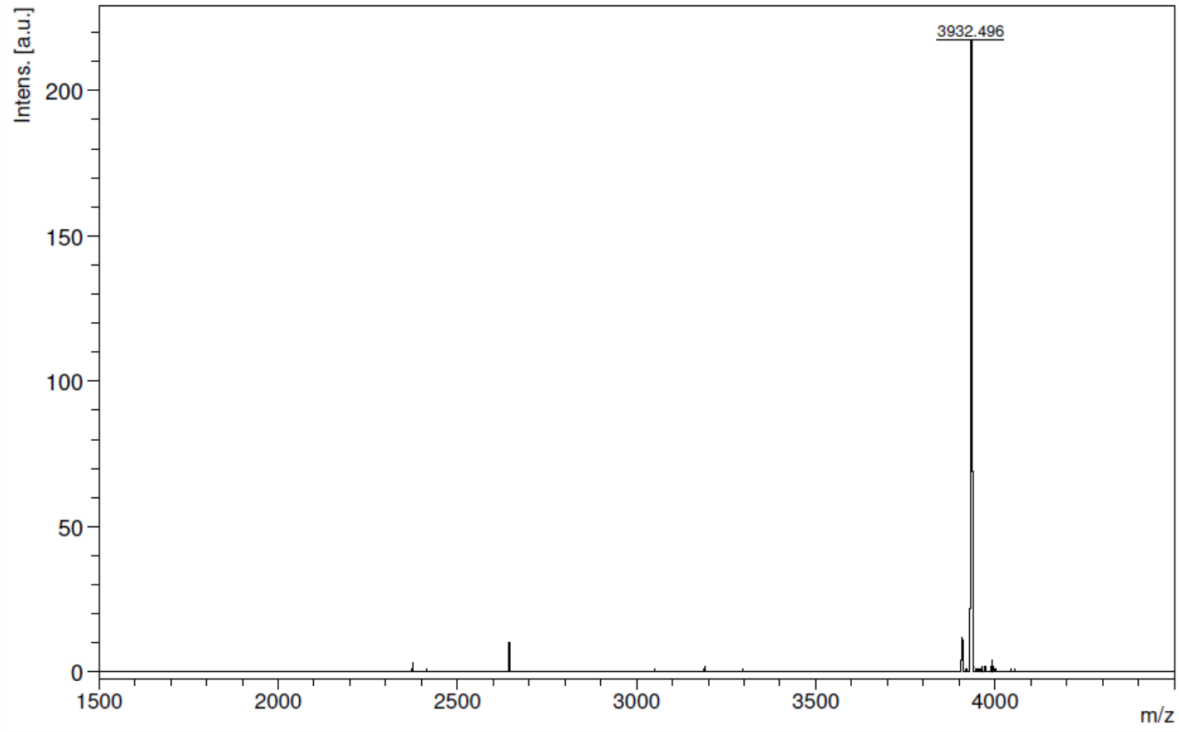

b) $(H\text{-}Stp)_2$-ssbb-C14

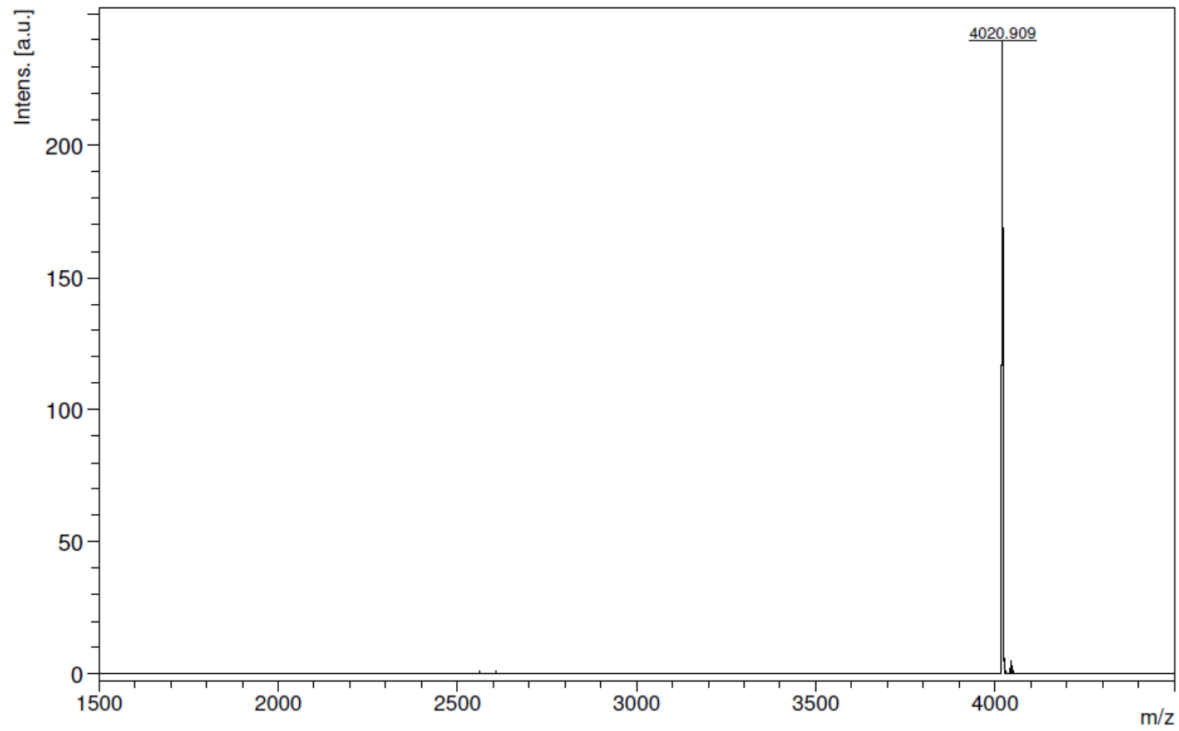

Figure 3.10. Mass spectra (MALDI-TOF MS). Example spectra of representative effective lipo-OAAs used in the *in vivo* study. (**a**) $(H\text{-}Stp)_2$-cys-C14; (**b**) $(H\text{-}Stp)_2$-ssbb-C14.

a) (H-Stp)$_2$-cys-C14

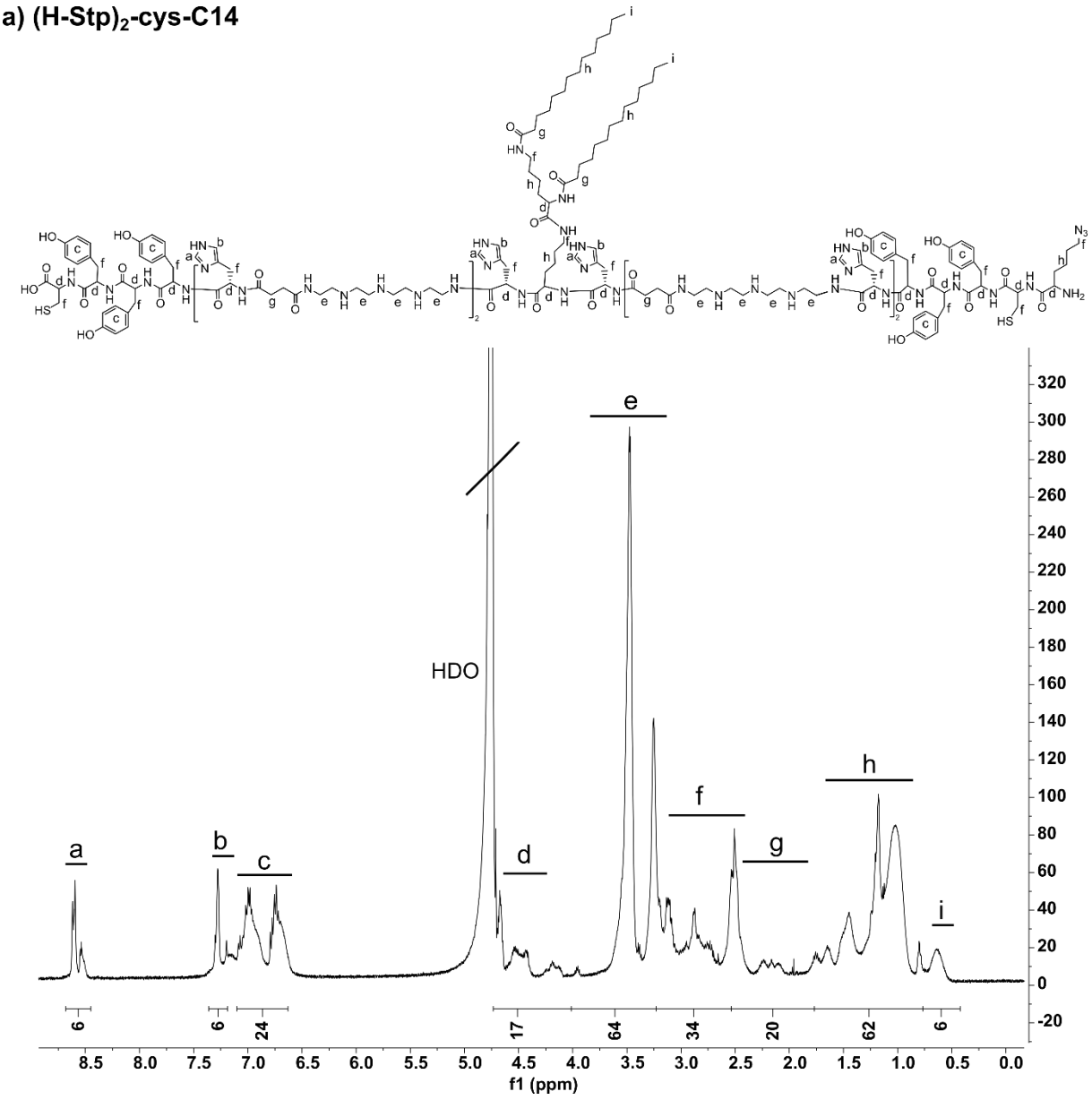

^{1}H NMR (500 MHz, deuterium oxide); δ (ppm) = 0.45-0.75 (s, 6 H, -CH_3 myristic acid), 0.75-1.75 (m, 62 H, βγδ H lysine, βγδ H azido-lysine, -CH_2- myristic acid), 1.75-2.55 (m, 20 H, -CO-CH_2-CH_2-CO- Stp, -CO-CH_2- myristic acid), 2.55-3.25 (m, 34 H, ε H lysine, ε H azido-lysine, β H tyrosine, β H histidine and β H cysteine), 3.25-4.00 (m, 64 H, -CH_2-Stp), 4.00-4.75 (m, 17 H, α H amino acids), 6.65-7.10 (m, 24 H, -CH- tyrosine), 7.20-7.35 (m, 6 H, aromatic H histidine), 8.45-8.70 (m, 6 H, aromatic H histidine).

Figure 3.11. ^{1}H NMR spectra. Example spectra of representative effective lipo-OAAs used in the *in vivo* study. (**a**) (H-Stp)$_2$-cys-C14.

b) (H-Stp)$_2$-ssbb-C14

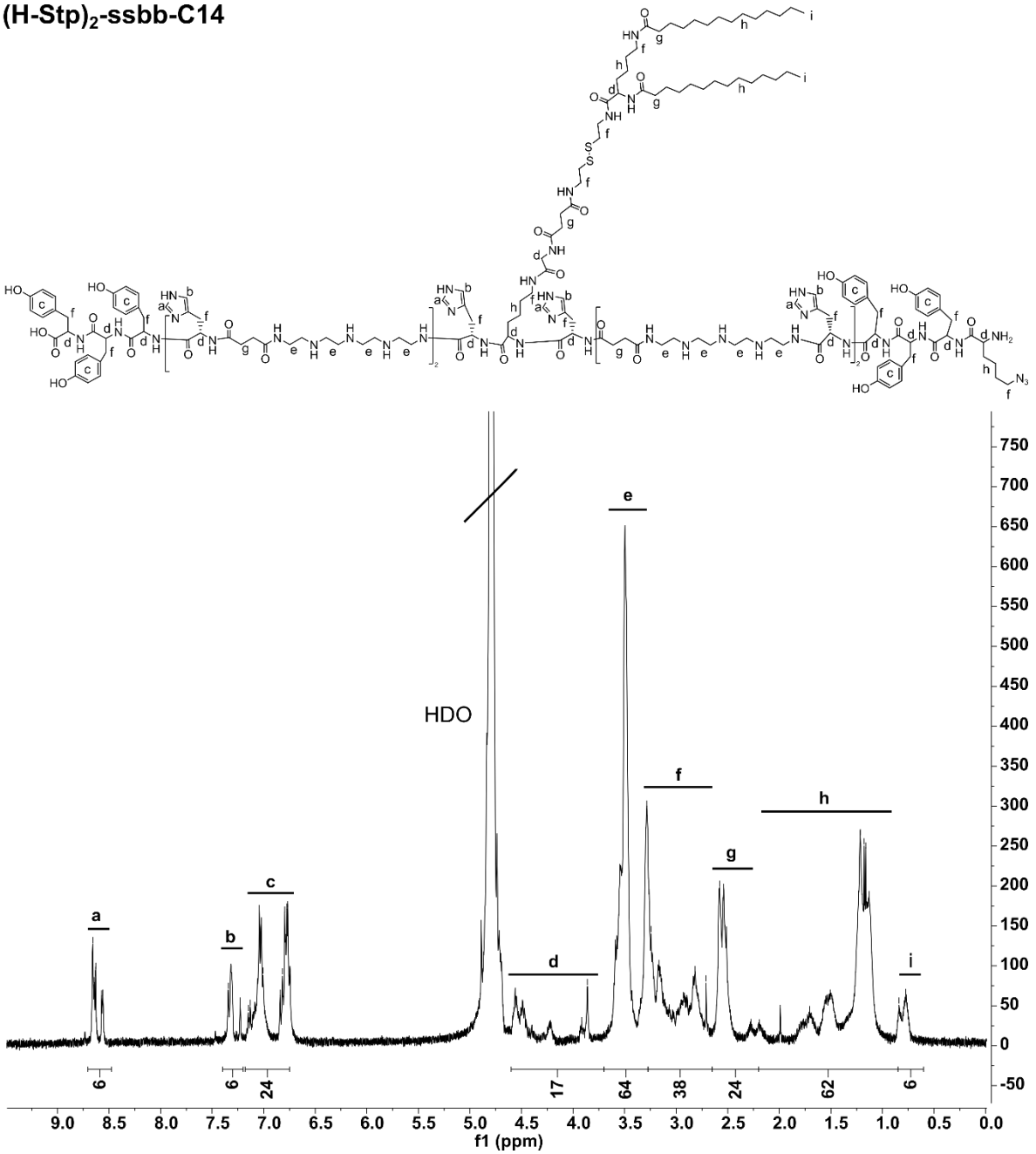

^{1}H NMR (500 MHz, deuterium oxide); δ (ppm) = 0.65-0.85 (s, 6 H, -CH_3 myristic acid), 0.85-2.20 (m, 62 H, βγδ H lysine, βγδ H azido-lysine, -CH_2- myristic acid), 2.20-2.65 (m, 24 H, -CO-CH_2-CH_2-CO- Stp and ssbb, -CO-CH_2- myristic acid), 2.65-3.25 (m, 38 H, ε H lysine, ε H azido-lysine, β H tyrosine, β H histidine and -CH_2-ssbb), 3.25-3.70 (m, 64 H, -CH_2-Stp), 3.70-4.60 (m, 17 H, α H amino acids), 6.75-7.20 (m, 24 H, -CH- tyrosine), 7.20-7.40 (m, 6 H, aromatic H histidine), 8.50-8.70 (m, 6 H, aromatic H histidine).

Figure 3.11. (*continued*) ^{1}H NMR spectra. Example spectra of representative effective lipo-OAAs used in the *in vivo* study. (**b**) (H-Stp)$_2$-ssbb-C14.

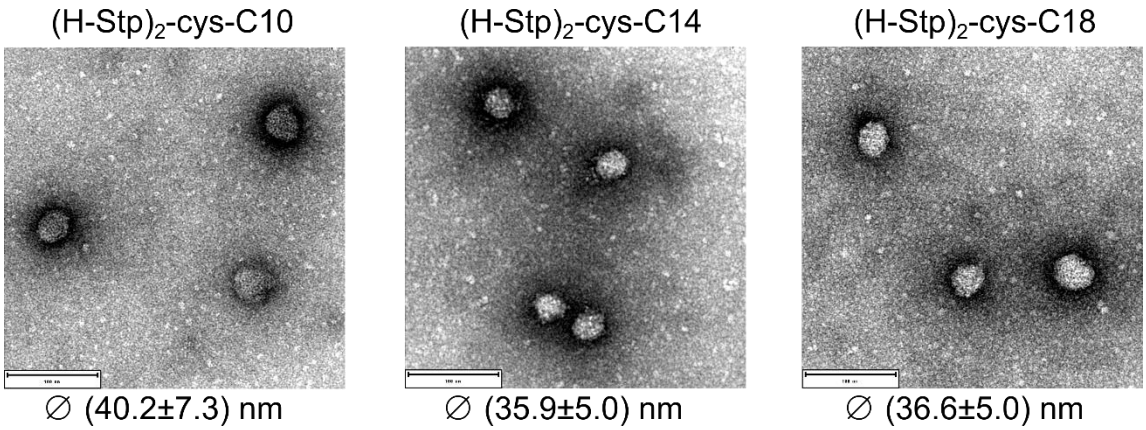

Figure 3.12. Representative TEM images of pDNA lipo-polyplexes (N/P = 12, H_2O) formed with selected $(H\text{-}Stp)_2$-cys carriers with shorter (C10), middle (C14) and longer fatty acids (C18), respectively. Average nanoparticle sizes are presented as diameters in nm (mean ± SD; *n* = 28 in the case of $(H\text{-}Stp)_2$-cys-C10; *n* = 29 in the case of $(H\text{-}Stp)_2$-cys-C14; *n* = 42 in the case of $(H\text{-}Stp)_2$-cys-C18). Scale bar = 100 nm. TEM measurements were performed by Susanne Kempter (Physics, LMU Munich) and analyzed by Özgür Öztürk (Pharmaceutical Biotechnology, LMU Munich).

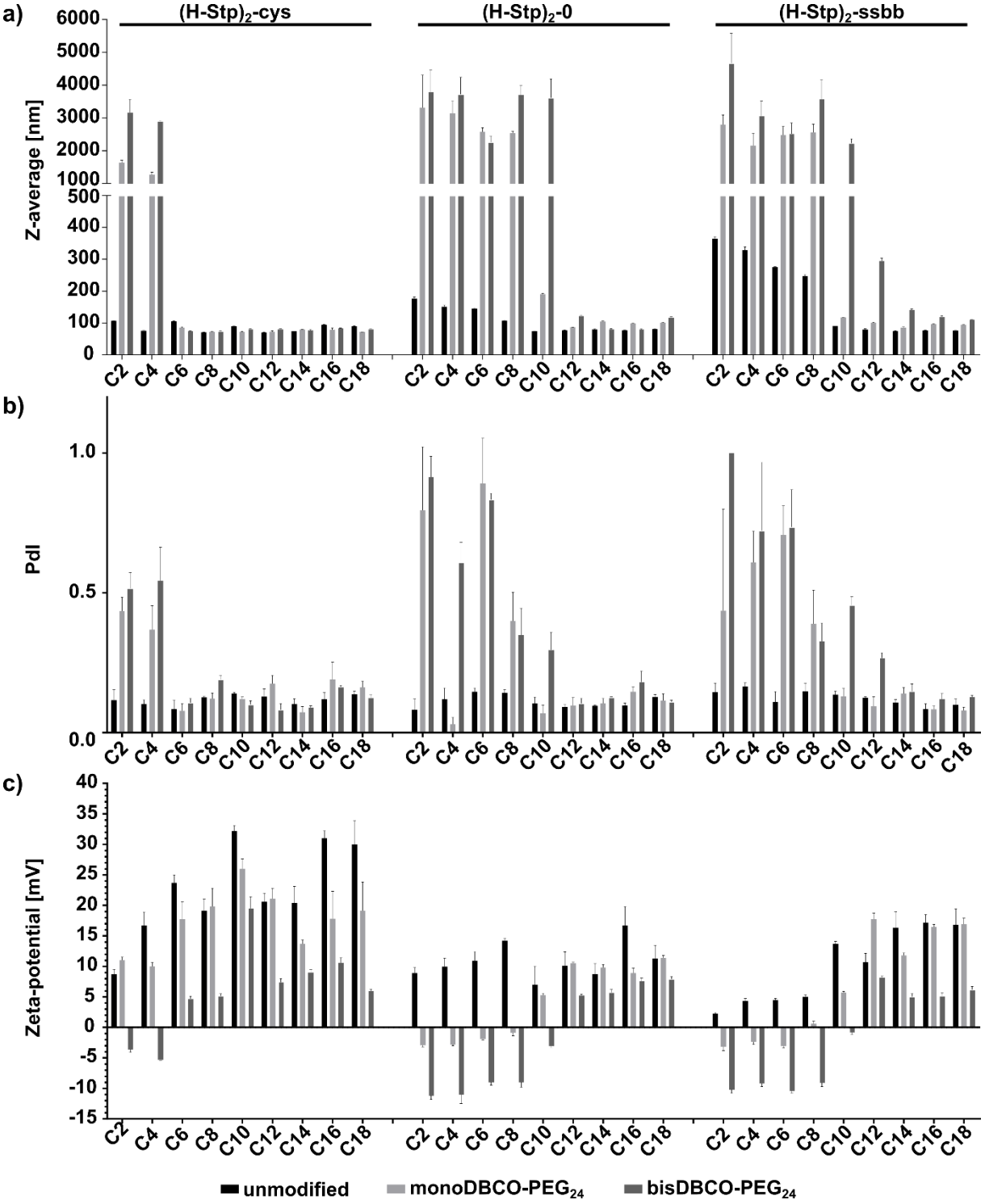

Figure 3.13. DLS and ELS results (mean + SD; *n* = 3) of pDNA polyplexes of the (H-Stp)$_2$-library (N/P = 12, HBG), unmodified or post-functionalized with 0.25 equiv of mono- or bisDBCO-PEG$_{24}$, respectively. (**a**) Size presented as z-average diameter in nm, (**b**) polydispersity index (PdI), and (**c**) zeta-potential in mV.

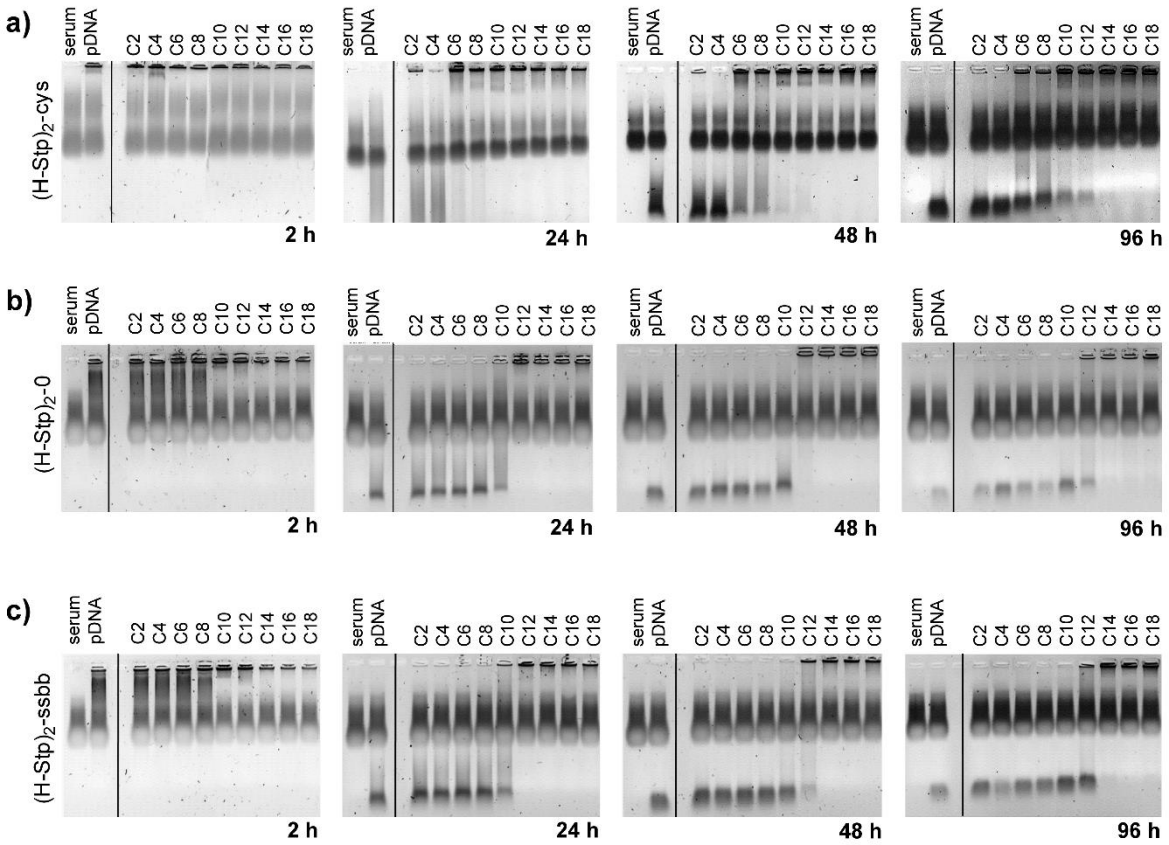

Figure 3.14. Serum agarose gel shift of pDNA polyplexes (N/P = 12, HBG) of the (H-Stp)$_2$-library after incubation for 2, 24, 48, and 96 h in 90% (v/v) serum (FBS) at 25 °C. (**a**) (H-Stp)$_2$-cys group, (**b**) (H-Stp)$_2$-0 group, (**c**) (H-Stp)$_2$-ssbb group.

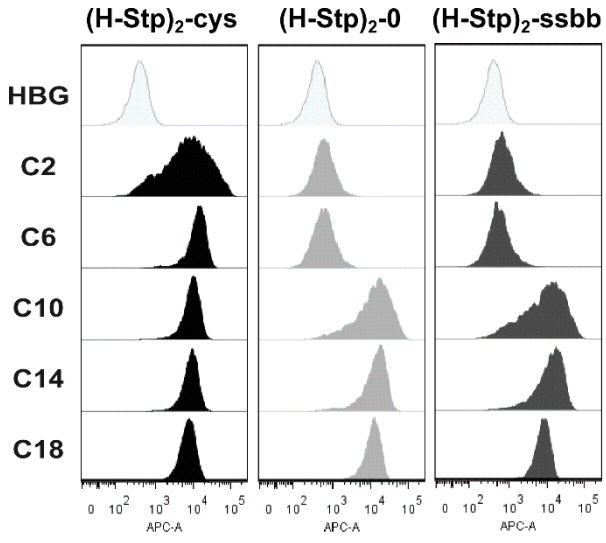

Figure 3.15. Cellular uptake of pDNA polyplexes (N/P = 12, HBG) of the (H-Stp)$_2$-library in N2a cells after 4 h, in comparison to HBG-treated control cells. Flow cytometry was done together with Dr. Ana Krhač Levačić (Pharmaceutical Biotechnology, LMU Munich).

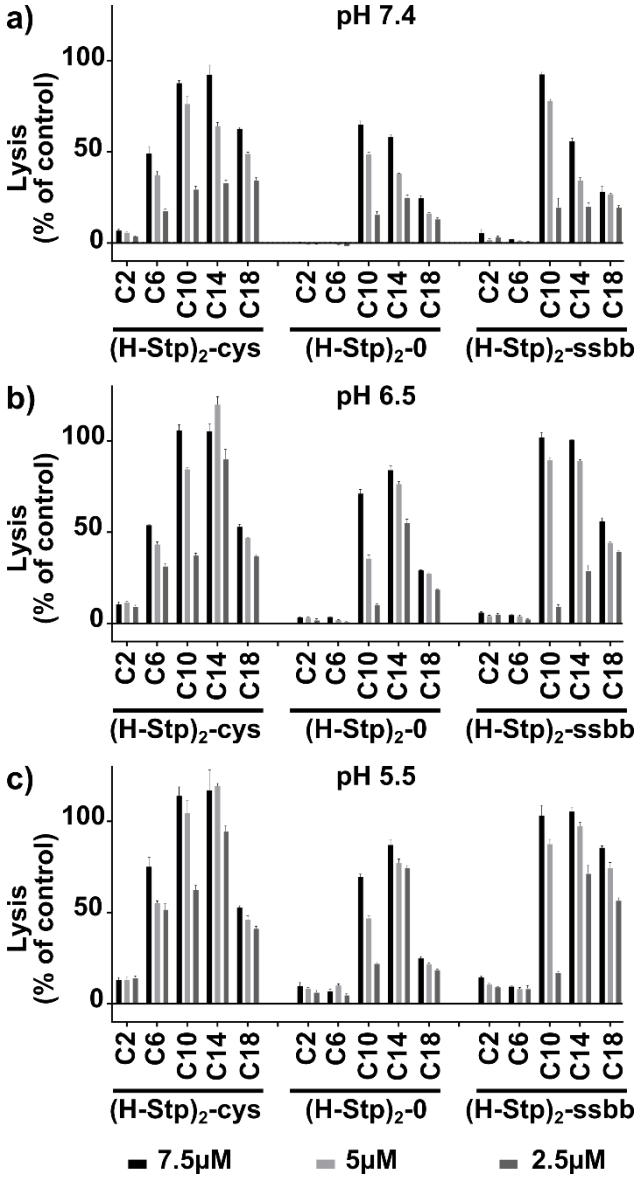

Figure 3.16. Lytic potential of the single OAAs of the $(H\text{-}Stp)_2$-library at different concentrations (7.5, 5, and 2.5 µM), measured in an erythrocyte leakage assay at different pH values: (**a**) pH 7.4, (**b**) pH 6.5, and (**c**) pH 5.5. Data are presented as mean + SD out of quadruplicates. The experiments were performed together with Dr. Ana Krhač Levačić (Pharmaceutical Biotechnology, LMU Munich).

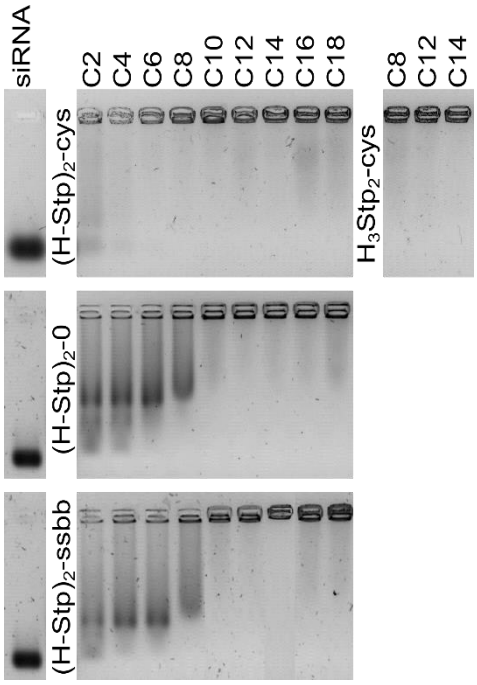

Figure 3.17. Standard agarose gel shift assay of siRNA polyplexes (N/P = 12, HBG) of the histidine library. The experiment was performed by Dr. Yanfang Wang (Pharmaceutical Biotechnology, LMU Munich).

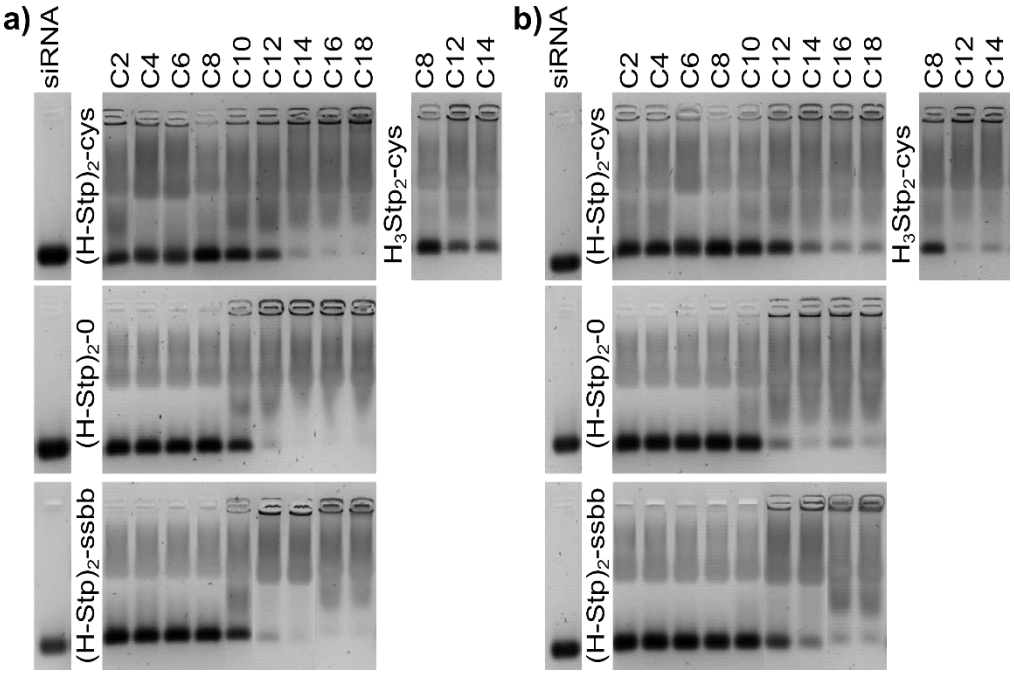

Figure 3.18. Serum agarose gel shift assay of siRNA polyplexes (N/P = 12, HBG) of the histidine library after (**a**) 4 h, and (**b**) 24 h incubation in 90% (v/v) serum (FBS) at 37 °C. The experiments were performed by Dr. Yanfang Wang (Pharmaceutical Biotechnology, LMU Munich).

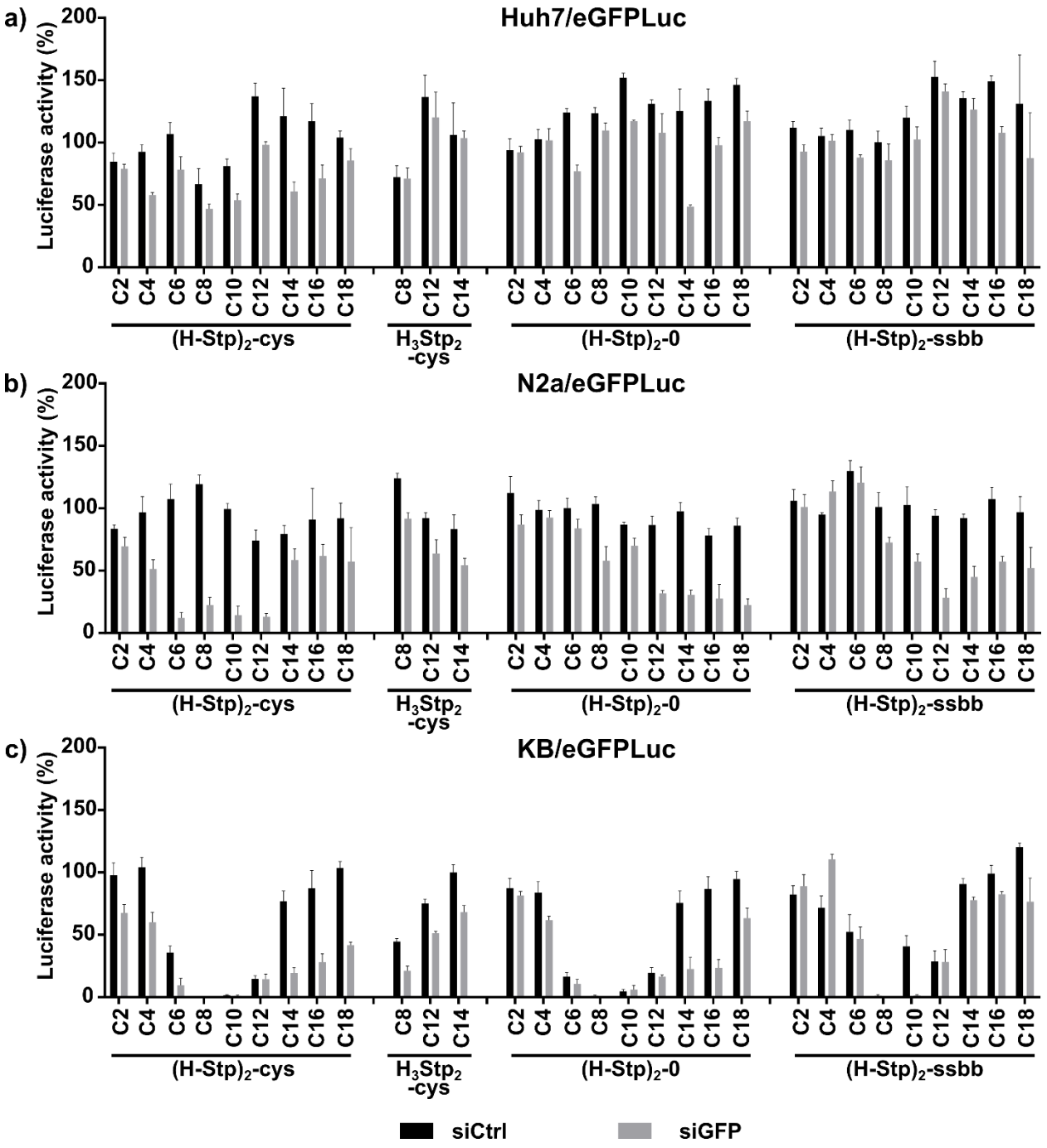

Figure 3.19. Gene silencing of siRNA polyplexes (N/P = 12, HBG) of the histidine library compared to HBG-treated cells, measured in a luciferase assay (mean + SD; *n* = 3) in three different cell lines. (**a**) Huh7/eGFPLuc cells, (**b**) N2a/eGFPLuc cells, and (**c**) KB/eGFPLuc cells. As siRNAs, eGFP-targeted siRNA (siGFP) and control siRNA (siCtrl) were used. Transfections were performed by Dr. Yanfang Wang (Pharmaceutical Biotechnology, LMU Munich).

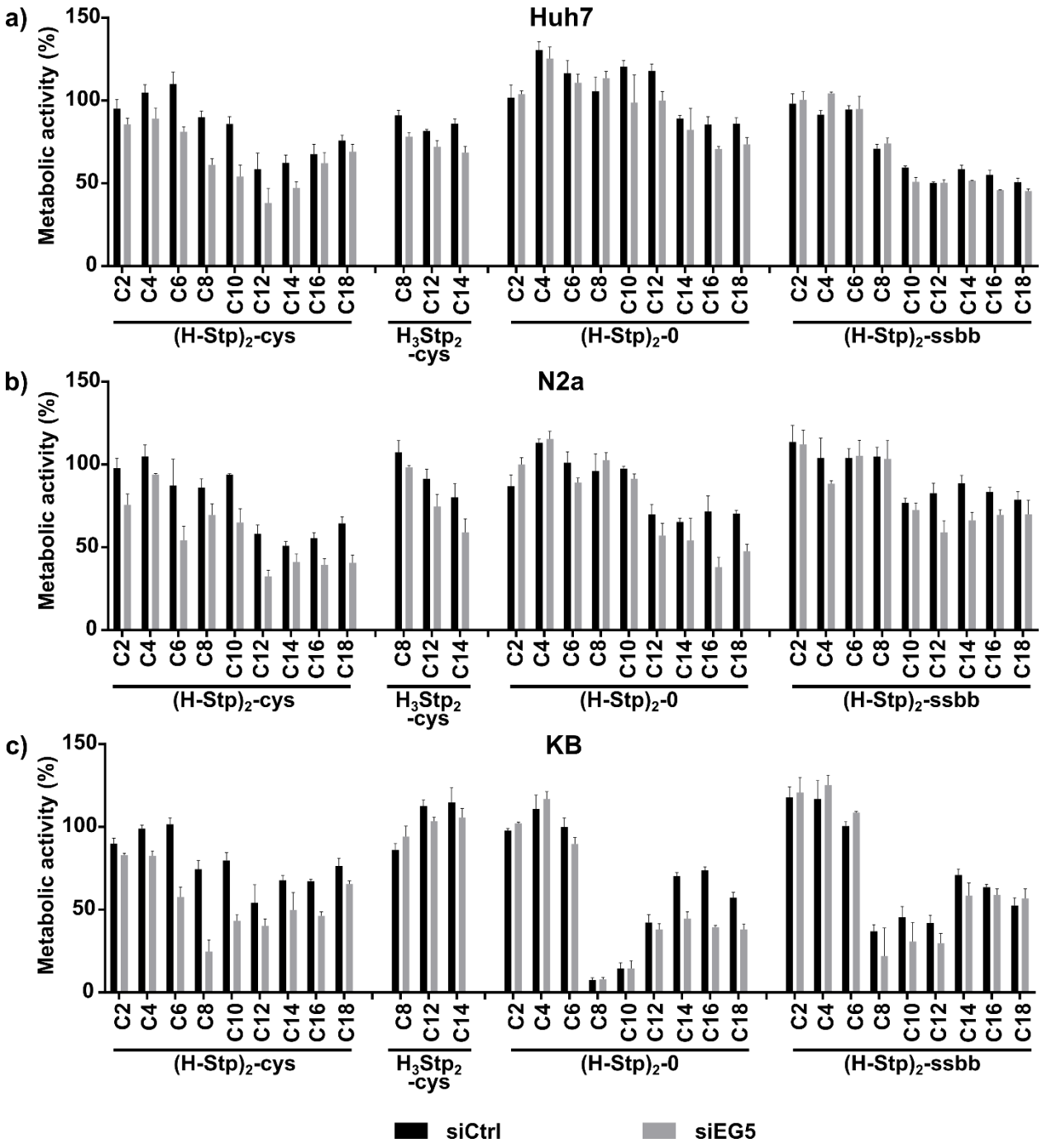

Figure 3.20. Metabolic activity compared to HBG-treated cells, determined by an MTT assay (mean + SD; *n* = 3) after incubation of three different cell lines with siRNA polyplexes (N/P = 12, HBG) of the histidine library. (**a**) Huh7 cells, (**b**) N2a cells, and (**c**) KB cells. Metabolic activities are presented as percentage relative to HBG buffer-treated control cells. As siRNAs, EG5-targeted siRNA (siEG5) and control siRNA (siCtrl) were used. Transfections were performed by Dr. Yanfang Wang (Pharmaceutical Biotechnology, LMU Munich).

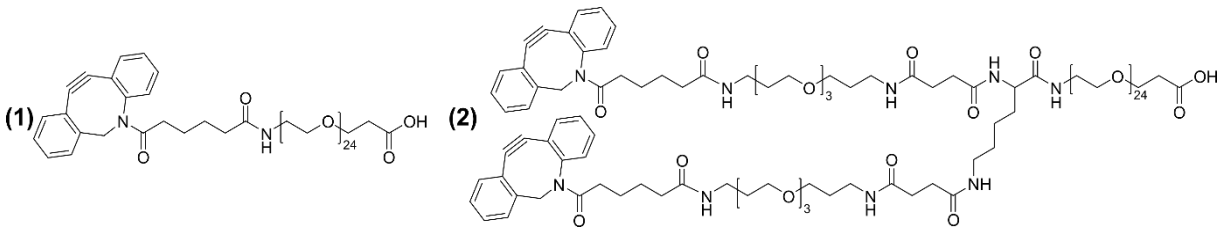

Figure 3.21. Chemical structures of the PEG shielding agents monoDBCO-PEG$_{24}$ (**1**) and bisDBCO-PEG$_{24}$ (**2**). Synthesis was done by Teoman Benli-Hoppe (Pharmaceutical Biotechnology, LMU Munich).

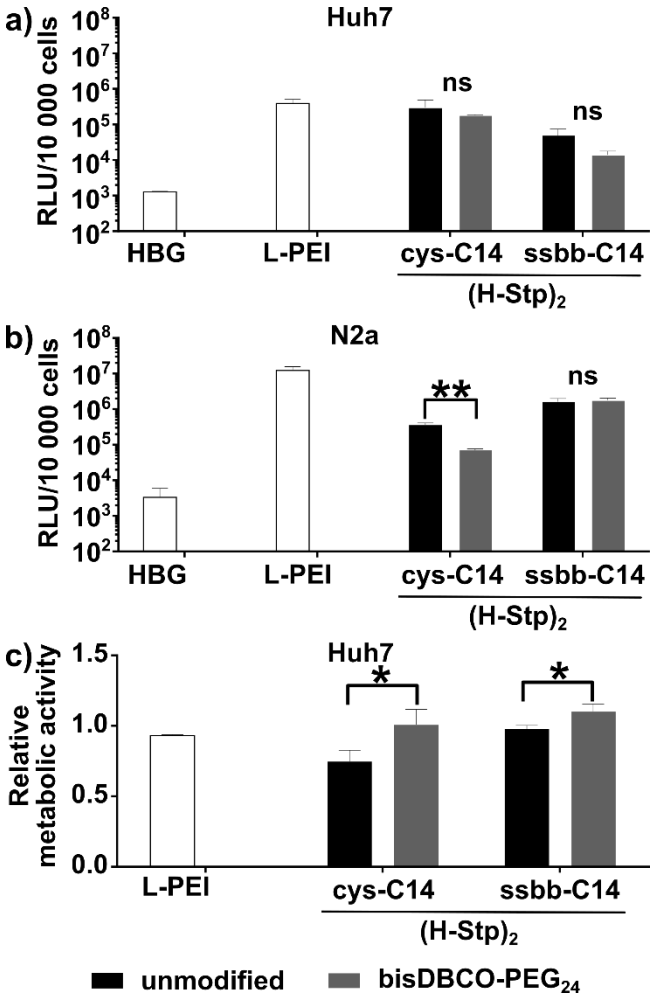

Figure 3.22. Transfection activity of selected pCMVLuc polyplexes of the (H-Stp)$_2$-library (N/P = 12, HBG), unmodified or post-functionalized with 0.25 equiv of DBCO agent. Luciferase gene expression was determined 24 h after transfection of Huh7 cells (**a**), and N2a cells (**b**) (mean + SD; *n* = 3). The CellTiter-Glo assay was performed 24 h after transfection of Huh7 cells (**c**) (mean + SD; *n* = 3). Metabolic activities, determined *via* CellTiter-Glo, are presented relative to HBG buffer-treated control cells. L-PEI pDNA polyplexes (N/P 6, HBG) served as positive control.

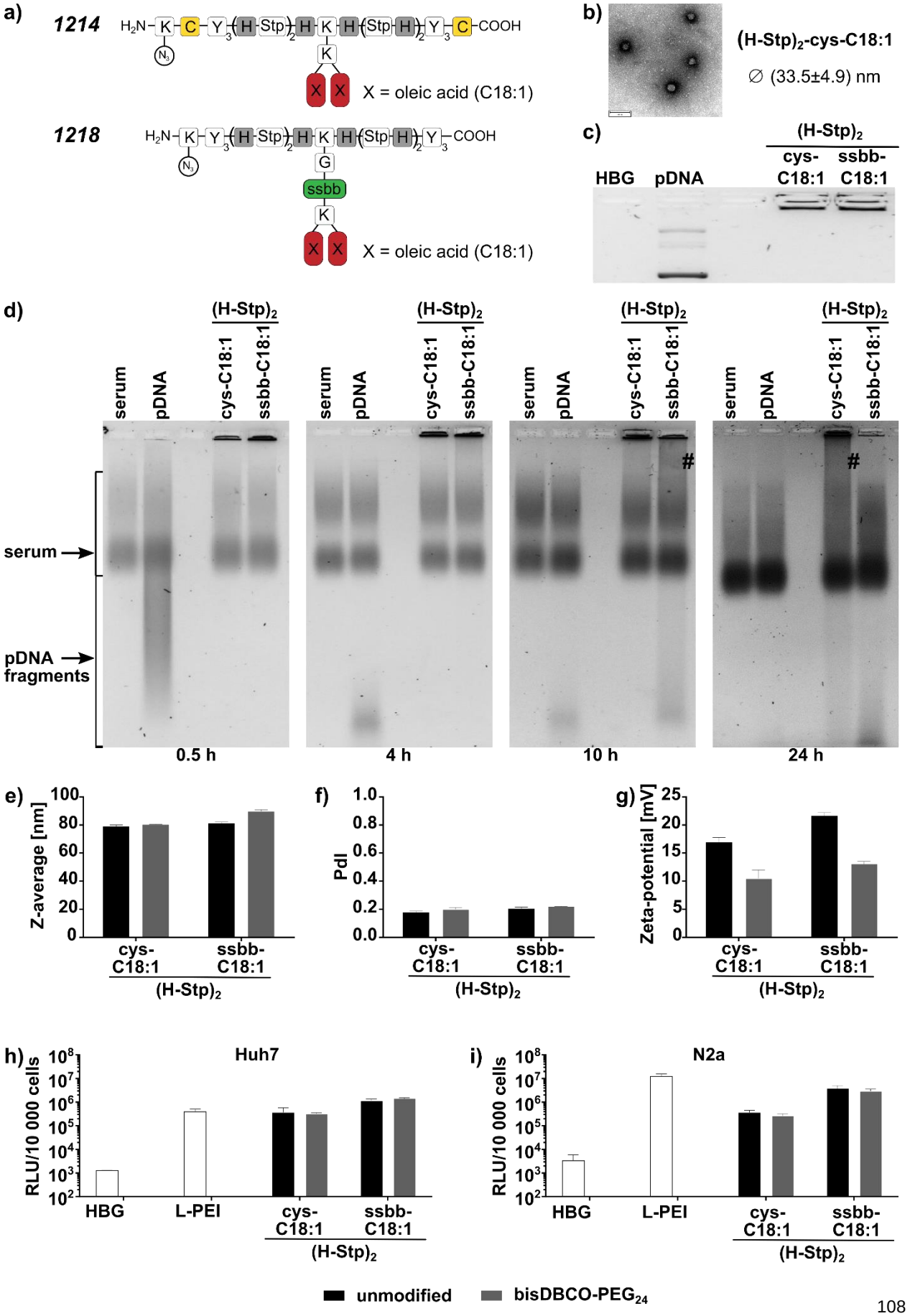
a)
1214
1218
X = oleic acid (C18:1)
X = oleic acid (C18:1)
b)
(H-Stp)2-cys-C18:1
∅ (33.5±4.9) nm
c)
(H-Stp)2
HBG
pDNA
cys-C18:1
ssbb-C18:1
d)
serum
pDNA
cys-C18:1
ssbb-C18:1
(H-Stp)2
serum
pDNA fragments
0.5 h
4 h
10 h
24 h
e)
Z-average [nm]
f)
PdI
g)
Zeta-potential [mV]
h)
Huh7
RLU/10 000 cells
HBG
L-PEI
i)
N2a
unmodified
bisDBCO-PEG24

Figure 3.23. Characterization of pDNA polyplexes formed with $(H\text{-}Stp)_2$-structures containing unsaturated fatty acid oleic acid (C18:1). (**a**) Structures of the two oleic acid T-Shape OAAs. $K(N_3)$: azido-lysine; K: lysine; C: cysteine; Y: tyrosine; H: histidine; G: glycine; Stp: succinoyl tetraethylene pentamine; ssbb: cystamine disulfide building block; X: residue = oleic acid. (**b**) Representative TEM image of pDNA lipo-polyplexes (N/P = 12, H_2O) formed with $(H\text{-}Stp)_2$-cys-C18:1. Scale bar = 100 nm. Average nanoparticle size is presented as diameter in nm (mean ± SD; *n* = 44). Standard agarose gel shift assay (**c**) and serum agarose gel shift assay (**d**) of corresponding unmodified pDNA lipo-polyplexes (N/P = 12, HBG). In case of the latter assay, polyplexes were incubated for 0.5, 4, 10, and 24 h in 90% (v/v) serum (FBS) at 37 °C prior to electrophoresis. Arrows label the bands caused by serum and degraded free pDNA. When pDNA is released from the polyplex, it gets degraded by serum enzymes (DNases, RNases), resulting in tailed lanes labeled with #. (**e**–**g**) DLS and ELS data of corresponding pDNA polyplexes (N/P = 12, HBG), unmodified and post-functionalized with 0.25 equiv of bisDBCO-PEG_{24} (mean + SD; *n* = 3). Gene-transfer efficiency of pCMVLuc polyplexes (N/P = 12, HBG), unmodified and post-functionalized with 0.25 equiv of bisDBCO-PEG_{24}, in Huh7 cells (**h**) and N2a cells (**i**), determined by a luciferase gene expression assay 24 h after transfection (mean + SD; *n* = 3). L-PEI pDNA polyplexes (N/P = 6, HBG) served as positive control. TEM measurements were performed by Susanne Kempter (Physics, LMU Munich) and analyzed by Özgür Öztürk (Pharmaceutical Biotechnology, LMU Munich).

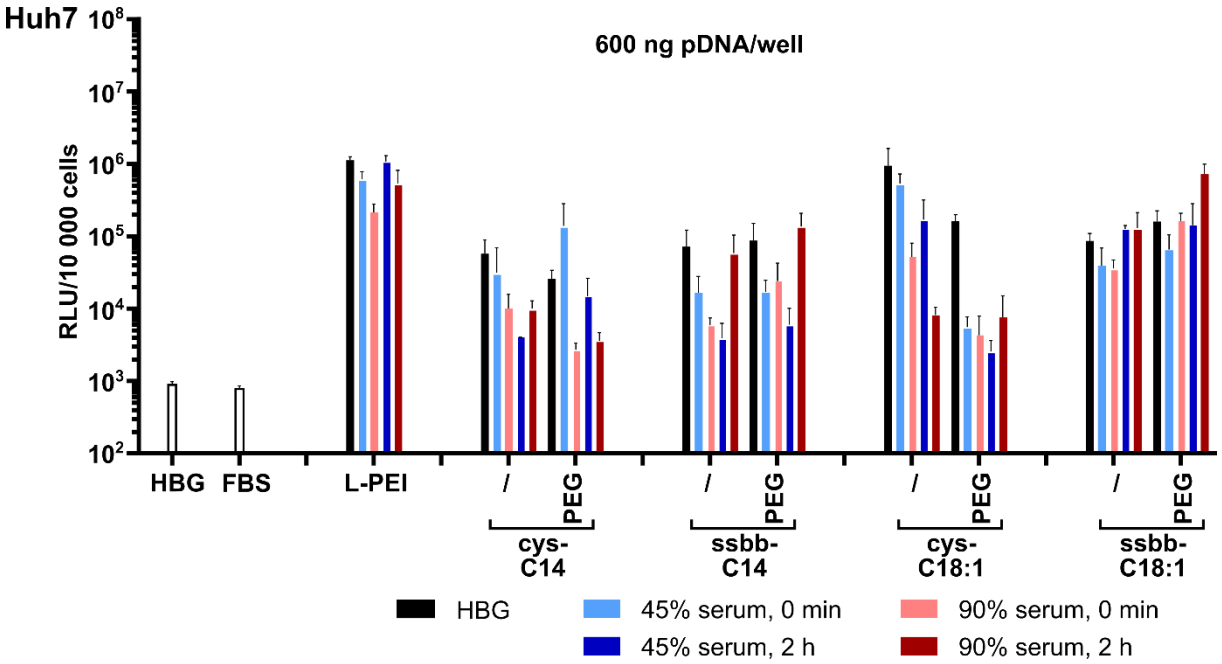

Figure 3.24. Gene-transfer performance in Huh7 cells in the presence of serum (FBS). Unmodified (/) and PEGylated (PEG; 0.25 equiv of bisDBCO-PEG_{24}) pCMVLuc polyplexes (N/P = 12, HBG; 600 ng pCMVLuc per well) formed with $(H\text{-}Stp)_2$-OAAs as well as L-PEI pDNA polyplexes (N/P = 6, HBG) were incubated in 45% (v/v) FBS, 90% (v/v) FBS, or HBG, respectively, for 0 min or 2 h at 37 °C (FBS) or RT (HBG) prior to transfection. The luciferase gene expression assay was performed 24 h after transfection (mean + SD; *n* = 3).

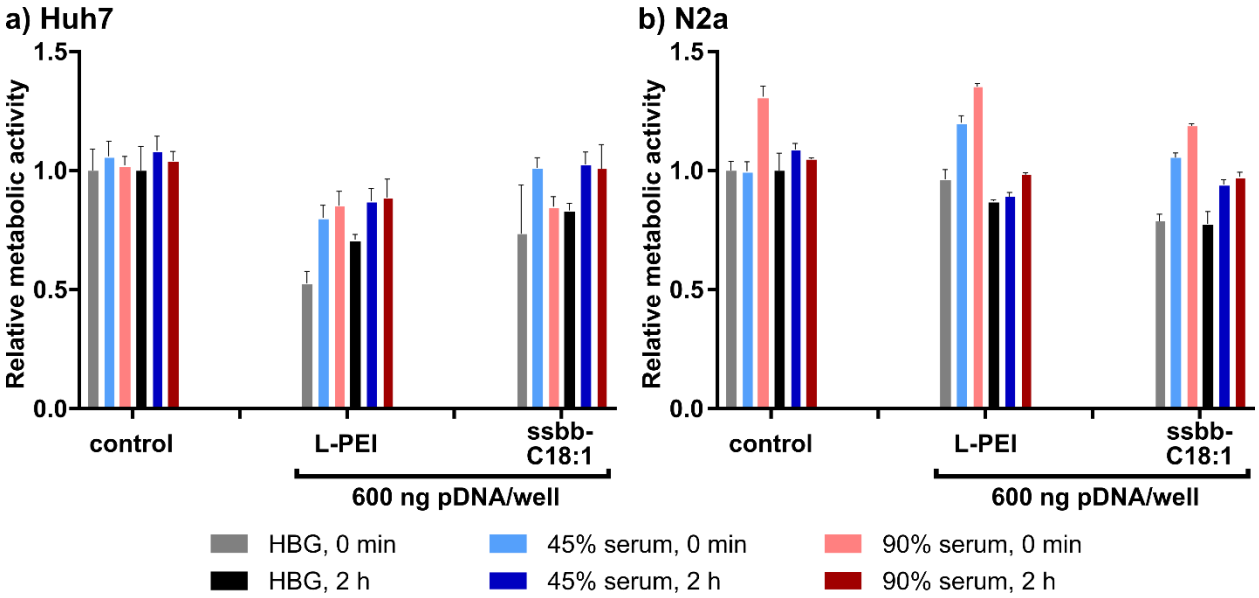

Figure 3.25. Cell viability of Huh7 cells (**a**) and N2a cells (**b**) after transfection with serum (FBS) incubated pCMVLuc polyplexes formed with $(H\text{-}Stp)_2$-ssbb-C18:1 (N/P = 12, HBG) or L-PEI (N/P = 6, HBG), respectively, containing 600 ng pDNA/well. Polyplexes were incubated in 45% (v/v) FBS, 90% (v/v) FBS or HBG, respectively, for 0 min or 2 h at 37°C (serum) or RT (HBG) prior to transfection. The CellTiter-Glo assay was performed 24 h after transfection (mean + SD; *n* = 3). The determined metabolic activities are presented relative to HBG buffer-treated control cells**.**

3.5.4 Supporting tables

Table 3.1. Structures plus abbreviation and compound ID numbers of the histidine library.

Abbreviation	Compound ID	Structure (N → C)
(H-Stp)$_2$-cys-C2	*1272*	K(N_3)-C-Y_3-(H-Stp)$_2$-H-K(K(AcA)$_2$)-H-(Stp-H)$_2$-Y_3-C
(H-Stp)$_2$-cys-C4	*1273*	K(N_3)-C-Y_3-(H-Stp)$_2$-H-K(K(ButA)$_2$)-H-(Stp-H)$_2$-Y_3-C
(H-Stp)$_2$-cys-C6	*1275*	K(N_3)-C-Y_3-(H-Stp)$_2$-H-K(K(HexA)$_2$)-H-(Stp-H)$_2$-Y_3-C
(H-Stp)$_2$-cys-C8	*1252*	K(N_3)-C-Y_3-(H-Stp)$_2$-H-K(K(OctA)$_2$)-H-(Stp-H)$_2$-Y_3-C
(H-Stp)$_2$-cys-C10	*1276*	K(N_3)-C-Y_3-(H-Stp)$_2$-H-K(K(DecA)$_2$)-H-(Stp-H)$_2$-Y_3-C
(H-Stp)$_2$-cys-C12	*1254*	K(N_3)-C-Y_3-(H-Stp)$_2$-H-K(K(LauA)$_2$)-H-(Stp-H)$_2$-Y_3-C
(H-Stp)$_2$-cys-C14	*1256*	K(N_3)-C-Y_3-(H-Stp)$_2$-H-K(K(MyrA)$_2$)-H-(Stp-H)$_2$-Y_3-C
(H-Stp)$_2$-cys-C16	*1277*	K(N_3)-C-Y_3-(H-Stp)$_2$-H-K(K(PalA)$_2$)-H-(Stp-H)$_2$-Y_3-C
(H-Stp)$_2$-cys-C18	*1278*	K(N_3)-C-Y_3-(H-Stp)$_2$-H-K(K(SteA)$_2$)-H-(Stp-H)$_2$-Y_3-C
(H-Stp)$_2$-cys-C18:1	*1214*	K(N_3)-C-Y_3-(H-Stp)$_2$-H-K(K(OleA)$_2$)-H-(Stp-H)$_2$-Y_3-C
H_3Stp$_2$-cys-C8	*1253*	K(N_3)-C-Y_3-H_3-Stp$_2$-K(K(OctA)$_2$)-Stp$_2$-H_3-Y_3-C
H_3Stp$_2$-cys-C12	*1255*	K(N_3)-C-Y_3-H_3-Stp$_2$-K(K(LauA)$_2$)-Stp$_2$-H_3-Y_3-C
H_3Stp$_2$-cys-C14	*1257*	K(N_3)-C-Y_3-H_3-Stp$_2$-K(K(MyrA)$_2$)-Stp$_2$-H_3-Y_3-C
(H-Stp)$_2$-0-C2	*1313*	K(N_3)-Y_3-(H-Stp)$_2$-H-K(K(AcA)$_2$)-H-(Stp-H)$_2$-Y_3
(H-Stp)$_2$-0-C4	*1314*	K(N_3)-Y_3-(H-Stp)$_2$-H-K(K(ButA)$_2$)-H-(Stp-H)$_2$-Y_3
(H-Stp)$_2$-0-C6	*1315*	K(N_3)-Y_3-(H-Stp)$_2$-H-K(K(HexA)$_2$)-H-(Stp-H)$_2$-Y_3
(H-Stp)$_2$-0-C8	*1316*	K(N_3)-Y_3-(H-Stp)$_2$-H-K(K(OctA)$_2$)-H-(Stp-H)$_2$-Y_3
(H-Stp)$_2$-0-C10	*1317*	K(N_3)-Y_3-(H-Stp)$_2$-H-K(K(DecA)$_2$)-H-(Stp-H)$_2$-Y_3
(H-Stp)$_2$-0-C12	*1318*	K(N_3)-Y_3-(H-Stp)$_2$-H-K(K(LauA)$_2$)-H-(Stp-H)$_2$-Y_3
(H-Stp)$_2$-0-C14	*1319*	K(N_3)-Y_3-(H-Stp)$_2$-H-K(K(MyrA)$_2$)-H-(Stp-H)$_2$-Y_3
(H-Stp)$_2$-0-C16	*1320*	K(N_3)-Y_3-(H-Stp)$_2$-H-K(K(PalA)$_2$)-H-(Stp-H)$_2$-Y_3
(H-Stp)$_2$-0-C18	*1321*	K(N_3)-Y_3-(H-Stp)$_2$-H-K(K(SteA)$_2$)-H-(Stp-H)$_2$-Y_3
(H-Stp)$_2$-ssbb-C2	*1279*	K(N_3)-Y_3-(H-Stp)$_2$-H-K(G-ssbb-K(AcA)$_2$)-H-(Stp-H)$_2$-Y_3
(H-Stp)$_2$-ssbb-C4	*1280*	K(N_3)-Y_3-(H-Stp)$_2$-H-K(G-ssbb-K(ButA)$_2$)-H-(Stp-H)$_2$-Y_3
(H-Stp)$_2$-ssbb-C6	*1281*	K(N_3)-Y_3-(H-Stp)$_2$-H-K(G-ssbb-K(HexA)$_2$)-H-(Stp-H)$_2$-Y_3
(H-Stp)$_2$-ssbb-C8	*1282*	K(N_3)-Y_3-(H-Stp)$_2$-H-K(G-ssbb-K(OctA)$_2$)-H-(Stp-H)$_2$-Y_3
(H-Stp)$_2$-ssbb-C10	*1284*	K(N_3)-Y_3-(H-Stp)$_2$-H-K(G-ssbb-K(DecA)$_2$)-H-(Stp-H)$_2$-Y_3
(H-Stp)$_2$-ssbb-C12	*1303*	K(N_3)-Y_3-(H-Stp)$_2$-H-K(G-ssbb-K(LauA)$_2$)-H-(Stp-H)$_2$-Y_3
(H-Stp)$_2$-ssbb-C14	*1304*	K(N_3)-Y_3-(H-Stp)$_2$-H-K(G-ssbb-K(MyrA)$_2$)-H-(Stp-H)$_2$-Y_3
(H-Stp)$_2$-ssbb-C16	*1305*	K(N_3)-Y_3-(H-Stp)$_2$-H-K(G-ssbb-K(PalA)$_2$)-H-(Stp-H)$_2$-Y_3
(H-Stp)$_2$-ssbb-C18	*1306*	K(N_3)-Y_3-(H-Stp)$_2$-H-K(G-ssbb-K(SteA)$_2$)-H-(Stp-H)$_2$-Y_3
(H-Stp)$_2$-ssbb-C18:1	*1218*	K(N_3)-Y_3-(H-Stp)$_2$-H-K(G-ssbb-K(OleA)$_2$)-H-(Stp-H)$_2$-Y_3

K(N_3): azido-lysine; K: lysine; C: cysteine; Y: tyrosine; H: histidine; G:glycine; Stp: succinoyl tetraethylene pentamine; ssbb: cystamine disulfide building block; AcA: Acetic acid (C2); ButA: Butanoic acid (C4); HexA: Hexanoic acid (C6); OctA: Octanoic acid (C8); DecA: Decanoic acid (C10); LauA: Lauric acid (C12); MyrA: Myristic acid (C14); PalA: Palmitic acid (C16); SteA: Stearic acid (C18); OleA: Oleic acid (C18:1).

Table 3.2. Structures plus abbreviation and compound ID numbers of the histidine-free library.

Abbreviation	Compound ID	Structure (N → C)
Stp_2-cys-C2	*1329*	$K(N_3)$-C-Y_3-Stp_2-K(K(AcA)$_2$)-Stp_2-Y_3-C
Stp_2-cys-C4	*1330*	$K(N_3)$-C-Y_3-Stp_2-K(K(ButA)$_2$)-Stp_2-Y_3-C
Stp_2-cys-C6	*1331*	$K(N_3)$-C-Y_3-Stp_2-K(K(HexA)$_2$)-Stp_2-Y_3-C
Stp_2-cys-C8	*1332*	$K(N_3)$-C-Y_3-Stp_2-K(K(OctA)$_2$)-Stp_2-Y_3-C
Stp_2-cys-C10	*1333*	$K(N_3)$-C-Y_3-Stp_2-K(K(DecA)$_2$)-Stp_2-Y_3-C
Stp_2-cys-C12	*1334*	$K(N_3)$-C-Y_3-Stp_2-K(K(LauA)$_2$)-Stp_2-Y_3-C
Stp_2-cys-C14	*1335*	$K(N_3)$-C-Y_3-Stp_2-K(K(MyrA)$_2$)-Stp_2-Y_3-C
Stp_2-cys-C16	*1336*	$K(N_3)$-C-Y_3-Stp_2-K(K(PalA)$_2$)-Stp_2-Y_3-C
Stp_2-cys-C18	*1337*	$K(N_3)$-C-Y_3-Stp_2-K(K(SteA)$_2$)-Stp_2-Y_3-C
Stp_2-0-C2	*1353*	$K(N_3)$-Y_3-Stp_2-K(K(AcA)$_2$)-Stp_2-Y_3
Stp_2-0-C4	*1354*	$K(N_3)$-Y_3-Stp_2-K(K(ButA)$_2$)-Stp_2-Y_3
Stp_2-0-C6	*1355*	$K(N_3)$-Y_3-Stp_2-K(K(HexA)$_2$)-Stp_2-Y_3
Stp_2-0-C8	*1356*	$K(N_3)$-Y_3-Stp_2-K(K(OctA)$_2$)-Stp_2-Y_3
Stp_2-0-C10	*1357*	$K(N_3)$-Y_3-Stp_2-K(K(DecA)$_2$)-Stp_2-Y_3
Stp_2-0-C12	*1358*	$K(N_3)$-Y_3-Stp_2-K(K(LauA)$_2$)-Stp_2-Y_3
Stp_2-0-C14	*1359*	$K(N_3)$-Y_3-Stp_2-K(K(MyrA)$_2$)-Stp_2-Y_3
Stp_2-0-C16	*1360*	$K(N_3)$-Y_3-Stp_2-K(K(PalA)$_2$)-Stp_2-Y_3
Stp_2-0-C18	*1361*	$K(N_3)$-Y_3-Stp_2-K(K(SteA)$_2$)-Stp_2-Y_3
Stp_2-ssbb-C2	*1341*	$K(N_3)$-Y_3-Stp_2-K(G-ssbb-K(AcA)$_2$)-Stp_2-Y_3
Stp_2-ssbb-C4	*1342*	$K(N_3)$-Y_3-Stp_2-K(G-ssbb-K(ButA)$_2$)-Stp_2-Y_3
Stp_2-ssbb-C6	*1343*	$K(N_3)$-Y_3-Stp_2-K(G-ssbb-K(HexA)$_2$)-Stp_2-Y_3
Stp_2-ssbb-C8	*1344*	$K(N_3)$-Y_3-Stp_2-K(G-ssbb-K(OctA)$_2$)-Stp_2-Y_3
Stp_2-ssbb-C10	*1345*	$K(N_3)$-Y_3-Stp_2-K(G-ssbb-K(DecA)$_2$)-Stp_2-Y_3
Stp_2-ssbb-C12	*1346*	$K(N_3)$-Y_3-Stp_2-K(G-ssbb-K(LauA)$_2$)-Stp_2-Y_3
Stp_2-ssbb-C14	*1347*	$K(N_3)$-Y_3-Stp_2-K(G-ssbb-K(MyrA)$_2$)-Stp_2-Y_3
Stp_2-ssbb-C16	*1348*	$K(N_3)$-Y_3-Stp_2-K(G-ssbb-K(PalA)$_2$)-Stp_2-Y_3
Stp_2-ssbb-C18	*1349*	$K(N_3)$-Y_3-Stp_2-K(G-ssbb-K(SteA)$_2$)-Stp_2-Y_3

$K(N_3)$: azido-lysine; K: lysine; C: cysteine; Y: tyrosine; G: glycine; Stp: succinoyl tetraethylene pentamine; ssbb: cystamine disulfide building block; AcA: Acetic acid (C2); ButA: Butanoic acid (C4); HexA: Hexanoic acid (C6); OctA: Octanoic acid (C8); DecA: Decanoic acid (C10); LauA: Lauric acid (C12); MyrA: Myristic acid (C14); PalA: Palmitic acid (C16); SteA: Stearic acid (C18).

Table 3.3. Structures plus abbreviation and compound ID numbers of the oligo-cysteine library.

Abbreviation	Compound ID	Structure (N → C)
C_3Y_3-C4	*1418*	$K(N_3)$-C_3-Y_3-(H-Stp)$_2$-H-K(K(ButA)$_2$)-H-(Stp-H)$_2$-Y_3-C_3
C_3Y_3-C8	*1419*	$K(N_3)$-C_3-Y_3-(H-Stp)$_2$-H-K(K(OctA)$_2$)-H-(Stp-H)$_2$-Y_3-C_3
C_3Y_3-C10	*1420*	$K(N_3)$-C_3-Y_3-(H-Stp)$_2$-H-K(K(DecA)$_2$)-H-(Stp-H)$_2$-Y_3-C_3
C_3Y_3-C14	*1421*	$K(N_3)$-C_3-Y_3-(H-Stp)$_2$-H-K(K(MyrA)$_2$)-H-(Stp-H)$_2$-Y_3-C_3
C_3Y_3-C18	*1422*	$K(N_3)$-C_3-Y_3-(H-Stp)$_2$-H-K(K(SteA)$_2$)-H-(Stp-H)$_2$-Y_3-C_3
C_3Y_3-C18:1	*1423*	$K(N_3)$-C_3-Y_3-(H-Stp)$_2$-H-K(K(OleA)$_2$)-H-(Stp-H)$_2$-Y_3-C_3
Y_3C_3-C4	*1424*	$K(N_3)$-Y_3-C_3-(H-Stp)$_2$-H-K(K(ButA)$_2$)-H-(Stp-H)$_2$-C_3-Y_3
Y_3C_3-C8	*1425*	$K(N_3)$-Y_3-C_3-(H-Stp)$_2$-H-K(K(OctA)$_2$)-H-(Stp-H)$_2$-C_3-Y_3
Y_3C_3-C10	*1426*	$K(N_3)$-Y_3-C_3-(H-Stp)$_2$-H-K(K(DecA)$_2$)-H-(Stp-H)$_2$-C_3-Y_3
Y_3C_3-C14	*1427*	$K(N_3)$-Y_3-C_3-(H-Stp)$_2$-H-K(K(MyrA)$_2$)-H-(Stp-H)$_2$-C_3-Y_3
Y_3C_3-C18	*1428*	$K(N_3)$-Y_3-C_3-(H-Stp)$_2$-H-K(K(SteA)$_2$)-H-(Stp-H)$_2$-C_3-Y_3
Y_3C_3-C18:1	*1429*	$K(N_3)$-Y_3-C_3-(H-Stp)$_2$-H-K(K(OleA)$_2$)-H-(Stp-H)$_2$-C_3-Y_3
(Y-C)$_3$-C4	*1430*	$K(N_3)$-(Y-C)$_3$-(H-Stp)$_2$-H-K(K(ButA)$_2$)-H-(Stp-H)$_2$-(C-Y)$_3$
(Y-C)$_3$-C8	*1431*	$K(N_3)$-(Y-C)$_3$-(H-Stp)$_2$-H-K(K(OctA)$_2$)-H-(Stp-H)$_2$-(C-Y)$_3$
(Y-C)$_3$-C10	*1432*	$K(N_3)$-(Y-C)$_3$-(H-Stp)$_2$-H-K(K(DecA)$_2$)-H-(Stp-H)$_2$-(C-Y)$_3$
(Y-C)$_3$-C14	*1433*	$K(N_3)$-(Y-C)$_3$-(H-Stp)$_2$-H-K(K(MyrA)$_2$)-H-(Stp-H)$_2$-(C-Y)$_3$
(Y-C)$_3$-C18	*1434*	$K(N_3)$-(Y-C)$_3$-(H-Stp)$_2$-H-K(K(SteA)$_2$)-H-(Stp-H)$_2$-(C-Y)$_3$
(Y-C)$_3$-C18:1	*1435*	$K(N_3)$-(Y-C)$_3$-(H-Stp)$_2$-H-K(K(OleA)$_2$)-H-(Stp-H)$_2$-(C-Y)$_3$
(C-Y)$_3$-C4	*1436*	$K(N_3)$-(C-Y)$_3$-(H-Stp)$_2$-H-K(K(ButA)$_2$)-H-(Stp-H)$_2$-(Y-C)$_3$
(C-Y)$_3$-C8	*1437*	$K(N_3)$-(C-Y)$_3$-(H-Stp)$_2$-H-K(K(OctA)$_2$)-H-(Stp-H)$_2$-(Y-C)$_3$
(C-Y)$_3$-C10	*1438*	$K(N_3)$-(C-Y)$_3$-(H-Stp)$_2$-H-K(K(DecA)$_2$)-H-(Stp-H)$_2$-(Y-C)$_3$
(C-Y)$_3$-C14	*1439*	$K(N_3)$-(C-Y)$_3$-(H-Stp)$_2$-H-K(K(MyrA)$_2$)-H-(Stp-H)$_2$-(Y-C)$_3$
(C-Y)$_3$-C18	*1440*	$K(N_3)$-(C-Y)$_3$-(H-Stp)$_2$-H-K(K(SteA)$_2$)-H-(Stp-H)$_2$-(Y-C)$_3$
(C-Y)$_3$-C18:1	*1441*	$K(N_3)$-(C-Y)$_3$-(H-Stp)$_2$-H-K(K(OleA)$_2$)-H-(Stp-H)$_2$-(Y-C)$_3$

$K(N_3)$: azido-lysine; K: lysine; C: cysteine; Y: tyrosine; H: histidine; Stp: succinoyl tetraethylene pentamine; ButA: Butanoic acid (C4); OctA: Octanoic acid (C8); DecA: Decanoic acid (C10); MyrA: Myristic acid (C14); SteA: Stearic acid (C18); OleA: Oleic acid (C18:1).

Table 3.4. Calculated and found masses (*via* MALDI-TOF MS) in Dalton [Da] of structures of the histidine library.

Abbreviation	Compound ID	Calculated mass [Da]	Found mass [Da]
(H-Stp)$_2$-cys-C2	*1272*	3603.86	3602.44
(H-Stp)$_2$-cys-C4	*1273*	3659.92	3656.96
(H-Stp)$_2$-cys-C6	*1275*	3715.99	3711.06
(H-Stp)$_2$-cys-C8	*1252*	3772.05	3767.06
(H-Stp)$_2$-cys-C10	*1276*	3828.11	3821.72
(H-Stp)$_2$-cys-C12	*1254*	3884.18	3879.36
(H-Stp)$_2$-cys-C14	*1256*	3940.24	3932.50
(H-Stp)$_2$-cys-C16	*1277*	3996.30	3990.11
(H-Stp)$_2$-cys-C18	*1278*	4052.36	4049.22
(H-Stp)$_2$-cys-C18:1	*1214*	4051.02	4050.10
H$_3$Stp$_2$-cys-C8	*1253*	3772.05	3767.80
H$_3$Stp$_2$-cys-C12	*1255*	3884.18	3879.38
H$_3$Stp$_2$-cys-C14	*1257*	3940.24	3936.58
(H-Stp)$_2$-0-C2	*1313*	3399.92	3397.57
(H-Stp)$_2$-0-C4	*1314*	3456.02	3453.59
(H-Stp)$_2$-0-C6	*1315*	3512.13	3509.55
(H-Stp)$_2$-0-C8	*1316*	3568.23	3568.53
(H-Stp)$_2$-0-C10	*1317*	3624.34	3616.09
(H-Stp)$_2$-0-C12	*1318*	3680.45	3678.95
(H-Stp)$_2$-0-C14	*1319*	3736.55	3731.22
(H-Stp)$_2$-0-C16	*1320*	3792.66	3789.96
(H-Stp)$_2$-0-C18	*1321*	3848.77	3846.06
(H-Stp)$_2$-ssbb-C2	*1279*	3684.31	3684.09
(H-Stp)$_2$-ssbb-C4	*1280*	3740.42	3740.04
(H-Stp)$_2$-ssbb-C6	*1281*	3796.53	3796.23
(H-Stp)$_2$-ssbb-C8	*1282*	3852.64	3851.75
(H-Stp)$_2$-ssbb-C10	*1284*	3908.74	3910.37
(H-Stp)$_2$-ssbb-C12	*1303*	3971.84	3970.17
(H-Stp)$_2$-ssbb-C14	*1304*	4027.94	4020.91
(H-Stp)$_2$-ssbb-C16	*1305*	4084.05	4083.15
(H-Stp)$_2$-ssbb-C18	*1306*	4140.16	4136.72
(H-Stp)$_2$-ssbb-C18:1	*1218*	4136.20	4135.00

Table 3.5. Calculated and found masses (*via* MALDI-TOF MS) in Dalton [Da] of structures of the histidine-free library.

Abbreviation	Compound ID	Calculated mass [Da]	Found mass [Da]
Stp_2-cys-C2	*1329*	2781.51	2778.75
Stp_2-cys-C4	*1330*	2837.57	2836.65
Stp_2-cys-C6	*1331*	2893.63	2891.66
Stp_2-cys-C8	*1332*	2949.70	2949.06
Stp_2-cys-C10	*1333*	3005.76	3004.02
Stp_2-cys-C12	*1334*	3061.82	3062.71
Stp_2-cys-C14	*1335*	3117.88	3117.57
Stp_2-cys-C16	*1336*	3173.95	3172.34
Stp_2-cys-C18	*1337*	3230.01	3229.14
Stp_2-0-C2	*1353*	2575.49	2575.67
Stp_2-0-C4	*1354*	2631.55	2632.13
Stp_2-0-C6	*1355*	2687.62	2686.54
Stp_2-0-C8	*1356*	2743.68	2743.84
Stp_2-0-C10	*1357*	2799.74	2797.06
Stp_2-0-C12	*1358*	2855.80	2854.33
Stp_2-0-C14	*1359*	2911.87	2910.52
Stp_2-0-C16	*1360*	2967.93	2968.75
Stp_2-0-C18	*1361*	3023.99	3023.43
Stp_2-ssbb-C2	*1341*	2866.56	2864.73
Stp_2-ssbb-C4	*1342*	2922.62	2919.16
Stp_2-ssbb-C6	*1343*	2978.69	2975.09
Stp_2-ssbb-C8	*1344*	3034.75	3030.97
Stp_2-ssbb-C10	*1345*	3090.81	3089.03
Stp_2-ssbb-C12	*1346*	3146.87	3143.17
Stp_2-ssbb-C14	*1347*	3202.94	3201.07
Stp_2-ssbb-C16	*1348*	3259.00	3256.56
Stp_2-ssbb-C18	*1349*	3315.06	3311.36

Table 3.6. Calculated and found masses (*via* MALDI-TOF MS) in Dalton [Da] of structures of the oligo-cysteine library.

Abbreviation	Compound ID	Calculated mass [Da]	Found mass [Da]
C_3Y_3-C4	*1418*	4071.96	4069.56
C_3Y_3-C8	*1419*	4184.09	4180.99
C_3Y_3-C10	*1420*	4240.15	4234.04
C_3Y_3-C14	*1421*	4352.27	4350.72
C_3Y_3-C18	*1422*	4464.40	4458.26
C_3Y_3-C18:1	*1423*	4460.37	4452.32
Y_3C_3-C4	*1424*	4071.96	4067.17
Y_3C_3-C8	*1425*	4184.09	4179.55
Y_3C_3-C10	*1426*	4240.15	4238.15
Y_3C_3-C14	*1427*	4352.27	4349.03
Y_3C_3-C18	*1428*	4464.40	4460.31
Y_3C_3-C18:1	*1429*	4460.37	4453.28
$(Y\text{-}C)_3$-C4	*1430*	4071.96	4067.28
$(Y\text{-}C)_3$-C8	*1431*	4184.09	4183.91
$(Y\text{-}C)_3$-C10	*1432*	4240.15	4237.15
$(Y\text{-}C)_3$-C14	*1433*	4352.27	4349.09
$(Y\text{-}C)_3$-C18	*1434*	4464.40	4458.89
$(Y\text{-}C)_3$-C18:1	*1435*	4460.37	4455.24
$(C\text{-}Y)_3$-C4	*1436*	4071.96	4065.04
$(C\text{-}Y)_3$-C8	*1437*	4184.09	4179.94
$(C\text{-}Y)_3$-C10	*1438*	4240.15	4237.04
$(C\text{-}Y)_3$-C14	*1439*	4352.27	4347.45
$(C\text{-}Y)_3$-C18	*1440*	4464.40	4459.91
$(C\text{-}Y)_3$-C18:1	*1441*	4460.37	4452.11

Table 3.7. DLS and ELS results of siRNA polyplexes formed at an N/P ratio of 12 in HBG (mean ± SD; *n* = 3).

siRNA polyplexes		Z-average diameter [nm]		PdI		Zeta-potential [mV]	
		mean	SD	mean	SD	mean	SD
$(H\text{-}Stp)_2$-cys	C2	152.3	2.7	0.105	0.020	17.2	1.0
	C4	166.3	1.8	0.186	0.013	23.6	0.5
	C6	178.6	0.9	0.206	0.014	28.0	1.5
	C8	160.2	2.7	0.198	0.010	31.4	0.9
	C10	168.2	3.0	0.245	0.013	29.2	1.6
	C12	160.7	2.7	0.179	0.018	31.9	2.3
	C14	176.2	6.3	0.299	0.051	29.6	1.2
	C16	245.0	15.6	0.352	0.031	27.8	1.6
	C18	250.7	13.7	0.405	0.027	25.6	1.8
H_3Stp_2-cys	C8	151.4	1.5	0.200	0.005	29.9	0.8
	C12	193.9	1.7	0.354	0.016	29.3	1.2
	C14	192.9	1.9	0.422	0.014	26.5	0.8
$(H\text{-}Stp)_2$-0	C2	234.8	7.9	0.133	0.023	6.8	0.3
	C4	238.5	4.6	0.111	0.028	6.3	0.4
	C6	197.4	1.8	0.047	0.049	7.7	0.9
	C8	149.7	2.0	0.126	0.033	12.9	0.1
	C10	165.9	1.3	0.168	0.022	32.4	1.2
	C12	148.3	2.0	0.149	0.009	34.1	1.1
	C14	160.9	0.2	0.165	0.027	32.9	1.1
	C16	154.6	0.6	0.158	0.022	31.4	0.6
	C18	174.6	1.5	0.156	0.017	32.8	2.1
$(H\text{-}Stp)_2$-ssbb	C2	224.5	8.0	0.080	0.044	6.9	0.2
	C4	187.1	4.1	0.082	0.018	9.3	0.4
	C6	191.3	3.5	0.047	0.013	8.4	1.2
	C8	147.2	1.8	0.108	0.032	16.1	2.1
	C10	149.8	0.5	0.152	0.012	32.6	0.9
	C12	156.1	1.0	0.161	0.008	33.7	1.1
	C14	166.9	1.2	0.192	0.011	30.5	1.7
	C16	151.2	2.0	0.153	0.023	28.9	0.6
	C18	152.4	2.5	0.157	0.011	28.6	1.0

Zetasizer measurements were performed by Dr. Yanfang Wang (Pharmaceutical Biotechnology, LMU Munich).

3.6 Abbreviations

DBCO, dibenzocyclooctyne; EtBr, ethidium bromide; L-PEI, linear polyethylenimine; OAA, oligoaminoamide; pDNA, plasmid DNA; PEG, polyethylene glycol; PdI, polydispersity index; siRNA, small-interfering RNA; SPAAC, strain-promoted alkyne-azide cycloaddition; SPPS, solid-phase assisted peptide synthesis; ssbb, cystamine disulfide building block; Stp, succinoyl tetraethylene pentamine.

3.7 Acknowledgements

We acknowledge the financial support by the German Research Foundation (DFG) SFB1032 (project-ID 201269156) sub-project B4, SFB824 sub-project C8, and DFG Excellence Cluster ‘Nanosystems Initiative Munich (NIM)’. Moreover, we thank Susanne Kempter (Physics, LMU Munich) for TEM measurements and helpful discussion of the results.

4. Performance of nanoparticles for biomedical applications: the *in vitro* / *in vivo* discrepancy

Simone Berger[a,], Martin Berger[b], Christoph Bantz[c], Michael Maskos[b,c], and Ernst Wagner[a]*

[a] Pharmaceutical Biotechnology, Department of Pharmacy, and Center for NanoScience (CeNS), Ludwig-Maximilians-Universität (LMU) Munich, Butenandtstr. 5-13, D-81377 Munich, Germany
[b] Department of Chemistry, Johannes Gutenberg-Universität Mainz, Duesbergweg 10-14, D-55128 Mainz, Germany
[c] Fraunhofer Institute for Microengineering and Microsystems IMM, Carl-Zeiss-Str. 18-20, D-55129 Mainz, Germany

* Corresponding author: S. Berger

This chapter is adapted from a pre-copy-edited version of a peer-reviewed review article published in ***Biophysics Reviews* 2022, 3, (1), 011303 (ref. [2]).**

Author contributions

Each author has substantially contributed to drafting this review. S. Berger, E. Wagner, and M. Maskos conceptualized the review topic. S. Berger, and M. Berger wrote and edited the original manuscript draft incl. illustrations, and S. Berger, E. Wagner, M. Berger, C. Bantz, and M. Maskos revised it. E. Wagner, and M. Maskos were responsible for funding acquisition. All authors have read and agreed to the published version of the manuscript.

Abstract

Nanomedicine has a great potential to revolutionize the therapeutic landscape. However, up-to-date, results obtained from *in vitro* experiments predict the *in vivo* performance of nanoparticles weakly or not at all. There is a need for *in vitro* experiments that better resemble the *in vivo* reality. As a result, animal experiments can be reduced, and potent *in vivo* candidates will not be missed. It is important to gain a deeper knowledge about nanoparticle characteristics in physiological environment. In this context, the protein corona plays a crucial role. Its formation process including driving forces, kinetics and influencing factors has to be explored in more detail. There exist different methods for the investigation of the protein corona and its impact on physico-chemical and biological properties of nanoparticles, which are compiled and critically reflected in this review

article. The obtained information about the protein corona can be exploited to optimize nanoparticles for *in vivo* application. Still, the translation from *in vitro* to *in vivo* remains challenging. Functional *in vitro* screening under physiological conditions such as in full serum, in 3D multicellular spheroids/organoids or under flow conditions is recommended. Innovative *in vivo* screening using barcoded nanoparticles can simultaneously test more than hundred samples regarding biodistribution and functional delivery within a single mouse.

Keywords

Nanoparticles, drug delivery, physiological environment, protein adsorption, protein corona, biomolecular corona, barcode DNA.

4.1 Introduction

Nanomedicine is an interesting, emerging field of modern medical care.[13, 234, 236, 237] Many nanotherapeutics are in clinical trials, and the number of approved nanoparticulate drug products is continuously growing. Liposomal doxorubicin (DOXIL®) was the first nano-drug to be approved by the United States Food and Drug Administration (FDA) in 1995.[238] Currently, messenger RNA (mRNA) vaccines are the big hope in the SARS-CoV-2 pandemic,[23] small-interfering RNA (siRNA) lipid nanoparticles (LNPs) reached the medical market,[17] and Cas9 mRNA LNPs have been applied for the first successful *in vivo* genetic correction by CRISPR Cas9/single guide RNA in patients.[24]

Despite the enormous potential, the progress in the development and application of nanoparticles as delivery vehicles for (bio)pharmaceutics (*e.g.*, chemotherapeutics, therapeutic nucleic acids or proteins) is rather slow and moderate. The production of such nanotherapeutics in pharmaceutical grade and scale is challenging.[13] Moreover, different cargos place different demands on their carriers.[3, 13, 26] Important is especially that the delivery system comprises extracellular stability and intracellular release of the cargo in its active form at the site of action. Bio-/stimuli-responsiveness can be a helpful tool for creating delivery systems, which change their properties in a dynamic mode upon specific endogenous or exogenous stimuli (*e.g.*, changes in pH, redox-potential, or temperature).[1] The probably most relevant reason for the slow progress, however, is the often weak to

absent translatability from obtained *in vitro* data to the *in vivo* situation,[27-33] which makes it hard to draw conclusions about the *in vivo* performance of nanoparticles from *in vitro* experiments.

After intravenous administration, the nanoparticles have to face several obstacles that differ from *in vitro* (**Figure 4.1**). Firstly, they get in contact with blood components. Usually, the nanoparticles are then covered by a biomolecular multi-layer (so-called protein corona or biomolecular corona),[34, 35] which creates a biological identity,[35, 36] thereby altering the physico-chemical properties, the pharmacokinetics, and toxicity profile of the nanoparticles.[37] Interaction with electrolytes, plasma proteins and blood cells (*e.g.*, erythrocytes and thrombocytes) can cause nanoparticle dissociation, self-aggregation, or aggregation with *e.g.*, erythrocytes.[3, 38] Cationic nanoparticles bind and activate complement blood proteins, thereby inducing innate immune responses with serious side effects.[39, 40] In addition, destabilizing shear forces within the blood stream act on the nanoparticles.[41, 42] Functionalization of the nanoparticle surface with shielding agents (*e.g.*, polyethylene glycol (PEG), poly(2-ethyl-2-oxazoline) (PetOx), or polysarcosine (pSar)) can reduce, but not completely prevent the protein corona formation and create a “stealth” character, by this hindering dissociation or aggregation.[36, 43-45, 239, 240] Secondly, the nanoparticles have to extravasate, penetrate and accumulate in the right tissue, followed by uptake in the target cells. Endothelial targeting as well as passive (*via* the so-called enhanced permeation and retention (EPR) effect) and/or active targeting can be helpful for efficient delivery *in vivo.*[1, 3, 28, 47] However, it has to be considered that the biomolecular corona can mask targeting ligands, thereby reducing the targeting capability.[37, 44, 50] Thirdly, endosomal escape and cargo release are necessary. Both processes are more or less comparable between *in vitro* and *in vivo* (single-cell level). But also here masked nanoparticles may be blocked *e.g.*, in their lytic activity, resulting in reduced release from the endosomes and thus reduced transfection efficiency.[29]

Also, for other application routes than intravenous (*e.g.*, inhalative, intravitreal, or transdermal) several biological barriers have to be overcome and the delivery system has to fulfill certain requirements.[54-56] Moreover, there can be difficulties to reach the target organ. The most prominent example is the systemic delivery to the brain, where the blood-brain-barrier (BBB) is a major hurdle.[57]

Due to the huge discrepancy between the *in vitro* and the *in vivo* situation, there is the

need for *in vitro* assays that resemble the *in vivo* situation more realistically. In this context, it is also necessary to gain a deeper knowledge about the interactions at the nano-bio interface, the protein corona formation, and the impact of physiological milieu on the nanoparticles. With better predictions of the *in vivo* efficacy, potent *in vivo* candidates that show only minor activity in standard *in vitro* assays will not be missed.[27, 30] In addition, such assays are also advantageous in regard to animal welfare and protection as ineffective carriers can be excluded from *in vivo* studies with greater certainty at an earlier point in time.

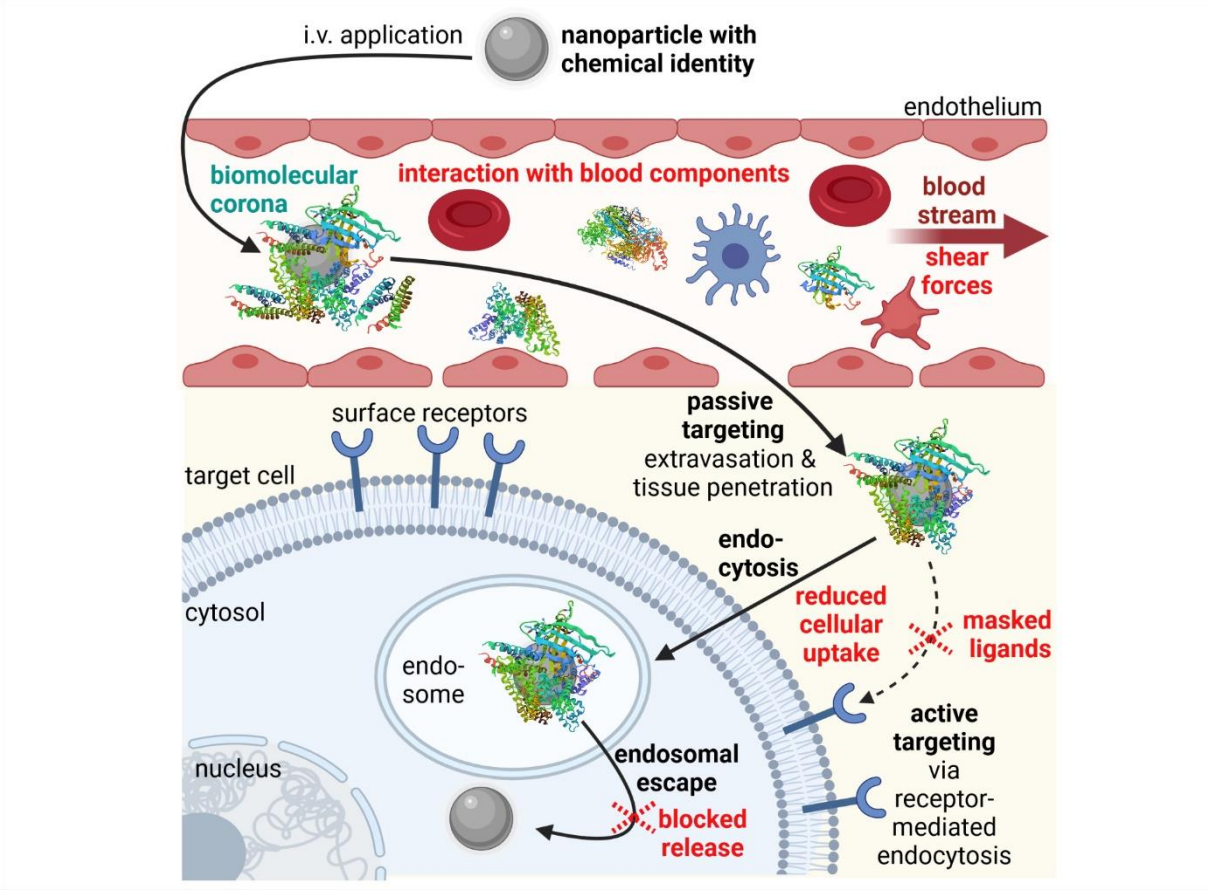

Figure 4.1. Obstacles (in red) in the *in vivo* delivery process of intravenously (i.v.) applied nanoparticles. Created with BioRender.com.

In recent years, several *in vitro* and *ex vivo* models have been developed, which mimic the *in vivo* situation with relevant biological barriers. However, these are not subject of the current review article as detailed reviews about such models can be found elsewhere – *e.g.*, about microfluidic organ-on-chip technology,[241-243] about lung and inhalation models,[54, 244] about skin models for transdermal application,[245, 246] and about BBB

models.[57] To briefly mention a practical example: Onyema *et al.* established a BBB model based on human induced pluripotent stem cells, which is suitable to study interactions with nanoparticles in correlation with their material, size, and protein corona composition.[247]

In the following, different methods for the characterization of the protein corona and its impact on nanoparticles' properties will be discussed and critically reflected. Moreover, a more advanced *in vivo* screening method using barcoded nanoparticles will be illustrated. With this method more than hundred samples can be simultaneously screened within a single mouse.[248] By this, the number of animals in the *in vivo* studies can be reduced, which is in line with a more reasonable and ethical use of animals.

4.2 Characterization of the protein corona and its impact on nanoparticle properties

In physiological environment, the nanoparticle surface gets coated inter alia with proteins [249-252], forming a so-called protein corona.[34, 253] The protein adsorption phenomenon was firstly described by Vroman *et al.* in 1962.[254] In 2012, the extended term "biomolecular corona" was introduced by Dawson and co-workers to underline the complexity of the nanoparticle corona in biological fluids, consisting not only of proteins but also of other biomolecules.[35] The chemical identity of the nanoparticles is changed towards a biological identity.[35, 36] Physico-chemical properties of the nanoparticles as well as their pharmacokinetics (*e.g.*, blood circulation time, clearance, biodistribution, targeting capability and drug release profiles) and biosafety (hemocompatibility, toxicity, immune response) are altered in biofluids.[36, 37, 44, 255-258] The corona formation is a dynamic process comprising physico-chemical interactions and thermodynamic exchanges [249], which evolves over time.[222, 258-266] The multi-layered structure of the protein corona can be subdivided into the inner tight hard corona (protein-nanoparticle interactions) and the outer looser soft corona (protein-protein interactions).[249] The properties of the formed protein corona depend on the nanoparticle composition,[44, 267-269] but also on additional nanoparticle properties such as size, surface charge, shape, nanoparticle surface, and functionalization (*e.g.*, PEGylation).[223, 249-252, 268, 270, 271] Moreover, experimental conditions (*e.g.*, biofluid, temperature, time, static versus dynamic incubation) can influence the protein adsorption.[251]

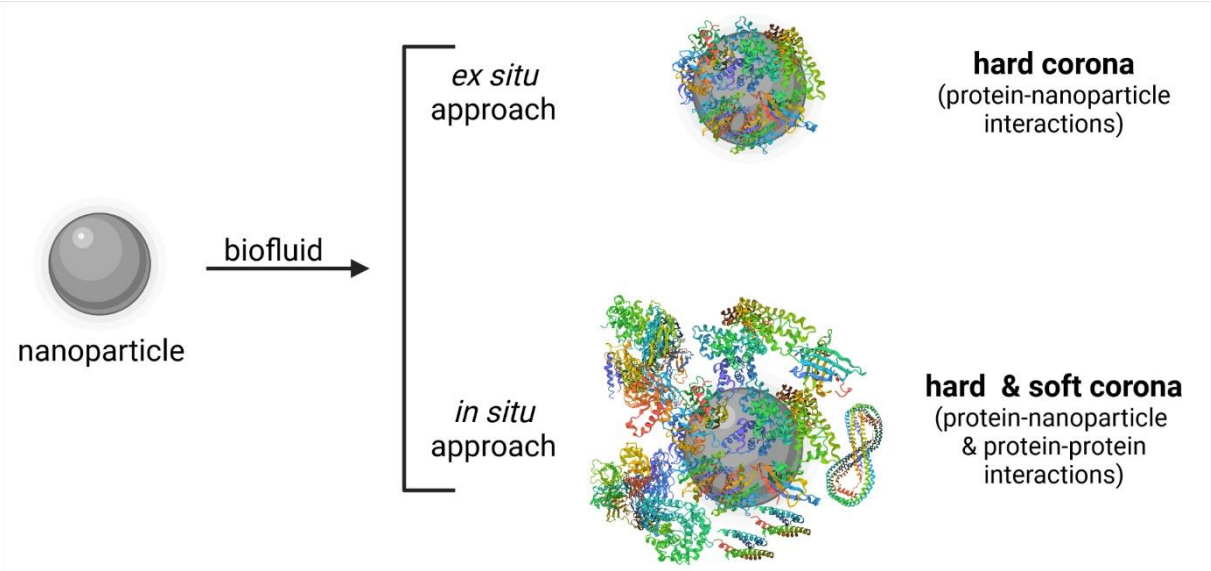

Figure 4.2. Protein corona investigation using *ex situ* or *in situ* approaches. While with the *ex situ* approach mainly the hard corona can be evaluated, *in situ* technologies allow for the characterization of the hard and soft corona. Created with BioRender.com.

4.2.1 General considerations for the experimental set-up of protein corona investigations

In general, the investigation of the hard corona is much easier and more accessible compared to the soft corona as the latter is of an unstable nature and difficult to isolate.[249] Thus, there exist only few attempts to evaluate the soft corona along with the hard corona using *in situ* techniques, where the protein corona is investigated immediately in the biofluid without prior separation of unbound proteins (**Figure 4.2**).[222, 249, 272-284] The classical *ex situ* approach consists of three steps: sample incubation in physiological fluids, followed by isolation and purification of nanoparticle-protein complexes from free proteins, and subsequent proteomic analysis and/or evaluation of physico-chemical and biological nanoparticle properties before and after protein interaction.[249, 285] With the *ex situ* approach, mainly the hard corona can be analyzed (**Figure 4.2**). Sample incubation conditions have to be carefully chosen,[249] *i.e.*, (*i*) sample concentration, (*ii*) biofluid – type (blood, plasma, serum, protein solutions, simulated body fluid, etc.), origin (*e.g.*, murine, bovine, human) and amount, (*iii*) temperature, (*iv*) time, (*v*) shaking speed. Dynamic incubation conditions (*e.g.*, peristaltic pumps for adjusting flow rates) may simulate more realistically the *in vivo* situation.[41, 42, 286, 287] Some research was also conducted investigating the *in vivo* protein corona of nanoparticles after blood circulation in mice.[261, 288-293] The different possible techniques for the isolation and purification of the

nanoparticle-protein complexes with all their advantages and limitations are reviewed in detail by Weber *et al.* [272] In short, the mostly used method is centrifugation,[285] often performed in presence of a sucrose cushion.[272] However, high centrifugal forces may alter the protein corona. Alternatively, chromatography-based methods such as asymmetrical flow field-flow fractionation (AF4), hydrodynamic chromatography (HDC) and size exclusion chromatography (SEC) can be utilized to purify the nanoparticle-protein complexes.[272] The very mild separation conditions of AF4 may allow to also isolate weakly bound proteins of the soft corona.[294] In the case of SEC, relatively high shear stress occurs that may influence the protein corona composition.[295] However, with this method dissociation rates can be investigated.[272] Moreover, special nanocarrier properties can be used for isolating the nanoparticle-protein complexes.[249, 272] Magnetic separation, for instance, can be an option for magnetic nanocarriers.[296-301]

After successful separation from free, unbound proteins, the protein corona can be analyzed with various techniques. **Figure 4.3** illustrates a typical experimental set-up for a protein corona investigation. Overall, in order to obtain as complete a picture as possible, a combination of *in situ* and *ex situ* technologies for the protein corona characterization is recommended, since each preparation method can have an influence on the tested system and findings.[272, 302]

In the following, such characterization methods will be discussed in detail with a focus on their advantages and limitations regarding protein corona analysis. Moreover, technologies for studying protein-nanoparticle interactions will be illustrated.

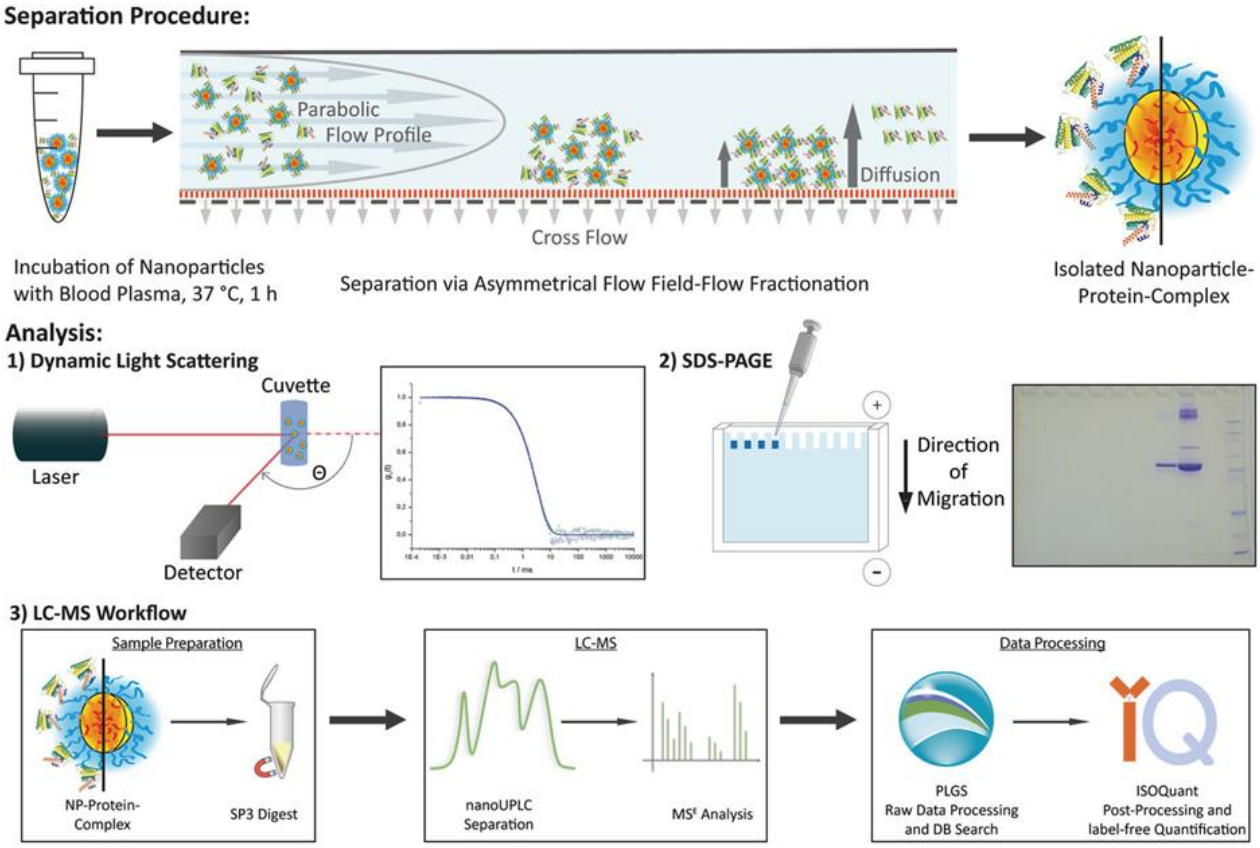

Figure 4.3. A typical experimental set-up for protein corona investigations. After incubation of nanoparticles in human blood plasma, nanoparticle-protein complexes are isolated by asymmetrical flow field-flow fractionation (AF4). The sizes can be assessed by dynamic light scattering (DLS). The protein corona composition and amount are analyzed by SDS-PAGE (sodium dodecyl sulfate polyacrylamide gel electrophoresis) and label-free quantitative proteomic analysis. LC-MS, liquid chromatography-mass spectrometry; UPLC, ultra-performance liquid chromatography. Reproduced with permission from Small 16, 1907574 (2020).[239] Copyright © 2021; John Wiley and Sons.

4.2.2 Investigation of protein-nanoparticle interactions

To gain a deeper knowledge about the protein corona formation process, it is important to comprehend the driving forces and kinetics of protein binding on nanoparticle surfaces. There exist several techniques to investigate single protein-nanoparticle interactions. Thermodynamic parameters such as affinity and stoichiometry of protein binding can be studied *via* isothermal titration calorimetry (ITC).[253, 303-305] Surface plasmon resonance (SPR) can help to assess association and dissociation rates.[253, 263, 306, 307] Multi-parametric SPR was utilized by Kari *et al.* for the *in situ* investigation of protein binding on biosensor-immobilized liposomes in undiluted protein solutions or human plasma.[274, 308] Oh *et al.* developed a new technique based on atomic force microscopy (AFM)-derived

recognition imaging to determine binding affinities by visualizing molecular bindings at the nanoscale, as demonstrated by means of DNA hybridization.[309] They state that this method is applicable to any receptor/ligand combination (*e.g.*, interaction between nanoparticles and plasma proteins), thus representing a potent alternative for next generation affinity sensors. Furthermore, different fluorescence spectroscopy-based methods can be used to characterize protein-nanoparticle interactions.[310-313] Boulos *et al.* studied the bovine serum albumin (BSA) adsorption on gold nanoparticles (kinetics, binding constants) *via* steady-state fluorescence spectroscopy, taking advantage of the fluorescence quenching capability of the tested gold nanoparticles.[311] They found that the nanoparticle shape and surface as well as PEGylation had no impact on the BSA binding affinity. This was confirmed by affinity capillary electrophoresis (ACE). Comparison of the binding constants derived from the two different methods, however, revealed orders of magnitude difference. Moreover, both techniques have their limitations: While fluorescence spectroscopy suffers from inner filter effects and gold nanoparticle optical interference, inner capillary wall effects are an issue in ACE. Therefore, combination of several methods is required to determine binding affinities as accurately as possible. A fluorescence polarization assay was developed by Gaus *et al.* to study protein binding towards antisense-oligonucleotides (ASO).[312] In a follow-up study, ASO-fatty acid conjugates showed in the fluorescence polarization assay improved protein binding affinities with increasing carbon chain length (optimum C16-C22).[313] The activity of ASO-fatty acid conjugates correlated with their affinity to albumin. The tighter the BSA binding, the greater the improvement in muscle activity.

When a protein binds on a nanoparticle, it can alter its structure/conformation in response to the nanoparticle surface, resulting in altered functionality.[251, 314, 315] Such changes can be examined by various spectroscopic methods. Circular dichroism (CD) spectroscopy can detect changes in the secondary structure of proteins in real-time and *in situ*.[251, 314, 316] By using synchrotron-radiation (SR) as light source for CD spectroscopy, measurements access much more of the vacuum ultra-violet (UV) wavelength range down to the extreme UV and even X-ray range.[317, 318] The SR-CD spectra are therefore richer in information than conventional CD spectra, including even electronic transitions of the polypeptide backbone.[318] By this, more precise determinations of changes within the secondary structure of proteins can be made. Sanchez-Guzman *et al.* used SR-CD to

investigate changes in structure and stability of weakly bound proteins on nanoparticles *in situ.*[319] In combination with computer simulation (molecular dynamics) and thermodynamic analysis, they concluded that nanoparticles altered weakly bound proteins by shifting the equilibrium towards the unfolded states at physiological temperature. Besides CD spectroscopy, several other techniques are used in literature to examine structural changes in proteins, *e.g.*, Fourier transform infrared (FT-IR) spectroscopy,[320, 321] Raman spectroscopy,[322] surface-enhanced Raman scattering (SERS),[323] differential scanning calorimetry (DSC),[250] nuclear magnetic resonance (NMR) spectroscopy,[324] or UV-vis spectroscopy.[325, 326]

4.2.3 Computational simulations of protein-nanoparticle interactions

Besides the aforementioned experimental techniques for the characterization of nanoparticle-protein interactions, *in silico* predictions *via* mathematical, theoretical modeling and computational simulations can be helpful to gain a better understanding of the complex processes happening at the nano-bio interface upon nanoparticle interaction with the physiological environment. There exist different simulation methods to comprehend the mechanistic properties (binding sites, functional units), (thermo-)dynamics and kinetics of protein-nanoparticle interactions. These are discussed in detail elsewhere.[250, 252, 327-329] However, since only single protein-nanoparticle interaction can be simulated, these computational studies fall short to completely depict the reality in a complex biological environment.[329] Great effort has been put into the development of simulation methods better resembling reality. To outline a few of those methods: (*i*) atomistic and coarse-grained molecular dynamics or Monte Carlo simulations help to predict details of nanoparticle-protein interactions at the molecular-to-particle level;[307, 329-336] (*ii*) the adopted Hill model can be utilized to assess equilibrium dissociation and kinetic coefficients for one or two protein species binding with one nanoparticle type;[337] (*iii*) with dynamic modeling Dell'Orco *et al.* predicted the corona formation process (evolution and equilibrium composition) based on affinities, stoichiometries, and rate constants;[263] (iv) statistical modeling can be another option for *in silico* predictions. Examples for this are statistical modeling of quantitative structure-activity relationships (QSAR) *via* linear and non-linear regression models,[338, 339] and statistical modeling of a so-called biological surface adsorption index (BSAI) based on multiple linear regression analysis and experimentally obtained binding coefficients.[340] With the rapid progress in electronic

development and the improvement of computing power, *in silico* predictions will gain more importance for protein corona investigations in the future.[252]

4.2.4 Identification and quantification of protein corona components

The commonly used techniques for the identification of protein corona components are SDS-PAGE (sodium dodecyl sulfate polyacrylamide gel electrophoresis) and MS (mass spectrometry) (**Figure 4.4**).[251, 341] The corona proteins have to be first eluted from the nanoparticles' surface under denaturing conditions and heating.[285] Then, in the case of SDS-PAGE, the detergent SDS (often together with a reducing agent like dithiothreitol) completely unfolds the proteins.[342] The negatively charged SDS-protein complexes are then separated by molecular weight. PAGE can be performed one-dimensionally (1D-PAGE, standard SDS-PAGE) [343] or two-dimensionally (2D-PAGE).[344] In the case of the latter, usually separation using isoelectric focusing (IEF) is followed by separation based on protein size (SDS-PAGE). This two-step separation process allows for the separation of complex protein mixtures into discrete spots but is more time consuming than 1D-PAGE.[344] Protein detection in the polyacrylamide gels is normally done by Coomassie Blue Staining, staining with SYPRO Ruby (a pre-formulated, noncovalent fluorescent stain), or Silver Staining.[345] By this, multi-protein identification is achieved; for the specific detection of single proteins, immunoblotting can be performed after SDS-PAGE.[341] Moreover, SDS-PAGE can be combined with liquid chromatography (LC)-MS or LC-tandem MS (LC-MS/MS).[251, 265, 271] For this, a trypsin-digest of the proteins has to be done beforehand.[346-348] Often used MS methods are such with soft ionization sources, *e.g.*, matrix-assisted laser desorption/ionization time-of-flight MS (MALDI-TOF MS),[349] quadrupole TOF MS,[265, 350] or electrospray ionization MS (ESI-MS).[271, 351] LC-MS of digested proteins[352] can be also performed without prior separation by SDS-PAGE.[239, 287, 341, 351] Advantage is the small sample volumes that are required.[249, 351] For the subsequent proteomics analysis, bioinformatic tools for data processing and database search (*e.g.*, Sequest,[353] Mascot,[354] or ProteinLynx Global Server[239, 270]), and specialized analyzing software (*e.g.*, Scaffold,[355] or Progenesis[356]) are inevitable.[249, 357] In the case of LC-MS, absolute in-sample amounts of proteins can be obtained by label-free quantification *e.g.*, as described in reference.[358] Whereas, in the case of SDS-PAGE, only the quantity of proteins with similar molecular weight can be assessed.[251] Alberg *et al.* quantified the human serum albumin (I) amount attached on nanoparticles by

performing a comparative SDS-PAGE based analysis with free, pure I at different concentrations.[239]

Bicinchoninic acid (BCA) assay is a standard protein quantification assay.[359, 360] With this assay, the total amount of corona proteins can be determined.[41, 293] Cysteines, tryptophans, tyrosines and the peptide bonds reduce Cu^{II} to Cu^{I} in an alkaline milieu, which then forms complexes with BCA.[361] However, drawbacks are the relatively low sensitivity and possible interference of the nanoparticles with this assay.[251, 361, 362]

Quartz crystal microbalance (QCM) can be used to predict the surface coverage on nanoparticles with proteins.[363, 364] This method is ultra-sensitive to total mass changes (down to the femto- to attogram range[273]), as measured by changes in the resonance frequency on a piezo-electric crystal.[365, 366] QCM can be measured *in vacuo* or in fluids.[366] With the further developed method termed QCM with dissipation monitoring (QCM-D), additional information about the viscoelastic properties of the adlayer can be derived in real-time and *in situ.*[365] By the way, QCM-D can be also used to study interactions between nanoparticles and membranes/lipid bilayers and how the protein corona influences these interactions.[367-369] Sebastiani *et al.* utilized QCM-D to screen various LNPs for their binding affinities to serum proteins in order to find the most promising candidates for subsequent *in vitro* and *in vivo* experiments.[370] For this purpose, they used gold sensors functionalized with antibodies against human ApoE or PEG. By this, binding affinities of LNPs towards ApoE as well as of PEGylated LNPs to serum proteins could be investigated.

Inductively coupled plasma mass spectrometry (ICP-MS) can be used to determine the stoichiometric composition of the protein corona of inorganic nanoparticles.[273] With ICP-MS, the metal (*e.g.*, gold) of the inorganic nanoparticles as well as sulfur of cysteine residues of proteins are detected, allowing for the calculation of the total concentrations of both elements.[371, 372] Together with results derived from classical protein quantification like BCA assay, the number of proteins per molecule can be determined.[372, 373]

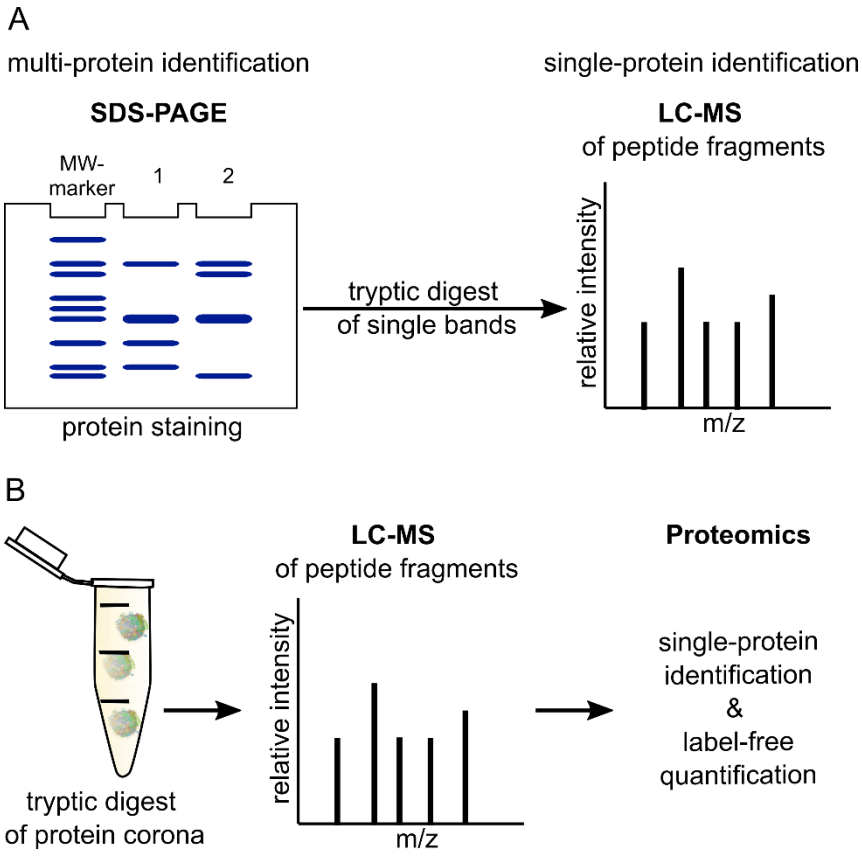

Figure 4.4. Classical approaches for the identification and quantification of protein corona components. (**A**) SDS-PAGE (sodium dodecyl sulfate polyacrylamide gel electrophoresis) followed by protein staining allows for multi-protein identification. Tryptic digest of single bands and subsequent LC-MS (liquid chromatography-mass spectrometry) analysis enables the identification of single proteins. (**B**) Trypsinized corona proteins can also be directly analyzed by LC-MS. With subsequent data processing and proteomic analysis, besides single-protein identification also label-free quantification is possible. MW-marker, molecular weight-marker. Nanoparticle-protein complexes (**B**) are created with BioRender.com.

4.2.5 Impact of the protein corona on the physico-chemical properties of nanoparticles

The protein corona determines inter alia physico-chemical properties (*e.g.*, size, surface charge and stability) of the nanoparticles in physiological environment.[36, 251, 374-376] The influence on the physico-chemical properties of the nanoparticles can be investigated using different characterization methods (**Table 4.1**). These can be divided into three general categories:[374] (*i*) scattering and correlation methods, (*ii*) microscopy-based methods, and (*iii*) fractionating methods based on hydrodynamic separation.

In the following, a closer look at the different characterization methods is taken. Practical examples for the methods with regard to protein corona investigations are listed in **Table 4.1**. A selection of these examples is also described in more detail in the text. **Table 4.2** summarizes the advantages and limitations of the different methods.

Table 4.1. Physico-chemical characterization methods for nanoparticles – practical examples with regard to protein corona investigations.

Characterization method		Information about	Practical examples – references
Scattering- and correlation-based	DLS, DDLS, SLS	size	[222, 239, 240, 266, 280, 376-382]
	ELS	zeta-potential	[222, 259, 271, 286, 297, 376, 381]
	SAXS, SANS	size	[381, 383-386]
	FCS	size	[275, 278, 387-389]
	PTV	size	[379, 390]
Microscopy-based	(Cryo-)TEM	size, shape	[43, 222, 293, 319, 378, 380, 381, 391-394]
	SEM		[395]
	AFM		[307, 396, 397]
Fractionating	AF4	size distribution	[239, 240, 378, 380, 398]
	SEC		[253, 312, 399]
	AUC		[396]
	DCS		[222, 332, 376, 400]
Others	TRPS	size, zeta-potential	[401-404]

AF4, asymmetrical flow field-flow fractionation; AFM, atomic force microscopy; AUC, analytical ultra-centrifugation; DCS, differential centrifugal sedimentation; DDLS, depolarized dynamic light scattering; DLS, dynamic light scattering; ELS, electrophoretic light scattering; FCS, fluorescence correlation spectroscopy; PTV, particle tracking velocimetry; SANS, small angle neutron scattering; SAXS, small angle X-ray scattering; SEC, size-exclusion chromatography; SEM, scanning electron microscopy; SLS, static light scattering; TEM, transmission electron microscopy; TRPS, tunable resistive pulse sensing.

Table 4.2. Advantages and limitations of the physico-chemical characterization methods.

Characterization method	Advantages	Limitations	References
DLS	Non-perturbative, fast, and accurate method to determine hydrodynamic radii (size range 1 nm – 10 µm); no calibration required	Hydrodynamic radii influenced by the formation of hydration shells, particle shapes, and counterion binding; high sensitivity towards the presence of larger particles; inability to characterize highly polydisperse systems	[329]
ELS	Straight forward method to measure surface charge and changes in surface charge; indicator of stability of NP dispersions	Minimum ionic strength required; only for monodisperse NPs (calculation of charge/size ratio)	[329]
SLS	Absolute method, no calibration required	Average values for Mw and Rg influenced by the sample's polydispersity	[405]
SAXS, SANS	High-resolved, in-depth structural characterization at the nanoscale	X-rays: possible radiation damage to the samples (not the case for non-destructive neutrons)	[406]
FCS	Sensitive method to measure minute changes in NP diffusivity; ability to quantify PC formation with high accuracy in the presence of free protein	Fluorescent label required	[329, 388]
PTV	Tracking of single NPs; potentially less sensitive to bigger particles (compared to *e.g.*, DLS)	Limited to analytes with low particle concentrations; loss of sensitivity in the case of small NP distances; sensitive to background scattering	[407-409]
TEM	Visualization of protein adsorption onto the NP surface	Negative staining of protein needed; shrinkage of vesicles due to drying process; cost- and time-intensive	[251, 407]
Cryo-TEM	Investigation of NPs in their natural surroundings	Cost- and time-intensive; contrast reduction caused by the water film	[391, 407, 410, 411]
SEM	Detailed 3D images; less prone to overestimate NP size (compared to *e.g.*, DLS)	Difficulties in the detection of proteins on the NP surface; staining with heavy metals required; shrinkage of vesicles during the drying process; cost- and time-intensive	[251, 407]
AFM	Visualization of the surface topography and properties (*e.g.*, hardness, texture, protein adsorption) with atomic resolution	Impossibility to distinguish hard and/or soft PC formation; difficult sample preparation; time consuming; matching of probe and operating mode to the specific sample required; various sources of artifacts (*e.g.*, tip and scanner)	[251, 407, 412, 413]
AF4	Characterization of soluble and insoluble sample specimen, and also of complex mixtures of colloids, particles or even cells (size range 1 nm – 100 µm); higher selectivity and greater resolution over a wider size range than SEC; low shear forces (soft corona investigation)	Strong dilution of the sample in the carrier liquid and incomplete particle recollection depending on the crossflow	[294, 407, 414]

Table 4.2 ***continued.***

SEC	Simplicity of the method; high speed and precision in separation; very small amounts of sample needed	Limited dynamic range; nonspecific interactions with the chromatographic material and column hardware; inaccuracy due to alteration of size distribution (*e.g.*, for reversible aggregates)	[295]
AUC	Hydrodynamic and thermodynamic characterization of macromolecules or colloids in situ; high resolution (Ångström range for NP size); no calibration necessary	Calculation of NP size distribution heavily depended on the knowledge of the sample's density; no fraction collection possible	[415]
DCS	Applicable to complex biological systems, without the need for fluorescent labels; high-resolution separation and detection of a small percentage of particle populations (size range 3 nm – 60 µm) within polydisperse colloidal samples	Identification of the "true" NP size relies on a simple core-shell model considering the new NP density; no fraction collection possible	[222, 400]
TRPS	High-resolution and accuracy in measurement of multimodal samples; measurement in complex biological media	Limited speed and detectable size range; no fraction collection possible	[401, 416, 417]

AF4, asymmetrical flow field-flow fractionation; AFM, atomic force microscopy; AUC, analytical ultra-centrifugation; DCS, differential centrifugal sedimentation; DLS, dynamic light scattering; ELS, electrophoretic light scattering; FCS, fluorescence correlation spectroscopy; NP, nanoparticle; PC, protein corona; PTV, particle tracking velocimetry; SANS, small angle neutron scattering; SAXS, small angle X-ray scattering; SEC, size-exclusion chromatography; SEM, scanning electron microscopy; SLS, static light scattering; TEM, transmission electron microscopy; TRPS, tunable resistive pulse sensing.

4.2.5.1 Scattering and correlation methods

In the case of static light scattering (SLS), a laser beam passes through the sample and the mean value of the intensity of the scattered light is measured at different angles. For particles larger than λ/20, the scattered light intensity depends on the detection angle θ. Using the Zimm equation one can derive the z-average of the squared radius of gyration $<R_g^2>_z$.[418] In dynamic light scattering (DLS) or quasi elastic light scattering (QELS), the fluctuation of the scattered light intensity is measured and autocorrelated. The autocorrelation function yields the z-average of the diffusion coefficient $<D>_z$. Using the Stokes-Einstein equation, the z-average of the reciprocal hydrodynamic radius $<1/R_h>_z$ can be calculated.[418] As a practical example, Alberg *et al.* could show by multiangle light scattering that incubation with 50% (v/v) human plasma did not affect the hydrodynamic radii and polydispersity of the tested polymeric micelles, which were surface modified with different hydrophilic shielding agents (PEG, poly(*N*-2-hydroxypropylmethacrylamide) (pHPMA), pSar).[239] Consecutive proteomic analysis confirmed that only a neglectable amount of plasma proteins was attached to the nanoparticles. This is especially preferable

for *in vivo* applications. A relatively new improvement of DLS is depolarized DLS (DDLS).[419] Hereby, the scattered light is divided into two beams (horizontally and vertically polarized), allowing the simultaneous determination of the translational and rotational diffusion. This enables the observation of nanoparticles with an optical anisotropy in a complex biological matrix, as the contribution to the scattered light intensity for particles without an optical anisotropy is negligible.[280]

The zeta-potential or effective charge of the nanoparticle can be measured with electrophoretic light scattering (ELS).[420-422] Sakulkhu and co-workers investigated the effect of serum on the zeta-potential of different polyvinyl alcohol (PVA)-coated superparamagnetic iron oxide nanoparticles (SPIONs).[297] The surface charge dropped in all cases due to the net-negative-charged layer of adsorbed serum proteins. At the same time, the hydrodynamic size of the SPIONs increased as determined by DLS measurements.

Small angle x-ray scattering (SAXS) and small angle neutron scattering (SANS) are also static light scattering experiments like SLS; the advantage of using neutrons or x-rays is that the de Broglie wavelengths are in the order of 0.1 to 10 nm as opposed to around 400 to 700 nm for the wavelength of visible light. This allows for a more detailed observation of structures.[423, 424] SAXS measurements were utilized, for instance, by Orts-Gil *et al.* to evaluate colloidal stability of silica nanoparticles in the presence of BSA.[381] The derived SAXS structure factor indicated a short-range attractive potential in the binary silica-BSA system, which is in line with observed agglomeration in DLS measurements. The authors hypothesized that protein bridging might be an explanation for the observed agglomeration. Sebastiani and co-workers examined the influence of ApoE binding to mRNA-LNPs *via* SANS.[383] They found that ApoE binding led to the re-arrangement of components both at the surface as well as in the LNP core.

Fluorescence correlation spectroscopy (FCS) autocorrelates the fluctuations of the intensity of fluorescent light, analog to DLS, caused by the diffusion of fluorescent nanoparticles through the observation volume.[388, 425] This method is limited to fluorescent particles but offers the advantage that non fluorescent components of the sample do not influence the autocorrelation function.[249] Negwer *et al.* developed a new method utilizing FCS for the direct characterization of nanoparticles in flowing blood.[275] For this purpose, they labeled the nanoparticles with near-infrared (NIR) fluorescent dyes and fitted the

autocorrelation functions with an analytical model accounting for the presence of blood cells.

Particle tracking velocimetry (PTV) can be used to track the Brownian motion of a single nanoparticle and calculate its diffusion coefficient from the obtained data.[408, 409] In this set-up, the particle suspension is illuminated, and the motion of individual scattering centers is tracked with multiple charge coupled device (CCD) cameras.[409] Due to the measurement principle, only analytes with a low particle concentration can be investigated by PTV. Di Silvio and co-workers used particle tracking analysis to investigate different nanoparticle-protein complexes isolated from complex biofluids by sucrose gradient ultracentrifugation.[379] The sizes of these complexes were comparable to that determined *in situ.* In contrast, isolation *via* conventional centrifugation had a bigger impact on the nanoparticle-protein complexes. The results were confirmed by DLS measurements. The authors concluded that ultracentrifugation could isolate and recover nanoparticle-protein complexes in stable form with high size-resolution.

4.2.5.2 Microscopy-based methods

Nanoparticles cannot be observed using light microscopy because they are a lot smaller than the abbe limit for visible light. Transmission electron microscopy (TEM) overcomes this limitation by using electrons instead of visible light, which have a very short de Broglie wavelength (around 3 pm depending on the acceleration voltage of the electron source) and therefore lower the abbe limit. This makes it possible to visualize structures with a resolution of a few nanometers.[426] One problem that arises with the typical dry preparation of samples for TEM imaging is the formation of artifacts formed during the drying process (*e.g.*, compaction of sample constituents in spots). The dry preparation is especially a problem for samples containing biological materials as such samples significantly change their appearance during the drying process. Cryo-TEM offers a solution to this problem.[391, 410, 411] Here, the sample is vitrified in a water film, which makes it possible to investigate the sample in its natural surroundings. A disadvantage of this preparation method is that the water film reduces the contrast of the sample. Hadjidemetriou *et al.*, for example, compared the structure and morphology of liposomes before and after protein corona formation *in vitro* and *in vivo* by TEM and cryo-TEM.[293] Structural integrity of the liposomes remained after isolation from both blood (*in vivo*) and plasma (*in vitro*), but the morphology of the protein coronas differed. The *in vitro* protein

corona consisted of a network of linear fibrillary structures, whereas the *in vivo* corona appeared more compact but not covering the whole liposome surface. The authors assumed that these morphological differences were due to the different protein corona compositions *in vitro* and *in vivo* (higher content of fibrinogen molecules in the case of *in vitro* protein coronas). Additional DLS measurements revealed a shrinkage of liposomes upon protein corona formation, which was more pronounced for the *in vivo* protein corona. This effect was most likely osmotically driven.[427]

A further microscopy-based method is scanning electron microscopy (SEM).[395] Here, the sample is scanned with an electron beam, and the intensity of the backscattered electrons is analyzed to create a topographic view of the sample.[428] This method again has certain limitations since the sample itself has to be conductive or it has to be coated with a thin layer of gold or carbon. Mirshafiee *et al.* used SEM to evaluate the influence of human plasma on the size of silica nanoparticles, which were either uncoated or pre-coated with γ-globulin (GG) or human serum albumin (I).[395] They found that the size changed only slightly (9 nm and 3 nm in the case of uncoated and I-coated nanoparticles) to not at all (in the case of GG-coated nanoparticles), but that there were less clustered nanoparticles, indicating that a protein corona was formed. Comparative analysis *via* DLS showed no increase but a decrease in size for I- and GG-coated nanoparticles, confirming the hypothesis of protein corona formation. In a next step, protein corona profiles were examined revealing an opsonin-rich corona for GG-coated but not for the other two nanoparticles. The expected enhanced uptake of GG-coated nanoparticles in macrophages, however, could not be observed, most probably due to unspecific absorption of other blocking plasma proteins.

Atomic force microscopy (AFM) is another method to obtain a topographic image of a sample.[413] Hereby, a small tip with a radius of around 10 nm is attached to a cantilever and rastered over the sample surface using piezo drives. The deflection of the cantilever is measured with a laser beam and a photo diode to calculate a topographic image of the sample. AFM can be used in a variety of different modes. The three most common modes are contact mode, non-contact mode and tapping mode. Dobrovolskaia *et al.* applied different size characterization methods (DLS, TEM, AFM) to investigate the influence of human plasma on the size of colloidal gold nanoparticles.[397] They found an almost 2-fold increase in the hydrodynamic size as measured by DLS but no effect on the nanoparticle

size as determined by TEM and AFM. The authors supposed that this is most probably due to the different sample preparation techniques.

4.2.5.3 Fractionating methods based on hydrodynamic separation

The family of field-flow fractionation (FFF) methods contains a wide variety of methods.[375, 429, 430] In general, the separation is achieved by the application of a physical field perpendicular to the direction the sample travels through a thin channel. This field leads to particle clouds of different heights for individual sample components. This in turn leads to different retention times because thicker particle clouds reach into regions of higher flow velocity in the parabolic flow profile, which is formed in the separation channel due to its small height.

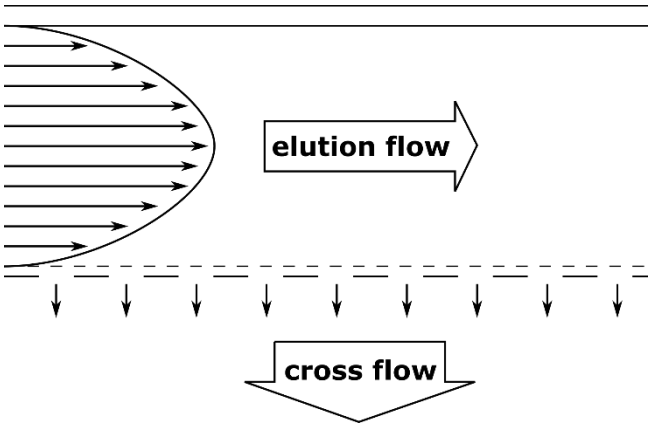

Figure 4.5. The principle of asymmetrical flow field-flow fractionation (AF4).

Examples for FFF methods are thermal FFF (Th-FFF),[405, 431-433] sedimentation FFF (Sd-FFF),[434] electric FFF (E-FFF),[435] and flow FFF (Fl-FFF).[436] One particularly interesting FFF method is asymmetrical flow field-flow fractionation (AF4), which is a variant of Fl-FFF.[380, 398, 432, 437-442] Here, the fractionation of the sample components is achieved by a flow field. The AF4 set-up consists of a separation channel with one permeable wall (the accumulation wall) through which a part of the eluent flows through and so creates the perpendicular flow field (**Figure 4.5**). Depending on the particles' diffusion coefficients (typically for particles smaller than 1 µm), the sample components accumulate in particle clouds of different thicknesses. The retention times of individual sample components depend on the height of the particle cloud (components with higher diffusion coefficients form higher particle clouds). A higher particle cloud reaches into regions of higher flow

velocity in the parabolic flow profile within the separation channel and thus elutes earlier. **Figure 4.6** illustrates the impact of the dissociation rates of nanoparticle-protein complexes on the elution profile. When there is no interaction between the proteins (fraction a) and the nanoparticles (fraction b), the two fractions can be separated completely (**Figure 4.6A**). For rapidly dissociating complexes, the particle cloud of fraction a (= proteins) is broadened a bit (**Figure 4.6B**). In the case of slow dissociation, this effect is even more pronounced (**Figure 4.6C**). With AF4 also weakly bound proteins and thus the soft corona can be investigated.[294] To mention a practical example, Bantz *et al.* used AF4, DLS and TEM to investigate the stability of various silicon oxide-based nanoparticles with different surface properties (different surface charges and polarities, PEGylation) under physiological conditions.[380] They showed that negatively charged silica nanoparticles were stable at physiological salt concentrations (150 mM sodium chloride) but aggregated in the presence of serum proteins. In contrast, positively charged poly(organosiloxane) nanoparticles macroscopically precipitated under physiological salt concentrations. In the presence of serum proteins, this was inhibited but still large particles were formed. PEGylation hindered aggregation to a great extent. Alkylation of secondary amines led to increased sizes at physiological salinity, which were not observable in the presence of serum. All in all, this study showed that different surface properties of the nanoparticles have a huge impact on the stability under physiological conditions, which has in the last consequence also an influence on the biological performance.

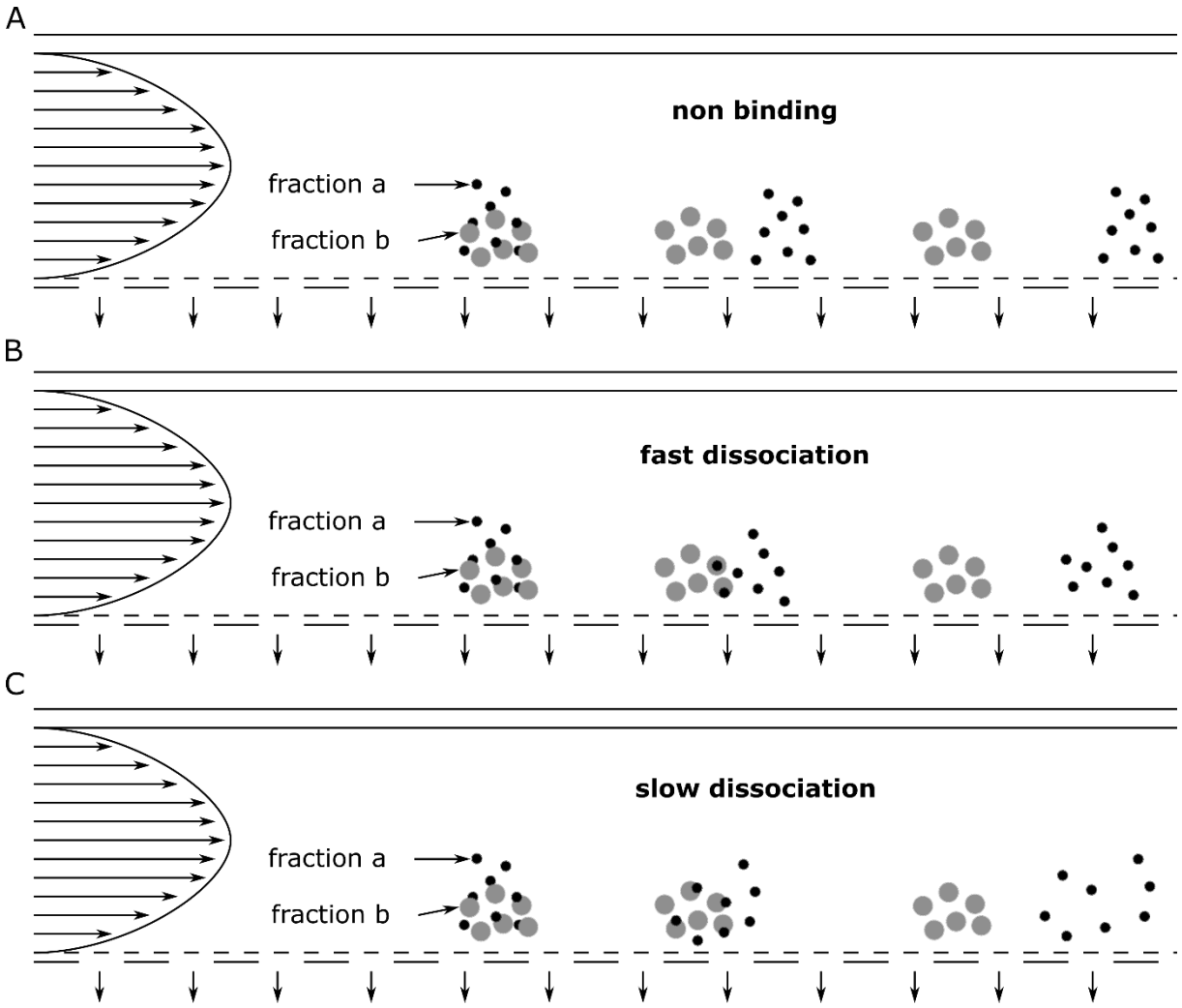

Figure 4.6. Impact of different dissociation rates of nanoparticle-protein complexes on the elution profile in asymmetrical flow field-flow fractionation (AF4). Fraction a in black represents proteins, fraction b in grey represents nanoparticles.

Size exclusion chromatography (SEC) is another fractionating method.[295] Here, the fractionation takes place in a column packed with porous beads made from polystyrene crosslinked with divinylbenzene. Smaller sample components can diffuse deeper into these pores and therefore remain in the column longer than larger particles. Particles of a certain size depending on the packing material of the column cannot diffuse into these pores and therefore no fractionation takes place.[295] This is called the upper exclusion limit. This problem does principally not occur in FFF methods due to the nature of its separation mechanism [414, 430]. A further advantage of FFF methods is the lower shear stress induced on the sample [272, 414], which is especially relevant for sensitive samples such as biological cells or nanoparticle-protein complexes. Nevertheless, Gaus *et al.*

successfully utilized SEC to investigate protein association with phosphorothioate modified antisense-oligonucleotides (ASOs) in plasma of different origin.[312] To identify binding of ASOs to plasma fractions, ASOs were spiked with ^{125}I-labelled ASOs; detection was done by UV-vis and β-RAM. The obtained binding profiles revealed species-specific differences. In the case of murine and human plasma, ASOs were mostly associated with albumin and histidine-rich glycopeptide (HRG). In contrast, ASOs complexed predominantly with HRG in monkey plasma. The authors found that HRG bound to ASOs with a very high affinity. They claimed that this could be of relevance for *in vivo* efficacy especially in monkeys, which showed highest HRG plasma levels among the tested species.

For both methods (FFF, SEC) the sample detection is done with a detector in line with the channel respectively column. Depending on the sample and the physical property of interest, a variety of different detection methods can be used *e.g.*, UV-absorbance, fluorescence detection, refractive index (RI), multi-angle laser light scattering (MALLS), SLS, DLS, or ICP-MS.[374] Comparing classical DLS (batch mode) with AF4 online DLS, the latter allows for a better assessment of the batch-to-batch variability and changes in the nanoparticle size induced by the interaction with serum proteins.[443] In general, fractionation coupled with light scattering methods has the advantage over batch mode measurements that the size distribution can be determined more realistically (**Figure 4.7**).

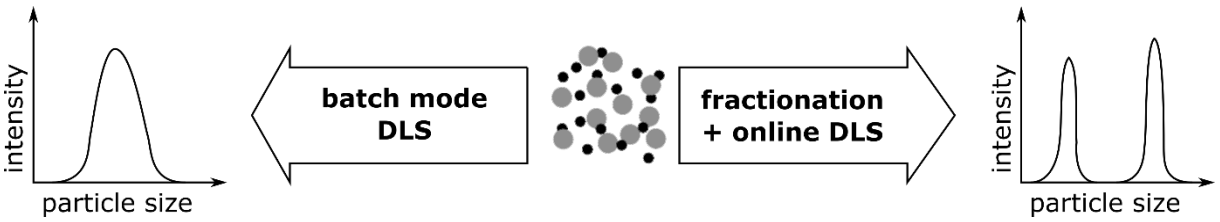

Figure 4.7. Comparison of the size determination of heterogeneous particle mixtures by dynamic light scattering (DLS) *via* batch mode measurement (*left*) versus prior fractionation (*right*).

Analytical ultra-centrifugation (AUC) is an absolute analytical method, which does not require a calibration with standards.[415, 444] In the experimental set-up, the sample is spun at high rotational speeds and the sample concentration along the radius is measured using *e.g.*, a UV-absorbance detector. The sample components start to move away from the rotational axis due to centrifugal forces, which causes a change of the sample

concentration along the radius. Generally, AUC can be used in two modes. The first mode is called sedimentation-diffusion equilibrium (SE) ultra-centrifugation. Here, the sample is spun until a concentration equilibrium between sedimentation and back diffusion is reached. The sample's molecular weight can be derived from this equilibrium concentration profile. The second mode is called sedimentation velocity (SV) ultra-centrifugation. In this mode, sedimentation coefficients can be determined by observing the change of the concentration profile in the sample cell over time. Schaefer *et al.* characterized the agglomeration state of four batches (A-C synthesized *via* flame pyrolysis; D synthesized *via* precipitation) of cerium oxide (CeO_2) nanoparticles in fetal calf serum by AUC with interference detection.[396] Two of these batches (A, B) showed low agglomeration tendency, indicating an effectively formed protein corona as adsorbed proteins are thought to promote stabilization. In contrast, the other two batches (C, D) showed a higher tendency to agglomerate, suggesting less effective protein corona formation. These results were in line with findings of AFM measurements with a BSA-modified tip. The first two batches (A, B) had a higher affinity towards BSA compared to the other two batches (C, D). In addition, densitometry revealed smaller Hill slopes for batches C and D compared to A and B, indicating once more a lower adsorption behavior. Altogether, the study demonstrated that there were big variations in the interaction with proteins between the different CeO_2 nanoparticle batches. This could not be explained by their intrinsic physico-chemical properties (hydrodynamic diameter, zeta potential, pH value) as these were only minimally different. The authors concluded that it is of great importance to investigate the *in situ* properties of nanoparticles with a combination of various proper characterization methods.

Differential centrifugal sedimentation (DCS) is a further fractionating analytical method, which can be used to determine the size distribution of a given sample.[445, 446] Here, the sample is injected in the center of a spinning disc containing a concentration gradient of an aqueous sucrose solution. A UV-absorbance detector located close to the outer circumference of the disc is used to measure the sedimentation time of the sample and its concentration. DCS can be used as a detection method not only for the hard corona but also for the soft corona.[446] Walczyk *et al.* applied various techniques (DCS, DLS, TEM) to characterize different polystyrene and silica nanoparticles in human plasma without (*in situ*) and with prior separation from excess plasma proteins (*ex situ*).[222] The

results of all three methods were consistent, demonstrating a robust protein coating on the nanoparticle surfaces upon plasma incubation with no significant difference between the *in situ* and the *ex situ* approach. This indicated that the nanoparticle-protein complexes could be physically isolated without changing the structure. Time-resolved studies, however, revealed a size increase for the *in situ* approach but no changes in nanoparticle size for the *ex vivo* approach.

Notably, in contrast to the other fractionating methods, AUC and DCS typically do not allow the collection of the fractionated sample.

4.2.5.4 Other methods for the characterization of physico-chemical nanoparticle properties influenced by biofluids

Tunable resistive pulse sensing (TRPS) is a high-resolution technique for size and zeta-potential measurements of nanoparticle dispersions in complex media (such as blood serum or plasma),[401, 402, 404] and has proved to be an alternative to other characterization methods as described in sections *4.2.5.1 – 4.2.5.3*.[402-404, 416] It works according to the Coulter Counter principle.[417, 447, 448] Hereby, changes in the ionic current, caused by (nano)particles passing through a single size-tunable elastomeric pore (“blockade” event), are detected particle-by-particle.[404] By monitoring the changes in blockade width, magnitude and frequency, zeta-potential, size, and concentration of colloidal dispersions can be determined *in situ*.[401] The sensitivity can be improved by adjusting the pore size.[449] Limitations of light scattering techniques (*e.g.*, DLS or PTV) like the high sensitivity towards the presence of larger particles/agglomerates as well as the inability to characterize highly polydisperse systems do not play a role in TRPS measurements.[402, 404, 416]

Agarose gel electrophoresis can be used to assess serum stability of nucleic acid delivery systems.[28, 29, 450-452] Free nucleic acid can be monitored by staining with *e.g.*, ethidium bromide or GelRed. Berger *et al.*, for example, tested the stability of plasmid DNA (pDNA) complexes in 90% serum.[29] The serum stability was strongly dependent on the backbone of the peptide-like carriers as well as the length of the lipidic unit within the carriers. Cysteine-containing carriers led through crosslinking to more stable complexes; and longer fatty acids provided higher stability by hydrophobic interactions. Karimov *et al.* formed complexes from tyrosine-modified linear polyethylenimine (LPEI) 10 kDa and siRNA, which displayed good stability in 50% serum as determined *via* agarose gel shift

assay.[451] By incubation of the complexes in tumor tissue and cell lysates, they demonstrated that the complexes at least partially disassembled at these conditions, confirming the possibility of siRNA release from the complexes upon cellular internalization.

A serum stability turbidity assay[453] was utilized by Kaczmarek *et al.* to detect serum-induced nanoparticle precipitation.[454] For this purpose, absorbance measurements at 660 nm (no interference with serum components at this wavelength) were done after indicated serum incubation times. A decrease in optical transmittance corresponded to nanoparticle precipitation, as confirmed by quantification of the cargo mRNA in the supernatant. With this assay, they optimized co-formulations of poly(β-amino esters) (PBAEs) with PEG-lipid for mRNA delivery. Serum stability was achieved by higher amounts of PEG-lipid. The optimized nanoparticles exhibited increased *in vitro* mRNA transfection efficiency and functional mRNA delivery to the lungs upon systemic application in mice.

X-ray based techniques (imaging, spectroscopy, scattering) to investigate the nano-bio interface are reviewed in detail by Sanchez-Cano *et al.*[455] The authors expect that with improved compact X-ray sources such methods can be applied to study the fate of nanoparticles *in situ* in animals and even humans.

4.3 Impact of the protein corona on the biological activity of nanoparticles

Besides the aforementioned impact of the protein corona on physico-chemical properties of the nanoparticles in physiological environment (section **4.2**), this protein corona also dictates the biological activity of the nanoparticles.[37] The *in vivo* performance of the nanoparticles can completely differ from their *in vitro* behavior. Pharmacokinetics and biosafety can be completely changed compared to the *in vitro* experimental results. Therefore, more efforts have been made in recent years to develop *in vitro* assays that better describe the *in vivo* situation. In this context, the focus is on the effects of the protein corona on cellular binding and internalization, targeting capability, drug release, transfection efficiency, and toxicity of the nanoparticles (**Figure 4.8**). **Table 4.3** gives an overview over selected examples, which are also described in more detail in the text.

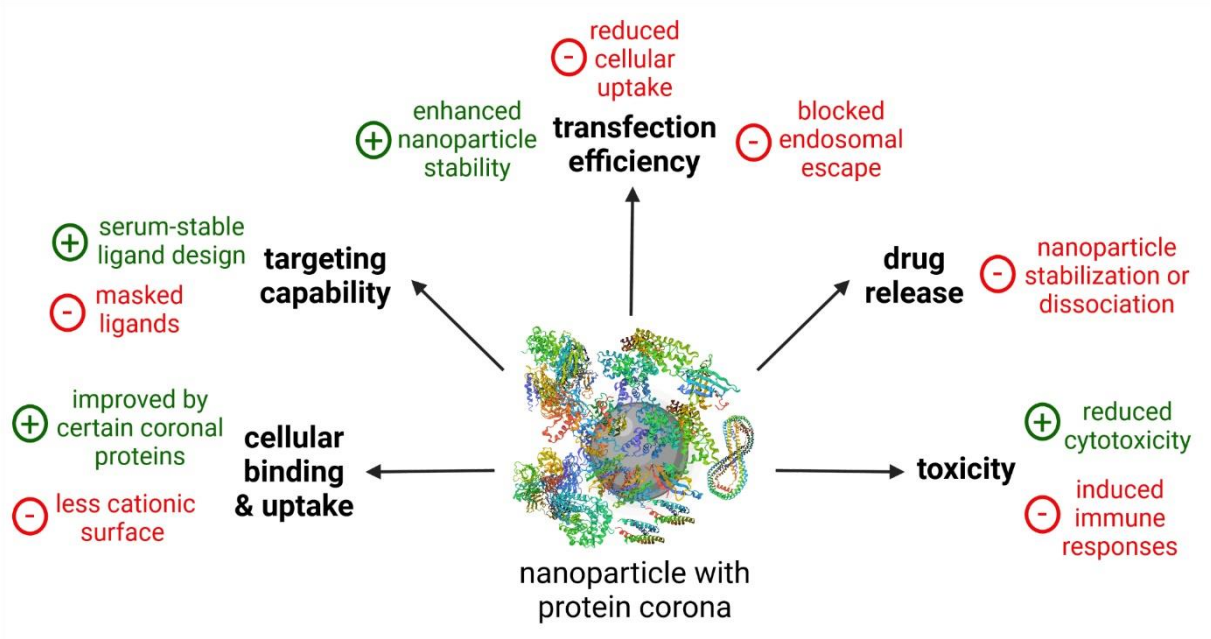

Figure 4.8. Effects of the protein corona on the biological activity of nanoparticles. Created with BioRender.com.

Table 4.3. Examples investigating the biological activity of nanoparticles in the presence of biofluids.

Nanoparticles	Biofluid	Protein corona	Biological impact	Reference
Cellular uptake and internalization				
Polystyrene NPs	10% FBS, static vs dynamic incubation	Dynamic incubation: protein-enriched corona (esp. plasminogen)	Dynamic incubation: reduced binding to HeLa cells	[41]
Unmodified LNPs	50% FBS, static vs dynamic incubation	Dynamic incubation: increased levels of α_1-antitrypsin in the PC	Dynamic incubation: increased uptake in HeLa cells, whereas decreased uptake in MCF-7 cells	[42]
Differently functionalized polystyrene NPs	HS, ratio of total particle-surface area to serum concentration = 5 mL/m^2	ApoH-enriched PC	Increased uptake in HeLa cells and hMSCs	[393]
		ApoA4- and ApoC3-enriched PC	Decreased uptake in HeLa cells and hMSCs	
Liposomes modified with PEG or hb-PG	5% and 100% HP	Neglectable PC formation	PEG: decreased uptake in RAW264.7 cells; hb-PG: increased uptake in RAW264.7 cells	[43]
Targeting capability				
hTf-functionalized silica NPs	10% FBS	n.d.	Abolished targeting efficiency	[50]
Tf-modified virus-like nanoparticles	55% FBS, murine, or chicken serum	Minor PC formation	No effect on targeting efficiency	[456]
	55% HS		Reduced targeting efficiency (competing hTf)	
mAB-conjugated liposomes	CD-1 mouse plasma *in vitro* vs *in vivo*	Amount of adsorbed proteins comparable for *in vitro* and *in vivo* PC, but *in vivo* PC composition more complex	No full inhibition of the targeting efficiency for the *in vivo* PC, but for the *in vitro PC*	[293]
Drug release				
4-nitroanisole loaded polymeric nanocapsules	10% or 100% FBS	n.d.	Minimal change in release profile	[255]
Tamoxifen-loaded SPIONs	10% or 100% FBS	n.d.	Reduced burst effect	
Albumin-bound paclitaxel drug (Abraxane®)	10% or 100% FBS or HP	n.d.		
Transfection efficiency				
Carboxymethyl poly(*L*-histidine)/ poly(β-amino ester) (PbAE)/pDNA ternary complexes	5 – 50% FBS	n.d.	HEK293 cells: improved serum-resistance and gene transfer	[457]
PEG-coated polyplex micelles loaded with bundled mRNA	50% FBS	n.d.	Improved serum stability and transfection efficiency (Huh7 cells)	[450]
T-Shape oligoaminoamides / pDNA complexes	45%, 90% FBS	n.d.	N2a and Huh7 cells: decreased transfection efficiency in high serum due to inhibited lytic activity	[29]
Gene transfectants histone H1 and cationic lipid DOSPER	> 10% FCS	n.d.	ECV 304 cells: inhibited transfection efficiency, remedy by addition of calcium ions or chloroquine	[458]

Table 4.3 *continued.*

Tyrosine-modified LPEI 10 kDa / siRNA complexes	50% FCS	n.d.	H441 cells: no decrease in transfection efficiency	[451]
Tyrosine-modified disulfide-crosslinked BPEI 2 kDa / pDNA complexes	50% FCS	n.d.	PC3 cells: no decrease in transfection efficiency	[452]
Toxicity				
Cationic polystyrene NPs	10% fluorescent labeled FBS	n.d.	1321N1 cells: reduced cytotoxicity due to masked cationic charges	[459]
Silica and polystyrene NPs	90% HP	Rapidly formed PC containing >300 different proteins	Reduced hemolysis, thrombocyte activation, and endothelial cell death	[258]
Magnetic NPs	2.5%, 10%, 40% HS	n.d.	No hemolytic effect	[460]
Silver NPs	1 or 10% FBS	Strongly attached PC	J774 cells: decreased cytotoxicity due to sulphidation	[257]
PEI 5 kDa; PEI 25 kDa PEG-free and PEGylated (2 kDa, 20 kDa; different grafting degrees (1; 10))	*In vitro:* HS; *in vivo:* pig model, *i.v.* injection	*In vitro*: formation of the complement terminal complex (SC5b-9); *in vivo*: cardiopulmonary changes in pigs	*In vitro:* complement activation only for PEG-free PEI 25 kDa; *in vivo*: PEG of ≥ 20 kDa may be favorable in terms of less complement activation	[40]

ApoA4/C3/H, apolipoprotein A4/C3/H; BPEI, branched polyethylenimine; pDNA, plasmid DNA; FBS, fetal bovine serum; FCS, fetal calf serum; hb-PG, hyper-branched polyglycerol; HP, human plasma; HS, human serum; *i.v.*, intravenous; LNPs, lipid nanoparticles; LPEI, linear polyethylenimine; mAB, monoclonal antibody; n.d., not determined; NPs, nanoparticles; PC, protein corona; PEG, polyethylene glycol; PEI, polyethylenimine; siRNA, small-interfering RNA; SPIONs, superparamagnetic iron oxide NPs; Tf, transferrin; hTf, human Tf.
Cell lines: 1321N1, human brain astrocytoma cell line; ECV 30, spontaneously transformed, human umbilical vein endothelial cell line; H441, human lung adenocarcinoma cell line; HEK293, human embryonic kidney cells; HeLa, human cervix carcinoma cells; hMSCs, human mesenchymal stem cells; Huh7, human hepatocellular carcinoma cell line; J774, murine macrophage cell line; MCF-7, human breast adenocarcinoma; N2a, murine neuroblastoma cell line Neuro2a; PC3, human prostate carcinoma cell line; RAW264.7, murine monocyte/macrophage-like cell line.

4.3.1 Cellular binding and uptake

The impact of the protein corona on the cellular uptake of nanoparticles can be studied by flow cytometry and confocal microscopy.[41, 43, 393, 461, 462] Silica nanoparticles for instance showed a stronger cell adhesion and enhanced cellular internalization under serum-free conditions as determined *via* flow cytometry, confocal and electron microscopy.[461] Another work evaluated the impact of static versus dynamic incubation with 10% fetal bovine serum (FBS) on protein corona formation and cellular binding efficiency of polystyrene nanoparticles.[41] The protein corona composition was highly dependent on the initial mixing. Incubation under flow resulted in nanoparticle-protein complexes with protein-enriched (especially plasminogen) corona. The binding of these complexes to

human cervical cancer cells (HeLa) was reduced compared to static incubation, as determined *via* flow cytometry. Palchetti *et al.* also found that changes in the protein corona induced by dynamic incubation with 50% FBS affected the uptake of unmodified LNPs in HeLa cells.[42] However, in this study dynamic flow led to an increased internalization in HeLa cells most likely due to increased levels of α_1-antitrypsin in the protein corona under flow conditions, an important promoter of nanoparticle-cell association [338]. These results were cell-line dependent. In a second tested cell line, human breast adenocarcinoma (MCF-7) cells, circulating FBS (especially at longer exposure time) had less effect on the cellular uptake, leading only to a small decrease.[42] Ritz *et al.* identified that cellular internalization of differently functionalized polystyrene nanoparticles is regulated by certain corona proteins.[393] Firstly, they determined the relative protein corona composition *via* quantitative LC-MS and correlated these findings with the cellular uptake into human cancer and bone marrow stem cells. In a next step, they validated key candidate proteins by artificially coating nanoparticles with the individual proteins. Apolipoprotein ApoH was found to increase cellular uptake, while apolipoproteins ApoA4 and ApoC3 acted rather as masking proteins and significantly decreased internalization. The effect of surface functionalization with two different hydrophilic polymers (PEG and hyper-branched polyglycerol (hb-PG)) on protein corona formation and internalization of liposomes in macrophages was investigated by Weber *et al.*[43] The low protein adsorption was comparable for unmodified as well as both functionalized liposomal formulations, whereas the cellular uptake completely differed. PEGylation led to the expected decreased internalization. Functionalization with hb-PG, however, surprisingly enhanced the uptake independent of the protein corona. Thus, it is assumed that this is a liposome-specific rather than a protein corona effect.

Protein corona may also be positively required for functional delivery, as highlighted for the case of LNPs with diffusible PEG-lipids.[24, 463, 464] *In vivo* accumulation and transfection potency of LNPs requires apolipoprotein E (ApoE) adsorption to the nanoparticle surface in the blood stream, resulting in receptor-mediated uptake by ApoE-dependent low density lipoprotein (LDL) receptors on the sinusoidal surface of hepatocytes. In an ApoE knockout mouse model the transfection activity was abolished.

4.3.2 Targeting capability

Ligands (especially peptide- and protein-ligands) are often not sufficiently stable in physiological environment and rapidly degraded (*e.g.*, by serum proteases). Cyclization, amino acid modifications or a so-called “retro-enantio” approach can be advantageous in terms of increased protease resistance and serum stability.[465, 466] In other cases, targeting ligands can be masked/blocked by components of the protein corona, which results in a reduced ligand recognition by receptors on the cell surface.[44, 467] By this, the targeting capability of nanoparticles can be drastically diminished in biological environment as proven in a model targeting reaction.[468] Both the presence of 10% (mimicking *in vitro* conditions) and 100% (mimicking *in vivo* conditions) serum inhibited the copper-free click reaction between fluorescent cycloalkyne-functionalized nanoparticles and azide-bearing silicon substrate monolayer as determined *via* fluorescent and scanning electron microscopy. Salvati *et al.* demonstrated *via* flow cytometry that the targeting specificity of silica nanoparticles functionalized with human transferrin disappeared in the presence of already 10% fetal bovine serum (FBS).[50] In contrast, Zackova Suchanova *et al.* showed that the protein corona formed in 55% FBS, mouse or chicken serum did not influence transferrin-receptor (TfR) targeting of transferrin-modified virus-like nanoparticles.[456] Serum proteins adsorbed only to a small extent as determined *via* SDS-PAGE, DLS and TEM. However, in human serum a decreased targeting capability was observed due to the high content of competing human transferrin. TfR targeting in the presence of serum (different types and amounts) with and without human transferrin competition was evaluated *via* an enzyme-linked immunosorbent assay (ELISA) as well as by uptake studies in TfR-expressing cells *via* flow cytometry and confocal microscopy. A comparison between the *in vitro* and *in vivo* formed protein coronas and their impact on the targeting capability of monoclonal antibody-conjugated liposomes was conducted by Hadjidemetriou and colleagues.[293] Both protein coronas significantly reduced cellular internalization as visualized with confocal microscopy. Interestingly, the *in vivo* protein corona, unlike the *in vitro* corona, did not lead to a full inhibition of the targeting efficiency. Last but not least, standard 2D cell culture systems do not at all represent the physiological real situation, with continuous blood flow and cells growing in all three dimensions. The ability of ligands to find and bind with their cellular targets can be more realistically evaluated in cellular adhesion models

under flow conditions.[469] Accessibility of target cells is better simulated in 3D multicellular spheroids and organoids.[470-473] Such 3D culture systems display heterogeneous cell populations, cell-to-cell and cell-to-extracellular matrix interactions.[472] Thus, they recapitulate the *in vivo* situation to a greater extent compared to 2D cell monolayers.[472] Spheroids are mostly used in cancer research. Whereas, the more advanced organoids, derived from pluripotent stem cells, progenitor cells of specific tissues or patients,[472, 474] can be used for different disease models.[475-478] Assembloids are generated by spatial organization of multiple cell types and are considered to even better mimic *in vivo* tissues.[474, 479] A combination of 3D cell culture and microfluidics can be realized with the "organ-on-a-chip" technology.[470, 472, 480] Bioengineering can help to construct more physiologically relevant spheroid/organoid models, *e.g.*, by incorporating vasculature,[480, 481] microenvironment,[472] or even the immune system.[482, 483] The microfluidic "organ-on-a-chip" systems enable high-throughput screening and are seen as potential alternative to animal models.[472, 478] This will speed up efficient preclinical research in the areas of drug discovery as well as precision, regenerative and personalized medicine.[474]

4.3.3 Drug release

Controlled drug release is important for successful delivery, an instant release has to be avoided.[255] The protein corona can affect the drug release profile of nanocarriers in two contrary directions by (*i*) destabilizing the delivery system leading to disassembly or aggregation,[284] or (*ii*) by additional shielding and stabilization [255]. Instability in physiological environment can result in immediate drug release. In the case of therapeutic nucleic acids, this would lead to rapid clearance and ineffectiveness. [3] Whereas, severe toxic effects would be the consequence in the case of chemotherapeutics (*i.e.*, burst effect).[255] Buyens *et al.* developed a fluorescence fluctuation spectroscopy-based *in situ* method to quantitatively investigate the integrity of siRNA-nanocarrier complexes in complex biological fluids like full human serum.[284] Amin *et al.* evaluated the stability of liposomal doxorubicin nano formulations in 30% serum by measuring the amount of free, released drug using high performance liquid chromatography (HPLC).[484] Detection of mRNA intactness after serum incubation *via* quantitative reverse transcriptase polymerase chain reaction (qRT-PCR) can be a method to assess serum stability (more precisely, serum-RNase resistance) of mRNA-nanocarrier systems.[450, 485-491] A detailed investigation of the influence of the protein corona on drug release profiles was performed

by Behzadi and co-workers.[255] They evaluated (*i*) tamoxifen-loaded SPIONs in 10% or 100% FBS, (*ii*) 4-nitroanisole loaded polymeric nanocapsules in 10% or 100% FBS, and (*iii*) albumin-bound paclitaxel drug (Abraxane®) in 10% or 100% FBS or human plasma. Drug release was determined by UV (in the case of tamoxifen) or HPLC (in the case of 4-nitroanisole and paclitaxel) after centrifugation or *in situ*. This study demonstrated that the drug release profiles are affected by the protein corona (*i.e.*, types and amounts of corona proteins), but to a different extent for the different nanocarrier types. In the case of SPIONs and Abraxane®, the protein corona could strongly reduce the burst effect. For polymeric nanocapsules, the protein corona only slightly changed the release profile.

4.3.4 Transfection efficiency

Transfection experiments in high serum can help to better predict *in vivo* efficacies of nucleic acid nanocarriers.[29, 458, 492] Read-out is done by reporter assays such as luciferase [29, 450-452, 458, 492] or eGFP (enhanced green fluorescent protein) expression assays.[457, 493] *In vitro* protocols often recommend transfection under serum-free conditions for optimum gene transfer, as transfection efficiency of lipidic nanocarriers was found to be inhibited even at the standard moderate amounts of ~10% serum in the transfection medium.[462, 492, 494] As prescreen for subsequent *in vivo* application, the use of 10% serum-supplemented medium has been frequently applied.[493, 495-497] However, optimization of nanocarriers for efficient delivery at high serum content (50% and higher), as done for instance by Chan *et al.* for their cationic liposome-DNA complexes,[492] is advisable for a more reliable prediction of the *in vivo* transfection performance. Gu *et al.* improved the serum-resistance and gene-transfer efficiency in 50% serum of DNA-poly(β-amino ester) (PBAE) complexes through electrostatic coating with carboxymethyl poly(*L*-histidine) (CM-PLH), as demonstrated *via* flow cytometry and fluorescence microscopy.[457] Koji *et al.* were able to improve serum stability and transfection efficiency in 50% serum by loading PEG-coated polyplex micelles with bundled mRNA (*i.e.*, sterically stabilized, tight mRNA structure).[450] Olden *et al.* needed higher polymer content in their mRNA and pDNA nano formulations to achieve transfection efficiency in medium supplemented with 10% FBS.[493] This can be explained by the fact that free polymers, known to facilitate gene transfer,[498] are partially blocked by serum components. Berger *et al.* made a similar observation that serum-treated (45% and 90% serum) carriers exhibited reduced transfection efficiency.[29] Cell culture screening in standard 10%

serum-supplemented medium had identified lipo-peptide nanocarriers with high gene transfer potency; subsequent evaluation in full serum blocked the lytic potential of such lipo-peptide carriers. As endosomolytic potential is one of the most important promoters for endosomal escape and thus gene delivery, a decreased *in vitro* gene-transfer performance was observed in full serum. This also explained the moderate *in vivo* results, which fell short of the expectations of standard *in vitro* transfections (in presence of 10% serum). Notably, *in vitro* gene transfer of gold standard LPEI 22 kDa was less to not affected by high serum content,[29] which is in line with the good *in vivo* performance as demonstrated in many publications.[143, 498-502] The endosomal release of LPEI complexes apparently works according to mechanisms different from membranolytic interactions.[88, 230] Haberland *et al.* also found for other gene transfectants (histone H1 and cationic lipid DOSPER) that the endosomal escape was responsible for the reduced transfection efficiency in serum of 10% and higher.[458] This serum-inhibition could be overcome by calcium ions (in the form of nascent calcium phosphate micro-precipitates) and chloroquine in the cell culture medium, which both promote endosomal/lysosomal release through their fusogenic and membranolytic activity.[503] Consistent with the above-mentioned good performance of LPEI in serum, Karimov *et al.* showed that the gene silencing efficiency of siRNA complexed with tyrosine-modified LPEI 10 kDa was not decreased in the presence of 50% serum.[451] On the contrary, serum may even be advantageous regarding preservation of bioactivity during prolonged storage of the complexes, as shown for storage for three days at 4 °C, room temperature and 37 °C. Similar findings were also made for pDNA complexed with disulfide-crosslinked, tyrosine-modified branched PEI 2 kDa.[452]

4.3.5 Toxicity

The protein corona impacts the biosafety and toxicity profile of nanoparticles.[256, 258] Especially cationic nanoparticles are prone to interfere with the (predominately) negatively charged bio membranes, resulting in membrane disruption at multiple stages.[3, 88] The formed protein corona can more or less shield the nanoparticles and by this reduce interactions with cell membranes (*e.g.*, of thrombocytes, erythrocytes, or endothelial cells). This protective effect of the protein corona was demonstrated for instance by Dawson and his team.[459] The adsorbed serum proteins on cationic polystyrene nanoparticles prevented cell damage induced by the bare nanoparticle surface until the

protein corona was enzymatically degraded in the lysosomes. In the context of pathophysiology, the protein corona can lower the risk for nanoparticle-induced thrombocyte activation/aggregation, erythrocyte aggregation or hemolysis, and cell death in general. Tenzer *et al.* demonstrated this and showed that the rapidly formed protein corona strongly improved the toxicity profile of the tested nanoparticles.[258] Cytotoxicity can be assessed inter alia by cell viability assays (*e.g.*, quantification of ATP)[29, 258] or by microscopic observation of cell morphology[504]. Thrombocyte aggregation can be evaluated *via* aggregometry measurements.[258] An assay to visualize nanoparticle-induced erythrocyte aggregation was developed by Ogris *et al.*[38] Yallapu *et al.* investigated the interaction of magnetic nanoparticles with erythrocytes *via* a hemolysis assay (spectrophotometric quantification of hemoglobin release) and SEM.[460] Both the nanoparticles without and with protein coronas showed no hemolytic activity. A detailed study on membrane interactions of gold nanoparticles was conducted by Wang *et al.*[336] They found a protective effect of the serum protein corona against cell membrane damage. Eventual cell membrane damage was evaluated by environmental SEM as well as TEM, and quantification of LDH (lactate dehydrogenase) release. Cytotoxicity was measured by an apoptosis/necrosis ratio analysis using flow cytometry, a CCK-8 assay to determine the activity of the mitochondrial dehydrogenase, and a live/dead assay.

The protein corona can also alter the biotransformation of the nanoparticles as found for instance for silver nanoparticles.[257] In this study, the hard corona mediated sulphidation, resulting in decreased cytotoxicity.

In contrast, immune responses (innate as well as adaptive) may be triggered by protein corona components (*e.g.*, by stimulation of immune cells or by complement activation), which may lead to immunotoxic effects.[256] Cationic nanoparticles, for example, can directly bind complement proteins and activate the alternative pathway of complement, or subsequent to protein binding the classical pathway, often resulting in serious toxicity.[39, 40]

4.4 *In vivo* screening using barcoded nanoparticles

Despite of all the additional information about nanoparticle properties in biofluids that can be obtained using the *in vitro* methods described in sections **4.2** and **4.3**, there are still uncertainties about the *in vivo* performance. Biodistribution and corresponding off-target effects, for example, can be hardly predicted with *in vitro* experiments alone, making *in vivo* studies inevitable. Dahlman and coworkers developed a high-throughput *in vivo* screening method, where simultaneously hundreds of nanoparticles can be tested within a single mouse.[248, 505] This not only accelerates the discovery of potent *in vivo* delivery systems and reduces the costs of *in vivo* studies but is also beneficial in view of the so-called “3R principle” (*i.e.*, replace, reduce, refine) for a rational use of animals. This technology utilizes DNA barcodes, which are individually formulated into chemically distinct nanoparticles. DNA barcodes are single-stranded DNA oligonucleotides (~ 60 nucleotides) with terminal stabilizing phosphorothioate-modifications, 8-10 central nucleotides serving as individual barcode, and the 3’- and 5’-ends as priming sites for next generation Illumina deep sequencing (**Figure 4.9A**).[248] The different barcoded nanoparticles are then co-administrated in mice and later on quantified simultaneously (**Figure 4.9B**). Initially, Dahlman *et al.* demonstrated the predictability of the *in vivo* biodistribution of siRNA LNPs by this DNA barcoding system.[248] In a follow-up study, this technique, which is named Joint Rapid DNA Analysis of Nanoparticles (JORDAN), proved to enable analysis of hundreds of nanoparticles at the same time.[30, 506] Subsequently, improvements were made regarding DNA barcode stability[507] and optimization of DNA-amplification (*e.g.*, QUANT barcodes for a more sensitive multiplexed analysis by Droplet Digital PCR).[508] In early works, only biodistribution was investigated,[30, 248, 505, 508] whereas later on functional testing was possible by using a high-throughput method to quantify functional mRNA[509-511] or siRNA delivery,[512, 513] which is termed Fast Identification of Nanoparticle Delivery (FIND). Individual DNA barcodes and the functional nucleic acid (*e.g.*, specific mRNA or siRNA) were co-formulated in single nanoparticles and applied in appropriate reporter mouse models (**Figure 4.9C**). After isolating successfully transfected cells by fluorescence-activated cell sorting (FACS), they were deep sequenced to identify the bioactive nanoparticles. To sum up, with this new high-throughput barcoding system, screening of several hundreds of nanoparticles at once *in vivo* is possible. It allows the investigation of functional delivery alongside biodistribution

[514]. By this, knowledge about the on-target to off-target ratio of nanoparticulate delivery systems can be gained, which is important for developing and improving therapeutics such as RNA therapeutics for COVID or cystic fibrosis.[514, 515]

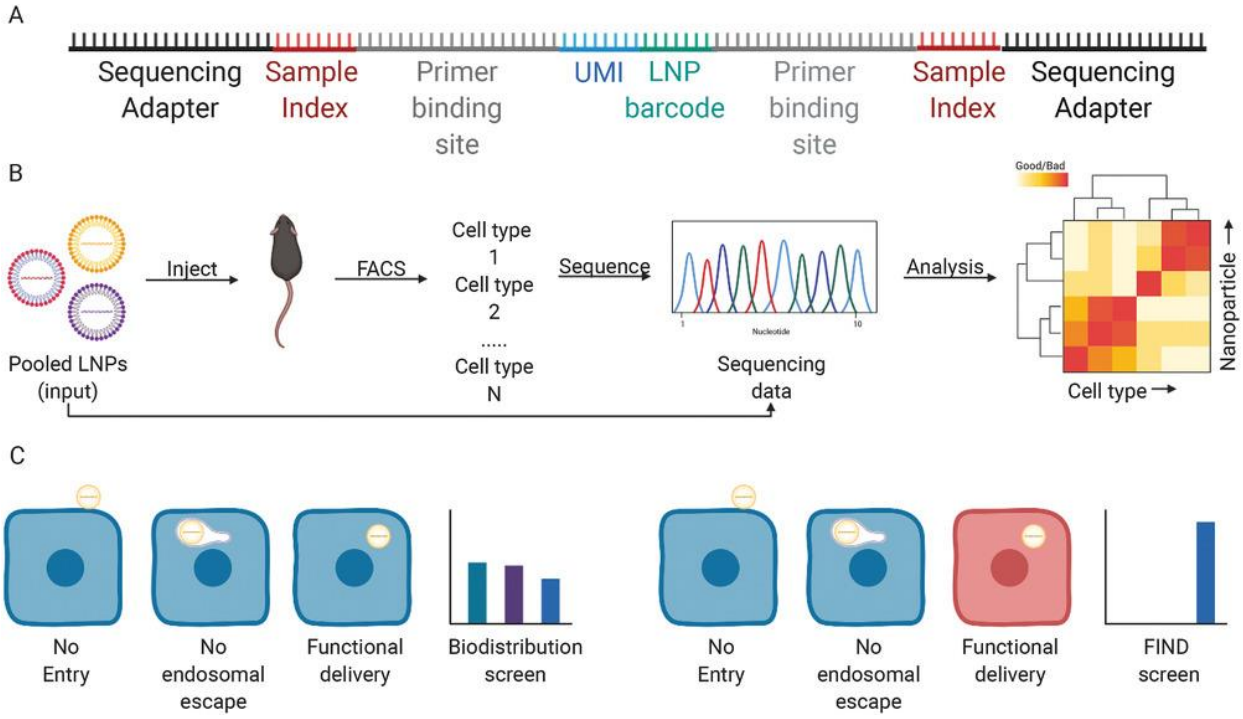

Figure 4.9. Principle of the high-throughput barcoding system developed by Dahlman and co-workers. (**A**) Structure of the DNA barcodes with 8-10 central nucleotides (green) as barcode region. (**B**) Several hundred different barcoded nanoparticles (*e.g.*, lipid nanoparticles, LNPs) are co-administrated in mice. With next generation sequencing, the *in vivo* biodistribution of the distinct barcoded nanoparticles can be analyzed simultaneously. This technology is termed Joint Rapid DNA Analysis of Nanoparticles (JORDAN). (**C**) JORDAN does not allow for functional delivery screening, as this method does not discriminate between nanoparticles outside or inside the cells (*left*). Fast Identification of Nanoparticle Delivery (FIND) provides a remedy (*right*). Here, successfully transfected reporter cells are identified. Reproduced with permission from Adv Healthcare Mater 10, e2002022 (2021).[514] Copyright © 2021; John Wiley and Sons.

Another barcoding system was developed by Yaari *et al.* to detect the therapeutic potential of different anticancer drugs (gemcitabine, doxorubicin, cisplatin) even at the single-cell level.[516] They loaded liposomes with various chemotherapeutics and corresponding double-stranded DNA barcodes, which differed in length, sequence, and primers. Detection of the distinct DNA barcodes was done – in contrast to the next generation sequencing used by Dahlman and co-workers – by real-time PCR, gel electrophoresis and conventional sequencing. A correlation was found between the barcode distribution

in cells and the therapeutic potency.

All in all, these barcoding techniques have the potential to make the preclinical pipeline more efficient[517] and, as a diagnostic tool, to lead to personalized therapy.[516]

4.5 Conclusion

When predicting *in vivo* performance from *in vitro* data, it has to be considered that each of the above-mentioned characterization methods has advantages and limitations. None of these methods is able to completely illustrate the nanoparticle properties in physiological environment.[374] The experimental set-up and the characterization technique chosen can have a huge impact on the outcome.[272, 302] Combination of several analytical and biological as well as *ex situ* and *in situ* methods is advisable to get a better and more detailed insight into the *in vivo* characteristics and behavior of the nanoparticles. In addition, the choice of the biofluid (serum, plasma, or full blood; animal origin) is of great importance as different biological fluids can have a huge impact on the resulting protein corona composition and thus also on the physicochemical and biological properties of the nanoparticle. This has been demonstrated in several publications.[518-525] However, up to now, this aspect has been rather neglected and biofluids have been used inconsistently and interchangeably. For the future, it is recommended that the biofluid source for *in vitro* investigation is selected matching to the *in vivo* studies.[518, 520, 521] Furthermore, testing in human plasma is considered to be one step closer to the translatability of the nanoparticles' performance in humans.[518, 520]

Physiologically relevant *in vitro* settings include, for example, screening in (*i*) full serum, [29] (*ii*) 3D multicellular spheroid and organoid cell culture,[472, 473, 480] (*iii*) static and dynamic air-liquid interfaces,[54, 526-529] (*iv*) BBB models [57, 247] and other disease models,[54, 242-244] or (*v*) cellular adhesion models under flow conditions.[469] Moreover, the gained knowledge about protein corona formation can be exploited to optimize carriers for nanomedical application.[37]

However, some information like *in vivo* biodistribution and off-target effects cannot be obtained from *in vitro* experiments. Consequently, *in vivo* studies are still necessary. With new high-throughput *in vivo* screening methods like the barcoding system of Dahlman and co-workers,[248] such *in vivo* investigations can be more effective, economical, and ethical.

The main goal is to generate large datasets about nanoparticle characteristic in physiological environment and analyze them appropriately.[517] In this respect, the establishment of standardized protocols is of great importance for more consistent, robust and comprehensive pre-clinical studies (*in vitro* characterization, animal models) with reproducible and reliable results.[412] By this, structure-activity relationships and *in vitro-in vivo* correlations can be derived.[32, 517] This knowledge can then be transferred to the rational design of nanoparticles for specific cargos and specific target cell types.

However, there is still an uncertainty about translatability from small to large animals and humans.[517, 530-532] So far, there are no systematic studies available, which address this subject. Species- and strain-dependent biological factors can influence the nanoparticle delivery. In the future, the question how well preclinical animal models predict nanoparticle performance in humans has to be investigated in more detail. Bioinformatics could help to identify best fitting animal models for certain diseases as recently shown for SARS-CoV-2.[533] Alternatives to animal models such as *in ovo* testing, microfluidic “human-organ-on-a-chip” technology as well as *in silico* predictions can be promising strategies for replacing animal studies in the future.[531, 534, 535]

Another aspect, which has to be considered, is that the protein corona differs between individuals and is disease-specific.[536-538] In this context, pharmacogenomics and personalized, patient-specific nanomedicine will gain importance.[44]

4.6 Abbreviations

ACE, affinity capillary electrophoresis; AF4, asymmetrical flow field-flow fractionation; AFM, atomic force microscopy; ASO, antisense-oligonucleotides; AUC, analytical ultra-centrifugation; BBB, blood-brain-barrier; BCA, bicinchoninic acid; BSA, bovine serum albumin; CD, circular dichroism; DCS, differential centrifugal sedimentation; DDLS, depolarized dynamic light scattering; DLS, dynamic light scattering; eGFP, enhanced green fluorescence protein; ELS, electrophoretic light scattering; ELISA, enzyme-linked immunosorbent assay; EPR, enhanced permeation and retention; ESI, electrospray ionization; FACS, fluorescence-activated cell sorting; FCS, fluorescence correlation spectroscopy; FFF, field-flow fractionation; FIND, Fast Identification of Nanoparticle Delivery; FT-IR, Fourier transform infrared; I, human serum albumin; HDC, hydrodynamic chromatography; ICP-MS, inductively coupled plasma mass spectrometry; IEF, isoelectric

focusing; ITC, isothermal titration calorimetry; JORDAN, Joint Rapid DNA Analysis of Nanoparticles; LC-MS, liquid chromatography-mass spectrometry; LDH, lactate dehydrogenase; LNP, lipid nanoparticle; MALDI matrix-assisted laser desorption/ionization; mRNA, messenger RNA; MS, mass spectrometry; MW, molecular weight; NMR, nuclear magnetic resonance; OAA, oligoaminoamide; pDNA, plasmid DNA; PEG, polyethylene glycol; PEI, polyethylenimine; PTV, particle tracking velocimetry; QCM, quartz crystal microbalance; QELS, quasi elastic light scattering; qRT-PCR, quantitative reverse transcriptase polymerase chain reaction; QSAR, quantitative structure-activity relationships; SANS, small angle neutron scattering; SAXS, small angle X-ray scattering; SDS-PAGE, sodium dodecyl sulfate polyacrylamide gel electrophoresis; SEC, size-exclusion chromatography; SEM, scanning electron microscopy; SERS, surface-enhanced Raman scattering; siRNA, small-interfering RNA; SLS, static light scattering; SPR, surface plasmon resonance; SR, synchrotron-radiation; TEM, transmission electron microscopy; TOF, time-of-flight; TRPS, tunable resistive pulse sensing; UPLC, ultra-performance liquid chromatography.

4.7 Acknowledgements

The authors are greatly thankful for support of their work by the German Research Foundation (DFG) *via* the Collaborative Research Center SFB 1066. Moreover, acknowledgements to the DFG SFB1032 sub-project B4 for the financial support of Prof. Dr. E. Wagner and his team.

5. Dynamic mRNA polyplexes benefiting from redox-sensitive cleavage sites for *in vitro* and *in vivo* transfer

Ana Krhač Levačić[a,‡] Simone Berger[a,‡], Judith Müller[b], Andrea Wegner[b], Ulrich Lächelt[a], Christian Dohmen[b], Carsten Rudolph[b], and Ernst Wagner[a,]*

[a] Pharmaceutical Biotechnology, Department of Pharmacy, and Center for NanoScience (CeNS), Ludwig-Maximilians-Universität (LMU) Munich, Butenandtstr. 5-13, D-81377 Munich, Germany
[b] Ethris GmbH, Semmelweisstr. 3, Planegg D-82152, Germany

‡ These authors contributed equally.
* Corresponding author: E. Wagner

This chapter is adapted from a pre-copy-edited version of a peer-reviewed research article published in ***J. Controlled Release* 2021, 339, 27-40 (ref. [539]).**

Author contributions

The manuscript was written through contributions of all authors. A. Krhač Levačić: Conceptualization, methodology, investigation, formal analysis, validation, visualization, writing and illustration – original draft, writing – review & editing; S. Berger: Conceptualization, investigation, resources, visualization, writing – original draft, writing – review & editing: J. Müller: Investigation; A. Wegner: Investigation, methodology; U. Lächelt: Conceptualization, writing – review & editing; C. Dohmen: Conceptualization, project administration; C. Rudolph: Conceptualization, project administration; E. Wagner: Conceptualization, project administration, supervision, writing – review & editing; funding acquisition. All authors gave approval to the final version of the manuscript.

Graphical abstract

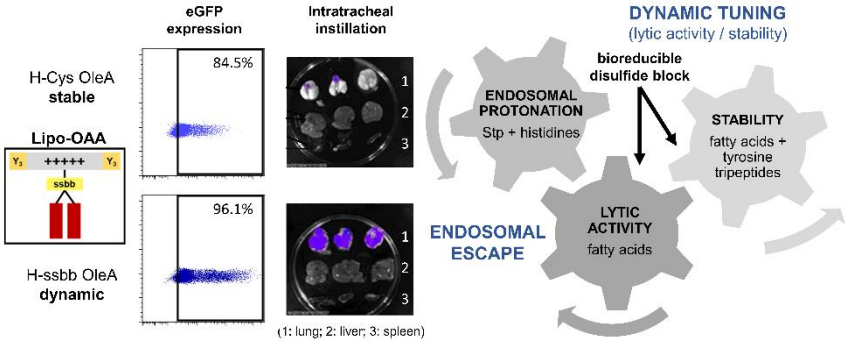

Highlights

- Succinylated branched polyethylenimine is a gold standard for mRNA delivery.
- A diverse library of polyethylenimine-like peptides was screened for mRNA delivery.
- Polyplex stability, endosomolytic activity, and intracellular release must be balanced.
- Incorporation of a dynamic bio-reducible motif was found to be most important.
- Intratracheal administration of mRNA complexes in mice confirmed the *in vitro* results.

Abstract

Currently, messenger RNA (mRNA)-based lipid nanoparticle formulations revolutionize the clinical field. Cationic polymer-based complexes (polyplexes) represent an alternative compound class for mRNA delivery. After establishing branched polyethylenimine with a succinylation degree of 10% (succPEI) as highly effective positive mRNA transfection standard, a diverse library of PEI-like peptides termed sequence-defined oligoaminoamides (OAAs) was screened for mRNA delivery. Notably, sequences, which had previously been identified as potent plasmid DNA (pDNA) or small-interfering RNA (siRNA) carriers, displayed only moderate mRNA transfection activity. A second round of screening combined the cationizable building block succinoyl tetraethylene pentamine and histidines for endosomal buffering, tyrosine tripeptides and various fatty acids for mRNA polyplex stabilization, as well as redox-sensitive units for programmed intracellular release. For the tested OAA carriers, balancing of extracellular stability, endosomal lytic activity, and intracellular release capability was found to be of utmost importance for optimum mRNA transfection efficiency. OAAs with T-shape topology containing two oleic acids as well-stabilizing fatty acids, attached *via* a dynamic bioreducible building block, displayed superior activity with up to 1000-fold increased transfection efficiency compared to their non-reducible analogs. In the absence of the dynamic linkage, incorporation of shorter less stabilizing fatty acids could only partly compensate for mRNA delivery. Highest GFP expression and the largest fraction of transfected cells (96%) could be detected for the bioreducible OAA with incorporated histidines and a dioleoyl motif, outperforming all other tested carriers as well as the positive control succPEI. The good *in vitro* performance of the dynamic lead structure was verified *in vivo* upon intratracheal administration of mRNA complexes in mice.

Keywords

mRNA, polyplexes, bioreducible, redox-sensitive, dynamic delivery.

5.1 Introduction

Messenger RNA (mRNA)-based drug technologies have attracted serious attention over the past years.[540, 541] Clinically relevant fields comprise vaccination,[9, 542-545] protein replacement therapy (*e.g.*, in case of genetic diseases),[546, 547] as well as cancer immunotherapy.[541, 548, 549] CRISPR/Cas9 gene editing based on co-delivery of Cas9 mRNA and single-guide RNA (sgRNA) is another interesting application of mRNA technology.[12, 550, 551] Nowadays, the development of mRNA therapeutics is progressing rapidly. More and more mRNA-based approaches are entering clinical trials with great potential in revolutionizing the therapeutic landscape.[547, 552, 553] In the current SARS-CoV-2 pandemic, mRNA-based vaccines are the big hope to defeat this highly infectious and deadly viral disease.[23, 554-556] Since major limitations of mRNA (limited stability and moderate effectivity) were largely resolved by various chemical modifications,[541, 546, 557, 558] an important restriction remains in the intracellular delivery.[559] Carrier systems need to be adjusted for effective mRNA delivery.[13, 26, 541, 559] As several barriers must be overcome for successful mRNA transfer into the cytoplasm, the multifunctional and dynamic nature of such carriers is of great importance.[3, 13, 26, 559-564] On the one hand, stability is important during the extracellular delivery steps to protect the fragile mRNA cargo. While on the other hand, the carrier must intracellularly release mRNA in a form which can be translated. Over the past decades, significant efforts have been put successfully into the development of effective delivery vehicles.[25] Lipoplexes and lipid nanoparticles (LNPs) have maturated into the most refined methods for mRNA delivery[541, 549, 551, 565-592] especially to the liver and in vaccination. Polyplexes (*i.e.*, complexes of negatively charged nucleic acid with cationic polymers or peptides) represent another promising approach for mRNA formulation.[450, 454, 487, 488, 493, 560-564, 578, 579, 593-613] Amongst polycations, pH-dependent cationizable molecules such as polyethylenimine (PEI) and its various derivatives have demonstrated promising transfection activity *in vitro* and *in vivo*.[88, 143, 614-617] In 2001, low molecular weight PEI and PEI-melittin conjugates were successfully introduced for mRNA transfection[618] and subsequently for effective double-stranded RNA delivery.[619] More recently, chemical backbone variations were found superior for mRNA delivery.[607] Multifunctional polymer structures, however, are chemically more complex than lipidic systems. Solid-phase assisted peptide synthesis (SPPS) offers the opportunity to combine the advantageous functional properties of PEI

with the precision of peptide synthesis.[62, 63] For this purpose, we had designed 'mini-PEI' artificial amino acids for the synthesis of structurally precise peptide-like carriers (so-called oligoaminoamides, OAAs) with varying sequences.[64] As described here, a variety of such sequence-defined OAAs was screened for mRNA delivery. Interestingly, the initial pre-screening revealed structure-activity relationships extremely different from those already found for plasmid DNA (pDNA) and small-interfering RNA (siRNA). The best working carriers for pDNA and siRNA showed no activity in mRNA delivery. It is known from literature that different nucleic acids require different properties of their delivery vehicles.[13, 26, 620, 621] Also consistent with recent literature, a dynamic intracellular release of mRNA appears as function boosting successful delivery.[561-564] Starting from first promising mRNA carrier candidates of the pre-screening, a new library of T-shaped OAAs was analyzed for successful mRNA delivery *in vitro* and subsequently *in vivo*.

5.2 Experimental section/methods

5.2.1 Materials

All cell culture consumables were obtained from Faust Lab Science (Klettgau, Germany). Cell culture media, fetal bovine serum (FBS) as well as paraformaldehyde (PFA) were purchased from Sigma Aldrich. Antibiotics were purchased from Invitrogen (Karlsruhe, Germany), trypsin/EDTA (ethylenediaminetetraacetic acid) from Biochrom (Berlin, Germany), HEPES from Biomol GmbH (Hamburg, Germany), glucose from Merck (Darmstadt, Germany) and water for injection (WFI) from B. Braun (Melsungen, Germany). Agarose BioReagent – low EEO as well as glutathione (GSH) were purchased from Sigma Aldrich (Munich, Germany), and GelRed 10,000x from VWR (Darmstadt, Germany). Citrate-buffered human blood was provided by the hospital of the Ludwig-Maximilians-Universität (Munich, Germany). Heparin sodium (5000 IU/mL) was purchased from Ratiopharm (Ulm, Germany). Cell culture 5x lysis buffer, *D*-luciferin sodium salt and CellTiter-Glo were obtained from Promega (Mannheim, Germany); DAPI (4′,6-diamidino-2-phenylindole) and ethidium bromide (EtBr) from Sigma-Aldrich (Munich, Germany). Branched PEI (brPEI) 25 kDa was obtained from Sigma-Aldrich (Munich, Germany). Unmodified linear polyethylenimine (linPEI) 22 kDa and succinylated branched PEI (succPEI) 25 kDa (succinylation degree of 10%, 20%, 30%, and 50%) were resynthesized as described before.[206, 622] Sequence-defined oligoaminoamides (OAAs) applied in the

current study were synthesized *via* standard Fmoc SPPS as described previously.[28, 29, 64, 123, 137, 138, 200, 202, 204, 208, 209, 623, 624] The sequences, internal ID numbers and references to all used structures can be found in **Table 5.3**. Chemically modified stabilized non-immunogenic messenger RNA encoding firefly luciferase (mRNA-luc) or encoding enhanced green fluorescent protein (mRNA-EGFP) were produced, purified, and provided by Ethris GmbH.

5.2.2 Polyplex formation

Indicated amounts of mRNA-luc or mRNA-EGFP and calculated amounts of OAA at indicated N/P (nitrogen/phosphate) ratios or w/w (weight/weight) ratios (in the case of succPEI) were diluted in separate tubes of equal volumes of HBG (20 mM of HEPES, 5% glucose; pH 7.4) each. Only protonatable nitrogens of the Stp (succinoyl tetraethylene pentamine) units and *N*-terminal amines were considered in the N/P ratio calculations. The nucleic acid solution was added to the OAA solution, mixed by rapid pipetting, and incubated for 30 min at RT under exposure to air oxidation in a closed Eppendorf reaction tube.

5.2.3 Particle size and zeta potential measurement

Particle size and zeta potential of mRNA (lipo)polyplexes were measured in a folded capillary cell (DTS1070) by dynamic and electrophoretic laser-light scattering (DLS, ELS) using a Zetasizer Nano ZS with backscatter detection (Malvern Instruments, Malvern, United Kingdom). mRNA polyplexes were prepared with 2.5 µg of mRNA-luc at indicated w/w or N/P ratios (succPEI, w/w = 4; linPEI, N/P = 9; brPEI, N/P = 10; lipo-OAAs, N/P = 12) in a total volume of 200 µL of HBG. For size measurements, the equilibration time was 0 min, the temperature was 25 °C, and an automatic attenuator was used. The refractive index of the solvent was 1.330, and the viscosity was 0.8872 mPa·s; the refractive index of polystyrene latex (1.590) was fixed. Results were plotted as z-average and standard deviation (SD) out of three runs, with 12 sub-runs each. For zeta potential measurements, the samples were diluted to 800 µL in HEPES buffer (20 mM; pH 7.4). Zeta potentials were calculated by the Smoluchowski equation and are displayed in mV as average ± SD of three runs with up to 15 sub-runs each.

5.2.4 Agarose gel shift assay for mRNA binding

A 1% (w/v) agarose gel was prepared by dissolving agarose in TBE buffer (trizma base

10.8 g, boric acid 5.5 g, disodium EDTA 0.75 g, in 1 L of water) and boiling it up to 100 °C. Afterwards, 1x GelRed for the detection of the nucleic acid was added, and the agarose solution was casted in the electrophoresis unit and left to form a gel. Polyplexes (succPEI, w/w = 4; lipo-OAAs, N/P = 12) were prepared as described in section 5.2.2 containing 250 ng of mRNA-luc in 20 µL of HBG. Then, 4 µL of loading buffer (prepared from 6 mL of glycerol, 1.2 mL of 0.5 M EDTA, 2.8 mL of H_2O, and 0.02 g of bromophenol blue) were added to each sample before they were placed into the sample pockets. Electrophoresis was performed at 120 V for 80 min.

5.2.5 Ethidium bromide exclusion assay

For the compaction study of mRNA nanoparticles, lipopolyplexes were prepared as described in section 5.2.2 with 2 µg of mRNA at N/P ratio = 12 in a total volume of 200 µL of HBG. In parallel to these polyplexes, the following were prepared; HBG buffer (blank), succPEI polyplexes (w/w = 4), and 2 µg of mRNA-luc in 200 µL of HBG buffer. The latter was considered as maximum ethidium bromide (EtBr) fluorescence intensity (100% value). After an incubation time of 30 min, 700 µL of EtBr solution (c = 0.5 µg/mL) were added to each sample. After an additional incubation for 3 min, the fluorescence intensity of EtBr was measured at the excitation wavelength λ_{ex} = 510 nm and emission wavelength λ_{em} = 590 nm using a Cary Eclipse spectrophotometer (Varian, Germany). The fluorescence intensity of EtBr for each sample was calculated in relation to the 100% value.

5.2.6 Ethidium bromide exclusion assay of mRNA lipopolyplexes under reductive conditions

Lipopolyplexes (N/P = 12) containing 2 µg of mRNA-luc were formed in a total volume of 200 µL of HBG. In parallel to these lipopolyplexes, the following were prepared: HBG buffer (blank value) and mRNA-luc in HBG (c = 10 µg/mL), which was considered as maximum EtBr fluorescence intensity (100% value). After lipopolyplex incubation, 50 µL of a glutathione (GSH) solution (50 mM; pH 7.4) was added to the lipopolyplex solution. Consequently, the resulting solutions had the final concentrations of 10 mM GSH. The solutions were incubated at 37 °C for 90 min. A volume of 700 µL of EtBr solution (c = 0.5 µg/mL) were added to each sample and an EtBr exclusion assay was performed as it is described in section 5.2.5.

5.2.7 Erythrocyte leakage assay with and without previous reductive treatment

Phosphate-buffered saline (PBS) was used for repeated washing of fresh, citrate-buffered

(25 mM citrate) human blood. After the last centrifugation step (2000 rpm, 4 °C, 10 min), when the supernatant was clear, the cell pellet was diluted to 5 × 10^7 erythrocytes per mL with PBS at different pH values (pH 7.4, 6.5, and 5.5). OAA solution, previously diluted with PBS of the respective pH value, was pipetted into a V-bottom 96-well plate (75 µL/well). The same volume of erythrocyte suspension at the same pH value was added to each well, resulting in a final concentration of 5 µM of OAA per well. In the case of GSH treatment, OAAs (c = 1 mg/mL) were pre-incubated with 10 mM of GSH in HEPES (20 mM; pH 7.4) at 37 °C for 90 min. To determine the lytic activity of the samples, the V-bottom 96-well plates were incubated at 37 °C under constant shaking for 1 h. After centrifugation (2000 rpm, 4 °C, 10 min), 100 µL of the supernatant were analyzed for hemoglobin release at wavelength λ = 405 nm using a microplate reader (Spectrafluor Plus, Tecan, Männedorf, Switzerland). PBS at the indicated pH values served as negative control (0% value), and TritonX-100 was used as positive control (100% value). Data are presented as mean value (± SD) out of quadruplicates.

5.2.8 Cell culture

The human prostate cancer cell line (DU145) was cultured in RPMI-1640 medium; mouse neuroblastoma (N2a), hepatocellular carcinoma (Huh7) and breast adenocarcinoma (MDA-MB-231) cells were grown in Dulbecco's modified Eagle's medium (DMEM)-low glucose (1 g/L of glucose), and cervix carcinoma (KB) cells were grown in folate free RPMI-1640 medium. All cell culture media were supplemented with 10% (v/v) FBS, 4 mM of stable glutamine, 100 U/mL of penicillin, and 100 µg/mL of streptomycin. All cell lines were cultured at 37 °C and 5% CO_2 in an incubator with a relative humidity of 95%.

5.2.9 Luciferase transfection efficiency of mRNA polyplexes and lipopolyplexes

One day prior to transfection, 10,000 DU145, N2a, Huh7 or MDA-MB-231, and 8,000 KB (on collagen coated plates) cells per well were seeded in 96-well plates. Transfection efficiency of OAAs was evaluated using 250 ng of mRNA-luc per well. Polyplexes were formed at N/P = 12 in a total volume of 20 µL of HBG. HBG buffer was used as negative control. SuccPEI (10% succinylation) was used at w/w = 4 as positive control. Before treatment, the cell culture medium was exchanged with 80 µL of fresh medium containing 10% (v/v) FBS. Polyplex solution was added to each well and incubated on cells at 37 °C for 24 h. All experiments were performed in triplicate. For all experiments, 24 h after initial

transfection, cells were treated with 100 µL of luciferase cell culture 0.5x lysis buffer. Luciferase activity in the cell lysate was measured by using a Centro LB 960 plate reader luminometer (Berthold Technologies, Bad Wildbad, Germany) and LAR buffer supplemented with 0.5 mM of *D*-luciferin. Transfection efficiency was evaluated as relative light units (RLU) per well (10,000 cells).

5.2.10 CellTiter-Glo assay

The cells were transfected as described in section 5.2.9. At 24 h after initial transfection, the medium in the well was replaced with 50 µL of fresh medium and 50 µL of CellTiter-Glo reagent. After 30 min incubation at RT under constant slight shaking, the relative metabolic activity was determined as the ratio of measured luminescent signal over the signal of untreated cells. For measuring the luminescent signals, which are proportional to the amount of ATP (adenosine triphosphate) present in the cells, a Centro LB 960 plate reader luminometer (Berthold Technologies, Bad Wildbad, Germany) was used.

5.2.11 EGFP expression

DU145 cells were seeded in 24-well plates at a density of 50,000 cells/well. On the following day, cells were transfected with lipopolyplexes formed with 1.5 µg of mRNA-EGFP at N/P = 12 in a total volume of 100 µL of HBG. SuccPEI (10% succinylation) was used at w/w = 4 as positive control. At 24 h after transfection, cells were washed with 500 µL of PBS, detached with trypsin/EDTA, and resuspended in PBS containing 10% (v/v) FBS. Samples were investigated for EGFP expression by collecting 10,000 events per sample *via* a BD-LSR Fortessa™ flow cytometer (BD Biosciences, Heidelberg, Germany) using BD FACSDiva software. Analysis was done with the FlowJo 7.6.5 flow cytometric analysis software (FlowJo, Ashland, OR, USA).

5.2.12 Fluorescence microscopy

DU145 cells were seeded in 8-well chamber slides at a density of 30,000 cells/well. The next day, cell culture medium was replaced with 240 µL of fresh growth medium. mRNA polyplexes (N/P = 12) containing 750 ng of mRNA-EGFP in 60 µL of HBG were added to each well and incubated at 37 °C for 24 h. SuccPEI (10% succinylation) was used at w/w = 4 as positive control. After 24 h, cells were washed twice with 500 µL of PBS and fixed with 4% PFA solution for 30 min at RT. Images were obtained using a Zeiss Axiovert 200 fluorescence microscope (Carl Zeiss AG, Germany).

5.2.13 *In vivo* performance of mRNA lipopolyplexes after intratracheal instillation and aspiration

All procedures were approved by the local animal welfare authorities (Regierung von Oberbayern; accreditation number: Vet_03-19-16) and were conducted according to the German animal protection law (Tierschutzgesetz). C57BL6/J mice were housed under specific pathogen-free conditions (facility tested negative for any FELASA listed pathogens according to the annual health and hygiene survey 2017) in individually ventilated cages under a circadian light cycle (lights on from 7 a.m. to 7 p.m.). Food and drinking water were provided *ad libitum*. After arrival, animals were given at least seven days for acclimatization until they entered the study. Prior to treatment, the animals were randomly divided into groups of three (n = 3). Animals were anesthetized by the inhalation of pure oxygen containing 4% isoflurane (Isothesia, Henry Shine, Germany). Unconscious animals were intubated using a 20-gauge catheter shortened to 37 mm. Lipopolyplexes (N/P = 12) containing 10 µg of mRNA-luc in a total volume of 50 µL of WFI were applied as one drop at the proximal tip of the tubus and thereby aspirated during the physiological inspiratory movement of the animal. Finally, 150 µL of air was applied to assure that no liquid remained within the catheter. After 4 h, animals were set under full anesthesia through intraperitoneal injection of fentanyl/midazolam/medetomidine (0.05/5.0/0.5 mg/kg bodyweight). *D*-Luciferin (3 mg/100 µL PBS) was applied by intraperitoneal injection and intranasally using the “sniffing method” (1.5 mg/5 µL PBS). After 10 min, mice were killed by cervical dislocation. The abdominal cavity was opened in the median axis. A careful cut was made in the diaphragm, which led to atmospheric pressure in the thoracal cavity and immediate collapse of the lungs. All rips were dissected, and the trachea was exposed. The left kidney artery was dissected. The small circulation was perfused using 5 mL of PBS, which was applied through the right ventricle. The lungs, livers, and spleens were explanted, placed on a petri dish on their ventral surface. *Ex vivo* imaging was performed using an IVIS 100 *In Vivo* Imaging System (Perkin Elmer, USA) using the parameters Binning: High, FOV, f_1, 1 min. In case of oversaturation, binning was reduced to Medium. In case that no signal was captured using high binning, exposure time was extended to 5 min. The frozen tissues were removed from the tube and cut in half using a scalpel. The whole organ and half of the organ that was analyzed were weighed. Subsequently, the sample was put into a homogenization tube (Lysing Matrix D) filled with 500 µL of cold

TritonX-100 lysis buffer (25 mM Tris-HCl, 0.1% (v/v) TritonX-100; pH 7.8). Homogenization was performed for 3x 20 s with a speed of 6.5 m/s in a tissue homogenizer (MP FastPrep-24 Tissue and Cell Homogenizer; MP Biomedicals, Eschwege, Germany). After homogenization, the samples were incubated for 10 min on ice and then centrifuged for 10 min at 4 °C in a Mikro 22R centrifuge (Hettich Zentrifugen, Tuttlingen, Germany) at maximum speed. Subsequently, 200 µL of the supernatant (without the layer of fat) were collected in a separate tube and stored on ice until measurement. Luciferase activity in tissue lysates was determined using the Lumat LB 9507 luminometer (Berthold Technologies, Bad Wildbad, Germany). Therefore, 75 µL of the lysates were pipetted into a test tube, 100 µL of luciferase assay buffer was added automatically by the machine, and the duration of luciferase activity was measured for 1 s. The mean of two measurements was calculated and extrapolated to the weight of the organ.

5.2.14 Statistical analysis

Results are presented as arithmetic mean ± SD and the number of replicates ($n \geq 3$). Statistical significances were analyzed using Student's two-tailed *t*-test. Significance levels were indicated with the following symbols: ns, $p > 0.05$; * $p \leq 0.05$; ** $p \leq 0.01$; *** $p \leq 0.001$; and **** $p \leq 0.0001$.

5.3 Results and discussion

5.3.1 Identifying succPEI as a “gold standard” for mRNA polyplexes

In previous studies, linear PEI of 22 kDa (linPEI) showed superior pDNA transfection activity over branched PEI of 25 kDa (brPEI).[499, 625] For siRNA, a succinylated form of brPEI (succPEI) outperformed the other derivatives in gene silencing activity.[622] Against first assumptions, the introduction of negative succinoyl charges on succPEI slightly enhanced siRNA polyplex stability, but as expected also strongly reduced cytotoxicity of PEI by 10-fold, resulting in potent gene silencing. In order to find the most suitable PEI-type positive control for mRNA polyplexes in the current study, the three previously successful pDNA and siRNA carriers linPEI, brPEI, and succPEI were tested for their potency in mRNA delivery (**Figure 5.1A**). As the aim was to identify the best positive control, the optimal conditions for each carrier were chosen. For unmodified linPEI and brPEI, their optimal N/P ratios of 9 (linPEI)[143] and 10 (brPEI)[626] were used. At higher N/P ratios, potential toxicity has to be considered.[88, 627] In the case of succPEI, the N/P ratio was considered to be not suitable for calculation of the amounts of succPEI to mRNA since some amino groups are substituted with succinic acid and thus not involved in nucleic acid binding. Therefore, the w/w ratio was used instead of the commonly used N/P ratio.[622] A w/w ratio of 1 would be an N/P ratio of 7.5 for an unsubstituted PEI. The transfection efficiency of succPEI (at optimal w/w = 4)[622] was superior compared to brPEI (at optimal N/P = 10)[626] and linPEI (at optimal N/P = 9),[143] as tested in five different cancer cell lines (**Figure 5.1B**).The zetasizer data of the three PEI polyplexes were as expected with sizes around 45 to 60 nm and positive surface charges around +20 to +28 mV (**Table 5.1**). Notably, no cytotoxicity was observed for all PEI-type polyplexes, even in the case of succPEI at the highest tested w/w ratio 8 (**Figure 5.1B, C,** *bottom*). The w/w ratio of 4 was finally chosen for succPEI mRNA polyplexes based on the transfection results of the w/w ratio titration as shown in **Figure 5.1C**. Among the evaluated succinylation degrees (10, 20, 30, and 50%), 10% turned out to be most effective with no significant difference recognizable between w/w ratio of 4 and 8 (**Figure 5.1C**). To sum up, succinylated polyethylenimine (succPEI, 10% succinylation; w/w = 4, HBG)[622] was found to be most suitable as positive control and thus was used as “gold standard” in all subsequent experiments.

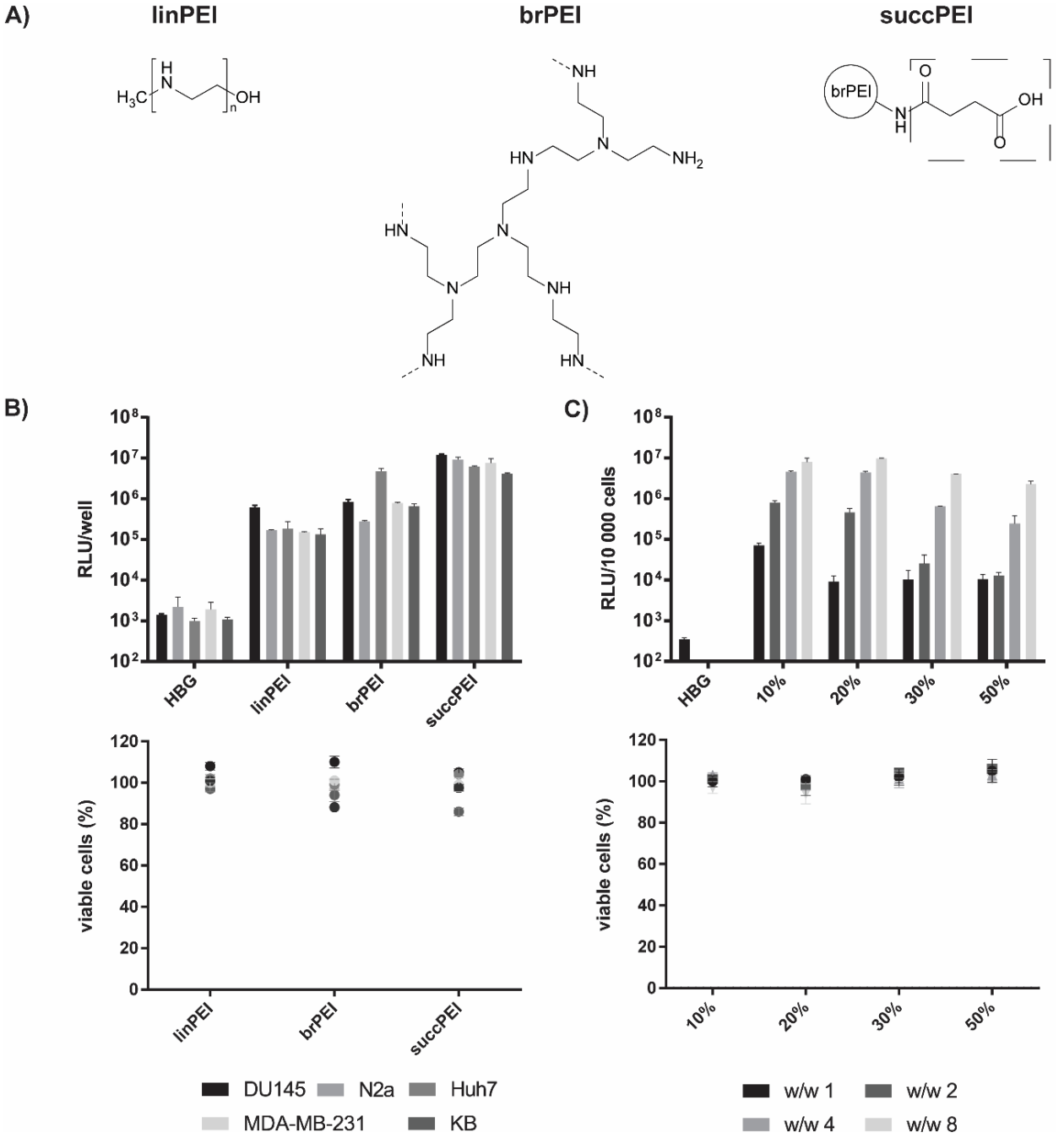

Figure 5.1. (**A**) Chemical structures of linear polyethylenimine (linPEI) 22 kDa,[206, 628] branched PEI (brPEI) 25 kDa,[628, 629] and succinylated PEI (succPEI) 25 kDa.[622] (**B**) Luciferase reporter expression assay (*top*) and corresponding cell metabolic activity assay (*bottom*) in five different cancer cell lines (DU145, N2a, Huh7, MDA-MB-231, KB) at 24 h after transfection with mRNA-luc polyplexes formed in HBG. LinPEI polyplexes were formed at N/P = 9, brPEI at N/P = 10, and succPEI at w/w = 4. (**C**) Transfection efficiency (luciferase reporter expression assay, *top*) and corresponding cell metabolic activity (*bottom*) in DU145 cells after 24 h of incubation with succPEI mRNA-luc polyplexes with different succinylation degrees (10 to 50%) of PEI. Cell metabolic activity was assessed by CellTiter-Glo assay (Promega, Mannheim, Germany) and calculated as percentage to cells treated with HBG. Data are presented as mean value (+ SD) out of triplicate. Transfections were performed by Dr. Ana Krhač Levačić (Pharmaceutical Biotechnology, LMU Munich).

Table 5.1. Results of DLS and ELS measurements (*n* = 3; mean ± SD) of mRNA polyplexes formed with different PEI derivatives in HBG.

	Z-average (nm)	Mean PDI	Mean zeta potential (mV)
linPEI (N/P = 9)	52.0 ± 2.9	0.30 ± 0.05	20.2 ± 3.9
brPEI (N/P = 10)	46.0 ± 3.0	0.27 ± 0.002	22.8 ± 2.2
succPEI (w/w = 4)	59.8 ± 0.9	0.29 ± 0.05	27.8 ± 3.9

5.3.2 Evaluation of an OAA library for mRNA-luc transfection efficiency

In the current work, a library of OAA based carriers with T-shape topology (**Scheme 5.1, Table 5.3A, B**) was evaluated for mRNA delivery. By this, appropriate carriers, beneficial structural motifs, and critical bottlenecks for mRNA delivery should be identified. The design of this library was based on an initial exploration of molecularly more diverse OAA structures with different sequences and topologies, which revealed encouraging activity of T-shape lipo-OAAs (**Figure 5.7, Table 5.3C**). Such OAA libraries are easily available by standard Fmoc solid-phase assisted peptide synthesis and were previously evaluated for delivery of nucleic acids like pDNA or siRNA.[64, 123, 137, 138, 200, 209, 623, 630, 631]

Scheme 5.1. Schematic structure of sequence-defined lipo-oligoaminoamides with T-shape topology and different modifications evaluated in the main screen.

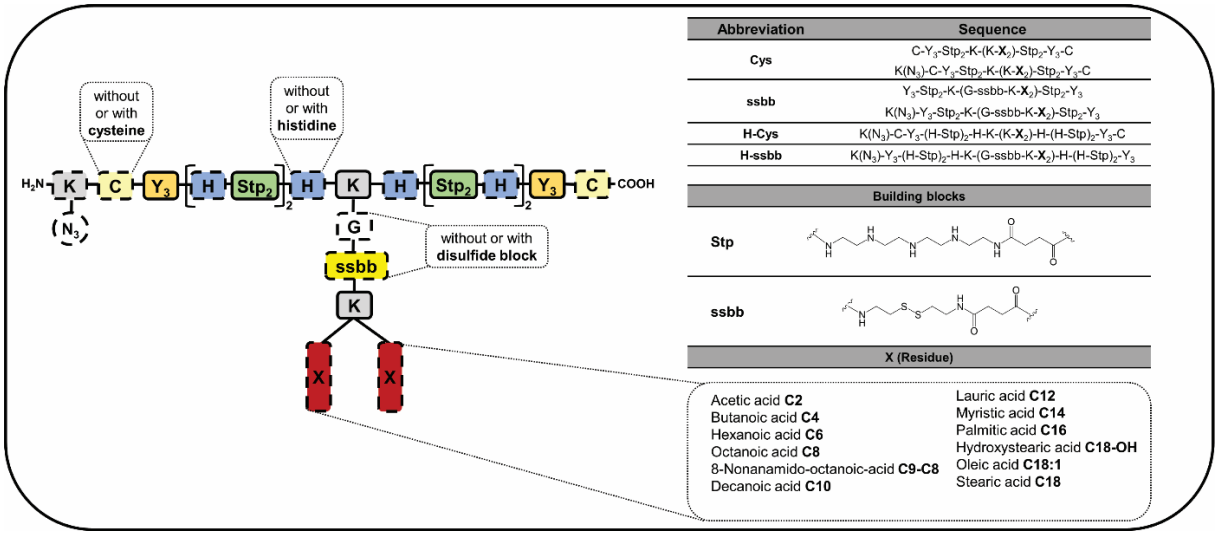

K(N_3): azido-lysine; C: cysteine; Y: tyrosine; H: histidine; K: lysine; G: glycine; ssbb: cystamine disulfide building block; Stp: succinoyl tetraethylene pentamine; X: residue with different fatty acids (saturated fatty acids of different chain lengths, unsaturated or modified fatty acids).

The pre-screening provided important information (**Figure 5.7, Table 5.3C**). Firstly, T-Shape topology seemed to be superior to others, such as 3- or 4-arm topology, which

were inefficient for mRNA delivery. Secondly, incorporation of either tyrosine-tripeptides (Y_3) or fatty acids in T-Shape structures was not sufficient; however, the combination of Y_3 plus fatty acids mediated successful mRNA delivery (**Figure 5.7C**). Both motifs have already been recognized as stabilizing domains for pDNA and siRNA polyplex formation by hydrophobic interactions.[137, 200, 630] It is also known from previous findings that the fatty acid type (saturated or unsaturated, different chain lengths) can affect the lipophilic interaction and therefore polyplex stability.[64, 136, 200] Furthermore, fatty acids exhibit lytic potential depending on their aliphatic chain length, and thus may help in endosomal release of the carrier system.[29] Thirdly, the incorporation of histidines (H) in alternating sequence with the artificial cationizable amino acid succinoyl tetraethylene pentamine (Stp) seemed to be beneficial (**Figure 5.7D**).[144, 184, 190] The $(H\text{-}Stp)_2$ motif was superior to the $(H\text{-}Stp)_4$ motif. Stp units promote nucleic acid packing, endosomal buffering, and endosomal escape.[64, 158, 183] Incorporation of histidines has been also previously reported advantageous for a series of transfection carriers, due to endosomal buffering and enhanced endosomal escape.[196, 593] Furthermore, an N/P ratio of 12 was figured out to be most suitable for the OAA/mRNA complexes (data not shown). It is known that free cationic OAAs are advantageous for transfection efficiency.[498] At low N/P ratios, less stability and almost neutral surface charge could lead to aggregate formation, especially in the case of lipo-OAAs with short fatty acids. At higher N/P ratios, in most cases no benefit in transfection efficiency could be obtained, but toxicity has to be considered. Therefore, the N/P ratio of 12 was selected for all lipo-OAAs in all experiments as best compromise between polyplex stability, transfection efficiency and cytotoxicity. Performing the experiments at the same N/P ratio enables to draw structure-activity relationships.

All OAA structures of the main screen (**Scheme 5.1, Table 5.3A, B**) had a polycationic backbone with four units of Stp, as well as Y_3 at each end of the linear backbone. An incorporated lysine in the middle of the backbone served as branching point, where the side chain with a diacyl domain was attached. By varying the fatty acids, the most suitable fatty acid for mRNA delivery should be revealed. In order to investigate the effect of histidines, structures with histidines and their analogs without histidines were included in the library. As hydrophobic stabilization *via* Y_3 and fatty acids seemed to be advantageous (**Figure 5.7C**), structures with cysteines (Cys) at the end of each polycationic arm for

further polyplex stabilization *via* redox-sensitive disulfide cross-links were tested. In addition, a disulfide building block (ssbb)[123] was evaluated for efficiency in mRNA delivery. While high extracellular stability of polyplexes is important, intracellular disassembly is required for the cytosolic release of mRNA. The incorporation of the ssbb between the cationic backbone and the hydrophobic domain should enhance release of the cargo in the intracellular reductive environment upon high concentrations of GSH.[123] To sum up, the new library of T-shaped OAAs can be divided in four main groups, namely, Cys group, H-Cys group, ssbb group and H-ssbb group (**Scheme 5.1**). In addition to these four main groups, structures without cysteines and without ssbb (0 and H-0 groups) were included in the study to emphasize the effects of the two structural modifications (**Table 5.3A, B**). The structures within each group differ only in the incorporated fatty acids (saturated or unsaturated, modified fatty acids, different chain lengths). For other nucleic acids, beneficial fatty acids have already been identified, but not for mRNA so far. Lipo-OAAs with cationic backbone and hydrophobic diacyl domain such as unsaturated fatty acid (oleic acid, linoleic acid) or sterically advanced fatty acids (*e.g.*, cholanic acid) are known as potent siRNA carriers because of strong electrostatic and hydrophobic lipopolyplex formation and endosomal membrane destabilization.[28, 64, 137, 147, 200, 202, 205, 208, 209] Saturated fatty acids of middle chain lengths (hexanoic to decanoic acid; C6–C10) recently proved to be very potent pDNA carriers.[29]

The library was investigated regarding mRNA transfection efficacy in cell culture (**Figure 5.2, Figure 5.8**). Transfections were performed in DU145 and N2a cell lines with (lipo)polyplexes (N/P = 12) formed in HBG. Cells were incubated with polyplexes for 24 h in 10% (v/v) FBS-supplemented medium, and afterwards luciferase expression as well as cell metabolic activity were recorded.

In general, the influence of different fatty acids, of redox-sensitive units (ssbb or cysteine cross-links) and of histidines was examined regarding transfection potency in DU145 and N2a cells (**Figure 5.2, Figure 5.8**). The relative transfection profiles of OAAs used in the study was similar in both tested cell lines.

Effect of fatty acids. In the case of Cys-containing polyplexes, transfection efficiency decreased in both cell lines with increasing acyl chain length, whereas it was vice versa in the case of ssbb-containing structures (**Figure 5.2A, Figure 5.8**). Here, the transfection efficiency increased with increasing acyl chain length. Cys-containing structures with C2–

C6 fatty acids as well as ssbb-containing structures with C6–C18 fatty acids mediated transfection efficiency comparable to the efficiency of the “gold standard” succPEI, especially in DU145 cells. Structures of the 0 and H-0 groups showed overall comparable results like their cysteine-analogs, except for short fatty acids (**Figure 5.8**). Here, cysteine-containing structures outperformed their cysteine-free counterparts by far. The high transfection results for Cys-containing polyplexes with fatty acids C2–C6 (histidine group; **Figure 5.2A**) or C2–C8 (histidine-free group; **Figure 5.8**) might be due to a beneficial effect of balanced stability (low, but not too low) analogously as it was already recognized for pDNA delivery.[29]

Effect of ssbb. Incorporation of the ssbb had an advantage for transfection efficiency over cysteine-containing analogs. Statistically significant enhanced luciferase expression was observed for fatty acids with chain lengths >C6 (histidine group; **Figure 5.2**) or >C8 (histidine-free group; **Figure 5.8**), respectively, as well as for unsaturated and modified fatty acids (OleA, NonOcA; **Figure 5.2, Figure 5.8**). The highest statistically significant difference in transfection efficiency between Cys- and ssbb-containing structures was observed for OleA (**Figure 5.2**). Although SteA-containing lipopolyplexes showed lower transfection efficiency at all, enhanced efficiency of bioreducible lipopolyplexes over their cysteine-analogs was achieved here as well. Also, SteA-containing structures of the 0 and H-0 groups exhibited comparable results like their ssbb-analogs.

On the one hand, low stability of nanoparticles is a critical issue for successful delivery, but on the other hand, too stable nanoparticles could also be problematic, resulting in low protein expression due to low mRNA release and translation in the cytosol. High polyplex stability might also be an explanation why the stability motifs CRC[138] or tyrosine-hexapeptides (Y_6) did not show any further advantage on transfection efficiency (**Figure 5.7D**). These results reveal once more the importance of balanced stability for optimum transfection results.

Effects of histidines. Interestingly, incorporation of histidines appeared to be beneficial for all Cys-containing OAAs, whereas in the case of ssbb-containing structure with longer fatty acids (MyrA, PalA, SteA), with unsaturated fatty acid OleA and also with the modified fatty acid NonOcA the beneficial effect of histidine was not noticed anymore (**Figure 5.2B, Figure 5.8**). For this reason, structures of the Cys, H-Cys, ssbb and H-ssbb groups containing NonOcA, MyrA, OleA or SteA were selected for more detailed investigation.

For further cell experiments, DU145 cells were chosen, as both tested cell lines showed same relative transfection profiles, but the overall expression was higher in DU145 cells.

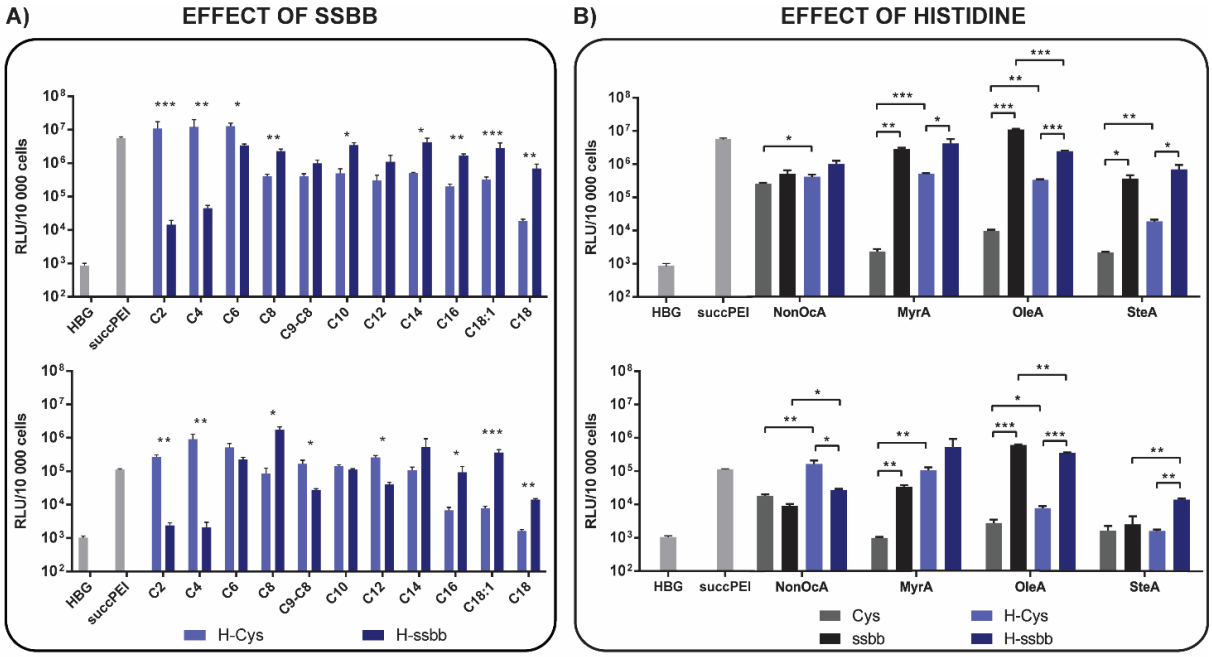

Figure 5.2. Luciferase reporter expression of mRNA lipopolyplexes formed with T-shape lipo-oligoaminoamides (N/P = 12, HBG) at 24 h after transfection in DU145 (*top*) and N2a cells (*bottom*). SuccPEI polyplexes (10% succinylation, w/w = 4, HBG) were used as positive control, HBG treated cells as background. Data are presented as mean value (+ SD) out of triplicate. Transfections were performed by Dr. Ana Krhač Levačić (Pharmaceutical Biotechnology, LMU Munich).

5.3.3 Biophysical characterization of mRNA lipopolyplexes

Compaction of mRNA with nucleic acid carriers into nanoparticles is an important requirement for successful mRNA delivery. Therefore, different characterization methods were used to compare various lipopolyplex formulations regarding their physicochemical properties.

Table 5.2. Results of DLS and ELS measurements (*n* = 3; mean ± SD) of mRNA lipopolyplexes (HBG, N/P = 12).

	Lipopolyplex	Z-average (nm)	Mean PDI	Mean zeta potential (mV)
NonOcA	Cys	86.4 ± 0.1	0.25 ± 0.01	37.6 ± 2.6
	ssbb	116.1 ± 0.6	0.11 ± 0.02	30.0 ± 1.6
	H-Cys	78.9 ± 5.2	0.31 ± 0.04	17.4 ± 1.4
	H-ssbb	79.1 ± 1.6	0.18 ± 0.01	10.5 ± 0.9
MyrA	Cys	79.0 ± 0.1	0.27 ± 0.01	39.3 ± 2.0
	ssbb	102.0 ± 0.7	0.21 ± 0.01	33.6 ± 1.5
	H-Cys	86.6 ± 2.7	0.28 ± 0.03	16.8 ± 1.0
	H-ssbb	78.7 ± 1.3	0.19 ± 0.01	17.8 ± 0.4
OleA	Cys	62.0 ± 0.9	0.16 ± 0.02	28.4 ± 1.5
	ssbb	77.1 ± 1.4	0.21 ± 0.01	41.1 ± 0.4
	H-Cys	78.1 ± 0.7	0.14 ± 0.01	18.5 ± 0.8
	H-ssbb	93.2 ± 0.5	0.11 ± 0.00	10.5 ± 0.2
SteA	Cys	69.8 ± 1.1	0.31 ± 0.02	37.2 ± 2.1
	ssbb	102.2 ± 0.8	0.21 ± 0.01	31.7 ± 0.7
	H-Cys	69.2 ± 4.2	0.28 ± 0.05	19.2 ± 2.5
	H-ssbb	70.2 ± 0.8	0.18 ± 0.01	16.4 ± 1.3

Particle sizes and zeta potentials of lipopolyplexes (N/P = 12, HBG) were determined by dynamic and electrophoretic light scattering (DLS, ELS) (**Table 5.2, Table 5.4**). Most of the carrier formulations exhibited well-defined particle sizes below 200 nm and positive surface charges between 10 and 40 mV, which may be beneficial for cellular uptake.[632] Nevertheless, OAAs of the H-ssbb group with fatty acids C2–C6 exhibited particle sizes bigger than 200 nm and low, almost neutral zeta potentials (**Table 5.4**), indicating less stability. The decreased stability in combination with the almost neutral surface charge might be the reason for the low transfection efficiency of those OAAs compared to the structures of the H-Cys group with the same fatty acids. Electrostatic membrane interaction as well as certain threshold stability is required for good transfection results.[3] Only one of the formulations displayed a particle size above 1 µm with still positive zeta potential, namely, the cysteine-structure with hydroxystearic acid (C18-OH). Therefore, this structure was excluded from further screening despite good transfection efficiency (**Figure 5.8**).

Gel shift assay analysis revealed complete binding of mRNA in the case of all lipo-OAAs at an N/P ratio of 12 (**Figure 5.3A, Figure 5.9**). To further investigate the mRNA compaction ability of different OAAs, an ethidium bromide (EtBr) exclusion assay was performed. In **Figure 5.3B**, the intensity of EtBr fluorescence normalized to fluorescence of uncomplexed mRNA is displayed. SuccPEI polyplexes (<5% EtBr fluorescence)

showed the best mRNA compaction. Interestingly, all lipopolyplexes showed sufficient mRNA compaction in the range between 10 and 25% EtBr fluorescence, while slightly lower compaction with around 30% EtBr fluorescence was observed for structures of the Cys-group with fatty acids NonOcA and MyrA. H-Cys analogs exhibited a better mRNA complexation and polyplex stabilization. Additionally, destabilization of bioreducible ssbb-containing lipopolyplexes at intracellular GSH concentrations (~10 mM) was examined *via* the EtBr exclusion assay, exemplarily for NonOcA- and OleA-containing lipo-OAAs (**Figure 5.3C**). Lipopolyplexes were incubated with 10 mM of physiological reducing agent GSH at 37 °C and pH 7.4 for 90 min. For OleA-containing OAAs, mRNA binding efficacy of carriers was significantly decreased for the reducible but not the analogous stable lipo-OAAs under reducing conditions. This could explain the better performance in the luciferase reporter expression assay of bioreducible lipopolyplexes over their non-reducible analogs (**Figure 5.2**). The position of the ssbb-linkage within the carrier allows the release of the diacyl domain from the small cationic backbone. This lipophilic part is a very important nanoparticle stabilization motif in T-shaped OAAs. However, a weak binding ability of the remaining cationic backbone still exists.[137, 138] Thus, destabilization of lipopolyplexes *via* reductive cleavage may ensure better availability of mRNA in the intracellular space. Surprisingly, this destabilizing effect could not be verified for all fatty acid groups. mRNA binding efficacy of reducible NonOcA-containing structures remained here unaffected from GSH reduction (**Figure 5.3C**). This is consistent with the transfection results (**Figure 5.2B**), where incorporation of the bioreducible building block did not improve the transfection efficiency of NonOcA-containing mRNA lipopolyplexes.

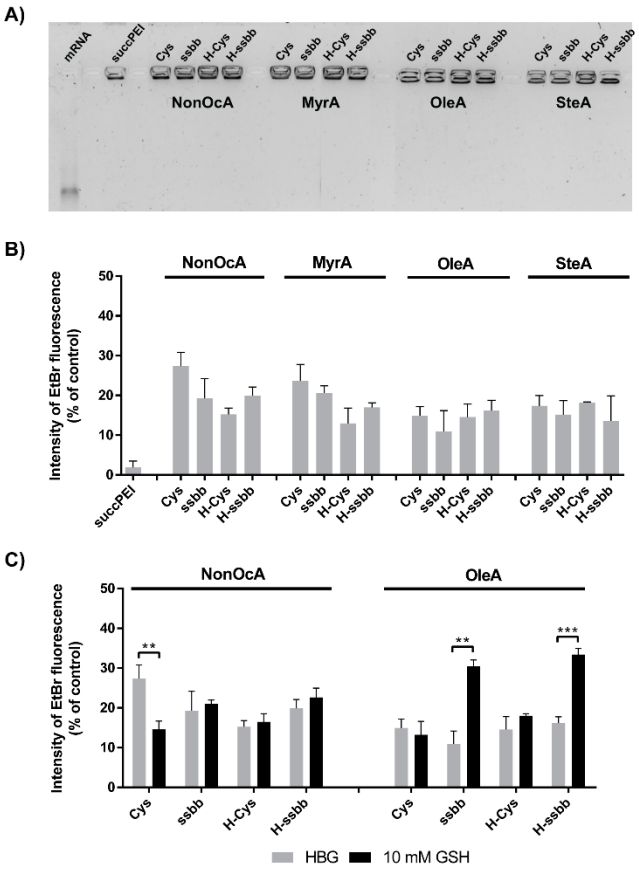

Figure 5.3. Physicochemical characterization of mRNA lipopolyplexes (N/P = 12; HBG). (**A**) Gel shift assay; (**B**) ethidium bromide (EtBr) assay (*n* = 3; mean + SD) under normal conditions as well as under prior treatment with 10 mM glutathione (GSH) (**C**). The experiments were carried out together with Dr. Ana Krhač Levačić (Pharmaceutical Biotechnology, LMU Munich).

Moreover, an erythrocyte leakage assay was performed comparing the lytic potential of the different fatty acids within the ssbb-containing lipo-OAAs and their stable cysteine-containing analogs at the three different physiological relevant pH values 5.5, 6.5, and 7.4 (**Figure 5.4**). Different fatty acids have a strong influence on the lytic properties of the carriers and may enhance endosomal escape. Nevertheless, unspecific membranolytic activity can cause toxicity. Therefore, pH dependent lytic activity is desirable showing lytic effects only in the acidic milieu of endosomes/lysosomes (pH 5.5–6.5) but not at physiological pH 7.4. Combination of the hydrophobic, membranolytic domain and increased cationization of the cationic parts at endosomal pH, facilitates endosomal membrane destabilization and escape of the delivery system into the cytosol.

In general, the ssbb-containing reducible structures showed lower lytic potential compared to their more stable Cys analogs (**Figure 5.4A**). Therefore, the backbone structure, apart

from the different fatty acids, also had an impact on the lytic activity. Higher lytic potential of stable Cys-analogs might be a consequence of higher fatty acid numbers per molecule due to prior formation of disulfide-based dimeric/oligomeric OAAs. Moreover, the ssbb-linker increases the distance between the hydrophilic and the lipophilic part, thereby reducing the amphiphilic character of the OAAs. The lytic potential was higher for structures with fatty acids NonOcA and MyrA than for structures with OleA and SteA. MyrA-containing structures (fatty acid with middle chain length) showed highest pH dependent lytic activity (40–50% higher at pH 5.5–6.5 compared to pH 7.4). Moreover, ssbb-containing structures with SteA also showed pH dependent lytic activity with an increase of around 50% from pH 7.4 to pH 5.5. While in the case of NonOcA and OleA, no notable difference in the lytic potential at the different pH values could be observed. Lowest lysis displayed the structure H-ssbb OleA with lytic activity less than 10% at pH 6.5–7.4 and less than 20% at pH 5.5. Lowest difference in lytic activity between ssbb-containing structures and their Cys-analogs was detected in the case of SteA. However, reducible structures with SteA exhibited a better pH dependent lytic profile than the stable analogs. Nevertheless, the overall lytic activity was rather low. The weak lytic activity for SteA-containing Cys-structures might explain the low transfection efficiency in comparison to the much better working bioreducible structures (**Figure 5.2**). High stability and low membrane interaction result in reduced mRNA release into the cytosol. In the case of the reducible OAAs with SteA, the stability is reduced and the lytic potential at endosomal pH is increased. Balancing of stability and lytic activity is therefore of great importance for optimum mRNA transfection. It seems that this balancing act is handled best in ssbb-containing structures with fatty acids NonOcA, OleA and MyrA. Furthermore, the OAAs were treated with GSH prior to the erythrocyte leakage assay (**Figure 5.4B**). The lytic activity of stable analogs remained unaffected, whereas a decrease in the case of almost all reducible lipo-OAAs could be recognized. Nevertheless, reducible OleA structures showed an even improved pH dependent lytic profile (increase of 45% from pH 7.4 to pH 5.5) at physiological relevant GSH concentrations, which can be valuable for mRNA delivery.

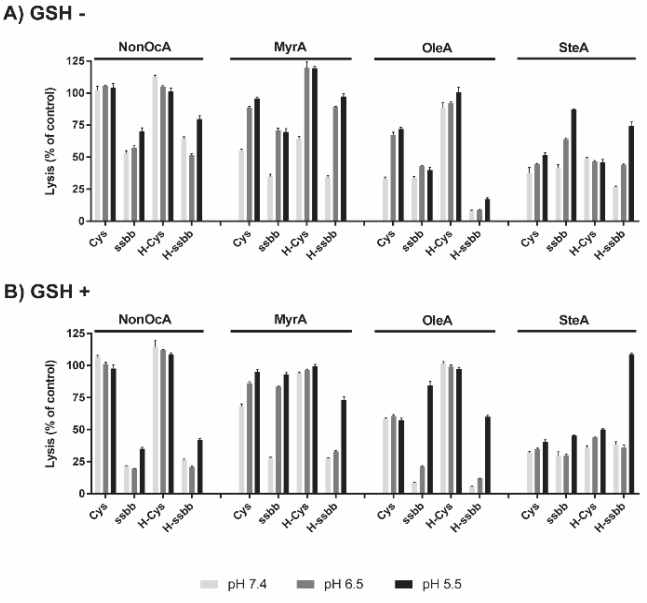

Figure 5.4. Lytic potential of the single lipo-oligoaminoamides at a concentration of 5 µM, measured in an erythrocyte leakage assay at different pH values (pH 7.4, 6.5, and 5.5) without (**A**) and with (**B**) prior reductive treatment with 10 mM glutathione (GSH). Data are presented as mean value (+ SD) out of quadruplicate. The experiments were carried out together with Dr. Ana Krhač Levačić (Pharmaceutical Biotechnology, LMU Munich).

One has to consider that higher lytic activity may increase cellular internalization, but it can also be a reason for unwanted cytotoxicity. However, the CellTiter-Glo assay, determining metabolic activity *via* ATP quantification, showed that cell viability of DU145 and N2a cells is well maintained in almost all cases (**Figure 5.8**). Slight toxicity was only noticed for histidine-containing groups with middle fatty acid chain lengths (C6–C14), when the bioreducible disulfide block was not incorporated. By integration of the ssbb into the structures the toxicity could be reduced. This goes along with our previous work.[123]

5.3.4 Evaluation of mRNA-EGFP transfection efficiency

In order to characterize the cellular mRNA expression in more detail, GFP gene expression was determined in DU145 cells at 24 h after transfection with mRNA-EGFP by flow cytometry and fluorescence microscopy (**Figure 5.5, Figure 5.10**). Again, (lipo)polyplexes were formed in HBG at N/P = 12.

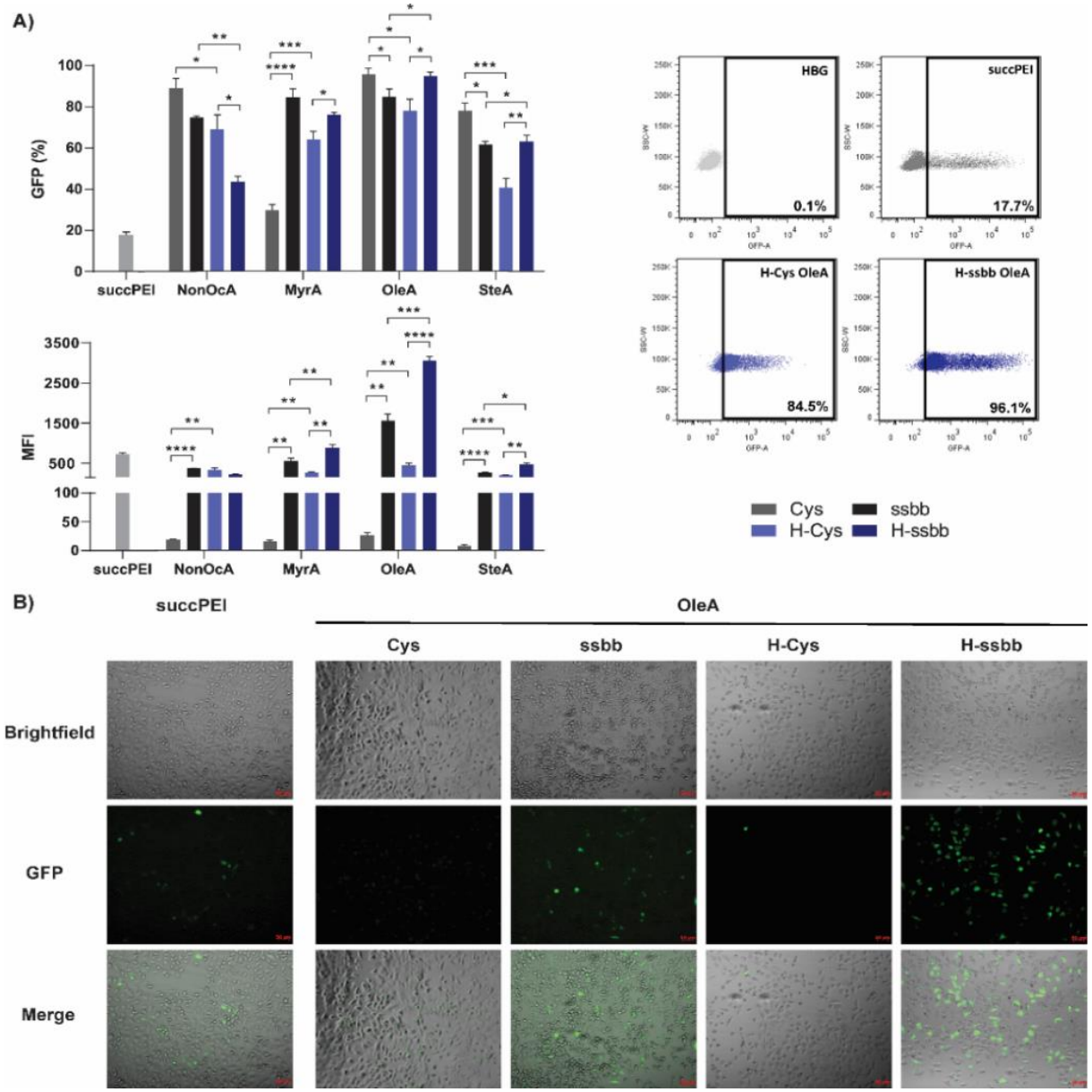

Figure 5.5. (**A**) GFP expression in DU145 cells after 24 h incubation of succPEI as well as Cys, ssbb, H-Cys, and H-ssbb mRNA lipopolyplexes containing NonOcA, MyrA, OleA, or SteA as determined by flow cytometry with corresponding mean fluorescence intensity (MFI) values (*n* = 3; mean + SD). (**B**) Fluorescence microscopy of fixed DU145 cells treated with succPEI or OleA lipopolyplexes for 24 h. *Top row*: brightfield images of the treated cells. *Middle row*: GFP fluorescence of the treated cells. *Bottom row*: merge. Scale bar = 50 µm. Flow cytometry as well as the fluorescence microscopic imaging was done together with Dr. Ana Krhač Levačić (Pharmaceutical Biotechnology, LMU Munich).

For the positive control succPEI, which can mediate high average luciferase activity in a cell population (**Figure 5.2**), flow cytometry with single cell resolution revealed a GFP expression characteristic also with high mean fluorescence intensity (MFI) but only

moderate number (only 17.7%) of GFP positive cells (**Figure 5.5A**). The same results were also confirmed *via* fluorescence microscopy (**Figure 5.5B**). For most of the screened OAAs, also a discrepancy between MFI expression values and population percentage of transfected cells was noticed (**Figure 5.5, Figure 5.10**). However, here a large number of transfected cells was recorded, with lower MFI intensity. Looking at the percentage of cells with GFP expression within the histidine groups (H-0, H-Cys, and H-ssbb), an increase with increasing acyl chain length was observed with a maximum for OleA-structures (**Figure 5.10**). Moreover, incorporated ssbb seems to be beneficial (**Figure 5.5A**). This fits well with the luciferase expression assay data (**Figure 5.2, Figure 5.8**). Even if similar transfection profiles of MyrA- and OleA-containing OAAs were obtained in the luciferase expression assay (**Figure 5.2B**), with the flow cytometry data the OleA-structures turned out to be more effective. The best transfection properties so far were recognized for H-ssbb OleA. This structure transfected almost 100% cells (96.1%) with the highest MFI value (3057) (**Figure 5.5, Figure 5.10**).

Fluorescence microscopy was performed with OleA-containing OAAs (**Figure 5.5B**). Polyplexes formed with non-reducible OAAs (Cys OleA, H-Cys OleA) transfected a high number of cells but with very poor GFP fluorescence intensity. Whereas in cells transfected *via* reducible OAAs (ssbb OleA, H-ssbb OleA) higher levels of GFP were observed and even a larger fraction of cells was transfected. Altogether, fluorescence microscopy results correlate well with the flow cytometry data.

5.3.5 *In vivo* performance of mRNA lipopolyplexes after intratracheal instillation and aspiration

The lipo-OAA structure H-ssbb OleA presented the most promising characteristics in the *in vitro* evaluation. To further investigate its potency in mRNA delivery, this lipo-OAA was selected for *in vivo* testing. In addition, its Cys-analog as well as its C14-analog were included in the study. By this, it was to be investigated, whether the bioreducible ssbb and the unsaturated fatty acid OleA were the most beneficial structural motifs also in the case of the *in vivo* situation. Polyplexes were formed with 10 µg mRNA in 50 µL of WFI at N/P = 12. The focus of this *in vivo* study lied on local administration into the lungs of mice by intratracheal instillation and aspiration (**Figure 5.6**).

Pre-experiments were performed to evaluate whether the mRNA lipopolyplexes still

exhibit the required properties when they were formed in WFI, which was the required solvent for the *in vivo* study. Furthermore, the stability of the lipopolyplexes was determined after a storage time of 4 h at room temperature (RT) or on ice (4 °C) in order to ensure complex stability during the handling and treatment procedure. Zetasizer measurements, determination of encapsulation efficiency (RiboGreen assay) and mRNA integrity (capillary gel electrophoresis, Fragment Analyzer) as well as comparative transfections of polyplexes after different storage conditions (30 min RT, 4 h RT, or 4 h 4 °C) as well as different formulation in HBG or WFI proved that formulation in WFI was comparable to formulation in HBG, and that stability over 4 h was given for all lipopolyplexes (**Figure 5.11**).

Afterwards, the mRNA lipopolyplexes were tested in mice (**Figure 5.6**). After 4 h, pulmonary delivery could be observed *via ex vivo* imaging for all three lipo-OAAs with no mRNA expression detectable in other examined organs (liver, spleen) (**Figure 5.6A**). That is desirable for selective local delivery to the lungs. Lipo-OAA H-ssbb OleA showed the best results (**Figure 5.6A, B**). This structure significantly outperformed the other two lipo-OAAs (**Figure 5.6B**). However, the overall expression, quantified by an *in vivo* luciferase assay, was rather low for all tested OAAs (**Figure 5.6B**). In addition, the nanoparticles seemed to be not well tolerated by the animals. With further improvement of the nanocarrier system, *e.g.*, by additional structural modifications and/or shielding and targeting, the mRNA expression levels might be increased, and the toxicity issue might be solved. PEGylation could be one possible option.[201, 454, 574, 633, 634] Nevertheless, for a first evaluation these results are promising. Local delivery to the lung with this kind of delivery system was achieved. As beneficial structural motifs, bioreducible disulfide block, tyrosine-tripeptides, and unsaturated fatty acid OleA were identified. The results fit quite well with the findings of the *in vitro* studies.

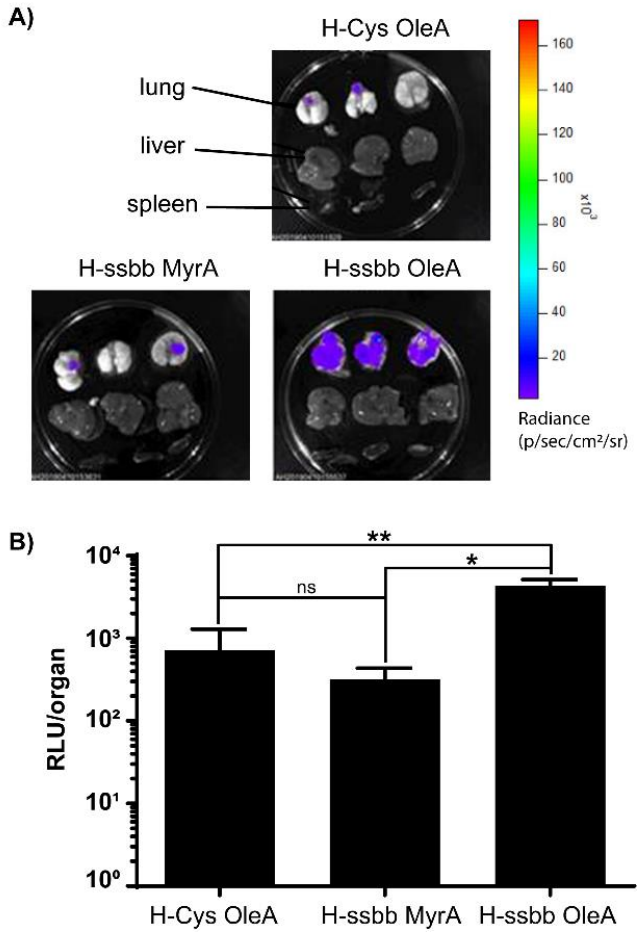

Figure 5.6. *In vivo* luciferase assay at 4 h after intratracheal instillation and aspiration. (**A**) Imaging of luciferase expression in lungs, liver, and spleen, and (**B**) quantification of luciferase expression in the lungs. mRNA lipopolyplexes (N/P = 12) were formed with 10 µg of mRNA-luc in 50 µL WFI. Luciferase expression is presented as relative light units (RLU) per organ (*i.e.,* per lungs; *n* = 3, mean ± SD). RLU values of the lysis buffer were subtracted. The *in vivo* study was conducted by Andrea Wegner and Dr. Günther Hasenpusch (both Ethris GmbH, Planegg).

5.4 Conclusion

Sequence-defined carriers represent a valuable strategy in the development of “smart” nucleic acid delivery systems. In the present study, the structure-activity relationship requirements of refined carriers for successful mRNA delivery *in vitro* and *in vivo* were evaluated. As positive control, succPEI polyplexes (10% succinylation, w/w = 4, HBG), previously established for siRNA delivery,[622] were figured out to be most suitable also in terms of mRNA transfection performance and biocompatibility. The key findings are summarized in **Scheme 5.2**. SPPS-derived cationic OAAs with T-shape topology and Stp as mRNA binding domain were recognized as potentially successful mRNA delivery

platform. Various modifications proved to be advantageous for further improvement of the carrier system. Histidines as endosomal buffering units can increase mRNA transfection efficiency by enhancing endosomal escape. This was especially observed for Cys-containing structures. Tyrosine-tripeptides as well as long-chain fatty acids present stability enhancing domains through hydrophobic interactions. However, too high stability can be counter-productive in terms of intracellular accessibility of mRNA for protein translation by the ribosomal machinery, as also observed for other recent polymer-based mRNA delivery systems.[560-564] Therefore, incorporation of the bioreducible disulfide building block (ssbb) was a required measure, leading to more effective release of mRNA into the intracellular cytosolic place in a dynamic manner. Carrier structures lacking this dynamic tuning element required less stabilizing shorter fatty acids to compensate for mRNA release from the complexes; but such carriers can cause cytotoxicity due to lytic effects. Altogether, best performer of the whole study was OAA H-ssbb OleA, which proved to be a potent carrier for mRNA also in the *in vivo* situation. Here, mRNA was delivered effectively to the lungs of mice after local application. Further optimization by shielding and targeting is well conceivable. An azide function incorporated in most of the tested OAAs will offer a straightforward opportunity to modify the lipopolyplexes with different targeting ligands and shielding agents *via* orthogonal copper-free click-chemistry.[635] By doing so, transfection efficiency as well as *in vivo* tolerability might be enhanced. Nevertheless, this study already demonstrated the unmodified lipopolyplexes as powerful delivery systems for mRNA.

Scheme 5.2. Beneficial structural motifs of T-Shape lipo-oligoaminoamides (lipo-OAAs) for successful mRNA delivery *in vitro* and *in vivo*.

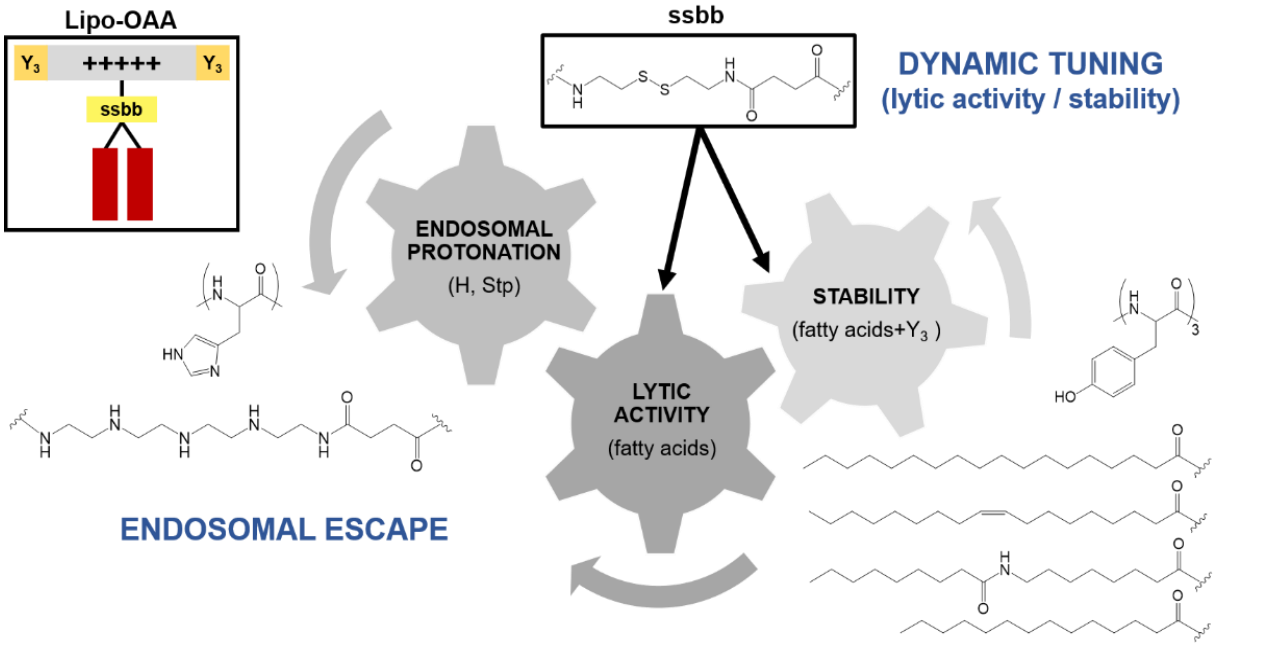

Stability, endosomal buffering properties, lytic activity, as well as bio-reducibility have to be balanced for optimum carrier performance. Tyrosine tripeptides as well as long-chain fatty acids can provide stability by hydrophobic interactions. Cationizable Stp (succinoyl tetraethylene pentamine) units together with histidines promote endosomal escape *via* endosomal protonation and buffering. Lytic activity of shorter and modified fatty acids can enhance the endosomal escape by lytic activity but also may cause toxicity. The bioreducible disulfide building block (ssbb) is cleaved upon high intracellular glutathione-concentrations and thus can release mRNA within the cytosol and reduce toxicity in a dynamic mode.

5.5 Supporting information

5.5.1 Supporting experimental section: Pre-experiments for the *in vivo* study

5.5.1.1 Encapsulation efficiency determined via RiboGreen assay

To determine the encapsulation efficiency, all samples were diluted to 4 µg/mL in water for injection (WFI). For “treated samples”, 50 µL of each sample as well as 50 µL of WFI as blank control were incubated with the same volume of heparin (c = 2.67 mg/mL) in 2% (v/v) TritonX-100 in a 96-well plate for 15 min at 70 °C and 300 rpm under constant shaking, followed by cooling to room temperature (RT). For “untreated samples”, 50 µL of each sample as well as 50 µL of WFI as blank control were diluted with the same volume of WFI. 100 µL of 100-fold diluted RiboGreen reagent (Quant-iT RiboGreen RNA Assay Kit; ThermoFisher, Waltham, Massachusetts, USA) in 1x TE buffer (10 mM Tris-HCl, 1 mM EDTA; pH 7.5 in diethylpyrocarbonate-treated water) were added into each well and incubated light-protected for 5 min at RT. The fluorescence intensity was measured on a Tecan plate reader (Perkin Elmer Life Science, Waltham, Massachusetts, USA) at excitation/emission wavelength of 785/535 nm, respectively. The encapsulation efficiency was expressed by following formula

$$100\% - \frac{emission_{"untreated\ sample"} - emission_{"untreated\ blank"}}{emission_{"treated\ sample"} - emission_{"treated\ blank"}} \times 100\%.$$

5.5.1.2 Measurement of relative mRNA integrity

The integrity of mRNA in the lipopolyplexes (N/P = 12, WFI) was determined *via* capillary gel electrophoresis using the Fragment Analyzer (Agilent Technologies, Santa Clara, California, USA). De-complexation of the nanoparticles (mRNA, c = 0.05 mg/mL) was carried out in heparin (c = 6 µg/µL), 0.2% (v/v) TritonX-100, and 50% (v/v) formamide. Samples were incubated for 15 min at 70 °C and 300 rpm. The mRNA reference was treated accordingly. For sample analysis, treated lipopolyplexes and the mRNA reference were diluted 1:4 in Diluent Marker (Standard Sensitivity RNA Diluent Marker (15nt); Agilent technologies, Santa Clara, California, USA).

5.5.2 Supporting figures

A)

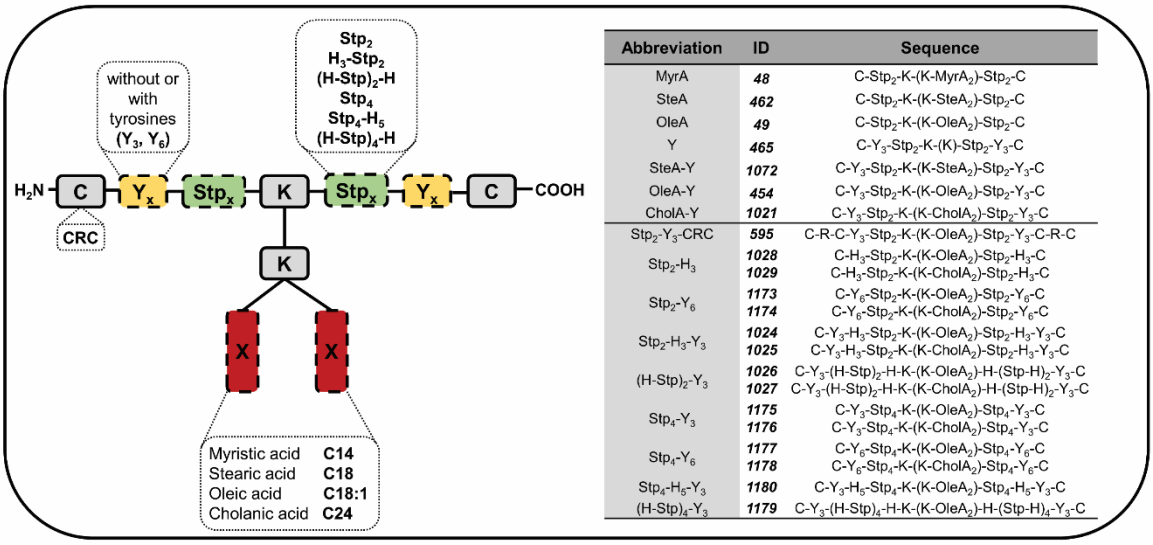

Abbreviation	ID	Sequence
MyrA	*48*	C-Stp_2-K-(K-$MyrA_2$)-Stp_2-C
SteA	*462*	C-Stp_2-K-(K-$SteA_2$)-Stp_2-C
OleA	*49*	C-Stp_2-K-(K-$OleA_2$)-Stp_2-C
Y	*465*	C-Y_3-Stp_2-K-(K)-Stp_2-Y_3-C
SteA-Y	*1072*	C-Y_3-Stp_2-K-(K-$SteA_2$)-Stp_2-Y_3-C
OleA-Y	*454*	C-Y_3-Stp_2-K-(K-$OleA_2$)-Stp_2-Y_3-C
CholA-Y	*1021*	C-Y_3-Stp_2-K-(K-$CholA_2$)-Stp_2-Y_3-C
Stp_2-Y_3-CRC	*595*	C-R-C-Y_3-Stp_2-K-(K-$OleA_2$)-Stp_2-Y_3-C-R-C
Stp_2-H_3	*1028*	C-H_3-Stp_2-K-(K-$OleA_2$)-Stp_2-H_3-C
	1029	C-H_3-Stp_2-K-(K-$CholA_2$)-Stp_2-H_3-C
Stp_2-Y_6	*1173*	C-Y_6-Stp_2-K-(K-$OleA_2$)-Stp_2-Y_6-C
	1174	C-Y_6-Stp_2-K-(K-$CholA_2$)-Stp_2-Y_6-C
Stp_2-H_3-Y_3	*1024*	C-Y_3-H_3-Stp_2-K-(K-$OleA_2$)-Stp_2-H_3-Y_3-C
	1025	C-Y_3-H_3-Stp_2-K-(K-$CholA_2$)-Stp_2-H_3-Y_3-C
(H-Stp)$_2$-Y_3	*1026*	C-Y_3-(H-Stp)$_2$-H-K-(K-$OleA_2$)-H-(Stp-H)$_2$-Y_3-C
	1027	C-Y_3-(H-Stp)$_2$-H-K-(K-$CholA_2$)-H-(Stp-H)$_2$-Y_3-C
Stp_4-Y_3	*1175*	C-Y_3-Stp_4-K-(K-$OleA_2$)-Stp_4-Y_3-C
	1176	C-Y_3-Stp_4-K-(K-$CholA_2$)-Stp_4-Y_3-C
Stp_4-Y_6	*1177*	C-Y_6-Stp_4-K-(K-$OleA_2$)-Stp_4-Y_6-C
	1178	C-Y_6-Stp_4-K-(K-$CholA_2$)-Stp_4-Y_6-C
Stp_4-H_5-Y_3	*1180*	C-Y_3-H_5-Stp_4-K-(K-$OleA_2$)-Stp_4-H_5-Y_3-C
(H-Stp)$_4$-Y_3	*1179*	C-Y_3-(H-Stp)$_4$-H-K-(K-$OleA_2$)-H-(Stp-H)$_4$-Y_3-C

B)

	Z-average (nm)	Mean PDI	Mean zeta potential (mV)
succPEI	59.8 ± 0.9	0.29 ± 0.05	27.8 ± 3.9
OleA-Y	46.0 ± 0.3	0.19 ± 0.01	27.9 ± 0.7
CholA-Y	89.8 ± 0.4	0.15 ± 0.01	20.5 ± 0.6

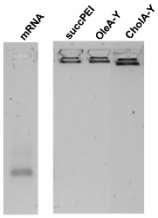

C)

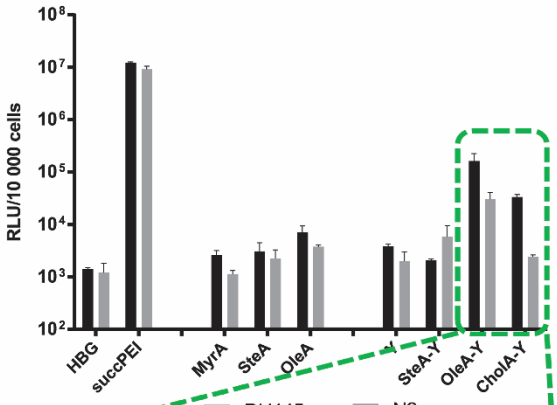

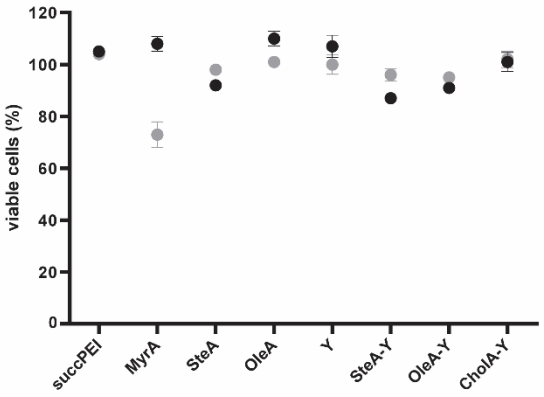

D)

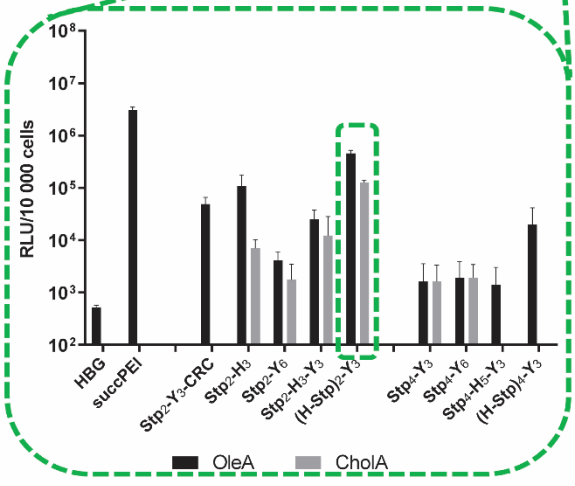

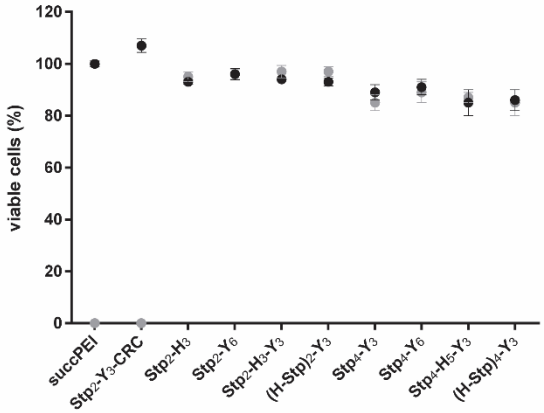

Figure 5.7. (**A**) Schematic structure of sequence-defined (lipo-)oligoaminoamides (OAAs) with T-shape topology and different modifications used in the pre-screening. (Stp: succinoyl tetraethylene pentamine, C: cysteine, K: lysine, Y: tyrosine, R: arginine, H: histidine, X: residue with different fatty acids, MyrA: myristic acid, SteA: stearic acid, OleA: oleic acid, CholA: 5β-cholanic acid). (**B**) Particle size (z-average in nm), polydispersity index (PDI) and zeta potential (in mV) of mRNA (lipo)polyplexes determined with DLS and ELS (*n* = 3; mean ± SD). Agarose gel shift assays for evaluation of mRNA binding efficiency of single (lipo-)OAAs. (Lipo)polyplexes were formed in HBG at N/P = 12 or at w/w = 4 in the case of succPEI polyplexes (10% succinylation). (**C**) Luciferase reporter expression assay and corresponding cell metabolic activity assay (CellTiter-Glo assay; Promega, Mannheim, Germany) of mRNA (lipo)polyplexes (N/P = 12, HBG) formed with T-shape (lipo-)OAAs at 24 h after transfection in DU145 and N2a cells. (**D**) Luciferase reporter expression assay and corresponding cell viability assay (CellTiter-Glo assay; Promega, Mannheim, Germany) of mRNA lipopolyplexes (N/P = 12, HBG) formed with T-shape lipo-OAAs with different structural motifs, both performed 24 h after transfection in DU145 cells. Cell viability was calculated as percentage to cells treated with HBG. SuccPEI polyplexes (10% succinylation, w/w = 4, HBG) were used as positive control, HBG treated cells as background (**C** and **D**). Transfection data are presented as mean value (+ SD) out of triplicate. Transfections were performed by Dr. Ana Krhač Levačić (Pharmaceutical Biotechnology, LMU Munich).

Note: In the pre-screening, several additional lipid-free OAAs were evaluated with topologies different from the T-Shape topology (3- and 4-arm structures) and with other cationic building blocks than Stp (Gtt: glutaryl triethylene tetramine; Sph: succinoyl pentaethylene hexamine). However, all of these carrier structures turned out to be ineffective in mRNA delivery.
The exact sequences of all OAAs evaluated in the pre-screening are listed in Table S1C together with their internal ID numbers and references.

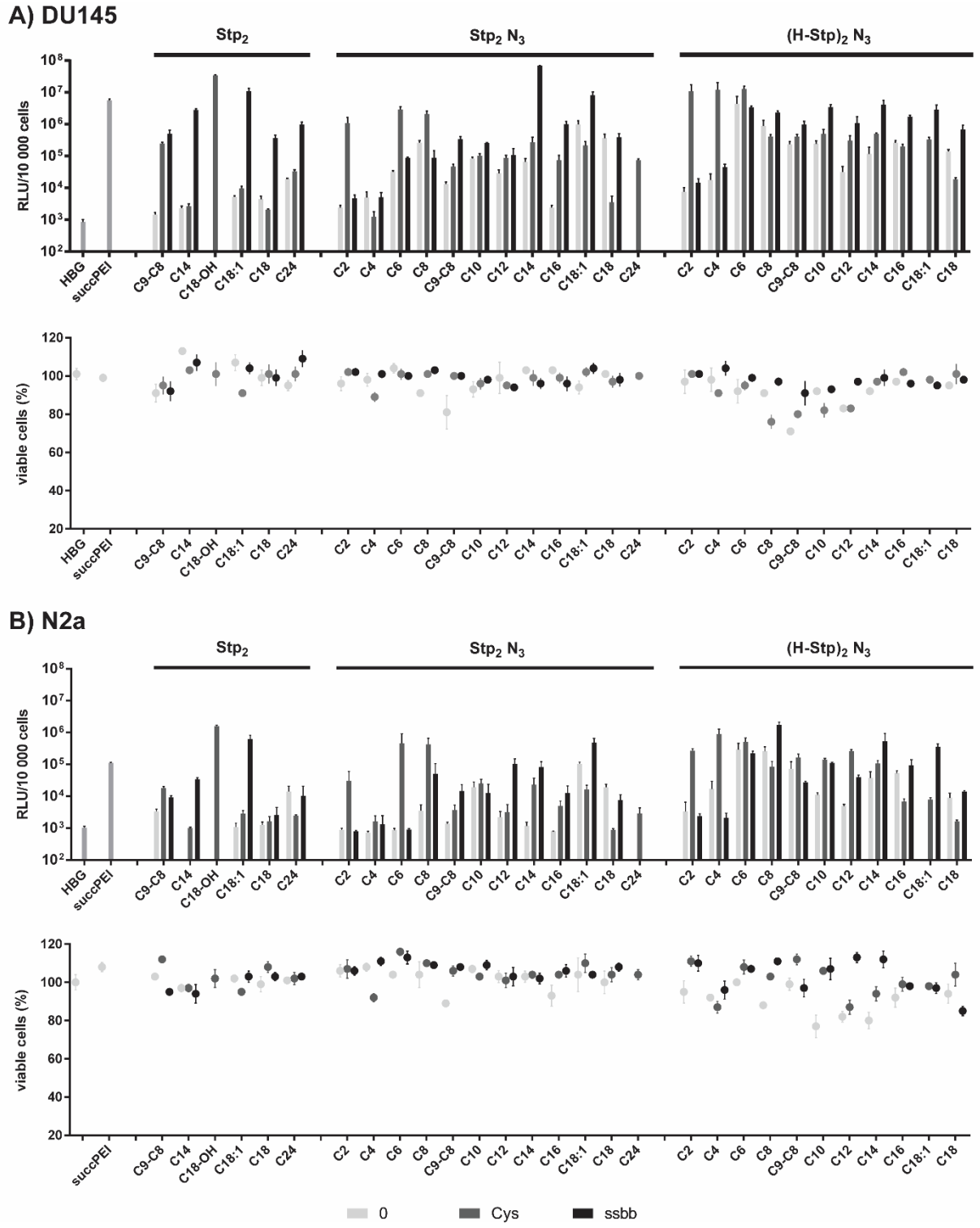

Figure 5.8. Luciferase reporter expression assay and corresponding cell metabolic activity assay (CellTiter-Glo assay; Promega, Mannheim, Germany) of mRNA (lipo)polyplexes (N/P = 12, HBG) formed with T-shape (lipo-)OAAs, both performed 24 h after transfection in (**A**) DU145, and (**B**) N2a cells. Cell viability was calculated as percentage to cells treated with HBG. SuccPEI polyplexes (10% succinylation, w/w = 4, HBG) were used as positive control, HBG treated cells as background. Data are presented as mean value (+SD) out of triplicate. Transfections were performed by Dr. Ana Krhač Levačić (Pharmaceutical Biotechnology, LMU Munich).

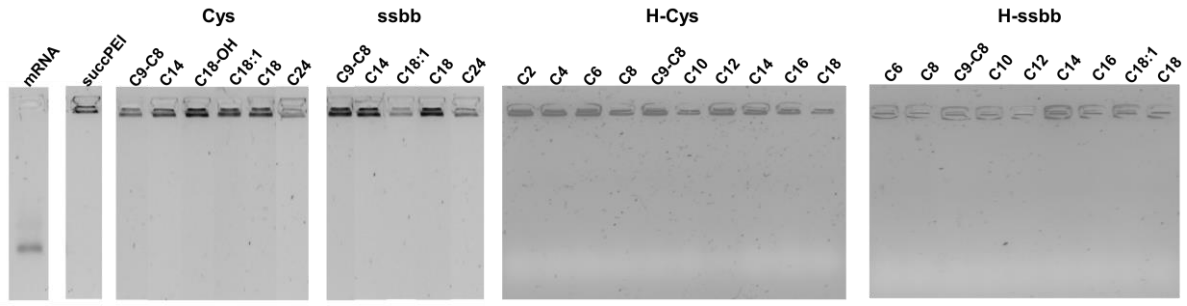

Figure 5.9. Standard agarose gel shift assay of mRNA (lipo)polyplexes formed at N/P = 12 in HBG. SuccPEI polyplexes (10% succinylation) were formed at w/w = 4 in HBG. The experiment was performed together with Dr. Ana Krhač Levačić (Pharmaceutical Biotechnology, LMU).

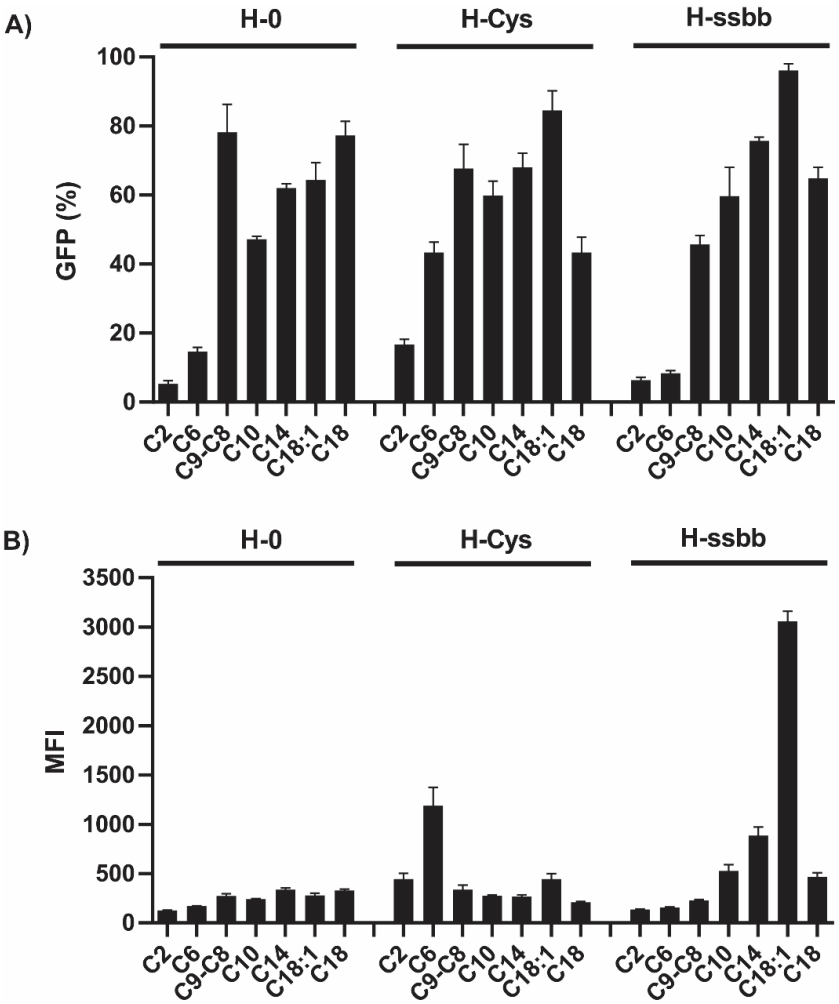

Figure 5.10. GFP expression in percentage after 24 h incubation of mRNA (lipo)polyplexes (N/P = 12, HBG) on DU145 cells as determined by flow cytometry (**A**) and corresponding mean fluorescence intensity (MFI) values (**B**). Data are presented as mean value (+ SD) out of triplicate. Flow cytometry was done together with Dr. Ana Krhač Levačić (Pharmaceutical Biotechnology, LMU Munich).

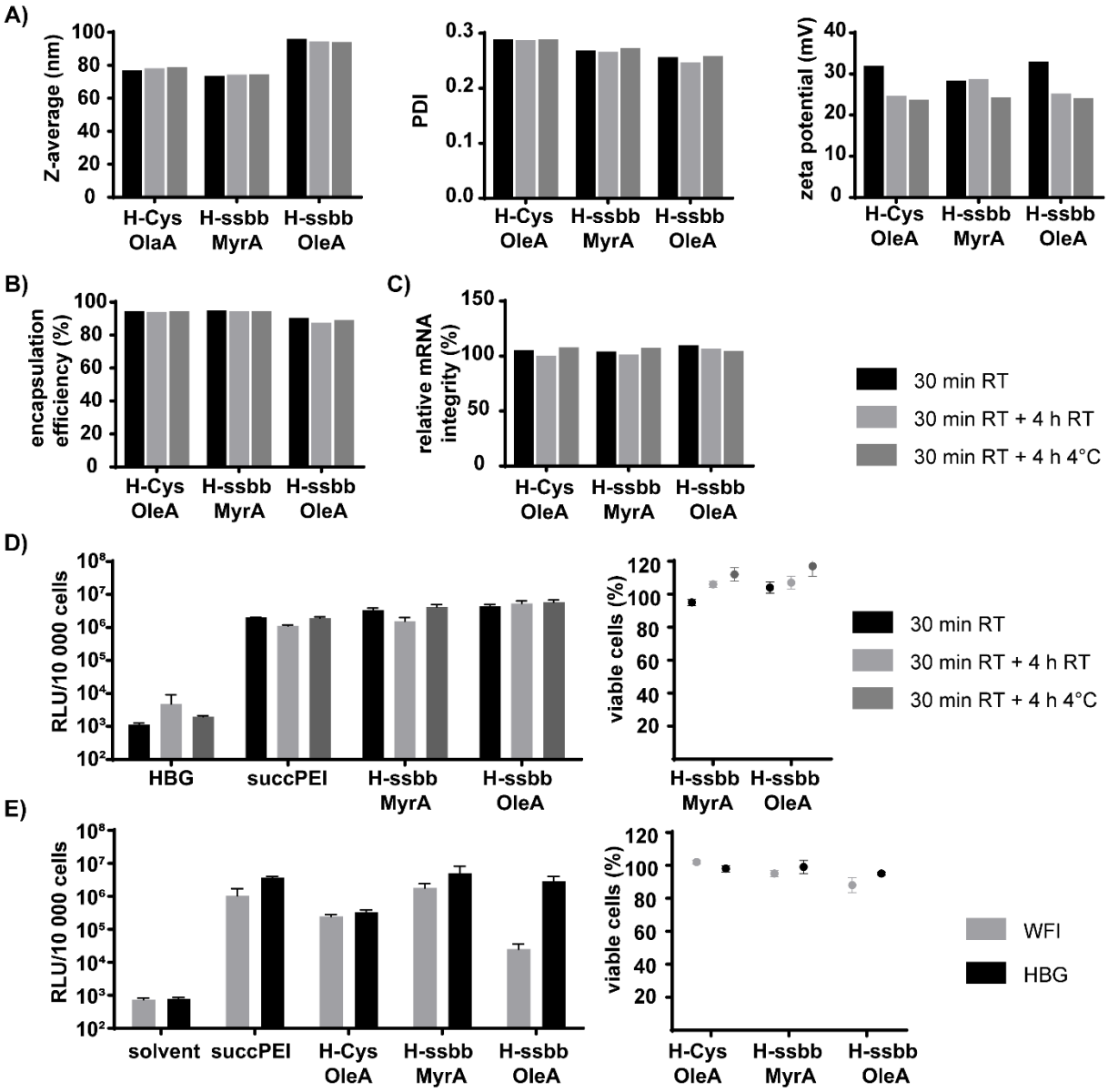

Figure 5.11. Pre-experiments for the *in vivo* study in order to evaluate the stability of mRNA lipopolyplexes (N/P = 12, WFI) after storage at RT or on ice (4 °C) for 4 h. (**A**) DLS and ELS results. (**B**) Encapsulation efficiency determined *via* RiboGreen assay (Quant-iT RiboGreen RNA Assay Kit; ThermoFisher, Waltham, Massachusetts, USA). (**C**) Relative mRNA integrity determined *via* capillary gel electrophoresis using the Fragment Analyzer (Agilent Technologies, Santa Clara, California, USA). (**D**) Luciferase reporter expression assay and corresponding cell metabolic activity assay (CellTiter-Glo assay; Promega, Mannheim, Germany), both performed 24 h after transfection in DU145 cells. Cell viability was calculated as percentage to cells treated with HBG. I Comparative transfection in DU145 cells with mRNA lipopolyplexes formulated at N/P = 12 in different solvents (WFI or HBG). Read-out was at 24 h after transfection. SuccPEI polyplexes (10% succinylation, w/w = 4) were used as positive control in the transfections. Transfection data are presented as mean value (+ SD) out of triplicate. Experiments A – C were performed with the help of Judith Müller (Ethris GmbH, Planegg). Transfections were performed by Dr. Ana Krhač Levačić (Pharmaceutical Biotechnology, LMU Munich).

5.5.3 Supporting tables

Table 5.3. List of all oligoaminoamides used in this study. Structures plus abbreviations, internal ID numbers and references of the histidine-free library (**A**) and of the histidine library (**B**), both evaluated in the main screen, as well as of the structures analyzed in the pre-screening (**C**).

A) Histidine-free library evaluated in the main screen.

Abbreviation		ID	Sequence (N→C)	Synthesis according to
0	C2	***1353***	$K(N_3)$-Y_3-Stp_2-$K(K(AcA)_2)$-Stp_2-Y_3	[29]
	C4	***1354***	$K(N_3)$-Y_3-Stp_2-$K(K(ButA)_2)$-Stp_2-Y_3	
	C6	***1355***	$K(N_3)$-Y_3-Stp_2-$K(K(HexA)_2)$-Stp_2-Y_3	
	C8	***1356***	$K(N_3)$-Y_3-Stp_2-$K(K(OctA)_2)$-Stp_2-Y_3	
	C9-C8	***1083***	Y_3-Stp_2-$K(G$-$K(NonOcA)_2)$-Stp_2-Y_3	[202, 209]
		1363	$K(N_3)$-Y_3-Stp_2-$K(K(NonOcA)_2)$-Stp_2-Y_3	
	C10	***1357***	$K(N_3)$-Y_3-Stp_2-$K(K(DecA)_2)$-Stp_2-Y_3	[29]
	C12	***1358***	$K(N_3)$-Y_3-Stp_2-$K(K(LauA)_2)$-Stp_2-Y_3	
	C14	***1081***	Y_3-Stp_2-$K(G$-$K(MyrA)_2)$-Stp_2-Y_3	[123]
		1359	$K(N_3)$-Y_3-Stp_2-$K(K(MyrA)_2)$-Stp_2-Y_3	[29]
	C16	***1360***	$K(N_3)$-Y_3-Stp_2-$K(K(PalA)_2)$-Stp_2-Y_3	[28]
	C18:1	***1107***	Y_3-Stp_2-$K(G$-$K(OleA)_2)$-Stp_2-Y_3	[123, 209]
		1208	$K(N_3)$-Y_3-Stp_2-$K(K(OleA)_2)$-Stp_2-Y_3	[208]
	C18	***989***	Y_3-Stp_2-$K(G$-$K(SteA)_2)$-Stp_2-Y_3	[123]
		1361	$K(N_3)$-Y_3-Stp_2-$K(K(SteA)_2)$-Stp_2-Y_3	[28]
	C24	***991***	Y_3-Stp_2-$K(G$-$K(CholA)_2)$-Stp_2-Y_3	[123]
Cys	C2	***1329***	$K(N_3)$-C-Y_3-Stp_2-$K(K(AcA)_2)$-Stp_2-Y_3-C	[29]
	C4	***1330***	$K(N_3)$-C-Y_3-Stp_2-$K(K(ButA)_2)$-Stp_2-Y_3-C	
	C6	***1331***	$K(N_3)$-C-Y_3-Stp_2-$K(K(HexA)_2)$-Stp_2-Y_3-C	
	C8	***1332***	$K(N_3)$-C-Y_3-Stp_2-$K(K(OctA)_2)$-Stp_2-Y_3-C	
	C9-C8	***1104***	C-Y_3-Stp_2-$K(K(NonOcA)_2)$-Stp_2-Y_3-C	[209]
		1339	$K(N_3)$-C-Y_3-Stp_2-$K(K(NonOcA)_2)$-Stp_2-Y_3-C	[202, 209]
	C10	***1333***	$K(N_3)$-C-Y_3-Stp_2-$K(K(DecA)_2)$-Stp_2-Y_3-C	[29]
	C12	***1334***	$K(N_3)$-C-Y_3-Stp_2-$K(K(LauA)_2)$-Stp_2-Y_3-C	
	C14	***1335***	$K(N_3)$-C-Y_3-Stp_2-$K(K(MyrA)_2)$-Stp_2-Y_3-C	
	C16	***1336***	$K(N_3)$-C-Y_3-Stp_2-$K(K(PalA)_2)$-Stp_2-Y_3-C	[28]
	C18-OH	***1105***	C-Y_3-Stp_2-$K(K(OHSteA)_2)$-Stp_2-Y_3-C	[209]
	C18:1	***454***	C-Y_3-Stp_2-$K(K(OleA)_2)$-Stp_2-Y_3-C	[137, 209]
		1198	$K(N_3)$-C-Y_3-Stp_2-$K(K(OleA)_2)$-Stp_2-Y_3-C	[204]
	C18	***1072***	C-Y_3-Stp_2-$K(K(SteA)_2)$-Stp_2-Y_3-C	[209]
		1337	$K(N_3)$-C-Y_3-Stp_2-$K(K(SteA)_2)$-Stp_2-Y_3-C	[28]
	C24	***1021***	C-Y_3-Stp_2-$K(K(CholA)_2)$-Stp_2-Y_3-C	[624]
		1340	$K(N_3)$-C-Y_3-Stp_2-$K(K(CholA)_2)$-Stp_2-Y_3-C	[202, 624]
ssbb	C2	***1341***	$K(N_3)$-Y_3-Stp_2-$K(G$-ssbb-$K(AcA)_2)$-Stp_2-Y_3	[29]
	C4	***1342***	$K(N_3)$-Y_3-Stp_2-$K(G$-ssbb-$K(ButA)_2)$-Stp_2-Y_3	
	C6	***1343***	$K(N_3)$-Y_3-Stp_2-$K(G$-ssbb-$K(HexA)_2)$-Stp_2-Y_3	
	C8	***1344***	$K(N_3)$-Y_3-Stp_2-$K(G$-ssbb-$K(OctA)_2)$-Stp_2-Y_3	
	C9-C8	***1084***	Y_3-Stp_2-$K(G$-ssbb-$K(NonOcA)_2)$-Stp_2-Y_3	[202, 209]
		1351	$K(N_3)$-Y_3-Stp_2-$K(G$-ssbb-$K(NonOcA)_2)$-Stp_2-Y_3	
	C10	***1345***	$K(N_3)$-Y_3-Stp_2-$K(G$-ssbb-$K(DecA)_2)$-Stp_2-Y_3	[29]
	C12	***1346***	$K(N_3)$-Y_3-Stp_2-$K(G$-ssbb-$K(LauA)_2)$-Stp_2-Y_3	
	C14	***1082***	Y_3-Stp_2-$K(G$-ssbb-$K(MyrA)_2)$-Stp_2-Y_3	[123]
		1347	$K(N_3)$-Y_3-Stp_2-$K(G$-ssbb-$K(MyrA)_2)$-Stp_2-Y_3	[29]
	C16	***1348***	$K(N_3)$-Y_3-Stp_2-$K(G$-ssbb-$K(PalA)_2)$-Stp_2-Y_3	[28]
	C18:1	***1108***	Y_3-Stp_2-$K(G$-ssbb-$K(OleA)_2)$-Stp_2-Y_3	[123, 209]
		1217	$K(N_3)$-Y_3-Stp_2-$K(G$-ssbb-$K(OleA)_2)$-Stp_2-Y_3	[208]

	C18	***990***	Y_3-Stp_2-K(G-ssbb-K(SteA)$_2$)-Stp_2-Y_3	[123]
		1349	K(N_3)-Y_3-Stp_2-K(G-ssbb-K(SteA)$_2$)-Stp_2-Y_3	[28]
	C24	***992***	Y_3-Stp_2-K(G-ssbb-K(CholA)$_2$)-Stp_2-Y_3	[123]

A: alanine; C: cysteine; G: glycine; H: histidine; K: lysine; K(N_3): azido-lysine; Y: tyrosine; Stp: succinoyl tetraethylene pentamine; Gtt: glutaryl triethylene tetramine; Sph: succinoyl pentaethylene hexamine; ssbb: cystamine disulfide building block; AcA: acetic acid (C2); ButA: butanoic acid (C4); HexA: hexanoic acid (C6); OctA: octanoic acid (C8); NonOcA: 8-nonanamido-octanoic acid (C9-C8); DecA: decanoic acid (C10); LauA: lauric acid (C12); MyrA: myristic acid (C14); PalA: palmitic acid (C16); OHSteA: hydroxystearic acid (C18-OH); OleA: oleic acid (C18:1); SteA: stearic acid (C18); CholA: 5β-cholanic acid.

Table 5.3 *continued.* B) Histidine library evaluated in the main screen.

Abbreviation		ID	Sequence (N→C)	Synthesis according to
H-0	C2	***1313***	$K(N_3)$-Y_3-(H-Stp)$_2$-H-K(K(AcA)$_2$)-H-(Stp-H)$_2$-Y_3	[29]
	C4	***1314***	$K(N_3)$-Y_3-(H-Stp)$_2$-H-K(K(ButA)$_2$)-H-(Stp-H)$_2$-Y_3	
	C6	***1315***	$K(N_3)$-Y_3-(H-Stp)$_2$-H-K(K(HexA)$_2$)-H-(Stp-H)$_2$-Y_3	
	C8	***1316***	$K(N_3)$-Y_3-(H-Stp)$_2$-H-K(K(OctA)$_2$)-H-(Stp-H)$_2$-Y_3	
	C9-C8	***1322***	$K(N_3)$-Y_3-(H-Stp)$_2$-H-K(K(NonOcA)$_2$)-H-(Stp-H)$_2$-Y_3	[202, 209]
	C10	***1317***	$K(N_3)$-Y_3-(H-Stp)$_2$-H-K(K(DecA)$_2$)-H-(Stp-H)$_2$-Y_3	[29]
	C12	***1318***	$K(N_3)$-Y_3-(H-Stp)$_2$-H-K(K(LauA)$_2$)-H-(Stp-H)$_2$-Y_3	
	C14	***1319***	$K(N_3)$-Y_3-(H-Stp)$_2$-H-K(K(MyrA)$_2$)-H-(Stp-H)$_2$-Y_3	
	C16	***1320***	$K(N_3)$-Y_3-(H-Stp)$_2$-H-K(K(PalA)$_2$)-H-(Stp-H)$_2$-Y_3	
	C18	***1321***	$K(N_3)$-Y_3-(H-Stp)$_2$-H-K(K(SteA)$_2$)-H-(Stp-H)$_2$-Y_3	
H-Cys	C2	***1272***	$K(N_3)$-C-Y_3-(H-Stp)$_2$-H-K(K(AcA)$_2$)-H-(Stp-H)$_2$-Y_3-C	[29]
	C4	***1273***	$K(N_3)$-C-Y_3-(H-Stp)$_2$-H-K(K(ButA)$_2$)-H-(Stp-H)$_2$-Y_3-C	
	C6	***1275***	$K(N_3)$-C-Y_3-(H-Stp)$_2$-H-K(K(HexA)$_2$)-H-(Stp-H)$_2$-Y_3-C	
	C8	***1252***	$K(N_3)$-C-Y_3-(H-Stp)$_2$-H-K(K(OctA)$_2$)-H-(Stp-H)$_2$-Y_3-C	
	C9-C8	***1258***	$K(N_3)$-C-Y_3-(H-Stp)$_2$-H-K(K(NonOcA)$_2$)-H-(Stp-H)$_2$-Y_3-C	[202, 209]
	C10	***1276***	$K(N_3)$-C-Y_3-(H-Stp)$_2$-H-K(K(DecA)$_2$)-H-(Stp-H)$_2$-Y_3-C	[29]
	C12	***1254***	$K(N_3)$-C-Y_3-(H-Stp)$_2$-H-K(K(LauA)$_2$)-H-(Stp-H)$_2$-Y_3-C	
	C14	***1256***	$K(N_3)$-C-Y_3-(H-Stp)$_2$-H-K(K(MyrA)$_2$)-H-(Stp-H)$_2$-Y_3-C	
	C16	***1277***	$K(N_3)$-C-Y_3-(H-Stp)$_2$-H-K(K(PalA)$_2$)-H-(Stp-H)$_2$-Y_3-C	
	C18:1	***1214***	$K(N_3)$-C-Y_3-(H-Stp)$_2$-H-K(K(OleA)$_2$)-H-(Stp-H)$_2$-Y_3-C	[28]
	C18	***1278***	$K(N_3)$-C-Y_3-(H-Stp)$_2$-H-K(K(SteA)$_2$)-H-(Stp-H)$_2$-Y_3-C	[29]
H-ssbb	C2	***1279***	$K(N_3)$-Y_3-(H-Stp)$_2$-H-K(G-ssbb-K(AcA)$_2$)-H-(Stp-H)$_2$-Y_3	[29]
	C4	***1280***	$K(N_3)$-Y_3-(H-Stp)$_2$-H-K(G-ssbb-K(ButA)$_2$)-H-(Stp-H)$_2$-Y_3	
	C6	***1281***	$K(N_3)$-Y_3-(H-Stp)$_2$-H-K(G-ssbb-K(HexA)$_2$)-H-(Stp-H)$_2$-Y_3	
	C8	***1282***	$K(N_3)$-Y_3-(H-Stp)$_2$-H-K(G-ssbb-K(OctA)$_2$)-H-(Stp-H)$_2$-Y_3	
	C9-C8	***1285***	$K(N_3)$-Y_3-(H-Stp)$_2$-H-K(G-ssbb-K(NonOcA)$_2$)-H-(Stp-H)$_2$-Y_3	[202, 209]
	C10	***1284***	$K(N_3)$-Y_3-(H-Stp)$_2$-H-K(G-ssbb-K(DecA)$_2$)-H-(Stp-H)$_2$-Y_3	[29]
	C12	***1303***	$K(N_3)$-Y_3-(H-Stp)$_2$-H-K(G-ssbb-K(LauA)$_2$)-H-(Stp-H)$_2$-Y_3	
	C14	***1304***	$K(N_3)$-Y_3-(H-Stp)$_2$-H-K(G-ssbb-K(MyrA)$_2$)-H-(Stp-H)$_2$-Y_3	
	C16	***1305***	$K(N_3)$-Y_3-(H-Stp)$_2$-H-K(G-ssbb-K(PalA)$_2$)-H-(Stp-H)$_2$-Y_3	
	C18:1	***1218***	$K(N_3)$-Y_3-(H-Stp)$_2$-H-K(G-ssbb-K(OleA)$_2$)-H-(Stp-H)$_2$-Y_3	[208]
	C18	***1306***	$K(N_3)$-Y_3-(H-Stp)$_2$-H-K(G-ssbb-K(SteA)$_2$)-H-(Stp-H)$_2$-Y_3	[29]

A: alanine; C: cysteine; G: glycine; H: histidine; K: lysine; $K(N_3)$: azido-lysine; Y: tyrosine; Stp: succinoyl tetraethylene pentamine; Gtt: glutaryl triethylene tetramine; Sph: succinoyl pentaethylene hexamine; ssbb: cystamine disulfide building block; AcA: acetic acid (C2); ButA: butanoic acid (C4); HexA: hexanoic acid (C6); OctA: octanoic acid (C8); NonOcA: 8-nonanamido-octanoic acid (C9-C8); DecA: decanoic acid (C10); LauA: lauric acid (C12); MyrA: myristic acid (C14); PalA: palmitic acid (C16); OHSteA: hydroxystearic acid (C18-OH); OleA: oleic acid (C18:1); SteA: stearic acid (C18); CholA: 5β-cholanic acid.

Table 5.3 *continued.* C) Structures analyzed in the pre-screening.

Abbreviation		ID	Sequence (N→C)	Synthesis according to
T-shape	MyrA	***48***	C-Stp$_2$-K(K-MyrA$_2$)-Stp$_2$-C	[200]
	SteA	***462***	C-Stp$_2$-K(K-SteA$_2$)-Stp$_2$-C	
	OleA	***49***	C-Stp$_2$-K(K-OleA$_2$)-Stp$_2$-C	
	Y	***465***	C-Y$_3$-Stp$_2$-K(K)-Stp$_2$-Y$_3$-C	[137]
	SteA-Y	***1072***	C-Y$_3$-Stp$_2$-K(K-SteA$_2$)-Stp$_2$-Y$_3$-C	[209]
	OleA-Y	***454***	C-Y$_3$-Stp$_2$-K(K-OleA$_2$)-Stp$_2$-Y$_3$-C	[137, 209]
	CholA-Y	***1021***	C-Y$_3$-Stp$_2$-K(K-CholA$_2$)-Stp$_2$-Y$_3$-C	[624]
	Stp$_2$-Y$_3$-CRC	***595***	C-R-C-Y$_3$-Stp$_2$-K(K-OleA$_2$)-Stp$_2$-Y$_3$-C-R-C	[138]
	Stp$_2$-H$_3$	***1028***	C-H$_3$-Stp$_2$-K(K-OleA$_2$)-Stp$_2$-H$_3$-C	[623]
		1029	C-H$_3$-Stp$_2$-K(K-CholA$_2$)-Stp$_2$-H$_3$-C	
	Stp$_2$-Y$_6$	***1173***	C-Y$_6$-Stp$_2$-K(K-OleA$_2$)-Stp$_2$-Y$_6$-C	
		1174	C-Y$_6$-Stp$_2$-K(K-CholA$_2$)-Stp$_2$-Y$_6$-C	
	Stp$_2$-H$_3$-Y$_3$	***1024***	C-Y$_3$-H$_3$-Stp$_2$-K(K-OleA$_2$)-Stp$_2$-H$_3$-Y$_3$-C	
		1025	C-Y$_3$-H$_3$-Stp$_2$-K(K-CholA$_2$)-Stp$_2$-H$_3$-Y$_3$-C	
	(Stp-H)$_2$-Y$_3$	***1026***	C-Y$_3$-(H-Stp)$_2$-H-K(K-OleA$_2$)-H-(Stp-H)$_2$-Y$_3$-C	
		1027	C-Y$_3$-(H-Stp)$_2$-H-K(K-CholA$_2$)-H-(Stp-H)$_2$-Y$_3$-C	[624]
	Stp$_4$-Y$_3$	***1175***	C-Y$_3$-Stp$_4$-K(K-OleA$_2$)-Stp$_4$-Y$_3$-C	[623]
		1176	C-Y$_3$-Stp$_4$-K(K-CholA$_2$)-Stp$_4$-Y$_3$-C	
	Stp$_4$-Y$_6$	***1177***	C-Y$_6$-Stp$_4$-K(K-OleA$_2$)-Stp$_4$-Y$_6$-C	
		1178	C-Y$_6$-Stp$_4$-K(K-CholA$_2$)-Stp$_4$-Y$_6$-C	
	Stp$_4$-H$_3$-Y$_3$	***1180***	C-Y$_3$-H$_3$-Stp$_4$-K(K-OleA$_2$)-Stp$_4$-H$_3$-Y$_3$-C	
	(Stp-H)$_4$-Y$_3$	***1179***	C-Y$_3$-(H-Stp)$_4$-H-K(K-OleA$_2$)-H-(Stp-H)$_4$-Y$_3$-C	
Abbreviation		**ID**	**Sequence (C→N)**	**Synthesis according to**
3-arm	3-arm Stp	***386***	C-Stp$_3$-K(Stp$_3$-C)$_2$	[64]
	3-arm H-Stp	***689***	C-H-(Stp-H)$_3$-K(H-(Stp-H)$_3$-C]$_2$	[184]
4-arm	4-arm H-Stp	***573***	A-K-[H-K-((H-Stp)$_3$-H-C)$_2$]$_2$	[144]
	4-arm H-Gtt	***577***	A-K-[H-K-((H-Gtt)$_3$-H-C)$_2$]$_2$	
	4-arm H-Sph-K	***784***	K-K-[H-K-((H-Sph-K)$_3$-H-C)$_2$]$_2$	[106]

A: alanine; C: cysteine; G: glycine; H: histidine; K: lysine; K(N$_3$): azido-lysine; Y: tyrosine; Stp: succinoyl tetraethylene pentamine; Gtt: glutaryl triethylene tetramine; Sph: succinoyl pentaethylene hexamine; ssbb: cystamine disulfide building block; AcA: acetic acid (C2); ButA: butanoic acid (C4); HexA: hexanoic acid (C6); OctA: octanoic acid (C8); NonOcA: 8-nonanamido-octanoic acid (C9-C8); DecA: decanoic acid (C10); LauA: lauric acid (C12); MyrA: myristic acid (C14); PalA: palmitic acid (C16); OHSteA: hydroxystearic acid (C18-OH); OleA: oleic acid (C18:1); SteA: stearic acid (C18); CholA: 5β-cholanic acid.

Table 5.4. Zetasizer results (*n* = 3; mean ± SD) of mRNA lipopolyplexes (N/P = 12, HBG) and succPEI polyplexes (10% succinylation, w/w = 4, HBG).

Polyplex/lipopolyplex		Z-average (nm)	Mean PDI	Mean zeta potential (mV)
succPEI		59.8 ± 0.9	0.29 ± 0.05	27.8 ± 3.9
Cys	C9-C8	86.4 ± 0.1	0.25 ± 0.01	37.6 ± 2.6
	C14	79.0 ± 0.1	0.27 ± 0.01	39.3 ± 2.0
	C18-OH	1360.3 ± 84.1	0.27 ± 0.02	16.6 ± 0.3
	C18:1	62.0 ± 0.9	0.16 ± 0.02	28.4 ± 1.5
	C18	69.8 ± 1.2	0.31 ± 0.02	37.2 ± 2.1
	C24	79.4 ± 1.3	0.27 ± 0.01	28.4 ± 0.6
ssbb	C9-C8	116.1 ± 0.6	0.11 ± 0.02	30.0 ± 1.6
	C14	102.0 ± 0.7	0.21 ± 0.01	33.6 ± 1.5
	C18:1	77.1 ± 1.4	0.21 ± 0.01	41.1 ± 0.4
	C18	102.2 ± 0.8	0.21 ± 0.01	31.7 ± 0.7
	C24	165.2 ± 5.3	0.11 ± 0.01	25.8 ± 1.0
H-Cys	C2	83.4 ± 3.0	0.19 ± 0.02	8.8 ± 0.6
	C4	77.3 ± 3.6	0.23 ± 0.01	7.8 ± 0.6
	C6	76.3 ± 2.0	0.24 ± 0.01	9.3 ± 0.3
	C8	136.4 ± 3.4	0.25 ± 0.02	7.7 ± 1.8
	C9-C8	78.9 ± 5.2	0.30 ± 0.04	17.4 ± 1.4
	C10	83.7 ± 1.0	0.27 ± 0.02	14.2 ± 0.7
	C12	63.9 ± 2.3	0.28 ± 0.00	17.8 ± 2.6
	C14	86.6 ± 2.7	0.28 ± 0.03	16.8 ± 1.0
	C16	86.4 ± 6.4	0.26 ± 0.01	18.3 ± 2.1
	C18	69.2 ± 4.2	0.28 ± 0.05	19.2 ± 2.5
H-ssbb	C2	857.4 ± 3.1	0.27 ± 0.06	0.3 ± 0.8
	C4	532.3 ± 10.2	0.25 ± 0.02	1.1 ± 0.2
	C6	233.9 ± 3.4	0.14 ± 0.01	- 3.7 ± 1.4
	C8	159.2 ± 1.2	0.17 ± 0.03	- 1.2 ± 0.4
	C9-C8	79.1 ± 1.6	0.18 ± 0.01	10.5 ± 0.9
	C10	69.0 ± 0.4	0.23 ± 0.00	7.4 ± 0.6
	C12	75.7 ± 0.9	0.21 ± 0.01	17.3 ± 0.9
	C14	78.7 ± 1.3	0.19 ± 0.01	17.8 ± 0.4
	C16	70.0 ± 1.9	0.20 ± 0.02	18.9 ± 0.2
	C18:1	93.2 ± 0.5	0.11 ± 0.00	10.5 ± 0.2
	C18	70.2 ± 0.8	0.18 ± 0.01	16.4 ± 1.3

Zetasizer measurements were performed together with Dr. Ana Krhač Levačić (Pharmaceutical Biotechnology, LMU Munich).

5.6 Abbreviations

brPEI, branched polyethylenimine 25 kDa; DAPI, 4′,6-diamidino-2-phenylindole; DLS, dynamic laser-light scattering; EGFP, enhanced green fluorescence protein; ELS, electrophoretic laser-light scattering; EtBr, ethidium bromide; FBS, fetal bovine serum; Gtt, glutaryl triethylene tetramine; GSH, glutathione; HBG, 20mM HEPES buffer with 5% glucose (pH 7.4); linPEI, linear polyethylenimine 22 kDa; mRNA, messenger RNA; N/P ratio, nitrogen-to-phosphate ratio; OAA, oligoaminoamide; PBS, phosphate-buffered saline (pH 7.4); pDNA, plasmid DNA; PEI, polyethylenimine; PFA, paraformaldehyde; RLU, relative light units, siRNA, small-interfering RNA; Sph, succinoyl pentaethylene hexamine; SPPS, solid-phase assisted peptide synthesis; ssbb, cystamine disulfide building block; Stp, succinoyl tetraethylene pentamine; succPEI, succinylated branched polyethylenimine 25 kDa; WFI, water for injection.

5.7 Acknowledgements

We thank Dr. Stephan Morys, Dr. Philipp Klein, Dr. Sören Reinhard, Dr. Dongsheng He, Dr. Christina Troiber and Dr. Jie Luo for the OAA synthesis, Wolfgang Rödl for technical support, and Dr. Günther Hasenpusch for support in the mouse study. Moreover, we gratefully acknowledge Prof. Christian Plank, shareholder of Ethris GmbH, for his helpful advice. In addition, we thank all other members of Ethris GmbH, which contributed to this study, for technical support and discussions.

6. Nucleic acid-based approaches for tumor therapy

Simone Hager[a,], Frederic Julien Fittler[b], Ernst Wagner[a], and Matthias Bros[b,*]*

[a] Pharmaceutical Biotechnology, Department of Pharmacy, and Center for NanoScience (CeNS), Ludwig-Maximilians-Universität (LMU) Munich, Butenandtstr. 5-13, D-81377 Munich, Germany
[b] Department of Dermatology, University Medical Center, 55131 Mainz, Germany

***** Corresponding authors: S. Hager and M. Bros

This chapter is adapted from pre-copy-edited version of a peer-reviewed research article published in ***Cells*** **2020, 9, (9), 2061 (ref. [234]).**

Author contributions

Each author has substantially contributed to drafting this review. S. Hager, E. Wagner, and M. Bros conceptualized the review topic. S. Hager, F.J. Fittler, E. Wagner, and M. Bros wrote the manuscript draft, and S. Hager, E. Wagner, and M. Bros revised it. E. Wagner, and M. Bros were responsible for funding acquisition. All authors have read and agreed to the published version of the manuscript.

Abstract

Within the last decade, the introduction of checkpoint inhibitors proposed to boost the patients' anti-tumor immune response has proven the efficacy of immunotherapeutic approaches for tumor therapy. Furthermore, especially in the context of the development of biocompatible, cell type targeting nano-carriers, nucleic acid-based drugs aimed to initiate and to enhance anti-tumor responses have come of age. This review intends to provide a comprehensive overview of the current state of the therapeutic use of nucleic acids for cancer treatment on various levels, comprising *i*) mRNA and DNA-based vaccines to be expressed by antigen presenting cells evoking sustained anti-tumor T cell responses, *ii*) molecular adjuvants, *iii*) strategies to inhibit/reprogram tumor-induced regulatory immune cells *e.g.*, by RNA interference (RNAi), *iv*) genetically tailored T cells and natural killer cells to directly recognize tumor antigens, and *v*) killing of tumor cells, and reprograming of constituents of the tumor microenvironment by gene transfer and RNAi. Aside from further improvements of individual nucleic acid-based drugs, the major perspective for successful cancer therapy will be combination treatments employing

conventional regimens as well as immunotherapeutics like checkpoint inhibitors and nucleic acid-based drugs, each acting on several levels to adequately counteract tumor immune evasion.

Keywords

Nucleic acids, nanoparticle, transgene, antigen, adjuvant, dendritic cell, tumor, immunotherapy.

6.1 Introduction

Cancer is a serious and life threatening disease with increasing incidence in today's world.[636-640] Depending on the tumor type, stage, and location, cancer therapy can be very challenging. Conventional treatments (surgery, chemotherapy, and irradiation) are often inefficient, resulting in recurrence and even death. The main reasons for therapy failure are chemoresistance as well as metastasis.[641, 642] Moreover, the patients often suffer from severe side-effects.[643] In the last 20–30 years, however, cancer treatment regimens have changed remarkably, based on the gained knowledge about molecular biology as well as tumor pathobiology and pathophysiology.[644-646] As a consequence of a better understanding of the tumor as a heterogeneous tissue with different types of cells, new strategies for cancer therapy have been developed, which are also applicable in combination with classical therapies.[5, 647-658] However, still only a limited number of patients responds to the already approved immunotherapies, and toxicity as well as induction of resistance towards treatment are often a problem.[659-663] Nanotechnology-based strategies, and in particular therapeutic nucleic acids, as well as combined immunotherapies may improve the therapeutic outcome in more patients for a broad range of tumors, even in late stage. In this regard, nucleic acid-based immunotherapeutic approaches have received growing interest.[5-7]

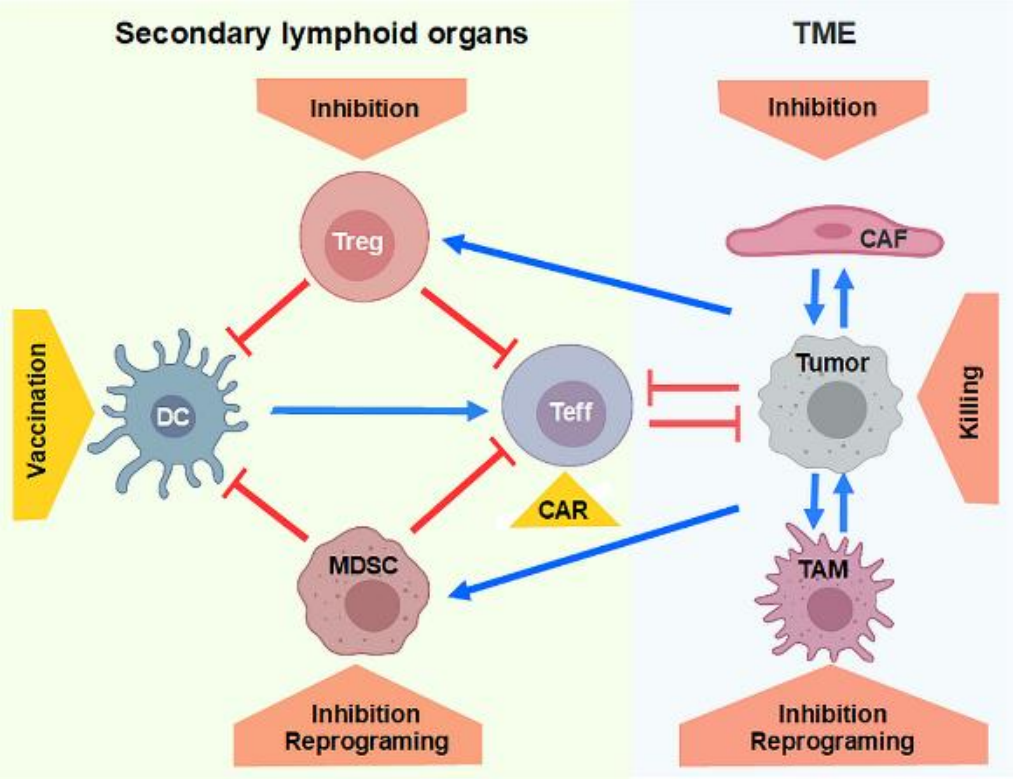

Figure 6.1. Nucleic acid-based strategies for tumor therapy. Vaccination of dendritic cells (DC) aims to induce tumor-specific effector T cells (Teff), which in turn kill tumor cells. Regulatory immune cells, regulatory T cells (Treg) and myeloid-derived suppressor cells (MDSC), are induced by the tumor and other cells of the tumor microenvironment (TME) and inhibit both DC and Teff. The expansion and suppressive activity of Treg/MDSC can be inhibited by RNA interference (RNAi) and MDSC may be reprogramed to yield antigen presenting cells by applying nucleic acid-based stimuli. Further, T cells can be transfected/transduced with chimeric antigen receptors (CAR) to gain tumor specificity. Teff are inhibited by factors within the TME. Tumor-specific delivery of nucleic acids (gene-coding or conferring RNAi) is aimed to induce apoptosis in tumor cells, and to inhibit or reprogram accessory cells within the TME, tumor-associated macrophages (TAM), and cancer-associated fibroblasts (CAF).

This review aims to present a comprehensive overview of the current state of nucleic acid-based anti-tumor therapeutics, and associated optimization strategies. As depicted in **Figure 6.1**, such strategies aim *i*) to deliver tumor-related antigen plus adjuvant to antigen presenting cells (APC) like dendritic cells (DC) that induce tumor-specific immune responses, *ii*) to either deplete or reprogram tumor-induced/expanded immunoregulatory cell types, especially regulatory T cells (Treg) and myeloid-derived suppressor cells (MDSC), which collectively inhibit the induction of adaptive immune reactions in the periphery, *iii*) to generate tumor-specific T cells and natural killer (NK) cells by genetic introduction of synthetic antigen receptors, termed CARs (chimeric antigen receptors),

and *iv*) at the tumor site itself to yield direct tumor cell killing, and to inhibit the tumor-promoting function of the tumor microenvironment (TME). It is worth mentioning that the first clinical trial ever using *in vivo* gene transfer was conducted by Nabel *et al.* in 1993 with an intratumorally applied liposomal formulation of immunotherapeutic DNA encoding for HLA (human leukocyte antigen)-B7.[664]

6.2 Nucleic acid-based strategies to induce adaptive anti-tumor responses

In the last decades, the potential to exploit the patients´ immune system to induce and shape anti-tumor responses has gained increasing interest.[665] The induction of tumor antigen-specific adaptive immune responses requires co-delivery of the antigen and of an immunostimulatory compound to evoke activation of a professional antigen presenting cell (APC).[666] In this regard, DC that are considered the most potent APC population at stimulated state are in the focus of interest.[667] In conventional vaccination approaches, the antigen is applied as a peptide/protein in combination with a structurally different adjuvant that specifically triggers a danger receptor expressed by DC (and other APC).[668] According vaccination approaches need to overcome several obstacles like *i*) unwanted uncoupling of antigen and adjuvant *in vivo*, which may contribute to unwanted immune reactions, *ii*) binding/uptake of the vaccine by non-APC, including regulatory immune cells like tumor-associated macrophages (TAM) and tumor-induced myeloid-derived suppressor cells (MDSC), which may result in the induction of tumor immune tolerance, and *iii*) limited presentation of the exogenous antigen *via* major histocompatibility complex class I (MHCI), yielding limited activation of $CD8^+$ T cells, and thereby insufficient induction of cytotoxic tumor lymphocytes (CTL). As outlined in the following, nucleic acids (plasmid DNA (pDNA), or messenger RNA (mRNA)) encoding for antigens and nucleic acid-based adjuvants, especially when encapsulated in APC-targeting nanoparticles (NP), provide an interesting alternative to conventional vaccination approaches.

So far, nucleic acid-based vaccines have been delivered largely by intramuscular, intradermal as well as subcutaneous injections, resulting in predominant transfection of myocytes[669] and keratinocytes,[670] respectively. Whereas mRNA-based transgenes are expressed directly in the cytoplasm of the transfected cell,[671] pDNA needs to translocate to the nucleus for transcription, followed by translation in the cytoplasm.[672] In case of intramuscular[673] as well as cutaneous[674] administration, directly transfected cells may

express the antigen. Antigen may be transferred to regional APC by the release of exosomes[675] or apoptotic bodies.[676] In either case, antigen of exogenous origin is presented largely on MHCII, resulting in the activation of antigen-specific $CD4^+$ T helper cells (Th).[677] Only subpopulations of DC are characterized by so-called cross priming activity, which means that antigen is shuttled/processed in such a manner that MHCI is loaded, resulting in $CD8^+$ T cell activation.[678] In case of direct APC transfection,[679] the antigen is expressed and processed like an endogenous gene, resulting in parallel loading onto MHCI and MHCII molecules.[680] APC that are sufficiently stimulated by pathogen-derived molecular patterns (PAMP) or endogenous danger signals, mimicked by the adjuvant, upregulate expression of MHC molecules, of costimulators and of soluble mediators (*i.e.*, cytokines), and migrate into the secondary lymphoid organs (draining lymph nodes, spleen) to prime antigen-specific T cells.[681] Activated $CD4^+$ T cells are required for full activation of $CD8^+$ T cells to yield CTL,[682] and to confer so-called B cell help.[683] Depending largely on the composition of cytokines released by activated APC, $CD4^+$ T cells polarize into various types of Th.[684] In case of tumor responses, the induction of Th1 cells, depending largely on IL-12, is paramount for CTL activation.[685]

6.2.1 Clinical trials using nucleic acid-based vaccines for tumor therapy

6.2.1.1 pDNA vaccines

In an early clinical phase I trial, stage IV melanoma patients were intranodally infused with pDNA encoding for melanoma-associated tyrosinase every two weeks for a total of four times.[686] This trial confirmed tolerability of pDNA administration, and some activation of tyrosinase-specific T cells, but no clinical responses were observed. In subsequent clinical trials DC were differentiated *in vitro* from peripheral blood monocytes of patients using GM-CSF (granulocyte macrophage colony–stimulating factor) plus interleukin (IL)-4, pulsed with tumor lysate/proteins, matured and reinfused.[687] In order to evaluate the suitability of nucleic acid-based vaccination, in a clinical phase I/II trial that enrolled stage IV melanoma patients, monocyte-derived DC were transfected *in vitro* with pDNA encoding melanoma-associated antigens melan A and gp100 using a cationic peptide for pDNA transfer, and chloroquine to promote endosomal escape, and were stimulated with TNF (tumor necrosis factor)-α and IL-1β.[688] Patients were vaccinated every three weeks for a total of three months. Whereas antigen-specific T cell responses were observed, the clinical response rate was only in the range of 10%, and not sustained. So far, similar

results have been obtained in most clinical studies on APC-focused pDNA vaccination (tabulated in [689]).

Only a few clinical trials have demonstrated therapeutic efficacy of pDNA vaccination. In a clinical phase I/II study, patients with carcinoembryonic antigen (CEA)-positive tumors (in most cases colorectal cancer) were repetitively treated with a pDNA vaccine that encoded for a MHCI-restricted CEA-derived peptide fused to an immunostimulatory domain derived from tetanus toxin fragment C as an adjuvant by intramuscular injection for three months.[690] About half of the patients developed diarrhea due to a break in tolerance towards CEA, which is also expressed by colonic mucosa. The group of patients that developed autoimmunity showed a prolonged overall survival over the 16 months' observation period.

Several reports have shown that combined treatment with a pDNA vaccine and a second drug exerted improved anti-tumor responses. In a clinical phase I trial, progression of metastatic prostate cancer was attenuated in more than half of the patients vaccinated for three months with a prostate acid phosphatase encoding pDNA plus recombinant GM-CSF as an adjuvant, co-applied intradermally, in combination with the programmed cell death protein (PD-)1 blocking antibody pembrolizumab.[691] This effect was not observed in case of sequential treatment with the antigen encoding vector/GM-CSF for three months followed by pembrolizumab application. In a phase IIB/III trial, treatment of non-small-cell lung cancer patients with a vaccinia virus encoding the tumor-associated antigen (TAA) Mucin-1, and IL-2 to stimulate T cells (TG4010) by repetitive subcutaneous injections yielded longer overall survival of patients upon co-treatment with first line chemotherapy (different drugs) as compared to patients that received chemotherapy only.[692] The efficacy of TG4010 in combination with checkpoint inhibitors is evaluated in ongoing phase II trials (NCT02823990, NCT03353675).

Due to the overall low efficacy of pDNA vaccination in clinical trials observed so far, pDNA vaccines need to be improved to yield stronger immunogenicity. In the following, various parameters that are important for the optimization of the design of pDNA vaccines as well as their delivery are discussed.

6.2.1.2 mRNA vaccines

Until a few years ago, mRNA-based anti-tumor vaccines were largely evaluated in clinical studies using patient-derived autologous DC electroporated *in vitro* with TAA-encoding mRNA either alone, in combination with adjuvant-encoding mRNA or subsequent stimulation with soluble mediators, followed by intradermal administration. In most of these trials, adaptive antigen-specific immune responses were detectable, but only some reached clinical responses (the outcome of these clinical trials is listed in [693]).

In an early phase II clinical trial, acute myeloid leukemia patients were vaccinated by intradermal injection with autologous DC electroporated *in vitro* with mRNA, encoding Wilms´ tumor 1 (WT1) antigen in bi-weekly intervals for four cycles.[694] About a third of the patients displayed complete remission after more than a year after the first vaccination. Therapeutic efficacy of vaccination with WT1-mRNA transfected DC was increased by including the lysosomal targeting signal of lysosomal-associated membrane protein (LAMP),[695] which previously demonstrated to achieve improved loading of antigen onto MHCII.[696] Similar results were achieved in another clinical phase II trial on patients with acute myeloid leukemia (AML) using human telomerase reverse transcriptase (hTERT) encoding mRNA for *ex vivo* electroporation of DC, followed by intradermal application.[697] The hTERT expression unit was fused to a LAMP minigene. Transfected DC were applied weekly for six weeks, followed by bi-weekly application for another six rounds. Recurrence-free survival of accordingly treated patients was prolonged as compared to historical controls.

Therapeutic efficacy of *ex vivo* mRNA-vaccinated DC was also demonstrated for glioblastoma, applied after surgical removal of the major tumor mass, and in combination with more conventional treatment regimens. In a phase II clinical trial, autologous DC were electroporated *ex vivo* with mRNA derived from surgically removed glioblastoma, and were maturated with a cocktail of proinflammatory mediators prior to intradermal application.[698] DC were applied six weeks after surgery and combined radiotherapy/chemotherapy (temozolomide), twice in the first week, and once per month afterwards (up to 18 treatments). All patients received chemotherapy throughout the vaccination period. The group of DC-treated patients showed prolonged progression-free survival. Strongly improved progression-free survival of glioblastoma patients vaccinated in a similar setting was also observed in a phase I clinical study using an mRNA encoding

cytomegalovirus (CMV) pp-65 for DC transfection and GM-CSF as an adjuvant.[699] CMV pp-65 was chosen based on the fact that glioblastoma cells expressed this protein, but no other brain cells.[700]

In melanoma therapy, efficacy of mRNA vaccines was observed in a study that enrolled stage III/IV melanoma patients after resection of metastases.[701] Autologous DC were co-transfected *ex vivo* with a mixture of four to six melanoma-associated antigen-encoding mRNAs (MAGE-A1/A3/C2, Melan A, gp100, tyrosinase) plus a mixture of adjuvants (either the toll-like receptor (TLR) 3 ligand polyriboinosinic:polyribocytidylic acid (poly(I:C)) plus CD40 ligand-mRNA, or TriMix-mRNA coding for CD40L, CD70, and a constitutively active TLR4 mutant). Transfected DC were applied intradermally in a bi-weekly cycle up to 12 times, and interferon (IFN)-α2b was administered concomitantly in most cases. Vaccinated patients showed an increased survival rate as compared to historical controls. In a follow-up study on stage III/IV melanoma patients, co-treatment of patients with DC co-electroporated with either of the melanoma antigen-mRNAs plus TriMix, and concomitant treatment with the checkpoint inhibitor ipilimumab (CTL-associated protein (CTLA-)4 blocking antibody), applied every three weeks for a total of four times yielded better long term survival rates than ipilimumab treatment alone.[702]

Within the last few years also some clinical trials assessing the potency of systemically applied mRNA-based vaccines (*e.g.*, NCT02410733; Lipo-MERIT) have been initiated, using lipoplexes to prevent mRNA degradation. The mRNA vaccine tested in the Lipo-MERIT study aims to directly target DC for melanoma therapy,[8] and is comprised of several mRNAs that encode four different TAA (MAGE-A3, NY-ESO-1, TPTE, and tyrosinase) to be presented *via* MHCI and MHCII, and induce IFN type I driven immune responses due to intrinsic stimulatory activity. In a preclinical setting, a liposomal formulation that specifically addressed DC was identified by testing the biodistribution and cell binding properties of a library of cationic liposomes consisting of DOTMA (1,2-di-O-octadecenyl-3-trimethylammonium propane) and DOPE (dioleoyl phosphatidylethanolamine), which differed in their size and zeta potential.[548] mRNA-loaded lipoplexes with a negative net charge and a diameter of around 300 nm almost exclusively accumulated in the spleen and were shown to address splenic and lymph node DC.

6.2.2 Optimization strategies for nucleic acid-based vaccines

6.2.2.1 Antigen

For tumor therapy, nucleic acid-based vaccines need to encode tumor-specific immunogenic peptides, which allows to comprise antigen-encoding sequences of different proteins within one minigene aimed to activate a broader number of $CD4^+$ and $CD8^+$ T cells.[703] In general, TAA may either constitute tumor-specific shared or tumor-specific unique antigens.[704] Whereas shared TAAs are also presented by normal cell types, albeit at lower extent, unique tumor antigens, also called neo-antigens, are exclusively expressed by tumors.[705] Especially in older studies, sequences encoding shared TAAs have been used,[706] but this may also result in autoimmune responses.[707] On the contrary, effector T cell responses towards neo-antigens, identified in a tumor-specific manner by mutagenome analysis, have been reported to be more potent.[708, 709] Moreover, antigens with a prolonged half-life have been shown to induce stronger CTL responses, and thereby increased immunogenicity.[710] To improve the presentation of (tumor) antigens, epitope-specific changes have been shown to increase MHC affinity,[711] including the use of xenogeneic antigens.[712] Loading of pDNA-encoded antigens onto MHCII was also demonstrated to be improved by inclusion of the coding sequence of the invariant chain.[713] mRNA-encoded antigens were shown to be presented at higher extent *via* MHCII when fused with the lysosomal targeting signal of LAMP.[696]

6.2.2.2 Adjuvant

Conventional pDNA was reported to possess intrinsic immunostimulatory activity due to a CpG-rich motif located within the ampicillin-resistance gene that triggered TLR9 in endo/lysosomes.[714] Besides, pDNA was also shown to bind cytosolic DNA sensors that mediate activation of the stimulator of IFN genes (STING) signaling pathway.[715] Moreover, physical stress associated with vaccination may also exert adjuvant effects as observed for gene gun-mediated delivery of gold particle adsorbed pDNA into the skin.[716]

However, nucleic acid-based vaccines normally contain an adjuvant, which is delivered as a separate unit, like the TLR3 agonist poly(I:C)[701] or CpG oligodeoxynucleotides (ODNs) that trigger TLR9,[717, 718] or more conventional adjuvants like Alum.[719] Whereas these moieties trigger danger receptors, in several studies the efficacy of transgenes that encode constitutively active mutants of danger receptors like TLR4, and receptors with co-stimulatory activity like CD40L and CD70[701] to confer APC

activation has been evaluated. Additionally, minigenes encoding signaling adaptors and transcription factors have been assessed in this regard. For example, Shedlock and co-workers reported that co-transfection of an NF-κB p65 expression plasmid and of a HIV protein encoding pDNA by *in vivo* electroporation of mice yielded stronger T cell responses.[720] Likewise, human monocyte-derived DC co-transfected *in vitro* with an mRNA encoding for a constitutively active form of IKKβ (inhibitor of nuclear factor kappa B kinase subunit beta) showed elevated upregulation of surface activation markers and cytokines like IL-12, and conferred stronger activation of co-cultured $CD8^+$ T cells[721] and NK cells.[722] Similarly, biolistic co-transfection of mice with an interferon regulatory transcription factor (IRF)-3 encoding pDNA enhanced T cell responses towards co-applied influenza antigen-encoding pDNA.[723]

Further, the suitability of pDNA[681] or mRNA[724] encoding cytokines intended to activate APC and to modulate T cells (in a paracrine manner) has been evaluated. For example, Li and co-workers co-administered healthy volunteers a multigene HIV DNA vaccine plus an IL-12 encoding pDNA by intramuscular injection, which conferred increased Th1/CTL responses.[725] Bontkes *et al.* demonstrated that human DC co-transfected *in vitro* with a TAA, and IL-12 as well as IL-18 encoding mRNA induced increased activity of co-cultured $CD8^+$ T cells and NK cells.[724] Similar findings were made in a preclinical mouse study upon intramuscular administration of a pDNA encoding mycobacteria antigen and IL-15, known to activate both APC as well as T cells and NK cells.[726] Further, administration of IL-2 and IL-7 pDNA expression constructs aimed to promote T cell activation and proliferation have been tested in preclinical studies.[727]

6.2.2.3 Inhibition of regulatory proteins in APC

In other studies, the potential of small-interfering RNA (siRNA) to inhibit the expression of endogenous inhibitory key factors in APC has been tested. For example, Luo and co-workers boosted anti-tumor responses using NPs that co-delivered the TLR3 ligand poly(I:C) and a siRNA specific for the transcription factor STAT (signal transducer and activators of transcription) 3,[728] which induces expression of anti-inflammatory factors like IL-10. Likewise, NPs delivering siRNA specific for the co-inhibitory receptor programmed cell death (PD) ligand 1 (PD-L1) have been evaluated in tumor studies.[729] More recently, also micro-RNA (miRNA) species, which constitute endogenously expressed small RNA species that inhibit gene expression (**Figure 6.2**), are considered

interesting candidates to modulate the activation state of APC.[730] For example, delivery of a plasmid harboring multiple miRNA consensus bindings sites, termed miRNA sponge,[731] and of anti-miRNA oligonucleotides,[732] is intended to limit the inhibitory effect of miRNAs on activation-associated mRNA targets.

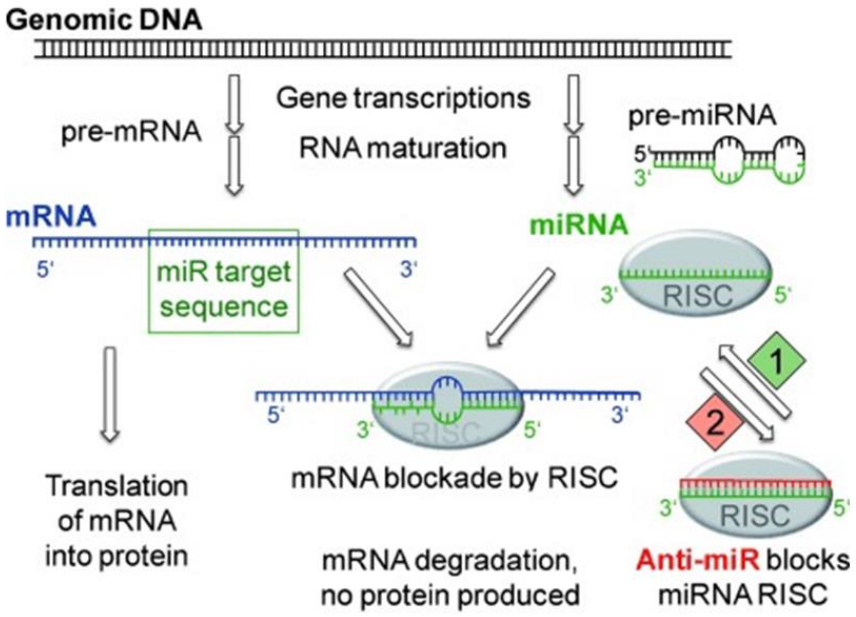

Figure 6.2. Mechanism of RNA interference (RNAi) and options for therapeutic intervention. (1) Substitution of tumor suppressor micro-RNA (miRNA, miR) in form of pre-miRNA or miRNA mimics, thereby inducing RNAi. (2) Blocking of oncogenic miRNA by miRNA-specific antagomirs (anti-miR). This figure is reprinted with permission from [733]. Copyright © 2020; John Wiley and Sons.

6.2.2.4 Structural optimization of pDNA vaccines

Expression units

In most of the aforementioned studies pDNA and mRNA species encoding antigen and adjuvant were applied as separate plasmids (in *trans*). However, the approach to integrate several transcription units into the same pDNA or mRNA in *cis* has received growing interest.[734] In case of pDNA, according vectors may either contain separate expression units each driven by another promoter, or a single promoter that regulates expression of the antigen and of molecular adjuvants. In case of the latter, which is also possible in case of mRNA vaccines, the different expression units may be separated either by an internal ribosomal entry site that confers cap-independent translation[735, 736] or virus-derived

recognition sites,[737] which in the derived long peptide are recognized by a ubiquitously expressed protease.[738]

Size reduction

A large part of pDNA is of prokaryotic origin and is required only for propagation in bacteria. It has been shown that after transfection prokaryotic parts are silenced by formation of heterochromatin, which may spread into the eukaryotic expression unit(s), and thereby limit transgene expression.[739] Therefore, the strategy to flank the expression cassette comprised of the promoter and the transgene-encoding part with phage recombinase-recognition sites has received growing interest. This configuration allows deletion of the prokaryotic part in the late phase of plasmid propagation by inducing phage recombinase. In several studies the derived mini-circle DNA (mcDNA) was reported to yield a higher transfection efficiency as well as a longer duration of gene expression as compared to the full length parental construct.[740]

Nuclear transfer

Moreover, in case of a pDNA vaccine its nuclear translocation is necessary for transcription of the encoded transgene(s), which constitutes a hurdle in mitotically inactive APC.[741] It was shown that transcription factors may bind recognition sites within the gene regulatory regions of the pDNA, and mediate nuclear import of the pDNA by their nuclear localization signal (NLS).[742] Especially the simian virus (SV)40 enhancer sequence was demonstrated to harbor several of these transcription factor binding sites, and inclusion of this region directly upstream or downstream of the transgene expression unit conferred enhanced nuclear import and elevated transfection efficiencies.[672] In a more controlled manner, viral peptides (*e.g.*, SV40 large T antigen) coupled to pDNA can facilitate its nuclear entry *via* their NLS.[743]

Transcriptional regulation

Expression units of pDNA-based vaccines are often under transcriptional control of virus-derived promotors characterized by ubiquitous activity at high level, like the human intermediate/early CMV or the SV40 promoter.[744] Since viral promoters may be subjected to methylation-mediated inactivation, both eukaryotic promoters, like the human elongation factor (EF)1α or beta-actin gene promoter, as well as viral/eukaryotic hybrid (*e.g.*, CMV/beta-actin) promoters have been introduced that allow long term transgene

expression.[745] These types of promoters are still widely used in preclinical and clinical studies. On the contrary, the potential of promoters that restrict gene expression to DC to avoid unwanted vaccine expression by regulatory immune cells (*e.g.*, TAM, MDSC) has been assessed in a limited number of preclinical studies only. The promoter of DC-STAMP (dendrocyte-expressed seven transmembrane proteins) is active in unstimulated human and mouse DC as well as in macrophages, and is downregulated upon stimulation.[746] Mice transduced with a lentivirus containing the DC-STAMP promoter displayed reporter activity in DC, monocytes, B cells, and NK cells.[747] Biolistic transfection of mice with a pDNA containing the promoter of the Langerhans cell (LC)-specifically active Dectin-2 gene resulted in LC-specific reporter activity,[748] and when employed in a lentiviral vector conferred both DC- and macrophage-restricted reporter expression.[749] In several studies the promoters of the evolutionarily conserved human[750] and mouse[751] fascin-1 genes were demonstrated to restrict gene expression to maturing DC. Biolistic transfection of mice with fascin-1 promoter driven antigen encoding pDNA yielded largely DC-restricted transgene expression, and conferred Th1-polarized immune responses in models of allergy,[752] and multiple sclerosis.[753] Furthermore, pDNA encoding for anti-inflammatory transforming growth factor (TGF)-β[753] and indoleamine 2,3-dioxygenase (IDO)[754] under transcriptional control of the fascin-1 promoter yielded tolerogenic effects.

6.2.2.5 NPs for APC-focused delivery of nucleic acids

Biocompatible NPs are highly interesting for cellular transfer of nucleic acids[755] in the context of nucleic acid-based tumor therapy,[756] since they offer protection against extracellular degradation by DNases[757] and RNases[758] either by dense complexation[759] or encapsulation[589] of nucleic acids. Especially in case of systemic application, NPs may confer either due to their intrinsic properties passive[548] or upon conjunction with surface receptor targeting moieties active[678] targeting of APC populations.

NP size and surface characteristics affecting biodistribution

With regard to the design of NPs it needs to be taken into account that DC as the often preferred target cell type internalize smaller particles (<200 nm) more efficiently,[760] whereas monocytes/macrophages preferably ingest larger ones (<5 µm) by means of receptor-mediated endocytosis and phagocytosis.[761] Besides size, also the shape of the NP may affect the efficacy of uptake as evaluated for gold-based NPs, which were

engulfed by macrophages more efficiently in case of spherical as compared to *e.g.*, elongated shape.[762] Both the cellular internalization of transfection complexes and the endosomal release of NP-complexed nucleic acids, can be increased by cell penetrating peptides (CPP) that are attached either *e.g.*, to the pDNA[763] or to the NP.[764]

Concerning the biodistribution of nucleic acid/NP transfection complexes, it was shown that small particles are easily transported into the lymph node, whereas larger particles remain longer at the site of administration.[765] Further, the route of administration can also account for the fate of NP delivery systems. After subcutaneous injection small PEGylated liposomes were found in a larger amount in the lymph node than after intravenous or intraperitoneal application.[766] Concerning NP clearance from the body, NPs that are smaller than 8 nm are cleared renally,[767] and the extent of renal clearance was shown to correlate with the extent of negative charge.[768] Biliary clearance was observed especially for particles over 200 nm, and for strongly charged particles.[769]

NP types suitable for APC transfection

By now, a large variety of materials and structures has been evaluated for transfer of nucleic acids into APC, comprising inorganic materials like solid core gold[770] and iron oxide-based,[771] mesoporous silica,[772] and graphene oxide[773] based NPs. The latter have repetitively shown to confer endosomal escape of nucleic acids.[774, 775] Polymer-based NPs bind nucleic acids by electrostatic interactions.[776] PLG (poly-*D,L*-lactide-co-glycolide),[777] PLGA (poly-*D,L*-lactic-co-glycolic acid),[778] and polyethylenimine (PEI)[625] are among the most intensely studied polymer-based NPs for delivery of nucleic acids. Of these, PEI by acting as a ‘proton sponge’ conferred the most pronounced endosomal release of nucleic acids,[126] but at the same time also mediated strong cytotoxicity.[779] Chitosan is a natural polysaccharide-based polymer, which has been evaluated for pDNA transfer,[780] and similar to PLGA,[781] was demonstrated to exert immunostimulatory activity.[782] Protein-based NPs offer the advantage of high biocompatibility.[783] For example, gelatin B (negatively charged) combined with protamine sulfate (positively charged) conferred DNA transfection, and mediated pDNA release under acidic conditions as apparent in endolysosomes.[784] Using endogenous proteins as nano-carriers may reduce potential immune reactions in response to repetitive application. In this regard, serum albumin coated with chitosan conferred DNA transfection.[785] NPs, consisting of albumin conjugated with cationic ethylenediamine complexed Bcl-2 specific siRNA,

intravenously injected into mice with established melanoma lung metastases successfully inhibited further tumor progression.[786] Cationic lipids complex negatively charged nucleic acids by electrostatic interactions, and by interaction with the negatively charged cell membrane confer internalization of lipoplexes.[787] DOTAP (*N*-[1-(2,3-dioleoyloxy)propyl]-*N,N,N*-trimethylammonium chloride) was the first lipid to be used for pDNA transfection,[788] and is still used either as a single component for complexation of nucleic acids or in combinations with helper lipids. With regard to the latter, neutral helper lipids like cholesterol have been included resulting in much stronger transfection efficiency presumably due to elevated endosomal escape of passenger DNA.[789] Incorporation of coiled-coil lipopeptides into liposomes resulted in direct release of the payload into the cytosol.[790]

Administration routes

Direct transfection of APC in secondary lymphoid organs can be achieved by intravenous application,[791] given that the nano-vaccine predominantly addresses APC by passive[548] or active[792] targeting. This would result in the induction of antigen-specific T effector cells, which can home to each tissue, and thereby also reach metastases irrespective of their location. However, as delineated in preclinical rodent biodistribution studies, systemically administered NPs of larger size (diameter ≥200 nm) may accumulate *e.g.*, in lung as reported *e.g.*, for mesoporous silica particles[793] or chitosan NPs.[794] Moreover, most NP formulations tested so far accumulate in the liver[795] as a consequence of the general clearance function of the liver,[796] conferred by Kupffer cells (KC) as the major liver-resident macrophage population[797] and liver sinusoidal endothelial cells (LSEC).[798] KC and LSEC are equipped with a number of danger receptors, including different C-type lectin receptors (CLR) as *e.g.*, the mannose receptor CD206,[799, 800] and scavenger receptors that broadly bind negatively charged ligands.[801, 802] Besides, KC[803] and LSEC[804] express high affinity Fc receptors, and KC also express complement receptors.[805] Therefore, it is conceivable that NPs, depending on the characteristics of the protein corona formed *in vivo*,[806] also including complement activation as shown for lectin-coated NP,[807] may be internalized preferentially by KC and LSEC. The formation of a pronounced protein corona may be attenuated by PEGylation, shown to reduce unwanted binding to KC[808] and LSEC,[809] and by conjugation with CD47, which serves as a ‘don’t-eat-me’ signal for macrophages as evaluated for liposomes.[810] Furthermore,

targeting moieties on NPs may engage according receptors on either non-parenchymal liver cell population. An example is mannose, which has frequently been used to address CD206-expressing APC of myeloid origin.[811, 812]

NP delivery *via* the skin constitutes an interesting alternative to systemic NP delivery for several reasons: *i*) topical application circumvents unwanted liver accumulation, *ii*) cutaneous DC, comprising Langerhans cells (LC) as the epidermal DC population, which form a dense network (200–1000 LC/mm^2 [813]), and dermal DC are apparent at rather high numbers in skin, and *iii*) targeting is not necessary since only DC, at activated state, are able to migrate to secondary lymphoid organs.[814] By now, several approaches for transfection of skin DC have been tested successfully in clinical trials concerning safety and tolerability and are used in preclinical studies to evaluate vaccines. These include conventional intradermal injection,[815] biolistic transfection of nucleic acids pre-adsorbed onto particles applied by gene gun[816] and PMED (particle-mediated epidermal delivery),[817] patches with dissolvable microneedles,[818, 819] and tattooing devices.[820] All of these transdermal delivery methods can transfer NP-complexed nucleic acids.[821] In case of biolistic transfection the method-associated physical stress was sufficient to confer activation and consequently emigration of transfected DC.[716] Further, administration of an electrical pulse just after intradermal[822] and intramuscular[823] injection, was shown to induce local inflammation, which activated APC at the according site, and to enhance overall transfection rates.[824] Consequently, electroporation devices that are applied in the context of intradermal injection are currently tested in clinical phase I (*e.g.,* NCT04336410) and phase II (NCT03180684) pDNA vaccination studies.

Other potential delivery routes for tumor vaccination comprise the respiratory system by applying nebulized pDNA or mRNA that largely transfect lung epithelia,[825] which has predominantly been employed for treatment of lung diseases like cystic fibrosis,[826] and oral vaccination approaches using attenuated bacteria (*e.g.*, Salmonella typhimurium) for pDNA transfer to APC in Payer's patches.[827]

Targeting of APC

Passive targeting of DC and monocytes/macrophages *in vivo* may be a consequence of the protein corona formed in case of many types of NPs due to adsorption of serum factors, which may constitute genuine ligands for cell surface receptors.[806] The composition of the protein corona is determined by several factors including *e.g.*, charge

and hydrophobicity of the particle surface. Further, serum factors due to interaction with the particle surface may alter their state of conformation, and thereby are recognized as 'new' ligands *e.g.,* by scavenger receptors.[828] Finally, NPs may be recognized as pathogen-like by the innate immune system, *e.g.*, in case of lectin surfaces intended to ensure biocompatibility of the NP, which however was found to trigger the lectin-dependent complement pathway.[829] This in turn resulted in adsorption of active complement C3 on the particle surface, and subsequent recognition of immune cells *via* complement receptors.[807] Unwanted adsorption of serum factors may be limited by conjugation with polyethylene glycol (PEG).[160] However, concerning the repetitive application of vaccines potential adverse reactions as *e.g.*, the induction of PEG-specific antibodies[830] need to be taken into account.

Active targeting of transfection complexes to DC and monocytes/macrophages can be achieved by conjugation of NPs with derivatives of natural ligands and antibodies that specifically bind endocytic surface receptors like C-type lectin receptors, which are expressed in a largely cell type-specific manner.**[831]** For example, the mannose receptor CD206 is highly expressed by macrophages (M2-like > M1-like), and is apparent at some extent on conventional DC,**[832]** whereas DC-SIGN is predominantly expressed by conventional DC populations, but only by a low fraction of macrophages.**[833]** In a preclinical study, intramuscular vaccination of mice with mannosylated cationic liposomes (distearoylphosphoethanolamine-polycarboxybetaine/DOTAP/cholesterol) that showed intrinsic DC stimulatory activity and complexed a HIV antigen-encoding pDNA improved HIV-specific T cell responses.**[834]** More recently, trimannosylated liposomes (1,2-bis(hexadecyl)glycerol/1,2-dioleoyl-*sn*-glycero-3-phosphocholine/cholesterol) were shown to specifically address DC-SIGN, and to accumulate at highest extent in the spleen after intravenous application, addressing predominantly DC.**[792]** While these approaches aimed to directly transfect APC *in vivo*, in an alternative approach, Wang and co-workers designed a pDNA that encoded a fusion protein consisting of a tumor antigen polypeptide and a single chain antibody fragment known to bind the murine DC-specific receptor CD11c.**[835]** Thereby, this pDNA was aimed to be expressed in non-APC, but the expressed fusion protein was meant to target DC. In a mouse breast cancer model, intramuscular injection of this pDNA prevented tumor growth when applied protectively prior to subcutaneous tumor cell inoculation, and attenuated tumor progression in a

therapeutic setting. As mentioned above, lipoplexes composed of DOTMA and DOPE loaded with mRNA with a negative net charge and a size of around 300 nm due to these characteristics predominantly targeted DC in secondary lymphoid organs.[548]

6.3 Inhibition of regulatory immune cells

The success of vaccination to induce a sustained antigen-specific anti-tumor response is limited by regulatory immune cells that are induced and expanded by tumors as part of their evasion strategy.[836] Both MDSC[837] and Treg[838] can attenuate the T cell stimulatory activity of APC, the activation of T cells as well as the anti-tumor function of Teff, and effector functions of NK cells. To counteract the suppressive effect of regulatory immune cells the suitability of RNAi has been delineated.[839, 840] Further, nucleic acids with immunostimulatory function were reported to reprogram MDSC to exert anti-tumor activity.[841]

6.3.1 Inhibition of Treg by RNA interference

Under homeostatic conditions, Treg ensure tolerance towards self-antigens to prohibit autoimmunity,[842] and against harmless antigens to prevent allergies.[843] Besides, as a negative feedback mechanism, Treg are expanded and are also induced *de novo* in the course of immune reactions in order to limit immune responses and thereby to minimize tissue damages. Under healthy conditions, Treg occur only in small numbers.[844] Depending on the place of origin, Treg can be differentiated in thymic Treg (tTreg), alternatively termed natural Treg,[845] and in Treg that are induced in the periphery (iTreg).[846] During thymopoieses, thymocytes which express a T cell receptor (TCR) with intermediate affinity for self-peptides, differentiate into immunosuppressive tTreg.[847] iTreg derive from $CD4^+$/$CD8^+$ T cells, whose TCR is not specific for self-antigens, but recognizes microbiota- and environmental antigens presented by DC in the periphery[848] in the context of low co-stimulation and/or Treg-promoting factors like retinoic acid, kynurenine and TGF-β.[849, 850] In mice, tTreg and some iTreg populations can be identified by constitutive expression of the IL-2 receptor CD25 and by co-expression of the transcription factor FoxP3,[851] whereas other iTreg populations are FoxP3-deficient, but may express anti-inflammatory mediators like IL-10 and TGF-β.[852]

In cancer, constituents of the TME produce anti-inflammatory mediators, which promote Treg expansion/induction in the periphery,[844] and release of chemokines as for example

the C-C motif chemokine ligand (CCL) 22, to recruit Treg to the tumor.[853] Treg suppress anti-tumor responses on the level of APC activity, T cell activation, T effector cell functions and the functions of NK cells by numerous mechanisms, as for example anti-inflammatory cytokines (*e.g.*, IL-10, TGF-β), surface receptor interactions (*e.g.*, negative cross-talk *via* CTLA-4), IL-2 depletion, and transfer of cyclic adenosine monophosphate (cAMP).[854]
There are different approaches to overcome the obstacle of Treg-mediated suppression of anti-tumor responses, including strategies to deplete Treg or to reduce their suppressive activity.[855] Concerning nucleic acid-based approaches to attenuate Treg induction, silencing of tumor-derived TGF-β in murine CT26 colon carcinoma cells by transfection with oligofectamine/TGF-β1 siRNA complexes suppressed Treg induction.[856] Most recently, Masjedi *et al*. reported that *ex vivo* silencing of the adenosine A2A receptor (A2AR) with an A2AR-specific siRNA complexed with PEG-chitosan-lactate (PCL) NPs inhibited the differentiation of $CD4^+CD25^-$ T cells derived from 4T1 breast tumor-bearing BALB/c mice toward Treg.[857] Alternative approaches have aimed to minimize the suppressive capability of Treg. For example, *in vitro* transfection of murine Treg with a Foxp3-specific siRNA resulted in profound inhibition of their suppressive capacity.[858] Another treatment option is to interfere with the recruitment of Treg to the tumor site. Kang and co-workers demonstrated that tumor infiltration with Treg in athymic nude mice, inoculated with human breast cancer cells, can be prohibited by tail vein injection of Treg transfected with a siRNA specific for CCL22.[859] Besides the use of synthetic siRNA for RNA interference, in recent years, miRNA (over)expression intended to alter the genetic program of Treg has gained increasing interest. In this regard, lentiviral transduction of Treg *in vitro* with miR-9 and miR-155 encoding vectors resulted in reduced expression of CTLA-4, which is a key factor for the immunosuppressive activity of Treg.[860] Also, Jonuleit *et al*. reported that in a mouse melanoma model systemic delivery of CTLA-4 specific siRNA by cationic lipid-assisted PEG–poly(lactic acid (PLA))-based NP resulted in reduced Treg numbers, and inhibited tumor growth.[861] Administration of miR-141 and miR-200a mimics in multiple sclerosis patients shifted the differentiation of naive T cells towards Th17, and at the same time inhibited Treg differentiation.[862] In a mouse model of epithelial ovarian cancer (EOC), *in vitro* transfection of $CD4^+$ T cells with miRNA 29a-3p and miR-21-5p mimics, complexed with the commercially available X-tremeGENE siRNA transfection reagent, and subsequent adoptive transfer into tumor-burdened mice

resulted in attenuated tumor growth.[863] This outcome was based on the inhibitory effects of both miRNA species on STAT3 expression, thereby favoring Th17 over Treg differentiation. In another study, transfection of Treg with miR-142-3p reduced the level of intracellular cAMP and adenylyl cyclase type 9 expression, which impaired their suppressive properties.[864] Treg-specific delivery of biologicals may be achieved by using IL-2-functionalized NPs as shown for hydroxyethyl starch nanocapsules that targeted Treg due to their constitutive high level expression of the IL-2 receptor CD25.[865]

Altogether, these studies demonstrate that nucleic acid-based strategies have a high potential to reduce overall Treg activity in cancer. However, it should be noted that Treg depletion may result in a compensatory induction of MDSC.[866]

6.3.2 Strategies for MDSC reprograming and depletion

MDSC derive from myeloid precursor cells during myelopoiesis.[867] Immunomodulatory factors generated by tumors like some cytokines, chemokines or colony-stimulating factors (CSF) are capable of stimulating expansion of MDSC on the expansion of monocytes, conventional DC, and neutrophils,[868] while chronic inflammations can lead to extramedullary myelopoiesis.[869] The expansion and activation of generated MDSC requires concerted interaction of several signaling pathways, like the NF-κB, JAK-STAT, HIF-1α, C/EBPβ and CHOP pathways. Based on the expression of plasma membrane markers, the amount of immune suppressive molecules as well as by functional analysis,[870] MDSC can be allocated to $CD11b^{+}Ly6G^{-}Ly6C^{hi}$ monocytic (m)MDSC and to $CD11b^{+}Ly6G^{+}Ly6C^{low}$ granulocytic (g)MDSC.[871] MDSC exert potent immune-suppressive activity against T cells[872] and NK cells.[873] Accordingly, MDSC contribute to control autoimmunity[874] and infections.[875] After activation, MDSC migrate to the site of inflammation or to the tumor site in response to a variety of chemokines.[876] There, MDSC generate an immune-suppressive milieu, which is enhanced by different cytokines.[869] The infiltration of mMDSC into a tumor leads to a distribution of tumor cells from the place of origin by induction of epithelial–mesenchymal transition (EMT), which generates a cancer stem cell (CSC) phenotype.[877] Tumor infiltration of gMDSC withdraws the CSC phenotype and leads to tumor cell proliferation and promotes metastasis. In secondary lymphoid organs, MDSC suppress APC, the activation of tumor antigen-specific T cells, and T effector cells by several mechanisms in an analogous manner as described for Treg.[878]

In some approaches, siRNA and miRNA have been applied to attenuate MDSC generation and their suppressive activity. For example, Boldin *et al*. have shown that miR-146a inhibited the proliferation of MDSC by targeting tumor necrosis factor receptor-associated factor 6 (TRAF6) and IL-1 receptor-associated kinase 1 (IRAK1).[879] Similarly, miR-424 was reported to interfere with MDSC differentiation.[840] In several mouse tumor models, intravenous application of oligofectamine/miR-223 complexes inhibited tumor-conferred MDSC generation by targeting myocyte enhancer factor 2C (MEF2C) in bone marrow progenitor cells.[880]

Moreover, some types of NPs as an intrinsic property have been reported to reprogram MDSC towards proinflammatory macrophages as shown *e.g.*, for cationic dextran- and PEI-based NPs[841] *in vitro,* and for NPs modified with a cationic polymer *in vivo.*[881] In addition, TLR agonists that address TLR7/8 (*e.g.*, R848) and TLR9 (CpG ODN) were shown to exert similar effects both *in vitro* and *in vivo,*[882] which may contribute to the overall immunostimulatory effect of these adjuvants.

6.3.3 Inhibition of Treg and MDSC by tumor-directed approaches

Besides direct targeting of Treg and MDSC *via* RNA interference, the induction/expansion and tumor infiltration of either regulatory cell type may also be controlled indirectly by affecting tumor gene expression and as a secondary effect in the course of inducing anti-tumor responses. Stem cell factor (SCF; c-kit ligand) is generated by tumors and confers MDSC infiltration.[883] In a mouse MCA26 colon tumor model, adenoviral transfer of SCF-specific siRNA resulted in reduced accumulation of MDSC at the tumor site.[884] Injection of a TNFAIP (TNF-α induced protein) 3-specific siRNA into E.G7 or B16-F10 melanoma induced apoptosis in MDSC *via* activation of the c-Jun *N*-terminal kinase (JNK) pathway.[885] Injection of vascular endothelial growth factor (VEGF)-specific siRNA, complexed with nanogels, into renal tumors significantly reduced MDSC numbers in that area.[886] Injection of a Newcastle Disease Virus Hemagglutinin–Neuraminidase encoding pDNA into the ear pinna of DA3 tumor bearing BALB/c mice promoted innate anti-tumor responses and reduced MDSC infiltration into the tumor site [887]. In humans suffering from pancreatic ductal adenocarcinoma (PDA), in many cases antibodies and T cells specific for α-enolase (ENO1) have been identified.[888] In a mouse model of autochthonous pancreatic cancer, injection/electroporation with a ENO1-encoding pDNA attenuated tumor growth and concomitantly also the expansion of Treg and MDSC.[889]

6.4 Generation of T cells and NK cells expressing CARs for tumor therapy

CARs are synthetic antigen receptors, which comprise an extracellular antibody domain, a transmembrane domain and an intracellular signaling domain, and recognize *e.g.*, tumor-associated antigens.[890] So-called CAR T cells (CAR-T) and CAR natural killer (CAR-NK) cells are generated by transfection of either cell type with a CAR-encoding pDNA, mRNA or are transduced with a CAR-encoding viral vector.[891] Therefore, CAR expressing cells are able to recognize antigens under tumor-induced immune-suppressive conditions and can exert a proper immune response. For CAR synthesis, the variable domains of an antibody's light and heavy chain are fused, for example by short glycine-serine linkers, to yield a single chain fragment variable (scFv).[892] The transmembrane domain is usually derived from CD28 or another membrane receptor.[893] In most cases, CD3ζ, which is a component of the endogenous TCR, serves as the signaling domain for CAR-T.[894] For CAR-NK, the transmembrane immune signaling adaptor chain is employed as the signaling domain.[890] The signaling domain is often combined with one or more co-stimulatory motifs[895] like CD28,[896] CD137, CD357, CD278, or CD134[897] for CAR-T, and CD28, CD137,[898] CD278, CD134,[899] or Dap10[896] in case of CAR-NK. The first generation of CARs contained only CD3 (ζ or γ chain) signaling motifs, which are able to activate murine CTL hybridoma cells, modified with chimeric genes for surface receptors, *e.g.*, to trigger IL-2 secretion, but these may be inactivated by tumors.[900] The second generation of CARs was equipped in addition with a co-stimulatory domain, and the third generation possessed more than one co-stimulatory domain.[901]

In an alternative approach, the signaling and the co-stimulatory domains are split between two different CARs, which is termed combinatorial targeting.[890] Until now, two CAR-T based immunotherapies have been approved by the United States Food and Drug Administration (FDA). Both are CD19-directed CAR-T immunotherapies, targeting the pan-B cell receptor CD19. They have shown significant results in the treatment of non-Hodgkin lymphoma (NHL), acute lymphoblastic leukemia (ALL), and chronic lymphocytic leukemia (CLL) [902]. Of these, treatment with tisagenlecleucel (T cells from the patients' blood are lentivirally transduced with CD19-specific CARs) yielded an overall remission rate of 81% after three months in patients suffering from relapsed or refractory ALL, but caused serious, mainly reversible toxic effects in children and young adults under 25 years.[903] In patients with NHL, axicabtagene ciloleucel (lentiviral transduction of patients'

blood T cells with CD19-specific CARs) resulted in an objective response rate of 82%, and a complete response in 54% of cases.[904] However, treatment with either CAR-T treatment can lead to serious and even life-threatening side effects, like the tumor lysis syndrome, a disease which can result from a tumor therapy, causing hyperuricemia, hyperkalemia, hyperphosphatemia, and hypocalcemia,[905] and the cytokine release syndrome that is induced by a cytokine storm,[906] leading to fever, hypotension and respiratory insufficiency.[907]

Another problem of CAR-Ts is the interaction of MDSC with CAR-Ts, which may lead to a reduction of CAR-T activation, to reduced proliferation after antigen stimulation, and lowered cytokine production.[908] MDSC in the liver, for example, suppress an anti-tumor response of CAR-Ts *via* binding of PD-L1 that engages PD-1 on T cells.[909] The expression of PD-L1 by MDSC in the liver is supported by GM-CSF and is largely regulated by the transcription factor STAT3. The negative effect of MDSC on CAR-T can be avoided by MDSC depletion, using therapeutic drugs like gemcitabine and 5-fluorouracil,[910] neutralization of GM-CSF, *e.g.,* by otilimab that is currently assessed in a clinical phase 3 study,[911] and PD-L1 blockade, *e.g.,* by checkpoint inhibitors like atezolizumab.[912] For example, Fultang and co-workers have recently shown that the activity of an anti-GD2-/mesothelin-/EGFRvIII-CAR-T was significantly enhanced when co-applied with the anti-MDSC drug gemtuzumab ozogamicin, an anti-CD33 antibody linked to cytostatic calicheamicin.[913] Altogether, due to the high potential of CARs for cancer treatment, improvement of CAR-based therapy is in the focus of research. For example, Wang *et al*. have recently generated CAR-T cells by electroporation-based transfection of T cells with non-viral mcDNA, which is considered much safer than virus-based chimeric antigen receptor-engineered CARs.[914]

6.5 Manipulating the TME using therapeutic nucleic acids

The TME is a complex, very heterogeneous network of stromal and endothelial cells as well as recruited immune cells.[915] It is characterized by leaky blood vessels, a special tumor-specific extracellular matrix (ECM), immunomodulatory agents/cytokines, and growth factors.[653, 915-917] The TME plays an important role during tumorigenesis as well as tumor progression and metastasis by supporting the tumor cells in evading the immune system[654, 918] and by contributing to chemoresistance.[919] Different cell types like CAF,[920]

TAM (pro-tumoral phenotype),[921-923] MDSC, and Treg (see section **6.3**)[653] as well as tolerogenic DC[653, 924] contribute to the establishment and maintenance of the immunosuppressive tumor surroundings. In addition, the TME inactivates effector functions of tumor-infiltrating lymphocytes (TIL) by various mechanisms, and thus undermines immunosurveillance.[918, 925, 926]

Further characteristics of the tumor tissue comprise acidity (~pH 6.5) due to the Warburg effect,[155, 156] hypoxia,[927] expression of distinct matrix enzymes like matrix metalloproteases (MMPs),[153] and an elevated redox potential[167] as well as increased levels of reactive oxygen species (ROS).[928] These properties display barriers in the delivery process of anti-tumor drugs, but can be also exploited for bio-responsive targeting of therapeutics to the tumor tissue.[1] By this, tumor selectivity and overall biocompatibility might be enhanced. Besides, passive targeting *via* the enhanced permeation and retention (EPR) effect,[47] and more effective tumor addressing *via* tumor homing peptides and CPPs can increase accumulation of (nano) formulations within the tumor.[46, 83, 84] In addition, active targeting mediated by ligands such as peptides, vitamins, or antibodies is often utilized to direct a therapeutic selectively to the target site.[3]

Immunotherapeutic approaches often aim to evoke a switch from immunosuppression to immune permission within the tumor tissue. By this, the tumor becomes immune-sensitive again, and then can be effectively combated by the innate and adaptive immune system. In the following, a selection of diverse strategies for TME manipulation is presented with a focus on nucleic acid-based approaches.

6.5.1 Modulation of intratumoral signaling by nucleic acids

In the immunosuppressive TME, a disproportion exists between soluble mediators (cytokines and growth factors) exerting pro- and anti-inflammatory properties, thereby promoting tumor immune escape and tumorigenesis.[929] There are two options to counteract this imbalance, resulting in effective anti-tumor activity.[929] On the one hand, the immune system can be stimulated by overexpression of pro-inflammatory cytokines. On the other hand, immunosuppression can be reduced by inhibition/neutralization of anti-inflammatory signals.

Cytokines are key mediators in the communication of immune cells and are crucially involved in controlling the intensity of an immune response.[930-932] Thus, it is not surprising that cytokine therapy has been pursued as a cancer immunotherapeutic approach for

more than 30 years now. However, in clinical studies, such cytokine therapies have not met the expectations based on the results of preclinical studies, especially when applied as monotherapies.[929] Only IFN-α[933] and IL-2 as high-dose therapy[934] have been approved for the systemic treatment of several cancers, based on moderate beneficial anti-tumor effects in clinical trials. Ongoing research is focused on increasing therapeutic efficacy and biocompatibility by developing recombinant cytokines with improved pharmacokinetics (*e.g.*, PEGylated or fused with targeting antibodies), combinations with other immunotherapeutic approaches such as immune checkpoint inhibitors, and local or specifically targeted administration of (recombinant) cytokines.[929] Besides that, cytokine gene therapy (using gene encoding pDNA or viral vectors) and other nucleic acid-based approaches (like RNAi or genome editing) are promising concepts.[5, 929, 932] **Table 6.1** summarizes such nucleic acid-based approaches evaluated in clinical trials. In the following, important signaling molecules and strategies (especially therapeutic nucleic acids) to modulate their levels within the tumor tissue are outlined.

IL-2 stimulates T-lymphocytes and NK cells, but also controls the duration and intensity of their activation, regulates immune homeostasis, and balances the Teff/Treg ratio.[929, 935] Various autologous/syngeneic as well as allogeneic IL-2 gene-modified tumor cell vaccines have been investigated in preclinical and clinical studies for their potential in prophylactic and therapeutic application for the treatment of advanced and metastatic cancers like melanoma.[936-942] *In vitro* transduction of tumor cells with the IL-2 gene was achieved using viral vectors (*e.g.*, retro-viral or adenoviral)[937, 939, 940] or by employment of advanced methods like the adenovirus-enhanced transferrinfection (AVET) system.[936, 938, 942, 943] The toxicity profile of systemic IL-2 gene therapy can be improved by transcriptional targeting of IL-2 to the tumor to ensure specific expression of the IL-2 gene within the tumor.[944-946]

TNF-α exhibits tumoricidal effects by inducing apoptosis and hemorrhagic necrosis of tumor cells.[947] GenVec's TNFerade is a replication-deficient adenoviral vector encoding for TNF-α under the control of a radiation-inducible promotor,[947, 948] applied by intratumoral injection. Phase III clinical trials have been terminated in 2010, as a study in locally advanced pancreatic cancer failed to show a significantly improved outcome of combination therapy with TNFerade in comparison to standard therapy alone.[949] Reduced transgene expression may be caused by (pre-existing) immune responses

against the adenoviral vector, mainly mediated by antibodies, limiting the option of repeated application.[950] Besides viral vectors, non-viral carrier systems for TNF-α delivery are subject of research as well. Kircheis *et al*. for example designed surface-shielded transferrin-PEI/DNA complexes for targeted TNF-α gene delivery after intravenous application in tumor-bearing mice.[951] Significant and selective TNF-α expression within the tumor without detectable serum levels could be demonstrated in three different tumor models. In a combination approach, Su *et al* evaluated to which extent systemic TNF-α gene therapy synergized with liposomal doxorubicin (Doxil®) to enhance tumor endothelium permeability, and thus would promote accumulation of the chemotherapeutic drug within the tumor.[952] Synthetic polymers based on amino ethylene units[221, 953] were used as pDNA carriers. The beneficial effect of TNF-α expression on concomitant Doxil® therapy was proven in all tested tumor models including metastases.[952] All in all, this combination approach offers great potential in treating metastases even with low doses of chemotherapeutic drugs. Quinn *et al.* achieved synergistic effects on tumor growth inhibition by combining systemic application of a previously evaluated RGD-targeted adeno-associated virus phage encoding for TNF-α [954, 955] with hypo-fractionated radiation for the therapy of disseminated melanoma.[956]

Another interesting candidate for cancer immunotherapy is IL-12 because of its ability to activate both the innate and the adaptive immune system.[957] In addition, IL-12 has anti-angiogenic properties by inducing IFN-γ, which in turn inhibits VEGF and MMPs.[929, 957-960] In early clinical trials, however, the anti-tumor activity of systemically applied IL-12 was found to be only moderate, and was accompanied by severe side effects.[957, 961] IFN-γ as induced by IL-12 is mainly responsible for the dose-related and schedule-dependent toxicity.[959, 962] New strategies focus on targeted and local delivery of IL-12 to minimize systemic toxicity and to improve specific tumor targeting by conjugating IL-12 to tumor antigen-specific monoclonal antibodies (so-called immunocytokines).[963, 964] Moreover, various IL-12 gene therapy approaches *ex vivo* and *in vivo* are pursued.[965, 966] Different delivery methods comprise viral vectors like adeno- or retroviral vectors,[967-973] and non-viral techniques such as electroporation,[974-980] or synthetic carrier systems like (lipo)polymer-DNA complexes and liposomes.[981-984] In order to increase the specificity of local IL-12 expression within the tumor, an IL-12 transgene with a ligand-inducible expression switch was designed.[970, 973] Another way to locally control *in situ* expression

of IL-12 is to engineer CAR- T cells, which release IL-12 in an inducible or constitutive manner.[985] Moreover, the IL-12 gene may be inserted in the genome of oncolytic viruses as an immune stimulatory component (see section 6.5.3).

GM-CSF has been investigated as an adjuvant for different types of vaccines because of its stimulatory effect on myeloid cell types like conventional DC and macrophages.[929] Unfortunately, GM-CSF activates TAM and MDSC as well, thereby supporting tumor growth. These opposing effects are mainly responsible for its only moderate clinical efficacy.[932] Combination therapy is an option to overcome this issue; *e.g.*, co-treatment with recombinant GM-CSF and immune checkpoint inhibitors led to prolonged survival of metastatic melanoma patients.[986] An example for a GM-CSF gene-based approach is the GVAX technology.[987-990] To this end, allogeneic pancreatic tumor cells have been transfected *ex vivo* with pDNA encoding GM-CSF. GVAX has been tested in combination with immune checkpoint inhibitors as well as with tumor vaccines. Moreover, oncolytic viruses often encode inter alia for GM-CSF (see section 6.5.3). GM-CSF is also addressed in strategies to improve the efficacy and to lower the toxicity of CAR-T cell therapies. However, in contrast to the aforementioned GM-CSF therapy concepts, here GM-CSF is not substituted, but knocked out for example *via* CRISPR/Cas9 technology.[991]

The CXCL12/CXCR4 (C-X-C motif chemokine 12/C-X-C motif chemokine receptor 4) axis plays a crucial role in tumorigenesis, metastasis and chemoresistance,[992, 993] and therefore is an ideal target for cancer immunotherapy. However, the toxicity of systemic anti-CXCL12 therapy approaches using small CXCR4 inhibitors like AMD3100[994] and monoclonal antibodies targeting CXCL12[995] is a serious issue. Transient and locally restricted expression of antibody-like trap proteins that bind and neutralize CXCL12 constitutes an option to increase systemic tolerability.[996, 997] For this purpose, NPs are used for target site-selective delivery of pCXCL12-trap encoding pDNA,[653] such as lipid NPs/liposomes.[996-998]

VEGF is crucial for neoangiogenesis, which is essential for tumor progression and metastasis.[999] Moreover, VEGF contributes to immunosuppression within the TME.[1000] Accordingly, several anti-VEGF therapeutics have already been clinically approved, and many pre-/clinical trials are currently carried out evaluating the VEGF trap protein aflibercept[1001, 1002] or monoclonal antibodies that target either VEGF itself (bevacizumab)[1003, 1004] and its receptor VEGFR (ramucirumab)[1005] in combination with

classical chemotherapeutics or immune checkpoint inhibitors.[1000, 1006] Another potent strategy is RNAi aimed to knock-down VEGF or VEGFR, which showed good anti-tumor results in many preclinical studies. In this regard, CPPs,[1007-1010] polymers like PEI[1011-1014] or chitosan,[1015] cationic liposomes,[1016, 1017] gold [1018] and graphene oxide NPs,[1019] often modified with shielding and targeting units, have been used as delivery systems.

TGF-β exhibits manifold functions regarding cell proliferation, differentiation, migration, and apoptosis.[1020-1022] In the context of cancer progression, an overexpression of TGF-β has been observed within the TME, promoting EMT, immunosuppression and metastasis. However, these tumor-promoting effects of TGF-β occur only in late-stage tumors, while in early stages its anti-tumor activity is more pronounced. Thus, anti-TGF-β therapy approaches aim to treat advanced cancers. A lot of preclinical and clinical research has been performed in the field of nucleic acid-based strategies ranging from siRNA[1023] over miRNA[1024-1026] to antisense oligonucleotides (ASO).[1027-1032] Belagenpneumatucel-L is an anti-TGF-β allogeneic tumor cell vaccine, based on non-small cell lung cancer cells genetically engineered to express ASO directed against TGF-β.[1033-1035] In a phase III clinical trial, however, no significant increase in the mean overall survival was achieved compared to placebo treatment, but *e.g.*, prior treatment with radiation therapy was found to have a positive effect on therapeutic outcome.[1035] Therefore, further investigation in clinical trials is necessary.

In addition to the mediators discussed above, many others can be addressed in immunotherapeutic approaches as well.[929, 932] For example, intramuscular IL-27 and intratumoral IFN-α gene delivery *via* viral vectors promoted Treg depletion in the TME.[1036-1038] This is favorable in view of the efficacy of cancer immunotherapy,[1039, 1040] suggesting that both approaches are valuable as adjuvant therapies. Moreover, IFN-α showed strong anti-proliferative, anti-angiogenic, and immunomodulatory activity.[1041, 1042] An IFN-α encoding adenoviral vector (rAdIFNα2b/Syn3, Instiladrin®) has been investigated in advanced clinical trials for intravesical treatment of BCG (Bacillus Calmette–Guerin) unresponsive bladder cancer.[1043]. Results of a phase III clinical trial that has been completed in 2018 are still pending (NCT02773849).

Table 6.1. Examples of clinical trials investigating nucleic acid-based approaches for adjusting intratumoral cytokine levels.

Signaling molecule	Therapy strategy	Application route	Treated cancer	Clinical state	References
IL-2	Syngeneic tumor cell vaccine modified with IL-2 gene *ex vivo*	Intradermal or subcutaneous injection	Metastatic melanoma	Phase I	[938]
	Allogeneic tumor cell vaccine modified with IL-2 gene *ex vivo*	Subcutaneous injection	Metastatic melanoma	Pilot study	[939]
				phase I-II	[941]
	Allogeneic tumor cell vaccine modified with IL-2 gene *ex vivo*	Subcutaneous injection	Relapsed neuroblastoma	Phase I	[940]
TNF-α	TNFerade, a replication-deficient adenoviral vector encoding for TNF-α under the control of a radiation inducible promotor (erg-1 gene promotor)	Intratumoral injection	Various cancer types, *e.g.*, advanced pancreatic cancer	Phase III	[947], [948]
IL-12	Ad–RTS–hIL-12, an adenoviral vector encoding for IL-12 transgene designed with a ligand-inducible expression switch	Injection in the resection cavity	Recurrent high-grade glioma	Phase I	[973]
GM-CSF	GVAX, an allogeneic tumor cell vaccine modified with GM-CSF gene *ex vivo*, (in combination with immune checkpoint inhibitors and/or cyclophosphamide and Listeria monocytogenes-expressing mesothelin [CRS-207])	Intradermal injection	Advanced pancreatic cancer	Phase I b	[987]
				Phase II	[988]
				Phase II b	[989]
				Phase II	[990]
IFN-α	Instiladrin® (rAdIFNα2b/Syn3), an IFN-α encoding adenoviral vector	Intravesical injection	BCG unresponsive bladder cancer	Phase III – results pending (NCT02773849)	[1043]
TGF-β (inhibition)	Belagenpneumatucel-L, an allogeneic tumor cell vaccine altered to express ASO directed against TGF-β	Intradermal injection	Advanced non-small cell lung cancer	Phase II	[1033], [1034]
				Phase III	[1035]

6.5.2 Nucleic acid-mediated immune checkpoint inhibition and T cell stimulation

Immune checkpoints regulate the intensity and the duration of immune responses.[1044, 1045] By this, self-tolerance is preserved, and hence tissue damage is minimized. Tumors often abuse such pathways in order to create an immunosuppressive surrounding, *e.g.*, by anergizing tumor-reactive Teff. Consequently, blockade of immune checkpoints presents a very promising method to restore immunity against the tumor and the TME. Among these CTLA-4 and PD-1 are the best characterized receptors.[1046, 1047] Intensive research led to therapy concepts of immune checkpoint inhibition, which revolutionized treatment especially of advanced cancers.[1048] Up to now, several antibodies addressing CTLA-4, PD-1, and its ligand PD-L1 have been implemented in cancer therapy regimens.[659, 660] However, response rates are quite low, and relapse often occurs due to resistance development.[1049-1053] Moreover, immune checkpoint blockade is effective only if the number of tumor-reactive Teff is high enough at the beginning of treatment.[1049, 1054-1057] In this regard, the T cell number in a patient can be increased by *ex vivo* expansion of TIL that are subsequently reinfused, or by prior treatment with tumor vaccines.[1053] Combinations of different immune checkpoint inhibitors as well as their combination with other (immuno)therapeutic approaches aim to overcome the resistance mechanisms.[1051, 1052, 1057]

Other major issues of checkpoint inhibitor therapy are immune-related adverse effects and toxicity.[1058, 1059] Systemic toxicity can be reduced by targeted delivery of checkpoint inhibitors using NPs and by nucleic acid-based approaches.[1057] Concerning the latter, mRNA encoding for an anti-CTLA-4 antibody,[1060] pDNA encoding for PD-L1 traps,[997, 1061, 1062] siRNA specific for PD-L1,[150, 1063-1066] and CRISPR/Cas9-mediated knock-out of the PD-1 gene in CAR-T cells[1067, 1068] have been tested so far (**Figure 6.3**).

For example, Pruitt *et al*. electroporated DC *ex vivo* with mRNA encoding heavy and light chains of blocking antibodies specific for CTLA-4 and glucocorticoid-induced TNFR-related protein,[1060] which are expressed by Treg at high level [1069]. Transfected DC were co-administrated with tumor antigen-transfected DC *via* subcutaneous injection into B16/F10.9 melanoma bearing C57BL/6 mice.[1060] Based on the encouraging results, a phase I clinical trial for treatment of metastatic melanoma has been initiated (NCT01216436).

Transient local expression of PD-L1 trap was pursued by Huang and co-workers.[1062] For

this purpose, pDNA encoding for PD-L1 trap fusion protein was loaded into lipid-protamine-DNA NPs, consisting of a DNA-protamine core within pre-formed DOTAP-cholesterol liposomes. These were optionally equipped with 1,2-distearoylphosphatidylethanolamine (DSPE)-PEG or DSPE-PEG-AEAA for shielding and targeting. These nano formulations were applied intravenously in combination with intraperitoneally administered oxaliplatin, a chemotherapeutic drug inducing immunogenic cell death and thereby activating DC. By this approach, synergistic effects on tumor inhibition were achieved in a colorectal cancer mouse model.

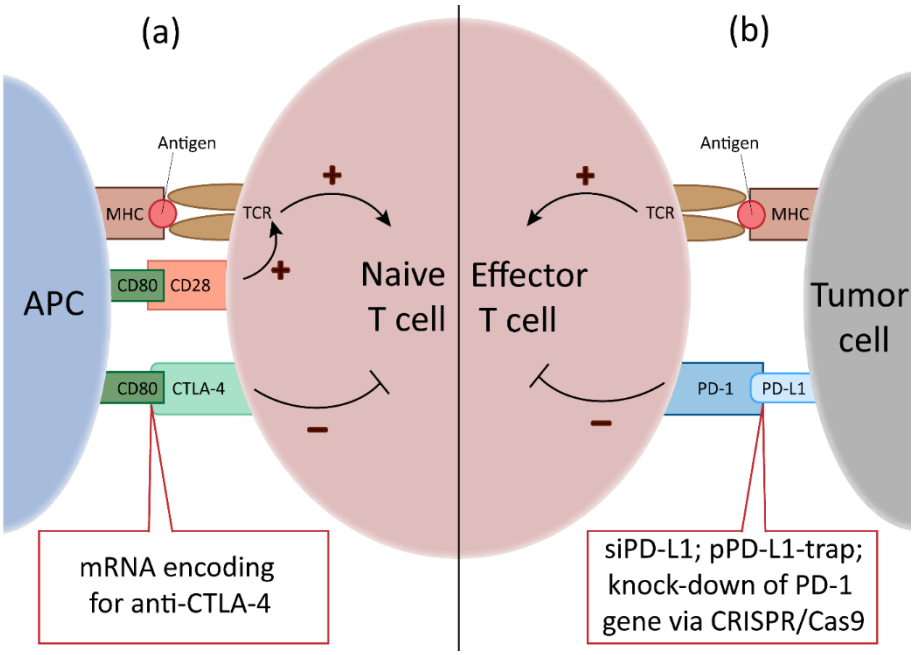

Figure 6.3. Immune checkpoint inhibition mediated by nucleic acid-based strategies. (**a**) Besides recognition of major histocompatibility complex (MHC)-bound antigen on the surface of APC *via* TCR, co-stimulatory signals – inter alia interaction of CD80 (B7-1) and CD28 – are required for full T cell activation. The duration and intensity of activation is regulated among other things by immune checkpoint CTLA-4 that binds with high affinity to CD80. Blocking of this interaction results in enhanced T cell activity. One therapeutic option is delivery of mRNA encoding for anti-CTLA-4 antibodies. (**b**) Tumor cells often upregulate PD-L1 that binds to PD-1 on effector T cells, thereby inhibiting the activity of effector T cells. Nucleic acid-based approaches for blocking this immune checkpoint comprise siRNA against PD-L1, pDNA encoding for PD-L1 trap proteins (pPD-L1-trap), and CRISPR/Cas9-mediated knock-down of PD-1 gene.

A further combination approach was conducted by Zhou *et al* by combined administration of doxorubicin and of PD-L1-specific siRNA delivered by stimuli-responsive NPs in a B16 melanoma tumor model.[1066] These NPs were dually sensitive towards the extracellular slightly acidic pH of tumor cells (pH-triggered detachment of the PEG layer) and their

elevated intracellular redox potential (reduction-sensitive polymer core of poly-*L*-lysine–lipoic acid). This combination therapy was superior to either monotherapy in terms of specificity, efficacy, and tolerability, proving once more the advantage of targeted combination therapies.

6.5.3 Multi-faceted combat of cancer by oncolytic virotherapy

Oncolytic viruses may constitute the next breakthrough in cancer immunotherapy.[1070] They comprise DNA and RNA viruses, which can be wild-type (*e.g.*, coxsackie virus, reovirus) or genetically modified (*e.g.*, herpes simplex virus (HSV), adenovirus, vaccinia virus).[1071] Oncolytic viruses selectively replicate in tumor tissue while destroying it.[649, 1072-1074] Moreover, they exhibit an immunostimulatory function. Infection and lysis of tumor cells lead to the release of ROS and proinflammatory cytokines as well as danger-associated molecular patterns and intracellular tumor antigens, stimulating both the innate and the adaptive immune system.[1074] By this, even immunological memory can be induced, resulting in long-lasting anti-tumor effects.[649, 1075]

In 1991, Martuza *et al*. succeeded in producing the first genetically modified HSV-1 characterized by a mutation in the thymidine kinase (TK) gene to ensure selective replication only in tumor cells.[1076] This pioneer work opened a new way for cancer treatment. The first clinical trial with an oncolytic virus started in mid-1990 [1077], followed quickly by many others.[1078] However, the clinical efficacy fell short of the expectations, but safety and synergism with standard cancer treatments could be demonstrated.[1078] Subsequent generations of oncolytic viruses have been developed by genetic engineering to enhance selectivity and efficiency while maintaining or even improving safety (**Figure 6.4**).[1071, 1073, 1079, 1080] Tumor selectivity can be enhanced at several levels (transduction, transcription, translation, post-translation) as well as *via* oncogenic targeting or insertion of miRNA targeting sequences.[1079, 1081] Oncolytic and immunogenic efficacy can be increased by insertion of certain transgenes encoding *i*) enzymes that convert pro-drugs to cytotoxic products (*e.g.*, HSV-TK or cytosine deaminase), *ii*) immunostimulatory cytokines (*e.g.*, GM-CSF or IL-12), or *iii*) TME/ECM-modifying peptides and enzymes (*e.g.*, MMP-9 or the anti-angiogenic peptide angiostatin).[1082] Safety can be ensured by mutations in pathogenic and virulence genes as well as in genes required for viral replication in normal cells.[1071, 1082]

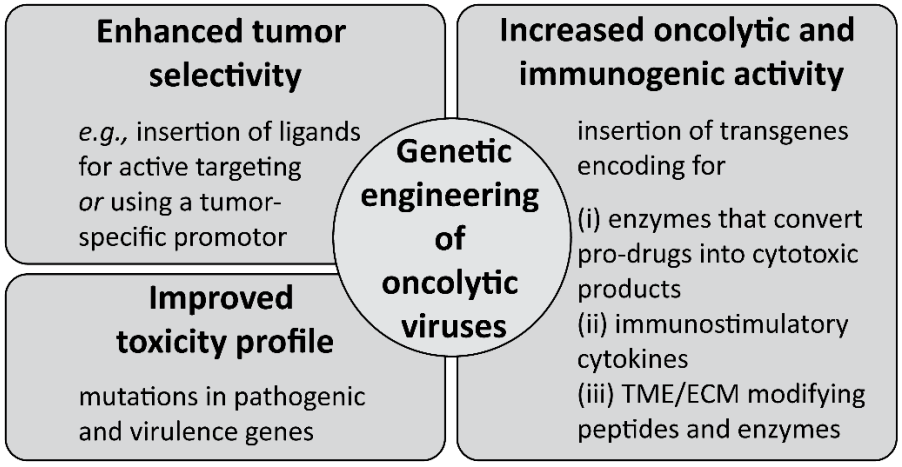

Figure 6.4. Genetic modifications to enhance selectivity, safety, and efficacy of oncolytic virotherapies.

Nowadays, a large repertoire of oncolytic viruses is available and oncolytic virotherapy has been intensively investigated in numerous preclinical and clinical studies, also in combination with other cancer therapies like chemotherapy, radiation therapy, or other immunotherapies.[1070-1074, 1083, 1084] **Table 6.2** displays approved oncolytic virotherapies and those that have been or are currently tested in clinical trials.

RIGVIR® was the first oncolytic virus being approved for therapy of melanoma in Latvia in 2004.[1085] This oncolytic virus, enteric cytopathogenic human orphan (ECHO)-7, is a wild-type virus. In 2005, the first genetically modified oncolytic virus (Oncorine®, a recombinant oncolytic adenovirus H101) was approved in China for the treatment of nasopharyngeal carcinoma.[1086, 1087] Ten years later, T-Vec (talminogene laherparepvec) achieved approval by the FDA and the European Medicines Agency (EMA) for treatment of advanced melanoma.[1088, 1089] This oncolytic virus is derived from HSV-1 and was genetically modified to mitigate pathogenicity as well as to increase tumor-selective replication and lysis.[1089] In addition, T-Vec expresses GM-CSF to enhance anti-tumor immunity.

Saha *et al*. conducted a preclinical study with a triple-mutated third generation oncolytic HSV-1 vector (G47Δ-mIL12), in which the murine IL-12 gene was inserted.[1090] This oncolytic virus was applied intratumorally, in combination with systemically applied immune checkpoint inhibitors. Only the triple combination of G47Δ-mIL12, anti-CTLA-4 and anti-PD-1 antibodies successfully cured glioblastoma in an immune-competent

glioblastoma mouse model.

Other oncolytic DNA viruses that are frequently used are genetically engineered adenovirus and vaccinia viruses.[1091, 1092] CG0070, an oncolytic adenovirus type 5 with an inserted GM-CSF gene, is currently investigated in advanced clinical trials for treatment of non-muscle invasive bladder cancer (BOND, NCT01438112; BOND2, NCT02365818).[1070] The BOND study (phase II/III clinical trial) demonstrated that intravesically applied CG0070 evoked a durable response in a subset of high-risk patients and was well tolerated.[1093] An example for an oncolytic vaccinia virus in clinical studies is pexastimogene devacirepvec (Pexa-Vec, JX-594), which bears a mutation in the TK gene for cancer cell targeting and an inserted GM-CSF gene to enhance immune stimulation.[1070, 1094-1097] In a phase III clinical trial, Pexa-Vec is currently evaluated in combination with the multi tyrosine kinase inhibitor sorafenib in patients with advanced hepatocellular carcinoma without prior systemic therapy.[1097]

Reolysin® (pelareorep) is a wild-type oncolytic RNA virus (type 3 Dearing (T3D) strain reovirus),[1071, 1098] which is extensively studied in clinical trials.[1070, 1099] In phase II and III clinical trials, Reolysin® showed encouraging clinical efficacy, especially in combination with chemotherapeutics (*e.g.*, carboplatin and paclitaxel) in patients with advanced malignancies.[1099, 1100]

Despite rapid progress in oncolytic virotherapy and encouraging results in clinical trials, there are still some obstacles.[1071] One shortcoming is the small genomic capacity of some oncolytic viruses.[1074] Moreover, deletion of pathogenic genes to reduce toxicity might also reduce oncolytic activity.[1101] Efficacy may be enhanced for instance by insertion of transgenes or combination with other therapies. In case of the latter, optimal therapy regimens and schedules have to be evaluated in terms of dosage, application routes and timing.[1071] Therefore, further investigations in clinical trials are needed.

Table 6.2. Examples of oncolytic virotherapies approved or in clinical trials.

Oncolytic virus	Genetic modification	Treated cancer	Clinical state	Reference
WILD-TYPE VIRUS				
RIGVIR® (wild-type ECHO-7; (+)ssRNA virus)	–	Melanoma	Approved in Lativa in 2004	[1085]
Reolysin® (pelareorep, type 3 Dearing [T3D] strain reovirus; dsRNA virus)	–	Many advanced malignancies (*e.g.*, melanoma, sarcomas, non-small cell lung cancer, pancreatic adenocarcinoma)	Phase I and II	[1071], [1099], [1100]
		Advanced, metastatic head and neck cancer	Phase III	[1099]
ONCOLYTIC ADENOVIRUS (dsDNA virus)				
Oncorine® (rAdV H101)	Deletion in E1B-55K and E3 genes	Nasopharyngeal carcinoma	Approved in China in 2005	[1086], [1087]
CG0070 (AdV-5)	Deletion in E3 gene; insertion of GM-CSF gene	Non-muscle-invasive bladder cancer	Phase II/III (BOND, NCT01438112); phase II (BOND2, NCT02365818)	[1070], [1093]
ONCOLYTIC HERPES SIMPLEX VIRUS, HSV-1 (dsDNA virus)				
T-Vec (talminogene laherparepvec)	Deletion in ICP34.5 and ICP47 genes; insertion of GM-CSF gene	Advanced melanoma	Approved by FDA and EMA in 2015	[1088], [1089]
M032	Deletion in ICP34.5 gene; insertion of IL-12 gene	Glioblastoma multiforme	Phase I	[1102]
G47Δ	Deletion in ICP34.5, ICP47 and ICP6 genes; insertion of GM-CSF gene	Recurrent glioblastoma, castration resistant prostate cancer, recurrent olfactory neuroblastoma	Clinical trials in Japan	[1070], [1103], [1104]
ONCOLYTIC VACCINIA VIRUS (dsDNA virus)				
Pexa-Vec (JX-594, pexastimogene devacirepvec)	Mutation in TK gene; insertion of GM-CSF gene	Advanced hepatocellular carcinoma	Phase III (in combination with sorafenib)	[1097]

6.5.4 Nucleic acid-based TLR agonists to boost anti-tumor immune response

PAMPs and other danger signals are recognized by the innate immune system *via* pattern recognition receptors such as TLRs.[1105, 1106] Subsequently, pro-inflammatory pathways and the innate immune system are activated to eradicate pathogens. The anti-tumor immune response can be augmented by mimicking PAMPs. Monophosphoryl lipid A, a modified lipopolysaccharide derivative that triggers TLR4, is used as the adjuvant component in the prophylactic cervix cancer vaccine Cervarix®.[1107] The successful application of this TLR ligand also reinforced further research in immunostimulatory nucleic acids like double-stranded RNA (dsRNA) or single-stranded DNA (ssDNA) for cancer immunotherapy.

Poly(I:C) is an artificial dsRNA analog that acts as a potent TLR3 agonist.[1105, 1108] Besides enhancement of the anti-tumor immune response, mainly by induction of IFN type I and chemokines especially in immune cells, poly(I:C) also directly induces apoptosis in cancer cells.[1109-1111] However, early clinical trials conducted in the 1970s using poly(I:C) for cancer treatment did not prove any clinical benefit,[1105, 1112-1114] most likely because of its fast degradation prior to cellular uptake.[1115, 1116] Consequently, a stabilized version of poly(I:C), polyriboinosinic:polyribocytidylic acid-polylysine carboxymethylcellulose (poly-ICLC, Hiltonol®), has been developed.[1116, 1117] However, toxicity was a big issue in early rounds of clinical testing, which could be reduced by administration of lower intravenous doses and by local application.[1105] Nowadays, poly-ICLC is intensively evaluated in phase I and II clinical trials, especially in combination with cancer vaccines and radiotherapy.[1105, 1106, 1109, 1118, 1119] Another concept to increase the stability and to improve the toxicity profile of TLR3 agonists is the employment of particulate formulations.[1120] Shir *et al*. designed poly(I:C) polyplexes using a polymer conjugate consisting of branched PEI, PEG, EGF for EGFR-targeting, and lytic melittin for improved endosomal escape.[619, 1121] Complete tumor elimination could be achieved *via* intratumoral application in three different tumor mouse models (glioblastoma, breast cancer, adenocarcinoma),[619] and in a disseminated EGFR overexpressing tumor mouse model.[1121] In the latter study, polyplexes were administered intravenously, followed by intraperitoneal injection of peripheral blood mononuclear cells into tumor bearing immune-deficient SCID mice. Tumor-targeted poly(I:C) mediated induction of chemokines and inflammatory cytokines selectively within the tumor tissue. This led to tumor homing of the injected immune cells as well as a strong anti-tumor and bystander killing effect. The latter might be advantageous in view of the heterogeneous tumor tissue. In this study, complete curation was achieved without adverse side effects.[1121] Schaffert *et al.* optimized the nano-carrier by using linear instead of branched PEI.[206] The improved carrier was effective even without the lytic melittin unit. In a follow-up study, GE11 peptide was used for EGFR targeting.[1122] In contrast to EGF, GE11 does not activate EGFR, and thus mitogenic activity of the tumor cells should be much lower. This could be an advantage in terms of clinical use. Other types of poly(I:C) polyplexes were formulated by Lächelt *et al*.[1123] using sequence-defined oligo(ethanamino)amides modified with PEG and the anti-folate drug methotrexate (MTX) with varying degrees of polyglutamylation. MTX exhibits

dual function by serving as ligand targeting the folate receptor and by exerting cytotoxic effects in the cytosol. The extent of polyplex uptake as well as MTX and poly(I:C) toxicities correlated with increasing amounts of glutamic acid. A synergism of the combined cytotoxic agents was observed.

CpG ODNs are another class of TLR agonists that imitate bacterial/viral genomic sequences and are recognized by TLR9 trough their unmethylated cytosine-guanine dinucleotide motif.[717, 1124-1126] TLR9 signaling results in the secretion of pro-inflammatory cytokines and the activation of APC and CTL. To improve the *in vivo* stability of CpG ODNs in most cases the phosphodiester backbone is replaced (at least in part) by a nuclease-resistant phosphorothioate backbone.[1125, 1127] Encouraging results in preclinical studies led to a series of clinical trials in the mid-2000s, testing CpG ODNs alone, in combination with cancer vaccines, or with chemo- and radiotherapy.[653, 1126, 1127] However, the clinical outcome fell far short of the hopes and expectations, especially in case of CpG ODN monotherapies, but safety and good tolerability were proved. Subsequent studies showed that TLR9 signaling was negatively influenced at several levels by the immunosuppressive TME.[1126] Consequently, CpG ODNs in combination with immune checkpoint inhibitors are currently evaluated in phase I and II clinical trials for treatment of advanced solid tumors like metastatic melanoma.[1126] Another dual immunotherapy strategy are conjugates of CpG ODN and either STAT3 siRNA or a STAT3 decoy ODN, respectively,[1126, 1128] as STAT3 is an oncogenic transcription factor that interferes with TLR9 signaling. Furthermore, NPs that deliver CpG ODN are under intensive investigation in several preclinical and also some clinical studies.[1125] The goal of all these NP-based approaches is to enhance the therapeutic efficacy of CpG ODNs by increasing their stability and protection against nucleases as well as to improve the uptake of CpG ODNs by target cells. In addition, NPs allow to use phosphodiesters instead of the commonly used phosphorothioate backbone.[1125] This may improve safety, as phosphorothioates are known to cause various adverse effects, especially in case of systemic application at higher doses.[1125, 1126] By now, several types of NPs have been evaluated for CpG ODN delivery.[653, 1125] Preclinical studies are conducted inter alia with polymeric NPs formed with polymers like poly(lactic-co-glycolic acid) or PEI,[1129, 1130] liposomal formulations,[1131-1133] carbon nanotubes,[1134, 1135] gold [1136, 1137] and silica mesoporous NPs,[1138] as well as DNA-based carriers.[1139, 1140] Near-infrared light responsive nanomaterials like copper

sulfide, graphene oxide or gold nanorods can be used for photothermal enhancing of CpG ODN immunogenicity.[1141-1143] Besides these preclinical studies, CpG ODN-loaded virus-like particles are already investigated in a phase I/II clinical trial.[1144] Furthermore, CpG ODNs can also be conjugated with antigen (peptide/protein) or human immunodeficiency virus-derived Tat-peptide.[1145, 1146] Self-assembled CpG ODNs like MGN1703 are another example, already tested in phase I and II clinical trials, for treatment of *e.g.*, metastatic colorectal carcinomas.[1147-1149]

6.5.5 Tumor suppression by RNA interference

The discovery of RNAi in 1998[1150] led to a better understanding of gene regulation mechanisms.[733] RNAi in humans and animals is mediated by miRNA (**Figure 6.2**).[1151] miRNAs influence many cellular functions like proliferation, differentiation, apoptosis, oncogenesis, and drug sensitivity.[1152-1155] Dysregulated miRNA expression is associated with the development and progress of various diseases.[1151, 1155, 1156] Calin *et al*. were the first to report involvement of miRNA in cancer progression.[1157] miRNAs can be used as diagnostic and prognostic biomarkers.[1158] For cancer therapy, oncogenic miRNAs can be blocked by antisense molecules (antagomirs), while attenuated levels of tumor suppressor miRNAs can be substituted by pre-miRNAs or miRNA mimics.[1151, 1155, 1159, 1160]

The major challenge in clinical translation of miRNA therapeutics is to ensure their efficient, specific, and safe delivery to the tumor.[1151, 1155, 1158, 1161] Chemical modifications can increase resistance of RNA to enzymatic degradation by nucleases. Examples for such structural alterations are modifications of the ribose 2'-OH group, the use of phosphorothioate instead of phosphodiester bonds, peptide nucleic acids, locked nucleic acids as well as conjugation with other moieties (*e.g.*, cholesterol, antibodies, or membrane translocation peptides).[733, 1151, 1162-1164]

For example, Cheng *et al*. conjugated peptide nucleic acid-based anti-miR-155 to a pH-sensitive membrane translocation peptide *via* a disulfide link.[733, 1164] In the acidic tumor tissue, the conformational change in this peptide promoted internalization of the antagomir, which was released intracellularly upon disulfide cleavage due to increased glutathione levels. In a lymphoma model, cell targeting, a significant inhibition of lymphoma proliferation as well as a good tolerability were demonstrated. It is also worth noting that the neutral charge of the peptide nucleic acid was decisive for success.

Viral as well as non-viral delivery systems such as liposomal or polymeric NPs are under investigation to prevent degradation of miRNA and to promote their targeted delivery.[1151, 1158, 1163] Loss of miR-200c expression is known to promote tumorigenic processes like tumor cell proliferation, EMT, migration and chemoresistance.[1151, 1165-1170] Müller *et al*. tested a cationic oligo(ethanamino)amide structure with T-shape topology, terminal cysteines, and a dioleoyl motif, post-functionalized with PEG-GE11 for shielding and EGFR targeting for delivery of a mimic of the tumor suppressor miR-200c.[217] In two different human tumor cell lines, these EGFR-targeting miRNA polyplexes conferred selective, enhanced delivery of miRNA-200c, leading to various anti-tumor effects, including decreased tumor cell proliferation and migration, and enhanced sensitivity towards doxorubicin.

Altogether, miRNA therapeutics hold great potential for efficient and safe cancer treatment, especially as multi-functional nano formulations, paving the way towards clinical translation. A liposomal formulation of miR-34a mimic (MRX34) for treatment of patients with advanced solid tumors was the first miRNA therapeutic entering phase I clinical studies in 2013 but was accompanied by severe immune-mediated adverse effects (NCT01829971).[1171, 1172] Nevertheless, the observed dose-dependent modulation of relevant target gene expression provided a proof-of-concept for miRNA-based cancer therapy.[1172] This raises hope that miRNA therapeutics will make the leap towards clinical application. Therefore, further optimization of cargo and delivery systems to improve clinical efficacy and toxicity profiles is necessary.

6.6 Conclusions

Until a few years ago, nucleic acid-based immunotherapeutics have proven successful in preclinical studies, but largely fell short of expectations when evaluated for therapeutic efficacy in clinical trials.[689, 693] One major limit has been the lack of appropriate delivery systems required to prevent degradation of pDNA/mRNA, and to enable cell type-specific delivery.[755, 756] Insofar, it is not surprising that by now virus-based gene therapies including oncolytic viruses,[1085-1089] and cell-based immunotherapeutics, namely CAR-T cell therapies, [662, 903, 1173-1175] demonstrated more successful for tumor therapy, and have been approved for clinical treatment. However, in the last years, the development of biocompatible, cell targeting NPs, especially of liposomal carriers,[1176] has strongly

improved the efficacy of *e.g.,* mRNA-based anti-tumor vaccines.[8, 548] Additionally, in case of CAR-T as an *ex vivo* gene therapy approach, non-viral delivery is currently tested.[1177] These developments, in combination with structural improvements in particular of gene encoding pDNA,[1178] and the proper choice of individual tumor-specific neoantigens for individualized vaccination,[709] are important factors to overcome the low therapeutic efficacy of most nucleic acid immunotherapeutics tested so far. Furthermore, as numerous clinical trials have repetitively shown, nucleic acid-based therapeutics were more efficient when co-applied with agents that act on other levels like immune checkpoint inhibitors[702, 709] or chemotherapeutics,[1086] and radiotherapy.[1179] Moreover, first preclinical studies have shown that also different kinds of nucleic acids that act on distinct levels of cancer treatment may be combined to yield synergistic effects. For example, co-administration of the adjuvant poly(I:C) enhanced the anti-tumor efficacy of CAR-T cells.[1180] Similarly, co-application of an oncolytic adenovirus and of CAR-T cells improved anti-tumor responses as compared to monotherapy.[1181]

Altogether, ongoing developments indicate that nucleic acid-based therapeutics will become essential tools for successful tumor therapy as part of combination therapies, comprising the induction of tumor antigen-specific immune reactions,[709] the enhancement of anti-tumor responses,[1126] the inhibition or reprograming of regulatory immune cells,[882] the generation of tumor killing immune cells (CAR),[910] and direct killing of tumor cells.[1097] The versatility of nucleic acids as a therapeutic mean is underscored by the fact that these can exert either of the aforementioned functions by serving as gene expression units in pDNA/mRNA vaccines, conferring RNAi (siRNA, miRNA), and adjuvant activity (*e.g.*, CpG ODN), and can be easily produced under GMP conditions.[1182] Therefore, it is conceivable that in the future nucleic acid-based therapeutics that act on different levels of cancer treatment will be part of combination therapies involving either also conventional therapeutics or distinct types of nucleic acids.

6.7 Abbreviations

A2AR, adenosine A2A receptor; ALL, acute lymphoblastic leukemia; AML, acute myeloid leukemia; APC, antigen presenting cell; ASO, antisense oligonucleotide; AVET, adenovirus-enhanced transferrinfection; CAR, chimeric antigen receptor; BCG, Bacillus Calmette–Guerin; CAF, cancer-associated fibroblast; cAMP, cyclic adenosine

monophosphate; CCL, C-C motif chemokine ligand; CLL, chronic lymphocytic leukemia; CLR, C-type lectin receptor; CPP, cell penetrating peptide; CEA, carcinoembryonic antigen; CSC, cancer stem cell; CTL, cytotoxic T lymphocyte; CTLA-4, CTL-associated protein 4; CXCL12, C-X-C motif chemokine 12; CXCR4, C-X-C motif chemokine receptor 4; DC, dendritic cell; DOPE, dioleoyl phosphatidylethanolamine; DOTAP, *N*-[1-(2,3-dioleoyloxy)propyl]-*N,N,N*-trimethylammonium chloride; DOTMA, 1,2-di-O-octadecenyl-3-trimethylammonium propane; DSPE, distearoylphosphatidylethanolamine; dsRNA, double-stranded RNA; ECHO-7, enteric cytopathogenic human orphan 7; ECM, extracellular matrix; EGFR, epidermal growth factor receptor; EMA, European Medicines Agency; EMT, epithelial–mesenchymal transition; ENO1, α-enolase; EPR, enhanced permeation and retention; FDA, united states food and drug administration; GM-CSF, granulocyte macrophage colony-stimulating factor; HD, hexanediol diacrylate; HSV, herpes simplex virus; IDO, indoleamine 2,3-dioxygenase; IFN-α, interferon alpha; IRF, interferon regulatory transcription factor; IL, interleukin; IRAK1, IL-1 receptor-associated kinase; JNK, c-Jun N-terminal kinase; KC, Kupffer cell; mcDNA, mini-circle DNA; LAMP, lysosomal-associated membrane protein; LSEC, liver sinusoidal endothelial cell; MHC, major histocompatibility complex; MDSC, myeloid-derived suppressor cell; MMP, matrix metalloprotease; MTX, methotrexate; NK, natural killer cell; NLS, nuclear localization signal; NP, nanoparticle; NHL, non-Hodgkin lymphoma; ODN, oligodeoxynucleotides; OEI, oligoethylenimine; PD-1, programmed cell death protein 1; PD-L1, PD ligand 1; PEG, polyethylene glycol; PEI, polyethylenimine; Pexa-Vec, pexastimogene devacirepvec; PLGA, poly-D,L-lactic-co-glycolic acid; poly(I:C), polyriboinosinic:polyribocytidylic acid; poly-ICLC, polyriboinosinic:polyribocytidylic acid-polylysine carboxymethylcellulose; RNAi, RNA interference; ROS, reactive oxygen species; SCF, stem cell factor; scFv, single chain fragment variable; ssDNA, single-stranded DNA; STAT, signal transducer and activator of transcription; STING, stimulator of IFN genes; SV40, simian virus 40; T-Vec, talminogene laherparepvec; T3D, type 3 Dearing; TAA, tumor-associated antigen; TAM, tumor-associated macrophage; TCR, T cell receptor; Teff, effector T cell; TGF-β, transforming growth factor beta; Th, T helper cell; TIL, tumor-infiltrating lymphocyte; TK, thymidine kinase; TLR, toll-like receptor; TNF-α, tumor necrosis factor alpha; TNFAIP3, TNF-α induced protein 3; TRAF6, tumor necrosis factor receptor-associated factor 6;

Treg, regulatory T cell; iTreg, induced Treg; tTreg, thymic Treg; VEGF, vascular endothelial growth factor; VEGFR, VEGF receptor; WT1, Wilms' tumor 1.

6.8 Acknowledgments

This work was funded by the Deutsche Forschungsgemeinschaft (SFB1066, project B05).

7. Transcriptional targeting of dendritic cells using an optimized human fascin1 gene promoter

Yanira Zeyn[1], Dominika Hobernik[1], Ulrich Wilk[2], Jana Pöhmerer[2], Christoph Hieber[1], Carolina Medina-Montano[1], Nadine Röhrig[1], Caroline F. Mohr[3], Andrea K. Thoma-Kress[4], Ernst Wagner[2], Matthias Bros[1,], and Simone Berger[2,*]*

[1] Department of Dermatology, University Medical Center of the Johannes Gutenberg University (JGU) Mainz, 55131 Mainz, Germany
[2] Pharmaceutical Biotechnology, Department of Pharmacy, Center for NanoScience, Ludwig-Maximilians-Universität (LMU) Munich, 81377 Munich, Germany
[3] Junior Group "Retroviral Pathogenesis" and BMBF Junior Research Group in Infection Research "Milk-Transmission of Viruses", Institute of Clinical and Molecular Virology, Friedrich-Alexander-Universität (FAU) Erlangen-Nürnberg, 91054 Erlangen, Germany
[4] Institute of Clinical and Molecular Virology, Friedrich-Alexander-Universität (FAU) Erlangen-Nürnberg, 91054 Erlangen, Germany

***** Corresponding authors: M. Bros and S. Berger

This chapter is adapted from a manuscript (research article) *in preparation*.

Author contributions

All authors contributed substantially to this work. Y. Zeyn: methodology, formal analysis, investigation, writing – original draft, visualization; D. Hobernik: methodology, formal analysis, investigation, resources; U. Wilk & J. Pöhmerer: methodology, formal analysis, investigation; C. Hieber, C. Medina-Montano, and N. Röhrig: methodology, formal analysis, investigation; C. F. Mohr: methodology, investigation, resources; A. K. Thoma-Kress: methodology, resources, supervision; E. Wagner: writing – review & editing, supervision, funding acquisition, project administration; M. Bros: conceptualization, project administration, writing – original draft / review & editing, supervision, funding acquisition; S. Berger: conceptualization, project administration, formal analysis, investigation, writing – original draft / review & editing, visualization, supervision, funding acquisition.

Abstract

Deeper knowledge about the role of the tumor microenvironment (TME) in cancer development and progression has resulted in new strategies such as gene-based cancer immunotherapy. Whereas some approaches focus on expression of tumoricidal genes within the TME, DNA-based vaccines are intended to be expressed in antigen-presenting cells (*e.g.*, dendritic cells, DCs) in secondary lymphoid organs, which in turn induce anti-tumor T cell responses. Besides effective delivery systems and the requirement of appropriate adjuvants, DNA vaccines themselves need to be optimized regarding efficacy and selectivity. In this work, the concept of DC-focused transcriptional targeting was tested by applying a plasmid encoding for the luciferase reporter gene under the control of a derivative of the human fascin1 gene promoter (pFscnLuc), comprising the proximal core promoter fused to the normally more distantly located DC enhancer region. DC-focused activity of this reporter construct was confirmed in cell culture in comparison to a standard reporter vector encoding for luciferase under the control of the strong ubiquitously active cytomegalovirus promoter and enhancer (pCMVLuc). Both plasmids were also compared upon intravenous administration in mice. The organ- and cell type-specific expression profile of pFscnLuc versus pCMVLuc demonstrated favorable activity especially in the spleen as a central immune organ, and within the spleen in DCs.

Keywords

Transcriptional targeting, DNA vaccine, dendritic cells, promoter, fascin1.

7.1 Introduction

Based on a deeper understanding of the pathophysiology and the important role of immune dysfunction in cancer development and progression, nucleic acid-based immunotherapeutic approaches have attracted growing interest in recent years.[234, 1183] Hereby, the aims are *i*) to modulate the immune system in such a way that it effectively fights the tumor, and *ii*) to create an immunological memory for long-term protection. DNA-based vaccination of dendritic cells (DCs) and other antigen-presenting cells (APCs) with transgenes that encode tumor-associated or -specific antigens aims to induce adaptive anti-tumor immune responses. So far, the overall efficacy of such DNA vaccines in clinical trials has been limited.[234, 689, 1184] Their combination with other immunotherapies (*e.g.*, check-point inhibitors, chimeric antigen receptor (CAR) T cells, or oncolytic viruses), or with conventional cancer treatments (*e.g.*, chemotherapy, irradiation) may improve the clinical outcome.[234] Moreover, DNA vaccines can be optimized by *i*) the careful choice of suitable antigens, *ii*) the selection of appropriate adjuvants, *iii*) the use of efficient delivery systems (*e.g.*, nanoparticles like polyplexes[25]), and *iv*) the structural optimization of the DNA itself. The latter can be achieved by using a strong APC-specific promoter that confines tumor antigen expression to APC. By this, unwanted gene expression in tumor-induced immune-regulatory cell types (*e.g.*, tumor-associated macrophages, or myeloid-derived suppressor cells), which in turn can induce tumor immune tolerance, may be prevented.[234] As DCs are the most potent T cell stimulatory APC population,[1185] they represent an ideal target for such an approach. Previously, the promoter of the murine fascin1 (Fscn1) gene was identified to be suitable for transcriptional targeting of activated DCs.[751] Fscn1, a cytoskeletal actin-bundling protein, is evolutionarily highly conserved, expressed upon activation of DCs, and is relevant for cell motility and migration.[1186] In the current work, also with regard to the translational perspective of DNA-based vaccination in the future, the Fscn1 gene promoters of both murine[751] and human[750] origin were compared. Hereby, the human promoter was superior in terms of activity and DC specificity even in murine cell lines (cross-species activity). The concept of DC-focused transcriptional targeting was tested *in vitro* and *in vivo* by using a plasmid encoding for the firefly luciferase reporter gene under the control of an optimized derivative of the human Fscn1 gene promoter (pFscnLuc), in comparison to a standard firefly luciferase encoding plasmid under the control of the strong ubiquitously active

cytomegalovirus promoter and enhancer (pCMVLuc). As effective non-viral plasmid DNA (pDNA) carriers *in vitro* and *in vivo*, linear polyethylenimine 22kDa (LPEI)[499, 502, 614] as well as succinylated branched polyethylenimine 25kDa (succPEI, 10% succinylation degree)[622] were used. Both cationic polymers are able to efficiently compact pDNA into nanoparticulate complexes (so-called polyplexes[25]) *via* electrostatic interactions.

7.2 Experimental section

7.2.1 Materials

Plasmids pCMVLuc[60] (encoding *Photinus pyralis* firefly luciferase under control of cytomegalovirus promotor and enhancer) and pFscnLuc[1187] (encoding *Photinus pyralis* firefly luciferase under control of a derivative of the human Fscn1 gene promotor) were obtained from Plasmid Factory GmbH (Bielefeld, Germany). Promoter-less expression vector pGL3-Basic (promoter-less expression vector encoding for *Photinus pyralis* firefly luciferase), and pGL3-Control (encoding *Photinus pyralis* firefly luciferase under control of the hybrid SV40 promoter/enhancer) (all from Promega, Mannheim, Germany) were obtained from Plasmid Factory GmbH (Bielefeld, Germany) as endotoxin-free preparations. The *Renilla reniformis* luciferase encoding vector pRL-EF1α[750] was amplified using the Endofree Plasmid Maxi Kit (Qiagen, Hilden, Germany).

HEPES (4-(2-hydroxyethyl)-1-piperazineethanesulfonic acid) was obtained from Biomol (Hamburg, Germany), disodium ethylenediaminetetraacetic acid (EDTA) as well as glucose from Merck (Darmstadt, Germany). Cell culture consumables were obtained from Faust Lab Science (Klettgau, Germany) or Greiner Bio-One (Frickenhausen, Germany). Cell culture media, bovine serum albumin (BSA), fetal bovine serum (FBS), antibiotics, and trypsin/EDTA were purchased from Sigma Aldrich (Munich, Germany) and PAN-Biotech (Aidenbach, Germany); β-mercaptoethanol was obtained from Roth (Karlsruhe, Germany). Cell culture 5× lysis buffer, CellTiter-Glo Reagent, and *D*-luciferin sodium salt were obtained from Promega (Mannheim, Germany); dithiothreitol (DTT), adenosine 5′-triphosphate (ATP) disodium salt trihydrate, coenzyme A trilithium salt, and protease and phosphatase inhibitor cocktail from Sigma-Aldrich (Munich, Germany). In case of co-transfection using firefly luciferase and renilla luciferase encoding vectors, luciferase activities were determined using the Dual-luciferase reporter assay kit (Promega, Fitchburg, WI, USA).

Succinylated branched PEI 25kDa (succPEI; succinylation degree of 10%) and unmodified linear PEI 22kDa (LPEI) were synthesized and analyzed as described previously.[206, 207, 622] Starting products branched PEI (brPEI) 25kDa as well as poly(2-ethyl-2-oxazoline) were purchased from Sigma Aldrich (Munich, Germany). The transfection reagent JetPEI (linear PEI) was obtained from Polyplus (Illkirch, France).

The murine neuroblastoma cell line Neuro2a (N2a), the murine macrophage-like cell line P388, and the murine B cell-like cell line A20 were purchased from the American Type Culture Collection (ATCC; Manassas, VA, USA). The murine hepatoma cell line Hepa1-6 was obtained from ATCC (Gaithersburg, MD, USA), and the murine DC-like cell line DC2.4 from Merck Millipore (Darmstadt, Germany).

PE-/APC- and PE-Cy7-labeled CD11c specific (clone N418), FITC-CD86 (GL-1), SB600-CD11b (M1/70), PE-NK1.1 (PK136), PE-eFl610-Ly6G (1A8-L6g), V500-B220 (RA3-6B2), SB702-CD45 (30-F11), eFl506- or FITC-CD3 (17-A2), AF647-Luciferase (EPR17789), eFl450-F4/80 (BM8), AF488-CD19 (6D5), AF647-XCR1 (ZET), PE-Cy7-CD172a (P84) and PE-CD32b (AT130-2) antibodies were used for flow cytometric analysis (FACS). FACS antibodies were purchased from BD Biosciences (Franklin Lakes, NJ, USA), BioLegend (San Diego, CA, USA) or ThermoFisher (Waltham, MA, USA). eFl780-FVD (fixable viability dye) used to identify dead cells was obtained from ThermoFisher. Unlabeled mouse anti-human Fscn1 antibody (55K2; Sigma-Aldrich), a corresponding isotype control antibody (mouse IgG1, clone MOPC-21, BioLegend), secondary AF488-labeled IgG goat anti-mouse antibody (948492) and HCS Cell Mask Orange Stain (both from ThermoFisher) were used for confocal laser scanning analysis (CLSM). For intracellular staining, Fluorofix Fixation Buffer, and Intracellular Staining Perm Wash Buffer (both from BioLegend) were used.

7.2.2 pDNA polyplex formation

pDNA and calculated amounts of LPEI at indicated N/P (nitrogen/phosphate) ratios or of succPEI at indicated w/w (weight/weight) ratios, respectively, were diluted with HBG (HEPES buffer with glucose; 20 mM of HEPES, 5% (w/v) glucose; pH 7.4) in separate vials at equal volumes. pDNA and LPEI or succPEI solutions were mixed by rapid pipetting and incubated for 30 min at room temperature (RT) in a closed vial.

Note: In the case of succPEI, the N/P ratio was considered to be not suitable for calculation of the amounts of succPEI to pDNA since some amino groups are substituted with succinic acid and thus not involved in

nucleic acid binding. Therefore, the w/w ratio was used instead of the commonly used N/P ratio.[622] A w/w ratio of 1 corresponds to an N/P ratio of ~7.5 for unsubstituted PEI.

7.2.3 Physico-chemical characterization of pDNA polyplexes – particle size and zeta-potential measurements

Polyplexes were formulated in HBG buffer as described above (method *7.2.2*) at pCMVLuc concentrations used for the *in vitro* experiments (*i.e.*, 10 µg mL^{-1} in the case of transfections in tumor cell lines N2a and Hepa1-6; 25 µg mL^{-1} in the case of transfections in the DC-like cell line DC2.4), and for the *in vivo* studies (*i.e.*, 300 µg mL^{-1}). Measurements of size and zeta-potential were performed by dynamic and electrophoretic laser-light scattering (DLS, ELS) using a Zetasizer Nano ZS (Malvern Instruments, Malvern, Worcestershire, U.K.) in a folded capillary cell (DTS1070). Size and polydispersity index were measured in 100 µL polyplex solution using the following instrument settings: equilibration time 30 sec, temperature 25 °C, refractive index 1.330, viscosity 0.8872 mPa*s. Samples were measured three times with six sub runs per measurement. For measurement of the zeta-potential, all samples were diluted to 800 µL with HBG directly before measurement. Parameters were identical to the size measurement apart from an equilibration time of 60 sec. Three measurements with 15 sub runs lasting 10 sec each were performed, and zeta-potentials were calculated by the Smoluchowski equation.

7.2.4 Cell culture

Cells were cultured at 37 °C and 5% CO_2 in an incubator with a relative humidity of 95%.

7.2.4.1 Immortalized cell lines

N2a and Hepa1-6 cells were grown in Dulbecco's Modified Eagle's Medium (DMEM)-low glucose (1 g L^{-1} glucose) supplemented with 10% (v/v) FBS, 4 mM of stable glutamine, 100 U mL^{-1} of penicillin, and 100 µg mL^{-1} of streptomycin. The DC2.4 cell line was grown in Iscove's Modified Dulbecco's Medium (IMDM) supplemented with 10% (v/v) FBS, 4 mM of stable L-glutamine, 100 U mL^{-1} of penicillin, and 100 µg mL^{-1} of streptomycin, and 50 µM of β-mercaptoethanol.

7.2.4.2 Primary cells

Bone marrow-derived cells (BMDCs, 2×10^5 mL^{-1}) were seeded in 12-well plates (Greiner Bio-One) in IMDM-based culture medium (see above) including recombinant murine granulocyte-macrophage colony-stimulating factor (GM-CSF; 10 ng mL^{-1}; Miltenyi Biotec)

to differentiate DCs. DC culture media was replenished on days 3 and 6 of culture.

7.2.5 Fscn1 staining of cell lines and confocal laser scanning microscopy (CLSM)

Cytospins were generated and Fscn1 expression was detected by CLSM as described previously.[1188] In brief, cells were re-suspended (5×10^5 mL^{-1}) in PBS (phosphate-buffered saline; 136.9 mM NaCl, 2.7 mM KCl, 8.1 mM Na_2HPO_4, 1.5 mM KH_2PO_4). Each 50,000 cells were cytospun (500 rpm, 5 min, RT) onto microscope slides (Superfrost Plus; VWR, Darmstadt, Germany) using a Cytospin 3 (ThermoFisher, Waltham, MA, USA), air-dried overnight, and stored at –20 °C. For staining, cytospins were incubated first with pre-cooled methanol (Roth, Karlsruhe, Germany) for 10 min to permeabilize the cell membrane and washed twice with PBS. During all subsequent incubation steps, samples were kept in a humidified chamber. Cytospins were incubated with a Fc receptor blocking antibody (clone 2.4-G2; 1:50-diluted in PBS/2% (v/v) BSA) for 10 min at RT. Then, Fscn1-specific or isotype control antibody (each 1:50-diluted in PBS/2% (v/v) FBS) was added, and samples were incubated for 20 min at RT. Afterwards, samples were washed and incubated with AF488-labeled secondary anti-mouse antibody (1:400-diluted in PBS/2% (v/v) FBS) for 20 min at RT. After two washing steps with PBS, HCS Cell Mask Orange (2 µg mL^{-1}, ThermoFisher) was applied, and samples were incubated for 30 min and finally washed with water. As a control, samples were left untreated or incubated with one agent only, respectively. All samples were covered with fluorescence mounting medium (DAKO; Agilent, Santa Clara, CA, USA) and a coverslip.

For CLSM, samples were imaged using a Leica SP8 confocal microscope (Mannheim, Germany) equipped with a 20/0.75 NA air objective using a 405 nm laser for transmission images, a 488 nm laser for AF488 (Fscn1) excitation (emission and detection within a spectral window of 499-581 nm), and 552 nm laser exposure for AF555 (HCS Cell Mask Orange) excitation (emission and detection within a spectral window of 562-632 nm). Cellular Fscn1 intensities were calculated using Imaris software version 9.3.1 (Bitplane, Zurich, Switzerland).

7.2.6 *In vitro* transfection efficiency of pDNA polyplexes – luciferase gene expression assay

One day prior to transfection, 10,000 N2a, 10,000 Hepa1-6, or 5000 DC2.4 cells were seeded per well into 96-well plates. For transfection, 200 ng (N2a; Hepa1-6), or 500 ng (DC2.4) pDNA per well were applied, respectively. HBG served as a negative control. All

transfection experiments were performed in biological triplicates. Medium was replaced with 80 µL of fresh medium containing 10% (v/v) FBS, and polyplexes formed at indicated N/P (LPEI) or w/w (succPEI) ratios in 20 µL HBG as described above (method 7.2.2) were added to each well. The plates were incubated at 37 °C without change of medium. After 24 h incubation, the medium was removed, cells were lyzed with 100 µL of cell culture 0.5× lysis buffer (Promega, Mannheim, Germany), and the samples were frozen at –80 °C at least overnight. Prior to measurement of luciferase activity, plates were equilibrated for 1 h at RT. Luciferase activity in 35 µL of the cell lysate was measured for 10 sec by using a Centro LB 960 plate reader luminometer (Berthold Technologies, Bad Wildbad, Germany) after addition of 100 µL LAR buffer (20 mM glycylglycine; 1 mM $MgCl_2$; 0.1 mM EDTA; 3.3 mM DTT; 0.55 mM ATP; 0.27 mM coenzyme A, pH 8-8.5) supplemented with 5% (v/v) of a mixture of 10 mM luciferin and 29 mM glycylglycine. Transfection efficiency was calculated for the seeded number of cells and presented as relative light units (RLU) per well.

In some experiments (results displayed in **Figure 7.1**), cells (DC2.4, P388, A20; each 20,000 per well in a 24 well plate) were co-transfected with firefly (950 ng of largest vector and equimolar amounts of smaller vector) and renilla luciferase (50 ng) encoding vectors using JetPEI (Polyplus) as recommended by the manufacturer. On the next day, plates were centrifuged, media was removed and 100 µL of Passive Lysis Buffer (Promega, Mannheim, Germany) was applied to each well. 10 µL of cell lysate were assayed for luciferase activities by subsequently applying firefly and renilla substrate as recommended by the manufacturer (Promega, Mannheim, Germany) and measuring luciferase activities for each 5 sec. Firefly luciferase activities were divided by renilla luciferase activities to account for differences in transfection efficacy.

7.2.7 Metabolic activity of pDNA polyplex-treated cells – CellTiter-Glo assay

Transfections were performed as described above (method 7.2.6). The supernatant was removed at 24 h after transfection, and 25 µL of medium as well as 25 µL of CellTiter-Glo Reagent were added to each well. After incubation on an orbital shaker for 30 min at RT, luminescence was recorded using a Centro LB 960 plate reader luminometer (Berthold Technologies, Bad Wildbad, Germany). The luminescent signals (in RLU) of the samples were set in relation to the luminescent signal of the negative control (HBG buffer-treated control cells). Results are presented as relative metabolic activity related to the negative

control. Experiments were performed in biological triplicate.

7.2.8 Assessment of live cells *via* flow cytometry

Cells were washed in staining buffer (PBS, 1% (v/v) FBS, 0.5 mM EDTA) and were incubated with Fc receptor blocking antibody (2.4-G2) for 15 min at RT. Then, samples were incubated with fluorescence-labeled antibodies (see above) for 20 min at 4 °C. Afterwards, samples were washed with PBS and subsequently incubated with eFl780-FVD to identify dead cells. Samples were assayed using an Attune NxT flow cytometer and data were analyzed using Attune NxT software (both ThermoFisher).

7.2.9 *In vivo* comparison of pCMVLuc and pFscnLuc polyplexes

In vivo experiments were performed according to the guidelines of the German Animal Welfare Act and were approved by the animal experiments ethical committee of the Government of Upper Bavaria (accreditation number Gz. ROB-55.2-2532.Vet_02-19-19). 6-week old female BALB/c mice (Janvier Labs, Le Genest-Saint-Isle, France) were randomly divided into groups of five. Mice were housed in isolated ventilated cages under specific pathogen-free conditions with a 12 h day/night interval, and food and water *ad libitum*. Weight and general well-being were monitored continuously. The experiments were performed by intravenous tail vein injection of polyplexes formed at indicated N/P (LPEI) or w/w (succPEI) ratio as described above (method 7.2.2), respectively, each containing 60 µg of pCMVLuc or pFscnLuc in 200 µL HBG. Mice were euthanized at 24 h after injection. The organs (lungs, liver, spleen) were dissected and washed carefully with PBS, followed by analysis *via* an *ex vivo* luciferase gene expression assay (method 7.2.10) as well as an immunostaining of single cell suspensions retrieved from dissected organs (lungs, liver, spleen, lymph nodes; method 7.2.11).

7.2.10 *In vivo* gene transfer efficiency of pDNA polyplexes – *ex vivo* luciferase gene expression assay

Organs were homogenized in Luciferase Cell Culture Lysis Reagent 1× (Promega, Mannheim, Germany), supplemented with 1% (v/v) protease and phosphatase inhibitor cocktail (Sigma-Aldrich, Munich, Germany) using a tissue and cell homogenizer (FastPrep®-24, MP Biomedicals, USA). Then, the samples were frozen overnight at –80 °C to ensure full lysis. The samples were thawed and centrifuged for 10 min at maximum speed (~13,000 rpm) at 4 °C. Luciferase activity in 25 µL supernatant was

measured for 10 sec as described above (method 7.2.6). The luciferase expression is presented as RLU per gram (g) organ after background subtraction (lysis buffer).

7.2.11 Immunostaining & gating strategy

Spleens and lymph nodes were meshed using a pestle and a 40 µM cell strainer (Greiner Bio-One, Frickenhausen, Germany) to yield a single-cell suspension. Spleen cells (2×10^6 500 μL^{-1}) were kept in FACS tubes overnight in medium (IMDM, containing 5% (v/v) FBS, 2 mM of L-glutamine, 100 U mL^{-1} of penicillin, 100 µg mL^{-1} of streptomycin, and 50 µM ß-mercaptoethanol).

Murine liver non-parenchymal cells (NPCs) were enriched by liver dissociation as described previously.[1189] In brief, livers were pre-incubated for 15 min in an enzyme-dependent dissociation mixture (Liver Dissociation Kit; Miltenyi Biotec, Bergisch-Gladbach, Germany). Then, the liver tissue was dissected in little pieces, which were transferred into prepared C tubes (Miltenyi Biotec). The C tubes were placed into a gentleMACS Dissociator to be minced (program m_liver_03). The derived cell suspension was incubated under continuous shaking (30 min at 37 °C), followed by another round of gentleMACS-mediated dissociation (m_liver_04). Afterwards, liver NPCs were enriched by density centrifugation employing 30% Histodenz-HBSS (both from Sigma-Aldrich).

Lung cell suspensions were obtained using the Lung Dissociation Kit (Miltenyi Biotec) according to the manufacturer's protocol.

Extracellular staining was performed as described above (method 7.2.8). For intracellular staining, samples were fixed with 0.5 mL Fluorofix Fixation Buffer for 20 min and washed twice with 0.5 mL Perm Wash Buffer. Then, the antibody for intracellular luciferase detection was added and the samples were incubated for 20 min at RT in the dark. Finally, samples were washed two times with each 1 mL Perm Wash Buffer. Gating was performed according to the strategies described in **Figure 7.13** and **Figure 7.14**. Samples were assayed using an Attune NxT flow cytometer and data were analyzed using Attune NxT software (both ThermoFisher).

7.2.12 Statistics

Results are presented as arithmetic mean and standard deviation (SD) or standard error of the mean (SEM), respectively, of at least three experiments. Unpaired Student's two-tailed *t*-test with Welch's correction, as well as ordinary one-way ANOVA (multiple

comparison, Tukey test), respectively, were performed using GraphPad Prism™ in order to analyze statistical significances between groups. Significance levels are indicated with symbols: ns $p > 0.05$; * $p \leq 0.05$; ** $p \leq 0.01$; *** $p \leq 0.001$; **** $p \leq 0.0001$.

7.3 Results and discussion

7.3.1 Evaluation of Fscn1 gene promoter constructs

We have previously reported that the murine[751, 1190] and human[750] Fscn1 gene promoters allowed for transcriptional targeting of DCs. Subsequent studies demonstrated that plasmids containing the murine Fscn1 promoter to drive antigen expression favorably stimulated a Th1-biased immune response.[674, 1190, 1191] In the current study, we compared the activity of both promoters in the murine DC-like cell line DC2.4 (**Figure 7.1A**). DC2.4 cells are known to be of mature phenotype,[751, 1192] and thus are considered to express Fscn1, which was confirmed by us *via* intracellular Fscn1 staining (**Figure 7.2, Figure 7.7**). Interestingly, the full length human Fscn1 promoter (phF3.1[750]) evoked 30-fold higher reporter gene expression than its murine counterpart (pmF2.6[751]), about 55-fold stronger than the promoter-less negative control (pGL3-Basic), and at similar extent as the hybrid SV40 promoter/enhancer (pGL3-Ctrl) serving as a positive control (**Figure 7.1A**). Since tumor cells are also able to *de novo* express Fscn1,[1188, 1193] murine B16 melanoma cells known to express Fscn1,[1194] were assayed as well. Similar to DC2.4, the human Fscn1 promoter mediated higher transgene expression than the murine Fscn1 promoter.

Due to the higher transcriptional activity of the human promoter and with regard to its translational use for DC-focused DNA vaccination in humans, we aimed to enhance its overall activity. The different human fascin1 gene promoter constructs (phF) are displayed in **Scheme 7.1**. We have previously shown that a 1.6 kb fragment of the human Fscn1 gene promoter (phF1.6) evoked strongest activity in human DCs,[750] and accordingly also exerted similar activity as the positive control (pGL3-Ctrl) in DC2.4 cells (**Figure 7.1B**, *left*). Further, we have reported that DC-specific activity was mediated by an enhancer region located within a 170 bp sequence stretch located downstream of phF1.6.[750] When fusing this enhancer sequence with the core promoter of the human Fscn1 gene promoter as apparent in phF0.21 (described in ref. [1187]), the resulting construct pFscnLuc exerted stronger transcriptional activity in DC2.4 cells than the parental constructs (2.5-fold higher

compared to phF1.6; 5-fold higher compared to phF0.21). This enhancer/core promoter hybrid retained DC-focused transcriptional activity as observed in Fscn1-negative cell lines [*i.e.*, macrophage-like P388 cells (**Figure 7.1B**, *middle*), and B cell-like A20 cells (**Figure 7.1B**, *right*)], yielding only about double activity as the negative control (pGL3-Basic) in either case.

Scheme 7.1. Human fascin1 gene promoter constructs (phF) encoding for luciferase reporter gene in comparison to control luciferase-encoding vectors pGL3-Basic (promoter-less) and pGL3-Ctrl (hybrid SV40 promoter/enhancer).

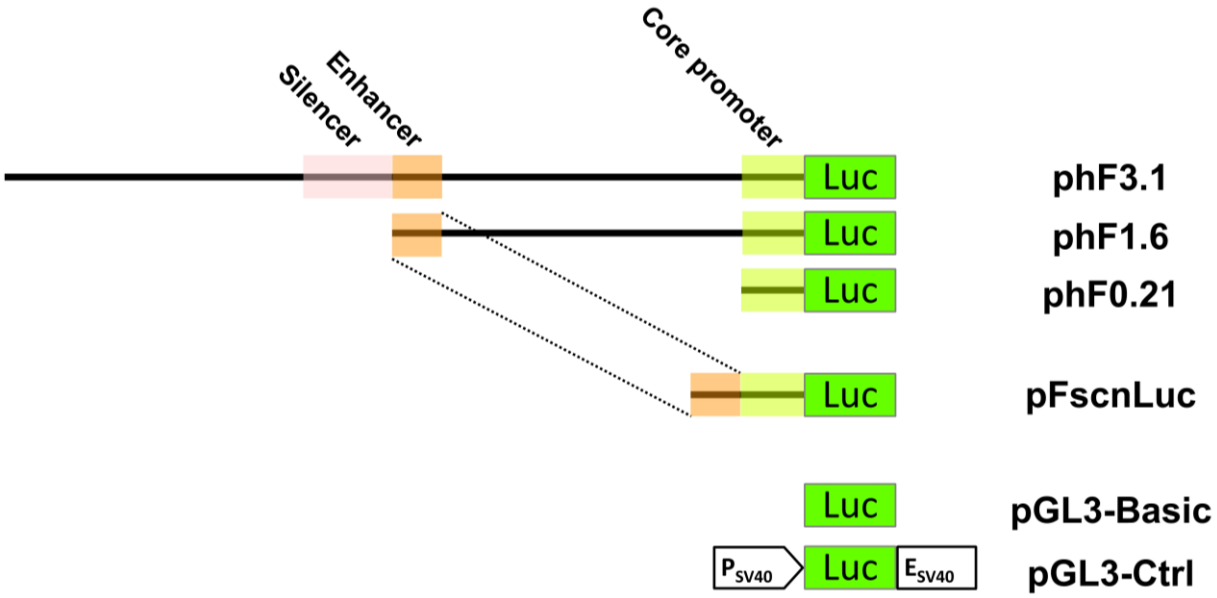

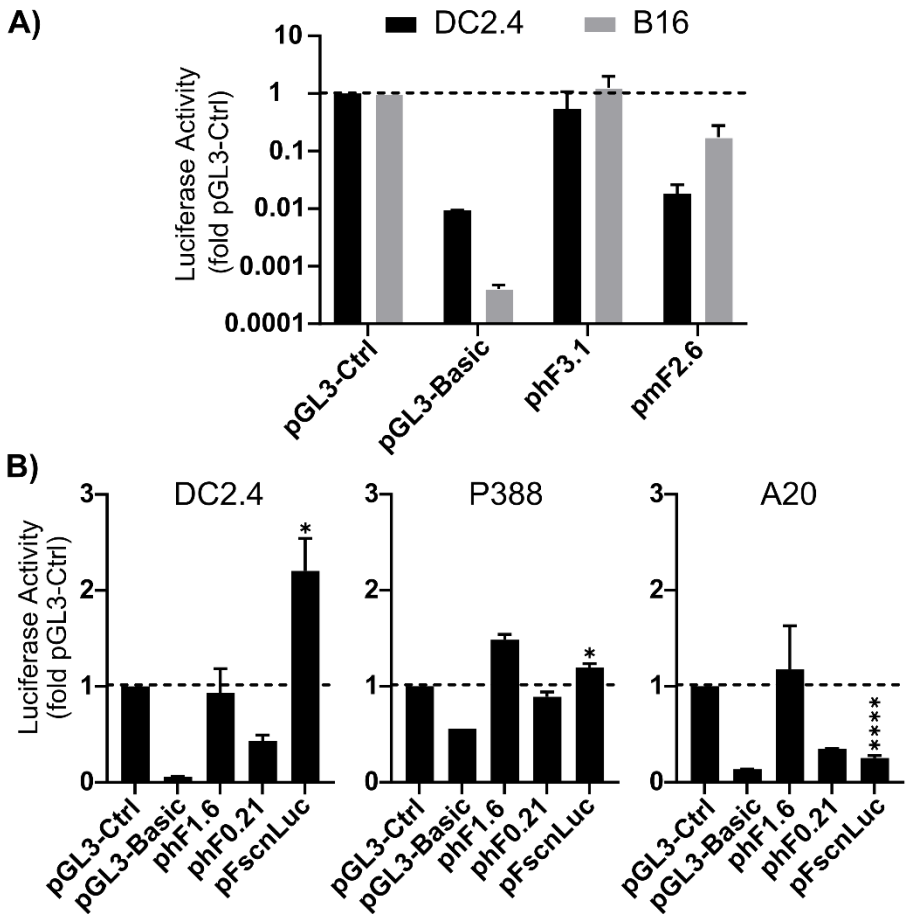

Figure 7.1. Transcriptional activity of various Fscn1 promoter luciferase reporter constructs. **A)** Comparison of Fscn1 promoter reporter constructs of human versus murine origin in DC-like DC2.4 cells, and B16 melanoma cells. **B)** Comparison of different human Fscn1 promoter reporter constructs in DC2.4 cells, macrophage-like P388 cells, and B cell-like A20 cells. Cell lines (all of murine origin; each 20,000 cells/well) were transfected with Fscn1 promoter firefly luciferase reporter constructs as indicated and control vectors (pGL3-Basic, pGL3-Ctrl) at equimolar amounts normalized to 950 ng of the largest plasmid, respectively, and a constant amount of 50 ng of a renilla luciferase encoding control vector (pRL-EF1α[750]) using the transfection reagent JetPEI according to the manufacturer's protocol. On the next day, firefly luciferase activities were determined. Data denote the relative luciferase activity (fold pGL3-Ctrl; *n*=4; mean + SEM). Significant differences versus pGL3-Ctrl: * $p \leq 0.05$; **** $p \leq 0.0001$ (unpaired Student's two-tailed *t*-test with Welch's correction; GraphPad Prism™).
The pFscnLuc construct was generated by Dr. Caroline F. Mohr and supervisor PD Dr. Andrea K. Thoma-Kress (both Institute of Clinical and Molecular Virology, FAU Erlangen-Nürnberg). Transfection experiments were performed by Dr. Dominika Hobernik (Department of Dermatology, University Medical Center, JGU Mainz).

In the following, the optimized human Fscn1 gene promoter was evaluated in comparison to the standard CMV promoter in terms of its transcriptional activity *in vitro* and *in vivo*.

7.3.2 Fscn1 expression in tumor cells in comparison to DCs

Under homoeostatic conditions, Fscn1 expression is mainly restricted to neuronal/glia cells and activated DCs, mediating membrane protrusions and the formation of filopodial extensions.[1188, 1195, 1196] Besides that, *de novo* expression of Fscn1 is also often found in tumor cells and correlates with cancer aggressiveness by promoting cancer progression, migration, and metastasis.[1188, 1193]

To prove that the neuroblastoma cell line N2a and the hepatoma cell line Hepa1-6 express Fscn1 and hence are suitable for pFscnLuc transfections, intracellular Fscn1 staining on cytospun cells was conducted. CLSM imaging revealed that both tumor cell lines indeed express Fscn1at a certain, yet lower extent compared to DC2.4 cells (**Figure 7.2, Figure 7.7**), and thus can be used for further evaluation of the human Fscn1 promoter.

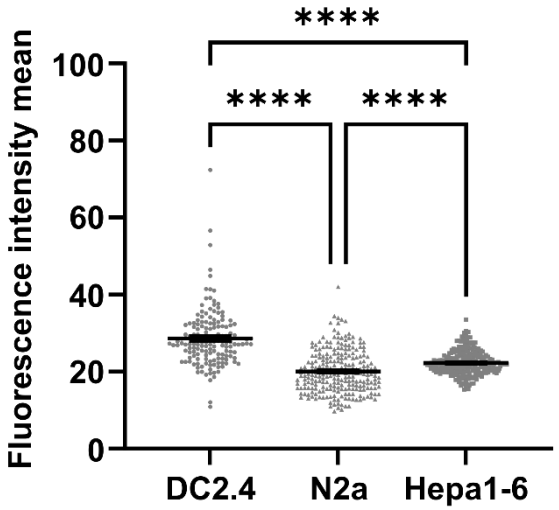

Figure 7.2. Quantification of Fscn1 levels in cell lines DC2.4, N2a, and Hepa1-6. Data denote the corresponding fluorescence intensities per cell and the mean ± SEM of 154-301 cells per group after CLSM imaging. Corresponding cytospin images are displayed in **Figure 7.7**.. Significance levels are indicated: **** $p \leq 0.0001$ (one-way ANOVA, Tukey test; GraphPad Prism™).
The experiments and analysis were done by Yanira Zeyn (Department of Dermatology, University Medical Center, JGU Mainz).

7.3.3 Suitability of carriers for pDNA delivery

For the comparison of the optimized human Fscn1 promoter with the standard CMV promoter *in vitro* and *in vivo*, LPEI[3, 88, 499, 502, 614] as the established gold standard for pDNA transfections as well as succPEI[622] were selected as pDNA carriers. Both cationic polymers were able to compact either plasmid at *in vitro* and *in vivo* concentrations into

well-defined, homogenous nanoparticles by electrostatic interactions with hydrodynamic diameters (z-average) between 55 and 140 nm, polydispersity indices (PdI) below 0.3, and a positive surface charge (zeta-potential ranging from + 10 to + 30 mV) (**Table 7.1**).

Despite the potent transfection capability of PEI, its multi-faceted cytotoxicity can be an issue.[88] Furthermore, PEI-mediated effects on the immune system such as complement activation[39, 40], or interactions with Toll-like receptors (TLRs)[1197-1199] have been reported, mediating either immune toxicity or immune stimulation.[88] Lowering the N/P ratio of LPEI pDNA complexes from highly effective N/P 9-10[143, 501, 502, 627] to N/P 6[210, 499] may be a compromise between efficacy and toxicity. Another option to reduce toxicity could be surface modification of PEI,[88] as for example demonstrated by succinylation of branched PEI (succPEI).[622]

In the following, LPEI and succPEI were tested regarding their possible toxicity and activation potential in DCs as the primarily intended target APC population. Therefore, the effects of LPEI and succPEI on viability and activation as deduced from upregulation of according markers (MHCII, major histocompatibility complex for antigen-presentation; CD80 and CD86 as costimulatory receptors for antigen-specific T cell activation)[849, 1200, 1201] in GM-CSF derived BMDCs were analyzed. To this end, pFscnLuc was complexed with the respective carrier at different N/P (LPEI; N/P 6 and 9, resp.) and w/w ratios (succPEI; w/w 1.5 and 4, resp.), and the BMDCs were incubated with these polyplexes overnight. Despite the far higher carrier amounts (w/w ratios of 1.5 and 4 represent N/P ratios of ~ 11.25 and ~ 30), succPEI polyplexes were well tolerated by the BMDCs, whereas LPEI especially at an N/P ratio of 9 significantly reduced their viability by around 30% (**Figure 7.3A**). Nevertheless, in contrast to succPEI, LPEI also enhanced expression of surface activation markers (**Figure 7.3B-D**), particularly of CD86 (at N/P 9, 1.5-fold increase compared to untreated control cells). This effect may be due to an intrinsic activating potential of the LPEI polyplexes. However, it is also possible that necrotic cells within the culture released endogenous danger factors like HMGB1 (high mobility group box-1 protein), which binds to TLR4,[1202] thereby triggering DC activation.

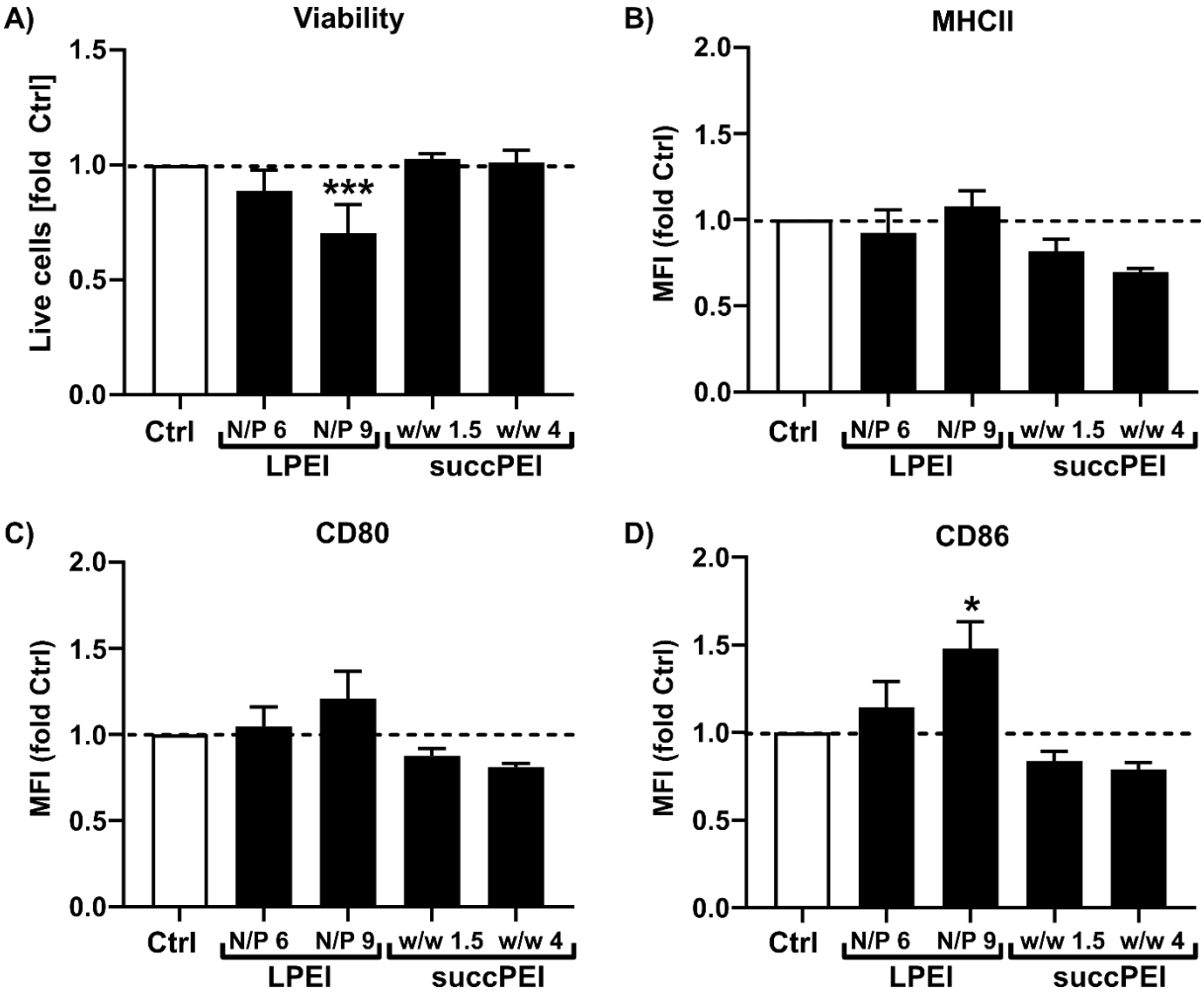

Figure 7.3. Viability and activation marker expression of BMDCs after incubation with LPEI and succPEI polyplexes. BMDCs (20,000 cells per well) were incubated overnight with LPEI (N/P 6 and 9, resp.) and succPEI (w/w 1.5 and 4, resp.) polyplexes at a concentration of 1 µg pFscnLuc/well. On the next day, samples were harvested, and both viability and activation marker surface expression were assayed by flow cytometry. Graph **A** denotes the frequencies of FVD-negative viable cells (*n*=4; mean + SEM), normalized to untreated cells (Ctrl). Graphs **B-D** denote the mean fluorescence intensity (MFI) (*n*=4; mean + SEM) in relation to the control (untreated cells). Significant differences versus Ctrl: * $p \leq 0.05$; *** $p \leq 0.001$ (one-way ANOVA, Tukey test; GraphPad Prism™). MHCII, major histocompatibility complex class 2; CD80 and CD86, costimulatory receptors for T cell activation.

Note: For succPEI, w/w ratios of 1.5 and 4 represent N/P ratios of ~ 11.25 and ~ 30 of an unsubstituted PEI.

The experiments were done by Yanira Zeyn (Department of Dermatology, University Medical Center, JGU Mainz).

The viability of DC-like DC2.4 cells treated with the various polyplexes was evaluated as well (**Figure 7.8**). The results were comparable to those received for BMDCs (~ 35% reduced cell viability compared to untreated control cells). Taken together, these results

indicate that the toxicity of LPEI-based polyplexes in DCs correlates with the N/P ratio. However, LPEI-mediated toxicity is only moderate even the higher N/P ratio of 9. To conclude, based on the findings regarding toxicity and activation potential, all four polyplex formulations were considered to be suitable as delivery systems in the following experiments.

7.3.4 *In vitro* performance of the optimized human Fscn1 promoter

The cell type-specific activity of pFscnLuc in comparison to standard plasmid pCMVLuc[60] was evaluated in different cell lines (**Figure 7.4**). In parallel assays, LPEI[3, 88, 143] as well as succPEI[622] were used as potent transfection agents at the indicated N/P (LPEI; N/P 6 and 9, resp.) or w/w ratios (succPEI; w/w 1.5 and 4, resp.).

The DC-focused activity of pFscnLuc was confirmed in a luciferase gene expression assay in DC2.4 cells for all four formulations. According polyplexes mediated up to 7.4-fold higher RLU values in DC2.4 cells compared to polyplexes formed with the standard plasmid pCMVLuc (**Figure 7.4A**).

Owed to the fact that Fscn1 is also expressed by (metastatic) tumor cells,[1188, 1193] pFscnLuc was additionally evaluated in the neuroblastoma cell line N2a (**Figure 7.4B**) and in the hepatoma cell line Hepa1-6 (**Figure 7.4C**) shown by us to express Fscn1. In contrast to DC2.4 cells, the preference for the Fscn1 promoter plasmid was here less pronounced. This is in line with the lower Fscn1 expression level compared to DC2.4 cells (**Figure 7.2**). Yet, pFscnLuc was expressed in both tumor cell lines at almost similar luciferase expression levels as the standard plasmid pCMVLuc (**Figure 7.4B, C**).

In addition, no plasmid-dependent differences in cytotoxicity were observed (**Figure 7.9**). Both tumor cell lines tolerated all tested polyplexes well (**Figure 7.9B, C**). DC2.4 cells were more sensitive towards the delivery systems and showed reduced metabolic activity. This was particularly the case for LPEI at higher carrier amounts (N/P 9), where only around 45% metabolic active cells were detected (**Figure 7.9A**). Nevertheless, a reduced metabolic activity does not necessarily correlate with more extensive cell death. Flow cytometric analysis of cell viability showed that succPEI polyplexes did not mediate cell killing in DC2.4 cells (**Figure 7.8**). Only LPEI, particularly at higher N/P ratio, attenuated cell viability by around 30%.

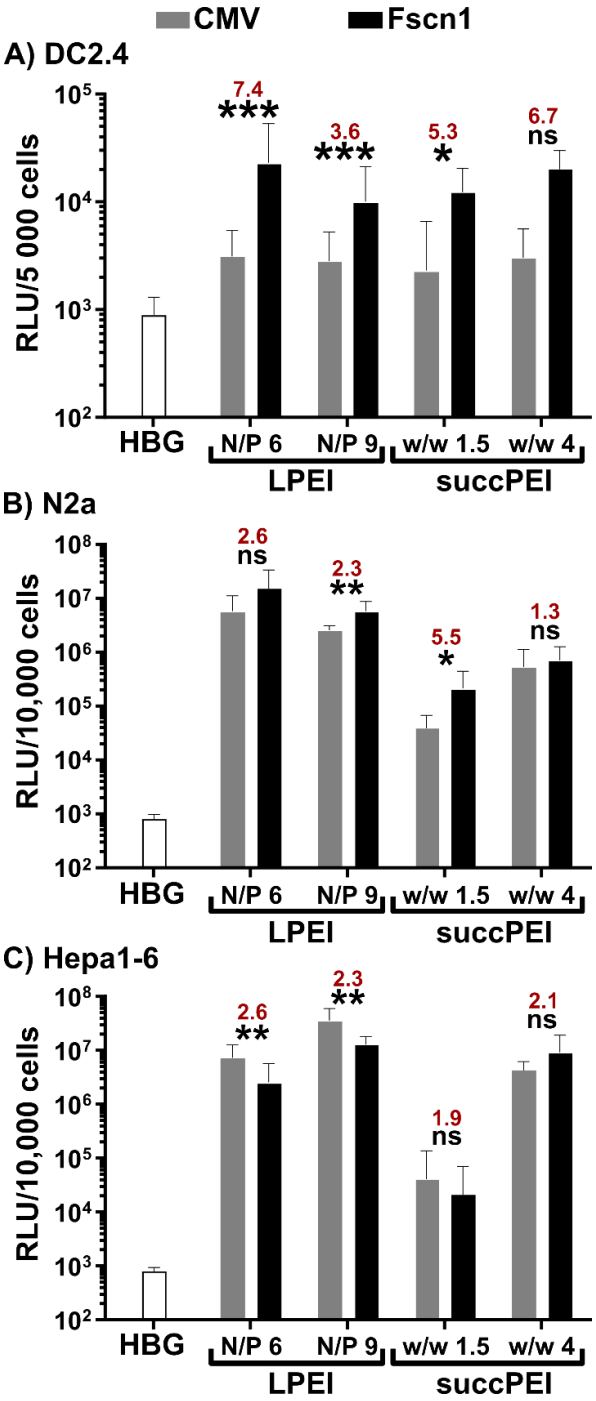

Figure 7.4. Comparison of promoter-dependent reporter activities in Fscn1-expressing cell types. Luciferase gene expression (*n*=3; mean + SD) was assayed at 24 h after transfection with LPEI (N/P 6 and 9, resp.) and succPEI (w/w 1.5 and 4, resp.) polyplexes containing pFscnLuc or pCMVLuc, resp., in the DC-like cell line DC2.4 (**A**) at a pDNA concentration of 500 ng/well, as well as in the neuroblastoma cell line N2a (**B**) and the hepatoma cell line Hepa1-6 (**C**) at a pDNA concentration of 200 ng/well. Red numbers indicate the fold difference in RLU values between pFscnLuc and pCMVLuc. Significant differences between both plasmids: ns $p > 0.05$; * $p \leq 0.05$; ** $p \leq 0.01$; *** $p \leq 0.001$ (unpaired Student's two-tailed *t*-test with Welch's correction; GraphPad Prism™). ns, not significant.

Note: For succPEI, w/w ratios of 1.5 and 4 represent N/P ratios of ~ 11.25 and ~ 30 of an unsubstituted PEI.

Altogether, these findings suggest on the one hand that the optimized Fscn1 promoter was suitable to drive stronger transgene expression in DCs as mediated by the standard CMV promoter/enhancer allowing for DC-focused DNA vaccination. On the other hand, the observation that the Fscn1 promoter was also highly active in tumor cells may pave the way to employ DNA therapeutics that (co-)target tumor cells. For example, transgenes under the control of the Fscn1 promoter encoding for anti-tumor cytokines (*e.g.*, tumor necrosis factor (TNF)-α) can be used to transcriptionally address tumor cells, leading to apoptosis.[234] Hence, one could envision a DNA vaccine which encodes for a tumor antigen and at the same time for TNF-α, driving activation of transfected DCs and at the same time exerting tumoricidal effects in case of transfected tumor cells.

7.3.5 *In vivo* performance of the optimized human Fscn1 promoter

7.3.5.1 Pre-evaluation of pDNA carriers regarding toxicity and activation potential on splenic immune cells

In light of the potential cytotoxicity of LPEI polyplexes on DCs (see section 7.3.3), effects of LPEI and succPEI on isolated murine primary splenic immune cells were evaluated in a pre-experiment for subsequent *in vivo* studies. Splenic immune cell types were distinguished based on the expression of according lineage surface markers. In accordance with moderate cytotoxicity of LPEI polyplexes at N/P 9 in DC2.4 cells and BMDCs (**Figure 7.3A, Figure 7.8**), we observed a decrease in the viability of primary DCs by around 30% as compared to untreated control cells (**Figure 7.10A**) and within the various DC subpopulations especially of type-2 conventional DCs (cDC2) when employing these polyplexes (**Figure 7.10B**). On the contrary, LPEI polyplexes at lower N/P ratio and succPEI polyplexes in general had no significant effect on DC viability. In contrast to DCs, the viability of other splenic immune cell types was not significantly affected by either polyplex as assessed for NK cells, neutrophils, B cells, and T cells (**Figure 7.10A**).

In accordance with the observations on BMDCs, LPEI polyplexes at an N/P ratio of 9 conferred a significant increase (~ 1.5-fold compared to untreated control cells) in CD86 activation marker expression on splenic DCs (**Figure 7.11**). Since only DCs were activated, it is more likely that LPEI at N/P 9 exerted intrinsic stimulatory activity than a release of broadly activating danger signals by necrotic cells.

7.3.5.2 Promoter-dependent reporter activity in spleen

The performance of the Fscn1 and the CMV promoter was compared also *in vivo* by intravenous administration of corresponding LPEI and succPEI pDNA polyplexes in BALB/c mice. Despite showing moderate toxicity in DCs (see sections 7.3.3 and *7.3.5.1*), LPEI polyplexes at an N/P ratio of 9 were considered as suitable for subsequent *in vivo* evaluation. It is known from literature that LPEI at N/P ratios of 9-10 is highly active *in vivo* and mediates only minor if any initial toxic effects.[501, 502, 627] For reasons of comparability and based on preliminary *in vivo* results (*data not shown*), a w/w ratio of 1.5 was chosen for succPEI polyplexes, which corresponds to an N/P ratio of ~ 11.25 for unsubstituted PEI. As compared with succPEI, LPEI showed a strong preference to confer luciferase reporter expression in the lungs (**Figure 7.5**). In the case of succPEI polyplexes, the Fscn1 promoter favored reporter gene expression in the spleen as a suitable target organ containing high numbers of APCs (12-fold higher RLU compared to CMV promoter). In the case of LPEI polyplexes, pFscnLuc exerted significantly lower lung and liver expression than pCMVLuc (10-fold less RLU). RLU levels in the other organs (*i.e.*, spleen in the LPEI group; lungs and liver in the succPEI group) remained constant, suggesting a preferable shift towards spleen expression mediated by pFscnLuc.

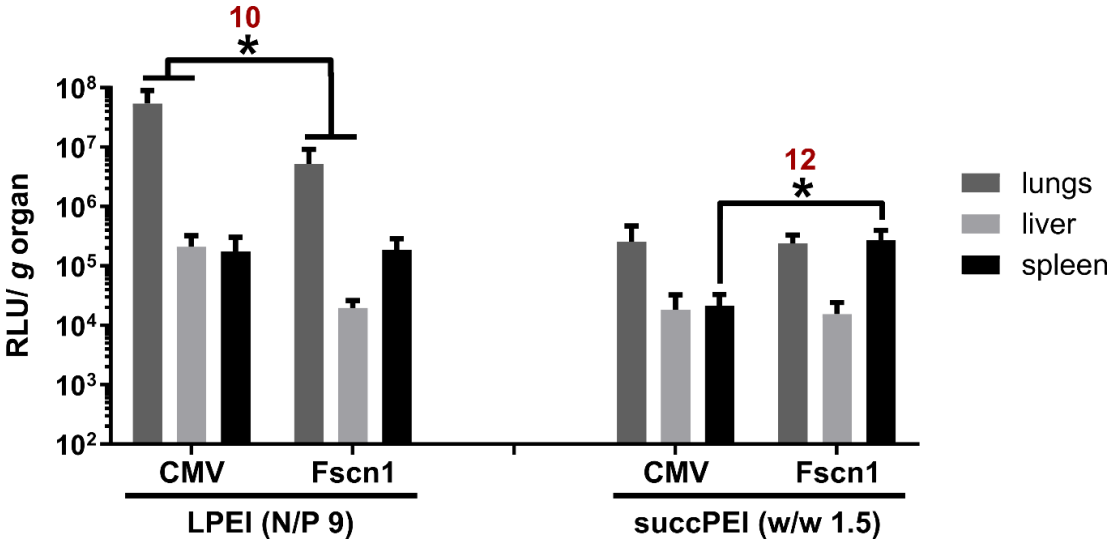

Figure 7.5. *In vivo* comparison of Fscn1 and CMV promoter activities in BALB/c mice. Luciferase expression within organs (*n*=5; mean + SD) assessed *via* an *ex vivo* luciferase assay at 24 h after intravenous injection of LPEI (N/P 9) and succPEI (w/w 1.5) polyplexes formed at a pDNA dose of 60 µg/animal in 200 µL of HBG buffer. Red numbers indicate the fold difference in RLU values between pFscnLuc and pCMVLuc. Significant differences: ns $p > 0.05$; * $p \leq 0.05$ (unpaired Student's two-tailed *t*-test with Welch's correction; GraphPad Prism™).
The *in vivo* study was conducted by Ulrich Wilk and Jana Pöhmerer (both Pharmaceutical Biotechnology, LMU Munich).

7.3.5.3 Promoter-dependent reporter activity in DCs in vivo

In addition, promoter-dependent reporter expression activity was examined in single cell suspensions retrieved from spleen, lymph nodes, liver, and lungs of accordingly treated BALB/c mice *via* intracellular immunostaining with a luciferase-specific antibody (**Figure 7.6, Figure 7.12**). succPEI was used as carrier for this evaluation, since it showed a more selective spleen activity compared to LPEI in the *ex vivo* luciferase assay (**Figure 7.5**). pFscnLuc expression was detected in DC populations of all tested organs (**Figure 7.12**). Standard plasmid pCMVLuc was also highly expressed due to the strong and ubiquitously active CMV promoter, not in favor of a real benefit of pFscnLuc at first glance. However, comparison of calculated ratios of luciferase expressing DC (dendritic cells) to MAC (macrophages) in the single organs revealed a slightly better performance of pFscnLuc with preferential luciferase expression in DCs, particularly in spleen and lymph nodes (**Figure 7.6**). For example, the DC:MAC ratio in the spleen was ~ 2.7 for pFscnLuc compared to ~ 1.9 for pCMVLuc.

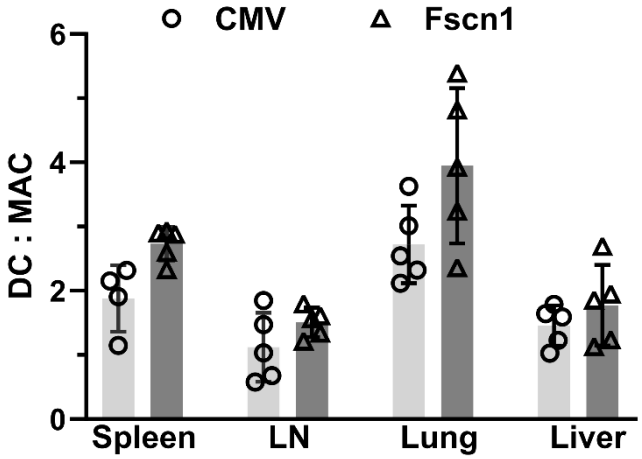

Figure 7.6. *In vivo* comparison of Fscn1 and CMV promoter activities on single cell level in BALB/c mice. *Ex vivo* analysis of single cell suspensions retrieved from different organs at 24 h after intravenous injection of 200 µL of succPEI polyplexes (w/w 1.5), containing 60 µg pDNA. Cells were isolated and subjected to flow cytometric analyses. Gating strategies for organs are pictured in **Figure 7.13** and **Figure 7.14**. Ratios of luciferase expressing DC (dendritic cells) to MAC (macrophages) of *n*=5 are displayed. The ratio calculation is based on the data shown in **Figure 7.12**. LN, lymph nodes.

The *in vivo* study was conducted by Ulrich Wilk and Jana Pöhmerer (both Pharmaceutical Biotechnology, LMU Munich). Subsequent analysis was carried out by Yanira Zeyn with the help of Christoph Hieber, Carolina Medina-Montano, and Nadine Röhrig, (all Department of Dermatology, University Medical Center, JGU Mainz).

7.4 Conclusion

The efficacy of DNA vaccines in clinical trials is still low.[234, 689, 1184] Improvement can be achieved by transcriptional targeting of DCs by using a DC-specific promoter. In the current study, we evaluated a hybrid enhancer/core human fascin1 gene promoter in this regard. This derivative showed preferable DC-focused activity *in vitro* compared to the standard CMV promoter. Upon systemic administration in mice, the expression profile of pFscnLuc was encouraging with favorable activity in the spleen as a central immune organ, and in DCs at somewhat higher level than in macrophages. This suggests that the human fascin1 gene promoter may be suitable for DC-focused transcriptional targeting. Moreover, pFscnLuc mediated high reporter gene expression in Fscn1-expressing tumor cells. Dual transcriptional targeting of DNA to both DCs and tumor cells may be an option to enhance the efficiency of DNA vaccines. By employing DNA vaccines that encode *i*) for a tumor antigen to induce anti-tumor T cell responses in case of transfected DCs, and *ii*) simultaneously for an anti-tumor cytokine, mediating tumoricidal effects in transfected tumor cells.

7.5 Supporting information

7.5.1 Supporting tables

Table 7.1. DLS and ELS measurements of LPEI and succPEI pDNA polyplexes.

		Z-average [nm]		Number mean [nm]		PdI		Zeta-potential [mV]	
		mean	SD	mean	SD	mean	SD	mean	SD
Different pDNA types (10 µg/mL pDNA)									
pCMVLuc	**LPEI (N/P 6)**	61.6	3.2	40.5	6.4	0.300	0.039	13.1	1.9
	SuccPEI (w/w 1.5)	54.1	2.0	35.0	3.4	0.248	0.027	11.4	1.7
pFscnLuc	**LPEI (N/P 6)**	70.6	0.6	47.4	2.3	0.138	0.012	11.4	1.4
	SuccPEI (w/w 1.5)	63.6	0.4	40.8	2.2	0.191	0.004	8.7	0.6
Different pDNA concentrations (*in vitro*, *in vivo*)									
10 µg/mL pCMVLuc	**LPEI (N/P 6)**	88.1	2.9	38.8	6.0	0.286	0.036	11.3	2.0
	LPEI (N/P 9)	105.4	1.0	47.9	15.1	0.253	0.010	20.4	3.1
	SuccPEI (w/w 1.5)	98.0	4.1	48.9	6.9	0.233	0.015	11.4	0.4
	SuccPEI (w/w 4)	77.5	3.0	32.8	2.1	0.265	0.007	23.2	2.3
25 µg/mL pCMVLuc	**LPEI (N/P 6)**	84.0	0.5	37.6	9.6	0.213	0.017	22.3	1.5
	LPEI (N/P 9)	72.4	0.1	44.4	2.8	0.159	0.014	17.5	2.7
	SuccPEI (w/w 1.5)	97.5	1.0	43.4	17.2	0.213	0.007	16.8	0.8
	SuccPEI (w/w 4)	68.7	0.6	38.7	0.6	0.172	0.015	15.5	1.8
300 µg/mL pCMVLuc	**LPEI (N/P 9)**	93.5	0.8	52.4	1.7	0.180	0.024	29.1	1.6
	succPEI (w/w 1.5)	138.3	5.3	89.4	3.5	0.147	0.009	25.7	1.4

DLS and ELS measurements (*n*=3, mean ± SD) of pDNA polyplexes formed with different pDNA types at indicated N/P (LPEI) or w/w (succPEI) ratios, respectively, and at different pDNA concentrations of 10 µg mL^{-1} (referring to *in vitro* transfections in tumor cell lines N2a and Hepa1-6), 25 µg mL^{-1} (referring to *in vitro* transfections in DC2.4 cells), and 300 µg mL^{-1} (referring to *in vivo* experiments).
Note: For succPEI, w/w ratios of 1.5 and 4 represent N/P ratios of ~ 11.25 and ~ 30 of an unsubstituted PEI.

7.5.2 Supporting figures

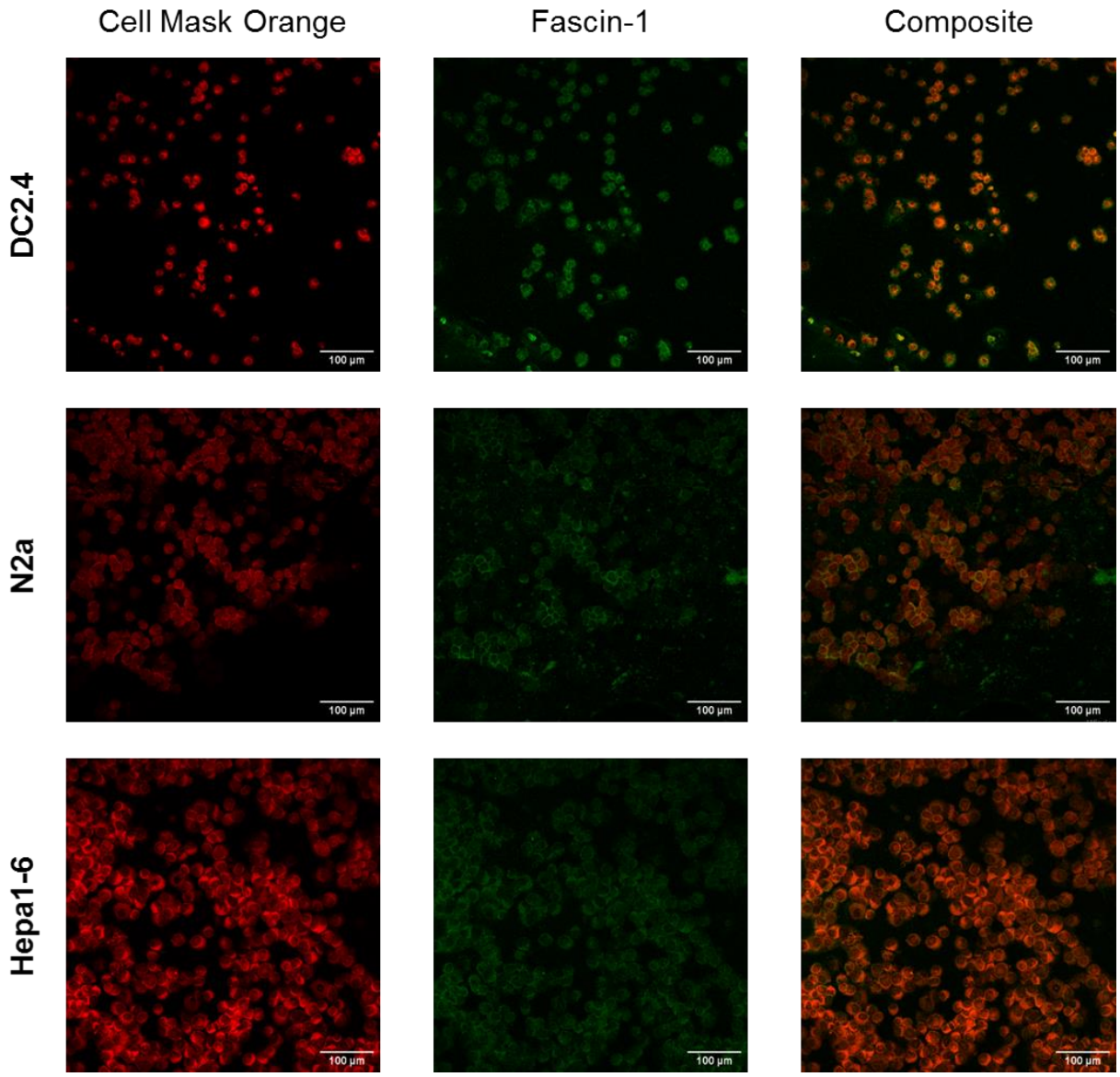

Figure 7.7. Intracellular fascin1 staining of DC2.4 (*top row*), N2a (*middle row)*, and Hepa1-6 cells (*bottom row*). CLSM images of cytospins after staining with Cell Mask Orange (*left column)* for membrane and nucleus staining, and a specific antibody for fascin1 (*middle column*); composite (*right column*).
The experiments were done by Yanira Zeyn (Department of Dermatology, University Medical Center, JGU Mainz).

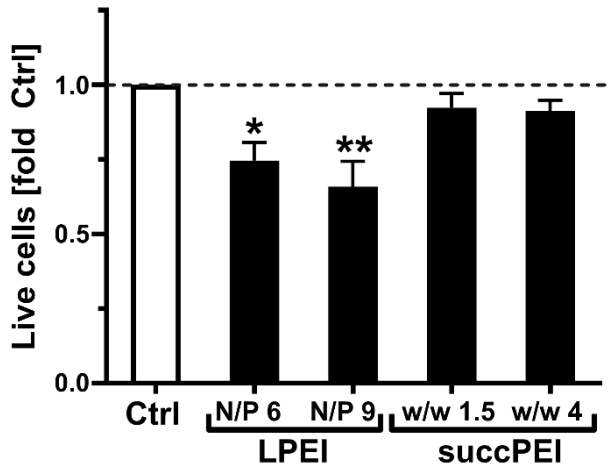

Figure 7.8. Viability of DC2.4 cells after incubation with polyplexes. DC2.4 cells (100,000 cells per well) were incubated overnight with LPEI (N/P 6 and 9, resp.) and succPEI (w/w 1.5 and 4, resp.) polyplexes at a concentration of 1 µg pFscnLuc/well. On the next day, samples were harvested, incubated with eFl780-FVD to delineate dead cells, and subjected to flow cytometric analysis. The graph denotes the frequencies of FVD-negative viable cells (*n*=4; mean + SEM), normalized to untreated cells (Ctrl). Significant differences versus Ctrl: * $p \leq 0.05$; ** $p \leq 0.01$ (one-way ANOVA, Tukey test; GraphPad Prism™).

Note: For succPEI, w/w ratios of 1.5 and 4 represent N/P ratios of ~ 11.25 and ~ 30 of an unsubstituted PEI.

The experiments were performed by Yanira Zeyn (Department of Dermatology, University Medical Center, JGU Mainz).

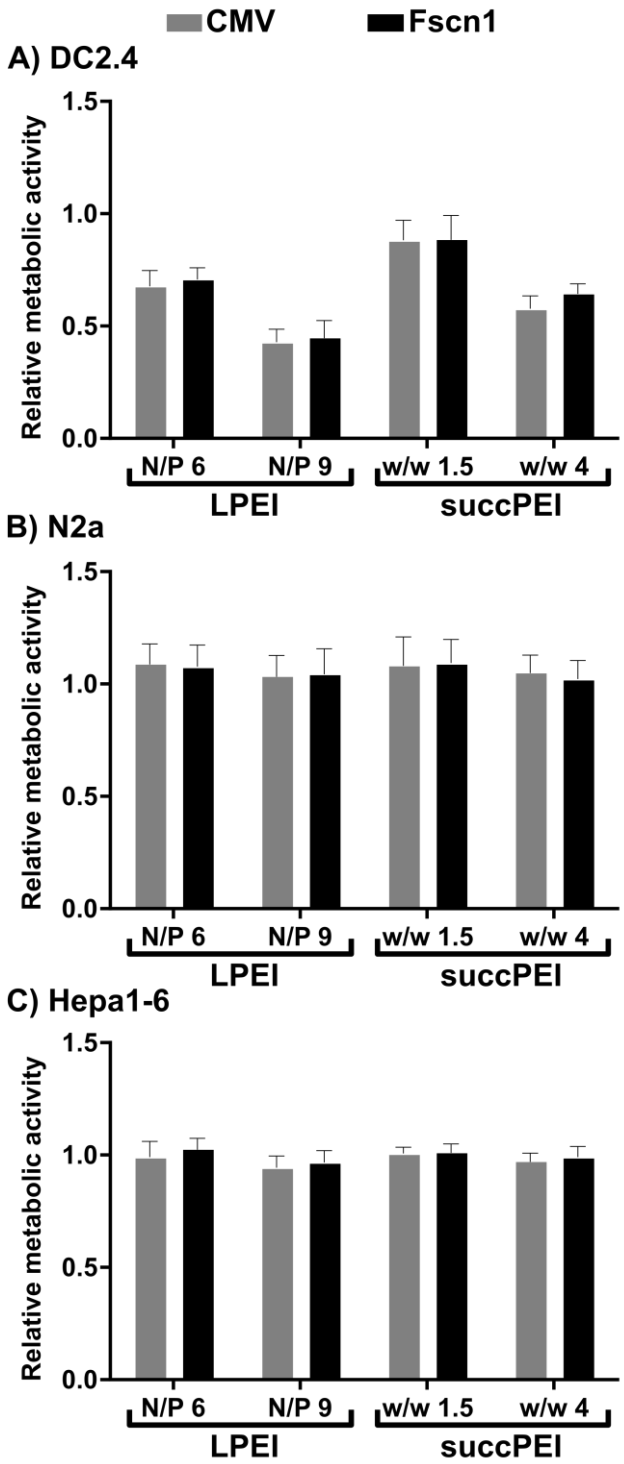

Figure 7.9. Comparison of pFscnLuc and pCMVLuc polyplexes in fascin1-expressing cell types. Metabolic activity was assessed *via* CellTiter-Glo assay (Promega) in relation to HBG-buffer treated control cells (*n*=3; mean + SD) at 24 h after transfection with LPEI (N/P 6 and 9, resp.) and succPEI (w/w 1.5 and 4, resp.) polyplexes in the DC-like cell line DC2.4 (**A**) at a pDNA concentration of 500 ng/well, as well as in the neuroblastoma cell line N2a (**B**) and the hepatoma cell line Hepa1-6 (**C**) at a pDNA concentration of 200 ng/well.
Note: For succPEI, w/w ratios of 1.5 and 4 represent N/P ratios of ~ 11.25 and ~ 30 of an unsubstituted PEI.

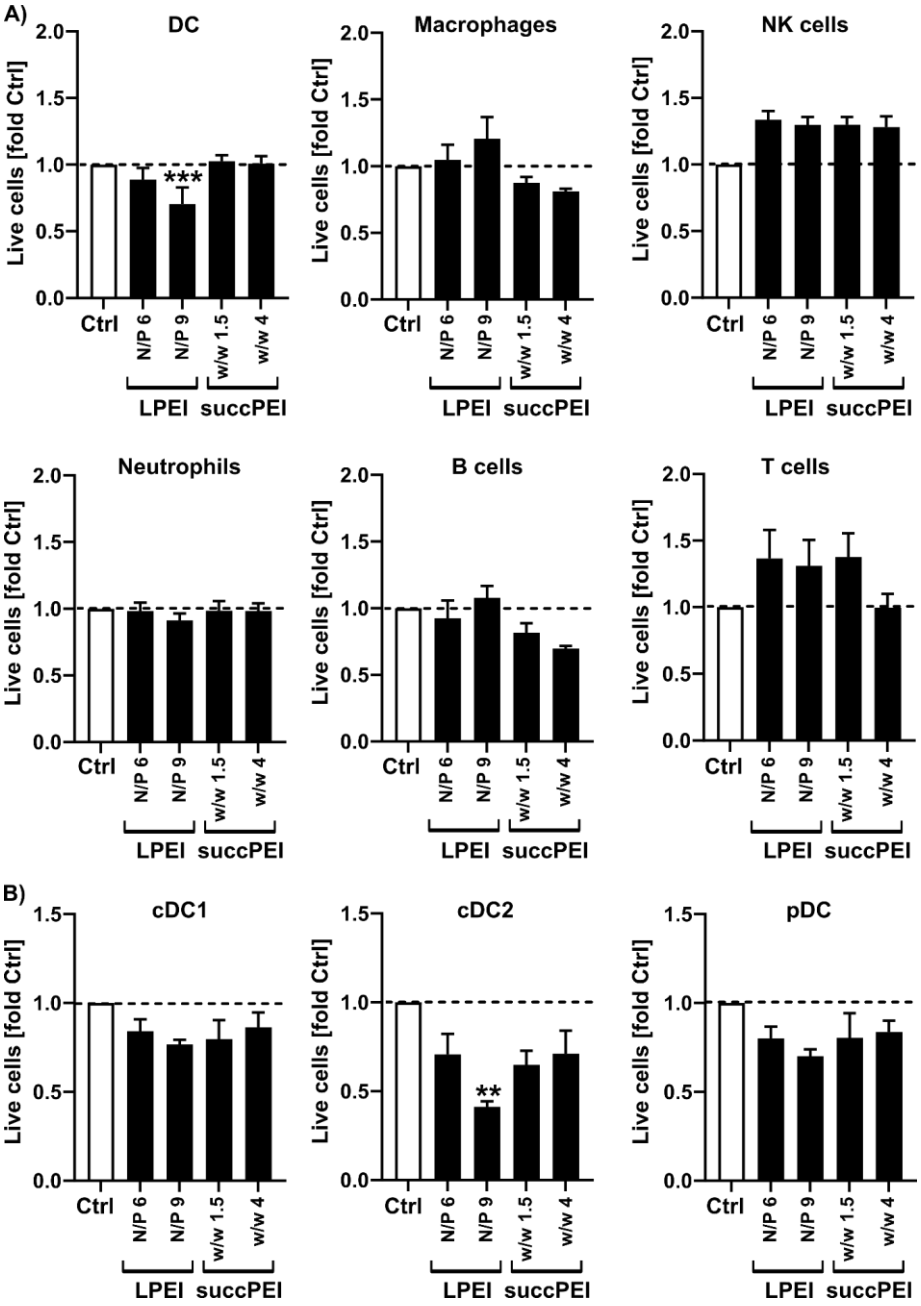

Figure 7.10. Effect of LPEI and succPEI polyplexes on the viability of splenic immune cells. Splenic immune cells (2×10^6 cells per well) were incubated with LPEI and succPEI polyplexes at indicated ratios and a concentration of 1 µg pFscnLuc/well. On the next day, the viability of various leukocyte populations was assessed by flow cytometry. **A)** Splenic immune cell populations were delineated by sequential gating as described in **Figure 7.13**. **B)** Splenic DC subpopulations were delineated by sequential gating as described in ref. [1188]. Graphs denote the frequencies of FVD-negative viable cells (*n*=4; mean + SEM), normalized to the untreated cells (Ctrl). Significant differences versus Ctrl: *** $p \leq 0.001$ (one-way ANOVA, Tukey test; GraphPad Prism™). DC, dendritic cells; cDC, conventional DCs; pDC, plasmacytoid DCs; NK, natural killer.
Note: For succPEI, w/w ratios of 1.5 and 4 represent N/P ratios of ~ 11.25 and ~ 30 of an unsubstituted PEI.
The experiments were done by Yanira Zeyn (Department of Dermatology, University Medical Center, JGU Mainz).

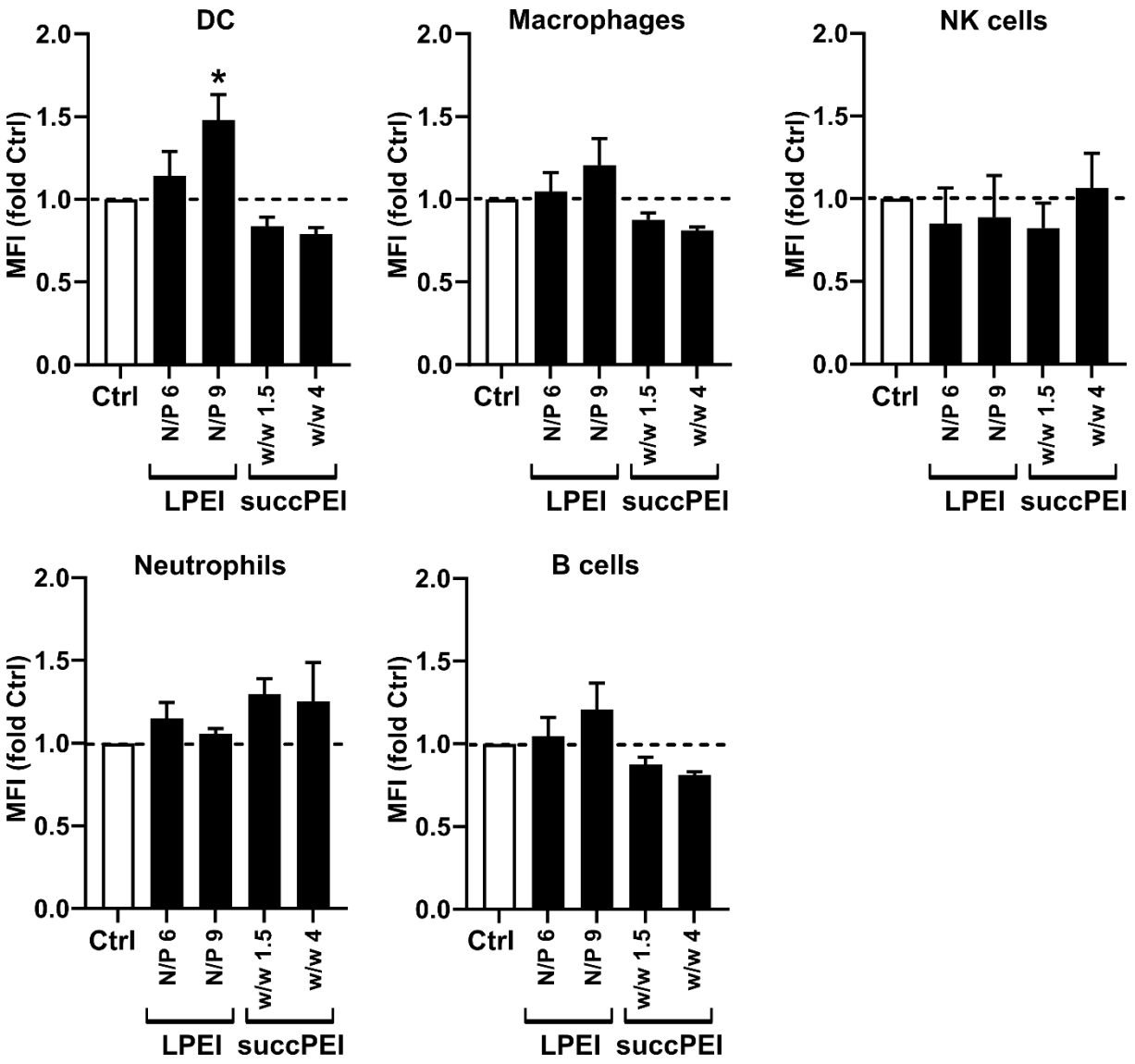

Figure 7.11. Effect of LPEI and succPEI polyplexes on CD86 activation marker expression of splenic immune cells. Expression of CD86 in splenic immune cell populations (2×10^6 cells per well) was monitored by flow cytometry after overnight incubation with LPEI and succPEI polyplexes at indicated ratios and a concentration of 1 µg pFscnLuc/well. Graphs denote the MFI (n=4; mean + SEM) in relation to the control (untreated cells). Significant differences versus Ctrl: * $p \leq 0.05$ (one-way ANOVA, Tukey test; GraphPad Prism™). DC, dendritic cells; NK, natural killer.

Note: For succPEI, w/w ratios of 1.5 and 4 represent N/P ratios of ~ 11.25 and ~ 30 of an unsubstituted PEI.

The experiments and analysis were done by Yanira Zeyn (Department of Dermatology, University Medical Center, JGU Mainz).

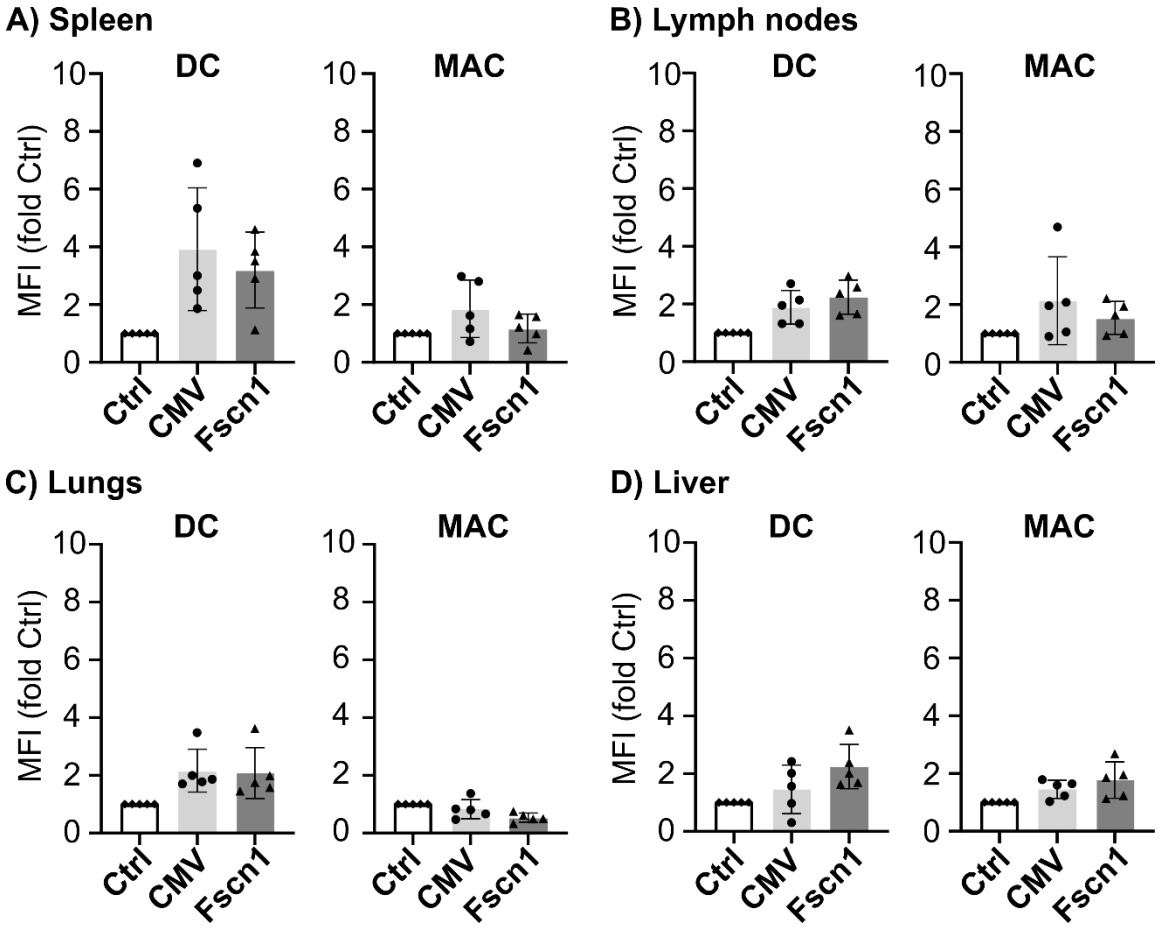

Figure 7.12. *In vivo* comparison of Fscn1 and CMV promoter activities on single cell level in BALB/c mice. *Ex vivo* analysis of single cell suspensions retrieved from different organs at 24 h after intravenous injection of 200 µL of succPEI polyplexes (w/w 1.5; HBG), containing 60 µg pDNA. Spleen (**A**), lymph nodes (**B**), lungs (**C**), and liver non-parenchymal cells (NPC; **D**) were processed to single cell suspensions, stained and subjected to flow cytometric analyses to monitor the luciferase signal. Gating strategy for **A) – C)** is described in **Figure 7.13**. Gating strategy for **D)** is described in **Figure 7.14**. MFI of luciferase of *n*=5 experiments is displayed in relation to HBG buffer treated animals (Ctrl). DC, dendritic cells; MAC, macrophages.
The *in vivo* study was conducted by Ulrich Wilk and Jana Pöhmerer (both Pharmaceutical Biotechnology, LMU Munich). Subsequent analysis was carried out by Yanira Zeyn with the help of Christoph Hieber, Carolina Medina-Montano, and Nadine Röhrig (all Department of Dermatology, University Medical Center, JGU Mainz).

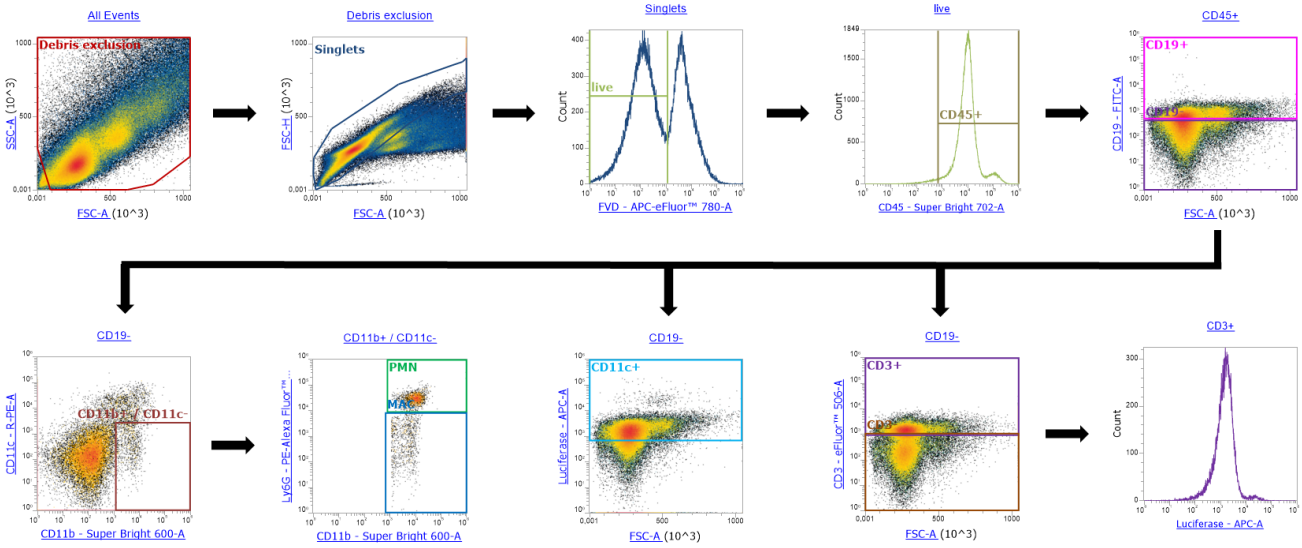

Figure 7.13. Gating strategy for cells of spleen, lymph nodes, and lungs delineated by lineage marker. First, debris and doublets were excluded from further analysis. Then cells were gated for FVD negative and CD45 positive fractions, to include only living immune cells. As next marker, B cells were identified as $CD19^+$. The $CD19^-$ fraction was further discriminated in $CD11c^+$ (DCs), $CD3^+$ (T cells), $CD11b^+/CD11^-$ [PMN (polymorpho nuclear neutrophils), and MAC (macrophages)]. The $CD11b^+/CD11^-$ fraction was further divided into PMN ($Ly6G^+$) and MAC ($Ly6G^-$). For all identified immune cell populations the MFI of luciferase antibody was determined.

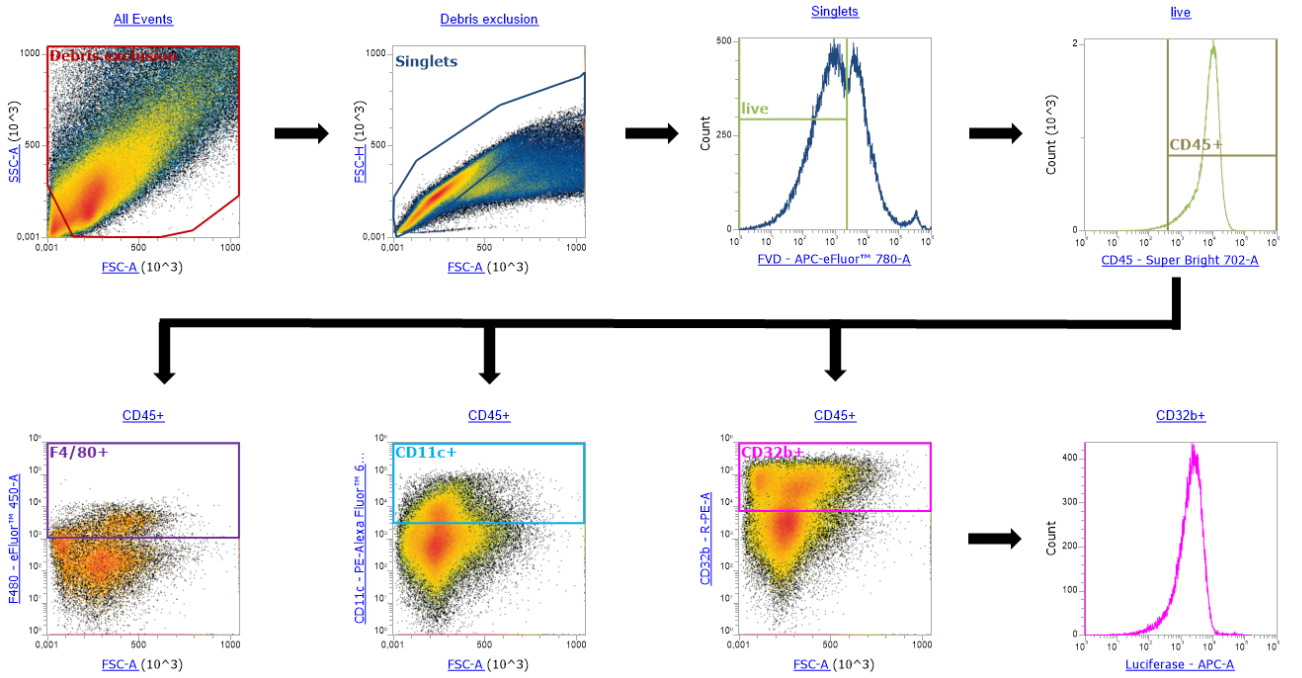

Figure 7.14. Gating strategy of liver immune cells delineated by liver NPC (non-parenchymal cells) marker. First, debris and doublets were excluded from further analysis. Then cells were gated for FVD negative and CD45 positive fractions, to include only living immune cells. As next markers, macrophages were identified as $F4/80^+$, DCs as $CD11c^+$, and liver sinusoidal endothelial cell (LSEC) as $CD32b^+$. For all identified immune cell populations the MFI of luciferase antibody was determined.

7.6 Abbreviations

APCs, antigen-presenting cells; ATP, adenosine 5′-triphosphate; BMDCs, bone marrow-derived cells; brPEI, branched polyethylenimine; CAR, chimeric antigen receptor; cDCs, conventional dendritic cells; CLSM, confocal laser scanning microscopy; DCs, dendritic cells; DTT, dithiothreitol; EDTA, ethylenediaminetetraacetic acid; FBS, fetal bovine serum; Fscn1, fascin1; FVD, fixable viability dye; GM-CSF, granulocyte-macrophage colony-stimulating factor; HBG, HEPES buffer with glucose; HEPES, 4-(2-hydroxyethyl)-1-piperazineethanesulfonic acid; HMGB1, high mobility group box-1 protein; LN, lymph node; LPEI, linear polyethylenimine 22kDa; LSEC, liver sinusoidal endothelial cell; MACs, macrophages; MFI, mean fluorescence intensity; N/P, nitrogen to phosphate; NPCs, liver non-parenchymal cells; PBS, phosphate-buffered saline; pDCs, plasmacytoid dendritic cells; pCMVLuc, standard reporter vector encoding for luciferase under the control of the strong ubiquitously active cytomegalovirus promoter and enhancer; PdI, polydispersity index; pDNA, plasmid DNA; pFscnLuc, plasmid encoding for the luciferase reporter gene under the control of a derivative of the human fascin1 gene promoter; pGL3-Basic, control luciferase-encoding vector (promoter-less); pGL3-Ctrl, control luciferase-encoding vector (hybrid SV40 promoter/enhancer); RLU, relative light units; RT, room temperature; SD, standard deviation; SEM, standard error of the mean; succPEI, succinylated branched polyethylenimine 25kDa (10% succinylation degree); TLR, toll-like receptor; TME, tumor microenvironment.

7.7 Acknowledgements

We acknowledge the financial support by the German Research Foundation (DFG), Collaborative Research Centers SFB1066 sub-project B5 (to MB and EW), and B15 (to MB) as well as SFB1032 sub-project B4 (to EW).

We thank Prof. Gregory Harms (Imaging Core Facility of the Research Center for Immunotherapy (FZI), University Medical Center Mainz, Germany) for assistance in CLSM.

We thank Wolfgang Rödl (Pharmaceutical Biotechnology, LMU Munich, Germany) for providing LPEI, and Janin Germer (PhD student, Pharmaceutical Biotechnology, LMU Munich, Germany) for providing succPEI.

8. Summary

In recent years, nucleic acid-based therapies have attracted more and more interest for a broad application field, ranging from gene therapies over cancer (immuno)therapies to vaccination approaches. Non-viral delivery systems (such as lipid nanoparticles, lipoplexes, or polyplexes) may be a safer alternative to viral vectors. However, their efficiency is still quite low. Optimization can be achieved by a so-called “bioinspired chemical evolution strategy”. Incorporation of bio-responsive elements within the non-viral carriers may help to imitate the dynamic, highly efficient delivery process of viral vectors. Chemical evolution is done by creating libraries of sequence-defined nanocarriers, followed by cycles of high-throughput screening (physicochemical and functional testing), rational selections, and systematic structural mutations. Future combination with computational simulations and machine learning approaches may make this whole optimization process more efficient and faster. Solid-phase assisted synthesis can generate peptide-based carrier libraries in a precise, sequence-defined way by modular design.

In the first part of the thesis, a library of sequence-defined oligoaminoamides (OAAs) was created *via* solid-phase assisted peptide synthesis as nanocarriers for nucleic acid delivery. Structure variations of a T-shaped artificial lipo-peptide carrier, based on four succinoyl tetraethylene pentamine (Stp) units and two terminal tyrosine tripeptide units, comprised *i*) histidines, *ii*) cysteines, *iii*) disulfide blocks, and *iv*) saturated fatty acids of different lengths in comparison to unsaturated fatty acid (namely, oleic acid) as well as modified fatty acids (namely, hydroxy-stearic acid, and 8-nonanamido-octanoic acid).

For successful pDNA delivery, a balancing act between extracellular polyplex stability, efficient uptake, endosomal escape, and intracellular cargo release was required. Cysteines as well as longer fatty acids improved polyplex stability. Histidines, in alternating sequence with Stp, were beneficial in terms of endosomal release. Highest pH-dependent lytic activity was observed for fatty acids of middle chain lengths (C8–C14), mediating efficient endosomal escape. Bio-responsive elements such as redox-sensitive disulfide blocks could reduce cytotoxicity by subsequent carrier degradation. Despite encouraging *in vitro* transfection results, the *in vivo* gene transfer performance of the lipo-OAAs was

only moderate. New *in vitro* assays were established investigating the influence of 90% full serum on the behavior of lipo-OAAs and corresponding pDNA polyplexes. Serum blocked the lytic activity of the T-shaped lipo-OAAs to a huge extent, by this lowering the transfection efficiency of corresponding pDNA polyplexes.
Also, for efficient mRNA delivery, stability, endosomal buffering properties, lytic activity as well as bio-reducibility had to be balanced for optimum carrier performance. Hereby, the most important measure was the incorporation of a bioreducible disulfide building block (ssbb), which led to more effective release of mRNA into the cytosol in a dynamic manner. Carriers lacking this dynamic tuning element required less stabilizing shorter fatty acids to compensate for mRNA release from the complexes; but such carriers might cause cytotoxicity due to lytic effects. Best performer was a T-shape lipo-OAA containing histidines, ssbb and oleic acid, which proved to be a potent carrier for mRNA also in the *in vivo* situation. Here, mRNA was delivered effectively to the lungs of mice upon local intratracheal application.
Altogether, the findings showed that fine-tuning of the required properties is necessary to optimize the carriers for every single nucleic acid type.

In the second part of the thesis, transcriptional targeting to dendritic cells (DCs) *in vitro* and *in vivo* was investigated as a potential DNA-based vaccination approach. Hereto, the human Fscn1 gene promoter was optimized by fusing the proximal core promoter with the normally more distantly located DC enhancer region. This optimized derivative showed preferable DC-focused activity *in vitro* and *in vivo* compared to the standard CMV promoter. Upon systemic administration in mice, the expression profile of pFscnLuc was encouraging with favorable activity in the spleen as a central immune organ, suggesting that the concept of DC-focused transcriptional targeting was successfully implemented. Moreover, pFscnLuc mediated high reporter gene expression in Fscn1-expressing tumor cells, opening up the possibility of a dual DNA vaccine approach by transcriptional targeting of DNA to both dendritic and tumor cells. The DNA might encode for a tumor antigen and simultaneously for an anti-tumor cytokine, mediating both activation of the immune system as well as tumoricidal effects in transfected tumor cells.

9. References

[1] Hager, S.; Wagner, E., Bioresponsive polyplexes - chemically programmed for nucleic acid delivery. *Expert Opin. Drug Delivery* **2018,** 15, (11), 1067-1083.
[2] Berger, S.; Berger, M.; Bantz, C.; Maskos, M.; Wagner, E., Performance of nanoparticles for biomedical applications: The in vitro/in vivo discrepancy. *Biophysics Reviews* **2022,** 3, (1), 011303.
[3] Lächelt, U.; Wagner, E., Nucleic Acid Therapeutics Using Polyplexes: A Journey of 50 Years (and Beyond). *Chem. Rev.* **2015,** 115, (19), 11043-78.
[4] Büning, H.; Fehse, B.; Ivics, Z.; Kochanek, S.; Koehl, U.; Kupatt, C.; Mussolino, C.; Nettelbeck, D. M.; Schambach, A.; Uckert, W.; Wagner, E.; Cathomen, T., Gene Therapy "Made in Germany": A Historical Perspective, Analysis of the Status Quo, and Recommendations for Action by the German Society for Gene Therapy. *Hum. Gene Ther.* **2021,** 32, (19-20), 987-996.
[5] Sun, W.; Shi, Q.; Zhang, H.; Yang, K.; Ke, Y.; Wang, Y.; Qiao, L., Advances in the techniques and methodologies of cancer gene therapy. *Discov. Med.* **2019,** 27, (146), 45-55.
[6] Ginn, S. L.; Amaya, A. K.; Alexander, I. E.; Edelstein, M.; Abedi, M. R., Gene therapy clinical trials worldwide to 2017: An update. *J. Gene Med.* **2018**, e3015.
[7] Hobernik, D.; Bros, M., DNA Vaccines—How Far From Clinical Use? *Int. J. Mol. Sci.* **2018,** 19, (11).
[8] Grabbe, S.; Haas, H.; Diken, M.; Kranz, L. M.; Langguth, P.; Sahin, U., Translating nanoparticulate-personalized cancer vaccines into clinical applications: case study with RNA-lipoplexes for the treatment of melanoma. *Nanomedicine* **2016,** 11, (20), 2723-2734.
[9] Tombácz, I.; Weissman, D.; Pardi, N., Vaccination with Messenger RNA: A Promising Alternative to DNA Vaccination. *Methods Mol. Biol.* **2021,** 2197, 13-31.
[10] Doudna, J. A.; Charpentier, E., Genome editing. The new frontier of genome engineering with CRISPR-Cas9. *Science* **2014,** 346, (6213), 1258096.
[11] Yin, H.; Song, C.-Q.; Dorkin, J. R.; Zhu, L. J.; Li, Y.; Wu, Q.; Park, A.; Yang, J.; Suresh, S.; Bizhanova, A.; Gupta, A.; Bolukbasi, M. F.; Walsh, S.; Bogorad, R. L.; Gao, G.; Weng, Z.; Dong, Y.; Koteliansky, V.; Wolfe, S. A.; Langer, R.; Xue, W.; Anderson, D. G., Therapeutic genome editing by combined viral and non-viral delivery of CRISPR system components in vivo. *Nat. Biotechnol.* **2016,** 34, 328.
[12] Lino, C. A.; Harper, J. C.; Carney, J. P.; Timlin, J. A., Delivering CRISPR: a review of the challenges and approaches. *Drug Delivery* **2018,** 25, (1), 1234-1257.
[13] Freitag, F.; Wagner, E., Optimizing synthetic nucleic acid and protein nanocarriers: The chemical evolution approach. *Adv. Drug Delivery Rev.* **2021,** 168, 30-54.
[14] Kulkarni, J. A.; Witzigmann, D.; Thomson, S. B.; Chen, S.; Leavitt, B. R.; Cullis, P. R.; van der Meel, R., The current landscape of nucleic acid therapeutics. *Nat. Nanotechnol.* **2021,** 16, (6), 630-643.
[15] Majeed, C. N.; Ma, C. D.; Xiao, T.; Rudnick, S.; Bonkovsky, H. L., Spotlight on Givosiran as a Treatment Option for Adults with Acute Hepatic Porphyria: Design, Development, and Place in Therapy. *Drug Des. Devel. Ther.* **2022,** 16, 1827-1845.
[16] Aartsma-Rus, A.; Corey, D. R., The 10th Oligonucleotide Therapy Approved: Golodirsen for Duchenne Muscular Dystrophy. *Nucleic Acid Ther.* **2020,** 30, (2), 67-70.
[17] Adams, D.; Gonzalez-Duarte, A.; O'Riordan, W. D.; Yang, C. C.; Ueda, M.; Kristen, A. V.; Tournev, I.; Schmidt, H. H.; Coelho, T.; Berk, J. L.; Lin, K. P.; Vita, G.; Attarian, S.; Planté-Bordeneuve, V.; Mezei, M. M.; Campistol, J. M.; Buades, J.; Brannagan, T. H., 3rd; Kim, B. J.; Oh, J.; Parman, Y.; Sekijima, Y.; Hawkins, P. N.; Solomon, S. D.; Polydefkis, M.; Dyck, P. J.; Gandhi, P. J.; Goyal, S.; Chen, J.; Strahs, A. L.; Nochur, S. V.; Sweetser, M. T.; Garg, P. P.; Vaishnaw, A. K.; Gollob, J. A.; Suhr, O. B., Patisiran, an RNAi Therapeutic, for Hereditary Transthyretin Amyloidosis. *N. Engl. J. Med.* **2018,** 379, (1), 11-21.
[18] Stein, C. A.; Castanotto, D., FDA-Approved Oligonucleotide Therapies in 2017. *Mol. Ther.* **2017,** 25, (5), 1069-1075.

[19] Titze-de-Almeida, R.; David, C.; Titze-de-Almeida, S. S., The Race of 10 Synthetic RNAi-Based Drugs to the Pharmaceutical Market. *Pharm. Res.* **2017,** 34, (7), 1339-1363.
[20] Trimble, C. L.; Morrow, M. P.; Kraynyak, K. A.; Shen, X.; Dallas, M.; Yan, J.; Edwards, L.; Parker, R. L.; Denny, L.; Giffear, M.; Brown, A. S.; Marcozzi-Pierce, K.; Shah, D.; Slager, A. M.; Sylvester, A. J.; Khan, A.; Broderick, K. E.; Juba, R. J.; Herring, T. A.; Boyer, J.; Lee, J.; Sardesai, N. Y.; Weiner, D. B.; Bagarazzi, M. L., Safety, efficacy, and immunogenicity of VGX-3100, a therapeutic synthetic DNA vaccine targeting human papillomavirus 16 and 18 E6 and E7 proteins for cervical intraepithelial neoplasia 2/3: a randomised, double-blind, placebo-controlled phase 2b trial. *Lancet* **2015,** 386, (10008), 2078-2088.
[21] Chen, C.; Yang, Z.; Tang, X., Chemical modifications of nucleic acid drugs and their delivery systems for gene-based therapy. *Med. Res. Rev.* **2018,** 38, (3), 829-869.
[22] Shen, X.; Corey, D. R., Chemistry, mechanism and clinical status of antisense oligonucleotides and duplex RNAs. *Nucleic Acids Res.* **2018,** 46, (4), 1584-1600.
[23] Verbeke, R.; Lentacker, I.; De Smedt, S. C.; Dewitte, H., The dawn of mRNA vaccines: The COVID-19 case. *J. Controlled Release* **2021,** 333, 511-520.
[24] Gillmore, J. D.; Gane, E.; Taubel, J.; Kao, J.; Fontana, M.; Maitland, M. L.; Seitzer, J.; O'Connell, D.; Walsh, K. R.; Wood, K.; Phillips, J.; Xu, Y.; Amaral, A.; Boyd, A. P.; Cehelsky, J. E.; McKee, M. D.; Schiermeier, A.; Harari, O.; Murphy, A.; Kyratsous, C. A.; Zambrowicz, B.; Soltys, R.; Gutstein, D. E.; Leonard, J.; Sepp-Lorenzino, L.; Lebwohl, D., CRISPR-Cas9 In Vivo Gene Editing for Transthyretin Amyloidosis. *N. Engl. J. Med.* **2021,** 385, (6), 493-502.
[25] Felgner, P. L.; Barenholz, Y.; Behr, J. P.; Cheng, S. H.; Cullis, P.; Huang, L.; Jessee, J. A.; Seymour, L.; Szoka, F.; Thierry, A. R.; Wagner, E.; Wu, G., Nomenclature for synthetic gene delivery systems. *Hum. Gene Ther.* **1997,** 8, (5), 511-2.
[26] Peng, L.; Wagner, E., Polymeric Carriers for Nucleic Acid Delivery: Current Designs and Future Directions. *Biomacromolecules* **2019,** 20, (10), 3613-3626.
[27] Leng, Q.; Chou, S. T.; Scaria, P. V.; Woodle, M. C.; Mixson, A. J., Increased tumor distribution and expression of histidine-rich plasmid polyplexes. *J. Gene Med.* **2014,** 16, (9-10), 317-28.
[28] Luo, J.; Schmaus, J.; Cui, M.; Hörterer, E.; Wilk, U.; Höhn, M.; Däther, M.; Berger, S.; Benli-Hoppe, T.; Peng, L.; Wagner, E., Hyaluronate siRNA nanoparticles with positive charge display rapid attachment to tumor endothelium and penetration into tumors. *J. Controlled Release* **2021,** 329, 919-933.
[29] Berger, S.; Krhač Levačić, A.; Hörterer, E.; Wilk, U.; Benli-Hoppe, T.; Wang, Y.; Öztürk, Ö.; Luo, J.; Wagner, E., Optimizing pDNA Lipo-polyplexes: A Balancing Act between Stability and Cargo Release. *Biomacromolecules* **2021,** 22, (3), 1282-1296.
[30] Paunovska, K.; Sago, C. D.; Monaco, C. M.; Hudson, W. H.; Castro, M. G.; Rudoltz, T. G.; Kalathoor, S.; Vanover, D. A.; Santangelo, P. J.; Ahmed, R.; Bryksin, A. V.; Dahlman, J. E., A Direct Comparison of in Vitro and in Vivo Nucleic Acid Delivery Mediated by Hundreds of Nanoparticles Reveals a Weak Correlation. *Nano Lett.* **2018,** 18, (3), 2148-2157.
[31] Zugates, G. T.; Peng, W.; Zumbuehl, A.; Jhunjhunwala, S.; Huang, Y. H.; Langer, R.; Sawicki, J. A.; Anderson, D. G., Rapid Optimization of Gene Delivery by Parallel End-modification of Poly(β-amino ester)s. *Mol. Ther.* **2007,** 15, (7), 1306-1312.
[32] Whitehead, K. A.; Matthews, J.; Chang, P. H.; Niroui, F.; Dorkin, J. R.; Severgnini, M.; Anderson, D. G., In vitro-in vivo translation of lipid nanoparticles for hepatocellular siRNA delivery. *ACS Nano* **2012,** 6, (8), 6922-9.
[33] Negron, K.; Khalasawi, N.; Lu, B.; Ho, C. Y.; Lee, J.; Shenoy, S.; Mao, H. Q.; Wang, T. H.; Hanes, J.; Suk, J. S., Widespread gene transfer to malignant gliomas with In vitro-to-In vivo correlation. *J. Controlled Release* **2019,** 303, 1-11.
[34] Lynch, I.; Cedervall, T.; Lundqvist, M.; Cabaleiro-Lago, C.; Linse, S.; Dawson, K. A., The nanoparticle-protein complex as a biological entity; a complex fluids and surface science challenge for the 21st century. *Adv. Colloid Interface Sci.* **2007,** 134-135, 167-74.

[35] Monopoli, M. P.; Aberg, C.; Salvati, A.; Dawson, K. A., Biomolecular coronas provide the biological identity of nanosized materials. *Nat. Nanotechnol.* **2012,** 7, (12), 779-86.
[36] Schöttler, S.; Becker, G.; Winzen, S.; Steinbach, T.; Mohr, K.; Landfester, K.; Mailänder, V.; Wurm, F. R., Protein adsorption is required for stealth effect of poly(ethylene glycol)- and poly(phosphoester)-coated nanocarriers. *Nat. Nanotechnol.* **2016,** 11, (4), 372-377.
[37] Cai, R.; Chen, C., The Crown and the Scepter: Roles of the Protein Corona in Nanomedicine. *Adv. Mater.* **2019,** 31, (45), e1805740.
[38] Ogris, M.; Brunner, S.; Schüller, S.; Kircheis, R.; Wagner, E., PEGylated DNA/transferrin-PEI complexes: reduced interaction with blood components, extended circulation in blood and potential for systemic gene delivery. *Gene Ther.* **1999,** 6, (4), 595-605.
[39] Plank, C.; Mechtler, K.; Szoka, F. C., Jr.; Wagner, E., Activation of the complement system by synthetic DNA complexes: a potential barrier for intravenous gene delivery. *Hum. Gene Ther.* **1996,** 7, (12), 1437-46.
[40] Merkel, O. M.; Urbanics, R.; Bedocs, P.; Rozsnyay, Z.; Rosivall, L.; Toth, M.; Kissel, T.; Szebeni, J., In vitro and in vivo complement activation and related anaphylactic effects associated with polyethylenimine and polyethylenimine-graft-poly(ethylene glycol) block copolymers. *Biomaterials* **2011,** 32, (21), 4936-42.
[41] Jayaram, D. T.; Pustulka, S. M.; Mannino, R. G.; Lam, W. A.; Payne, C. K., Protein Corona in Response to Flow: Effect on Protein Concentration and Structure. *Biophys J* **2018,** 115, (2), 209-216.
[42] Palchetti, S.; Pozzi, D.; Capriotti, A. L.; Barbera, G.; Chiozzi, R. Z.; Digiacomo, L.; Peruzzi, G.; Caracciolo, G.; Laganà, A., Influence of dynamic flow environment on nanoparticle-protein corona: From protein patterns to uptake in cancer cells. *Colloids Surf., B* **2017,** 153, 263-271.
[43] Weber, C.; Voigt, M.; Simon, J.; Danner, A. K.; Frey, H.; Mailänder, V.; Helm, M.; Morsbach, S.; Landfester, K., Functionalization of Liposomes with Hydrophilic Polymers Results in Macrophage Uptake Independent of the Protein Corona. *Biomacromolecules* **2019,** 20, (8), 2989-2999.
[44] Caracciolo, G., Clinically approved liposomal nanomedicines: lessons learned from the biomolecular corona. *Nanoscale* **2018,** 10, (9), 4167-4172.
[45] Pozzi, D.; Colapicchioni, V.; Caracciolo, G.; Piovesana, S.; Capriotti, A. L.; Palchetti, S.; De Grossi, S.; Riccioli, A.; Amenitsch, H.; Laganà, A., Effect of polyethyleneglycol (PEG) chain length on the bio-nano-interactions between PEGylated lipid nanoparticles and biological fluids: from nanostructure to uptake in cancer cells. *Nanoscale* **2014,** 6, (5), 2782-92.
[46] Ruoslahti, E., Tumor penetrating peptides for improved drug delivery. *Adv. Drug Delivery Rev.* **2017,** 110-111, 3-12.
[47] Maeda, H., Toward a full understanding of the EPR effect in primary and metastatic tumors as well as issues related to its heterogeneity. *Adv. Drug Delivery Rev.* **2015,** 91, 3-6.
[48] Steffens, R. C.; Wagner, E., Directing the Way-Receptor and Chemical Targeting Strategies for Nucleic Acid Delivery. *Pharm. Res.* **2022**, 1-30.
[49] Vetter, V. C.; Wagner, E., Targeting nucleic acid-based therapeutics to tumors: Challenges and strategies for polyplexes. *J. Controlled Release* **2022,** 346, 110-135.
[50] Salvati, A.; Pitek, A. S.; Monopoli, M. P.; Prapainop, K.; Bombelli, F. B.; Hristov, D. R.; Kelly, P. M.; Åberg, C.; Mahon, E.; Dawson, K. A., Transferrin-functionalized nanoparticles lose their targeting capabilities when a biomolecule corona adsorbs on the surface. *Nat. Nanotechnol.* **2013,** 8, (2), 137-43.
[51] Duncan, R.; Richardson, S. C. W., Endocytosis and Intracellular Trafficking as Gateways for Nanomedicine Delivery: Opportunities and Challenges. *Mol. Pharmaceutics* **2012,** 9, (9), 2380-2402.
[52] Degors, I. M. S.; Wang, C.; Rehman, Z. U.; Zuhorn, I. S., Carriers Break Barriers in Drug Delivery: Endocytosis and Endosomal Escape of Gene Delivery Vectors. *Acc. Chem. Res.* **2019,** 52, (7), 1750-1760.

[53] Winkeljann, B.; Keul, D. C.; Merkel, O. M., Engineering poly- and micelleplexes for nucleic acid delivery - A reflection on their endosomal escape. *J. Controlled Release* **2022,** 353, 518-534.
[54] Selo, M. A.; Sake, J. A.; Kim, K. J.; Ehrhardt, C., In vitro and ex vivo models in inhalation biopharmaceutical research - advances, challenges and future perspectives. *Adv. Drug Delivery Rev.* **2021,** 177, 113862.
[55] Martens, T. F.; Vercauteren, D.; Forier, K.; Deschout, H.; Remaut, K.; Paesen, R.; Ameloot, M.; Engbersen, J. F.; Demeester, J.; De Smedt, S. C.; Braeckmans, K., Measuring the intravitreal mobility of nanomedicines with single-particle tracking microscopy. *Nanomedicine* **2013,** 8, (12), 1955-68.
[56] Neupane, R.; Boddu, S. H. S.; Abou-Dahech, M. S.; Bachu, R. D.; Terrero, D.; Babu, R. J.; Tiwari, A. K., Transdermal Delivery of Chemotherapeutics: Strategies, Requirements, and Opportunities. *Pharmaceutics* **2021,** 13, (7), 960.
[57] Hanafy, A. S.; Dietrich, D.; Fricker, G.; Lamprecht, A., Blood-brain barrier models: Rationale for selection. *Adv. Drug Delivery Rev.* **2021,** 176, 113859.
[58] Wagner, E., Polymers for siRNA Delivery: Inspired by Viruses to be Targeted, Dynamic, and Precise. *Acc. Chem. Res.* **2012,** 45, (7), 1005-1013.
[59] Wagner, E.; Plank, C.; Zatloukal, K.; Cotten, M.; Birnstiel, M. L., Influenza virus hemagglutinin HA-2 N-terminal fusogenic peptides augment gene transfer by transferrin-polylysine-DNA complexes: toward a synthetic virus-like gene-transfer vehicle. *Proc. Natl. Acad. Sci. U.S.A.* **1992,** 89, (17), 7934-7938.
[60] Plank, C.; Zatloukal, K.; Cotten, M.; Mechtler, K.; Wagner, E., Gene transfer into hepatocytes using asialoglycoprotein receptor mediated endocytosis of DNA complexed with an artificial tetra-antennary galactose ligand. *Bioconjugate Chem.* **1992,** 3, (6), 533-539.
[61] Morys, S.; Wagner, E.; Lächelt, U., From Artificial Amino Acids to Sequence-Defined Targeted Oligoaminoamides. *Methods Mol. Biol.* **2016,** 1445, 235-58.
[62] Hartmann, L.; Krause, E.; Antonietti, M.; Börner, H. G., Solid-Phase Supported Polymer Synthesis of Sequence-Defined, Multifunctional Poly(amidoamines). *Biomacromolecules* **2006,** 7, (4), 1239-1244.
[63] Hill SA, G. C., Hartmann L, Recent Developments in Solid-Phase Strategies towards Synthetic, Sequence-Defined Macromolecules. *Chem. Asian J.* **2018,** 13, 3611-3622.
[64] Schaffert, D.; Troiber, C.; Salcher, E. E.; Fröhlich, T.; Martin, I.; Badgujar, N.; Dohmen, C.; Edinger, D.; Kläger, R.; Maiwald, G.; Farkasova, K.; Seeber, S.; Jahn-Hofmann, K.; Hadwiger, P.; Wagner, E., Solid-Phase Synthesis of Sequence-Defined T-, i-, and U-Shape Polymers for pDNA and siRNA Delivery. *Angew. Chem., Int. Ed. Engl.* **2011,** 50, (38), 8986-8989.
[65] Ritt, N.; Berger, S.; Wagner, E.; Zentel, R., Versatile, Multifunctional Block Copolymers for the Self-Assembly of Well-Defined, Nontoxic pDNA Polyplexes. *ACS Appl. Polym. Mater.* **2020,** 2, (12), 5469-5481.
[66] Belliveau, N. M.; Huft, J.; Lin, P. J.; Chen, S.; Leung, A. K.; Leaver, T. J.; Wild, A. W.; Lee, J. B.; Taylor, R. J.; Tam, Y. K.; Hansen, C. L.; Cullis, P. R., Microfluidic Synthesis of Highly Potent Limit-size Lipid Nanoparticles for In Vivo Delivery of siRNA. *Mol. Ther.-Nucleic Acids* **2012,** 1, (8), e37.
[67] Leung, A. K.; Hafez, I. M.; Baoukina, S.; Belliveau, N. M.; Zhigaltsev, I. V.; Afshinmanesh, E.; Tieleman, D. P.; Hansen, C. L.; Hope, M. J.; Cullis, P. R., Lipid Nanoparticles Containing siRNA Synthesized by Microfluidic Mixing Exhibit an Electron-Dense Nanostructured Core. *J. Phys. Chem. C* **2012,** 116, (34), 18440-18450.
[68] Leung, A. K.; Tam, Y. Y.; Chen, S.; Hafez, I. M.; Cullis, P. R., Microfluidic Mixing: A General Method for Encapsulating Macromolecules in Lipid Nanoparticle Systems. *J. Phys. Chem. B* **2015,** 119, (28), 8698-706.
[69] Song, Y.; Hormes, J.; Kumar, C. S., Microfluidic synthesis of nanomaterials. *Small* **2008,** 4, (6), 698-711.

[70] Kastner, E.; Kaur, R.; Lowry, D.; Moghaddam, B.; Wilkinson, A.; Perrie, Y., High-throughput manufacturing of size-tuned liposomes by a new microfluidics method using enhanced statistical tools for characterization. *Int. J. Pharm.* **2014,** 477, (1-2), 361-8.
[71] Damiati, S.; Kompella, U. B.; Damiati, S. A.; Kodzius, R., Microfluidic Devices for Drug Delivery Systems and Drug Screening. *Genes* **2018,** 9, (2).
[72] Feldmann, D. P.; Xie, Y.; Jones, S. K.; Yu, D.; Moszczynska, A.; Merkel, O. M., The impact of microfluidic mixing of triblock micelleplexes on in vitroin vivo gene silencing and intracellular trafficking. *Nanotechnology* **2017,** 28, (22), 224001.
[73] Feldmann, D. P.; Jones, S.; Douglas, K.; Shields, A. F.; Merkel, O. M., Microfluidic Assembly of siRNA-Loaded Micelleplexes for Tumor Targeting in an Orthotopic Model of Ovarian Cancer. In *RNA Interference and Cancer Therapy: Methods and Protocols*, Dinesh Kumar, L., Ed. Springer New York: New York, NY, 2019; pp 355-369.
[74] Kumar, R.; Le, N.; Oviedo, F.; Brown, M. E.; Reineke, T. M., Combinatorial Polycation Synthesis and Causal Machine Learning Reveal Divergent Polymer Design Rules for Effective pDNA and Ribonucleoprotein Delivery. *JACS Au* **2022,** 2, (2), 428-442.
[75] Liang, H.; Hu, A.; Chen, X.; Jin, R.; Wang, K.; Ke, B.; Nie, Y., Structure optimization of dendritic lipopeptide based gene vectors with the assistance from molecular dynamic simulation. *Journal of materials chemistry. B* **2019,** 7, (6), 915-926.
[76] Tavares Luiz, M.; Santos Rosa Viegas, J.; Palma Abriata, J.; Viegas, F.; Testa Moura de Carvalho Vicentini, F.; Lopes Badra Bentley, M. V.; Chorilli, M.; Maldonado Marchetti, J.; Tapia-Blácido, D. R., Design of experiments (DoE) to develop and to optimize nanoparticles as drug delivery systems. *Eur. J. Pharm. Biopharm.* **2021,** 165, 127-148.
[77] Terada, T.; Kulkarni, J. A.; Huynh, A.; Chen, S.; van der Meel, R.; Tam, Y. Y. C.; Cullis, P. R., Characterization of Lipid Nanoparticles Containing Ionizable Cationic Lipids Using Design-of-Experiments Approach. *Langmuir* **2021,** 37, (3), 1120-1128.
[78] Politis, S. N.; Colombo, P.; Colombo, G.; M. Rekkas, D., Design of experiments (DoE) in pharmaceutical development. *Drug Dev. Ind. Pharm.* **2017,** 43, (6), 889-901.
[79] Bevers, S.; Kooijmans, S. A. A.; Van de Velde, E.; Evers, M. J. W.; Seghers, S.; Gitz-Francois, J. J. J. M.; van Kronenburg, N. C. H.; Fens, M. H. A. M.; Mastrobattista, E.; Hassler, L.; Sork, H.; Lehto, T.; Ahmed, K. E.; El Andaloussi, S.; Fiedler, K.; Breckpot, K.; Maes, M.; Van Hoorick, D.; Bastogne, T.; Schiffelers, R. M.; De Koker, S., mRNA-LNP vaccines tuned for systemic immunization induce strong antitumor immunity by engaging splenic immune cells. *Mol. Ther.* **2022,** 30, (9), 3078-3094.
[80] Wang, Y.; Lamim Ribeiro, J. M.; Tiwary, P., Machine learning approaches for analyzing and enhancing molecular dynamics simulations. *Curr. Opin. Struct. Biol.* **2020,** 61, 139-145.
[81] Zhang, P.; Wagner, E., History of Polymeric Gene Delivery Systems. *Top. Curr. Chem.* **2017,** 375, (2), 26.
[82] Matsumura, Y.; Maeda, H., A New Concept for Macromolecular Therapeutics in Cancer Chemotherapy: Mechanism of Tumoritropic Accumulation of Proteins and the Antitumor Agent Smancs. *Cancer Res.* **1986,** 46, (12 Part 1), 6387.
[83] Ruoslahti, E., Peptides as targeting elements and tissue penetration devices for nanoparticles. *Adv. Mater.* **2012,** 24, (28), 3747-56.
[84] Ramsey, J. D.; Flynn, N. H., Cell-penetrating peptides transport therapeutics into cells. *Pharmacol. Ther.* **2015,** 154, 78-86.
[85] Symens, N.; Soenen, S. J.; Rejman, J.; Braeckmans, K.; De Smedt, S. C.; Remaut, K., Intracellular partitioning of cell organelles and extraneous nanoparticles during mitosis. *Adv. Drug Delivery Rev.* **2012,** 64, (1), 78-94.
[86] Scholz, C.; Wagner, E., Therapeutic plasmid DNA versus siRNA delivery: Common and different tasks for synthetic carriers. *J. Controlled Release* **2012,** 161, (2), 554-565.
[87] Wang, T.; Upponi, J. R.; Torchilin, V. P., Design of multifunctional non-viral gene vectors to overcome physiological barriers: Dilemmas and strategies. *Int. J. Pharm.* **2012,** 427, (1), 3-20.

[88] Hall, A.; Lächelt, U.; Bartek, J.; Wagner, E.; Moghimi, S. M., Polyplex Evolution: Understanding Biology, Optimizing Performance. *Mol. Ther.* **2017,** 25, (7), 1476-1490.
[89] Wagner, E., Programmed drug delivery: nanosystems for tumor targeting. *Expert Opin. Biol. Ther.* **2007,** 7, (5), 587-593.
[90] Sun, M.; Wang, K.; Oupický, D., Advances in Stimulus-Responsive Polymeric Materials for Systemic Delivery of Nucleic Acids. *Adv. Healthcare Mater.* **2017,** 7, (4), 1701070.
[91] Veiman, K.-L.; Künnapuu, K.; Lehto, T.; Kiisholts, K.; Pärn, K.; Langel, Ü.; Kurrikoff, K., PEG shielded MMP sensitive CPPs for efficient and tumor specific gene delivery in vivo. *J. Controlled Release* **2015,** 209, 238-247.
[92] Huang, S.; Shao, K.; Kuang, Y.; Liu, Y.; Li, J.; An, S.; Guo, Y.; Ma, H.; He, X.; Jiang, C., Tumor targeting and microenvironment-responsive nanoparticles for gene delivery. *Biomaterials* **2013,** 34, (21), 5294-5302.
[93] Wang, H.-X.; Yang, X.-Z.; Sun, C.-Y.; Mao, C.-Q.; Zhu, Y.-H.; Wang, J., Matrix metalloproteinase 2-responsive micelle for siRNA delivery. *Biomaterials* **2014,** 35, (26), 7622-7634.
[94] Zhu, L.; Perche, F.; Wang, T.; Torchilin, V. P., Matrix metalloproteinase 2-sensitive multifunctional polymeric micelles for tumor-specific co-delivery of siRNA and hydrophobic drugs. *Biomaterials* **2014,** 35, (13), 4213-4222.
[95] Li, J.; Ge, Z.; Liu, S., PEG-sheddable polyplex micelles as smart gene carriers based on MMP-cleavable peptide-linked block copolymers. *Chem. Commun.* **2013,** 49, (62), 6974-6976.
[96] Qiu, N.; Liu, X.; Zhong, Y.; Zhou, Z.; Piao, Y.; Miao, L.; Zhang, Q.; Tang, J.; Huang, L.; Shen, Y., Esterase-Activated Charge-Reversal Polymer for Fibroblast-Exempt Cancer Gene Therapy. *Adv. Mater.* **2016,** 28, (48), 10613-10622.
[97] Chu, D. S. H.; Johnson, R. N.; Pun, S. H., Cathepsin B-sensitive polymers for compartment-specific degradation and nucleic acid release. *J. Controlled Release* **2012,** 157, (3), 445-454.
[98] Meyer, M.; Wagner, E., pH-responsive shielding of non-viral gene vectors. *Expert Opin. Drug Delivery* **2006,** 3, (5), 563-571.
[99] Guan, X.; Guo, Z.; Wang, T.; Lin, L.; Chen, J.; Tian, H.; Chen, X., A pH-Responsive Detachable PEG Shielding Strategy for Gene Delivery System in Cancer Therapy. *Biomacromolecules* **2017,** 18, (4), 1342-1349.
[100] Xu, C.; Guan, X.; Lin, L.; Wang, Q.; Gao, B.; Zhang, S.; Li, Y.; Tian, H., pH-Responsive Natural Polymeric Gene Delivery Shielding System Based on Dynamic Covalent Chemistry. *ACS Biomater. Sci. Eng.* **2018,** 4, (1), 193-199.
[101] Cheng, Y.; Sellers, D. L.; Tan, J.-K. Y.; Peeler, D. J.; Horner, P. J.; Pun, S. H., Development of switchable polymers to address the dilemma of stability and cargo release in polycationic nucleic acid carriers. *Biomaterials* **2017,** 127, 89-96.
[102] Kim, J.; Lee, Y. M.; Kim, H.; Park, D.; Kim, J.; Kim, W. J., Phenylboronic acid-sugar grafted polymer architecture as a dual stimuli-responsive gene carrier for targeted anti-angiogenic tumor therapy. *Biomaterials* **2016,** 75, 102-111.
[103] Fan, B.; Kang, L.; Chen, L.; Sun, P.; Jin, M.; Wang, Q.; Bae, Y. H.; Huang, W.; Gao, Z., Systemic siRNA Delivery with a Dual pH-Responsive and Tumor-targeted Nanovector for Inhibiting Tumor Growth and Spontaneous Metastasis in Orthotopic Murine Model of Breast Carcinoma. *Theranostics* **2017,** 7, (2), 357-376.
[104] Meyer, M.; Dohmen, C.; Philipp, A.; Kiener, D.; Maiwald, G.; Scheu, C.; Ogris, M.; Wagner, E., Synthesis and Biological Evaluation of a Bioresponsive and Endosomolytic siRNA−Polymer Conjugate. *Mol. Pharmaceutics* **2009,** 6, (3), 752-762.
[105] Rozema, D. B.; Lewis, D. L.; Wakefield, D. H.; Wong, S. C.; Klein, J. J.; Roesch, P. L.; Bertin, S. L.; Reppen, T. W.; Chu, Q.; Blokhin, A. V.; Hagstrom, J. E.; Wolff, J. A., Dynamic PolyConjugates for targeted in vivo delivery of siRNA to hepatocytes. *Proc. Natl. Acad. Sci. U.S.A.* **2007,** 104, (32), 12982.

[106] Beckert, L.; Kostka, L.; Kessel, E.; Krhac Levacic, A.; Kostkova, H.; Etrych, T.; Lächelt, U.; Wagner, E., Acid-labile pHPMA modification of four-arm oligoaminoamide pDNA polyplexes balances shielding and gene transfer activity in vitro and in vivo. *Eur. J. Pharm. Biopharm.* **2016,** 105, 85-96.
[107] Sun, C.-Y.; Shen, S.; Xu, C.-F.; Li, H.-J.; Liu, Y.; Cao, Z.-T.; Yang, X.-Z.; Xia, J.-X.; Wang, J., Tumor Acidity-Sensitive Polymeric Vector for Active Targeted siRNA Delivery. *J. Am. Chem. Soc.* **2015,** 137, (48), 15217-15224.
[108] Xu, C.-F.; Zhang, H.-B.; Sun, C.-Y.; Liu, Y.; Shen, S.; Yang, X.-Z.; Zhu, Y.-H.; Wang, J., Tumor acidity-sensitive linkage-bridged block copolymer for therapeutic siRNA delivery. *Biomaterials* **2016,** 88, 48-59.
[109] Chen, S.; Rong, L.; Lei, Q.; Cao, P.-X.; Qin, S.-Y.; Zheng, D.-W.; Jia, H.-Z.; Zhu, J.-Y.; Cheng, S.-X.; Zhuo, R.-X.; Zhang, X.-Z., A surface charge-switchable and folate modified system for co-delivery of proapoptosis peptide and p53 plasmid in cancer therapy. *Biomaterials* **2016,** 77, 149-163.
[110] Wooddell, C. I.; Rozema, D. B.; Hossbach, M.; John, M.; Hamilton, H. L.; Chu, Q.; Hegge, J. O.; Klein, J. J.; Wakefield, D. H.; Oropeza, C. E.; Deckert, J.; Roehl, I.; Jahn-Hofmann, K.; Hadwiger, P.; Vornlocher, H.-P.; McLachlan, A.; Lewis, D. L., Hepatocyte-targeted RNAi Therapeutics for the Treatment of Chronic Hepatitis B Virus Infection. *Mol. Ther.* **2013,** 21, (5), 973-985.
[111] Wooddell, C. I.; Yuen, M.-F.; Chan, H. L.-Y.; Gish, R. G.; Locarnini, S. A.; Chavez, D.; Ferrari, C.; Given, B. D.; Hamilton, J.; Kanner, S. B.; Lai, C.-L.; Lau, J. Y. N.; Schluep, T.; Xu, Z.; Lanford, R. E.; Lewis, D. L., RNAi-based treatment of chronically infected patients and chimpanzees reveals that integrated hepatitis B virus DNA is a source of HBsAg. *Sci. Transl. Med.* **2017,** 9, (409).
[112] Neu, M.; Germershaus, O.; Mao, S.; Voigt, K.-H.; Behe, M.; Kissel, T., Crosslinked nanocarriers based upon poly(ethylene imine) for systemic plasmid delivery: In vitro characterization and in vivo studies in mice. *J. Controlled Release* **2007,** 118, (3), 370-380.
[113] Russ, V.; Fröhlich, T.; Li, Y.; Halama, A.; Ogris, M.; Wagner, E., Improved in vivo gene transfer into tumor tissue by stabilization of pseudodendritic oligoethylenimine-based polyplexes. *J. Gene Med.* **2010,** 12, (2), 180-93.
[114] Klein, P. M.; Wagner, E., Bioreducible polycations as shuttles for therapeutic nucleic acid and protein transfection. *Antioxid Redox Signal* **2014,** 21, (5), 804-817.
[115] Dohmen, C.; Edinger, D.; Fröhlich, T.; Schreiner, L.; Lächelt, U.; Troiber, C.; Rädler, J.; Hadwiger, P.; Vornlocher, H.-P.; Wagner, E., Nanosized Multifunctional Polyplexes for Receptor-Mediated SiRNA Delivery. *ACS Nano* **2012,** 6, (6), 5198-5208.
[116] Parmar, R. G.; Busuek, M.; Walsh, E. S.; Leander, K. R.; Howell, B. J.; Sepp-Lorenzino, L.; Kemp, E.; Crocker, L. S.; Leone, A.; Kochansky, C. J.; Carr, B. A.; Garbaccio, R. M.; Colletti, S. L.; Wang, W., Endosomolytic Bioreducible Poly(amido amine disulfide) Polymer Conjugates for the in Vivo Systemic Delivery of siRNA Therapeutics. *Bioconjugate Chem.* **2013,** 24, (4), 640-647.
[117] Choi, S.; Lee, K.-D., Enhanced gene delivery using disulfide-crosslinked low molecular weight polyethylenimine with listeriolysin o-polyethylenimine disulfide conjugate. *J. Controlled Release* **2008,** 131, (1), 70-76.
[118] Saito, G.; Amidon, G. L.; Lee, K. D., Enhanced cytosolic delivery of plasmid DNA by a sulfhydryl-activatable listeriolysin O/protamine conjugate utilizing cellular reducing potential. *Gene Ther.* **2003,** 10, 72.
[119] Chen, C.-P.; Kim, J.-s.; Steenblock, E.; Liu, D.; Rice, K. G., Gene Transfer with Poly-Melittin Peptides. *Bioconjugate Chem.* **2006,** 17, (4), 1057-1062.
[120] Ping, Y.; Hu, Q.; Tang, G.; Li, J., FGFR-targeted gene delivery mediated by supramolecular assembly between β-cyclodextrin-crosslinked PEI and redox-sensitive PEG. *Biomaterials* **2013,** 34, (27), 6482-6494.

[121] Liu, J.; Jiang, X.; Hennink, W. E.; Zhuo, R., A modular approach toward multifunctional supramolecular nanopolyplexes for targeting gene delivery. *J. Controlled Release* **2015,** 213, e123-e124.
[122] Li, J.; Zhu, Y.; Hazeldine, S. T.; Li, C.; Oupický, D., Dual-Function CXCR4 Antagonist Polyplexes To Deliver Gene Therapy and Inhibit Cancer Cell Invasion. *Angew. Chem., Int. Ed. Engl.* **2012,** 51, (35), 8740-8743.
[123] Klein, P. M.; Reinhard, S.; Lee, D.-J.; Müller, K.; Ponader, D.; Hartmann, L.; Wagner, E., Precise redox-sensitive cleavage sites for improved bioactivity of siRNA lipopolyplexes. *Nanoscale* **2016,** 8, (42), 18098-18104.
[124] Zheng, M.; Zhong, Y.; Meng, F.; Peng, R.; Zhong, Z., Lipoic Acid Modified Low Molecular Weight Polyethylenimine Mediates Nontoxic and Highly Potent in Vitro Gene Transfection. *Mol. Pharm.* **2011,** 8, (6), 2434-2443.
[125] He, Y.; Nie, Y.; Cheng, G.; Xie, L.; Shen, Y.; Gu, Z., Viral Mimicking Ternary Polyplexes: A Reduction-Controlled Hierarchical Unpacking Vector for Gene Delivery. *Adv. Mater.* **2013,** 26, (10), 1534-1540.
[126] Zhu, J.; Qiao, M.; Wang, Q.; Ye, Y.; Ba, S.; Ma, J.; Hu, H.; Zhao, X.; Chen, D., Dual-responsive polyplexes with enhanced disassembly and endosomal escape for efficient delivery of siRNA. *Biomaterials* **2018,** 162, 47-59.
[127] Yang, Z.; Li, Y.; Gao, J.; Cao, Z.; Jiang, Q.; Liu, J., pH and redox dual-responsive multifunctional gene delivery with enhanced capability of transporting DNA into the nucleus. *Colloids Surf., B* **2017,** 153, 111-122.
[128] Jiang, Q.; Nie, Y.; Chen, X.; He, Y.; Yue, D.; Gu, Z., pH-Triggered Pinpointed Cascading Charge-Conversion and Redox-Controlled Gene Release Design: Modularized Fabrication for Nonviral Gene Transfection. *Adv. Funct. Mater.* **2017,** 27, (26), 1701571.
[129] Shim, M. S.; Xia, Y., A Reactive Oxygen Species (ROS)-Responsive Polymer for Safe, Efficient, and Targeted Gene Delivery in Cancer Cells. *Angew. Chem., Int. Ed. Engl.* **2013,** 52, (27), 6926-6929.
[130] Ruan, C.; Liu, L.; Wang, Q.; Chen, X.; Chen, Q.; Lu, Y.; Zhang, Y.; He, X.; Zhang, Y.; Guo, Q.; Sun, T.; Jiang, C., Reactive Oxygen Species-Biodegradable Gene Carrier for the Targeting Therapy of Breast Cancer. *ACS Appl. Mater. Interfaces* **2018,** 10, (12), 10398-10408.
[131] Zhu, D.; Yan, H.; Liu, X.; Xiang, J.; Zhou, Z.; Tang, J.; Liu, X.; Shen, Y., Intracellularly Disintegratable Polysulfoniums for Efficient Gene Delivery. *Adv. Funct. Mater.* **2017,** 27, (16), 1606826.
[132] Gupta, M. K.; Lee, S. H.; Crowder, S. W.; Wang, X.; Hofmeister, L. H.; Nelson, C. E.; Bellan, L. M.; Duvall, C. L.; Sung, H.-J., Oligoproline-derived nanocarrier for dual stimuli-responsive gene delivery. *Journal of materials chemistry. B* **2015,** 3, (36), 7271-7280.
[133] Naito, M.; Ishii, T.; Matsumoto, A.; Miyata, K.; Miyahara, Y.; Kataoka, K., A Phenylboronate-Functionalized Polyion Complex Micelle for ATP-Triggered Release of siRNA. *Angew. Chem., Int. Ed. Engl.* **2012,** 51, (43), 10751-10755.
[134] Naito, M.; Yoshinaga, N.; Ishii, T.; Matsumoto, A.; Miyahara, Y.; Miyata, K.; Kataoka, K., Enhanced Intracellular Delivery of siRNA by Controlling ATP-Responsivity of Phenylboronic Acid-Functionalized Polyion Complex Micelles. *Macromol. Biosci.* **2018,** 18, (1), 1700357.
[135] Perche, F.; Biswas, S.; Wang, T.; Zhu, L.; Torchilin, V. P., Hypoxia-Targeted siRNA Delivery. *Angew. Chem., Int. Ed. Engl.* **2014,** 53, (13), 3362-3366.
[136] Schaffert, D.; Troiber, C.; Wagner, E., New sequence-defined polyaminoamides with tailored endosomolytic properties for plasmid DNA delivery. *Bioconjugate Chem.* **2012,** 23, (6), 1157-65.
[137] Troiber, C.; Edinger, D.; Kos, P.; Schreiner, L.; Kläger, R.; Herrmann, A.; Wagner, E., Stabilizing effect of tyrosine trimers on pDNA and siRNA polyplexes. *Biomaterials* **2013,** 34, (5), 1624-1633.
[138] Klein, P. M.; Müller, K.; Gutmann, C.; Kos, P.; Krhac Levacic, A.; Edinger, D.; Höhn, M.; Leroux, J. C.; Gauthier, M. A.; Wagner, E., Twin disulfides as opportunity for improving stability

and transfection efficiency of oligoaminoethane polyplexes. *J. Controlled Release* **2015,** 205, 109-19.
[139] Takemoto, H.; Miyata, K.; Nishiyama, N.; Kataoka, K., Chapter Ten - Bioresponsive Polymer-Based Nucleic Acid Carriers. In *Adv. Genet.*, Huang, L.; Liu, D.; Wagner, E., Eds. Academic Press: 2014; Vol. 88, pp 289-323.
[140] Takemoto, H.; Miyata, K.; Hattori, S.; Ishii, T.; Suma, T.; Uchida, S.; Nishiyama, N.; Kataoka, K., Acidic pH-Responsive siRNA Conjugate for Reversible Carrier Stability and Accelerated Endosomal Escape with Reduced IFNα-Associated Immune Response. *Angew. Chem., Int. Ed. Engl.* **2013,** 52, (24), 6218-6221.
[141] Klibanov Alexander, L.; Maruyama, K.; Torchilin Vladimir, P.; Huang, L., Amphipathic polyethyleneglycols effectively prolong the circulation time of liposomes. *FEBS Lett.* **1990,** 268, (1), 235-237.
[142] Ogris, M.; Wagner, E., To Be Targeted: Is the Magic Bullet Concept a Viable Option for Synthetic Nucleic Acid Therapeutics? *Hum. Gene Ther.* **2011,** 22, (7), 799-807.
[143] Boussif, O.; Lezoualc; h, F.; Zanta, M. A.; Mergny, M. D.; Scherman, D.; Demeneix, B.; Behr, J. P., A versatile vector for gene and oligonucleotide transfer into cells in culture and in vivo: polyethylenimine. *Proc. Natl. Acad. Sci. U.S.A.* **1995,** 92, (16), 7297.
[144] Lächelt, U.; Kos, P.; Mickler, F. M.; Herrmann, A.; Salcher, E. E.; Rödl, W.; Badgujar, N.; Bräuchle, C.; Wagner, E., Fine-tuning of proton sponges by precise diaminoethanes and histidines in pDNA polyplexes. *Nanomedicine* **2014,** 10, (1), 35-44.
[145] Plank, C.; Zauner, W.; Wagner, E., Application of membrane-active peptides for drug and gene delivery across cellular membranes. *Adv. Drug Delivery Rev.* **1998,** 34, (1), 21-35.
[146] Sawant, R.; Torchilin, V., Intracellular transduction using cell-penetrating peptides. *Mol. BioSyst.* **2010,** 6, (4), 628-640.
[147] Zhang, W.; Müller, K.; Kessel, E.; Reinhard, S.; He, D.; Klein, P. M.; Höhn, M.; Rödl, W.; Kempter, S.; Wagner, E., Targeted siRNA Delivery Using a Lipo-Oligoaminoamide Nanocore with an Influenza Peptide and Transferrin Shell. *Adv. Healthcare Mater.* **2016,** 5, (12), 1493-504.
[148] Oude Blenke, E.; Sleszynska, M.; Evers, M. J. W.; Storm, G.; Martin, N. I.; Mastrobattista, E., Strategies for the Activation and Release of the Membranolytic Peptide Melittin from Liposomes Using Endosomal pH as a Trigger. *Bioconjugate Chem.* **2017,** 28, (2), 574-582.
[149] Cheng, Y.; Yumul, R. C.; Pun, S. H., Virus-Inspired Polymer for Efficient In Vitro and In Vivo Gene Delivery. *Angew. Chem., Int. Ed. Engl.* **2016,** 55, (39), 12013-7.
[150] Wang, D.; Wang, T.; Liu, J.; Yu, H.; Jiao, S.; Feng, B.; Zhou, F.; Fu, Y.; Yin, Q.; Zhang, P.; Zhang, Z.; Zhou, Z.; Li, Y., Acid-Activatable Versatile Micelleplexes for PD-L1 Blockade-Enhanced Cancer Photodynamic Immunotherapy. *Nano Lett.* **2016,** 16, (9), 5503-13.
[151] Zhang, J.; Wang, Y.; Chen, J.; Liang, X.; Han, H.; Yang, Y.; Li, Q.; Wang, Y., Inhibition of cell proliferation through an ATP-responsive co-delivery system of doxorubicin and Bcl-2 siRNA. *Int. J. Nanomed.* **2017,** 12, 4721-4732.
[152] Liu, H.-M.; Zhang, Y.-F.; Xie, Y.-D.; Cai, Y.-F.; Li, B.-Y.; Li, W.; Zeng, L.-Y.; Li, Y.-L.; Yu, R.-T., Hypoxia-responsive ionizable liposome delivery siRNA for glioma therapy. *Int. J. Nanomed.* **2017,** 12, 1065-1083.
[153] Gialeli, C.; Theocharis, A. D.; Karamanos, N. K., Roles of matrix metalloproteinases in cancer progression and their pharmacological targeting. *FEBS J.* **2011,** 278, (1), 16-27.
[154] Mellman, I.; Fuchs, R.; Helenius, A., Acidification of the Endocytic and Exocytic Pathways. *Annu. Rev. Biochem.* **1986,** 55, (1), 663-700.
[155] Warburg, O., The Metabolism of Carcinoma Cells. *Cancer Res.* **1925,** 9, (1), 148.
[156] Ferreira, L. M. R., Cancer metabolism: The Warburg effect today. *Exp. Mol. Pathol.* **2010,** 89, (3), 372-380.
[157] Nelson, C. E.; Kintzing, J. R.; Hanna, A.; Shannon, J. M.; Gupta, M. K.; Duvall, C. L., Balancing Cationic and Hydrophobic Content of PEGylated siRNA Polyplexes Enhances Endosome Escape, Stability, Blood Circulation Time, and Bioactivity In Vivo. *ACS Nano* **2013,** 7, (10), 10.1021/nn403325f.

[158] Schaffert, D.; Badgujar, N.; Wagner, E., Novel Fmoc-polyamino acids for solid-phase synthesis of defined polyamidoamines. *Org. Lett.* **2011,** 13, (7), 1586-9.
[159] Schellinger, J. G.; Pahang, J. A.; Johnson, R. N.; Chu, D. S. H.; Sellers, D. L.; Maris, D. O.; Convertine, A. J.; Stayton, P. S.; Horner, P. J.; Pun, S. H., Melittin-grafted HPMA-oligolysine based copolymers for gene delivery. *Biomaterials* **2013,** 34, (9), 2318-2326.
[160] Khalil, I. A.; Harashima, H., An efficient PEGylated gene delivery system with improved targeting: Synergism between octaarginine and a fusogenic peptide. *Int. J. Pharm.* **2018,** 538, (1), 179-187.
[161] Zhou, K.; Wang, Y.; Huang, X.; Luby-Phelps, K.; Sumer, B. D.; Gao, J., Tunable, ultrasensitive pH-responsive nanoparticles targeting specific endocytic organelles in living cells. *Angew. Chem., Int. Ed. Engl.* **2011,** 50, (27), 6109-14.
[162] Wang, Y.; Zhou, K.; Huang, G.; Hensley, C.; Huang, X.; Ma, X.; Zhao, T.; Sumer, B. D.; DeBerardinis, R. J.; Gao, J., A nanoparticle-based strategy for the imaging of a broad range of tumours by nonlinear amplification of microenvironment signals. *Nat. Mater.* **2014,** 13, (2), 204-12.
[163] Arunachalam, B.; Phan, U. T.; Geuze, H. J.; Cresswell, P., Enzymatic reduction of disulfide bonds in lysosomes: Characterization of a Gamma-interferon-inducible lysosomal thiol reductase (GILT). *Proc. Natl. Acad. Sci. U.S.A.* **2000,** 97, (2), 745.
[164] Brülisauer, L.; Kathriner, N.; Prenrecaj, M.; Gauthier, M. A.; Leroux, J.-C., Tracking the Bioreduction of Disulfide-Containing Cationic Dendrimers. *Angew. Chem., Int. Ed. Engl.* **2012,** 51, (50), 12454-12458.
[165] Bellocq, N. C.; Pun, S. H.; Jensen, G. S.; Davis, M. E., Transferrin-Containing, Cyclodextrin Polymer-Based Particles for Tumor-Targeted Gene Delivery. *Bioconjugate Chem.* **2003,** 14, (6), 1122-1132.
[166] Davis, M. E.; Zuckerman, J. E.; Choi, C. H. J.; Seligson, D.; Tolcher, A.; Alabi, C. A.; Yen, Y.; Heidel, J. D.; Ribas, A., Evidence of RNAi in humans from systemically administered siRNA via targeted nanoparticles. *Nature* **2010,** 464, 1067.
[167] Kuppusamy, P.; Li, H.; Ilangovan, G.; Cardounel, A. J.; Zweier, J. L.; Yamada, K.; Krishna, M. C.; Mitchell, J. B., Noninvasive Imaging of Tumor Redox Status and Its Modification by Tissue Glutathione Levels. *Cancer Res.* **2002,** 62, (1), 307.
[168] Lü, R., Reaction-based small-molecule fluorescent probes for dynamic detection of ROS and transient redox changes in living cells and small animals. *J. Mol. Cell. Cardiol.* **2017,** 110, 96-108.
[169] Traut, T. W., Physiological concentrations of purines and pyrimidines. *Mol. Cell. Biochem.* **1994,** 140, (1), 1-22.
[170] Wilson, W. R.; Hay, M. P., Targeting hypoxia in cancer therapy. *Nat. Rev. Cancer* **2011,** 11, 393.
[171] Nair, J. K.; Willoughby, J. L. S.; Chan, A.; Charisse, K.; Alam, M. R.; Wang, Q.; Hoekstra, M.; Kandasamy, P.; Kel'in, A. V.; Milstein, S.; Taneja, N.; O'Shea, J.; Shaikh, S.; Zhang, L.; van der Sluis, R. J.; Jung, M. E.; Akinc, A.; Hutabarat, R.; Kuchimanchi, S.; Fitzgerald, K.; Zimmermann, T.; van Berkel, T. J. C.; Maier, M. A.; Rajeev, K. G.; Manoharan, M., Multivalent N-Acetylgalactosamine-Conjugated siRNA Localizes in Hepatocytes and Elicits Robust RNAi-Mediated Gene Silencing. *J. Am. Chem. Soc.* **2014,** 136, (49), 16958-16961.
[172] Huang, Y., Preclinical and Clinical Advances of GalNAc-Decorated Nucleic Acid Therapeutics. *Mol. Ther.-Nucleic Acids* **2017,** 6, 116-132.
[173] Foster, D. J.; Brown, C. R.; Shaikh, S.; Trapp, C.; Schlegel, M. K.; Qian, K.; Sehgal, A.; Rajeev, K. G.; Jadhav, V.; Manoharan, M.; Kuchimanchi, S.; Maier, M. A.; Milstein, S., Advanced siRNA Designs Further Improve In Vivo Performance of GalNAc-siRNA Conjugates. *Mol. Ther.* **2018,** 26, (3), 708-717.
[174] FDA approves first-of-its kind targeted RNA-based therapy to treat a rare disease. In Springfield, Maryland: U.S. Food and Drug Administration: FDA News Release – Press Announcements. , 2018.

[175] Zhang, Y.; Satterlee, A.; Huang, L., In vivo gene delivery by nonviral vectors: overcoming hurdles? *Mol. Ther.* **2012,** 20, (7), 1298-1304.
[176] Kulkarni, J. A.; Darjuan, M. M.; Mercer, J. E.; Chen, S.; van der Meel, R.; Thewalt, J. L.; Tam, Y. Y. C.; Cullis, P. R., On the Formation and Morphology of Lipid Nanoparticles Containing Ionizable Cationic Lipids and siRNA. *ACS Nano* **2018,** 12, (5), 4787-4795.
[177] Khalil, I. A.; Yamada, Y.; Harashima, H., Optimization of siRNA delivery to target sites: issues and future directions. *Expert Opin. Drug Delivery* **2018,** 15, (11), 1053-1065.
[178] Uchida, S.; Kataoka, K., Design concepts of polyplex micelles for in vivo therapeutic delivery of plasmid DNA and messenger RNA. *J. Biomed. Mater. Res. A* **2019,** 107, (5), 978-990.
[179] Luo, T.; Liang, H.; Jin, R.; Nie, Y., Virus-inspired and mimetic designs in non-viral gene delivery. *J. Gene Med.* **2019,** 21, (7), e3090.
[180] Dong, Y.; Siegwart, D. J.; Anderson, D. G., Strategies, design, and chemistry in siRNA delivery systems. *Adv. Drug Delivery Rev.* **2019,** 144, 133-147.
[181] Zhang, P.; Wagner, E., History of Polymeric Gene Delivery Systems. In *Polymeric Gene Delivery Systems*, Cheng, Y., Ed. Springer International Publishing: Cham, 2018; pp 1-39.
[182] Blakney, A. K.; Yilmaz, G.; McKay, P. F.; Becer, C. R.; Shattock, R. J., One Size Does Not Fit All: The Effect of Chain Length and Charge Density of Poly(ethylene imine) Based Copolymers on Delivery of pDNA, mRNA, and RepRNA Polyplexes. *Biomacromolecules* **2018,** 19, (7), 2870-2879.
[183] Salcher, E. E.; Kos, P.; Fröhlich, T.; Badgujar, N.; Scheible, M.; Wagner, E., Sequence-defined four-arm oligo(ethanamino)amides for pDNA and siRNA delivery: Impact of building blocks on efficacy. *J. Controlled Release* **2012,** 164, (3), 380-6.
[184] Kos, P.; Lächelt, U.; Herrmann, A.; Mickler, F. M.; Döblinger, M.; He, D.; Krhač Levačić, A.; Morys, S.; Bräuchle, C.; Wagner, E., Histidine-rich stabilized polyplexes for cMet-directed tumor-targeted gene transfer. *Nanoscale* **2015,** 7, (12), 5350-5362.
[185] He, D. Combinatorial optimization of nucleic acid carriers for folate-targeted delivery. Ludwig-Maximilians-Universität Munich, Munich, 2016.
[186] Wang, C. Y.; Huang, L., Polyhistidine mediates an acid-dependent fusion of negatively charged liposomes. *Biochemistry* **1984,** 23, (19), 4409-16.
[187] Uster, P. S.; Deamer, D. W., pH-dependent fusion of liposomes using titratable polycations. *Biochemistry* **1985,** 24, (1), 1-8.
[188] Midoux, P.; Kichler, A.; Boutin, V.; Maurizot, J. C.; Monsigny, M., Membrane permeabilization and efficient gene transfer by a peptide containing several histidines. *Bioconjugate Chem.* **1998,** 9, (2), 260-7.
[189] Midoux, P.; Pichon, C.; Yaouanc, J.-J.; Jaffrès, P.-A., Chemical vectors for gene delivery: a current review on polymers, peptides and lipids containing histidine or imidazole as nucleic acids carriers. *Br J Pharmacol* **2009,** 157, (2), 166-178.
[190] He, J.; Xu, S.; Mixson, A. J., The Multifaceted Histidine-Based Carriers for Nucleic Acid Delivery: Advances and Challenges. *Pharmaceutics* **2020,** 12, (8).
[191] Midoux, P.; Monsigny, M., Efficient gene transfer by histidylated polylysine/pDNA complexes. *Bioconjugate Chem.* **1999,** 10, (3), 406-11.
[192] Gonçalves, C.; Pichon, C.; Guérin, B.; Midoux, P., Intracellular processing and stability of DNA complexed with histidylated polylysine conjugates. *J. Gene Med.* **2002,** 4, (3), 271-81.
[193] Pichon, C.; Gonçalves, C.; Midoux, P., Histidine-rich peptides and polymers for nucleic acids delivery. *Adv. Drug Delivery Rev.* **2001,** 53, (1), 75-94.
[194] Hwang, H. S.; Hu, J.; Na, K.; Bae, Y. H., Role of polymeric endosomolytic agents in gene transfection: a comparative study of poly(L-lysine) grafted with monomeric L-histidine analogue and poly(L-histidine). *Biomacromolecules* **2014,** 15, (10), 3577-86.
[195] Bertrand, E.; Gonçalves, C.; Billiet, L.; Gomez, J. P.; Pichon, C.; Cheradame, H.; Midoux, P.; Guégan, P., Histidinylated linear PEI: a new efficient non-toxic polymer for gene transfer. *Chem. Commun.* **2011,** 47, (46), 12547-9.

[196] Gomez, J. P.; Tresset, G.; Pichon, C.; Midoux, P., Improved histidinylated lPEI polyplexes for skeletal muscle cells transfection. *Int. J. Nanomed.* **2019,** 559, 58-67.
[197] Leng, Q.; Mixson, A. J., Modified branched peptides with a histidine-rich tail enhance in vitro gene transfection. *Nucleic Acids Res.* **2005,** 33, (4), e40-e40.
[198] Chen, Q.-R.; Zhang, L.; Luther, P. W.; Mixson, A. J., Optimal transfection with the HK polymer depends on its degree of branching and the pH of endocytic vesicles. *Nucleic Acids Res.* **2002,** 30, (6), 1338-1345.
[199] McKenzie, D. L.; Kwok, K. Y.; Rice, K. G., A Potent New Class of Reductively Activated Peptide Gene Delivery Agents. *J. Biol. Chem.* **2000,** 275, 9970-9977.
[200] Fröhlich, T.; Edinger, D.; Kläger, R.; Troiber, C.; Salcher, E.; Badgujar, N.; Martin, I.; Schaffert, D.; Cengizeroglu, A.; Hadwiger, P.; Vornlocher, H.-P.; Wagner, E., Structure–activity relationships of siRNA carriers based on sequence-defined oligo (ethane amino) amides. *J. Controlled Release* **2012,** 160, (3), 532-541.
[201] Suk, J. S.; Xu, Q.; Kim, N.; Hanes, J.; Ensign, L. M., PEGylation as a strategy for improving nanoparticle-based drug and gene delivery. *Adv. Drug Delivery Rev.* **2016,** 99, (Pt A), 28-51.
[202] Klein, P. M.; Kern, S.; Lee, D.-J.; Schmaus, J.; Höhn, M.; Gorges, J.; Kazmaier, U.; Wagner, E., Folate receptor-directed orthogonal click-functionalization of siRNA lipopolyplexes for tumor cell killing in vivo. *Biomaterials* **2018,** 178, 630-642.
[203] Klein, P. M.; Wagner, E., Click-Shielded and Targeted Lipopolyplexes. In *Oligonucleotide-Based Therapies: Methods and Protocols*, Gissberg, O.; Zain, R.; Lundin, K. E., Eds. Springer New York: New York, NY, 2019; pp 141-164.
[204] Truebenbach, I.; Zhang, W.; Wang, Y.; Kern, S.; Höhn, M.; Reinhard, S.; Gorges, J.; Kazmaier, U.; Wagner, E., Co-delivery of pretubulysin and siEG5 to EGFR overexpressing carcinoma cells. *Int. J. Pharm.* **2019,** 569, 118570.
[205] Wang, Y.; Luo, J.; Truebenbach, I.; Reinhard, S.; Klein, P. M.; Höhn, M.; Kern, S.; Morys, S.; Loy, D. M.; Wagner, E.; Zhang, W., Double Click-Functionalized siRNA Polyplexes for Gene Silencing in Epidermal Growth Factor Receptor-Positive Tumor Cells. *ACS Biomater. Sci. Eng.* **2020,** 6, (2), 1074-1089.
[206] Schaffert, D.; Kiss, M.; Rödl, W.; Shir, A.; Levitzki, A.; Ogris, M.; Wagner, E., Poly(I:C)-mediated tumor growth suppression in EGF-receptor overexpressing tumors using EGF-polyethylene glycol-linear polyethylenimine as carrier. *Pharm. Res.* **2011,** 28, (4), 731-41.
[207] Rödl, W.; Taschauer, A.; Schaffert, D.; Wagner, E.; Ogris, M., Synthesis of Polyethylenimine-Based Nanocarriers for Systemic Tumor Targeting of Nucleic Acids. In *Nanotechnology for Nucleic Acid Delivery: Methods and Protocols*, Ogris, M.; Sami, H., Eds. Springer New York: New York, NY, 2019; pp 83-99.
[208] Luo, J.; Höhn, M.; S., R.; M., L. D.; M., K. P.; E., W., IL4-Receptor-Targeted Dual Antitumoral Apoptotic Peptide—siRNA Conjugate Lipoplexes. *Adv. Funct. Mater.* **2019,** 29, 18.
[209] Reinhard, S.; Zhang, W.; Wagner, E., Optimized Solid-Phase-Assisted Synthesis of Oleic Acid Containing siRNA Nanocarriers. *ChemMedChem* **2017,** 12, (17), 1464-1470.
[210] Russ, V.; Elfberg, H.; Thoma, C.; Kloeckner, J.; Ogris, M.; Wagner, E., Novel degradable oligoethylenimine acrylate ester-based pseudodendrimers for in vitro and in vivo gene transfer. *Gene Ther.* **2008,** 15, (1), 18-29.
[211] Morys, S.; Urnauer, S.; Spitzweg, C.; Wagner, E., EGFR Targeting and Shielding of pDNA Lipopolyplexes via Bivalent Attachment of a Sequence-Defined PEG Agent. *Macromol. Biosci.* **2018,** 18, (1), 1700203.
[212] Klein, P. M. Redox-sensitive and receptor-targeted sequence-defined, cationic carriers for nucleic acid delivery. Thesis, Ludwig-Maximilians-Universität Munich, Munich, Germany, 2017.
[213] Chiper, M.; Tounsi, N.; Kole, R.; Kichler, A.; Zuber, G., Self-aggregating 1.8kDa polyethylenimines with dissolution switch at endosomal acidic pH are delivery carriers for plasmid DNA, mRNA, siRNA and exon-skipping oligonucleotides. *J. Controlled Release* **2017,** 246, 60-70.

[214] Hama, S.; Akita, H.; Ito, R.; Mizuguchi, H.; Hayakawa, T.; Harashima, H., Quantitative comparison of intracellular trafficking and nuclear transcription between adenoviral and lipoplex systems. *Mol. Ther.* **2006,** 13, (4), 786-794.
[215] Hama, S.; Akita, H.; Iida, S.; Mizuguchi, H.; Harashima, H., Quantitative and mechanism-based investigation of post-nuclear delivery events between adenovirus and lipoplex. *Nucleic Acids Res.* **2007,** 35, (5), 1533-1543.
[216] Takeda, K. M.; Osada, K.; Tockary, T. A.; Dirisala, A.; Chen, Q.; Kataoka, K., Poly(ethylene glycol) Crowding as Critical Factor To Determine pDNA Packaging Scheme into Polyplex Micelles for Enhanced Gene Expression. *Biomacromolecules* **2017,** 18, (1), 36-43.
[217] Müller, K.; Klein, P. M.; Heissig, P.; Roidl, A.; Wagner, E., EGF receptor targeted lipo-oligocation polyplexes for antitumoral siRNA and miRNA delivery. *Nanotechnology* **2016,** 27, (46), 464001.
[218] Novo, L.; van Gaal, E. V.; Mastrobattista, E.; van Nostrum, C. F.; Hennink, W. E., Decationized crosslinked polyplexes for redox-triggered gene delivery. *J. Controlled Release* **2013,** 169, (3), 246-56.
[219] Shin, M. L.; Hänsch, G.; Mayer, M. M., Effect of agents that produce membrane disorder on lysis of erythrocytes by complement. *Proc. Natl. Acad. Sci. U.S.A.* **1981,** 78, (4), 2522.
[220] Reinhard, S.; Wagner, E., Sequence-Defined Cationic Lipo-Oligomers Containing Unsaturated Fatty Acids for Transfection. *Methods Mol. Biol.* **2019,** 1943, 1-25.
[221] Russ, V.; Günther, M.; Halama, A.; Ogris, M.; Wagner, E., Oligoethylenimine-grafted polypropylenimine dendrimers as degradable and biocompatible synthetic vectors for gene delivery. *J. Controlled Release* **2008,** 132, (2), 131-40.
[222] Walczyk, D.; Bombelli, F. B.; Monopoli, M. P.; Lynch, I.; Dawson, K. A., What the cell "sees" in bionanoscience. *J. Am. Chem. Soc.* **2010,** 132, (16), 5761-8.
[223] Treuel, L.; Docter, D.; Maskos, M.; Stauber, R. H., Protein corona - from molecular adsorption to physiological complexity. *Beilstein J. Nanotechnol.* **2015,** 6, 857-73.
[224] Schöttler, S.; Landfester, K.; Mailänder, V., Controlling the Stealth Effect of Nanocarriers through Understanding the Protein Corona. *Angew. Chem., Int. Ed. Engl.* **2016,** 55, (31), 8806-15.
[225] Gref, R.; Lück, M.; Quellec, P.; Marchand, M.; Dellacherie, E.; Harnisch, S.; Blunk, T.; Müller, R. H., 'Stealth' corona-core nanoparticles surface modified by polyethylene glycol (PEG): influences of the corona (PEG chain length and surface density) and of the core composition on phagocytic uptake and plasma protein adsorption. *Colloids Surf., B* **2000,** 18, (3-4), 301-313.
[226] Kim, H. R.; Andrieux, K.; Delomenie, C.; Chacun, H.; Appel, M.; Desmaële, D.; Taran, F.; Georgin, D.; Couvreur, P.; Taverna, M., Analysis of plasma protein adsorption onto PEGylated nanoparticles by complementary methods: 2-DE, CE and Protein Lab-on-chip system. *Electrophoresis* **2007,** 28, (13), 2252-61.
[227] Walkey, C. D.; Olsen, J. B.; Guo, H.; Emili, A.; Chan, W. C., Nanoparticle size and surface chemistry determine serum protein adsorption and macrophage uptake. *J. Am. Chem. Soc.* **2012,** 134, (4), 2139-47.
[228] Kichler, A.; Leborgne, C.; Coeytaux, E.; Danos, O., Polyethylenimine-mediated gene delivery: a mechanistic study. *J. Gene Med.* **2001,** 3, (2), 135-144.
[229] Akinc, A.; Thomas, M.; Klibanov, A. M.; Langer, R., Exploring polyethylenimine-mediated DNA transfection and the proton sponge hypothesis. *J. Gene Med.* **2005,** 7, (5), 657-663.
[230] Sonawane, N. D.; Szoka, F. C., Jr.; Verkman, A. S., Chloride accumulation and swelling in endosomes enhances DNA transfer by polyamine-DNA polyplexes. *J. Biol. Chem.* **2003,** 278, (45), 44826-31.
[231] Reinhard, S.; Wang, Y.; Dengler, S.; Wagner, E., Precise Enzymatic Cleavage Sites for Improved Bioactivity of siRNA Lipo-Polyplexes. *Bioconjugate Chem.* **2018,** 29, (11), 3649-3657.
[232] Kuhn, J.; Klein, P. M.; Al Danaf, N.; Nordin, J. Z.; Reinhard, S.; Loy, D. M.; Höhn, M.; El Andaloussi, S.; Lamb, D. C.; Wagner, E.; Aoki, Y.; Lehto, T.; Lächelt, U., Supramolecular

Assembly of Aminoethylene-Lipopeptide PMO Conjugates into RNA Splice-Switching Nanomicelles. *Adv. Funct. Mater.* **2019,** 29, (48), 1906432.
[233] Mastrobattista, E.; Kapel, R. H.; Eggenhuisen, M. H.; Roholl, P. J.; Crommelin, D. J.; Hennink, W. E.; Storm, G., Lipid-coated polyplexes for targeted gene delivery to ovarian carcinoma cells. *Cancer Gene Ther.* **2001,** 8, (6), 405-13.
[234] Hager, S.; Fittler, F. J.; Wagner, E.; Bros, M., Nucleic Acid-Based Approaches for Tumor Therapy. *Cells* **2020,** 9, (9), 2061.
[235] Fröhlich, T.; Edinger, D.; Russ, V.; Wagner, E., Stabilization of polyplexes via polymer crosslinking for efficient siRNA delivery. *Eur. J. Pharm. Sci.* **2012,** 47, (5), 914-20.
[236] Cheng, Z.; Li, M.; Dey, R.; Chen, Y., Nanomaterials for cancer therapy: current progress and perspectives. *J. Hematol. Oncol.* **2021,** 14, (1), 85.
[237] Shi, J.; Kantoff, P. W.; Wooster, R.; Farokhzad, O. C., Cancer nanomedicine: progress, challenges and opportunities. *Nat. Rev. Cancer* **2017,** 17, (1), 20-37.
[238] Barenholz, Y., Doxil®--the first FDA-approved nano-drug: lessons learned. *J. Controlled Release* **2012,** 160, (2), 117-34.
[239] Alberg, I.; Kramer, S.; Schinnerer, M.; Hu, Q.; Seidl, C.; Leps, C.; Drude, N.; Möckel, D.; Rijcken, C.; Lammers, T.; Diken, M.; Maskos, M.; Morsbach, S.; Landfester, K.; Tenzer, S.; Barz, M.; Zentel, R., Polymeric Nanoparticles with Neglectable Protein Corona. *Small* **2020,** 16, (18), 1907574.
[240] Koshkina, O.; Westmeier, D.; Lang, T.; Bantz, C.; Hahlbrock, A.; Würth, C.; Resch-Genger, U.; Braun, U.; Thiermann, R.; Weise, C.; Eravci, M.; Mohr, B.; Schlaad, H.; Stauber, R. H.; Docter, D.; Bertin, A.; Maskos, M., Tuning the Surface of Nanoparticles: Impact of Poly(2-ethyl-2-oxazoline) on Protein Adsorption in Serum and Cellular Uptake. *Macromol. Biosci.* **2016,** 16, (9), 1287-300.
[241] Bhatia, S. N.; Ingber, D. E., Microfluidic organs-on-chips. *Nat. Biotechnol.* **2014,** 32, (8), 760-72.
[242] Zheng, F.; Fu, F.; Cheng, Y.; Wang, C.; Zhao, Y.; Gu, Z., Organ-on-a-Chip Systems: Microengineering to Biomimic Living Systems. *Small* **2016,** 12, (17), 2253-82.
[243] Wang, D.; Cong, Y.; Deng, Q.; Han, X.; Zhang, S.; Zhao, L.; Luo, Y.; Zhang, X., Physiological and Disease Models of Respiratory System Based on Organ-on-a-Chip Technology. *Micromachines* **2021,** 12, (9), 1106.
[244] Primavessy, D.; Metz, J.; Schnur, S.; Schneider, M.; Lehr, C.-M.; Hittinger, M., Pulmonary in vitro instruments for the replacement of animal experiments. *Eur. J. Pharm. Biopharm.* **2021,** 168, 62-75.
[245] Abd, E.; Yousef, S. A.; Pastore, M. N.; Telaprolu, K.; Mohammed, Y. H.; Namjoshi, S.; Grice, J. E.; Roberts, M. S., Skin models for the testing of transdermal drugs. *Clin. Pharmacol.* **2016,** 8, 163-176.
[246] Garcia, M. T. J.; de Vasconcellos, F. L. L.; Raffier, C. P.; Roberts, M. S.; Grice, J. E.; Benson, H. A. E.; Leite-Silva, V. R., Alternative Methods to Animal Studies for the Evaluation of Topical/ Transdermal Drug Delivery Systems. *Curr. Top. Med. Chem.* **2018,** 18, (4), 287-299.
[247] Onyema, H. N.; Berger, M.; Musyanovych, A.; Bantz, C.; Maskos, M.; Freese, C., Uptake of polymeric nanoparticles in a human induced pluripotent stem cell-based blood-brain barrier model: Impact of size, material, and protein corona. *Biointerphases* **2021,** 16, (2), 021004.
[248] Dahlman, J. E.; Kauffman, K. J.; Xing, Y.; Shaw, T. E.; Mir, F. F.; Dlott, C. C.; Langer, R.; Anderson, D. G.; Wang, E. T., Barcoded nanoparticles for high throughput in vivo discovery of targeted therapeutics. *Proc. Natl. Acad. Sci. U.S.A.* **2017,** 114, (8), 2060-2065.
[249] García-Álvarez, R.; Vallet-Regí, M., Hard and Soft Protein Corona of Nanomaterials: Analysis and Relevance. *Nanomaterials* **2021,** 11, (4), 888.
[250] Ghosh, G.; Panicker, L., Protein-nanoparticle interactions and a new insight. *Soft Matter* **2021,** 17, (14), 3855-3875.
[251] Baimanov, D.; Cai, R.; Chen, C., Understanding the Chemical Nature of Nanoparticle-Protein Interactions. *Bioconjugate Chem.* **2019,** 30, (7), 1923-1937.

[252] Ke, P. C.; Lin, S.; Parak, W. J.; Davis, T. P.; Caruso, F., A Decade of the Protein Corona. *ACS Nano* **2017,** 11, (12), 11773-11776.
[253] Cedervall, T.; Lynch, I.; Lindman, S.; Berggård, T.; Thulin, E.; Nilsson, H.; Dawson, K. A.; Linse, S., Understanding the nanoparticle–protein corona using methods to quantify exchange rates and affinities of proteins for nanoparticles. *Proc. Natl. Acad. Sci. U.S.A.* **2007,** 104, (7), 2050.
[254] Vroman, L., Effect of Adsorbed Proteins on the Wettability of Hydrophilic and Hydrophobic Solids. *Nature* **1962,** 196, (4853), 476-477.
[255] Behzadi, S.; Serpooshan, V.; Sakhtianchi, R.; Müller, B.; Landfester, K.; Crespy, D.; Mahmoudi, M., Protein corona change the drug release profile of nanocarriers: The “overlooked” factor at the nanobio interface. *Colloids Surf., B* **2014,** 123, 143-149.
[256] Corbo, C.; Molinaro, R.; Parodi, A.; Toledano Furman, N. E.; Salvatore, F.; Tasciotti, E., The impact of nanoparticle protein corona on cytotoxicity, immunotoxicity and target drug delivery. *Nanomedicine* **2016,** 11, (1), 81-100.
[257] Miclăuş, T.; Beer, C.; Chevallier, J.; Scavenius, C.; Bochenkov, V. E.; Enghild, J. J.; Sutherland, D. S., Dynamic protein coronas revealed as a modulator of silver nanoparticle sulphidation in vitro. *Nat. Commun.* **2016,** 7, 11770.
[258] Tenzer, S.; Docter, D.; Kuharev, J.; Musyanovych, A.; Fetz, V.; Hecht, R.; Schlenk, F.; Fischer, D.; Kiouptsi, K.; Reinhardt, C.; Landfester, K.; Schild, H.; Maskos, M.; Knauer, S. K.; Stauber, R. H., Rapid formation of plasma protein corona critically affects nanoparticle pathophysiology. *Nat. Nanotechnol.* **2013,** 8, (10), 772-81.
[259] Casals, E.; Pfaller, T.; Duschl, A.; Oostingh, G. J.; Puntes, V., Time Evolution of the Nanoparticle Protein Corona. *ACS Nano* **2010,** 4, (7), 3623-3632.
[260] Pisani, C.; Gaillard, J. C.; Odorico, M.; Nyalosaso, J. L.; Charnay, C.; Guari, Y.; Chopineau, J.; Devoisselle, J. M.; Armengaud, J.; Prat, O., The timeline of corona formation around silica nanocarriers highlights the role of the protein interactome. *Nanoscale* **2017,** 9, (5), 1840-1851.
[261] Hadjidemetriou, M.; Al-Ahmady, Z.; Kostarelos, K., Time-evolution of in vivo protein corona onto blood-circulating PEGylated liposomal doxorubicin (DOXIL) nanoparticles. *Nanoscale* **2016,** 8, (13), 6948-6957.
[262] Weiss, A. C. G.; Krüger, K.; Besford, Q. A.; Schlenk, M.; Kempe, K.; Förster, S.; Caruso, F., In Situ Characterization of Protein Corona Formation on Silica Microparticles Using Confocal Laser Scanning Microscopy Combined with Microfluidics. *ACS Appl. Mater. Interfaces* **2019,** 11, (2), 2459-2469.
[263] Dell'Orco, D.; Lundqvist, M.; Oslakovic, C.; Cedervall, T.; Linse, S., Modeling the time evolution of the nanoparticle-protein corona in a body fluid. *PLoS One* **2010,** 5, (6), e10949.
[264] Lundqvist, M., Nanoparticles: Tracking protein corona over time. *Nat. Nanotechnol.* **2013,** 8, (10), 701-2.
[265] Lundqvist, M.; Stigler, J.; Cedervall, T.; Berggård, T.; Flanagan, M. B.; Lynch, I.; Elia, G.; Dawson, K., The evolution of the protein corona around nanoparticles: a test study. *ACS Nano* **2011,** 5, (9), 7503-9.
[266] Barrán-Berdón, A. L.; Pozzi, D.; Caracciolo, G.; Capriotti, A. L.; Caruso, G.; Cavaliere, C.; Riccioli, A.; Palchetti, S.; Laganà, A., Time evolution of nanoparticle-protein corona in human plasma: relevance for targeted drug delivery. *Langmuir* **2013,** 29, (21), 6485-94.
[267] Chen, D.; Parayath, N.; Ganesh, S.; Wang, W.; Amiji, M., The role of apolipoprotein- and vitronectin-enriched protein corona on lipid nanoparticles for in vivo targeted delivery and transfection of oligonucleotides in murine tumor models. *Nanoscale* **2019,** 11, (40), 18806-18824.
[268] Chen, D.; Ganesh, S.; Wang, W.; Amiji, M., The role of surface chemistry in serum protein corona-mediated cellular delivery and gene silencing with lipid nanoparticles. *Nanoscale* **2019,** 11, (18), 8760-8775.
[269] Pozzi, D.; Caracciolo, G.; Capriotti, A. L.; Cavaliere, C.; La Barbera, G.; Anchordoquy, T. J.; Laganà, A., Surface chemistry and serum type both determine the nanoparticle-protein corona. *J. Proteomics* **2015,** 119, 209-17.

[270] Tenzer, S.; Docter, D.; Rosfa, S.; Wlodarski, A.; Kuharev, J.; Rekik, A.; Knauer, S. K.; Bantz, C.; Nawroth, T.; Bier, C.; Sirirattanapan, J.; Mann, W.; Treuel, L.; Zellner, R.; Maskos, M.; Schild, H.; Stauber, R. H., Nanoparticle size is a critical physicochemical determinant of the human blood plasma corona: a comprehensive quantitative proteomic analysis. *ACS Nano* **2011,** 5, (9), 7155-67.
[271] Lundqvist, M.; Stigler, J.; Elia, G.; Lynch, I.; Cedervall, T.; Dawson, K. A., Nanoparticle size and surface properties determine the protein corona with possible implications for biological impacts. *Proc. Natl. Acad. Sci. U.S.A.* **2008,** 105, (38), 14265-70.
[272] Weber, C.; Morsbach, S.; Landfester, K., Possibilities and Limitations of Different Separation Techniques for the Analysis of the Protein Corona. *Angew. Chem., Int. Ed. Engl.* **2019,** 58, (37), 12787-12794.
[273] Carrillo-Carrion, C.; Carril, M.; Parak, W. J., Techniques for the experimental investigation of the protein corona. *Curr. Opin. Biotechnol.* **2017,** 46, 106-113.
[274] Kari, O. K.; Ndika, J.; Parkkila, P.; Louna, A.; Lajunen, T.; Puustinen, A.; Viitala, T.; Alenius, H.; Urtti, A., In situ analysis of liposome hard and soft protein corona structure and composition in a single label-free workflow. *Nanoscale* **2020,** 12, (3), 1728-1741.
[275] Negwer, I.; Best, A.; Schinnerer, M.; Schäfer, O.; Capeloa, L.; Wagner, M.; Schmidt, M.; Mailänder, V.; Helm, M.; Barz, M.; Butt, H. J.; Koynov, K., Monitoring drug nanocarriers in human blood by near-infrared fluorescence correlation spectroscopy. *Nat. Commun.* **2018,** 9, (1), 5306.
[276] Carril, M.; Padro, D.; Del Pino, P.; Carrillo-Carrion, C.; Gallego, M.; Parak, W. J., In situ detection of the protein corona in complex environments. *Nat. Commun.* **2017,** 8, (1), 1542.
[277] Frost, R.; Langhammer, C.; Cedervall, T., Real-time in situ analysis of biocorona formation and evolution on silica nanoparticles in defined and complex biological environments. *Nanoscale* **2017,** 9, (10), 3620-3628.
[278] Shang, L.; Nienhaus, G. U., In Situ Characterization of Protein Adsorption onto Nanoparticles by Fluorescence Correlation Spectroscopy. *Acc. Chem. Res.* **2017,** 50, (2), 387-395.
[279] Lo Giudice, M. C.; Herda, L. M.; Polo, E.; Dawson, K. A., In situ characterization of nanoparticle biomolecular interactions in complex biological media by flow cytometry. *Nat. Commun.* **2016,** 7, 13475.
[280] Balog, S.; Rodriguez-Lorenzo, L.; Monnier, C. A.; Obiols-Rabasa, M.; Rothen-Rutishauser, B.; Schurtenberger, P.; Petri-Fink, A., Characterizing nanoparticles in complex biological media and physiological fluids with depolarized dynamic light scattering. *Nanoscale* **2015,** 7, (14), 5991-5997.
[281] Nuhn, L.; Gietzen, S.; Mohr, K.; Fischer, K.; Toh, K.; Miyata, K.; Matsumoto, Y.; Kataoka, K.; Schmidt, M.; Zentel, R., Aggregation behavior of cationic nanohydrogel particles in human blood serum. *Biomacromolecules* **2014,** 15, (4), 1526-33.
[282] Pitek, A. S.; O'Connell, D.; Mahon, E.; Monopoli, M. P.; Baldelli Bombelli, F.; Dawson, K. A., Transferrin coated nanoparticles: study of the bionano interface in human plasma. *PLoS One* **2012,** 7, (7), e40685-e40685.
[283] Rausch, K.; Reuter, A.; Fischer, K.; Schmidt, M., Evaluation of nanoparticle aggregation in human blood serum. *Biomacromolecules* **2010,** 11, (11), 2836-9.
[284] Buyens, K.; Lucas, B.; Raemdonck, K.; Braeckmans, K.; Vercammen, J.; Hendrix, J.; Engelborghs, Y.; De Smedt, S. C.; Sanders, N. N., A fast and sensitive method for measuring the integrity of siRNA-carrier complexes in full human serum. *J. Controlled Release* **2008,** 126, (1), 67-76.
[285] Monopoli, M. P.; Pitek, A. S.; Lynch, I.; Dawson, K. A., Formation and Characterization of the Nanoparticle–Protein Corona. In *Nanomaterial Interfaces in Biology: Methods and Protocols*, Bergese, P.; Hamad-Schifferli, K., Eds. Humana Press: Totowa, NJ, 2013; pp 137-155.
[286] Pozzi, D.; Caracciolo, G.; Digiacomo, L.; Colapicchioni, V.; Palchetti, S.; Capriotti, A. L.; Cavaliere, C.; Zenezini Chiozzi, R.; Puglisi, A.; Laganà, A., The biomolecular corona of nanoparticles in circulating biological media. *Nanoscale* **2015,** 7, (33), 13958-13966.

[287] Palchetti, S.; Colapicchioni, V.; Digiacomo, L.; Caracciolo, G.; Pozzi, D.; Capriotti, A. L.; La Barbera, G.; Laganà, A., The protein corona of circulating PEGylated liposomes. *Biochim. Biophys. Acta Biomembr.* **2016,** 1858, (2), 189-196.
[288] Simon, J.; Kuhn, G.; Fichter, M.; Gehring, S.; Landfester, K.; Mailänder, V., Unraveling the In Vivo Protein Corona. *Cells* **2021,** 10, (1), 132.
[289] Bai, X.; Wang, J.; Mu, Q.; Su, G., In vivo Protein Corona Formation: Characterizations, Effects on Engineered Nanoparticles' Biobehaviors, and Applications. *Front. Bioeng. Biotechnol.* **2021,** 9, (263), 646708.
[290] García-Álvarez, R.; Hadjidemetriou, M.; Sánchez-Iglesias, A.; Liz-Marzán, L. M.; Kostarelos, K., In vivo formation of protein corona on gold nanoparticles. The effect of their size and shape. *Nanoscale* **2018,** 10, (3), 1256-1264.
[291] Bertrand, N.; Grenier, P.; Mahmoudi, M.; Lima, E. M.; Appel, E. A.; Dormont, F.; Lim, J. M.; Karnik, R.; Langer, R.; Farokhzad, O. C., Mechanistic understanding of in vivo protein corona formation on polymeric nanoparticles and impact on pharmacokinetics. *Nat. Commun.* **2017,** 8, (1), 777.
[292] Corbo, C.; Molinaro, R.; Taraballi, F.; Toledano Furman, N. E.; Hartman, K. A.; Sherman, M. B.; De Rosa, E.; Kirui, D. K.; Salvatore, F.; Tasciotti, E., Unveiling the in Vivo Protein Corona of Circulating Leukocyte-like Carriers. *ACS Nano* **2017,** 11, (3), 3262-3273.
[293] Hadjidemetriou, M.; Al-Ahmady, Z.; Mazza, M.; Collins, R. F.; Dawson, K.; Kostarelos, K., In Vivo Biomolecule Corona around Blood-Circulating, Clinically Used and Antibody-Targeted Lipid Bilayer Nanoscale Vesicles. *ACS Nano* **2015,** 9, (8), 8142-56.
[294] Weber, C.; Simon, J.; Mailänder, V.; Morsbach, S.; Landfester, K., Preservation of the soft protein corona in distinct flow allows identification of weakly bound proteins. *Acta Biomater.* **2018,** 76, 217-224.
[295] Brusotti, G.; Calleri, E.; Colombo, R.; Massolini, G.; Rinaldi, F.; Temporini, C., Advances on Size Exclusion Chromatography and Applications on the Analysis of Protein Biopharmaceuticals and Protein Aggregates: A Mini Review. *Chromatographia* **2018,** 81, (1), 3-23.
[296] Sakulkhu, U.; Maurizi, L.; Mahmoudi, M.; Motazacker, M.; Vries, M.; Gramoun, A.; Ollivier Beuzelin, M.-G.; Vallée, J.-P.; Rezaee, F.; Hofmann, H., Ex situ evaluation of the composition of protein corona of intravenously injected superparamagnetic nanoparticles in rats. *Nanoscale* **2014,** 6, (19), 11439-11450.
[297] Sakulkhu, U.; Mahmoudi, M.; Maurizi, L.; Salaklang, J.; Hofmann, H., Protein corona composition of superparamagnetic iron oxide nanoparticles with various physico-chemical properties and coatings. *Sci. Rep.* **2014,** 4, 5020.
[298] Hu, Z.; Zhang, H.; Zhang, Y.; Wu, R.; Zou, H., Nanoparticle size matters in the formation of plasma protein coronas on Fe3O4 nanoparticles. *Colloids Surf., B* **2014,** 121, 354-61.
[299] Raesch, S. S.; Tenzer, S.; Storck, W.; Rurainski, A.; Selzer, D.; Ruge, C. A.; Perez-Gil, J.; Schaefer, U. F.; Lehr, C. M., Proteomic and Lipidomic Analysis of Nanoparticle Corona upon Contact with Lung Surfactant Reveals Differences in Protein, but Not Lipid Composition. *ACS Nano* **2015,** 9, (12), 11872-85.
[300] Bonvin, D.; Chiappe, D.; Moniatte, M.; Hofmann, H.; Mionić Ebersold, M., Methods of protein corona isolation for magnetic nanoparticles. *Analyst* **2017,** 142, (20), 3805-3815.
[301] Cursi, L.; Vercellino, S.; McCafferty, M. M.; Sheridan, E.; Petseva, V.; Adumeau, L.; Dawson, K. A., Multifunctional superparamagnetic nanoparticles with a fluorescent silica shell for the in vitro study of bio-nano interactions at the subcellular scale. *Nanoscale* **2021,** 13, 16324-16338.
[302] Winzen, S.; Schoettler, S.; Baier, G.; Rosenauer, C.; Mailaender, V.; Landfester, K.; Mohr, K., Complementary analysis of the hard and soft protein corona: sample preparation critically effects corona composition. *Nanoscale* **2015,** 7, (7), 2992-3001.
[303] Ding, Z.; Ma, H.; Chen, Y., Interaction of graphene oxide with human serum albumin and its mechanism. *RSC Adv.* **2014,** 4, (98), 55290-55295.

[304] Fleischer, C. C.; Payne, C. K., Secondary structure of corona proteins determines the cell surface receptors used by nanoparticles. *J. Phys. Chem. B* **2014,** 118, (49), 14017-26.
[305] Lindman, S.; Lynch, I.; Thulin, E.; Nilsson, H.; Dawson, K. A.; Linse, S., Systematic investigation of the thermodynamics of HSA adsorption to N-iso-propylacrylamide/N-tert-butylacrylamide copolymer nanoparticles. Effects of particle size and hydrophobicity. *Nano Lett.* **2007,** 7, (4), 914-20.
[306] de Puig, H.; Federici, S.; Baxamusa, S. H.; Bergese, P.; Hamad-Schifferli, K., Quantifying the nanomachinery of the nanoparticle-biomolecule interface. *Small* **2011,** 7, (17), 2477-84.
[307] Chong, Y.; Ge, C.; Yang, Z.; Garate, J. A.; Gu, Z.; Weber, J. K.; Liu, J.; Zhou, R., Reduced Cytotoxicity of Graphene Nanosheets Mediated by Blood-Protein Coating. *ACS Nano* **2015,** 9, (6), 5713-24.
[308] Kari, O. K.; Rojalin, T.; Salmaso, S.; Barattin, M.; Jarva, H.; Meri, S.; Yliperttula, M.; Viitala, T.; Urtti, A., Multi-parametric surface plasmon resonance platform for studying liposome-serum interactions and protein corona formation. *Drug Delivery Transl. Res.* **2017,** 7, (2), 228-240.
[309] Oh, Y. J.; Koehler, M.; Lee, Y.; Mishra, S.; Park, J. W.; Hinterdorfer, P., Ultra-Sensitive and Label-Free Probing of Binding Affinity Using Recognition Imaging. *Nano Lett.* **2019,** 19, (1), 612-617.
[310] Röcker, C.; Pötzl, M.; Zhang, F.; Parak, W. J.; Nienhaus, G. U., A quantitative fluorescence study of protein monolayer formation on colloidal nanoparticles. *Nat. Nanotechnol.* **2009,** 4, (9), 577-80.
[311] Boulos, S. P.; Davis, T. A.; Yang, J. A.; Lohse, S. E.; Alkilany, A. M.; Holland, L. A.; Murphy, C. J., Nanoparticle-protein interactions: a thermodynamic and kinetic study of the adsorption of bovine serum albumin to gold nanoparticle surfaces. *Langmuir* **2013,** 29, (48), 14984-96.
[312] Gaus, H. J.; Gupta, R.; Chappell, A. E.; Østergaard, M. E.; Swayze, E. E.; Seth, P. P., Characterization of the interactions of chemically-modified therapeutic nucleic acids with plasma proteins using a fluorescence polarization assay. *Nucleic Acids Res.* **2019,** 47, (3), 1110-1122.
[313] Prakash, T. P.; Mullick, A. E.; Lee, R. G.; Yu, J.; Yeh, S. T.; Low, A.; Chappell, A. E.; Østergaard, M. E.; Murray, S.; Gaus, H. J.; Swayze, E. E.; Seth, P. P., Fatty acid conjugation enhances potency of antisense oligonucleotides in muscle. *Nucleic Acids Res.* **2019,** 47, (12), 6029-6044.
[314] Park, S. J., Protein-Nanoparticle Interaction: Corona Formation and Conformational Changes in Proteins on Nanoparticles. *Int. J. Nanomed.* **2020,** 15, 5783-5802.
[315] Wang, J.; Jensen, U. B.; Jensen, G. V.; Shipovskov, S.; Balakrishnan, V. S.; Otzen, D.; Pedersen, J. S.; Besenbacher, F.; Sutherland, D. S., Soft interactions at nanoparticles alter protein function and conformation in a size dependent manner. *Nano Lett.* **2011,** 11, (11), 4985-91.
[316] Greenfield, N. J., Using circular dichroism spectra to estimate protein secondary structure. *Nat. Protoc.* **2006,** 1, (6), 2876-2890.
[317] Sutherland, J. C., Circular Dichroism Using Synchrotron Radiation. In *Circular Dichroism and the Conformational Analysis of Biomolecules*, Fasman, G. D., Ed. Springer US: Boston, MA, 1996; pp 599-633.
[318] Wallace, B. A., Conformational changes by synchrotron radiation circular dichroism spectroscopy. *Nat. Struct. Biol.* **2000,** 7, (9), 708-709.
[319] Sanchez-Guzman, D.; Giraudon-Colas, G.; Marichal, L.; Boulard, Y.; Wien, F.; Degrouard, J.; Baeza-Squiban, A.; Pin, S.; Renault, J. P.; Devineau, S., In Situ Analysis of Weakly Bound Proteins Reveals Molecular Basis of Soft Corona Formation. *ACS Nano* **2020,** 14, (7), 9073-9088.
[320] Yang, H.; Yang, S.; Kong, J.; Dong, A.; Yu, S., Obtaining information about protein secondary structures in aqueous solution using Fourier transform IR spectroscopy. *Nat. Protoc.* **2015,** 10, (3), 382-96.
[321] Wang, M.; Fu, C.; Liu, X.; Lin, Z.; Yang, N.; Yu, S., Probing the mechanism of plasma protein adsorption on Au and Ag nanoparticles with FT-IR spectroscopy. *Nanoscale* **2015,** 7, (37), 15191-6.

[322] Shashilov, V. A.; Sikirzhytski, V.; Popova, L. A.; Lednev, I. K., Quantitative methods for structural characterization of proteins based on deep UV resonance Raman spectroscopy. *Methods* **2010,** 52, (1), 23-37.
[323] Zhang, D.; Neumann, O.; Wang, H.; Yuwono, V. M.; Barhoumi, A.; Perham, M.; Hartgerink, J. D.; Wittung-Stafshede, P.; Halas, N. J., Gold nanoparticles can induce the formation of protein-based aggregates at physiological pH. *Nano Lett.* **2009,** 9, (2), 666-71.
[324] Assfalg, M.; Ragona, L.; Pagano, K.; D'Onofrio, M.; Zanzoni, S.; Tomaselli, S.; Molinari, H., The study of transient protein-nanoparticle interactions by solution NMR spectroscopy. *Biochim. Biophys. Acta. Proteins Proteomics* **2016,** 1864, (1), 102-14.
[325] Deka, J.; Paul, A.; Chattopadhyay, A., Estimating conformation content of a protein using citrate-stabilized Au nanoparticles. *Nanoscale* **2010,** 2, (8), 1405-12.
[326] Xu, L.; Dong, S.; Hao, J.; Cui, J.; Hoffmann, H., Surfactant-Modified Ultrafine Gold Nanoparticles with Magnetic Responsiveness for Reversible Convergence and Release of Biomacromolecules. *Langmuir* **2017,** 33, (12), 3047-3055.
[327] Casalini, T.; Limongelli, V.; Schmutz, M.; Som, C.; Jordan, O.; Wick, P.; Borchard, G.; Perale, G., Molecular Modeling for Nanomaterial-Biology Interactions: Opportunities, Challenges, and Perspectives. *Front. Bioeng. Biotechnol.* **2019,** 7, 268.
[328] Kharazian, B.; Hadipour, N. L.; Ejtehadi, M. R., Understanding the nanoparticle-protein corona complexes using computational and experimental methods. *Int. J. Biochem. Cell Biol.* **2016,** 75, 162-74.
[329] Mahmoudi, M.; Lynch, I.; Ejtehadi, M. R.; Monopoli, M. P.; Bombelli, F. B.; Laurent, S., Protein-nanoparticle interactions: opportunities and challenges. *Chem. Rev.* **2011,** 111, (9), 5610-37.
[330] Tavanti, F.; Pedone, A.; Menziani, M. C., Multiscale Molecular Dynamics Simulation of Multiple Protein Adsorption on Gold Nanoparticles. *Int. J. Mol. Sci.* **2019,** 20, (14), 3539.
[331] Brancolini, G.; Tozzini, V., Multiscale modeling of proteins interaction with functionalized nanoparticles. *Curr. Opin. Colloid Interface Sci.* **2019,** 41, 66-73.
[332] Vilanova, O.; Mittag, J. J.; Kelly, P. M.; Milani, S.; Dawson, K. A.; Rädler, J. O.; Franzese, G., Understanding the Kinetics of Protein-Nanoparticle Corona Formation. *ACS Nano* **2016,** 10, (12), 10842-10850.
[333] Settanni, G.; Zhou, J.; Suo, T.; Schöttler, S.; Landfester, K.; Schmid, F.; Mailänder, V., Protein corona composition of poly(ethylene glycol)- and poly(phosphoester)-coated nanoparticles correlates strongly with the amino acid composition of the protein surface. *Nanoscale* **2017,** 9, (6), 2138-2144.
[334] Settanni, G.; Zhou, J.; Schmid, F., Interactions between proteins and poly(ethylene-glycol) investigated using molecular dynamics simulations. *J. Phys: Conf. Ser.* **2017,** 921, 012002.
[335] Settanni, G.; Schäfer, T.; Muhl, C.; Barz, M.; Schmid, F., Poly-sarcosine and Poly(Ethylene-Glycol) Interactions with Proteins Investigated Using Molecular Dynamics Simulations. *Comput. Struct. Biotechnol. J.* **2018,** 16, 543-550.
[336] Wang, L.; Li, J.; Pan, J.; Jiang, X.; Ji, Y.; Li, Y.; Qu, Y.; Zhao, Y.; Wu, X.; Chen, C., Revealing the binding structure of the protein corona on gold nanorods using synchrotron radiation-based techniques: understanding the reduced damage in cell membranes. *J. Am. Chem. Soc.* **2013,** 135, (46), 17359-68.
[337] Pino, P. d.; Pelaz, B.; Zhang, Q.; Maffre, P.; Nienhaus, G. U.; Parak, W. J., Protein corona formation around nanoparticles – from the past to the future. *Mater. Horiz.* **2014,** 1, (3), 301-313.
[338] Liu, R.; Jiang, W.; Walkey, C. D.; Chan, W. C.; Cohen, Y., Prediction of nanoparticles-cell association based on corona proteins and physicochemical properties. *Nanoscale* **2015,** 7, (21), 9664-75.
[339] Bigdeli, A.; Palchetti, S.; Pozzi, D.; Hormozi-Nezhad, M. R.; Baldelli Bombelli, F.; Caracciolo, G.; Mahmoudi, M., Exploring Cellular Interactions of Liposomes Using Protein Corona Fingerprints and Physicochemical Properties. *ACS Nano* **2016,** 10, (3), 3723-37.

[340] Xia, X. R.; Monteiro-Riviere, N. A.; Riviere, J. E., An index for characterization of nanomaterials in biological systems. *Nat. Nanotechnol.* **2010,** 5, (9), 671-5.
[341] Docter, D.; Distler, U.; Storck, W.; Kuharev, J.; Wünsch, D.; Hahlbrock, A.; Knauer, S. K.; Tenzer, S.; Stauber, R. H., Quantitative profiling of the protein coronas that form around nanoparticles. *Nat. Protoc.* **2014,** 9, (9), 2030-44.
[342] Svasti, J.; Panijpan, B., SDS-polyacrylamide gel electrophoresis. A simple explanation of why it works. *J. Chem. Educ.* **1977,** 54, (9), 560.
[343] Gallagher, S. R., One-Dimensional SDS Gel Electrophoresis of Proteins. *Curr. Protoc. Protein Sci.* **2012,** 68, (1), 10.1.1-10.1.44.
[344] Harper, S.; W. Speicher, D., Comparing Complex Protein Samples Using Two-Dimensional Polyacrylamide Gels. *Curr. Protoc. Protein Sci.* **2019,** 96, (1), e87.
[345] Beer, L. A.; Speicher, D. W., Protein Detection in Gels Using Fixation. *Curr. Protoc. Protein Sci.* **2018,** 91, (1), 10.5.1-10.5.20.
[346] Rosenfeld, J.; Capdevielle, J.; Guillemot, J. C.; Ferrara, P., In-gel digestion of proteins for internal sequence analysis after one- or two-dimensional gel electrophoresis. *Anal. Biochem.* **1992,** 203, (1), 173-179.
[347] Jeno, P.; Mini, T.; Moes, S.; Hintermann, E.; Horst, M., Internal Sequences from Proteins Digested in Polyacrylamide Gels. *Anal. Biochem.* **1995,** 224, (1), 75-82.
[348] Shevchenko, A.; Wilm, M.; Vorm, O.; Mann, M., Mass spectrometric sequencing of proteins silver-stained polyacrylamide gels. *Anal. Chem.* **1996,** 68, (5), 850-8.
[349] Wang, H.; Shang, L.; Maffre, P.; Hohmann, S.; Kirschhöfer, F.; Brenner-Weiß, G.; Nienhaus, G. U., The Nature of a Hard Protein Corona Forming on Quantum Dots Exposed to Human Blood Serum. *Small* **2016,** 12, (42), 5836-5844.
[350] Cedervall, T.; Lynch, I.; Foy, M.; Berggård, T.; Donnelly, S. C.; Cagney, G.; Linse, S.; Dawson, K. A., Detailed identification of plasma proteins adsorbed on copolymer nanoparticles. *Angew. Chem., Int. Ed. Engl.* **2007,** 46, (30), 5754-6.
[351] Gaspari, M.; Cuda, G., Nano LC-MS/MS: a robust setup for proteomic analysis. *Methods Mol. Biol.* **2011,** 790, 115-26.
[352] Sielaff, M.; Kuharev, J.; Bohn, T.; Hahlbrock, J.; Bopp, T.; Tenzer, S.; Distler, U., Evaluation of FASP, SP3, and iST Protocols for Proteomic Sample Preparation in the Low Microgram Range. *J. Proteome Res.* **2017,** 16, (11), 4060-4072.
[353] Eng, J. K.; McCormack, A. L.; Yates, J. R., An approach to correlate tandem mass spectral data of peptides with amino acid sequences in a protein database. *J. Am. Soc. Mass Spectrom.* **1994,** 5, (11), 976-89.
[354] Perkins, D. N.; Pappin, D. J.; Creasy, D. M.; Cottrell, J. S., Probability-based protein identification by searching sequence databases using mass spectrometry data. *Electrophoresis* **1999,** 20, (18), 3551-67.
[355] Searle, B. C., Scaffold: A bioinformatic tool for validating MS/MS-based proteomic studies. *Proteomics* **2010,** 10, (6), 1265-1269.
[356] Zhang, R.; Barton, A.; Brittenden, J.; Huang, J. T.-J.; Crowther, D., Evaluation for computational platforms of LC-MS based label-free quantitative proteomics - A global view. *J. Proteomics Bioinf.* **2010,** 3, (9), 260-265.
[357] Pozzi, D.; Caracciolo, G.; Capriotti, A. L.; Cavaliere, C.; Piovesana, S.; Colapicchioni, V.; Palchetti, S.; Riccioli, A.; Laganà, A., A proteomics-based methodology to investigate the protein corona effect for targeted drug delivery. *Mol. BioSyst.* **2014,** 10, (11), 2815-9.
[358] Silva, J. C.; Gorenstein, M. V.; Li, G. Z.; Vissers, J. P.; Geromanos, S. J., Absolute quantification of proteins by LCMSE: a virtue of parallel MS acquisition. *Mol. Cell. Proteomics* **2006,** 5, (1), 144-56.
[359] Brown, R. E.; Jarvis, K. L.; Hyland, K. J., Protein measurement using bicinchoninic acid: elimination of interfering substances. *Anal. Biochem.* **1989,** 180, (1), 136-139.

[360] Smith, P. K.; Krohn, R. I.; Hermanson, G. T.; Mallia, A. K.; Gartner, F. H.; Provenzano, M. D.; Fujimoto, E. K.; Goeke, N. M.; Olson, B. J.; Klenk, D. C., Measurement of protein using bicinchoninic acid. *Anal. Biochem.* **1985,** 150, (1), 76-85.
[361] Wiechelman, K. J.; Braun, R. D.; Fitzpatrick, J. D., Investigation of the bicinchoninic acid protein assay: Identification of the groups responsible for color formation. *Anal. Biochem.* **1988,** 175, (1), 231-237.
[362] Kessler, R. J.; Fanestil, D. D., Interference by lipids in the determination of protein using bicinchoninic acid. *Anal. Biochem.* **1986,** 159, (1), 138-142.
[363] Kaufman, E. D.; Belyea, J.; Johnson, M. C.; Nicholson, Z. M.; Ricks, J. L.; Shah, P. K.; Bayless, M.; Pettersson, T.; Feldotö, Z.; Blomberg, E.; Claesson, P.; Franzen, S., Probing protein adsorption onto mercaptoundecanoic acid stabilized gold nanoparticles and surfaces by quartz crystal microbalance and zeta-potential measurements. *Langmuir* **2007,** 23, (11), 6053-62.
[364] Brewer, S. H.; Glomm, W. R.; Johnson, M. C.; Knag, M. K.; Franzen, S., Probing BSA binding to citrate-coated gold nanoparticles and surfaces. *Langmuir* **2005,** 21, (20), 9303-7.
[365] Dixon, M. C., Quartz crystal microbalance with dissipation monitoring: enabling real-time characterization of biological materials and their interactions. *J. Biomol. Tech.* **2008,** 19, (3), 151-8.
[366] Chen, Q.; Xu, S.; Liu, Q.; Masliyah, J.; Xu, Z., QCM-D study of nanoparticle interactions. *Adv. Colloid Interface Sci.* **2016,** 233, 94-114.
[367] Di Silvio, D.; Maccarini, M.; Parker, R.; Mackie, A.; Fragneto, G.; Baldelli Bombelli, F., The effect of the protein corona on the interaction between nanoparticles and lipid bilayers. *J. Colloid Interface Sci.* **2017,** 504, 741-750.
[368] Wang, X.; Wang, M.; Lei, R.; Zhu, S. F.; Zhao, Y.; Chen, C., Chiral Surface of Nanoparticles Determines the Orientation of Adsorbed Transferrin and Its Interaction with Receptors. *ACS Nano* **2017,** 11, (5), 4606-4616.
[369] Wang, Q.; Lim, M.; Liu, X.; Wang, Z.; Chen, K. L., Influence of Solution Chemistry and Soft Protein Coronas on the Interactions of Silver Nanoparticles with Model Biological Membranes. *Environ. Sci. Technol.* **2016,** 50, (5), 2301-2309.
[370] Sebastiani, F.; Yanez Arteta, M.; Lindfors, L.; Cárdenas, M., Screening of the binding affinity of serum proteins to lipid nanoparticles in a cell free environment. *J. Colloid Interface Sci.* **2021**.
[371] Matczuk, M.; Legat, J.; Shtykov, S. N.; Jarosz, M.; Timerbaev, A. R., Characterization of the protein corona of gold nanoparticles by an advanced treatment of CE-ICP-MS data. *Electrophoresis* **2016,** 37, (15-16), 2257-2259.
[372] Fernández-Iglesias, N.; Bettmer, J., Complementary mass spectrometric techniques for the quantification of the protein corona: a case study on gold nanoparticles and human serum proteins. *Nanoscale* **2015,** 7, (34), 14324-31.
[373] Costa-Fernández, J. M.; Menéndez-Miranda, M.; Bouzas-Ramos, D.; Encinar, J. R.; Sanz-Medel, A., Mass spectrometry for the characterization and quantification of engineered inorganic nanoparticles. *TrAC Trends Anal. Chem.* **2016,** 84, 139-148.
[374] Eslahian, K. A.; Lang, T.; Bantz, C.; Keller, R.; Sperling, R.; Docter, D.; Stauber, R.; Maskos, M., Characterization of Nanoparticles Under Physiological Conditions. In *Measuring Biological Impacts of Nanomaterials*, Wegener, J., Ed. Springer International Publishing: Cham, 2016; pp 1-29.
[375] Maskos, M.; Stauber, R. H., Characterization of nanoparticles in biological environments. In *Comprehensive Biomaterials*, Ducheyne, P.; Healy, K. E.; Hutmacher, D. W.; Grainger, D. W.; Kirkpatrick, C. J., Eds. Elsevier: 2011; Vol. 3, pp 329-339.
[376] Monopoli, M. P.; Walczyk, D.; Campbell, A.; Elia, G.; Lynch, I.; Bombelli, F. B.; Dawson, K. A., Physical-chemical aspects of protein corona: relevance to in vitro and in vivo biological impacts of nanoparticles. *J. Am. Chem. Soc.* **2011,** 133, (8), 2525-34.

[377] Grun, M. K.; Suberi, A.; Shin, K.; Lee, T.; Gomerdinger, V.; Moscato, Z. M.; Piotrowski-Daspit, A. S.; Saltzman, W. M., PEGylation of poly(amine-co-ester) polyplexes for tunable gene delivery. *Biomaterials* **2021,** 272, 120780.
[378] Koshkina, O.; Lang, T.; Thiermann, R.; Docter, D.; Stauber, R. H.; Secker, C.; Schlaad, H.; Weidner, S.; Mohr, B.; Maskos, M.; Bertin, A., Temperature-Triggered Protein Adsorption on Polymer-Coated Nanoparticles in Serum. *Langmuir* **2015,** 31, (32), 8873-8881.
[379] Di Silvio, D.; Rigby, N.; Bajka, B.; Mayes, A.; Mackie, A.; Baldelli Bombelli, F., Technical tip: high-resolution isolation of nanoparticle-protein corona complexes from physiological fluids. *Nanoscale* **2015,** 7, (28), 11980-90.
[380] Bantz, C.; Koshkina, O.; Lang, T.; Galla, H.-J.; Kirkpatrick, C. J.; Stauber, R. H.; Maskos, M., The surface properties of nanoparticles determine the agglomeration state and the size of the particles under physiological conditions. *Beilstein J. Nanotechnol.* **2014,** 5, 1774-1786.
[381] Orts-Gil, G.; Natte, K.; Thiermann, R.; Girod, M.; Rades, S.; Kalbe, H.; Thünemann, A. F.; Maskos, M.; Österle, W., On the role of surface composition and curvature on biointerface formation and colloidal stability of nanoparticles in a protein-rich model system. *Colloids Surf., B* **2013,** 108, 110-119.
[382] Bello Roufaï, M.; Midoux, P., Histidylated polylysine as DNA vector: elevation of the imidazole protonation and reduced cellular uptake without change in the polyfection efficiency of serum stabilized negative polyplexes. *Bioconjugate Chem.* **2001,** 12, (1), 92-9.
[383] Sebastiani, F.; Yanez Arteta, M.; Lerche, M.; Porcar, L.; Lang, C.; Bragg, R. A.; Elmore, C. S.; Krishnamurthy, V. R.; Russell, R. A.; Darwish, T.; Pichler, H.; Waldie, S.; Moulin, M.; Haertlein, M.; Forsyth, V. T.; Lindfors, L.; Cárdenas, M., Apolipoprotein E Binding Drives Structural and Compositional Rearrangement of mRNA-Containing Lipid Nanoparticles. *ACS Nano* **2021,** 15, (4), 6709-6722.
[384] Waldie, S.; Sebastiani, F.; Moulin, M.; Del Giudice, R.; Paracini, N.; Roosen-Runge, F.; Gerelli, Y.; Prevost, S.; Voss, J. C.; Darwish, T. A.; Yepuri, N.; Pichler, H.; Maric, S.; Forsyth, V. T.; Haertlein, M.; Cárdenas, M., ApoE and ApoE Nascent-Like HDL Particles at Model Cellular Membranes: Effect of Protein Isoform and Membrane Composition. *Front. Chem.* **2021,** 9, (249), 630152.
[385] Marichal, L.; Giraudon-Colas, G.; Cousin, F.; Thill, A.; Labarre, J.; Boulard, Y.; Aude, J. C.; Pin, S.; Renault, J. P., Protein-Nanoparticle Interactions: What Are the Protein-Corona Thickness and Organization? *Langmuir* **2019,** 35, (33), 10831-10837.
[386] Meissner, J.; Wu, Y.; Jestin, J.; Shelton, W. A.; Findenegg, G. H.; Bharti, B., pH-Induced reorientation of cytochrome c on silica nanoparticles. *Soft Matter* **2019,** 15, (3), 350-354.
[387] Klapper, Y.; Maffre, P.; Shang, L.; Ekdahl, K. N.; Nilsson, B.; Hettler, S.; Dries, M.; Gerthsen, D.; Nienhaus, G. U., Low affinity binding of plasma proteins to lipid-coated quantum dots as observed by in situ fluorescence correlation spectroscopy. *Nanoscale* **2015,** 7, (22), 9980-9984.
[388] Maffre, P.; Brandholt, S.; Nienhaus, K.; Shang, L.; Parak, W. J.; Nienhaus, G. U., Effects of surface functionalization on the adsorption of human serum albumin onto nanoparticles – a fluorescence correlation spectroscopy study. *Beilstein J. Nanotechnol.* **2014,** 5, 2036-2047.
[389] Milani, S.; Bombelli, F. B.; Pitek, A. S.; Dawson, K. A.; Rädler, J., Reversible versus irreversible binding of transferrin to polystyrene nanoparticles: soft and hard corona. *ACS Nano* **2012,** 6, (3), 2532-41.
[390] Kittler, S.; Greulich, C.; Gebauer, J.; Diendorf, J.; Treuel, L.; Ruiz, L.; Gonzalez-Calbet, J.; Vallet-Regi, M.; Zellner, R.; Köller, M., The influence of proteins on the dispersability and cell-biological activity of silver nanoparticles. *J. Mater. Chem.* **2010,** 20, (3), 512-518.
[391] Sheibani, S.; Basu, K.; Farnudi, A.; Ashkarran, A.; Ichikawa, M.; Presley, J. F.; Bui, K. H.; Ejtehadi, M. R.; Vali, H.; Mahmoudi, M., Nanoscale characterization of the biomolecular corona by cryo-electron microscopy, cryo-electron tomography, and image simulation. *Nat. Commun.* **2021,** 12, (1), 573.

[392] Klepac, D.; Kostková, H.; Petrova, S.; Chytil, P.; Etrych, T.; Kereïche, S.; Raška, I.; Weitz, D. A.; Filippov, S. K., Interaction of spin-labeled HPMA-based nanoparticles with human blood plasma proteins - the introduction of protein-corona-free polymer nanomedicine. *Nanoscale* **2018,** 10, (13), 6194-6204.
[393] Ritz, S.; Schöttler, S.; Kotman, N.; Baier, G.; Musyanovych, A.; Kuharev, J.; Landfester, K.; Schild, H.; Jahn, O.; Tenzer, S.; Mailänder, V., Protein corona of nanoparticles: distinct proteins regulate the cellular uptake. *Biomacromolecules* **2015,** 16, (4), 1311-21.
[394] Schäffler, M.; Semmler-Behnke, M.; Sarioglu, H.; Takenaka, S.; Wenk, A.; Schleh, C.; Hauck, S. M.; Johnston, B. D.; Kreyling, W. G., Serum protein identification and quantification of the corona of 5, 15 and 80 nm gold nanoparticles. *Nanotechnology* **2013,** 24, (26), 265103.
[395] Mirshafiee, V.; Kim, R.; Park, S.; Mahmoudi, M.; Kraft, M. L., Impact of protein pre-coating on the protein corona composition and nanoparticle cellular uptake. *Biomaterials* **2016,** 75, 295-304.
[396] Schaefer, J.; Schulze, C.; Marxer, E. E.; Schaefer, U. F.; Wohlleben, W.; Bakowsky, U.; Lehr, C. M., Atomic force microscopy and analytical ultracentrifugation for probing nanomaterial protein interactions. *ACS Nano* **2012,** 6, (6), 4603-14.
[397] Dobrovolskaia, M. A.; Patri, A. K.; Zheng, J.; Clogston, J. D.; Ayub, N.; Aggarwal, P.; Neun, B. W.; Hall, J. B.; McNeil, S. E., Interaction of colloidal gold nanoparticles with human blood: effects on particle size and analysis of plasma protein binding profiles. *Nanomedicine* **2009,** 5, (2), 106-117.
[398] Ashby, J.; Schachermeyer, S.; Pan, S.; Zhong, W., Dissociation-based screening of nanoparticle-protein interaction via flow field-flow fractionation. *Anal. Chem.* **2013,** 85, (15), 7494-501.
[399] Osborn, M. F.; Coles, A. H.; Biscans, A.; Haraszti, R. A.; Roux, L.; Davis, S.; Ly, S.; Echeverria, D.; Hassler, M. R.; Godinho, B.; Nikan, M.; Khvorova, A., Hydrophobicity drives the systemic distribution of lipid-conjugated siRNAs via lipid transport pathways. *Nucleic Acids Res.* **2019,** 47, (3), 1070-1081.
[400] Perez-Potti, A.; Lopez, H.; Pelaz, B.; Abdelmonem, A.; Soliman, M. G.; Schoen, I.; Kelly, P. M.; Dawson, K. A.; Parak, W. J.; Krpetic, Z.; Monopoli, M. P., In depth characterisation of the biomolecular coronas of polymer coated inorganic nanoparticles with differential centrifugal sedimentation. *Sci. Rep.* **2021,** 11, (1), 6443.
[401] Blundell, E.; Healey, M. J.; Holton, E.; Sivakumaran, M.; Manstana, S.; Platt, M., Characterisation of the protein corona using tunable resistive pulse sensing: determining the change and distribution of a particle's surface charge. *Anal. Bioanal. Chem.* **2016,** 408, (21), 5757-5768.
[402] Sikora, A.; Shard, A. G.; Minelli, C., Size and ζ-Potential Measurement of Silica Nanoparticles in Serum Using Tunable Resistive Pulse Sensing. *Langmuir* **2016,** 32, (9), 2216-2224.
[403] Sikora, A.; Bartczak, D.; Geißler, D.; Kestens, V.; Roebben, G.; Ramaye, Y.; Varga, Z.; Palmai, M.; Shard, A. G.; Goenaga-Infante, H.; Minelli, C., A systematic comparison of different techniques to determine the zeta potential of silica nanoparticles in biological medium. *Anal. Methods* **2015,** 7, (23), 9835-9843.
[404] Pal, A. K.; Aalaei, I.; Gadde, S.; Gaines, P.; Schmidt, D.; Demokritou, P.; Bello, D., High Resolution Characterization of Engineered Nanomaterial Dispersions in Complex Media Using Tunable Resistive Pulse Sensing Technology. *ACS Nano* **2014,** 8, (9), 9003-9015.
[405] Eslahian, K. A.; Majee, A.; Maskos, M.; Würger, A., Specific salt effects on thermophoresis of charged colloids. *Soft Matter* **2014,** 10, (12), 1931-1936.
[406] Di Cola, E.; Grillo, I.; Ristori, S., Small Angle X-ray and Neutron Scattering: Powerful Tools for Studying the Structure of Drug-Loaded Liposomes. *Pharmaceutics* **2016,** 8, (2), 10.
[407] Mast, M.-P.; Modh, H.; Champanhac, C.; Wang, J.-W.; Storm, G.; Krämer, J.; Mailänder, V.; Pastorin, G.; Wacker, M. G., Nanomedicine at the crossroads – a quick guide for ivivc. *Adv. Drug Delivery Rev.* **2021**, 113829.

[408] Matsuura, Y.; Nakamura, A.; Kato, H., Nanoparticle tracking velocimetry by observing light scattering from individual particles. *Sens. Actuators, B* **2018,** 256, 1078-1085.
[409] Maas, H.; Gruen, A.; Papantoniou, D., Particle tracking velocimetry in three-dimensional flows. *Exp. Fluids* **1993,** 15, (2), 133-146.
[410] Subramaniam, S.; Earl, L. A.; Falconieri, V.; Milne, J. L.; Egelman, E. H., Resolution advances in cryo-EM enable application to drug discovery. *Curr. Opin. Struct. Biol.* **2016,** 41, 194-202.
[411] Milne, J. L.; Borgnia, M. J.; Bartesaghi, A.; Tran, E. E.; Earl, L. A.; Schauder, D. M.; Lengyel, J.; Pierson, J.; Patwardhan, A.; Subramaniam, S., Cryo-electron microscopy--a primer for the non-microscopist. *FEBS J.* **2013,** 280, (1), 28-45.
[412] Mahmoudi, M., The need for robust characterization of nanomaterials for nanomedicine applications. *Nat. Commun.* **2021,** 12, (1), 5246.
[413] Giessibl, F. J., Advances in atomic force microscopy. *Rev. Mod. Phys.* **2003,** 75, (3), 949-983.
[414] Fraunhofer, W.; Winter, G., The use of asymmetrical flow field-flow fractionation in pharmaceutics and biopharmaceutics. *Eur. J. Pharm. Biopharm.* **2004,** 58, (2), 369-83.
[415] Planken, K. L.; Cölfen, H., Analytical ultracentrifugation of colloids. *Nanoscale* **2010,** 2, (10), 1849-69.
[416] Anderson, W.; Kozak, D.; Coleman, V. A.; Jämting, Å. K.; Trau, M., A comparative study of submicron particle sizing platforms: Accuracy, precision and resolution analysis of polydisperse particle size distributions. *J. Colloid Interface Sci.* **2013,** 405, 322-330.
[417] Kozak, D.; Anderson, W.; Vogel, R.; Trau, M., Advances in resistive pulse sensors: Devices bridging the void between molecular and microscopic detection. *Nano Today* **2011,** 6, (5), 531-545.
[418] Schärtl, W., *Light Scattering from Polymer Solutions and Nanoparticle Dispersions*. 1 ed.; Springer, Berlin, Heidelberg: Springer-Verlag Berlin Heidelberg, 2007.
[419] Meyer, A.; Dierks, K.; Betzel, C., Depolarized Dynamic Light Scattering a method to analyse Particle Shape and Size. *Acta Crystallogr. Sect. A* **2014,** 70, (a1), C1749.
[420] Delgado, Á. V.; González-Caballero, F.; Hunter, R.; Koopal, L.; Lyklema, J., Measurement and interpretation of electrokinetic phenomena. *J. Colloid Interface Sci.* **2007,** 309, (2), 194-224.
[421] Hunter, R. J., *Introduction to modern colloid science*. Oxford University Press: 1993.
[422] Varenne, F.; Botton, J.; Merlet, C.; Vachon, J.-J.; Geiger, S.; Infante, I. C.; Chehimi, M. M.; Vauthier, C., Standardization and validation of a protocol of zeta potential measurements by electrophoretic light scattering for nanomaterial characterization. *Colloids Surf., A* **2015,** 486, 218-231.
[423] Guinier, A.; Fournet, G.; Yudowitch, K. L., *Small-angle scattering of X-rays*. John Wiley & Sons Inc.: 1955.
[424] Glatter, O., A new method for the evaluation of small-angle scattering data. *J. Appl. Crystallogr.* **1977,** 10, (5), 415-421.
[425] Wang, H.; Lin, Y.; Nienhaus, K.; Nienhaus, G. U., The protein corona on nanoparticles as viewed from a nanoparticle-sizing perspective. *Wiley Interdiscip. Rev. Nanomed. Nanobiotechnol.* **2018,** 10, (4), e1500.
[426] Pennycook, S. J.; David, B.; Williams, C. B., Transmission electron microscopy: a textbook for materials science. *Microsc. Microanal.* **2010,** 16, (1), 111.
[427] Wolfram, J.; Suri, K.; Yang, Y.; Shen, J.; Celia, C.; Fresta, M.; Zhao, Y.; Shen, H.; Ferrari, M., Shrinkage of pegylated and non-pegylated liposomes in serum. *Colloids Surf., B* **2014,** 114, 294-300.
[428] Smith, K.; Oatley, C., The scanning electron microscope and its fields of application. *Br. J. Appl. Phys.* **1955,** 6, (11), 391.
[429] Schimpf, M. E.; Caldwell, K.; Giddings, J. C., *Field-flow fractionation handbook*. John Wiley & Sons: 2000.

[430] Giddings, J. C., Field-flow fractionation: analysis of macromolecular, colloidal, and particulate materials. *Science* **1993,** 260, (5113), 1456-65.
[431] Eslahian, K. A.; Maskos, M., Thermal Field-Flow Fractionation of Colloidal Suspensions. In *Encyclopedia of Analytical Chemistry*, Meyers, R. A., Ed. John Wiley & Sons, Ltd: 2015; pp 1-27.
[432] Lang, T.; Eslahian, K. A.; Maskos, M., Ion Effects in Field-Flow Fractionation of Aqueous Colloidal Polystyrene. *Macromol. Chem. Phys.* **2012,** 213, (22), 2353-2361.
[433] Liu, G.; Giddings, J., Separation of particles in aqueous suspensions by thermal field-flow fractionation. Measurement of thermal diffusion coefficients. *Chromatographia* **1992,** 34, (9), 483-492.
[434] Giddings, J. C.; Karaiskakis, G.; Caldwell, K. D.; Myers, M. N., Colloid characterization by sedimentation field-flow fractionation: I. Monodisperse populations. *J. Colloid Interface Sci.* **1983,** 92, (1), 66-80.
[435] Tri, N.; Caldwell, K.; Beckett, R., Development of electrical field-flow fractionation. *Anal. Chem.* **2000,** 72, (8), 1823-1829.
[436] Giddings, J. C.; Yang, F. J.; Myers, M. N., Flow field-flow fractionation as a methodology for protein separation and characterization. *Anal. Biochem.* **1977,** 81, (2), 394-407.
[437] Berger, M.; Scherer, C.; Noskov, S.; Bantz, C.; Nickel, C.; Schupp, W.; Maskos, M., Influence of oscillating main flow on separation efficiency in asymmetrical flow field-flow fractionation. *J. Chromatogr. A* **2021,** 1640, 461941.
[438] Nickel, C.; Scherer, C.; Noskov, S.; Bantz, C.; Berger, M.; Schupp, W.; Maskos, M., Observation of interaction forces by investigation of the influence of eluent additives on the retention behavior of aqueous nanoparticle dispersions in asymmetrical flow field-flow fractionation. *J. Chromatogr. A* **2021,** 1637, 461840.
[439] Noskov, S.; Scherer, C.; Maskos, M., Determination of Hamaker constants of polymeric nanoparticles in organic solvents by asymmetrical flow field-flow fractionation. *J. Chromatogr. A* **2013,** 1274, 151-158.
[440] Scherer, C.; Noskov, S.; Utech, S.; Bantz, C.; Mueller, W.; Krohne, K.; Maskos, M., Characterization of Polymer Nanoparticles by Asymmetrical Flow Field Flow Fractionation (AF-FFF). *J. Nanosci. Nanotechnol.* **2010,** 10, (10), 6834-6839.
[441] Jungmann, N.; Schmidt, M.; Maskos, M., Characterization of Polyorganosiloxane Nanoparticles in Aqueous Dispersion by Asymmetrical Flow Field-Flow Fractionation. *Macromolecules* **2001,** 34, (23), 8347-8353.
[442] Wahlund, K. G.; Giddings, J. C., Properties of an asymmetrical flow field-flow fractionation channel having one permeable wall. *Anal. Chem.* **1987,** 59, (9), 1332-1339.
[443] Caputo, F.; Arnould, A.; Bacia, M.; Ling, W. L.; Rustique, E.; Texier, I.; Mello, A. P.; Couffin, A.-C., Measuring Particle Size Distribution by Asymmetric Flow Field Flow Fractionation: A Powerful Method for the Preclinical Characterization of Lipid-Based Nanoparticles. *Mol. Pharmaceutics* **2019,** 16, (2), 756-767.
[444] Scott, D. J.; Schuck, P., *A brief introduction to the analytical ultracentrifugation of proteins for beginners*. RSC Publishing: 2005; p 1-25.
[445] Krpetić, Z.; Davidson, A. M.; Volk, M.; Lévy, R.; Brust, M.; Cooper, D. L., High-resolution sizing of monolayer-protected gold clusters by differential centrifugal sedimentation. *ACS Nano* **2013,** 7, (10), 8881-90.
[446] Davidson, A. M.; Brust, M.; Cooper, D. L.; Volk, M., Sensitive Analysis of Protein Adsorption to Colloidal Gold by Differential Centrifugal Sedimentation. *Anal. Chem.* **2017,** 89, (12), 6807-6814.
[447] Bayley, H.; Martin, C. R., Resistive-Pulse Sensing-From Microbes to Molecules. *Chem. Rev.* **2000,** 100, (7), 2575-2594.
[448] Henriquez, R. R.; Ito, T.; Sun, L.; Crooks, R. M., The resurgence of Coulter counting for analyzing nanoscale objects. *Analyst* **2004,** 129, (6), 478-482.

[449] Kozak, D.; Anderson, W.; Vogel, R.; Chen, S.; Antaw, F.; Trau, M., Simultaneous size and ζ-potential measurements of individual nanoparticles in dispersion using size-tunable pore sensors. *ACS Nano* **2012,** 6, (8), 6990-7.
[450] Koji, K.; Yoshinaga, N.; Mochida, Y.; Hong, T.; Miyazaki, T.; Kataoka, K.; Osada, K.; Cabral, H.; Uchida, S., Bundling of mRNA strands inside polyion complexes improves mRNA delivery efficiency in vitro and in vivo. *Biomaterials* **2020,** 261, 120332.
[451] Karimov, M.; Schulz, M.; Kahl, T.; Noske, S.; Kubczak, M.; Gockel, I.; Thieme, R.; Büch, T.; Reinert, A.; Ionov, M.; Bryszewska, M.; Franke, H.; Krügel, U.; Ewe, A.; Aigner, A., Tyrosine-modified linear PEIs for highly efficacious and biocompatible siRNA delivery in vitro and in vivo. *Nanomedicine* **2021,** 36, 102403.
[452] Karimov, M.; Appelhans, D.; Ewe, A.; Aigner, A., The combined disulfide cross-linking and tyrosine-modification of very low molecular weight linear PEI synergistically enhances transfection efficacies and improves biocompatibility. *Eur. J. Pharm. Biopharm.* **2021,** 161, 56-65.
[453] Lauraeus, S.; Holopainen, J. M.; Taskinen, M.-R.; Kinnunen, P. K. J., Aggregation of dimyristoylphosphatidylglycerol liposomes by human plasma low density lipoprotein. *Biochim. Biophys. Acta Biomembr.* **1998,** 1373, (1), 147-162.
[454] Kaczmarek, J. C.; Patel, A. K.; Kauffman, K. J.; Fenton, O. S.; Webber, M. J.; Heartlein, M. W.; DeRosa, F.; Anderson, D. G., Polymer-Lipid Nanoparticles for Systemic Delivery of mRNA to the Lungs. *Angew. Chem., Int. Ed. Engl.* **2016,** 55, (44), 13808-13812.
[455] Sanchez-Cano, C.; Alvarez-Puebla, R. A.; Abendroth, J. M.; Beck, T.; Blick, R.; Cao, Y.; Caruso, F.; Chakraborty, I.; Chapman, H. N.; Chen, C.; Cohen, B. E.; Conceição, A. L. C.; Cormode, D. P.; Cui, D.; Dawson, K. A.; Falkenberg, G.; Fan, C.; Feliu, N.; Gao, M.; Gargioni, E.; Glüer, C. C.; Grüner, F.; Hassan, M.; Hu, Y.; Huang, Y.; Huber, S.; Huse, N.; Kang, Y.; Khademhosseini, A.; Keller, T. F.; Körnig, C.; Kotov, N. A.; Koziej, D.; Liang, X. J.; Liu, B.; Liu, S.; Liu, Y.; Liu, Z.; Liz-Marzán, L. M.; Ma, X.; Machicote, A.; Maison, W.; Mancuso, A. P.; Megahed, S.; Nickel, B.; Otto, F.; Palencia, C.; Pascarelli, S.; Pearson, A.; Peñate-Medina, O.; Qi, B.; Rädler, J.; Richardson, J. J.; Rosenhahn, A.; Rothkamm, K.; Rübhausen, M.; Sanyal, M. K.; Schaak, R. E.; Schlemmer, H. P.; Schmidt, M.; Schmutzler, O.; Schotten, T.; Schulz, F.; Sood, A. K.; Spiers, K. M.; Staufer, T.; Stemer, D. M.; Stierle, A.; Sun, X.; Tsakanova, G.; Weiss, P. S.; Weller, H.; Westermeier, F.; Xu, M.; Yan, H.; Zeng, Y.; Zhao, Y.; Zhao, Y.; Zhu, D.; Zhu, Y.; Parak, W. J., X-ray-Based Techniques to Study the Nano-Bio Interface. *ACS Nano* **2021,** 15, (3), 3754-3807.
[456] Zackova Suchanova, J.; Hejtmankova, A.; Neburkova, J.; Cigler, P.; Forstova, J.; Spanielova, H., The Protein Corona Does Not Influence Receptor-Mediated Targeting of Virus-like Particles. *Bioconjugate Chem.* **2020,** 31, (5), 1575-1585.
[457] Gu, J.; Chen, X.; Xin, H.; Fang, X.; Sha, X., Serum-resistant complex nanoparticles functionalized with imidazole-rich polypeptide for gene delivery to pulmonary metastatic melanoma. *Int. J. Pharm.* **2014,** 461, (1-2), 559-69.
[458] Haberland, A.; Knaus, T.; Zaitsev, S. V.; Buchberger, B.; Lun, A.; Haller, H.; Böttger, M., Histone H1-mediated transfection: serum inhibition can be overcome by Ca2+ ions. *Pharm. Res.* **2000,** 17, (2), 229-35.
[459] Wang, F.; Yu, L.; Monopoli, M. P.; Sandin, P.; Mahon, E.; Salvati, A.; Dawson, K. A., The biomolecular corona is retained during nanoparticle uptake and protects the cells from the damage induced by cationic nanoparticles until degraded in the lysosomes. *Nanomedicine* **2013,** 9, (8), 1159-68.
[460] Yallapu, M. M.; Chauhan, N.; Othman, S. F.; Khalilzad-Sharghi, V.; Ebeling, M. C.; Khan, S.; Jaggi, M.; Chauhan, S. C., Implications of protein corona on physico-chemical and biological properties of magnetic nanoparticles. *Biomaterials* **2015,** 46, 1-12.
[461] Lesniak, A.; Fenaroli, F.; Monopoli, M. P.; Åberg, C.; Dawson, K. A.; Salvati, A., Effects of the presence or absence of a protein corona on silica nanoparticle uptake and impact on cells. *ACS Nano* **2012,** 6, (7), 5845-57.

[462] Zelphati, O.; Uyechi, L. S.; Barron, L. G.; Szoka, F. C., Jr., Effect of serum components on the physico-chemical properties of cationic lipid/oligonucleotide complexes and on their interactions with cells. *Biochim. Biophys. Acta* **1998,** 1390, (2), 119-33.
[463] Kulkarni, J. A.; Witzigmann, D.; Chen, S.; Cullis, P. R.; van der Meel, R., Lipid Nanoparticle Technology for Clinical Translation of siRNA Therapeutics. *Acc. Chem. Res.* **2019,** 52, (9), 2435-2444.
[464] Akinc, A.; Maier, M. A.; Manoharan, M.; Fitzgerald, K.; Jayaraman, M.; Barros, S.; Ansell, S.; Du, X.; Hope, M. J.; Madden, T. D.; Mui, B. L.; Semple, S. C.; Tam, Y. K.; Ciufolini, M.; Witzigmann, D.; Kulkarni, J. A.; van der Meel, R.; Cullis, P. R., The Onpattro story and the clinical translation of nanomedicines containing nucleic acid-based drugs. *Nat. Nanotechnol.* **2019,** 14, (12), 1084-1087.
[465] Prades, R.; Oller-Salvia, B.; Schwarzmaier, S. M.; Selva, J.; Moros, M.; Balbi, M.; Grazú, V.; de La Fuente, J. M.; Egea, G.; Plesnila, N.; Teixidó, M.; Giralt, E., Applying the retro-enantio approach to obtain a peptide capable of overcoming the blood-brain barrier. *Angew. Chem., Int. Ed. Engl.* **2015,** 54, (13), 3967-72.
[466] Cardle, I. I.; Jensen, M. C.; Pun, S. H.; Sellers, D. L., Optimized serum stability and specificity of an αvβ6 integrin-binding peptide for tumor targeting. *J. Biol. Chem.* **2021,** 296, 100657.
[467] Mahon, E.; Salvati, A.; Baldelli Bombelli, F.; Lynch, I.; Dawson, K. A., Designing the nanoparticle-biomolecule interface for "targeting and therapeutic delivery". *J. Controlled Release* **2012,** 161, (2), 164-74.
[468] Mirshafiee, V.; Mahmoudi, M.; Lou, K.; Cheng, J.; Kraft, M. L., Protein corona significantly reduces active targeting yield. *Chem. Commun.* **2013,** 49, (25), 2557-2559.
[469] Broda, E.; Mickler, F. M.; Lächelt, U.; Morys, S.; Wagner, E.; Bräuchle, C., Assessing potential peptide targeting ligands by quantification of cellular adhesion of model nanoparticles under flow conditions. *J. Controlled Release* **2015,** 213, 79-85.
[470] Jensen, C.; Shay, C.; Teng, Y., The New Frontier of Three-Dimensional Culture Models to Scale-Up Cancer Research. In *Physical Exercise and Natural and Synthetic Products in Health and Disease*, Guest, P. C., Ed. Springer US: New York, NY, 2022; pp 3-18.
[471] Elter, J. K.; Quader, S.; Eichhorn, J.; Gottschaldt, M.; Kataoka, K.; Schacher, F. H., Core-Crosslinked Fluorescent Worm-Like Micelles for Glucose-Mediated Drug Delivery. *Biomacromolecules* **2021,** 22, (4), 1458-1471.
[472] Wu, Y.; Zhou, Y.; Qin, X.; Liu, Y., From cell spheroids to vascularized cancer organoids: Microfluidic tumor-on-a-chip models for preclinical drug evaluations. *Biomicrofluidics* **2021,** 15, (6), 061503.
[473] Han, M.; Bae, Y.; Nishiyama, N.; Miyata, K.; Oba, M.; Kataoka, K., Transfection study using multicellular tumor spheroids for screening non-viral polymeric gene vectors with low cytotoxicity and high transfection efficiencies. *J. Controlled Release* **2007,** 121, (1-2), 38-48.
[474] Wu, X.; Su, J.; Wei, J.; Jiang, N.; Ge, X., Recent Advances in Three-Dimensional Stem Cell Culture Systems and Applications. *Stem Cells Int.* **2021,** 2021, 9477332.
[475] Chew, L.; Añonuevo, A.; Knock, E., Generating Cerebral Organoids from Human Pluripotent Stem Cells. *Methods Mol. Biol.* **2022,** 2389, 177-199.
[476] Salem, T.; Frankman, Z.; Churko, J. M., Tissue Engineering Techniques for Induced Pluripotent Stem Cell Derived Three-Dimensional Cardiac Constructs. *Tissue Eng. Part B* **2021**.
[477] Brighi, C.; Cordella, F.; Chiriatti, L.; Soloperto, A.; Di Angelantonio, S., Retinal and Brain Organoids: Bridging the Gap Between in vivo Physiology and in vitro Micro-Physiology for the Study of Alzheimer's Diseases. *Front. Neurosci.* **2020,** 14, 655.
[478] Rossi, G.; Manfrin, A.; Lutolf, M. P., Progress and potential in organoid research. *Nat. Rev. Genet.* **2018,** 19, (11), 671-687.
[479] Vogt, N., Assembloids. *Nat. Methods* **2021,** 18, (1), 27.
[480] Mansouri, M.; Leipzig, N. D., Advances in removing mass transport limitations for more physiologically relevant in vitro 3D cell constructs. *Biophysics Reviews* **2021,** 2, (2), 021305.

[481] Bhat, S. M.; Badiger, V. A.; Vasishta, S.; Chakraborty, J.; Prasad, S.; Ghosh, S.; Joshi, M. B., 3D tumor angiogenesis models: recent advances and challenges. *J. Cancer Res. Clin. Oncol.* **2021,** 147, (12), 3477-3494.
[482] Yuki, K.; Cheng, N.; Nakano, M.; Kuo, C. J., Organoid Models of Tumor Immunology. *Trends Immunol.* **2020,** 41, (8), 652-664.
[483] Sherman, H.; Gitschier, H. J.; Rossi, A. E., A Novel Three-Dimensional Immune Oncology Model for High-Throughput Testing of Tumoricidal Activity. *Front. Immunol.* **2018,** 9, 857.
[484] Amin, M.; Mansourian, M.; Koning, G. A.; Badiee, A.; Jaafari, M. R.; Ten Hagen, T. L. M., Development of a novel cyclic RGD peptide for multiple targeting approaches of liposomes to tumor region. *J. Controlled Release* **2015,** 220, (Pt A), 308-315.
[485] Uchida, H.; Itaka, K.; Nomoto, T.; Ishii, T.; Suma, T.; Ikegami, M.; Miyata, K.; Oba, M.; Nishiyama, N.; Kataoka, K., Modulated protonation of side chain aminoethylene repeats in N-substituted polyaspartamides promotes mRNA transfection. *J. Am. Chem. Soc.* **2014,** 136, (35), 12396-405.
[486] Yoshinaga, N.; Cho, E.; Koji, K.; Mochida, Y.; Naito, M.; Osada, K.; Kataoka, K.; Cabral, H.; Uchida, S., Bundling mRNA Strands to Prepare Nano-Assemblies with Enhanced Stability Towards RNase for In Vivo Delivery. *Angew. Chem., Int. Ed. Engl.* **2019,** 58, (33), 11360-11363.
[487] Yoshinaga, N.; Uchida, S.; Naito, M.; Osada, K.; Cabral, H.; Kataoka, K., Induced packaging of mRNA into polyplex micelles by regulated hybridization with a small number of cholesteryl RNA oligonucleotides directed enhanced in vivo transfection. *Biomaterials* **2019,** 197, 255-267.
[488] Miyazaki, T.; Uchida, S.; Nagatoishi, S.; Koji, K.; Hong, T.; Fukushima, S.; Tsumoto, K.; Ishihara, K.; Kataoka, K.; Cabral, H., Polymeric Nanocarriers with Controlled Chain Flexibility Boost mRNA Delivery In Vivo through Enhanced Structural Fastening. *Adv. Healthcare Mater.* **2020,** 9, (16), e2000538.
[489] Miyazaki, T.; Uchida, S.; Miyahara, Y.; Matsumoto, A.; Cabral, H., Development of Flexible Polycation-Based mRNA Delivery Systems for In Vivo Applications. *Mater. Proc.* **2021,** 4, (1), 5.
[490] Uchida, S.; Koji, K.; Yoshinaga, N.; Mochida, Y.; Hong, T.; Cabral, H., mRNA Structuring for Stabilizing mRNA Nanocarriers and Improving Their Delivery Efficiency. *Mater. Proc.* **2021,** 4, (1), 82.
[491] Yoshinaga, N.; Naito, M.; Tachihara, Y.; Boonstra, E.; Osada, K.; Cabral, H.; Uchida, S., PEGylation of mRNA by Hybridization of Complementary PEG-RNA Oligonucleotides Stabilizes mRNA without Using Cationic Materials. *Pharmaceutics* **2021,** 13, (6), 800.
[492] Chan, C. L.; Ewert, K. K.; Majzoub, R. N.; Hwu, Y. K.; Liang, K. S.; Leal, C.; Safinya, C. R., Optimizing cationic and neutral lipids for efficient gene delivery at high serum content. *J. Gene Med.* **2014,** 16, (3-4), 84-96.
[493] Olden, B. R.; Cheng, Y.; Yu, J. L.; Pun, S. H., Cationic polymers for non-viral gene delivery to human T cells. *J. Controlled Release* **2018,** 282, 140-147.
[494] Turek, J.; Dubertret, C.; Jaslin, G.; Antonakis, K.; Scherman, D.; Pitard, B., Formulations which increase the size of lipoplexes prevent serum-associated inhibition of transfection. *J. Gene Med.* **2000,** 2, (1), 32-40.
[495] Kursa, M.; Walker, G. F.; Roessler, V.; Ogris, M.; Roedl, W.; Kircheis, R.; Wagner, E., Novel shielded transferrin-polyethylene glycol-polyethylenimine/DNA complexes for systemic tumor-targeted gene transfer. *Bioconjugate Chem.* **2003,** 14, (1), 222-31.
[496] Warriner, L. W.; Duke, J. R.; Pack, D. W.; DeRouchey, J. E., Succinylated Polyethylenimine Derivatives Greatly Enhance Polyplex Serum Stability and Gene Delivery In Vitro. *Biomacromolecules* **2018,** 19, (11), 4348-4357.
[497] Uddin, N.; Warriner, L. W.; Pack, D. W.; DeRouchey, J. E., Enhanced Gene Delivery and CRISPR/Cas9 Homology-Directed Repair in Serum by Minimally Succinylated Polyethylenimine. *Mol. Pharmaceutics* **2021,** 18, (9), 3452-3463.

[498] Boeckle, S.; von Gersdorff, K.; van der Piepen, S.; Culmsee, C.; Wagner, E.; Ogris, M., Purification of polyethylenimine polyplexes highlights the role of free polycations in gene transfer. *J. Gene Med.* **2004,** 6, (10), 1102-11.
[499] Wightman, L.; Kircheis, R.; Rössler, V.; Carotta, S.; Ruzicka, R.; Kursa, M.; Wagner, E., Different behavior of branched and linear polyethylenimine for gene delivery in vitro and in vivo. *J. Gene Med.* **2001,** 3, (4), 362-372.
[500] Kircheis, R.; Wightman, L.; Schreiber, A.; Robitza, B.; Rössler, V.; Kursa, M.; Wagner, E., Polyethylenimine/DNA complexes shielded by transferrin target gene expression to tumors after systemic application. *Gene Ther.* **2001,** 8, (1), 28-40.
[501] Coll, J. L.; Chollet, P.; Brambilla, E.; Desplanques, D.; Behr, J. P.; Favrot, M., In vivo delivery to tumors of DNA complexed with linear polyethylenimine. *Hum. Gene Ther.* **1999,** 10, (10), 1659-66.
[502] Zou, S. M.; Erbacher, P.; Remy, J. S.; Behr, J. P., Systemic linear polyethylenimine (L-PEI)-mediated gene delivery in the mouse. *J. Gene Med.* **2000,** 2, (2), 128-34.
[503] Haberland, A.; Knaus, T.; Zaitsev, S. V.; Stahn, R.; Mistry, A. R.; Coutelle, C.; Haller, H.; Böttger, M., Calcium ions as efficient cofactor of polycation-mediated gene transfer. *Biochim. Biophys. Acta* **1999,** 1445, (1), 21-30.
[504] Docter, D.; Bantz, C.; Westmeier, D.; Galla, H. J.; Wang, Q.; Kirkpatrick, J. C.; Nielsen, P.; Maskos, M.; Stauber, R. H., The protein corona protects against size- and dose-dependent toxicity of amorphous silica nanoparticles. *Beilstein J. Nanotechnol.* **2014,** 5, 1380-92.
[505] Lokugamage, M. P.; Sago, C. D.; Dahlman, J. E., Testing thousands of nanoparticles in vivo using DNA barcodes. *Curr. Opin. Biomed. Eng.* **2018,** 7, 1-8.
[506] Paunovska, K.; Gil, C. J.; Lokugamage, M. P.; Sago, C. D.; Sato, M.; Lando, G. N.; Gamboa Castro, M.; Bryksin, A. V.; Dahlman, J. E., Analyzing 2000 in Vivo Drug Delivery Data Points Reveals Cholesterol Structure Impacts Nanoparticle Delivery. *ACS Nano* **2018,** 12, (8), 8341-8349.
[507] Sago, C. D.; Kalathoor, S.; Fitzgerald, J. P.; Lando, G. N.; Djeddar, N.; Bryksin, A. V.; Dahlman, J. E., Barcoding chemical modifications into nucleic acids improves drug stability in vivo. *Journal of materials chemistry. B* **2018,** 6, (44), 7197-7203.
[508] Sago, C. D.; Lokugamage, M. P.; Lando, G. N.; Djeddar, N.; Shah, N. N.; Syed, C.; Bryksin, A. V.; Dahlman, J. E., Modifying a Commonly Expressed Endocytic Receptor Retargets Nanoparticles in Vivo. *Nano Lett.* **2018,** 18, (12), 7590-7600.
[509] Sago, C. D.; Lokugamage, M. P.; Paunovska, K.; Vanover, D. A.; Monaco, C. M.; Shah, N. N.; Gamboa Castro, M.; Anderson, S. E.; Rudoltz, T. G.; Lando, G. N.; Munnilal Tiwari, P.; Kirschman, J. L.; Willett, N.; Jang, Y. C.; Santangelo, P. J.; Bryksin, A. V.; Dahlman, J. E., High-throughput in vivo screen of functional mRNA delivery identifies nanoparticles for endothelial cell gene editing. *Proc. Natl. Acad. Sci. U.S.A.* **2018,** 115, (42), E9944-e9952.
[510] Paunovska, K.; Da Silva Sanchez, A. J.; Sago, C. D.; Gan, Z.; Lokugamage, M. P.; Islam, F. Z.; Kalathoor, S.; Krupczak, B. R.; Dahlman, J. E., Nanoparticles Containing Oxidized Cholesterol Deliver mRNA to the Liver Microenvironment at Clinically Relevant Doses. *Adv. Mater.* **2019,** 31, (14), e1807748.
[511] Gan, Z.; Lokugamage, M. P.; Hatit, M. Z. C.; Loughrey, D.; Paunovska, K.; Sato, M.; Cristian, A.; Dahlman, J. E., Nanoparticles containing constrained phospholipids deliver mRNA to liver immune cells in vivo without targeting ligands. *Bioeng. Transl. Med.* **2020,** 5, (3), e10161-e10161.
[512] Sago, C. D.; Lokugamage, M. P.; Islam, F. Z.; Krupczak, B. R.; Sato, M.; Dahlman, J. E., Nanoparticles That Deliver RNA to Bone Marrow Identified by in Vivo Directed Evolution. *J. Am. Chem. Soc.* **2018,** 140, (49), 17095-17105.
[513] Lokugamage, M. P.; Sago, C. D.; Gan, Z.; Krupczak, B. R.; Dahlman, J. E., Constrained Nanoparticles Deliver siRNA and sgRNA to T Cells In Vivo without Targeting Ligands. *Adv. Mater.* **2019,** 31, (41), e1902251-e1902251.

[514] Dobrowolski, C.; Paunovska, K.; Hatit, M. Z. C.; Lokugamage, M. P.; Dahlman, J. E., Therapeutic RNA Delivery for COVID and Other Diseases. *Adv. Healthcare Mater.* **2021,** 10, (15), e2002022-e2002022.
[515] Da Silva Sanchez, A.; Paunovska, K.; Cristian, A.; Dahlman, J. E., Treating Cystic Fibrosis with mRNA and CRISPR. *Hum. Gene Ther.* **2020,** 31, (17-18), 940-955.
[516] Yaari, Z.; da Silva, D.; Zinger, A.; Goldman, E.; Kajal, A.; Tshuva, R.; Barak, E.; Dahan, N.; Hershkovitz, D.; Goldfeder, M.; Roitman, J. S.; Schroeder, A., Theranostic barcoded nanoparticles for personalized cancer medicine. *Nat. Commun.* **2016,** 7, 13325.
[517] Paunovska, K.; Loughrey, D.; Sago, C. D.; Langer, R.; Dahlman, J. E., Using Large Datasets to Understand Nanotechnology. *Adv. Mater.* **2019,** 31, (43), e1902798-e1902798.
[518] Yang, K.; Reker-Smit, C.; Stuart, M. C. A.; Salvati, A., Effects of Protein Source on Liposome Uptake by Cells: Corona Composition and Impact of the Excess Free Proteins. *Adv. Healthcare Mater.* **2021,** 10, (14), e2100370.
[519] Lee, S. Y.; Son, J. G.; Moon, J. H.; Joh, S.; Lee, T. G., Comparative study on formation of protein coronas under three different serum origins. *Biointerphases* **2020,** 15, (6), 061002.
[520] Müller, L. K.; Simon, J.; Rosenauer, C.; Mailänder, V.; Morsbach, S.; Landfester, K., The Transferability from Animal Models to Humans: Challenges Regarding Aggregation and Protein Corona Formation of Nanoparticles. *Biomacromolecules* **2018,** 19, (2), 374-385.
[521] Lundqvist, M.; Augustsson, C.; Lilja, M.; Lundkvist, K.; Dahlbäck, B.; Linse, S.; Cedervall, T., The nanoparticle protein corona formed in human blood or human blood fractions. *PLoS One* **2017,** 12, (4), e0175871.
[522] Solorio-Rodríguez, A.; Escamilla-Rivera, V.; Uribe-Ramírez, M.; Chagolla, A.; Winkler, R.; García-Cuellar, C. M.; De Vizcaya-Ruiz, A., A comparison of the human and mouse protein corona profiles of functionalized SiO(2) nanocarriers. *Nanoscale* **2017,** 9, (36), 13651-13660.
[523] Schöttler, S.; Klein, K.; Landfester, K.; Mailänder, V., Protein source and choice of anticoagulant decisively affect nanoparticle protein corona and cellular uptake. *Nanoscale* **2016,** 8, (10), 5526-36.
[524] Mirshafiee, V.; Kim, R.; Mahmoudi, M.; Kraft, M. L., The importance of selecting a proper biological milieu for protein corona analysis in vitro: Human plasma versus human serum. *Int. J. Biochem. Cell Biol.* **2016,** 75, 188-95.
[525] Laurent, S.; Burtea, C.; Thirifays, C.; Rezaee, F.; Mahmoudi, M., Significance of cell "observer" and protein source in nanobiosciences. *J. Colloid Interface Sci.* **2013,** 392, 431-445.
[526] Dvorak, A.; Tilley, A. E.; Shaykhiev, R.; Wang, R.; Crystal, R. G., Do airway epithelium air-liquid cultures represent the in vivo airway epithelium transcriptome? *Am. J. Respir. Cell Mol. Biol.* **2011,** 44, (4), 465-73.
[527] Baldassi, D.; Gabold, B.; Merkel, O. M., Air−Liquid Interface Cultures of the Healthy and Diseased Human Respiratory Tract: Promises, Challenges, and Future Directions. *Adv. Nanobiomed. Res.* **2021,** 1, (6), 2000111.
[528] Bennet, T. J.; Randhawa, A.; Hua, J.; Cheung, K. C., Airway-On-A-Chip: Designs and Applications for Lung Repair and Disease. *Cells* **2021,** 10, (7), 1602.
[529] Carius, P.; Dubois, A.; Ajdarirad, M.; Artzy-Schnirman, A.; Sznitman, J.; Schneider-Daum, N.; Lehr, C.-M., PerfuPul—A Versatile Perfusable Platform to Assess Permeability and Barrier Function of Air Exposed Pulmonary Epithelia. *Front. Bioeng. Biotechnol.* **2021,** 9, (904), 743236.
[530] McGonigle, P.; Ruggeri, B., Animal models of human disease: Challenges in enabling translation. *Biochem. Pharmacol.* **2014,** 87, (1), 162-171.
[531] Mak, I. W.; Evaniew, N.; Ghert, M., Lost in translation: animal models and clinical trials in cancer treatment. *Am. J. Transl. Res.* **2014,** 6, (2), 114-8.
[532] Perel, P.; Roberts, I.; Sena, E.; Wheble, P.; Briscoe, C.; Sandercock, P.; Macleod, M.; Mignini, L. E.; Jayaram, P.; Khan, K. S., Comparison of treatment effects between animal experiments and clinical trials: systematic review. *BMJ* **2007,** 334, (7586), 197.
[533] Liu, B.; Liu, S.; Zhang, S.; Bai, L.; Liu, E., Bioinformatic evaluation of the potential animal models for studying SARS-Cov-2. *Heliyon* **2020,** 6, (12), e05725.

[534] Preis, E.; Schulze, J.; Gutberlet, B.; Pinnapireddy, S. R.; Jedelská, J.; Bakowsky, U., The chorioallantoic membrane as a bio-barrier model for the evaluation of nanoscale drug delivery systems for tumour therapy. *Adv. Drug Delivery Rev.* **2021,** 174, 317-336.
[535] Schulze, J.; Lehmann, J.; Agel, S.; Amin, M. U.; Schaefer, J.; Bakowsky, U., In Ovo Testing Method for Inhalants on a Chorio-Allantoic Membrane. *ACS Appl. Bio. Mater.* **2021,** 4, (11), 7764-7768.
[536] Hajipour, M. J.; Laurent, S.; Aghaie, A.; Rezaee, F.; Mahmoudi, M., Personalized protein coronas: a "key" factor at the nanobiointerface. *Biomater. Sci.* **2014,** 2, (9), 1210-1221.
[537] Hajipour, M. J.; Raheb, J.; Akhavan, O.; Arjmand, S.; Mashinchian, O.; Rahman, M.; Abdolahad, M.; Serpooshan, V.; Laurent, S.; Mahmoudi, M., Personalized disease-specific protein corona influences the therapeutic impact of graphene oxide. *Nanoscale* **2015,** 7, (19), 8978-8994.
[538] Corbo, C.; Molinaro, R.; Tabatabaei, M.; Farokhzad, O. C.; Mahmoudi, M., Personalized protein corona on nanoparticles and its clinical implications. *Biomater. Sci.* **2017,** 5, (3), 378-387.
[539] Krhač Levačić, A.; Berger, S.; Müller, J.; Wegner, A.; Lächelt, U.; Dohmen, C.; Rudolph, C.; Wagner, E., Dynamic mRNA polyplexes benefit from bioreducible cleavage sites for in vitro and in vivo transfer. *J. Controlled Release* **2021,** 339, 27-40.
[540] Hajj, K. A. W., Kathryn A. , Tools for translation: non-viral materials for therapeutic mRNA delivery. *Nat. Rev. Mater.* **2017,** 2, 1-17.
[541] Kowalski, P. S.; Rudra, A.; Miao, L.; Anderson, D. G., Delivering the Messenger: Advances in Technologies for Therapeutic mRNA Delivery. *Mol. Ther.* **2019,** 27, (4), 710-728.
[542] Zeng, C.; Zhang, C.; Walker, P. G.; Dong, Y., Formulation and Delivery Technologies for mRNA Vaccines. *Curr. Top. Microbiol. Immunol.* **2020**.
[543] Pardi, N.; Hogan, M. J.; Weissman, D., Recent advances in mRNA vaccine technology. *Curr. Opin. Immunol.* **2020,** 65, 14-20.
[544] Alameh, M. G.; Weissman, D.; Pardi, N., Messenger RNA-Based Vaccines Against Infectious Diseases. *Curr. Top. Microbiol. Immunol.* **2020**.
[545] Wadhwa, A.; Aljabbari, A.; Lokras, A.; Foged, C.; Thakur, A., Opportunities and Challenges in the Delivery of mRNA-based Vaccines. *Pharmaceutics* **2020,** 12, (2), 102.
[546] Trepotec, Z.; Lichtenegger, E.; Plank, C.; Aneja, M. K.; Rudolph, C., Delivery of mRNA Therapeutics for the Treatment of Hepatic Diseases. *Mol. Ther.* **2019,** 27, (4), 794-802.
[547] Sahu, I.; Haque, A.; Weidensee, B.; Weinmann, P.; Kormann, M. S. D., Recent Developments in mRNA-Based Protein Supplementation Therapy to Target Lung Diseases. *Mol. Ther.* **2019,** 27, (4), 803-823.
[548] Kranz, L. M.; Diken, M.; Haas, H.; Kreiter, S.; Loquai, C.; Reuter, K. C.; Meng, M.; Fritz, D.; Vascotto, F.; Hefesha, H.; Grunwitz, C.; Vormehr, M.; Husemann, Y.; Selmi, A.; Kuhn, A. N.; Buck, J.; Derhovanessian, E.; Rae, R.; Attig, S.; Diekmann, J.; Jabulowsky, R. A.; Heesch, S.; Hassel, J.; Langguth, P.; Grabbe, S.; Huber, C.; Tureci, O.; Sahin, U., Systemic RNA delivery to dendritic cells exploits antiviral defence for cancer immunotherapy. *Nature* **2016,** 534, (7607), 396-401.
[549] Guevara, M. L.; Persano, F.; Persano, S., Advances in Lipid Nanoparticles for mRNA-Based Cancer Immunotherapy. *Front. Chem.* **2020,** 8, 589959.
[550] Miller, J. B.; Zhang, S.; Kos, P.; Xiong, H.; Zhou, K.; Perelman, S. S.; Zhu, H.; Siegwart, D. J., Non-Viral CRISPR/Cas Gene Editing In Vitro and In Vivo Enabled by Synthetic Nanoparticle Co-Delivery of Cas9 mRNA and sgRNA. *Angew. Chem., Int. Ed. Engl.* **2017,** 56, (4), 1059-1063.
[551] Cheng, Q.; Wei, T.; Farbiak, L.; Johnson, L. T.; Dilliard, S. A.; Siegwart, D. J., Selective organ targeting (SORT) nanoparticles for tissue-specific mRNA delivery and CRISPR-Cas gene editing. *Nat. Nanotechnol.* **2020,** 15, (4), 313-320.
[552] Weissman, D., mRNA transcript therapy. *Expert Rev. Vaccines* **2015,** 14, 265-281.
[553] Kaczmarek, J. C.; Kowalski, P. S.; Anderson, D. G., Advances in the delivery of RNA therapeutics: from concept to clinical reality. *Genome Med.* **2017,** 9, (1), 60.
[554] Chung, Y. H.; Beiss, V.; Fiering, S. N.; Steinmetz, N. F., COVID-19 Vaccine Frontrunners and Their Nanotechnology Design. *ACS Nano* **2020,** 14, (10), 12522-12537.

[555] Dong, Y.; Dai, T.; Wei, Y.; Zhang, L.; Zheng, M.; Zhou, F., A systematic review of SARS-CoV-2 vaccine candidates. *Signal Transduction Targeted Ther.* **2020,** 5, (1), 237.
[556] Yi, C.; Yi, Y.; Li, J., mRNA Vaccines: Possible Tools to Combat SARS-CoV-2. *Virol. Sin.* **2020,** 35, (3), 259-262.
[557] Kormann, M. S.; Hasenpusch, G.; Aneja, M. K.; Nica, G.; Flemmer, A. W.; Herber-Jonat, S.; Huppmann, M.; Mays, L. E.; Illenyi, M.; Schams, A.; Griese, M.; Bittmann, I.; Handgretinger, R.; Hartl, D.; Rosenecker, J.; Rudolph, C., Expression of therapeutic proteins after delivery of chemically modified mRNA in mice. *Nat. Biotechnol.* **2011,** 29, (2), 154-7.
[558] Li, B.; Luo, X.; Dong, Y., Effects of Chemically Modified Messenger RNA on Protein Expression. *Bioconjugate Chem.* **2016,** 27, (3), 849-53.
[559] Dowdy, S. F., Overcoming cellular barriers for RNA therapeutics. *Nat. Biotechnol.* **2017,** 35, (3), 222-229.
[560] Yoshinaga, N.; Uchida, S.; Dirisala, A.; Naito, M.; Osada, K.; Cabral, H.; Kataoka, K., mRNA loading into ATP-responsive polyplex micelles with optimal density of phenylboronate ester crosslinking to balance robustness in the biological milieu and intracellular translational efficiency. *J. Controlled Release* **2020,** 330, 317-328.
[561] Dirisala, A.; Uchida, S.; Tockary, T. A.; Yoshinaga, N.; Li, J.; Osawa, S.; Gorantla, L.; Fukushima, S.; Osada, K.; Kataoka, K., Precise tuning of disulphide crosslinking in mRNA polyplex micelles for optimising extracellular and intracellular nuclease tolerability. *J. Drug Targeting* **2019,** 27, (5-6), 670-680.
[562] Haabeth, O. A. W.; Blake, T. R.; McKinlay, C. J.; Waymouth, R. M.; Wender, P. A.; Levy, R., mRNA vaccination with charge-altering releasable transporters elicits human T cell responses and cures established tumors in mice. *Proc. Natl. Acad. Sci. U.S.A.* **2018,** 115, (39), E9153.
[563] McKinlay, C. J.; Benner, N. L.; Haabeth, O. A.; Waymouth, R. M.; Wender, P. A., Enhanced mRNA delivery into lymphocytes enabled by lipid-varied libraries of charge-altering releasable transporters. *Proc. Natl. Acad. Sci. U.S.A.* **2018,** 115, (26), E5859.
[564] McKinlay, C. J.; Vargas, J. R.; Blake, T. R.; Hardy, J. W.; Kanada, M.; Contag, C. H.; Wender, P. A.; Waymouth, R. M., Charge-altering releasable transporters (CARTs) for the delivery and release of mRNA in living animals. *Proc. Natl. Acad. Sci. U.S.A.* **2017,** 114, (4), E448-e456.
[565] Cullis, P. R.; Hope, M. J., Lipid Nanoparticle Systems for Enabling Gene Therapies. *Mol. Ther.* **2017,** 25, (7), 1467-1475.
[566] Blakney, A. K.; Deletic, P.; McKay, P. F.; Bouton, C. R.; Ashford, M.; Shattock, R. J.; Sabirsh, A., Effect of complexing lipids on cellular uptake and expression of messenger RNA in human skin explants. *J. Controlled Release* **2020**.
[567] Billingsley, M. M.; Singh, N.; Ravikumar, P.; Zhang, R.; June, C. H.; Mitchell, M. J., Ionizable Lipid Nanoparticle-Mediated mRNA Delivery for Human CAR T Cell Engineering. *Nano Lett.* **2020,** 20, (3), 1578-1589.
[568] Eygeris, Y.; Patel, S.; Jozic, A.; Sahay, G., Deconvoluting Lipid Nanoparticle Structure for Messenger RNA Delivery. *Nano Lett.* **2020,** 20, (6), 4543-4549.
[569] Gaspar, R.; Coelho, F.; Silva, B. F. B., Lipid-Nucleic Acid Complexes: Physicochemical Aspects and Prospects for Cancer Treatment. *Molecules* **2020,** 25, (21).
[570] Kim, J.; Jozic, A.; Sahay, G., Naturally Derived Membrane Lipids Impact Nanoparticle-Based Messenger RNA Delivery. *Cell Mol. Bioeng.* **2020,** 13, (5), 1-12.
[571] Lee, S. M.; Cheng, Q.; Yu, X.; Liu, S.; Johnson, L. T.; Siegwart, D. J., A Systematic Study of Unsaturation in Lipid Nanoparticles Leads to Improved mRNA Transfection In Vivo. *Angew. Chem., Int. Ed. Engl.* **2020**.
[572] Miao, L.; Lin, J.; Huang, Y.; Li, L.; Delcassian, D.; Ge, Y.; Shi, Y.; Anderson, D. G., Synergistic lipid compositions for albumin receptor mediated delivery of mRNA to the liver. *Nat. Commun.* **2020,** 11, (1), 2424.
[573] Patel, S.; Ashwanikumar, N.; Robinson, E.; Xia, Y.; Mihai, C.; Griffith, J. P., 3rd; Hou, S.; Esposito, A. A.; Ketova, T.; Welsher, K.; Joyal, J. L.; Almarsson, Ö.; Sahay, G., Naturally-occurring

cholesterol analogues in lipid nanoparticles induce polymorphic shape and enhance intracellular delivery of mRNA. *Nat. Commun.* **2020,** 11, (1), 983.
[574] Zhang, H.; Leal, J.; Soto, M. R.; Smyth, H. D. C.; Ghosh, D., Aerosolizable Lipid Nanoparticles for Pulmonary Delivery of mRNA through Design of Experiments. *Pharmaceutics* **2020,** 12, (11), 1042.
[575] Zhang, X.; Zhao, W.; Nguyen, G. N.; Zhang, C.; Zeng, C.; Yan, J.; Du, S.; Hou, X.; Li, W.; Jiang, J.; Deng, B.; McComb, D. W.; Dorkin, R.; Shah, A.; Barrera, L.; Gregoire, F.; Singh, M.; Chen, D.; Sabatino, D. E.; Dong, Y., Functionalized lipid-like nanoparticles for in vivo mRNA delivery and base editing. *Science advances* **2020,** 6, (34), eabc2315.
[576] Guimaraes, P. P. G.; Zhang, R.; Spektor, R.; Tan, M.; Chung, A.; Billingsley, M. M.; El-Mayta, R.; Riley, R. S.; Wang, L.; Wilson, J. M.; Mitchell, M. J., Ionizable lipid nanoparticles encapsulating barcoded mRNA for accelerated in vivo delivery screening. *J. Controlled Release* **2019,** 316, 404-417.
[577] Ball, R. L.; Hajj, K. A.; Vizelman, J.; Bajaj, P.; Whitehead, K. A., Lipid Nanoparticle Formulations for Enhanced Co-delivery of siRNA and mRNA. *Nano Lett.* **2018,** 18, (6), 3814-3822.
[578] Kaczmarek, J. C.; Kauffman, K. J.; Fenton, O. S.; Sadtler, K.; Patel, A. K.; Heartlein, M. W.; DeRosa, F.; Anderson, D. G., Optimization of a Degradable Polymer-Lipid Nanoparticle for Potent Systemic Delivery of mRNA to the Lung Endothelium and Immune Cells. *Nano Lett.* **2018,** 18, (10), 6449-6454.
[579] Kowalski, P. S.; Capasso Palmiero, U.; Huang, Y.; Rudra, A.; Langer, R.; Anderson, D. G., Ionizable Amino-Polyesters Synthesized via Ring Opening Polymerization of Tertiary Amino-Alcohols for Tissue Selective mRNA Delivery. *Adv. Mater.* **2018**, e1801151.
[580] Yanez Arteta, M.; Kjellman, T.; Bartesaghi, S.; Wallin, S.; Wu, X.; Kvist, A. J.; Dabkowska, A.; Székely, N.; Radulescu, A.; Bergenholtz, J.; Lindfors, L., Successful reprogramming of cellular protein production through mRNA delivered by functionalized lipid nanoparticles. *Proc. Natl. Acad. Sci. U.S.A.* **2018,** 115, (15), E3351-e3360.
[581] Sabnis, S.; Kumarasinghe, E. S.; Salerno, T.; Mihai, C.; Ketova, T.; Senn, J. J.; Lynn, A.; Bulychev, A.; McFadyen, I.; Chan, J.; Almarsson, Ö.; Stanton, M. G.; Benenato, K. E., A Novel Amino Lipid Series for mRNA Delivery: Improved Endosomal Escape and Sustained Pharmacology and Safety in Non-human Primates. *Mol. Ther.* **2018,** 26, (6), 1509-1519.
[582] Abraham, M. K.; Peter, K.; Michel, T.; Wendel, H. P.; Krajewski, S.; Wang, X., Nanoliposomes for Safe and Efficient Therapeutic mRNA Delivery: A Step Toward Nanotheranostics in Inflammatory and Cardiovascular Diseases as well as Cancer. *Nanotheranostics* **2017,** 1, (2), 154-165.
[583] Oberli, M. A.; Reichmuth, A. M.; Dorkin, J. R.; Mitchell, M. J.; Fenton, O. S.; Jaklenec, A.; Anderson, D. G.; Langer, R.; Blankschtein, D., Lipid Nanoparticle Assisted mRNA Delivery for Potent Cancer Immunotherapy. *Nano Lett.* **2017,** 17, (3), 1326-1335.
[584] Pardi, N.; Hogan, M. J.; Pelc, R. S.; Muramatsu, H.; Andersen, H.; DeMaso, C. R.; Dowd, K. A.; Sutherland, L. L.; Scearce, R. M.; Parks, R.; Wagner, W.; Granados, A.; Greenhouse, J.; Walker, M.; Willis, E.; Yu, J.-S.; McGee, C. E.; Sempowski, G. D.; Mui, B. L.; Tam, Y. K.; Huang, Y.-J.; Vanlandingham, D.; Holmes, V. M.; Balachandran, H.; Sahu, S.; Lifton, M.; Higgs, S.; Hensley, S. E.; Madden, T. D.; Hope, M. J.; Karikó, K.; Santra, S.; Graham, B. S.; Lewis, M. G.; Pierson, T. C.; Haynes, B. F.; Weissman, D., Zika virus protection by a single low-dose nucleoside-modified mRNA vaccination. *Nature* **2017,** 543, (7644), 248-251.
[585] Patel, S.; Ashwanikumar, N.; Robinson, E.; DuRoss, A.; Sun, C.; Murphy-Benenato, K. E.; Mihai, C.; Almarsson, Ö.; Sahay, G., Boosting Intracellular Delivery of Lipid Nanoparticle-Encapsulated mRNA. *Nano Lett.* **2017,** 17, (9), 5711-5718.
[586] Utzinger, M.; Jarzebinska, A.; Haag, N.; Schweizer, M.; Winter, G.; Dohmen, C.; Rudolph, C.; Plank, C., cmRNA/lipoplex encapsulation in PLGA microspheres enables transfection via calcium phosphate cement (CPC)/PLGA composites. *J. Controlled Release* **2017,** 249, 143-149.
[587] Badieyan, Z. S.; Berezhanskyy, T.; Utzinger, M.; Aneja, M. K.; Emrich, D.; Erben, R.; Schuler, C.; Altpeter, P.; Ferizi, M.; Hasenpusch, G.; Rudolph, C.; Plank, C., Transcript-activated

collagen matrix as sustained mRNA delivery system for bone regeneration. *J. Controlled Release* **2016,** 239, 137-48.
[588] Kauffman, K. J.; Dorkin, J. R.; Yang, J. H.; Heartlein, M. W.; DeRosa, F.; Mir, F. F.; Fenton, O. S.; Anderson, D. G., Optimization of Lipid Nanoparticle Formulations for mRNA Delivery in Vivo with Fractional Factorial and Definitive Screening Designs. *Nano Lett.* **2015,** 15, (11), 7300-6.
[589] Midoux, P.; Pichon, C., Lipid-based mRNA vaccine delivery systems. *Expert Rev. Vaccines* **2015,** 14, (2), 221-234.
[590] Su, X.; Fricke, J.; Kavanagh, D. G.; Irvine, D. J., In vitro and in vivo mRNA delivery using lipid-enveloped pH-responsive polymer nanoparticles. *Mol. Pharmaceutics* **2011,** 8, (3), 774-87.
[591] Rejman, J.; Tavernier, G.; Bavarsad, N.; Demeester, J.; De Smedt, S. C., mRNA transfection of cervical carcinoma and mesenchymal stem cells mediated by cationic carriers. *J. Controlled Release* **2010,** 147, (3), 385-91.
[592] Anderson, D. M.; Hall, L. L.; Ayyalapu, A. R.; Irion, V. R.; Nantz, M. H.; Hecker, J. G., Stability of mRNA/cationic lipid lipoplexes in human and rat cerebrospinal fluid: methods and evidence for nonviral mRNA gene delivery to the central nervous system. *Hum. Gene Ther.* **2003,** 14, (3), 191-202.
[593] He, J.; Xu, S.; Leng, Q.; Mixson, A. J., Location of a single histidine within peptide carriers increases mRNA delivery. *J. Gene Med.* **2021,** 23, (2), e3295.
[594] van den Berg, A. I. S.; Yun, C. O.; Schiffelers, R. M.; Hennink, W. E., Polymeric delivery systems for nucleic acid therapeutics: Approaching the clinic. *J. Controlled Release* **2021,** 331, 121-141.
[595] Blakney, A. K.; Abdouni, Y.; Yilmaz, G.; Liu, R.; McKay, P. F.; Bouton, C. R.; Shattock, R. J.; Becer, C. R., Mannosylated Poly(ethylene imine) Copolymers Enhance saRNA Uptake and Expression in Human Skin Explants. *Biomacromolecules* **2020,** 21, (6), 2482-2492.
[596] Siewert, C. D.; Haas, H.; Cornet, V.; Nogueira, S. S.; Nawroth, T.; Uebbing, L.; Ziller, A.; Al-Gousous, J.; Radulescu, A.; Schroer, M. A.; Blanchet, C. E.; Svergun, D. I.; Radsak, M. P.; Sahin, U.; Langguth, P., Hybrid Biopolymer and Lipid Nanoparticles with Improved Transfection Efficacy for mRNA. *Cells* **2020,** 9, (9), 2034.
[597] Son, S.; Nam, J.; Zenkov, I.; Ochyl, L. J.; Xu, Y.; Scheetz, L.; Shi, J.; Farokhzad, O. C.; Moon, J. J., Sugar-Nanocapsules Imprinted with Microbial Molecular Patterns for mRNA Vaccination. *Nano Lett.* **2020,** 20, (3), 1499-1509.
[598] Patel, A. K.; Kaczmarek, J. C.; Bose, S.; Kauffman, K. J.; Mir, F.; Heartlein, M. W.; DeRosa, F.; Langer, R.; Anderson, D. G., Inhaled Nanoformulated mRNA Polyplexes for Protein Production in Lung Epithelium. *Adv. Mater.* **2019,** 31, (8), e1805116.
[599] Chen, Q.; Qi, R.; Chen, X.; Yang, X.; Wu, S.; Xiao, H.; Dong, W., A Targeted and Stable Polymeric Nanoformulation Enhances Systemic Delivery of mRNA to Tumors. *Mol. Ther.* **2017,** 25, (1), 92-101.
[600] Li, J.; He, Y.; Wang, W.; Wu, C.; Hong, C.; Hammond, P. T., Polyamine-Mediated Stoichiometric Assembly of Ribonucleoproteins for Enhanced mRNA Delivery. *Angew. Chem., Int. Ed. Engl.* **2017,** 56, (44), 13709-13712.
[601] Li, J.; Wang, W.; He, Y.; Li, Y.; Yan, E. Z.; Zhang, K.; Irvine, D. J.; Hammond, P. T., Structurally Programmed Assembly of Translation Initiation Nanoplex for Superior mRNA Delivery. *ACS Nano* **2017,** 11, (3), 2531-2544.
[602] Liu, Y.; Krishnan, M. N.; Phua, K. K. L., Suppression of mRNA Nanoparticle Transfection in Human Fibroblasts by Selected Interferon Inhibiting Small Molecule Compounds. *Biomolecules* **2017,** 7, (3), 56.
[603] Meng, Z.; O'Keeffe-Ahern, J.; Lyu, J.; Pierucci, L.; Zhou, D.; Wang, W., A new developing class of gene delivery: messenger RNA-based therapeutics. *Biomater. Sci.* **2017,** 5, (12), 2381-2392.
[604] Udhayakumar, V. K.; De Beuckelaer, A.; McCaffrey, J.; McCrudden, C. M.; Kirschman, J. L.; Vanover, D.; Van Hoecke, L.; Roose, K.; Deswarte, K.; De Geest, B. G.; Lienenklaus, S.; Santangelo, P. J.; Grooten, J.; McCarthy, H. O.; De Koker, S., Arginine-Rich Peptide-Based

mRNA Nanocomplexes Efficiently Instigate Cytotoxic T Cell Immunity Dependent on the Amphipathic Organization of the Peptide. *Adv. Healthcare Mater.* **2017,** 6, (13), 1601412.
[605] Yan, Y.; Xiong, H.; Zhang, X.; Cheng, Q.; Siegwart, D. J., Systemic mRNA Delivery to the Lungs by Functional Polyester-based Carriers. *Biomacromolecules* **2017,** 18, (12), 4307-4315.
[606] Chahal, J. S.; Khan, O. F.; Cooper, C. L.; McPartlan, J. S.; Tsosie, J. K.; Tilley, L. D.; Sidik, S. M.; Lourido, S.; Langer, R.; Bavari, S.; Ploegh, H. L.; Anderson, D. G., Dendrimer-RNA nanoparticles generate protective immunity against lethal Ebola, H1N1 influenza, and Toxoplasma gondii challenges with a single dose. *Proc. Natl. Acad. Sci. U.S.A.* **2016,** 113, (29), E4133.
[607] Jarzebinska, A.; Pasewald, T.; Lambrecht, J.; Mykhaylyk, O.; Kummerling, L.; Beck, P.; Hasenpusch, G.; Rudolph, C.; Plank, C.; Dohmen, C., A Single Methylene Group in Oligoalkylamine-Based Cationic Polymers and Lipids Promotes Enhanced mRNA Delivery. *Angew. Chem., Int. Ed. Engl.* **2016,** 55, (33), 9591-5.
[608] Nuhn, L.; Kaps, L.; Diken, M.; Schuppan, D.; Zentel, R., Reductive Decationizable Block Copolymers for Stimuli-Responsive mRNA Delivery. *Macromol. Rapid Commun.* **2016,** 37, (11), 924-33.
[609] Nathan J. Oldenhuis, A. C. E., Alan O. Burts, Keun Ah Ryu, Jae Chung, Mark E. Johnson, and Zhibin Guan, Biodegradable Dendronized Polymers for Efficient mRNA Delivery. *ChemistrySelect* **2016,** 1, 4413-4417.
[610] Uchida, S.; Kinoh, H.; Ishii, T.; Matsui, A.; Tockary, T. A.; Takeda, K. M.; Uchida, H.; Osada, K.; Itaka, K.; Kataoka, K., Systemic delivery of messenger RNA for the treatment of pancreatic cancer using polyplex nanomicelles with a cholesterol moiety. *Biomaterials* **2016,** 82, 221-228.
[611] Baba, M.; Itaka, K.; Kondo, K.; Yamasoba, T.; Kataoka, K., Treatment of neurological disorders by introducing mRNA in vivo using polyplex nanomicelles. *J. Controlled Release* **2015,** 201, 41-8.
[612] Islam, M. A.; Reesor, E. K.; Xu, Y.; Zope, H. R.; Zetter, B. R.; Shi, J., Biomaterials for mRNA delivery. *Biomater. Sci.* **2015,** 3, (12), 1519-33.
[613] Debus, H.; Baumhof, P.; Probst, J.; Kissel, T., Delivery of messenger RNA using poly(ethylene imine)-poly(ethylene glycol)-copolymer blends for polyplex formation: biophysical characterization and in vitro transfection properties. *J. Controlled Release* **2010,** 148, (3), 334-43.
[614] Kircheis, R.; Wightman, L.; Wagner, E., Design and gene delivery activity of modified polyethylenimines. *Adv. Drug Delivery Rev.* **2001,** 53, (3), 341-58.
[615] Kim, H. J.; Ogura, S.; Otabe, T.; Kamegawa, R.; Sato, M.; Kataoka, K.; Miyata, K., Fine-Tuning of Hydrophobicity in Amphiphilic Polyaspartamide Derivatives for Rapid and Transient Expression of Messenger RNA Directed Toward Genome Engineering in Brain. *ACS Cent. Sci.* **2019,** 5, (11), 1866-1875.
[616] Xie, Y.; Kim, N. H.; Nadithe, V.; Schalk, D.; Thakur, A.; Kılıç, A.; Lum, L. G.; Bassett, D. J. P.; Merkel, O. M., Targeted delivery of siRNA to activated T cells via transferrin-polyethylenimine (Tf-PEI) as a potential therapy of asthma. *J. Controlled Release* **2016,** 229, 120-129.
[617] Abbasi, S.; Uchida, S.; Toh, K.; Tockary, T. A.; Dirisala, A.; Hayashi, K.; Fukushima, S.; Kataoka, K., Co-encapsulation of Cas9 mRNA and guide RNA in polyplex micelles enables genome editing in mouse brain. *J. Controlled Release* **2021,** 332, 260-268.
[618] Bettinger, T.; Carlisle, R. C.; Read, M. L.; Ogris, M.; Seymour, L. W., Peptide-mediated RNA delivery: a novel approach for enhanced transfection of primary and post-mitotic cells. *Nucleic Acids Res.* **2001,** 29, (18), 3882-91.
[619] Shir, A.; Ogris, M.; Wagner, E.; Levitzki, A., EGF receptor-targeted synthetic double-stranded RNA eliminates glioblastoma, breast cancer, and adenocarcinoma tumors in mice. *PLoS Med.* **2006,** 3, (1), e6.
[620] Youn, H.; Chung, J. K., Modified mRNA as an alternative to plasmid DNA (pDNA) for transcript replacement and vaccination therapy. *Expert Opin. Biol. Ther.* **2015,** 15, (9), 1337-48.

[621] Yamamoto, A.; Kormann, M.; Rosenecker, J.; Rudolph, C., Current prospects for mRNA gene delivery. *Eur. J. Pharm. Biopharm.* **2009,** 71, (3), 484-9.
[622] Zintchenko, A.; Philipp, A.; Dehshahri, A.; Wagner, E., Simple modifications of branched PEI lead to highly efficient siRNA carriers with low toxicity. *Bioconjugate Chem.* **2008,** 19, (7), 1448-55.
[623] Morys, S., Optimization of shielding and targeting domains within sequence-defined, cationic carriers for pDNA delivery. *Dissertation, LMU München: : Fakultät für Chemie und Pharmazie* **2018**.
[624] Steinborn, B.; Truebenbach, I.; Morys, S.; Lächelt, U.; Wagner, E.; Zhang, W., Epidermal growth factor receptor targeted methotrexate and small interfering RNA co-delivery. *J. Gene Med.* **2018,** 20, (7-8), e3041.
[625] Itaka, K.; Harada, A.; Yamasaki, Y.; Nakamura, K.; Kawaguchi, H.; Kataoka, K., In situ single cell observation by fluorescence resonance energy transfer reveals fast intra-cytoplasmic delivery and easy release of plasmid DNA complexed with linear polyethylenimine. *J. Gene Med.* **2004,** 6, (1), 76-84.
[626] Boletta, A.; Benigni, A.; Lutz, J.; Remuzzi, G.; Soria, M. R.; Monaco, L., Nonviral gene delivery to the rat kidney with polyethylenimine. *Hum. Gene Ther.* **1997,** 8, (10), 1243-51.
[627] Chollet, P.; Favrot, M. C.; Hurbin, A.; Coll, J. L., Side-effects of a systemic injection of linear polyethylenimine-DNA complexes. *J. Gene Med.* **2002,** 4, (1), 84-91.
[628] Lungwitz, U.; Breunig, M.; Blunk, T.; Göpferich, A., Polyethylenimine-based non-viral gene delivery systems. *Eur. J. Pharm. Biopharm.* **2005,** 60, (2), 247-66.
[629] von Harpe, A.; Petersen, H.; Li, Y.; Kissel, T., Characterization of commercially available and synthesized polyethylenimines for gene delivery. *J. Controlled Release* **2000,** 69, (2), 309-322.
[630] He, D.; Müller, K.; Krhac Levacic, A.; Kos, P.; Lächelt, U.; Wagner, E., Combinatorial Optimization of Sequence-Defined Oligo(ethanamino)amides for Folate Receptor-Targeted pDNA and siRNA Delivery. *Bioconjugate Chem.* **2016,** 27, (3), 647-59.
[631] Levacic, A. K.; Morys, S.; Kempter, S.; Lächelt, U.; Wagner, E., Minicircle Versus Plasmid DNA Delivery by Receptor-Targeted Polyplexes. *Hum. Gene Ther.* **2017,** 28, (10), 862-874.
[632] Rejman, J.; Oberle, V.; Zuhorn, I. S.; Hoekstra, D., Size-dependent internalization of particles via the pathways of clathrin- and caveolae-mediated endocytosis. *Biochem. J.* **2004,** 377, (Pt 1), 159-169.
[633] Qiu, Y.; Man, R. C. H.; Liao, Q.; Kung, K. L. K.; Chow, M. Y. T.; Lam, J. K. W., Effective mRNA pulmonary delivery by dry powder formulation of PEGylated synthetic KL4 peptide. *J. Controlled Release* **2019,** 314, 102-115.
[634] Osman, G.; Rodriguez, J.; Chan, S. Y.; Chisholm, J.; Duncan, G.; Kim, N.; Tatler, A. L.; Shakesheff, K. M.; Hanes, J.; Suk, J. S.; Dixon, J. E., PEGylated enhanced cell penetrating peptide nanoparticles for lung gene therapy. *J. Controlled Release* **2018,** 285, 35-45.
[635] Klein, P. M.; Wagner, E., Click-Shielded and Targeted Lipopolyplexes. *Methods Mol. Biol.* **2019,** 2036, 141-164.
[636] Siegel, R. L.; Miller, K. D.; Jemal, A., Cancer statistics, 2019. *Ca-Cancer J. Clin.* **2019,** 69, (1), 7-34.
[637] Think globally about cancer. *Nat. Med.* **2019,** 25, (3), 351-351.
[638] Ferlay, J.; Colombet, M.; Soerjomataram, I.; Mathers, C.; Parkin, D. M.; Piñeros, M.; Znaor, A.; Bray, F., Estimating the global cancer incidence and mortality in 2018: GLOBOCAN sources and methods. *Int. J. Cancer* **2019,** 144, (8), 1941-1953.
[639] Ferlay, J.; Colombet, M.; Soerjomataram, I.; Dyba, T.; Randi, G.; Bettio, M.; Gavin, A.; Visser, O.; Bray, F., Cancer incidence and mortality patterns in Europe: Estimates for 40 countries and 25 major cancers in 2018. *Eur. J. Cancer* **2018,** 103, 356-387.
[640] Bray, F.; Ferlay, J.; Soerjomataram, I.; Siegel, R. L.; Torre, L. A.; Jemal, A., Global cancer statistics 2018: GLOBOCAN estimates of incidence and mortality worldwide for 36 cancers in 185 countries. *Ca-Cancer J. Clin.* **2018,** 68, (6), 394-424.

[641] Zheng, H. C., The molecular mechanisms of chemoresistance in cancers. *Oncotarget* **2017,** 8, (35), 59950-59964.
[642] Liu, Q.; Zhang, H.; Jiang, X.; Qian, C.; Liu, Z.; Luo, D., Factors involved in cancer metastasis: a better understanding to “seed and soil” hypothesis. *Mol. Cancer* **2017,** 16, (1), 176.
[643] Schirrmacher, V., From chemotherapy to biological therapy: A review of novel concepts to reduce the side effects of systemic cancer treatment (Review). *Int. J. Oncol.* **2019,** 54, (2), 407-419.
[644] Rosenberg, S. A., A New Era for Cancer Immunotherapy Based on the Genes that Encode Cancer Antigens. *Immunity* **1999,** 10, (3), 281-287.
[645] Zugazagoitia, J.; Guedes, C.; Ponce, S.; Ferrer, I.; Molina-Pinelo, S.; Paz-Ares, L., Current Challenges in Cancer Treatment. *Clin. Ther.* **2016,** 38, (7), 1551-66.
[646] Tariman, J. D., Changes in Cancer Treatment: Mabs, Mibs, Mids, Nabs, and Nibs. *Nurs. Clin. North Am.* **2017,** 52, (1), 65-81.
[647] Farkona, S.; Diamandis, E. P.; Blasutig, I. M., Cancer immunotherapy: the beginning of the end of cancer? *BMC Med.* **2016,** 14, (1), 73.
[648] Saleh, T.; Shojaosadati, S. A., Multifunctional nanoparticles for cancer immunotherapy. *Hum. Vaccines Immunother.* **2016,** 12, (7), 1863-1875.
[649] Sami, H.; Ogris, M., Biopharmaceuticals and gene vectors opening new avenues in cancer immune therapy. *Ther. Delivery* **2016,** 7, (7), 419-422.
[650] Emens, L. A.; Ascierto, P. A.; Darcy, P. K.; Demaria, S.; Eggermont, A. M. M.; Redmond, W. L.; Seliger, B.; Marincola, F. M., Cancer immunotherapy: Opportunities and challenges in the rapidly evolving clinical landscape. *Eur. J. Cancer* **2017,** 81, 116-129.
[651] Rangel-Sosa, M. M.; Aguilar-Córdova, E.; Rojas-Martínez, A., Immunotherapy and gene therapy as novel treatments for cancer. *Colomb Med (Cali)* **2017,** 48, (3), 138-147.
[652] Song, W.; Musetti, S. N.; Huang, L., Nanomaterials for cancer immunotherapy. *Biomaterials* **2017,** 148, 16-30.
[653] Musetti, S.; Huang, L., Nanoparticle-Mediated Remodeling of the Tumor Microenvironment to Enhance Immunotherapy. *ACS Nano* **2018,** 12, (12), 11740-11755.
[654] Sau, S.; Alsaab, H. O.; Bhise, K.; Alzhrani, R.; Nabil, G.; Iyer, A. K., Multifunctional nanoparticles for cancer immunotherapy: A groundbreaking approach for reprogramming malfunctioned tumor environment. *J. Controlled Release* **2018,** 274, 24-34.
[655] Bai, Y.; Wang, Y.; Zhang, X.; Fu, J.; Xing, X.; Wang, C.; Gao, L.; Liu, Y.; Shi, L., Potential applications of nanoparticles for tumor microenvironment remodeling to ameliorate cancer immunotherapy. *Int. J. Pharm.* **2019,** 570, 118636.
[656] Luo, Q.; Zhang, L.; Luo, C.; Jiang, M., Emerging strategies in cancer therapy combining chemotherapy with immunotherapy. *Cancer Lett.* **2019,** 454, 191-203.
[657] Salvioni, L.; Rizzuto, A. M.; Bertolini, A. J.; Pandolfi, L.; Colombo, M.; Prosperi, D., Thirty Years of Cancer Nanomedicine: Success, Frustration, and Hope. *Cancers* **2019,** 11, (12).
[658] Shi, Y.; Lammers, T., Combining Nanomedicine and Immunotherapy. *Acc. Chem. Res.* **2019,** 52, (6), 1543-1554.
[659] Hargadon, K. M.; Johnson, C. E.; Williams, C. J., Immune checkpoint blockade therapy for cancer: An overview of FDA-approved immune checkpoint inhibitors. *Int. Immunopharmacol.* **2018,** 62, 29-39.
[660] Wilky, B. A., Immune checkpoint inhibitors: The linchpins of modern immunotherapy. *Immunol. Rev.* **2019,** 290, (1), 6-23.
[661] Chen, Q.; Wang, C.; Chen, G.; Hu, Q.; Gu, Z., Delivery Strategies for Immune Checkpoint Blockade. *Adv. Healthcare Mater.* **2018,** 7, (20), e1800424.
[662] Sermer, D.; Brentjens, R., CAR T-cell therapy: Full speed ahead. *Hematol. Oncol.* **2019,** 37 Suppl 1, 95-100.
[663] Shah, N. N.; Fry, T. J., Mechanisms of resistance to CAR T cell therapy. *Nat. Rev. Clin. Oncol.* **2019,** 16, (6), 372-385.

[664] Nabel, G. J.; Nabel, E. G.; Yang, Z. Y.; Fox, B. A.; Plautz, G. E.; Gao, X.; Huang, L.; Shu, S.; Gordon, D.; Chang, A. E., Direct gene transfer with DNA-liposome complexes in melanoma: expression, biologic activity, and lack of toxicity in humans. *Proc. Natl. Acad. Sci. U.S.A.* **1993,** 90, (23), 11307.
[665] Goldberg, M. S., Improving cancer immunotherapy through nanotechnology. *Nat. Rev. Cancer* **2019,** 19, (10), 587-602.
[666] Shae, D.; Baljon, J. J.; Wehbe, M.; Becker, K. W.; Sheehy, T. L.; Wilson, J. T., At the bench: Engineering the next generation of cancer vaccines. *J. Leukocyte Biol.* **2019**.
[667] Sadeghzadeh, M.; Bornehdeli, S.; Mohahammadrezakhani, H.; Abolghasemi, M.; Poursaei, E.; Asadi, M.; Zafari, V.; Aghebati-Maleki, L.; Shanehbandi, D., Dendritic cell therapy in cancer treatment; the state-of-the-art. *Life Sci.* **2020,** 254, 117580.
[668] Bastola, R.; Noh, G.; Keum, T.; Bashyal, S.; Seo, J. E.; Choi, J.; Oh, Y.; Cho, Y.; Lee, S., Vaccine adjuvants: smart components to boost the immune system. *Arch. Pharm. Res.* **2017,** 40, (11), 1238-1248.
[669] Marino, M.; Scuderi, F.; Provenzano, C.; Bartoccioni, E., Skeletal muscle cells: from local inflammatory response to active immunity. *Gene Ther.* **2011,** 18, (2), 109-16.
[670] Hengge, U. R.; Chan, E. F.; Foster, R. A.; Walker, P. S.; Vogel, J. C., Cytokine gene expression in epidermis with biological effects following injection of naked DNA. *Nat. Genet.* **1995,** 10, (2), 161-6.
[671] Oh, S.; Kessler, J. A., Design, Assembly, Production, and Transfection of Synthetic Modified mRNA. *Methods* **2018,** 133, 29-43.
[672] Bai, H.; Lester, G. M. S.; Petishnok, L. C.; Dean, D. A., Cytoplasmic transport and nuclear import of plasmid DNA. *Biosci. Rep.* **2017,** 37, (6).
[673] Lazzaro, S.; Giovani, C.; Mangiavacchi, S.; Magini, D.; Maione, D.; Baudner, B.; Geall, A. J.; De Gregorio, E.; D'Oro, U.; Buonsanti, C., CD8 T-cell priming upon mRNA vaccination is restricted to bone-marrow-derived antigen-presenting cells and may involve antigen transfer from myocytes. *Immunology* **2015,** 146, (2), 312-26.
[674] Sudowe, S.; Dominitzki, S.; Montermann, E.; Bros, M.; Grabbe, S.; Reske-Kunz, A. B., Uptake and presentation of exogenous antigen and presentation of endogenously produced antigen by skin dendritic cells represent equivalent pathways for the priming of cellular immune responses following biolistic DNA immunization. *Immunology* **2009,** 128, (1 Suppl), e193-205.
[675] Li, Q.; Wang, H.; Peng, H.; Huyan, T.; Cacalano, N. A., Exosomes: Versatile Nano Mediators of Immune Regulation. *Cancers* **2019,** 11, (10).
[676] Chen, Z.; Larregina, A. T.; Morelli, A. E., Impact of extracellular vesicles on innate immunity. *Curr. Opin. Organ Transplant.* **2019,** 24, (6), 670-678.
[677] den Haan, J. M.; Arens, R.; van Zelm, M. C., The activation of the adaptive immune system: cross-talk between antigen-presenting cells, T cells and B cells. *Immunol. Lett.* **2014,** 162, (2 Pt B), 103-12.
[678] Macri, C.; Dumont, C.; Johnston, A. P.; Mintern, J. D., Targeting dendritic cells: a promising strategy to improve vaccine effectiveness. *Clin. Transl. Immunol.* **2016,** 5, (3), e66.
[679] Porgador, A.; Irvine, K. R.; Iwasaki, A.; Barber, B. H.; Restifo, N. P.; Germain, R. N., Predominant role for directly transfected dendritic cells in antigen presentation to CD8+ T cells after gene gun immunization. *J. Exp. Med.* **1998,** 188, (6), 1075-82.
[680] Coban, C.; Kobiyama, K.; Jounai, N.; Tozuka, M.; Ishii, K. J., DNA vaccines: a simple DNA sensing matter? *Hum. Vaccines Immunother.* **2013,** 9, (10), 2216-21.
[681] Joffre, O.; Nolte, M. A.; Sporri, R.; Reis e Sousa, C., Inflammatory signals in dendritic cell activation and the induction of adaptive immunity. *Immunol. Rev.* **2009,** 227, (1), 234-47.
[682] Maecker, H. T.; Umetsu, D. T.; DeKruyff, R. H.; Levy, S., Cytotoxic T cell responses to DNA vaccination: dependence on antigen presentation via class II MHC. *Journal of immunology (Baltimore, Md. : 1950)* **1998,** 161, (12), 6532-6.
[683] Aloulou, M.; Fazilleau, N., Regulation of B cell responses by distinct populations of CD4 T cells. *Biomed. J.* **2019,** 42, (4), 243-251.

[684] Fu, S. H.; Chien, M. W.; Hsu, C. Y.; Liu, Y. W.; Sytwu, H. K., Interplay between Cytokine Circuitry and Transcriptional Regulation Shaping Helper T Cell Pathogenicity and Plasticity in Inflammatory Bowel Disease. *Int. J. Mol. Sci.* **2020,** 21, (9).
[685] Farhood, B.; Najafi, M.; Mortezaee, K., CD8(+) cytotoxic T lymphocytes in cancer immunotherapy: A review. *J. Cell. Physiol.* **2019,** 234, (6), 8509-8521.
[686] Tagawa, S. T.; Lee, P.; Snively, J.; Boswell, W.; Ounpraseuth, S.; Lee, S.; Hickingbottom, B.; Smith, J.; Johnson, D.; Weber, J. S., Phase I study of intranodal delivery of a plasmid DNA vaccine for patients with Stage IV melanoma. *Cancer* **2003,** 98, (1), 144-54.
[687] Proudfoot, O.; Apostolopoulos, V.; Pietersz, G. A., Receptor-mediated delivery of antigens to dendritic cells: anticancer applications. *Mol. Pharmaceutics* **2007,** 4, (1), 58-72.
[688] Steele, J. C.; Rao, A.; Marsden, J. R.; Armstrong, C. J.; Berhane, S.; Billingham, L. J.; Graham, N.; Roberts, C.; Ryan, G.; Uppal, H.; Walker, C.; Young, L. S.; Steven, N. M., Phase I/II trial of a dendritic cell vaccine transfected with DNA encoding melan A and gp100 for patients with metastatic melanoma. *Gene Ther.* **2011,** 18, (6), 584-93.
[689] Lopes, A.; Vandermeulen, G.; Préat, V., Cancer DNA vaccines: current preclinical and clinical developments and future perspectives. *J. Exp. Clin. Cancer Res.* **2019,** 38, (1), 146.
[690] McCann, K. J.; Mander, A.; Cazaly, A.; Chudley, L.; Stasakova, J.; Thirdborough, S.; King, A.; Lloyd-Evans, P.; Buxton, E.; Edwards, C.; Halford, S.; Bateman, A.; O'Callaghan, A.; Clive, S.; Anthoney, A.; Jodrell, D. I.; Weinschenk, T.; Simon, P.; Sahin, U.; Thomas, G. J.; Stevenson, F. K.; Ottensmeier, C. H., Targeting Carcinoembryonic Antigen with DNA Vaccination: On-Target Adverse Events Link with Immunologic and Clinical Outcomes. *Clin. Cancer Res.* **2016,** 22, (19), 4827-4836.
[691] McNeel, D. G.; Eickhoff, J. C.; Wargowski, E.; Zahm, C.; Staab, M. J.; Straus, J.; Liu, G., Concurrent, but not sequential, PD-1 blockade with a DNA vaccine elicits anti-tumor responses in patients with metastatic, castration-resistant prostate cancer. *Oncotarget* **2018,** 9, (39), 25586-25596.
[692] Tosch, C.; Bastien, B.; Barraud, L.; Grellier, B.; Nourtier, V.; Gantzer, M.; Limacher, J. M.; Quemeneur, E.; Bendjama, K.; Préville, X., Viral based vaccine TG4010 induces broadening of specific immune response and improves outcome in advanced NSCLC. *J. Immunother. Cancer* **2017,** 5, (1), 70.
[693] Dörrie, J.; Schaft, N.; Schuler, G.; Schuler-Thurner, B., Therapeutic Cancer Vaccination with Ex Vivo RNA-Transfected Dendritic Cells-An Update. *Pharmaceutics* **2020,** 12, (2).
[694] Van Tendeloo, V. F.; Van de Velde, A.; Van Driessche, A.; Cools, N.; Anguille, S.; Ladell, K.; Gostick, E.; Vermeulen, K.; Pieters, K.; Nijs, G.; Stein, B.; Smits, E. L.; Schroyens, W. A.; Gadisseur, A. P.; Vrelust, I.; Jorens, P. G.; Goossens, H.; de Vries, I. J.; Price, D. A.; Oji, Y.; Oka, Y.; Sugiyama, H.; Berneman, Z. N., Induction of complete and molecular remissions in acute myeloid leukemia by Wilms' tumor 1 antigen-targeted dendritic cell vaccination. *Proc. Natl. Acad. Sci. U.S.A.* **2010,** 107, (31), 13824-9.
[695] Anguille, S.; Van de Velde, A. L.; Smits, E. L.; Van Tendeloo, V. F.; Juliusson, G.; Cools, N.; Nijs, G.; Stein, B.; Lion, E.; Van Driessche, A.; Vandenbosch, I.; Verlinden, A.; Gadisseur, A. P.; Schroyens, W. A.; Muylle, L.; Vermeulen, K.; Maes, M. B.; Deiteren, K.; Malfait, R.; Gostick, E.; Lammens, M.; Couttenye, M. M.; Jorens, P.; Goossens, H.; Price, D. A.; Ladell, K.; Oka, Y.; Fujiki, F.; Oji, Y.; Sugiyama, H.; Berneman, Z. N., Dendritic cell vaccination as postremission treatment to prevent or delay relapse in acute myeloid leukemia. *Blood* **2017,** 130, (15), 1713-1721.
[696] Su, Z.; Vieweg, J.; Weizer, A. Z.; Dahm, P.; Yancey, D.; Turaga, V.; Higgins, J.; Boczkowski, D.; Gilboa, E.; Dannull, J., Enhanced induction of telomerase-specific CD4(+) T cells using dendritic cells transfected with RNA encoding a chimeric gene product. *Cancer Res.* **2002,** 62, (17), 5041-8.
[697] Khoury, H. J.; Collins, R. H., Jr.; Blum, W.; Stiff, P. S.; Elias, L.; Lebkowski, J. S.; Reddy, A.; Nishimoto, K. P.; Sen, D.; Wirth, E. D., 3rd; Case, C. C.; DiPersio, J. F., Immune responses

and long-term disease recurrence status after telomerase-based dendritic cell immunotherapy in patients with acute myeloid leukemia. *Cancer* **2017,** 123, (16), 3061-3072.
[698] Vik-Mo, E. O.; Nyakas, M.; Mikkelsen, B. V.; Moe, M. C.; Due-Tønnesen, P.; Suso, E. M.; Sæbøe-Larssen, S.; Sandberg, C.; Brinchmann, J. E.; Helseth, E.; Rasmussen, A. M.; Lote, K.; Aamdal, S.; Gaudernack, G.; Kvalheim, G.; Langmoen, I. A., Therapeutic vaccination against autologous cancer stem cells with mRNA-transfected dendritic cells in patients with glioblastoma. *Cancer Immunol. Immunother.* **2013,** 62, (9), 1499-509.
[699] Batich, K. A.; Reap, E. A.; Archer, G. E.; Sanchez-Perez, L.; Nair, S. K.; Schmittling, R. J.; Norberg, P.; Xie, W.; Herndon, J. E., 2nd; Healy, P.; McLendon, R. E.; Friedman, A. H.; Friedman, H. S.; Bigner, D.; Vlahovic, G.; Mitchell, D. A.; Sampson, J. H., Long-term Survival in Glioblastoma with Cytomegalovirus pp65-Targeted Vaccination. *Clin. Cancer Res.* **2017,** 23, (8), 1898-1909.
[700] Rahman, M.; Dastmalchi, F.; Karachi, A.; Mitchell, D., The role of CMV in glioblastoma and implications for immunotherapeutic strategies. *OncoImmunology* **2019,** 8, (1), e1514921.
[701] Wilgenhof, S.; Corthals, J.; Van Nuffel, A. M.; Benteyn, D.; Heirman, C.; Bonehill, A.; Thielemans, K.; Neyns, B., Long-term clinical outcome of melanoma patients treated with messenger RNA-electroporated dendritic cell therapy following complete resection of metastases. *Cancer Immunol. Immunother.* **2015,** 64, (3), 381-8.
[702] Wilgenhof, S.; Corthals, J.; Heirman, C.; van Baren, N.; Lucas, S.; Kvistborg, P.; Thielemans, K.; Neyns, B., Phase II Study of Autologous Monocyte-Derived mRNA Electroporated Dendritic Cells (TriMixDC-MEL) Plus Ipilimumab in Patients With Pretreated Advanced Melanoma. *J. Clin. Oncol.* **2016,** 34, (12), 1330-8.
[703] Nazarkina Zh, K.; Khar'kova, M. V.; Antonets, D. V.; Morozkin, E. S.; Bazhan, S. I.; Karpenko, L. I.; Vlasov, V. V.; Ilyichev, A. A.; Laktionov, P. P., Design of Polyepitope DNA Vaccine against Breast Carcinoma Cells and Analysis of Its Expression in Dendritic Cells. *Bull. Exp. Biol. Med.* **2016,** 160, (4), 486-90.
[704] Hirayama, M.; Nishimura, Y., The present status and future prospects of peptide-based cancer vaccines. *International immunology* **2016,** 28, (7), 319-28.
[705] Brennick, C. A.; George, M. M.; Corwin, W. L.; Srivastava, P. K.; Ebrahimi-Nik, H., Neoepitopes as cancer immunotherapy targets: key challenges and opportunities. *Immunotherapy* **2017,** 9, (4), 361-371.
[706] Kiyotani, K.; Chan, H. T.; Nakamura, Y., Immunopharmacogenomics towards personalized cancer immunotherapy targeting neoantigens. *Cancer Sci.* **2018,** 109, (3), 542-549.
[707] Sultan, H.; Trillo-Tinoco, J.; Rodriguez, P.; Celis, E., Effective antitumor peptide vaccines can induce severe autoimmune pathology. *Oncotarget* **2017,** 8, (41), 70317-70331.
[708] Lu, Y. C.; Yao, X.; Crystal, J. S.; Li, Y. F.; El-Gamil, M.; Gross, C.; Davis, L.; Dudley, M. E.; Yang, J. C.; Samuels, Y.; Rosenberg, S. A.; Robbins, P. F., Efficient identification of mutated cancer antigens recognized by T cells associated with durable tumor regressions. *Clin. Cancer Res.* **2014,** 20, (13), 3401-10.
[709] Sahin, U.; Derhovanessian, E.; Miller, M.; Kloke, B. P.; Simon, P.; Löwer, M.; Bukur, V.; Tadmor, A. D.; Luxemburger, U.; Schrörs, B.; Omokoko, T.; Vormehr, M.; Albrecht, C.; Paruzynski, A.; Kuhn, A. N.; Buck, J.; Heesch, S.; Schreeb, K. H.; Müller, F.; Ortseifer, I.; Vogler, I.; Godehardt, E.; Attig, S.; Rae, R.; Breitkreuz, A.; Tolliver, C.; Suchan, M.; Martic, G.; Hohberger, A.; Sorn, P.; Diekmann, J.; Ciesla, J.; Waksmann, O.; Brück, A. K.; Witt, M.; Zillgen, M.; Rothermel, A.; Kasemann, B.; Langer, D.; Bolte, S.; Diken, M.; Kreiter, S.; Nemecek, R.; Gebhardt, C.; Grabbe, S.; Höller, C.; Utikal, J.; Huber, C.; Loquai, C.; Türeci, Ö., Personalized RNA mutanome vaccines mobilize poly-specific therapeutic immunity against cancer. *Nature* **2017,** 547, (7662), 222-226.
[710] Bins, A. D.; Wolkers, M. C.; van den Boom, M. D.; Haanen, J. B.; Schumacher, T. N., In vivo antigen stability affects DNA vaccine immunogenicity. *Journal of immunology (Baltimore, Md. : 1950)* **2007,** 179, (4), 2126-33.
[711] Hoppes, R.; Oostvogels, R.; Luimstra, J. J.; Wals, K.; Toebes, M.; Bies, L.; Ekkebus, R.; Rijal, P.; Celie, P. H.; Huang, J. H.; Emmelot, M. E.; Spaapen, R. M.; Lokhorst, H.; Schumacher, T. N.; Mutis, T.; Rodenko, B.; Ovaa, H., Altered peptide ligands revisited: vaccine design through

chemically modified HLA-A2-restricted T cell epitopes. *Journal of immunology (Baltimore, Md. : 1950)* **2014,** 193, (10), 4803-13.
[712] Seledtsova, G. V.; Shishkov, A. A.; Kaschenko, E. A.; Goncharov, A. G.; Gazatova, N. D.; Seledtsov, V. I., Xenogeneic cell-based vaccine therapy for stage III melanoma: safety, immune-mediated responses and survival benefits. *Eur. J. Dermatol.* **2016,** 26, (2), 138-43.
[713] Sponaas, A.; Carstens, C.; Koch, N., C-terminal extension of the MHC class II-associated invariant chain by an antigenic sequence triggers activation of naive T cells. *Gene Ther.* **1999,** 6, (11), 1826-34.
[714] Tudor, D.; Dubuquoy, C.; Gaboriau, V.; Lefevre, F.; Charley, B.; Riffault, S., TLR9 pathway is involved in adjuvant effects of plasmid DNA-based vaccines. *Vaccine* **2005,** 23, (10), 1258-64.
[715] Suschak, J. J.; Wang, S.; Fitzgerald, K. A.; Lu, S., A cGAS-Independent STING/IRF7 Pathway Mediates the Immunogenicity of DNA Vaccines. *Journal of immunology (Baltimore, Md. : 1950)* **2016,** 196, (1), 310-6.
[716] Larregina, A. T.; Watkins, S. C.; Erdos, G.; Spencer, L. A.; Storkus, W. J.; Beer Stolz, D.; Falo, L. D., Jr., Direct transfection and activation of human cutaneous dendritic cells. *Gene Ther.* **2001,** 8, (8), 608-17.
[717] Hemmi, H.; Takeuchi, O.; Kawai, T.; Kaisho, T.; Sato, S.; Sanjo, H.; Matsumoto, M.; Hoshino, K.; Wagner, H.; Takeda, K.; Akira, S., A Toll-like receptor recognizes bacterial DNA. *Nature* **2000,** 408, (6813), 740-5.
[718] Scheiermann, J.; Klinman, D. M., Clinical evaluation of CpG oligonucleotides as adjuvants for vaccines targeting infectious diseases and cancer. *Vaccine* **2014,** 32, (48), 6377-89.
[719] Garg, R.; Kaur, M.; Saxena, A.; Prasad, R.; Bhatnagar, R., Alum adjuvanted rabies DNA vaccine confers 80% protection against lethal 50 LD50 rabies challenge virus standard strain. *Mol. Immunol.* **2017,** 85, 166-173.
[720] Shedlock, D. J.; Tingey, C.; Mahadevan, L.; Hutnick, N.; Reuschel, E. L.; Kudchodkar, S.; Flingai, S.; Yan, J.; Kim, J. J.; Ugen, K. E.; Weiner, D. B.; Muthumani, K., Co-Administration of Molecular Adjuvants Expressing NF-Kappa B Subunit p65/RelA or Type-1 Transactivator T-bet Enhance Antigen Specific DNA Vaccine-Induced Immunity. *Vaccines* **2014,** 2, (2), 196-215.
[721] Pfeiffer, I. A.; Hoyer, S.; Gerer, K. F.; Voll, R. E.; Knippertz, I.; Gückel, E.; Schuler, G.; Schaft, N.; Dörrie, J., Triggering of NF-κB in cytokine-matured human DCs generates superior DCs for T-cell priming in cancer immunotherapy. *Eur. J. Immunol.* **2014,** 44, (11), 3413-28.
[722] Bosch, N. C.; Voll, R. E.; Voskens, C. J.; Gross, S.; Seliger, B.; Schuler, G.; Schaft, N.; Dörrie, J., NF-κB activation triggers NK-cell stimulation by monocyte-derived dendritic cells. *Ther. Adv. Med. Oncol.* **2019,** 11, 1758835919891622.
[723] Sasaki, S.; Amara, R. R.; Yeow, W. S.; Pitha, P. M.; Robinson, H. L., Regulation of DNA-raised immune responses by cotransfected interferon regulatory factors. *J. Virol.* **2002,** 76, (13), 6652-9.
[724] Bontkes, H. J.; Kramer, D.; Ruizendaal, J. J.; Meijer, C. J.; Hooijberg, E., Tumor associated antigen and interleukin-12 mRNA transfected dendritic cells enhance effector function of natural killer cells and antigen specific T-cells. *Clin. Immunol.* **2008,** 127, (3), 375-84.
[725] Li, S. S.; Kochar, N. K.; Elizaga, M.; Hay, C. M.; Wilson, G. J.; Cohen, K. W.; De Rosa, S. C.; Xu, R.; Ota-Setlik, A.; Morris, D.; Finak, G.; Allen, M.; Tieu, H. V.; Frank, I.; Sobieszczyk, M. E.; Hannaman, D.; Gottardo, R.; Gilbert, P. B.; Tomaras, G. D.; Corey, L.; Clarke, D. K.; Egan, M. A.; Eldridge, J. H.; McElrath, M. J.; Frahm, N., DNA Priming Increases Frequency of T-Cell Responses to a Vesicular Stomatitis Virus HIV Vaccine with Specific Enhancement of CD8(+) T-Cell Responses by Interleukin-12 Plasmid DNA. *Clin. Vaccine Immunol.* **2017,** 24, (11).
[726] Sun, L.; Yuan, Q.; Xu, T.; Yao, L.; Feng, J.; Ma, J.; Wang, L.; Lv, C.; Wang, D., Novel adjuvant for immunization against tuberculosis: DNA vaccine expressing Mycobacterium tuberculosis antigen 85A and interleukin-15 fusion product elicits strong immune responses in mice. *Biotechnol. Lett.* **2017,** 39, (8), 1159-1166.
[727] Zhang, Y.; Liang, S.; Li, X.; Wang, L.; Zhang, J.; Xu, J.; Huo, S.; Cao, X.; Zhong, Z.; Zhong, F., Mutual enhancement of IL-2 and IL-7 on DNA vaccine immunogenicity mainly involves

regulations on their receptor expression and receptor-expressing lymphocyte generation. *Vaccine* **2015,** 33, (30), 3480-7.
[728] Luo, Z.; Wang, C.; Yi, H.; Li, P.; Pan, H.; Liu, L.; Cai, L.; Ma, Y., Nanovaccine loaded with poly I:C and STAT3 siRNA robustly elicits anti-tumor immune responses through modulating tumor-associated dendritic cells in vivo. *Biomaterials* **2015,** 38, 50-60.
[729] Luo, X.; Peng, X.; Hou, J.; Wu, S.; Shen, J.; Wang, L., Folic acid-functionalized polyethylenimine superparamagnetic iron oxide nanoparticles as theranostic agents for magnetic resonance imaging and PD-L1 siRNA delivery for gastric cancer. *Int. J. Nanomed.* **2017,** 12, 5331-5343.
[730] Self-Fordham, J. B.; Naqvi, A. R.; Uttamani, J. R.; Kulkarni, V.; Nares, S., MicroRNA: Dynamic Regulators of Macrophage Polarization and Plasticity. *Front. Immunol.* **2017,** 8, 1062.
[731] Migault, M.; Donnou-Fournet, E.; Galibert, M. D.; Gilot, D., Definition and identification of small RNA sponges: Focus on miRNA sequestration. *Methods* **2017,** 117, 35-47.
[732] Lima, J. F.; Cerqueira, L.; Figueiredo, C.; Oliveira, C.; Azevedo, N. F., Anti-miRNA oligonucleotides: A comprehensive guide for design. *RNA Biol.* **2018,** 15, (3), 338-352.
[733] Wagner, E., Tumor-targeted Delivery of Anti-microRNA for Cancer Therapy: pHLIP is Key. *Angew. Chem., Int. Ed. Engl.* **2015,** 54, (20), 5824-6.
[734] Vargas, J. E.; Salton, G.; Sodre de Castro Laino, A.; Pires, T. D.; Bonamino, M.; Lenz, G.; Delgado-Canedo, A., pLR: a lentiviral backbone series to stable transduction of bicistronic genes and exchange of promoters. *Plasmid* **2012,** 68, (3), 179-85.
[735] Terenin, I. M.; Smirnova, V. V.; Andreev, D. E.; Dmitriev, S. E.; Shatsky, I. N., A researcher's guide to the galaxy of IRESs. *Cell. Mol. Life Sci.* **2017,** 74, (8), 1431-1455.
[736] Ko, H. L.; Park, H. J.; Kim, J.; Kim, H.; Youn, H.; Nam, J. H., Development of an RNA Expression Platform Controlled by Viral Internal Ribosome Entry Sites. *J. Microbiol. Biotechnol.* **2019,** 29, (1), 127-140.
[737] Chng, J.; Wang, T.; Nian, R.; Lau, A.; Hoi, K. M.; Ho, S. C.; Gagnon, P.; Bi, X.; Yang, Y., Cleavage efficient 2A peptides for high level monoclonal antibody expression in CHO cells. *mAbs* **2015,** 7, (2), 403-12.
[738] Kim, J. H.; Lee, S. R.; Li, L. H.; Park, H. J.; Park, J. H.; Lee, K. Y.; Kim, M. K.; Shin, B. A.; Choi, S. Y., High cleavage efficiency of a 2A peptide derived from porcine teschovirus-1 in human cell lines, zebrafish and mice. *PLoS One* **2011,** 6, (4), e18556.
[739] Gracey Maniar, L. E.; Maniar, J. M.; Chen, Z. Y.; Lu, J.; Fire, A. Z.; Kay, M. A., Minicircle DNA vectors achieve sustained expression reflected by active chromatin and transcriptional level. *Mol. Ther.* **2013,** 21, (1), 131-8.
[740] Stenler, S.; Blomberg, P.; Smith, C. I., Safety and efficacy of DNA vaccines: plasmids vs. minicircles. *Hum. Vaccines Immunother.* **2014,** 10, (5), 1306-8.
[741] Lechardeur, D.; Lukacs, G. L., Nucleocytoplasmic transport of plasmid DNA: a perilous journey from the cytoplasm to the nucleus. *Hum. Gene Ther.* **2006,** 17, (9), 882-9.
[742] Dean, D. A.; Dean, B. S.; Muller, S.; Smith, L. C., Sequence requirements for plasmid nuclear import. *Exp. Cell Res.* **1999,** 253, (2), 713-22.
[743] Kanazawa, T.; Yamazaki, M.; Fukuda, T.; Takashima, Y.; Okada, H., Versatile nuclear localization signal-based oligopeptide as a gene vector. *Biol. Pharm. Bull.* **2015,** 38, (4), 559-65.
[744] Grubor-Bauk, B.; Yu, W.; Wijesundara, D.; Gummow, J.; Garrod, T.; Brennan, A. J.; Voskoboinik, I.; Gowans, E. J., Intradermal delivery of DNA encoding HCV NS3 and perforin elicits robust cell-mediated immunity in mice and pigs. *Gene Ther.* **2016,** 23, (1), 26-37.
[745] Krinner, S.; Heitzer, A.; Asbach, B.; Wagner, R., Interplay of Promoter Usage and Intragenic CpG Content: Impact on GFP Reporter Gene Expression. *Hum. Gene Ther.* **2015,** 26, (12), 826-40.
[746] Yagi, M.; Miyamoto, T.; Toyama, Y.; Suda, T., Role of DC-STAMP in cellular fusion of osteoclasts and macrophage giant cells. *J. Bone Miner. Metab.* **2006,** 24, (5), 355-8.

[747] Dresch, C.; Edelmann, S. L.; Marconi, P.; Brocker, T., Lentiviral-mediated transcriptional targeting of dendritic cells for induction of T cell tolerance in vivo. *Journal of immunology (Baltimore, Md. : 1950)* **2008,** 181, (7), 4495-506.
[748] Bonkobara, M.; Zukas, P. K.; Shikano, S.; Nakamura, S.; Cruz, P. D., Jr.; Ariizumi, K., Epidermal Langerhans cell-targeted gene expression by a dectin-2 promoter. *Journal of immunology (Baltimore, Md. : 1950)* **2001,** 167, (12), 6893-900.
[749] Lopes, A.; Vanvarenberg, K.; Preat, V.; Vandermeulen, G., Codon-Optimized P1A-Encoding DNA Vaccine: Toward a Therapeutic Vaccination against P815 Mastocytoma. *Mol. Ther.-Nucleic Acids* **2017,** 8, 404-415.
[750] Bros, M.; Ross, X. L.; Pautz, A.; Reske-Kunz, A. B.; Ross, R., The human fascin gene promoter is highly active in mature dendritic cells due to a stage-specific enhancer. *Journal of immunology (Baltimore, Md. : 1950)* **2003,** 171, (4), 1825-34.
[751] Ross, R.; Sudowe, S.; Beisner, J.; Ross, X. L.; Ludwig-Portugall, I.; Steitz, J.; Tuting, T.; Knop, J.; Reske-Kunz, A. B., Transcriptional targeting of dendritic cells for gene therapy using the promoter of the cytoskeletal protein fascin. *Gene Ther.* **2003,** 10, (12), 1035-40.
[752] Raker, V.; Maxeiner, J.; Reske-Kunz, A. B.; Sudowe, S., Efficiency of biolistic DNA vaccination in experimental type I allergy. *Methods Mol. Biol.* **2013,** 940, 357-70.
[753] Castor, T.; Yogev, N.; Blank, T.; Barwig, C.; Prinz, M.; Waisman, A.; Bros, M.; Reske-Kunz, A. B., Inhibition of experimental autoimmune encephalomyelitis by tolerance-promoting DNA vaccination focused to dendritic cells. *PLoS One* **2018,** 13, (2), e0191927.
[754] Sudowe, S.; Höhn, Y.; Renzing, A.; Maxeiner, J.; Montermann, E.; Habermeier, A.; Closs, E.; Bros, M.; Reske-Kunz, A. B., Inhibition of antigen-specific immune responses by co-application of an indoleamine 2,3-dioxygenase (IDO)-encoding vector requires antigen transgene expression focused on dendritic cells. *Amino Acids* **2020,** 52, (3), 411-424.
[755] Angell, C.; Xie, S.; Zhang, L.; Chen, Y., DNA Nanotechnology for Precise Control over Drug Delivery and Gene Therapy. *Small* **2016,** 12, (9), 1117-32.
[756] Das, S. K.; Menezes, M. E.; Bhatia, S.; Wang, X. Y.; Emdad, L.; Sarkar, D.; Fisher, P. B., Gene Therapies for Cancer: Strategies, Challenges and Successes. *J. Cell. Physiol.* **2015,** 230, (2), 259-71.
[757] Cai, P.; Zhang, X.; Wang, M.; Wu, Y. L.; Chen, X., Combinatorial Nano-Bio Interfaces. *ACS Nano* **2018**.
[758] Houseley, J.; Tollervey, D., The many pathways of RNA degradation. *Cell* **2009,** 136, (4), 763-76.
[759] Li, B.; Zhang, X.; Dong, Y., Nanoscale platforms for messenger RNA delivery. *Wiley Interdiscip. Rev. Nanomed. Nanobiotechnol.* **2019,** 11, (2), e1530.
[760] Foged, C.; Brodin, B.; Frokjaer, S.; Sundblad, A., Particle size and surface charge affect particle uptake by human dendritic cells in an in vitro model. *Int. J. Pharm.* **2005,** 298, (2), 315-22.
[761] Xiang, S. D.; Scholzen, A.; Minigo, G.; David, C.; Apostolopoulos, V.; Mottram, P. L.; Plebanski, M., Pathogen recognition and development of particulate vaccines: does size matter? *Methods* **2006,** 40, (1), 1-9.
[762] Niikura, K.; Matsunaga, T.; Suzuki, T.; Kobayashi, S.; Yamaguchi, H.; Orba, Y.; Kawaguchi, A.; Hasegawa, H.; Kajino, K.; Ninomiya, T.; Ijiro, K.; Sawa, H., Gold nanoparticles as a vaccine platform: influence of size and shape on immunological responses in vitro and in vivo. *ACS Nano* **2013,** 7, (5), 3926-38.
[763] Radis-Baptista, G.; Campelo, I. S.; Morlighem, J. R. L.; Melo, L. M.; Freitas, V. J. F., Cell-penetrating peptides (CPPs): From delivery of nucleic acids and antigens to transduction of engineered nucleases for application in transgenesis. *J. Biotechnol.* **2017,** 252, 15-26.
[764] Falanga, A.; Galdiero, S., Peptide chemistry encounters nanomedicine: recent applications and upcoming scenarios in cancer. *Future Med. Chem.* **2018,** 10, (16), 1877-1880.
[765] Dane, K. Y.; Nembrini, C.; Tomei, A. A.; Eby, J. K.; O'Neil, C. P.; Velluto, D.; Swartz, M. A.; Inverardi, L.; Hubbell, J. A., Nano-sized drug-loaded micelles deliver payload to lymph node immune cells and prolong allograft survival. *J. Controlled Release* **2011,** 156, (2), 154-60.

[766] Allen, T. M.; Hansen, C. B.; Guo, L. S., Subcutaneous administration of liposomes: a comparison with the intravenous and intraperitoneal routes of injection. *Biochim. Biophys. Acta* **1993,** 1150, (1), 9-16.
[767] Longmire, M.; Choyke, P. L.; Kobayashi, H., Clearance properties of nano-sized particles and molecules as imaging agents: considerations and caveats. *Nanomedicine* **2008,** 3, (5), 703-17.
[768] Hu, J.; Sheng, Y.; Shi, J.; Yu, B.; Yu, Z.; Liao, G., Long circulating polymeric nanoparticles for gene/drug delivery. *Curr. Drug Metab.* **2017**.
[769] He, C.; Hu, Y.; Yin, L.; Tang, C.; Yin, C., Effects of particle size and surface charge on cellular uptake and biodistribution of polymeric nanoparticles. *Biomaterials* **2010,** 31, (13), 3657-66.
[770] Fogli, S.; Montis, C.; Paccosi, S.; Silvano, A.; Michelucci, E.; Berti, D.; Bosi, A.; Parenti, A.; Romagnoli, P., Inorganic nanoparticles as potential regulators of immune response in dendritic cells. *Nanomedicine* **2017,** 12, (14), 1647-1660.
[771] Svoboda, O.; Fohlerova, Z.; Baiazitova, L.; Mlynek, P.; Samouylov, K.; Provaznik, I.; Hubalek, J., Transfection by Polyethyleneimine-Coated Magnetic Nanoparticles: Fine-Tuning the Condition for Electrophysiological Experiments. *J. Biomed. Nanotechnol.* **2018,** 14, (8), 1505-1514.
[772] Xiong, L.; Qiao, S. Z., A mesoporous organosilica nano-bowl with high DNA loading capacity - a potential gene delivery carrier. *Nanoscale* **2016,** 8, (40), 17446-17450.
[773] Singh, D. P.; Herrera, C. E.; Singh, B.; Singh, S.; Singh, R. K.; Kumar, R., Graphene oxide: An efficient material and recent approach for biotechnological and biomedical applications. *Mater. Sci. Eng., C* **2018,** 86, 173-197.
[774] Kim, H.; Kim, J.; Lee, M.; Choi, H. C.; Kim, W. J., Stimuli-Regulated Enzymatically Degradable Smart Graphene-Oxide-Polymer Nanocarrier Facilitating Photothermal Gene Delivery. *Adv. Healthcare Mater.* **2016,** 5, (15), 1918-30.
[775] Yue, H.; Zhou, X.; Cheng, M.; Xing, D., Graphene oxide-mediated Cas9/sgRNA delivery for efficient genome editing. *Nanoscale* **2018,** 10, (3), 1063-1071.
[776] Quader, S.; Kataoka, K., Nanomaterial-Enabled Cancer Therapy. *Mol. Ther.* **2017,** 25, (7), 1501-1513.
[777] Jang, H. J.; Jeong, E. J.; Lee, K. Y., Carbon Dioxide-Generating PLG Nanoparticles for Controlled Anti-Cancer Drug Delivery. *Pharm. Res.* **2018,** 35, (3), 59.
[778] Li, Z.; Xiong, F.; He, J.; Dai, X.; Wang, G., Surface-functionalized, pH-responsive poly(lactic-co-glycolic acid)-based microparticles for intranasal vaccine delivery: Effect of surface modification with chitosan and mannan. *Eur. J. Pharm. Biopharm.* **2016,** 109, 24-34.
[779] Hao, F.; Li, Y.; Zhu, J.; Sun, J.; Marshall, B.; Lee, R. J.; Teng, L.; Yang, Z.; Xie, J., Polyethylenimine-based Formulations for Delivery of Oligonucleotides. *Curr. Med. Chem.* **2019,** 26, (13), 2264-2284.
[780] Erbacher, P.; Zou, S.; Bettinger, T.; Steffan, A. M.; Remy, J. S., Chitosan-based vector/DNA complexes for gene delivery: biophysical characteristics and transfection ability. *Pharm. Res.* **1998,** 15, (9), 1332-9.
[781] Liu, Q.; Chen, X.; Jia, J.; Zhang, W.; Yang, T.; Wang, L.; Ma, G., pH-Responsive Poly(D,L-lactic-co-glycolic acid) Nanoparticles with Rapid Antigen Release Behavior Promote Immune Response. *ACS Nano* **2015,** 9, (5), 4925-38.
[782] Slutter, B.; Plapied, L.; Fievez, V.; Sande, M. A.; des Rieux, A.; Schneider, Y. J.; Van Riet, E.; Jiskoot, W.; Preat, V., Mechanistic study of the adjuvant effect of biodegradable nanoparticles in mucosal vaccination. *J. Controlled Release* **2009,** 138, (2), 113-21.
[783] Lohcharoenkal, W.; Wang, L.; Chen, Y. C.; Rojanasakul, Y., Protein nanoparticles as drug delivery carriers for cancer therapy. *Biomed. Res. Int.* **2014,** 2014, 180549.
[784] Moran, M. C.; Rosell, N.; Ruano, G.; Busquets, M. A.; Vinardell, M. P., Gelatin-based nanoparticles as DNA delivery systems: Synthesis, physicochemical and biocompatible characterization. *Colloids Surf., B* **2015,** 134, 156-68.

[785] Kumari, M.; Liu, C. H.; Wu, W. C., Efficient gene delivery by oligochitosan conjugated serum albumin: Facile synthesis, polyplex stability, and transfection. *Carbohydr. Polym.* **2018,** 183, 37-49.
[786] Han, J.; Wang, Q.; Zhang, Z.; Gong, T.; Sun, X., Cationic bovine serum albumin based self-assembled nanoparticles as siRNA delivery vector for treating lung metastatic cancer. *Small* **2014,** 10, (3), 524-35.
[787] Rezaee, M.; Oskuee, R. K.; Nassirli, H.; Malaekeh-Nikouei, B., Progress in the development of lipopolyplexes as efficient non-viral gene delivery systems. *J. Controlled Release* **2016,** 236, 1-14.
[788] Felgner, P. L.; Gadek, T. R.; Holm, M.; Roman, R.; Chan, H. W.; Wenz, M.; Northrop, J. P.; Ringold, G. M.; Danielsen, M., Lipofection: a highly efficient, lipid-mediated DNA-transfection procedure. *Proc. Natl. Acad. Sci. U.S.A.* **1987,** 84, (21), 7413-7.
[789] Mevel, M.; Haudebourg, T.; Colombani, T.; Peuziat, P.; Dallet, L.; Chatin, B.; Lambert, O.; Berchel, M.; Montier, T.; Jaffres, P. A.; Lehn, P.; Pitard, B., Important role of phosphoramido linkage in imidazole-based dioleyl helper lipids for liposome stability and primary cell transfection. *J. Gene Med.* **2016,** 18, (1-3), 3-15.
[790] Yang, J.; Bahreman, A.; Daudey, G.; Bussmann, J.; Olsthoorn, R. C.; Kros, A., Drug Delivery via Cell Membrane Fusion Using Lipopeptide Modified Liposomes. *ACS Cent. Sci.* **2016,** 2, (9), 621-630.
[791] Glass, J. J.; Kent, S. J.; De Rose, R., Enhancing dendritic cell activation and HIV vaccine effectiveness through nanoparticle vaccination. *Expert Rev. Vaccines* **2016,** 15, (6), 719-29.
[792] Wagener, K.; Bros, M.; Krumb, M.; Langhanki, J.; Pektor, S.; Worm, M.; Schinnerer, M.; Montermann, E.; Miederer, M.; Frey, H.; Opatz, T.; Rösch, F., Targeting of Immune Cells with Trimannosylated Liposomes. *Adv. Ther.* **2020,** 3, (6), 1900185.
[793] Lindén, M., Biodistribution and Excretion of Intravenously Injected Mesoporous Silica Nanoparticles: Implications for Drug Delivery Efficiency and Safety. *Enzymes* **2018,** 43, 155-180.
[794] Guo, X.; Zhuang, Q.; Ji, T.; Zhang, Y.; Li, C.; Wang, Y.; Li, H.; Jia, H.; Liu, Y.; Du, L., Multi-functionalized chitosan nanoparticles for enhanced chemotherapy in lung cancer. *Carbohydr. Polym.* **2018,** 195, 311-320.
[795] Meng, H.; Leong, W.; Leong, K. W.; Chen, C.; Zhao, Y., Walking the line: The fate of nanomaterials at biological barriers. *Biomaterials* **2018,** 174, 41-53.
[796] Zhang, Y. N.; Poon, W.; Tavares, A. J.; McGilvray, I. D.; Chan, W. C. W., Nanoparticle-liver interactions: Cellular uptake and hepatobiliary elimination. *J. Controlled Release* **2016,** 240, 332-348.
[797] Li, P.; He, K.; Li, J.; Liu, Z.; Gong, J., The role of Kupffer cells in hepatic diseases. *Mol. Immunol.* **2017,** 85, 222-229.
[798] Sago, C. D.; Krupczak, B. R.; Lokugamage, M. P.; Gan, Z.; Dahlman, J. E., Cell Subtypes Within the Liver Microenvironment Differentially Interact with Lipid Nanoparticles. *Cell. Mol. Bioeng.* **2019,** 12, (5), 389-397.
[799] Pustylnikov, S.; Sagar, D.; Jain, P.; Khan, Z. K., Targeting the C-type lectins-mediated host-pathogen interactions with dextran. *J. Pharm. Pharm. Sci.* **2014,** 17, (3), 371-92.
[800] Elvevold, K.; Simon-Santamaria, J.; Hasvold, H.; McCourt, P.; Smedsrød, B.; Sørensen, K. K., Liver sinusoidal endothelial cells depend on mannose receptor-mediated recruitment of lysosomal enzymes for normal degradation capacity. *Hepatology* **2008,** 48, (6), 2007-15.
[801] Hughes, D. A.; Fraser, I. P.; Gordon, S., Murine macrophage scavenger receptor: in vivo expression and function as receptor for macrophage adhesion in lymphoid and non-lymphoid organs. *Eur. J. Immunol.* **1995,** 25, (2), 466-73.
[802] Poisson, J.; Lemoinne, S.; Boulanger, C.; Durand, F.; Moreau, R.; Valla, D.; Rautou, P. E., Liver sinusoidal endothelial cells: Physiology and role in liver diseases. *J. Hepatol.* **2017,** 66, (1), 212-227.

[803] Gül, N.; Babes, L.; Siegmund, K.; Korthouwer, R.; Bögels, M.; Braster, R.; Vidarsson, G.; ten Hagen, T. L.; Kubes, P.; van Egmond, M., Macrophages eliminate circulating tumor cells after monoclonal antibody therapy. *J. Clin. Invest.* **2014,** 124, (2), 812-23.
[804] Ganesan, L. P.; Kim, J.; Wu, Y.; Mohanty, S.; Phillips, G. S.; Birmingham, D. J.; Robinson, J. M.; Anderson, C. L., FcγRIIb on liver sinusoidal endothelium clears small immune complexes. *Journal of immunology (Baltimore, Md. : 1950)* **2012,** 189, (10), 4981-8.
[805] Hinglais, N.; Kazatchkine, M. D.; Mandet, C.; Appay, M. D.; Bariety, J., Human liver Kupffer cells express CR1, CR3, and CR4 complement receptor antigens. An immunohistochemical study. *Lab. Invest.* **1989,** 61, (5), 509-14.
[806] Bros, M.; Nuhn, L.; Simon, J.; Moll, L.; Mailander, V.; Landfester, K.; Grabbe, S., The Protein Corona as a Confounding Variable of Nanoparticle-Mediated Targeted Vaccine Delivery. *Front. Immunol.* **2018,** 9, 1760.
[807] Shen, L.; Tenzer, S.; Storck, W.; Hobernik, D.; Raker, V. K.; Fischer, K.; Decker, S.; Dzionek, A.; Krauthauser, S.; Diken, M.; Nikolaev, A.; Maxeiner, J.; Schuster, P.; Kappel, C.; Verschoor, A.; Schild, H.; Grabbe, S.; Bros, M., Protein corona-mediated targeting of nanocarriers to B cells allows redirection of allergic immune responses. *J. Allergy Clin. Immunol.* **2018**.
[808] Sun, X.; Wang, G.; Zhang, H.; Hu, S.; Liu, X.; Tang, J.; Shen, Y., The Blood Clearance Kinetics and Pathway of Polymeric Micelles in Cancer Drug Delivery. *ACS Nano* **2018,** 12, (6), 6179-6192.
[809] Zhou, H.; Fan, Z.; Li, P. Y.; Deng, J.; Arhontoulis, D. C.; Li, C. Y.; Bowne, W. B.; Cheng, H., Dense and Dynamic Polyethylene Glycol Shells Cloak Nanoparticles from Uptake by Liver Endothelial Cells for Long Blood Circulation. *ACS Nano* **2018,** 12, (10), 10130-10141.
[810] Hayat, S. M. G.; Jaafari, M. R.; Hatamipour, M.; Penson, P. E.; Sahebkar, A., Liposome Circulation Time is Prolonged by CD47 Coating. *Protein Pept. Lett.* **2020**.
[811] Gulla, S. K.; Rao, B. R.; Moku, G.; Jinka, S.; Nimmu, N. V.; Khalid, S.; Patra, C. R.; Chaudhuri, A., In vivo targeting of DNA vaccines to dendritic cells using functionalized gold nanoparticles. *Biomater. Sci.* **2019,** 7, (3), 773-788.
[812] Wi, T. I.; Byeon, Y.; Won, J. E.; Lee, J. M.; Kang, T. H.; Lee, J. W.; Lee, Y. J.; Sood, A. K.; Han, H. D.; Park, Y. M., Selective Tumor-Specific Antigen Delivery to Dendritic Cells Using Mannose-Labeled Poly(d, l-lactide-co-glycolide) Nanoparticles for Cancer Immunotherapy. *J. Biomed. Nanotechnol.* **2020,** 16, (2), 201-211.
[813] Chen, H.; Yuan, J.; Wang, Y.; Silvers, W. K., Distribution of ATPase-positive Langerhans cells in normal adult human skin. *Br. J. Dermatol.* **1985,** 113, (6), 707-11.
[814] Russo, E.; Nitschke, M.; Halin, C., Dendritic cell interactions with lymphatic endothelium. *Lymphatic Res. Biol.* **2013,** 11, (3), 172-82.
[815] Fernando, G. J.; Zhang, J.; Ng, H. I.; Haigh, O. L.; Yukiko, S. R.; Kendall, M. A., Influenza nucleoprotein DNA vaccination by a skin targeted, dry coated, densely packed microprojection array (Nanopatch) induces potent antibody and CD8(+) T cell responses. *J. Controlled Release* **2016,** 237, 35-41.
[816] Lambracht-Washington, D.; Fu, M.; Frost, P.; Rosenberg, R. N., Evaluation of a DNA Aβ42 vaccine in adult rhesus monkeys (Macaca mulatta): antibody kinetics and immune profile after intradermal immunization with full-length DNA Aβ42 trimer. *Alzheimers Res. Ther.* **2017,** 9, (1), 30.
[817] Alvarez, R. D.; Huh, W. K.; Bae, S.; Lamb, L. S., Jr.; Conner, M. G.; Boyer, J.; Wang, C.; Hung, C. F.; Sauter, E.; Paradis, M.; Adams, E. A.; Hester, S.; Jackson, B. E.; Wu, T. C.; Trimble, C. L., A pilot study of pNGVL4a-CRT/E7(detox) for the treatment of patients with HPV16+ cervical intraepithelial neoplasia 2/3 (CIN2/3). *Gynecologic oncology* **2016,** 140, (2), 245-52.
[818] Duong, H. T. T.; Yin, Y.; Thambi, T.; Nguyen, T. L.; Giang Phan, V. H.; Lee, M. S.; Lee, J. E.; Kim, J.; Jeong, J. H.; Lee, D. S., Smart vaccine delivery based on microneedle arrays decorated with ultra-pH-responsive copolymers for cancer immunotherapy. *Biomaterials* **2018,** 185, 13-24.

[819] Cole, G.; Ali, A. A.; McErlean, E.; Mulholland, E. J.; Short, A.; McCrudden, C. M.; McCaffrey, J.; Robson, T.; Kett, V. L.; Coulter, J. A.; Dunne, N. J.; Donnelly, R. F.; McCarthy, H. O., DNA vaccination via RALA nanoparticles in a microneedle delivery system induces a potent immune response against the endogenous prostate cancer stem cell antigen. *Acta Biomater.* **2019,** 96, 480-490.
[820] Samuels, S.; Marijne Heeren, A.; Zijlmans, H.; Welters, M. J. P.; van den Berg, J. H.; Philips, D.; Kvistborg, P.; Ehsan, I.; Scholl, S. M. E.; Nuijen, B.; Schumacher, T. N. M.; van Beurden, M.; Jordanova, E. S.; Haanen, J.; van der Burg, S. H.; Kenter, G. G., HPV16 E7 DNA tattooing: safety, immunogenicity, and clinical response in patients with HPV-positive vulvar intraepithelial neoplasia. *Cancer Immunol. Immunother.* **2017,** 66, (9), 1163-1173.
[821] Bernelin-Cottet, C.; Urien, C.; McCaffrey, J.; Collins, D.; Donadei, A.; McDaid, D.; Jakob, V.; Barnier-Quer, C.; Collin, N.; Bouguyon, E.; Bordet, E.; Barc, C.; Boulesteix, O.; Leplat, J. J.; Blanc, F.; Contreras, V.; Bertho, N.; Moore, A. C.; Schwartz-Cornil, I., Electroporation of a nanoparticle-associated DNA vaccine induces higher inflammation and immunity compared to its delivery with microneedle patches in pigs. *J. Controlled Release* **2019,** 308, 14-28.
[822] Schultheis, K.; Smith, T. R. F.; Kiosses, W. B.; Kraynyak, K. A.; Wong, A.; Oh, J.; Broderick, K. E., Delineating the Cellular Mechanisms Associated with Skin Electroporation. *Hum. Gene Ther: Methods.* **2018,** 29, (4), 177-188.
[823] Lamolinara, A.; Stramucci, L.; Hysi, A.; Iezzi, M.; Marchini, C.; Mariotti, M.; Amici, A.; Curcio, C., Intradermal DNA Electroporation Induces Cellular and Humoral Immune Response and Confers Protection against HER2/neu Tumor. *J. Immunol. Res.* **2015,** 2015, 159145.
[824] Lee, S. H.; Danishmalik, S. N.; Sin, J. I., DNA vaccines, electroporation and their applications in cancer treatment. *Hum. Vaccines Immunother.* **2015,** 11, (8), 1889-900.
[825] Katz, M. G.; Fargnoli, A. S.; Gubara, S. M.; Fish, K.; Weber, T.; Bridges, C. R.; Hajjar, R. J.; Ishikawa, K., Targeted Gene Delivery through the Respiratory System: Rationale for Intratracheal Gene Transfer. *J. Cardiovasc. Dev. Dis.* **2019,** 6, (1).
[826] Davies, L. A.; Nunez-Alonso, G. A.; McLachlan, G.; Hyde, S. C.; Gill, D. R., Aerosol delivery of DNA/liposomes to the lung for cystic fibrosis gene therapy. *Hum. Gene Ther.: Clin. Dev.* **2014,** 25, (2), 97-107.
[827] Zheng, Z.; Diaz-Arevalo, D.; Guan, H.; Zeng, M., Noninvasive vaccination against infectious diseases. *Hum. Vaccines Immunother.* **2018,** 14, (7), 1717-1733.
[828] Mortimer, G. M.; Butcher, N. J.; Musumeci, A. W.; Deng, Z. J.; Martin, D. J.; Minchin, R. F., Cryptic epitopes of albumin determine mononuclear phagocyte system clearance of nanomaterials. *ACS Nano* **2014,** 8, (4), 3357-66.
[829] Huang, G.; Huang, H., Application of dextran as nanoscale drug carriers. *Nanomedicine* **2018,** 13, (24), 3149-3158.
[830] Zhang, P.; Sun, F.; Liu, S.; Jiang, S., Anti-PEG antibodies in the clinic: Current issues and beyond PEGylation. *J. Controlled Release* **2016,** 244, (Pt B), 184-193.
[831] Frenz, T.; Grabski, E.; Duran, V.; Hozsa, C.; Stepczynska, A.; Furch, M.; Gieseler, R. K.; Kalinke, U., Antigen presenting cell-selective drug delivery by glycan-decorated nanocarriers. *Eur. J. Pharm. Biopharm.* **2015,** 95, (Pt A), 13-7.
[832] Burgdorf, S.; Lukacs-Kornek, V.; Kurts, C., The Mannose Receptor Mediates Uptake of Soluble but Not of Cell-Associated Antigen for Cross-Presentation. *Journal of immunology (Baltimore, Md. : 1950)* **2006,** 176, (11), 6770.
[833] Appelmelk, B. J.; van Die, I.; van Vliet, S. J.; Vandenbroucke-Grauls, C. M.; Geijtenbeek, T. B.; van Kooyk, Y., Cutting edge: carbohydrate profiling identifies new pathogens that interact with dendritic cell-specific ICAM-3-grabbing nonintegrin on dendritic cells. *Journal of immunology (Baltimore, Md. : 1950)* **2003,** 170, (4), 1635-9.
[834] Qiao, C.; Liu, J.; Yang, J.; Li, Y.; Weng, J.; Shao, Y.; Zhang, X., Enhanced non-inflammasome mediated immune responses by mannosylated zwitterionic-based cationic liposomes for HIV DNA vaccines. *Biomaterials* **2016,** 85, 1-17.

[835] Wang, Q.; Cao, W.; Yang, Z. G.; Zhao, G. F., DC targeting DNA vaccines induce protective and therapeutic antitumor immunity in mice. *Int. J. Clin. Exp. Med.* **2015,** 8, (10), 17565-77.
[836] Shimizu, K.; Iyoda, T.; Okada, M.; Yamasaki, S.; Fujii, S. I., Immune suppression and reversal of the suppressive tumor microenvironment. *International immunology* **2018,** 30, (10), 445-454.
[837] Weber, R.; Fleming, V.; Hu, X.; Nagibin, V.; Groth, C.; Altevogt, P.; Utikal, J.; Umansky, V., Myeloid-Derived Suppressor Cells Hinder the Anti-Cancer Activity of Immune Checkpoint Inhibitors. *Front. Immunol.* **2018,** 9, 1310.
[838] Ahrends, T.; Borst, J., The opposing roles of CD4(+) T cells in anti-tumour immunity. *Immunology* **2018**.
[839] Hippen, K. L.; Loschi, M.; Nicholls, J.; MacDonald, K. P. A.; Blazar, B. R., Effects of MicroRNA on Regulatory T Cells and Implications for Adoptive Cellular Therapy to Ameliorate Graft-versus-Host Disease. *Front. Immunol.* **2018,** 9, 57.
[840] Zhang, C.; Wang, S.; Liu, Y.; Yang, C., Epigenetics in myeloid derived suppressor cells: a sheathed sword towards cancer. *Oncotarget* **2016,** 7, (35), 57452-57463.
[841] He, W.; Liang, P.; Guo, G.; Huang, Z.; Niu, Y.; Dong, L.; Wang, C.; Zhang, J., Re-polarizing Myeloid-derived Suppressor Cells (MDSCs) with Cationic Polymers for Cancer Immunotherapy. *Sci. Rep.* **2016,** 6, 24506.
[842] Li, W.; Deng, C.; Yang, H.; Wang, G., The Regulatory T Cell in Active Systemic Lupus Erythematosus Patients: A Systemic Review and Meta-Analysis. *Front. Immunol.* **2019,** 10, 159.
[843] Bacher, P.; Scheffold, A., Antigen-specific regulatory T-cell responses against aeroantigens and their role in allergy. *Mucosal Immunol.* **2018,** 11, (6), 1537-1550.
[844] Najafi, M.; Farhood, B.; Mortezaee, K., Contribution of regulatory T cells to cancer: A review. *J. Cell. Physiol.* **2019,** 234, (6), 7983-7993.
[845] Attias, M.; Al-Aubodah, T.; Piccirillo, C. A., Mechanisms of human FoxP3(+) T(reg) cell development and function in health and disease. *Clin. Exp. Immunol.* **2019,** 197, (1), 36-51.
[846] Yang, S.; Xie, C.; Chen, Y.; Wang, J.; Chen, X.; Lu, Z.; June, R. R.; Zheng, S. G., Differential roles of TNFα-TNFR1 and TNFα-TNFR2 in the differentiation and function of CD4(+)Foxp3(+) induced Treg cells in vitro and in vivo periphery in autoimmune diseases. *Cell Death Dis.* **2019,** 10, (1), 27.
[847] Oh, J.; Wang, W.; Thomas, R.; Su, D. M., Capacity of tTreg generation is not impaired in the atrophied thymus. *PLoS Biol.* **2017,** 15, (11), e2003352.
[848] Zhong, H.; Liu, Y.; Xu, Z.; Liang, P.; Yang, H.; Zhang, X.; Zhao, J.; Chen, J.; Fu, S.; Tang, Y.; Lv, J.; Wang, J.; Olsen, N.; Xu, A.; Zheng, S. G., TGF-β-Induced CD8(+)CD103(+) Regulatory T Cells Show Potent Therapeutic Effect on Chronic Graft-versus-Host Disease Lupus by Suppressing B Cells. *Front. Immunol.* **2018,** 9, 35.
[849] Devi, K. S.; Anandasabapathy, N., The origin of DCs and capacity for immunologic tolerance in central and peripheral tissues. *Semin. Immunopathol.* **2017,** 39, (2), 137-152.
[850] Takenaka, M. C.; Quintana, F. J., Tolerogenic dendritic cells. *Semin. Immunopathol.* **2017,** 39, (2), 113-120.
[851] Hall, B. M.; Robinson, C. M.; Plain, K. M.; Verma, N. D.; Tran, G. T.; Nomura, M.; Carter, N.; Boyd, R.; Hodgkinson, S. J., Changes in Reactivity In Vitro of CD4(+)CD25(+) and CD4(+)CD25(-) T Cell Subsets in Transplant Tolerance. *Front. Immunol.* **2017,** 8, 994.
[852] Sun, X.; He, S.; Lv, C.; Sun, X.; Wang, J.; Zheng, W.; Wang, D., Analysis of murine and human Treg subsets in inflammatory bowel disease. *Mol. Med. Rep.* **2017,** 16, (3), 2893-2898.
[853] Huang, Y. H.; Chang, C. Y.; Kuo, Y. Z.; Fang, W. Y.; Kao, H. Y.; Tsai, S. T.; Wu, L. W., Cancer-associated fibroblast-derived interleukin-1β activates protumor C-C motif chemokine ligand 22 signaling in head and neck cancer. *Cancer Sci.* **2019,** 110, (9), 2783-2793.
[854] Siede, J.; Fröhlich, A.; Datsi, A.; Hegazy, A. N.; Varga, D. V.; Holecska, V.; Saito, H.; Nakae, S.; Löhning, M., IL-33 Receptor-Expressing Regulatory T Cells Are Highly Activated, Th2 Biased and Suppress CD4 T Cell Proliferation through IL-10 and TGFβ Release. *PLoS One* **2016,** 11, (8), e0161507.

[855] Tanaka, A.; Sakaguchi, S., Targeting Treg cells in cancer immunotherapy. *Eur. J. Immunol.* **2019,** 49, (8), 1140-1146.
[856] Conroy, H.; Galvin, K. C.; Higgins, S. C.; Mills, K. H., Gene silencing of TGF-β1 enhances antitumor immunity induced with a dendritic cell vaccine by reducing tumor-associated regulatory T cells. *Cancer Immunol. Immunother.* **2012,** 61, (3), 425-31.
[857] Masjedi, A.; Ahmadi, A.; Ghani, S.; Malakotikhah, F.; Nabi Afjadi, M.; Irandoust, M.; Karoon Kiani, F.; Heydarzadeh Asl, S.; Atyabi, F.; Hassannia, H.; Hojjat-Farsangi, M.; Namdar, A.; Ghalamfarsa, G.; Jadidi-Niaragh, F., Silencing adenosine A2a receptor enhances dendritic cell-based cancer immunotherapy. *Nanomedicine* **2020,** 29, 102240.
[858] Zhang, H. H.; Fei, R.; Xie, X. W.; Wang, L.; Luo, H.; Wang, X. Y.; Wei, L.; Chen, H. S., [Specific suppression in regulatory T cells by Foxp3 siRNA contributes to enhance the in vitro anti-tumor immune response in hepatocellular carcinoma patients]. *Beijing Da Xue Xue Bao Yi Xue Ban* **2009,** 41, (3), 313-8.
[859] Kang, S.; Xie, J.; Ma, S.; Liao, W.; Zhang, J.; Luo, R., Targeted knock down of CCL22 and CCL17 by siRNA during DC differentiation and maturation affects the recruitment of T subsets. *Immunobiology* **2010,** 215, (2), 153-62.
[860] Jebbawi, F.; Fayyad-Kazan, H.; Merimi, M.; Lewalle, P.; Verougstraete, J. C.; Leo, O.; Romero, P.; Burny, A.; Badran, B.; Martiat, P.; Rouas, R., A microRNA profile of human CD8(+) regulatory T cells and characterization of the effects of microRNAs on Treg cell-associated genes. *J. Transl. Med.* **2014,** 12, 218.
[861] Jonuleit, H.; Bopp, T.; Becker, C., Treg cells as potential cellular targets for functionalized nanoparticles in cancer therapy. *Nanomedicine* **2016,** 11, (20), 2699-2709.
[862] Naghavian, R.; Ghaedi, K.; Kiani-Esfahani, A.; Ganjalikhani-Hakemi, M.; Etemadifar, M.; Nasr-Esfahani, M. H., miR-141 and miR-200a, Revelation of New Possible Players in Modulation of Th17/Treg Differentiation and Pathogenesis of Multiple Sclerosis. *PLoS One* **2015,** 10, (5), e0124555.
[863] Zhou, J.; Li, X.; Wu, X.; Zhang, T.; Zhu, Q.; Wang, X.; Wang, H.; Wang, K.; Lin, Y.; Wang, X., Exosomes Released from Tumor-Associated Macrophages Transfer miRNAs That Induce a Treg/Th17 Cell Imbalance in Epithelial Ovarian Cancer. *Cancer Immunol. Res.* **2018,** 6, (12), 1578-1592.
[864] Klein, M.; Bopp, T., Cyclic AMP Represents a Crucial Component of Treg Cell-Mediated Immune Regulation. *Front. Immunol.* **2016,** 7, 315.
[865] Frick, S. U.; Domogalla, M. P.; Baier, G.; Wurm, F. R.; Mailänder, V.; Landfester, K.; Steinbrink, K., Interleukin-2 Functionalized Nanocapsules for T Cell-Based Immunotherapy. *ACS Nano* **2016,** 10, (10), 9216-9226.
[866] Woller, N.; Knocke, S.; Mundt, B.; Gürlevik, E.; Strüver, N.; Kloos, A.; Boozari, B.; Schache, P.; Manns, M. P.; Malek, N. P.; Sparwasser, T.; Zender, L.; Wirth, T. C.; Kubicka, S.; Kühnel, F., Virus-induced tumor inflammation facilitates effective DC cancer immunotherapy in a Treg-dependent manner in mice. *J. Clin. Invest.* **2011,** 121, (7), 2570-82.
[867] Al Sayed, M. F.; Amrein, M. A.; Bührer, E. D.; Huguenin, A. L.; Radpour, R.; Riether, C.; Ochsenbein, A. F., T-cell-Secreted TNFα Induces Emergency Myelopoiesis and Myeloid-Derived Suppressor Cell Differentiation in Cancer. *Cancer Res.* **2019,** 79, (2), 346-359.
[868] Keskinov, A. A.; Shurin, M. R., Myeloid regulatory cells in tumor spreading and metastasis. *Immunobiology* **2015,** 220, (2), 236-42.
[869] Salminen, A.; Kauppinen, A.; Kaarniranta, K., AMPK activation inhibits the functions of myeloid-derived suppressor cells (MDSC): impact on cancer and aging. *J. Mol. Med.* **2019,** 97, (8), 1049-1064.
[870] Bruger, A. M.; Dorhoi, A.; Esendagli, G.; Barczyk-Kahlert, K.; van der Bruggen, P.; Lipoldova, M.; Perecko, T.; Santibanez, J.; Saraiva, M.; Van Ginderachter, J. A.; Brandau, S., How to measure the immunosuppressive activity of MDSC: assays, problems and potential solutions. *Cancer Immunol. Immunother.* **2019,** 68, (4), 631-644.

[871] Zeng, Y.; Hahn, S.; Stokes, J.; Hoffman, E. A.; Schmelz, M.; Proytcheva, M.; Chernoff, J.; Katsanis, E., Pak2 regulates myeloid-derived suppressor cell development in mice. *Blood Adv.* **2017,** 1, (22), 1923-1933.
[872] Fleet, J. C.; Burcham, G. N.; Calvert, R. D.; Elzey, B. D.; Ratliff, T. L., 1α, 25 Dihydroxyvitamin D (1,25(OH)(2)D) inhibits the T cell suppressive function of myeloid derived suppressor cells (MDSC). *J. Steroid Biochem. Mol. Biol.* **2020,** 198, 105557.
[873] Finn, O. J.; Ochoa, A. C., Editorial: Myeloid Derived Suppressor Cells as Disease Modulators. *Front. Immunol.* **2020,** 11, 90.
[874] Boros, P.; Ochando, J.; Zeher, M., Myeloid derived suppressor cells and autoimmunity. *Hum. Immunol.* **2016,** 77, (8), 631-636.
[875] Medina, E.; Hartl, D., Myeloid-Derived Suppressor Cells in Infection: A General Overview. *J. Innate Immun.* **2018,** 10, (5-6), 407-413.
[876] Li, B. H.; Garstka, M. A.; Li, Z. F., Chemokines and their receptors promoting the recruitment of myeloid-derived suppressor cells into the tumor. *Mol. Immunol.* **2020,** 117, 201-215.
[877] Ouzounova, M.; Lee, E.; Piranlioglu, R.; El Andaloussi, A.; Kolhe, R.; Demirci, M. F.; Marasco, D.; Asm, I.; Chadli, A.; Hassan, K. A.; Thangaraju, M.; Zhou, G.; Arbab, A. S.; Cowell, J. K.; Korkaya, H., Monocytic and granulocytic myeloid derived suppressor cells differentially regulate spatiotemporal tumour plasticity during metastatic cascade. *Nat. Commun.* **2017,** 8, 14979.
[878] Veglia, F.; Perego, M.; Gabrilovich, D., Myeloid-derived suppressor cells coming of age. *Nat. Immunol.* **2018,** 19, (2), 108-119.
[879] Boldin, M. P.; Taganov, K. D.; Rao, D. S.; Yang, L.; Zhao, J. L.; Kalwani, M.; Garcia-Flores, Y.; Luong, M.; Devrekanli, A.; Xu, J.; Sun, G.; Tay, J.; Linsley, P. S.; Baltimore, D., miR-146a is a significant brake on autoimmunity, myeloproliferation, and cancer in mice. *J. Exp. Med.* **2011,** 208, (6), 1189-201.
[880] Liu, Q.; Zhang, M.; Jiang, X.; Zhang, Z.; Dai, L.; Min, S.; Wu, X.; He, Q.; Liu, J.; Zhang, Y.; Zhang, Z.; Yang, R., miR-223 suppresses differentiation of tumor-induced $CD11b^+$ $Gr1^+$ myeloid-derived suppressor cells from bone marrow cells. *Int. J. Cancer* **2011,** 129, (11), 2662-73.
[881] Wu, C.; Muroski, M. E.; Miska, J.; Lee-Chang, C.; Shen, Y.; Rashidi, A.; Zhang, P.; Xiao, T.; Han, Y.; Lopez-Rosas, A.; Cheng, Y.; Lesniak, M. S., Repolarization of myeloid derived suppressor cells via magnetic nanoparticles to promote radiotherapy for glioma treatment. *Nanomedicine* **2019,** 16, 126-137.
[882] Shirota, H.; Tross, D.; Klinman, D. M., CpG Oligonucleotides as Cancer Vaccine Adjuvants. *Vaccines* **2015,** 3, (2), 390-407.
[883] Lee, W. C.; Hsu, P. Y.; Hsu, H. Y., Stem cell factor produced by tumor cells expands myeloid-derived suppressor cells in mice. *Sci. Rep.* **2020,** 10, (1), 11257.
[884] Kao, J.; Ko, E. C.; Eisenstein, S.; Sikora, A. G.; Fu, S.; Chen, S. H., Targeting immune suppressing myeloid-derived suppressor cells in oncology. *Crit. Rev. Oncol./Hematol.* **2011,** 77, (1), 12-9.
[885] Shao, B.; Wei, X.; Luo, M.; Yu, J.; Tong, A.; Ma, X.; Ye, T.; Deng, H.; Sang, Y.; Liang, X.; Ma, Y.; Wu, Q.; Du, W.; Du, J.; Gao, X.; Wen, Y.; Fu, P.; Shi, H.; Luo, S.; Wei, Y., Inhibition of A20 expression in tumor microenvironment exerts anti-tumor effect through inducing myeloid-derived suppressor cells apoptosis. *Sci. Rep.* **2015,** 5, 16437.
[886] Fujii, H.; Shin-Ya, M.; Takeda, S.; Hashimoto, Y.; Mukai, S. A.; Sawada, S.; Adachi, T.; Akiyoshi, K.; Miki, T.; Mazda, O., Cycloamylose-nanogel drug delivery system-mediated intratumor silencing of the vascular endothelial growth factor regulates neovascularization in tumor microenvironment. *Cancer Sci.* **2014,** 105, (12), 1616-25.
[887] Ni, J.; Galani, I. E.; Cerwenka, A.; Schirrmacher, V.; Fournier, P., Antitumor vaccination by Newcastle Disease Virus Hemagglutinin-Neuraminidase plasmid DNA application: changes in tumor microenvironment and activation of innate anti-tumor immunity. *Vaccine* **2011,** 29, (6), 1185-93.

[888] Principe, M.; Ceruti, P.; Shih, N. Y.; Chattaragada, M. S.; Rolla, S.; Conti, L.; Bestagno, M.; Zentilin, L.; Yang, S. H.; Migliorini, P.; Cappello, P.; Burrone, O.; Novelli, F., Targeting of surface alpha-enolase inhibits the invasiveness of pancreatic cancer cells. *Oncotarget* **2015,** 6, (13), 11098-113.
[889] Cappello, P.; Rolla, S.; Chiarle, R.; Principe, M.; Cavallo, F.; Perconti, G.; Feo, S.; Giovarelli, M.; Novelli, F., Vaccination with ENO1 DNA prolongs survival of genetically engineered mice with pancreatic cancer. *Gastroenterology* **2013,** 144, (5), 1098-106.
[890] Arndt, C.; Bachmann, M.; Bergmann, R.; Berndt, N.; Feldmann, A.; Koristka, S., Theranostic CAR T cell targeting: A brief review. *J. Labelled Compd. Radiopharm.* **2019,** 62, (8), 533-540.
[891] Newick, K.; O'Brien, S.; Sun, J.; Kapoor, V.; Maceyko, S.; Lo, A.; Puré, E.; Moon, E.; Albelda, S. M., Augmentation of CAR T-cell Trafficking and Antitumor Efficacy by Blocking Protein Kinase A Localization. *Cancer Immunol. Res.* **2016,** 4, (6), 541-51.
[892] Darowski, D.; Jost, C.; Stubenrauch, K.; Wessels, U.; Benz, J.; Ehler, A.; Freimoser-Grundschober, A.; Brünker, P.; Mössner, E.; Umaña, P.; Kobold, S.; Klein, C., P329G-CAR-J: a novel Jurkat-NFAT-based CAR-T reporter system recognizing the P329G Fc mutation. *Protein Eng., Des. Sel.* **2019,** 32, (5), 207-218.
[893] Chung, S. H.; Hughes, G.; Koffman, B.; Turtle, C. J.; Maloney, D. G.; Acharya, U. H., Not so crystal clear: observations from a case of crystalline arthritis with cytokine release syndrome (CRS) after chimeric antigen receptor (CAR)-T cell therapy. *Bone Marrow Transplant.* **2019,** 54, (4), 632-634.
[894] Rohrs, J. A.; Siegler, E. L.; Wang, P.; Finley, S. D., ERK Activation in CAR T Cells Is Amplified by CD28-Mediated Increase in CD3ζ Phosphorylation. *iScience* **2020,** 23, (4), 101023.
[895] Kintz, H.; Nylen, E.; Barber, A., Inclusion of Dap10 or 4-1BB costimulation domains in the chPD1 receptor enhances anti-tumor efficacy of T cells in murine models of lymphoma and melanoma. *Cell Immunol.* **2020,** 351, 104069.
[896] Li, Y.; Hermanson, D. L.; Moriarity, B. S.; Kaufman, D. S., Human iPSC-Derived Natural Killer Cells Engineered with Chimeric Antigen Receptors Enhance Anti-tumor Activity. *Cell Stem Cell* **2018,** 23, (2), 181-192.e5.
[897] Strohl, W. R.; Naso, M., Bispecific T-Cell Redirection versus Chimeric Antigen Receptor (CAR)-T Cells as Approaches to Kill Cancer Cells. *Antibodies* **2019,** 8, (3).
[898] Oelsner, S.; Friede, M. E.; Zhang, C.; Wagner, J.; Badura, S.; Bader, P.; Ullrich, E.; Ottmann, O. G.; Klingemann, H.; Tonn, T.; Wels, W. S., Continuously expanding CAR NK-92 cells display selective cytotoxicity against B-cell leukemia and lymphoma. *Cytotherapy* **2017,** 19, (2), 235-249.
[899] Hu, W.; Wang, G.; Huang, D.; Sui, M.; Xu, Y., Cancer Immunotherapy Based on Natural Killer Cells: Current Progress and New Opportunities. *Front. Immunol.* **2019,** 10, 1205.
[900] Oberschmidt, O.; Kloess, S.; Koehl, U., Redirected Primary Human Chimeric Antigen Receptor Natural Killer Cells As an "Off-the-Shelf Immunotherapy" for Improvement in Cancer Treatment. *Front. Immunol.* **2017,** 8, 654.
[901] Sievers, N. M.; Dörrie, J.; Schaft, N., CARs: Beyond T Cells and T Cell-Derived Signaling Domains. *Int. J. Mol. Sci.* **2020,** 21, (10).
[902] Hirayama, A. V.; Turtle, C. J., Toxicities of CD19 CAR-T cell immunotherapy. *Am. J. Hematol.* **2019,** 94, (S1), S42-s49.
[903] Maude, S. L.; Laetsch, T. W.; Buechner, J.; Rives, S.; Boyer, M.; Bittencourt, H.; Bader, P.; Verneris, M. R.; Stefanski, H. E.; Myers, G. D.; Qayed, M.; De Moerloose, B.; Hiramatsu, H.; Schlis, K.; Davis, K. L.; Martin, P. L.; Nemecek, E. R.; Yanik, G. A.; Peters, C.; Baruchel, A.; Boissel, N.; Mechinaud, F.; Balduzzi, A.; Krueger, J.; June, C. H.; Levine, B. L.; Wood, P.; Taran, T.; Leung, M.; Mueller, K. T.; Zhang, Y.; Sen, K.; Lebwohl, D.; Pulsipher, M. A.; Grupp, S. A., Tisagenlecleucel in Children and Young Adults with B-Cell Lymphoblastic Leukemia. *N. Engl. J. Med.* **2018,** 378, (5), 439-448.

[904] Locke, F. L.; Neelapu, S. S.; Bartlett, N. L.; Siddiqi, T.; Chavez, J. C.; Hosing, C. M.; Ghobadi, A.; Budde, L. E.; Bot, A.; Rossi, J. M.; Jiang, Y.; Xue, A. X.; Elias, M.; Aycock, J.; Wiezorek, J.; Go, W. Y., Phase 1 Results of ZUMA-1: A Multicenter Study of KTE-C19 Anti-CD19 CAR T Cell Therapy in Refractory Aggressive Lymphoma. *Mol. Ther.* **2017,** 25, (1), 285-295.
[905] Belay, Y.; Yirdaw, K.; Enawgaw, B., Tumor Lysis Syndrome in Patients with Hematological Malignancies. *J. Oncol.* **2017,** 2017, 9684909.
[906] Shimabukuro-Vornhagen, A.; Gödel, P.; Subklewe, M.; Stemmler, H. J.; Schlößer, H. A.; Schlaak, M.; Kochanek, M.; Böll, B.; von Bergwelt-Baildon, M. S., Cytokine release syndrome. *J. Immunother. Cancer* **2018,** 6, (1), 56.
[907] Giavridis, T.; van der Stegen, S. J. C.; Eyquem, J.; Hamieh, M.; Piersigilli, A.; Sadelain, M., CAR T cell-induced cytokine release syndrome is mediated by macrophages and abated by IL-1 blockade. *Nat. Med.* **2018,** 24, (6), 731-738.
[908] Cervantes, E. V.; Boucher, J. C.; Lee, S. B.; Spitler, K.; Reid, K.; Davila, M. L., MDSC Suppression of CAR T Cells Can be Reduced By Targeted Signaling Disruption. *Blood* **2019,** 134, (Supplement_1), 4438-4438.
[909] Burga, R. A.; Thorn, M.; Point, G. R.; Guha, P.; Nguyen, C. T.; Licata, L. A.; DeMatteo, R. P.; Ayala, A.; Joseph Espat, N.; Junghans, R. P.; Katz, S. C., Liver myeloid-derived suppressor cells expand in response to liver metastases in mice and inhibit the anti-tumor efficacy of anti-CEA CAR-T. *Cancer Immunol. Immunother.* **2015,** 64, (7), 817-29.
[910] Wang, Z.; Liu, Y.; Zhang, Y.; Shang, Y.; Gao, Q., MDSC-decreasing chemotherapy increases the efficacy of cytokine-induced killer cell immunotherapy in metastatic renal cell carcinoma and pancreatic cancer. *Oncotarget* **2016,** 7, (4), 4760-9.
[911] Crotti, C.; Agape, E.; Becciolini, A.; Biggioggero, M.; Favalli, E. G., Targeting Granulocyte-Monocyte Colony-Stimulating Factor Signaling in Rheumatoid Arthritis: Future Prospects. *Drugs* **2019,** 79, (16), 1741-1755.
[912] Alsaab, H. O.; Sau, S.; Alzhrani, R.; Tatiparti, K.; Bhise, K.; Kashaw, S. K.; Iyer, A. K., PD-1 and PD-L1 Checkpoint Signaling Inhibition for Cancer Immunotherapy: Mechanism, Combinations, and Clinical Outcome. *Front. Pharmacol.* **2017,** 8, 561.
[913] Fultang, L.; Panetti, S.; Ng, M.; Collins, P.; Graef, S.; Rizkalla, N.; Booth, S.; Lenton, R.; Noyvert, B.; Shannon-Lowe, C.; Middleton, G.; Mussai, F.; De Santo, C., MDSC targeting with Gemtuzumab ozogamicin restores T cell immunity and immunotherapy against cancers. *EBioMedicine* **2019,** 47, 235-246.
[914] Wang, H.; Ye, X.; Ju, Y.; Cai, Z.; Wang, X.; Du, P.; Zhang, M.; Li, Y.; Cai, J., Minicircle DNA-Mediated CAR T Cells Targeting CD44 Suppressed Hepatocellular Carcinoma Both in vitro and in vivo. *OncoTargets Ther.* **2020,** 13, 3703-3716.
[915] Wu, T.; Dai, Y., Tumor microenvironment and therapeutic response. *Cancer Lett.* **2017,** 387, 61-68.
[916] Hanahan, D.; Coussens, L. M., Accessories to the crime: functions of cells recruited to the tumor microenvironment. *Cancer Cell* **2012,** 21, (3), 309-22.
[917] Chen, D. S.; Mellman, I., Elements of cancer immunity and the cancer-immune set point. *Nature* **2017,** 541, (7637), 321-330.
[918] Beatty, G. L.; Gladney, W. L., Immune Escape Mechanisms as a Guide for Cancer Immunotherapy. *Clin. Cancer Res.* **2015,** 21, (4), 687.
[919] Östman, A., The tumor microenvironment controls drug sensitivity. *Nat. Med.* **2012,** 18, (9), 1332-1334.
[920] Chen, X.; Song, E., Turning foes to friends: targeting cancer-associated fibroblasts. *Nat. Rev. Drug Discovery* **2019,** 18, (2), 99-115.
[921] Qian, B.-Z.; Pollard, J. W., Macrophage Diversity Enhances Tumor Progression and Metastasis. *Cell* **2010,** 141, (1), 39-51.
[922] Pathria, P.; Louis, T. L.; Varner, J. A., Targeting Tumor-Associated Macrophages in Cancer. *Trends Immunol.* **2019,** 40, (4), 310-327.

[923] Prenen, H.; Mazzone, M., Tumor-associated macrophages: a short compendium. *Cell. Mol. Life Sci.* **2019,** 76, (8), 1447-1458.
[924] Swiecki, M.; Colonna, M., The multifaceted biology of plasmacytoid dendritic cells. *Nat. Rev. Immunol.* **2015,** 15, (8), 471-485.
[925] Anderson, K. G.; Stromnes, I. M.; Greenberg, P. D., Obstacles Posed by the Tumor Microenvironment to T cell Activity: A Case for Synergistic Therapies. *Cancer Cell* **2017,** 31, (3), 311-325.
[926] Badalamenti, G.; Fanale, D.; Incorvaia, L.; Barraco, N.; Listì, A.; Maragliano, R.; Vincenzi, B.; Calò, V.; Iovanna, J. L.; Bazan, V.; Russo, A., Role of tumor-infiltrating lymphocytes in patients with solid tumors: Can a drop dig a stone? *Cell Immunol.* **2019,** 343, 103753.
[927] Wilson, W. R.; Hay, M. P., Targeting hypoxia in cancer therapy. *Nat. Rev. Cancer* **2011,** 11, (6), 393-410.
[928] Reuter, S.; Gupta, S. C.; Chaturvedi, M. M.; Aggarwal, B. B., Oxidative stress, inflammation, and cancer: how are they linked? *Free Radical Biol. Med.* **2010,** 49, (11), 1603-16.
[929] Berraondo, P.; Sanmamed, M. F.; Ochoa, M. C.; Etxeberria, I.; Aznar, M. A.; Pérez-Gracia, J. L.; Rodríguez-Ruiz, M. E.; Ponz-Sarvise, M.; Castañón, E.; Melero, I., Cytokines in clinical cancer immunotherapy. *Br. J. Cancer* **2019,** 120, (1), 6-15.
[930] Cao, L.; Kulmburg, P.; Veelken, H.; Mackensen, A.; Mézes, B.; Lindemann, A.; Mertelsmann, R.; Rosenthal, F. M., Cytokine gene transfer in cancer therapy. *Stem Cells* **1998,** 16 Suppl 1, 251-60.
[931] Parmiani, G.; Rivoltini, L.; Andreola, G.; Carrabba, M., Cytokines in cancer therapy. *Immunol. Lett.* **2000,** 74, (1), 41-44.
[932] Conlon, K. C.; Miljkovic, M. D.; Waldmann, T. A., Cytokines in the Treatment of Cancer. *J. Interferon Cytokine Res.* **2019,** 39, (1), 6-21.
[933] Golomb, H. M.; Jacobs, A.; Fefer, A.; Ozer, H.; Thompson, J.; Portlock, C.; Ratain, M.; Golde, D.; Vardiman, J.; Burke, J. S., Alpha-2 interferon therapy of hairy-cell leukemia: a multicenter study of 64 patients. *J. Clin. Oncol.* **1986,** 4, (6), 900-905.
[934] Antony, G. K.; Dudek, A. Z., Interleukin 2 in Cancer Therapy. *Curr. Med. Chem.* **2010,** 17, (29), 3297-3302.
[935] Xu, L.; Song, X.; Su, L.; Zheng, Y.; Li, R.; Sun, J., New therapeutic strategies based on IL-2 to modulate Treg cells for autoimmune diseases. *Int. Immunopharmacol.* **2019,** 72, 322-329.
[936] Kircheis, R.; Küpcü, Z.; Wallner, G.; Wagner, E., Cytokine gene-modified tumor cells for prophylactic and therapeutic vaccination: IL-2, IFN-gamma, or combination IL-2 + IFN-gamma. *Cytokines, Cell. Mol. Ther.* **1998,** 4, (2), 95-103.
[937] Rosenberg, S. A.; Anderson, W. F.; Blaese, M. R.; Ettinghausen, S. E.; Hwu, P.; Karp, S. E.; Kasid, A.; Mule, J. J.; Parkinson, D. R.; Salo, J. C.; Schwartzentruber, D. J.; Topalian, S. L.; Weber, J. S.; Yannelli, J. R.; Yang, J. C.; Linehan, W. M., Immunization of Cancer Patients Using Autologous Cancer Cells Modified by Insertion of the Gene for Interleukin-2 (National Institutes of Health). *Hum. Gene Ther.* **1992,** 3, (1), 75-90.
[938] Schreiber, S.; Kämpgen, E.; Wagner, E.; Pirkhammer, D.; Trcka, J.; Korschan, H.; Lindemann, A.; Dorffner, R.; Kittler, H.; Kasteliz, F.; Küpcü, Z.; Sinski, A.; Zatloukal, K.; Buschle, M.; Schmidt, W.; Birnstiel, M.; Kempe, R. E.; Voigt, T.; Weber, H. A.; Pehamberger, H.; Mertelsmann, R.; Bröcker, E. B.; Wolff, K.; Stingl, G., Immunotherapy of metastatic malignant melanoma by a vaccine consisting of autologous interleukin 2-transfected cancer cells: outcome of a phase I study. *Hum. Gene Ther.* **1999,** 10, (6), 983-93.
[939] Gansbacher, B.; Houghton, A.; Livingston, P.; Minasian, L.; Rosenthal, F.; Gilboa, E.; Oettgen, H.; Steffens, T.; Yang, S. Y.; Wong, G., A Pilot Study of Immunization with HLA-A2 Matched Allogeneic Melanoma Cells That Secrete Interleukin-2 in Patients with Metastatic Melanoma. *Hum. Gene Ther.* **1992,** 3, (6), 677-690.
[940] Bowman, L. C.; Grossmann, M.; Rill, D.; Brown, M.; Zhong, W. Y.; Alexander, B.; Leimig, T.; Coustan-Smith, E.; Campana, D.; Jenkins, J.; Woods, D.; Brenner, M., Interleukin-2 gene-

modified allogeneic tumor cells for treatment of relapsed neuroblastoma. *Hum. Gene Ther.* **1998,** 9, (9), 1303-11.
[941] Osanto, S.; Brouwenstÿn, N.; Vaessen, N.; Figdor, C. G.; Melief, C. J.; Schrier, P. I., Immunization with interleukin-2 transfected melanoma cells. A phase I-II study in patients with metastatic melanoma. *Hum. Gene Ther.* **1993,** 4, (3), 323-30.
[942] Kircheis, R.; Küpcü, Z.; Wallner, G.; Rössler, V.; Schweighoffer, T.; Wagner, E., Interleukin-2 gene-modified allogeneic melanoma cell vaccines can induce cross-protection against syngeneic tumors in mice. *Cancer Gene Ther.* **2000,** 7, (6), 870-878.
[943] Wagner, E.; Zatloukal, K.; Cotten, M.; Kirlappos, H.; Mechtler, K.; Curiel, D. T.; Birnstiel, M. L., Coupling of adenovirus to transferrin-polylysine/DNA complexes greatly enhances receptor-mediated gene delivery and expression of transfected genes. *Proc. Natl. Acad. Sci. U.S.A.* **1992,** 89, (13), 6099-103.
[944] Vile, R.; Miller, N.; Chernajovsky, Y.; Hart, I., A comparison of the properties of different retroviral vectors containing the murine tyrosinase promoter to achieve transcriptionally targeted expression of the HSVtk or IL-2 genes. *Gene Ther.* **1994,** 1, (5), 307-16.
[945] He, P.; Tang, Z. Y.; Liu, B. B.; Ye, S. L.; Liu, Y. K., The targeted expression of the human interleukin-2/interferon alpha2b fused gene in alpha-fetoprotein-expressing hepatocellular carcinoma cells. *J. Cancer Res. Clin. Oncol.* **1999,** 125, (2), 77-82.
[946] Chaurasiya, S.; Hew, P.; Crosley, P.; Sharon, D.; Potts, K.; Agopsowicz, K.; Long, M.; Shi, C.; Hitt, M. M., Breast cancer gene therapy using an adenovirus encoding human IL-2 under control of mammaglobin promoter/enhancer sequences. *Cancer Gene Ther.* **2016,** 23, (6), 178-87.
[947] Kali, A., TNFerade, an innovative cancer immunotherapeutic. *Indian J. Pharmacol.* **2015,** 47, (5), 479-483.
[948] Kircheis, R.; Wagner, E., Technology evaluation: TNFerade, GenVec. *Curr. Opin. Mol. Ther.* **2003,** 5, (4), 437-47.
[949] Herman, J. M.; Wild, A. T.; Wang, H.; Tran, P. T.; Chang, K. J.; Taylor, G. E.; Donehower, R. C.; Pawlik, T. M.; Ziegler, M. A.; Cai, H.; Savage, D. T.; Canto, M. I.; Klapman, J.; Reid, T.; Shah, R. J.; Hoffe, S. E.; Rosemurgy, A.; Wolfgang, C. L.; Laheru, D. A., Randomized phase III multi-institutional study of TNFerade biologic with fluorouracil and radiotherapy for locally advanced pancreatic cancer: final results. *J. Clin. Oncol.* **2013,** 31, (7), 886-894.
[950] Bottermann, M.; Foss, S.; van Tienen, L. M.; Vaysburd, M.; Cruickshank, J.; O'Connell, K.; Clark, J.; Mayes, K.; Higginson, K.; Hirst, J. C.; McAdam, M. B.; Slodkowicz, G.; Hutchinson, E.; Kozik, P.; Andersen, J. T.; James, L. C., TRIM21 mediates antibody inhibition of adenovirus-based gene delivery and vaccination. *Proc. Natl. Acad. Sci. U.S.A.* **2018,** 115, (41), 10440-10445.
[951] Kircheis, R.; Ostermann, E.; Wolschek, M. F.; Lichtenberger, C.; Magin-Lachmann, C.; Wightman, L.; Kursa, M.; Wagner, E., Tumor-targeted gene delivery of tumor necrosis factor-α induces tumor necrosis and tumor regression without systemic toxicity. *Cancer Gene Ther.* **2002,** 9, (8), 673-680.
[952] Su, B.; Cengizeroglu, A.; Farkasova, K.; Viola, J. R.; Anton, M.; Ellwart, J. W.; Haase, R.; Wagner, E.; Ogris, M., Systemic TNFα Gene Therapy Synergizes With Liposomal Doxorubicine in the Treatment of Metastatic Cancer. *Mol. Ther.* **2013,** 21, (2), 300-308.
[953] Schäfer, A.; Pahnke, A.; Schaffert, D.; van Weerden, W. M.; de Ridder, C. M.; Rödl, W.; Vetter, A.; Spitzweg, C.; Kraaij, R.; Wagner, E.; Ogris, M., Disconnecting the yin and yang relation of epidermal growth factor receptor (EGFR)-mediated delivery: a fully synthetic, EGFR-targeted gene transfer system avoiding receptor activation. *Hum. Gene Ther.* **2011,** 22, (12), 1463-73.
[954] Tandle, A.; Hanna, E.; Lorang, D.; Hajitou, A.; Moya, C. A.; Pasqualini, R.; Arap, W.; Adem, A.; Starker, E.; Hewitt, S.; Libutti, S. K., Tumor vasculature-targeted delivery of tumor necrosis factor-α*. *Cancer* **2009,** 115, (1), 128-139.
[955] Yuan, Z.; Syrkin, G.; Adem, A.; Geha, R.; Pastoriza, J.; Vrikshajanani, C.; Smith, T.; Quinn, T. J.; Alemu, G.; Cho, H.; Barrett, C. J.; Arap, W.; Pasqualini, R.; Libutti, S. K., Blockade of

inhibitors of apoptosis (IAPs) in combination with tumor-targeted delivery of tumor necrosis factor-α leads to synergistic antitumor activity. *Cancer Gene Ther.* **2013,** 20, (1), 46-56.
[956] Quinn, T. J.; Healy, N.; Sara, A.; Maggi, E.; Claros, C. S.; Kabarriti, R.; Scandiuzzi, L.; Liu, L.; Gorecka, J.; Adem, A.; Basu, I.; Yuan, Z.; Guha, C., Preclinical evaluation of radiation and systemic, RGD-targeted, adeno-associated virus phage-TNF gene therapy in a mouse model of spontaneously metastatic melanoma. *Cancer Gene Ther.* **2017,** 24, (1), 13-19.
[957] Lasek, W.; Zagożdżon, R.; Jakobisiak, M., Interleukin 12: still a promising candidate for tumor immunotherapy? *Cancer Immunol. Immunother.* **2014,** 63, (5), 419-35.
[958] Voest, E. E.; Kenyon, B. M.; O'Reilly, M. S.; Truitt, G.; D'Amato, R. J.; Folkman, J., Inhibition of angiogenesis in vivo by interleukin 12. *J. Natl. Cancer Inst.* **1995,** 87, (8), 581-6.
[959] Dias, S.; Boyd, R.; Balkwill, F., IL-12 regulates VEGF and MMPs in a murine breast cancer model. *Int. J. Cancer* **1998,** 78, (3), 361-365.
[960] Del Vecchio, M.; Bajetta, E.; Canova, S.; Lotze, M. T.; Wesa, A.; Parmiani, G.; Anichini, A., Interleukin-12: biological properties and clinical application. *Clin. Cancer Res.* **2007,** 13, (16), 4677-85.
[961] Cohen, J., IL-12 Deaths: Explanation and a Puzzle. *Science* **1995,** 270, (5238), 908.
[962] Leonard, J. P.; Sherman, M. L.; Fisher, G. L.; Buchanan, L. J.; Larsen, G.; Atkins, M. B.; Sosman, J. A.; Dutcher, J. P.; Vogelzang, N. J.; Ryan, J. L., Effects of single-dose interleukin-12 exposure on interleukin-12-associated toxicity and interferon-gamma production. *Blood* **1997,** 90, (7), 2541-8.
[963] Pasche, N.; Neri, D., Immunocytokines: a novel class of potent armed antibodies. *Drug Discovery Today* **2012,** 17, (11-12), 583-90.
[964] Rudman, S. M.; Jameson, M. B.; McKeage, M. J.; Savage, P.; Jodrell, D. I.; Harries, M.; Acton, G.; Erlandsson, F.; Spicer, J. F., A phase 1 study of AS1409, a novel antibody-cytokine fusion protein, in patients with malignant melanoma or renal cell carcinoma. *Clin. Cancer Res.* **2011,** 17, (7), 1998-2005.
[965] Hernandez-Alcoceba, R.; Poutou, J.; Ballesteros-Briones, M. C.; Smerdou, C., Gene therapy approaches against cancer using in vivo and ex vivo gene transfer of interleukin-12. *Immunotherapy* **2016,** 8, (2), 179-98.
[966] Tugues, S.; Burkhard, S. H.; Ohs, I.; Vrohlings, M.; Nussbaum, K.; vom Berg, J.; Kulig, P.; Becher, B., New insights into IL-12-mediated tumor suppression. *Cell Death Differ.* **2015,** 22, (2), 237-246.
[967] Sangro, B.; Mazzolini, G.; Ruiz, J.; Herraiz, M.; Quiroga, J.; Herrero, I.; Benito, A.; Larrache, J.; Pueyo, J.; Subtil, J. C.; Olagüe, C.; Sola, J.; Sádaba, B.; Lacasa, C.; Melero, I.; Qian, C.; Prieto, J., Phase I Trial of Intratumoral Injection of an Adenovirus Encoding Interleukin-12 for Advanced Digestive Tumors. *J. Clin. Oncol.* **2004,** 22, (8), 1389-1397.
[968] Triozzi, P. L.; Strong, T. V.; Bucy, R. P.; Allen, K. O.; Carlisle, R. R.; Moore, S. E.; Lobuglio, A. F.; Conry, R. M., Intratumoral administration of a recombinant canarypox virus expressing interleukin 12 in patients with metastatic melanoma. *Hum. Gene Ther.* **2005,** 16, (1), 91-100.
[969] Triozzi, P. L.; Allen, K. O.; Carlisle, R. R.; Craig, M.; LoBuglio, A. F.; Conry, R. M., Phase I study of the intratumoral administration of recombinant canarypox viruses expressing B7.1 and interleukin 12 in patients with metastatic melanoma. *Clin. Cancer Res.* **2005,** 11, (11), 4168-75.
[970] Linette, G. P.; Hamid, O.; Whitman, E. D.; Nemunaitis, J. J.; Chesney, J.; Agarwala, S. S.; Starodub, A.; Barrett, J. A.; Marsh, A.; Martell, L. A.; Cho, A.; Reed, T. D.; Youssoufian, H.; Vergara-Silva, A., A phase I open-label study of Ad-RTS-hIL-12, an adenoviral vector engineered to express hIL-12 under the control of an oral activator ligand, in subjects with unresectable stage III/IV melanoma. *J. Clin. Oncol.* **2013,** 31, (15_suppl), 3022-3022.
[971] Quetglas, J. I.; Labiano, S.; Aznar, M. Á.; Bolaños, E.; Azpilikueta, A.; Rodriguez, I.; Casales, E.; Sánchez-Paulete, A. R.; Segura, V.; Smerdou, C.; Melero, I., Virotherapy with a Semliki Forest Virus–Based Vector Encoding IL12 Synergizes with PD-1/PD-L1 Blockade. *Cancer Immunol. Res.* **2015,** 3, (5), 449.

[972] Yang, X.; Yu, X.; Wei, Y., Lentiviral delivery of novel fusion protein IL12/FasTI for cancer immune/gene therapy. *PLoS One* **2018,** 13, (7), e0201100.
[973] Chiocca, E. A.; Yu, J. S.; Lukas, R. V.; Solomon, I. H.; Ligon, K. L.; Nakashima, H.; Triggs, D. A.; Reardon, D. A.; Wen, P.; Stopa, B. M.; Naik, A.; Rudnick, J.; Hu, J. L.; Kumthekar, P.; Yamini, B.; Buck, J. Y.; Demars, N.; Barrett, J. A.; Gelb, A. B.; Zhou, J.; Lebel, F.; Cooper, L. J. N., Regulatable interleukin-12 gene therapy in patients with recurrent high-grade glioma: Results of a phase 1 trial. *Sci. Transl. Med.* **2019,** 11, (505).
[974] Lucas, M. L.; Heller, L.; Coppola, D.; Heller, R., IL-12 plasmid delivery by in vivo electroporation for the successful treatment of established subcutaneous B16.F10 melanoma. *Mol. Ther.* **2002,** 5, (6), 668-75.
[975] Heinzerling, L.; Burg, G.; Dummer, R.; Maier, T.; Oberholzer, P. A.; Schultz, J.; Elzaouk, L.; Pavlovic, J.; Moelling, K., Intratumoral injection of DNA encoding human interleukin 12 into patients with metastatic melanoma: clinical efficacy. *Hum. Gene Ther.* **2005,** 16, (1), 35-48.
[976] Mahvi, D. M.; Henry, M. B.; Albertini, M. R.; Weber, S.; Meredith, K.; Schalch, H.; Rakhmilevich, A.; Hank, J.; Sondel, P., Intratumoral injection of IL-12 plasmid DNA--results of a phase I/IB clinical trial. *Cancer Gene Ther.* **2007,** 14, (8), 717-23.
[977] Daud, A. I.; DeConti, R. C.; Andrews, S.; Urbas, P.; Riker, A. I.; Sondak, V. K.; Munster, P. N.; Sullivan, D. M.; Ugen, K. E.; Messina, J. L.; Heller, R., Phase I trial of interleukin-12 plasmid electroporation in patients with metastatic melanoma. *J. Clin. Oncol.* **2008,** 26, (36), 5896-903.
[978] Cutrera, J.; King, G.; Jones, P.; Kicenuik, K.; Gumpel, E.; Xia, X.; Li, S., Safety and efficacy of tumor-targeted interleukin 12 gene therapy in treated and non-treated, metastatic lesions. *Curr. Gene Ther.* **2015,** 15, (1), 44-54.
[979] Cemazar, M.; Ambrozic Avgustin, J.; Pavlin, D.; Sersa, G.; Poli, A.; Krhac Levacic, A.; Tesic, N.; Lampreht Tratar, U.; Rak, M.; Tozon, N., Efficacy and safety of electrochemotherapy combined with peritumoral IL-12 gene electrotransfer of canine mast cell tumours. *Vet. Comp. Oncol.* **2017,** 15, (2), 641-654.
[980] Cicchelero, L.; Denies, S.; Haers, H.; Vanderperren, K.; Stock, E.; Van Brantegem, L.; de Rooster, H.; Sanders, N. N., Intratumoural interleukin 12 gene therapy stimulates the immune system and decreases angiogenesis in dogs with spontaneous cancer. *Vet. Comp. Oncol.* **2017,** 15, (4), 1187-1205.
[981] Rodrigo-Garzón, M.; Berraondo, P.; Ochoa, L.; Zulueta, J. J.; González-Aseguinolaza, G., Antitumoral efficacy of DNA nanoparticles in murine models of lung cancer and pulmonary metastasis. *Cancer Gene Ther.* **2010,** 17, (1), 20-7.
[982] Anwer, K.; Barnes, M. N.; Fewell, J.; Lewis, D. H.; Alvarez, R. D., Phase-I clinical trial of IL-12 plasmid/lipopolymer complexes for the treatment of recurrent ovarian cancer. *Gene Ther.* **2010,** 17, (3), 360-9.
[983] Anwer, K.; Kelly, F. J.; Chu, C.; Fewell, J. G.; Lewis, D.; Alvarez, R. D., Phase I trial of a formulated IL-12 plasmid in combination with carboplatin and docetaxel chemotherapy in the treatment of platinum-sensitive recurrent ovarian cancer. *Gynecologic oncology* **2013,** 131, (1), 169-73.
[984] Men, K.; Huang, R.; Zhang, X.; Zhang, R.; Zhang, Y.; He, M.; Tong, R.; Yang, L.; Wei, Y.; Duan, X., Local and Systemic Delivery of Interleukin-12 Gene by Cationic Micelles for Cancer Immunogene Therapy. *J. Biomed. Nanotechnol.* **2018,** 14, (10), 1719-1730.
[985] Chmielewski, M.; Abken, H., CAR T cells transform to trucks: chimeric antigen receptor-redirected T cells engineered to deliver inducible IL-12 modulate the tumour stroma to combat cancer. *Cancer Immunol. Immunother.* **2012,** 61, (8), 1269-77.
[986] Hodi, F. S.; Lee, S.; McDermott, D. F.; Rao, U. N.; Butterfield, L. H.; Tarhini, A. A.; Leming, P.; Puzanov, I.; Shin, D.; Kirkwood, J. M., Ipilimumab plus sargramostim vs ipilimumab alone for treatment of metastatic melanoma: a randomized clinical trial. *JAMA* **2014,** 312, (17), 1744-53.
[987] Le, D. T.; Lutz, E.; Uram, J. N.; Sugar, E. A.; Onners, B.; Solt, S.; Zheng, L.; Diaz, L. A., Jr.; Donehower, R. C.; Jaffee, E. M.; Laheru, D. A., Evaluation of ipilimumab in combination with

allogeneic pancreatic tumor cells transfected with a GM-CSF gene in previously treated pancreatic cancer. *J. Immunother.* **2013,** 36, (7), 382-9.
[988] Le, D. T.; Wang-Gillam, A.; Picozzi, V.; Greten, T. F.; Crocenzi, T.; Springett, G.; Morse, M.; Zeh, H.; Cohen, D.; Fine, R. L.; Onners, B.; Uram, J. N.; Laheru, D. A.; Lutz, E. R.; Solt, S.; Murphy, A. L.; Skoble, J.; Lemmens, E.; Grous, J.; Dubensky, T., Jr.; Brockstedt, D. G.; Jaffee, E. M., Safety and survival with GVAX pancreas prime and Listeria Monocytogenes-expressing mesothelin (CRS-207) boost vaccines for metastatic pancreatic cancer. *J. Clin. Oncol.* **2015,** 33, (12), 1325-33.
[989] Le, D. T.; Picozzi, V. J.; Ko, A. H.; Wainberg, Z. A.; Kindler, H.; Wang-Gillam, A.; Oberstein, P.; Morse, M. A.; Zeh, H. J., 3rd; Weekes, C.; Reid, T.; Borazanci, E.; Crocenzi, T.; LoConte, N. K.; Musher, B.; Laheru, D.; Murphy, A.; Whiting, C.; Nair, N.; Enstrom, A.; Ferber, S.; Brockstedt, D. G.; Jaffee, E. M., Results from a Phase IIb, Randomized, Multicenter Study of GVAX Pancreas and CRS-207 Compared with Chemotherapy in Adults with Previously Treated Metastatic Pancreatic Adenocarcinoma (ECLIPSE Study). *Clin. Cancer Res.* **2019,** 25, (18), 5493-5502.
[990] Tsujikawa, T.; Crocenzi, T.; Durham, J. N.; Sugar, E. A.; Wu, A. A.; Onners, B.; Nauroth, J. M.; Anders, R. A.; Fertig, E. J.; Laheru, D. A.; Reiss, K.; Vonderheide, R. H.; Ko, A. H.; Tempero, M. A.; Fisher, G. A.; Considine, M.; Danilova, L.; Brockstedt, D. G.; Coussens, L. M.; Jaffee, E. M.; Le, D. T., Evaluation of Cyclophosphamide/GVAX Pancreas Followed by Listeria-Mesothelin (CRS-207) with or without Nivolumab in Patients with Pancreatic Cancer. *Clin. Cancer Res.* **2020**.
[991] Sterner, R. M.; Cox, M. J.; Sakemura, R.; Kenderian, S. S., Using CRISPR/Cas9 to Knock Out GM-CSF in CAR-T Cells. *J. Visualized Exp.* **2019**, (149).
[992] Teicher, B. A.; Fricker, S. P., CXCL12 (SDF-1)/CXCR4 pathway in cancer. *Clin. Cancer Res.* **2010,** 16, (11), 2927-31.
[993] Meng, W.; Xue, S.; Chen, Y., The role of CXCL12 in tumor microenvironment. *Gene* **2018,** 641, 105-110.
[994] Feig, C.; Jones, J. O.; Kraman, M.; Wells, R. J.; Deonarine, A.; Chan, D. S.; Connell, C. M.; Roberts, E. W.; Zhao, Q.; Caballero, O. L.; Teichmann, S. A.; Janowitz, T.; Jodrell, D. I.; Tuveson, D. A.; Fearon, D. T., Targeting CXCL12 from FAP-expressing carcinoma-associated fibroblasts synergizes with anti-PD-L1 immunotherapy in pancreatic cancer. *Proc. Natl. Acad. Sci. U.S.A.* **2013,** 110, (50), 20212-7.
[995] Zhong, C.; Wang, J.; Li, B.; Xiang, H.; Ultsch, M.; Coons, M.; Wong, T.; Chiang, N. Y.; Clark, S.; Clark, R.; Quintana, L.; Gribling, P.; Suto, E.; Barck, K.; Corpuz, R.; Yao, J.; Takkar, R.; Lee, W. P.; Damico-Beyer, L. A.; Carano, R. D.; Adams, C.; Kelley, R. F.; Wang, W.; Ferrara, N., Development and preclinical characterization of a humanized antibody targeting CXCL12. *Clin. Cancer Res.* **2013,** 19, (16), 4433-45.
[996] Goodwin, T. J.; Zhou, Y.; Musetti, S. N.; Liu, R.; Huang, L., Local and transient gene expression primes the liver to resist cancer metastasis. *Sci. Transl. Med.* **2016,** 8, (364), 364ra153.
[997] Miao, L.; Li, J.; Liu, Q.; Feng, R.; Das, M.; Lin, C. M.; Goodwin, T. J.; Dorosheva, O.; Liu, R.; Huang, L., Transient and Local Expression of Chemokine and Immune Checkpoint Traps To Treat Pancreatic Cancer. *ACS Nano* **2017,** 11, (9), 8690-8706.
[998] Hu, Y.; Haynes, M. T.; Wang, Y.; Liu, F.; Huang, L., A highly efficient synthetic vector: nonhydrodynamic delivery of DNA to hepatocyte nuclei in vivo. *ACS Nano* **2013,** 7, (6), 5376-84.
[999] Weis, S. M.; Cheresh, D. A., Tumor angiogenesis: molecular pathways and therapeutic targets. *Nat. Med.* **2011,** 17, (11), 1359-1370.
[1000] Ott, P. A.; Hodi, F. S.; Buchbinder, E. I., Inhibition of Immune Checkpoints and Vascular Endothelial Growth Factor as Combination Therapy for Metastatic Melanoma: An Overview of Rationale, Preclinical Evidence, and Initial Clinical Data. *Front. Oncol.* **2015,** 5, 202-202.
[1001] Lockhart, A. C.; Rothenberg, M. L.; Dupont, J.; Cooper, W.; Chevalier, P.; Sternas, L.; Buzenet, G.; Koehler, E.; Sosman, J. A.; Schwartz, L. H.; Gultekin, D. H.; Koutcher, J. A.; Donnelly, E. F.; Andal, R.; Dancy, I.; Spriggs, D. R.; Tew, W. P., Phase I Study of Intravenous Vascular Endothelial Growth Factor Trap, Aflibercept, in Patients With Advanced Solid Tumors. *J. Clin. Oncol.* **2009,** 28, (2), 207-214.

[1002] Tarhini, A. A.; Frankel, P.; Margolin, K. A.; Christensen, S.; Ruel, C.; Shipe-Spotloe, J.; Gandara, D. R.; Chen, A.; Kirkwood, J. M., Aflibercept (VEGF Trap) in Inoperable Stage III or Stage IV Melanoma of Cutaneous or Uveal Origin. *Clin. Cancer Res.* **2011,** 17, (20), 6574.
[1003] Ferrara, N.; Hillan, K. J.; Novotny, W., Bevacizumab (Avastin), a humanized anti-VEGF monoclonal antibody for cancer therapy. *Biochem. Biophys. Res. Commun.* **2005,** 333, (2), 328-335.
[1004] Melosky, B.; Reardon, D. A.; Nixon, A. B.; Subramanian, J.; Bair, A. H.; Jacobs, I., Bevacizumab biosimilars: scientific justification for extrapolation of indications. *Future Oncol.* **2018,** 14, (24), 2507-2520.
[1005] Vennepureddy, A.; Singh, P.; Rastogi, R.; Atallah, J. P.; Terjanian, T., Evolution of ramucirumab in the treatment of cancer - A review of literature. *J. Oncol. Pharm. Pract.* **2017,** 23, (7), 525-539.
[1006] Tekade, R. K.; Tekade, M.; Kesharwani, P.; D'Emanuele, A., RNAi-combined nano-chemotherapeutics to tackle resistant tumors. *Drug Discovery Today* **2016,** 21, (11), 1761-1774.
[1007] Kanazawa, T.; Sugawara, K.; Tanaka, K.; Horiuchi, S.; Takashima, Y.; Okada, H., Suppression of tumor growth by systemic delivery of anti-VEGF siRNA with cell-penetrating peptide-modified MPEG-PCL nanomicelles. *Eur. J. Pharm. Biopharm.* **2012,** 81, (3), 470-7.
[1008] Egorova, A.; Shubina, A.; Sokolov, D.; Selkov, S.; Baranov, V.; Kiselev, A., CXCR4-targeted modular peptide carriers for efficient anti-VEGF siRNA delivery. *Int. J. Pharm.* **2016,** 515, (1-2), 431-440.
[1009] Chung, J. Y.; Ul Ain, Q.; Lee, H. L.; Kim, S. M.; Kim, Y. H., Enhanced Systemic Anti-Angiogenic siVEGF Delivery Using PEGylated Oligo-d-arginine. *Mol. Pharmaceutics* **2017,** 14, (9), 3059-3068.
[1010] Lee, Y. W.; Hwang, Y. E.; Lee, J. Y.; Sohn, J. H.; Sung, B. H.; Kim, S. C., VEGF siRNA Delivery by a Cancer-Specific Cell-Penetrating Peptide. *J. Microbiol. Biotechnol.* **2018,** 28, (3), 367-374.
[1011] Schiffelers, R. M.; Ansari, A.; Xu, J.; Zhou, Q.; Tang, Q.; Storm, G.; Molema, G.; Lu, P. Y.; Scaria, P. V.; Woodle, M. C., Cancer siRNA therapy by tumor selective delivery with ligand-targeted sterically stabilized nanoparticle. *Nucleic Acids Res.* **2004,** 32, (19), e149-e149.
[1012] Kim, S. H.; Jeong, J. H.; Lee, S. H.; Kim, S. W.; Park, T. G., Local and systemic delivery of VEGF siRNA using polyelectrolyte complex micelles for effective treatment of cancer. *J. Controlled Release* **2008,** 129, (2), 107-116.
[1013] Jiang, G.; Park, K.; Kim, J.; Kim, K. S.; Hahn, S. K., Target specific intracellular delivery of siRNA/PEI-HA complex by receptor mediated endocytosis. *Mol. Pharmaceutics* **2009,** 6, (3), 727-37.
[1014] Zhao, Z.; Li, Y.; Shukla, R.; Liu, H.; Jain, A.; Barve, A.; Cheng, K., Development of a Biocompatible Copolymer Nanocomplex to Deliver VEGF siRNA for Triple Negative Breast Cancer. *Theranostics* **2019,** 9, (15), 4508-4524.
[1015] Kim, M. G.; Jo, S. D.; Yhee, J. Y.; Lee, B. S.; Lee, S. J.; Park, S. G.; Kang, S. W.; Kim, S. H.; Jeong, J. H., Synergistic anti-tumor effects of bevacizumab and tumor targeted polymerized VEGF siRNA nanoparticles. *Biochem. Biophys. Res. Commun.* **2017,** 489, (1), 35-41.
[1016] Yang, Z. Z.; Li, J. Q.; Wang, Z. Z.; Dong, D. W.; Qi, X. R., Tumor-targeting dual peptides-modified cationic liposomes for delivery of siRNA and docetaxel to gliomas. *Biomaterials* **2014,** 35, (19), 5226-39.
[1017] Li, F.; Wang, Y.; Chen, W. L.; Wang, D. D.; Zhou, Y. J.; You, B. G.; Liu, Y.; Qu, C. X.; Yang, S. D.; Chen, M. T.; Zhang, X. N., Co-delivery of VEGF siRNA and Etoposide for Enhanced Anti-angiogenesis and Anti-proliferation Effect via Multi-functional Nanoparticles for Orthotopic Non-Small Cell Lung Cancer Treatment. *Theranostics* **2019,** 9, (20), 5886-5898.
[1018] Conde, J.; Bao, C.; Tan, Y.; Cui, D.; Edelman, E. R.; Azevedo, H. S.; Byrne, H. J.; Artzi, N.; Tian, F., Dual targeted immunotherapy via in vivo delivery of biohybrid RNAi-peptide nanoparticles to tumour-associated macrophages and cancer cells. *Adv. Funct. Mater.* **2015,** 25, (27), 4183-4194.

[1019] Sun, Q.; Wang, X.; Cui, C.; Li, J.; Wang, Y., Doxorubicin and anti-VEGF siRNA co-delivery via nano-graphene oxide for enhanced cancer therapy in vitro and in vivo. *Int. J. Nanomed.* **2018,** 13, 3713-3728.
[1020] Akhurst, R. J.; Hata, A., Targeting the TGFβ signalling pathway in disease. *Nat. Rev. Drug Discovery* **2012,** 11, (10), 790-811.
[1021] Haque, S.; Morris, J. C., Transforming growth factor-β: A therapeutic target for cancer. *Hum. Vaccines Immunother.* **2017,** 13, (8), 1741-1750.
[1022] Ahmadi, A.; Najafi, M.; Farhood, B.; Mortezaee, K., Transforming growth factor-β signaling: Tumorigenesis and targeting for cancer therapy. *J. Cell. Physiol.* **2019,** 234, (8), 12173-12187.
[1023] Xu, Z.; Wang, Y.; Zhang, L.; Huang, L., Nanoparticle-delivered transforming growth factor-β siRNA enhances vaccination against advanced melanoma by modifying tumor microenvironment. *ACS Nano* **2014,** 8, (4), 3636-45.
[1024] Cao, Q.; Liu, F.; Ji, K.; Liu, N.; He, Y.; Zhang, W.; Wang, L., MicroRNA-381 inhibits the metastasis of gastric cancer by targeting TMEM16A expression. *J. Exp. Clin. Cancer Res.* **2017,** 36, (1), 29.
[1025] Shu, Y. J.; Bao, R. F.; Jiang, L.; Wang, Z.; Wang, X. A.; Zhang, F.; Liang, H. B.; Li, H. F.; Ye, Y. Y.; Xiang, S. S.; Weng, H.; Wu, X. S.; Li, M. L.; Hu, Y. P.; Lu, W.; Zhang, Y. J.; Zhu, J.; Dong, P.; Liu, Y. B., MicroRNA-29c-5p suppresses gallbladder carcinoma progression by directly targeting CPEB4 and inhibiting the MAPK pathway. *Cell Death Differ.* **2017,** 24, (3), 445-457.
[1026] Fang, F.; Huang, B.; Sun, S.; Xiao, M.; Guo, J.; Yi, X.; Cai, J.; Wang, Z., miR-27a inhibits cervical adenocarcinoma progression by downregulating the TGF-βRI signaling pathway. *Cell Death Dis.* **2018,** 9, (3), 395.
[1027] Schlingensiepen, R.; Goldbrunner, M.; Szyrach, M. N.; Stauder, G.; Jachimczak, P.; Bogdahn, U.; Schulmeyer, F.; Hau, P.; Schlingensiepen, K. H., Intracerebral and intrathecal infusion of the TGF-beta 2-specific antisense phosphorothioate oligonucleotide AP 12009 in rabbits and primates: toxicology and safety. *Oligonucleotides* **2005,** 15, (2), 94-104.
[1028] Schlingensiepen, K. H.; Schlingensiepen, R.; Steinbrecher, A.; Hau, P.; Bogdahn, U.; Fischer-Blass, B.; Jachimczak, P., Targeted tumor therapy with the TGF-beta 2 antisense compound AP 12009. *Cytokine Growth Factor Rev.* **2006,** 17, (1-2), 129-39.
[1029] Schlingensiepen, K. H.; Jaschinski, F.; Lang, S. A.; Moser, C.; Geissler, E. K.; Schlitt, H. J.; Kielmanowicz, M.; Schneider, A., Transforming growth factor-beta 2 gene silencing with trabedersen (AP 12009) in pancreatic cancer. *Cancer Sci.* **2011,** 102, (6), 1193-200.
[1030] Hau, P.; Jachimczak, P.; Schlingensiepen, R.; Schulmeyer, F.; Jauch, T.; Steinbrecher, A.; Brawanski, A.; Proescholdt, M.; Schlaier, J.; Buchroithner, J.; Pichler, J.; Wurm, G.; Mehdorn, M.; Strege, R.; Schuierer, G.; Villarrubia, V.; Fellner, F.; Jansen, O.; Straube, T.; Nohria, V.; Goldbrunner, M.; Kunst, M.; Schmaus, S.; Stauder, G.; Bogdahn, U.; Schlingensiepen, K. H., Inhibition of TGF-beta2 with AP 12009 in recurrent malignant gliomas: from preclinical to phase I/II studies. *Oligonucleotides* **2007,** 17, (2), 201-12.
[1031] Nagaraj, N. S.; Datta, P. K., Targeting the transforming growth factor-beta signaling pathway in human cancer. *Expert Opin. Invest. Drugs* **2010,** 19, (1), 77-91.
[1032] Bogdahn, U.; Hau, P.; Stockhammer, G.; Venkataramana, N. K.; Mahapatra, A. K.; Suri, A.; Balasubramaniam, A.; Nair, S.; Oliushine, V.; Parfenov, V.; Poverennova, I.; Zaaroor, M.; Jachimczak, P.; Ludwig, S.; Schmaus, S.; Heinrichs, H.; Schlingensiepen, K. H., Targeted therapy for high-grade glioma with the TGF-β2 inhibitor trabedersen: results of a randomized and controlled phase IIb study. *Neuro Oncol.* **2011,** 13, (1), 132-42.
[1033] Nemunaitis, J.; Dillman, R. O.; Schwarzenberger, P. O.; Senzer, N.; Cunningham, C.; Cutler, J.; Tong, A.; Kumar, P.; Pappen, B.; Hamilton, C.; DeVol, E.; Maples, P. B.; Liu, L.; Chamberlin, T.; Shawler, D. L.; Fakhrai, H., Phase II study of belagenpumatucel-L, a transforming growth factor beta-2 antisense gene-modified allogeneic tumor cell vaccine in non-small-cell lung cancer. *J. Clin. Oncol.* **2006,** 24, (29), 4721-30.
[1034] Nemunaitis, J.; Nemunaitis, M.; Senzer, N.; Snitz, P.; Bedell, C.; Kumar, P.; Pappen, B.; Maples, P. B.; Shawler, D.; Fakhrai, H., Phase II trial of Belagenpumatucel-L, a TGF-beta2

antisense gene modified allogeneic tumor vaccine in advanced non small cell lung cancer (NSCLC) patients. *Cancer Gene Ther.* **2009,** 16, (8), 620-4.
[1035] Giaccone, G.; Bazhenova, L. A.; Nemunaitis, J.; Tan, M.; Juhász, E.; Ramlau, R.; van den Heuvel, M. M.; Lal, R.; Kloecker, G. H.; Eaton, K. D.; Chu, Q.; Dunlop, D. J.; Jain, M.; Garon, E. B.; Davis, C. S.; Carrier, E.; Moses, S. C.; Shawler, D. L.; Fakhrai, H., A phase III study of belagenpumatucel-L, an allogeneic tumour cell vaccine, as maintenance therapy for non-small cell lung cancer. *Eur. J. Cancer* **2015,** 51, (16), 2321-9.
[1036] Zhu, J.; Liu, J. Q.; Shi, M.; Cheng, X.; Ding, M.; Zhang, J. C.; Davis, J. P.; Varikuti, S.; Satoskar, A. R.; Lu, L.; Pan, X.; Zheng, P.; Liu, Y.; Bai, X. F., IL-27 gene therapy induces depletion of Tregs and enhances the efficacy of cancer immunotherapy. *JCI Insight* **2018,** 3, (7).
[1037] Hashimoto, H.; Ueda, R.; Narumi, K.; Heike, Y.; Yoshida, T.; Aoki, K., Type I IFN gene delivery suppresses regulatory T cells within tumors. *Cancer Gene Ther.* **2014,** 21, (12), 532-541.
[1038] Hirata, A.; Hashimoto, H.; Shibasaki, C.; Narumi, K.; Aoki, K., Intratumoral IFN-α gene delivery reduces tumor-infiltrating regulatory T cells through the downregulation of tumor CCL17 expression. *Cancer Gene Ther.* **2019,** 26, (9-10), 334-343.
[1039] Byrne, W. L.; Mills, K. H. G.; Lederer, J. A.; Sullivan, G. C., Targeting Regulatory T Cells in Cancer. *Cancer Res.* **2011,** 71, (22), 6915.
[1040] Jacobs, J. F. M.; Nierkens, S.; Figdor, C. G.; de Vries, I. J. M.; Adema, G. J., Regulatory T cells in melanoma: the final hurdle towards effective immunotherapy? *Lancet Oncol.* **2012,** 13, (1), e32-e42.
[1041] Pfeffer, L. M.; Dinarello, C. A.; Herberman, R. B.; Williams, B. R. G.; Borden, E. C.; Bordens, R.; Walter, M. R.; Nagabhushan, T. L.; Trotta, P. P.; Pestka, S., Biological Properties of Recombinant α-Interferons: 40th Anniversary of the Discovery of Interferons. *Cancer Res.* **1998,** 58, (12), 2489.
[1042] Iqbal Ahmed, C. M.; Johnson, D. E.; Demers, G. W.; Engler, H.; Howe, J. A.; Wills, K. N.; Wen, S. F.; Shinoda, J.; Beltran, J.; Nodelman, M.; Machemer, T.; Maneval, D. C.; Nagabhushan, T. L.; Sugarman, B. J., Interferon alpha2b gene delivery using adenoviral vector causes inhibition of tumor growth in xenograft models from a variety of cancers. *Cancer Gene Ther.* **2001,** 8, (10), 788-95.
[1043] Duplisea, J. J.; Mokkapati, S.; Plote, D.; Schluns, K. S.; McConkey, D. J.; Yla-Herttuala, S.; Parker, N. R.; Dinney, C. P., The development of interferon-based gene therapy for BCG unresponsive bladder cancer: from bench to bedside. *World J. Urol.* **2019,** 37, (10), 2041-2049.
[1044] Pardoll, D. M., The blockade of immune checkpoints in cancer immunotherapy. *Nat. Rev. Cancer* **2012,** 12, (4), 252-64.
[1045] Sadreddini, S.; Baradaran, B.; Aghebati-Maleki, A.; Sadreddini, S.; Shanehbandi, D.; Fotouhi, A.; Aghebati-Maleki, L., Immune checkpoint blockade opens a new way to cancer immunotherapy. *J. Cell. Physiol.* **2019,** 234, (6), 8541-8549.
[1046] Brunet, J. F.; Denizot, F.; Luciani, M. F.; Roux-Dosseto, M.; Suzan, M.; Mattei, M. G.; Golstein, P., A new member of the immunoglobulin superfamily--CTLA-4. *Nature* **1987,** 328, (6127), 267-70.
[1047] Ishida, Y.; Agata, Y.; Shibahara, K.; Honjo, T., Induced expression of PD-1, a novel member of the immunoglobulin gene superfamily, upon programmed cell death. *EMBO J.* **1992,** 11, (11), 3887-95.
[1048] Taams, L. S.; de Gruijl, T. D., Immune checkpoint inhibition: from molecules to clinical application. *Clin. Exp. Immunol.* **2020,** 200, (2), 105-107.
[1049] Chen, P.-L.; Roh, W.; Reuben, A.; Cooper, Z. A.; Spencer, C. N.; Prieto, P. A.; Miller, J. P.; Bassett, R. L.; Gopalakrishnan, V.; Wani, K.; De Macedo, M. P.; Austin-Breneman, J. L.; Jiang, H.; Chang, Q.; Reddy, S. M.; Chen, W.-S.; Tetzlaff, M. T.; Broaddus, R. J.; Davies, M. A.; Gershenwald, J. E.; Haydu, L.; Lazar, A. J.; Patel, S. P.; Hwu, P.; Hwu, W.-J.; Diab, A.; Glitza, I. C.; Woodman, S. E.; Vence, L. M.; Wistuba, I. I.; Amaria, R. N.; Kwong, L. N.; Prieto, V.; Davis, R. E.; Ma, W.; Overwijk, W. W.; Sharpe, A. H.; Hu, J.; Futreal, P. A.; Blando, J.; Sharma, P.; Allison, J. P.; Chin, L.; Wargo, J. A., Analysis of Immune Signatures in Longitudinal Tumor

Samples Yields Insight into Biomarkers of Response and Mechanisms of Resistance to Immune Checkpoint Blockade. *Cancer Discovery* **2016,** 6, (8), 827.
[1050] Jenkins, R. W.; Barbie, D. A.; Flaherty, K. T., Mechanisms of resistance to immune checkpoint inhibitors. *Br. J. Cancer* **2018,** 118, (1), 9-16.
[1051] Barrueto, L.; Caminero, F.; Cash, L.; Makris, C.; Lamichhane, P.; Deshmukh, R. R., Resistance to Checkpoint Inhibition in Cancer Immunotherapy. *Transl. Oncol.* **2020,** 13, (3), 100738.
[1052] Kalbasi, A.; Ribas, A., Tumour-intrinsic resistance to immune checkpoint blockade. *Nat. Rev. Immunol.* **2020,** 20, (1), 25-39.
[1053] van Elsas, M. J.; van Hall, T.; van der Burg, S. H., Future Challenges in Cancer Resistance to Immunotherapy. *Cancers* **2020,** 12, (4).
[1054] Ji, R.-R.; Chasalow, S. D.; Wang, L.; Hamid, O.; Schmidt, H.; Cogswell, J.; Alaparthy, S.; Berman, D.; Jure-Kunkel, M.; Siemers, N. O.; Jackson, J. R.; Shahabi, V., An immune-active tumor microenvironment favors clinical response to ipilimumab. *Cancer Immunol. Immunother.* **2012,** 61, (7), 1019-1031.
[1055] Tumeh, P. C.; Harview, C. L.; Yearley, J. H.; Shintaku, I. P.; Taylor, E. J. M.; Robert, L.; Chmielowski, B.; Spasic, M.; Henry, G.; Ciobanu, V.; West, A. N.; Carmona, M.; Kivork, C.; Seja, E.; Cherry, G.; Gutierrez, A. J.; Grogan, T. R.; Mateus, C.; Tomasic, G.; Glaspy, J. A.; Emerson, R. O.; Robins, H.; Pierce, R. H.; Elashoff, D. A.; Robert, C.; Ribas, A., PD-1 blockade induces responses by inhibiting adaptive immune resistance. *Nature* **2014,** 515, (7528), 568-571.
[1056] Granier, C.; De Guillebon, E.; Blanc, C.; Roussel, H.; Badoual, C.; Colin, E.; Saldmann, A.; Gey, A.; Oudard, S.; Tartour, E., Mechanisms of action and rationale for the use of checkpoint inhibitors in cancer. *ESMO Open* **2017,** 2, (2), e000213.
[1057] Lamichhane, P.; Amin, N. P.; Agarwal, M.; Lamichhane, N., Checkpoint Inhibition: Will Combination with Radiotherapy and Nanoparticle-Mediated Delivery Improve Efficacy? *Medicines* **2018,** 5, (4).
[1058] Wang, D. Y.; Salem, J.-E.; Cohen, J. V.; Chandra, S.; Menzer, C.; Ye, F.; Zhao, S.; Das, S.; Beckermann, K. E.; Ha, L.; Rathmell, W. K.; Ancell, K. K.; Balko, J. M.; Bowman, C.; Davis, E. J.; Chism, D. D.; Horn, L.; Long, G. V.; Carlino, M. S.; Lebrun-Vignes, B.; Eroglu, Z.; Hassel, J. C.; Menzies, A. M.; Sosman, J. A.; Sullivan, R. J.; Moslehi, J. J.; Johnson, D. B., Fatal Toxic Effects Associated With Immune Checkpoint Inhibitors: A Systematic Review and Meta-analysis. *JAMA Oncol.* **2018,** 4, (12), 1721-1728.
[1059] Urwyler, P.; Earnshaw, I.; Bermudez, M.; Perucha, E.; Wu, W.; Ryan, S.; McDonald, L.; Karagiannis, S. N.; Taams, L. S.; Powell, N.; Cope, A.; Papa, S., Mechanisms of checkpoint inhibition-induced adverse events. *Clin. Exp. Immunol.* **2020,** 200, (2), 141-154.
[1060] Pruitt, S. K.; Boczkowski, D.; de Rosa, N.; Haley, N. R.; Morse, M. A.; Tyler, D. S.; Dannull, J.; Nair, S., Enhancement of anti-tumor immunity through local modulation of CTLA-4 and GITR by dendritic cells. *Eur. J. Immunol.* **2011,** 41, (12), 3553-63.
[1061] Goodwin, T. J.; Shen, L.; Hu, M.; Li, J.; Feng, R.; Dorosheva, O.; Liu, R.; Huang, L., Liver specific gene immunotherapies resolve immune suppressive ectopic lymphoid structures of liver metastases and prolong survival. *Biomaterials* **2017,** 141, 260-271.
[1062] Song, W.; Shen, L.; Wang, Y.; Liu, Q.; Goodwin, T. J.; Li, J.; Dorosheva, O.; Liu, T.; Liu, R.; Huang, L., Synergistic and low adverse effect cancer immunotherapy by immunogenic chemotherapy and locally expressed PD-L1 trap. *Nat. Commun.* **2018,** 9, (1), 2237.
[1063] Teo, P. Y.; Yang, C.; Whilding, L. M.; Parente-Pereira, A. C.; Maher, J.; George, A. J.; Hedrick, J. L.; Yang, Y. Y.; Ghaem-Maghami, S., Ovarian cancer immunotherapy using PD-L1 siRNA targeted delivery from folic acid-functionalized polyethylenimine: strategies to enhance T cell killing. *Adv. Healthcare Mater.* **2015,** 4, (8), 1180-9.
[1064] Kwak, G.; Kim, D.; Nam, G. H.; Wang, S. Y.; Kim, I. S.; Kim, S. H.; Kwon, I. C.; Yeo, Y., Programmed Cell Death Protein Ligand-1 Silencing with Polyethylenimine-Dermatan Sulfate Complex for Dual Inhibition of Melanoma Growth. *ACS Nano* **2017,** 11, (10), 10135-10146.

[1065] Li, G.; Gao, Y.; Gong, C.; Han, Z.; Qiang, L.; Tai, Z.; Tian, J.; Gao, S., Dual-Blockade Immune Checkpoint for Breast Cancer Treatment Based on a Tumor-Penetrating Peptide Assembling Nanoparticle. *ACS Appl. Mater. Interfaces* **2019,** 11, (43), 39513-39524.
[1066] Zhou, Y. J.; Wan, W. J.; Tong, Y.; Chen, M. T.; Wang, D. D.; Wang, Y.; You, B. G.; Liu, Y.; Zhang, X. N., Stimuli-responsive nanoparticles for the codelivery of chemotherapeutic agents doxorubicin and siPD-L1 to enhance the antitumor effect. *J. Biomed. Mater. Res., Part B* **2020,** 108, (4), 1710-1724.
[1067] Rupp, L. J.; Schumann, K.; Roybal, K. T.; Gate, R. E.; Ye, C. J.; Lim, W. A.; Marson, A., CRISPR/Cas9-mediated PD-1 disruption enhances anti-tumor efficacy of human chimeric antigen receptor T cells. *Sci. Rep.* **2017,** 7, (1), 737.
[1068] Hu, B.; Zou, Y.; Zhang, L.; Tang, J.; Niedermann, G.; Firat, E.; Huang, X.; Zhu, X., Nucleofection with Plasmid DNA for CRISPR/Cas9-Mediated Inactivation of Programmed Cell Death Protein 1 in CD133-Specific CAR T Cells. *Hum. Gene Ther.* **2019,** 30, (4), 446-458.
[1069] Wing, J. B.; Tay, C.; Sakaguchi, S., Control of Regulatory T Cells by Co-signal Molecules. *Adv. Exp. Med. Biol.* **2019,** 1189, 179-210.
[1070] Fukuhara, H.; Ino, Y.; Todo, T., Oncolytic virus therapy: A new era of cancer treatment at dawn. *Cancer Sci.* **2016,** 107, (10), 1373-1379.
[1071] Lan, Q.; Xia, S.; Wang, Q.; Xu, W.; Huang, H.; Jiang, S.; Lu, L., Development of oncolytic virotherapy: from genetic modification to combination therapy. *Front. Med.* **2020,** 14, (2), 160-184.
[1072] Kaufman, H. L.; Kohlhapp, F. J.; Zloza, A., Oncolytic viruses: a new class of immunotherapy drugs. *Nat. Rev. Drug Discovery* **2015,** 14, (9), 642-62.
[1073] Marchini, A.; Scott, E. M.; Rommelaere, J., Overcoming Barriers in Oncolytic Virotherapy with HDAC Inhibitors and Immune Checkpoint Blockade. *Viruses* **2016,** 8, (1).
[1074] Bommareddy, P. K.; Shettigar, M.; Kaufman, H. L., Integrating oncolytic viruses in combination cancer immunotherapy. *Nat. Rev. Immunol.* **2018,** 18, (8), 498-513.
[1075] Saha, D.; Wakimoto, H.; Rabkin, S. D., Oncolytic herpes simplex virus interactions with the host immune system. *Curr. Opin. Virol.* **2016,** 21, 26-34.
[1076] Martuza, R. L.; Malick, A.; Markert, J. M.; Ruffner, K. L.; Coen, D. M., Experimental therapy of human glioma by means of a genetically engineered virus mutant. *Science* **1991,** 252, (5007), 854-6.
[1077] Ganly, I.; Kirn, D.; Eckhardt, S. G.; Rodriguez, G. I.; Soutar, D. S.; Otto, R.; Robertson, A. G.; Park, O.; Gulley, M. L.; Heise, C.; Von Hoff, D. D.; Kaye, S. B., A Phase I Study of Onyx-015, an E1B Attenuated Adenovirus, Administered Intratumorally to Patients with Recurrent Head and Neck Cancer. *Clin. Cancer Res.* **2000,** 6, (3), 798.
[1078] Aghi, M.; Martuza, R. L., Oncolytic viral therapies - the clinical experience. *Oncogene* **2005,** 24, (52), 7802-16.
[1079] Vacchelli, E.; Eggermont, A.; Sautès-Fridman, C.; Galon, J.; Zitvogel, L.; Kroemer, G.; Galluzzi, L., Trial watch. *OncoImmunology* **2013,** 2, (6), e24612.
[1080] Miest, T. S.; Cattaneo, R., New viruses for cancer therapy: meeting clinical needs. *Nat. Rev. Microbiol.* **2014,** 12, (1), 23-34.
[1081] Russell, S. J.; Peng, K.-W.; Bell, J. C., Oncolytic virotherapy. *Nat. Biotechnol.* **2012,** 30, (7), 658-670.
[1082] Peters, C.; Rabkin, S. D., Designing Herpes Viruses as Oncolytics. *Molecular therapy oncolytics* **2015,** 2, 15010-.
[1083] Achard, C.; Surendran, A.; Wedge, M.-E.; Ungerechts, G.; Bell, J.; Ilkow, C. S., Lighting a Fire in the Tumor Microenvironment Using Oncolytic Immunotherapy. *EBioMedicine* **2018,** 31, 17-24.
[1084] Lemay, C. G.; Keller, B. A.; Edge, R. E.; Abei, M.; Bell, J. C., Oncolytic Viruses: The Best is Yet to Come. *Curr. Cancer Drug Targets* **2018,** 18, (2), 109-123.
[1085] Alberts, P.; Tilgase, A.; Rasa, A.; Bandere, K.; Venskus, D., The advent of oncolytic virotherapy in oncology: The Rigvir® story. *Eur. J. Pharmacol.* **2018,** 837, 117-126.

[1086] Xia, Z. J.; Chang, J. H.; Zhang, L.; Jiang, W. Q.; Guan, Z. Z.; Liu, J. W.; Zhang, Y.; Hu, X. H.; Wu, G. H.; Wang, H. Q.; Chen, Z. C.; Chen, J. C.; Zhou, Q. H.; Lu, J. W.; Fan, Q. X.; Huang, J. J.; Zheng, X., [Phase III randomized clinical trial of intratumoral injection of E1B gene-deleted adenovirus (H101) combined with cisplatin-based chemotherapy in treating squamous cell cancer of head and neck or esophagus]. *Ai Zheng* **2004,** 23, (12), 1666-70.
[1087] Liang, M., Oncorine, the World First Oncolytic Virus Medicine and its Update in China. *Curr. Cancer Drug Targets* **2018,** 18, (2), 171-176.
[1088] Andtbacka, R. H.; Kaufman, H. L.; Collichio, F.; Amatruda, T.; Senzer, N.; Chesney, J.; Delman, K. A.; Spitler, L. E.; Puzanov, I.; Agarwala, S. S.; Milhem, M.; Cranmer, L.; Curti, B.; Lewis, K.; Ross, M.; Guthrie, T.; Linette, G. P.; Daniels, G. A.; Harrington, K.; Middleton, M. R.; Miller, W. H., Jr.; Zager, J. S.; Ye, Y.; Yao, B.; Li, A.; Doleman, S.; VanderWalde, A.; Gansert, J.; Coffin, R. S., Talimogene Laherparepvec Improves Durable Response Rate in Patients With Advanced Melanoma. *J. Clin. Oncol.* **2015,** 33, (25), 2780-8.
[1089] Harrington, K. J.; Puzanov, I.; Hecht, J. R.; Hodi, F. S.; Szabo, Z.; Murugappan, S.; Kaufman, H. L., Clinical development of talimogene laherparepvec (T-VEC): a modified herpes simplex virus type-1-derived oncolytic immunotherapy. *Expert Rev. Anticancer Ther.* **2015,** 15, (12), 1389-403.
[1090] Saha, D.; Martuza, R. L.; Rabkin, S. D., Oncolytic herpes simplex virus immunovirotherapy in combination with immune checkpoint blockade to treat glioblastoma. *Immunotherapy* **2018,** 10, (9), 779-786.
[1091] Niemann, J.; Kühnel, F., Oncolytic viruses: adenoviruses. *Virus Genes* **2017,** 53, (5), 700-706.
[1092] Yang, X.; Huang, B.; Deng, L.; Hu, Z., Progress in gene therapy using oncolytic vaccinia virus as vectors. *J. Cancer Res. Clin. Oncol.* **2018,** 144, (12), 2433-2440.
[1093] Packiam Vignesh, T.; Campanile Alexa, N.; Barocas Daniel, A.; Chamie, K.; Davis, I. I. I. R. L.; Kader, A. K.; Lamm Donald, L.; Yeung Alex, W.; Steinberg Gary, D., MP13-19 A PHASE II/III TRIAL OF CG0070, AN ONCOLYTIC ADENOVIRUS, FOR BCG-REFRACTORY NON-MUSCLE-INVASIVE BLADDER CANCER (NMIBC). *J. Urol.* **2016,** 195, (4S), e142-e142.
[1094] Hwang, T.-H.; Moon, A.; Burke, J.; Ribas, A.; Stephenson, J.; Breitbach, C. J.; Daneshmand, M.; De Silva, N.; Parato, K.; Diallo, J.-S.; Lee, Y.-S.; Liu, T.-C.; Bell, J. C.; Kirn, D. H., A Mechanistic Proof-of-concept Clinical Trial With JX-594, a Targeted Multi-mechanistic Oncolytic Poxvirus, in Patients With Metastatic Melanoma. *Mol. Ther.* **2011,** 19, (10), 1913-1922.
[1095] Breitbach, C. J.; Bell, J. C.; Hwang, T. H.; Kirn, D. H.; Burke, J., The emerging therapeutic potential of the oncolytic immunotherapeutic Pexa-Vec (JX-594). *Oncolytic Virother.* **2015,** 4, 25-31.
[1096] Breitbach, C. J.; Parato, K.; Burke, J.; Hwang, T. H.; Bell, J. C.; Kirn, D. H., Pexa-Vec double agent engineered vaccinia: oncolytic and active immunotherapeutic. *Curr. Opin. Virol.* **2015,** 13, 49-54.
[1097] Abou-Alfa, G. K.; Galle, P. R.; Chao, Y.; Brown, K. T.; Heo, J.; Borad, M. J.; Luca, A.; Pelusio, A.; Agathon, D.; Lusky, M.; Breitbach, C.; Burke, J.; Qin, S., PHOCUS: A phase 3 randomized, open-label study comparing the oncolytic immunotherapy Pexa-Vec followed by sorafenib (SOR) vs SOR in patients with advanced hepatocellular carcinoma (HCC) without prior systemic therapy. *J. Clin. Oncol.* **2016,** 34, (15_suppl), TPS4146-TPS4146.
[1098] Bourhill, T.; Mori, Y.; Rancourt, D. E.; Shmulevitz, M.; Johnston, R. N., Going (Reo)Viral: Factors Promoting Successful Reoviral Oncolytic Infection. *Viruses* **2018,** 10, (8).
[1099] Gong, J.; Sachdev, E.; Mita, A. C.; Mita, M. M., Clinical development of reovirus for cancer therapy: An oncolytic virus with immune-mediated antitumor activity. *World J. Methodol.* **2016,** 6, (1), 25-42.
[1100] Mahalingam, D.; Fountzilas, C.; Moseley, J.; Noronha, N.; Tran, H.; Chakrabarty, R.; Selvaggi, G.; Coffey, M.; Thompson, B.; Sarantopoulos, J., A phase II study of REOLYSIN(®) (pelareorep) in combination with carboplatin and paclitaxel for patients with advanced malignant melanoma. *Cancer Chemother. Pharmacol.* **2017,** 79, (4), 697-703.

[1101] Abdullahi, S.; Jäkel, M.; Behrend, S. J.; Steiger, K.; Topping, G.; Krabbe, T.; Colombo, A.; Sandig, V.; Schiergens, T. S.; Thasler, W. E.; Werner, J.; Lichtenthaler, S. F.; Schmid, R. M.; Ebert, O.; Altomonte, J., A Novel Chimeric Oncolytic Virus Vector for Improved Safety and Efficacy as a Platform for the Treatment of Hepatocellular Carcinoma. *J. Virol.* **2018,** 92, (23).
[1102] Patel, D. M.; Foreman, P. M.; Nabors, L. B.; Riley, K. O.; Gillespie, G. Y.; Markert, J. M., Design of a Phase I Clinical Trial to Evaluate M032, a Genetically Engineered HSV-1 Expressing IL-12, in Patients with Recurrent/Progressive Glioblastoma Multiforme, Anaplastic Astrocytoma, or Gliosarcoma. *Hum. Gene Ther.: Clin. Dev.* **2016,** 27, (2), 69-78.
[1103] Todo, T.; Martuza, R. L.; Rabkin, S. D.; Johnson, P. A., Oncolytic herpes simplex virus vector with enhanced MHC class I presentation and tumor cell killing. *Proc. Natl. Acad. Sci. U.S.A.* **2001,** 98, (11), 6396-401.
[1104] Ino, Y.; Todo, T., CLINICAL DEVELOPMENT OF A THIRD-GENERATION ONCOLYTIC HSV-1 (G47Δ) FOR MALIGNANT GLIOMA. *Gene Ther. Regul.* **2010,** 05, (01), 101-111.
[1105] Ammi, R.; De Waele, J.; Willemen, Y.; Van Brussel, I.; Schrijvers, D. M.; Lion, E.; Smits, E. L., Poly(I:C) as cancer vaccine adjuvant: knocking on the door of medical breakthroughs. *Pharmacol. Ther.* **2015,** 146, 120-31.
[1106] Smith, M.; García-Martínez, E.; Pitter, M. R.; Fucikova, J.; Spisek, R.; Zitvogel, L.; Kroemer, G.; Galluzzi, L., Trial Watch: Toll-like receptor agonists in cancer immunotherapy. *OncoImmunology* **2018,** 7, (12), e1526250-e1526250.
[1107] Schwarz, T. F., Clinical update of the AS04-adjuvanted human papillomavirus-16/18 cervical cancer vaccine, Cervarix. *Adv. Ther.* **2009,** 26, (11), 983-98.
[1108] 'Mac' Cheever, M. A., Twelve immunotherapy drugs that could cure cancers. *Immunol. Rev.* **2008,** 222, (1), 357-368.
[1109] Bianchi, F.; Pretto, S.; Tagliabue, E.; Balsari, A.; Sfondrini, L., Exploiting poly(I:C) to induce cancer cell apoptosis. *Cancer Biol. Ther.* **2017,** 18, (10), 747-756.
[1110] Salaun, B.; Coste, I.; Rissoan, M. C.; Lebecque, S. J.; Renno, T., TLR3 can directly trigger apoptosis in human cancer cells. *Journal of immunology (Baltimore, Md. : 1950)* **2006,** 176, (8), 4894-901.
[1111] Estornes, Y.; Toscano, F.; Virard, F.; Jacquemin, G.; Pierrot, A.; Vanbervliet, B.; Bonnin, M.; Lalaoui, N.; Mercier-Gouy, P.; Pachéco, Y.; Salaun, B.; Renno, T.; Micheau, O.; Lebecque, S., dsRNA induces apoptosis through an atypical death complex associating TLR3 to caspase-8. *Cell Death Differ.* **2012,** 19, (9), 1482-94.
[1112] Feldman, S.; Hughes, W. T.; Darlington, R. W.; Kim, H. K., Evaluation of Topical Polyinosinic Acid-Polycytidylic Acid in Treatment of Localized Herpes Zoster in Children with Cancer: a Randomized, Double-Blind Controlled Study. *Antimicrob. Agents Chemother.* **1975,** 8, (3), 289.
[1113] Robinson, R. A.; DeVita, V. T.; Levy, H. B.; Baron, S.; Hubbard, S. P.; Levine, A. S., A Phase I–II Trial of Multiple-Dose Polyriboinosinic-Polyribocytidylic Acid in Patients With Leukemia or Solid Tumors. *J. Natl. Cancer Inst.* **1976,** 57, (3), 599-602.
[1114] Herr, H. W.; Kemeny, N.; Yagoda, A.; Whitmore, W. F., Jr., Poly I:C immunotherapy in patients with papillomas or superficial carcinomas of the bladder. *Natl. Cancer Inst. Monogr.* **1978**, (49), 325.
[1115] Nordlund, J. J.; Wolff, S. M.; Levy, H. B., Inhibition of biologic activity of poly I: poly C by human plasma. *Proc. Soc. Exp. Biol. Med.* **1970,** 133, (2), 439-44.
[1116] Levy, H. B.; Baer, G.; Baron, S.; Buckler, C. E.; Gibbs, C. J.; Iadarola, M. J.; London, W. T.; Rice, J., A Modified Polyriboinosinic-Polyribocytidylic Acid Complex That Induces Interferon in Primates. *J. Infect. Dis.* **1975,** 132, (4), 434-439.
[1117] Levine, A. S.; Sivulich, M.; Wiernik, P. H.; Levy, H. B., Initial clinical trials in cancer patients of polyriboinosinic-polyribocytidylic acid stabilized with poly-L-lysine, in carboxymethylcellulose [poly(ICLC)], a highly effective interferon inducer. *Cancer Res.* **1979,** 39, (5), 1645-50.

[1118] Patchett, A. L.; Tovar, C.; Corcoran, L. M.; Lyons, A. B.; Woods, G. M., The toll-like receptor ligands Hiltonol® (polyICLC) and imiquimod effectively activate antigen-specific immune responses in Tasmanian devils (Sarcophilus harrisii). *Dev. Comp. Immunol.* **2017,** 76, 352-360.
[1119] Rodríguez-Ruiz, M. E.; Perez-Gracia, J. L.; Rodríguez, I.; Alfaro, C.; Oñate, C.; Pérez, G.; Gil-Bazo, I.; Benito, A.; Inogés, S.; López-Diaz de Cerio, A.; Ponz-Sarvise, M.; Resano, L.; Berraondo, P.; Barbés, B.; Martin-Algarra, S.; Gúrpide, A.; Sanmamed, M. F.; de Andrea, C.; Salazar, A. M.; Melero, I., Combined immunotherapy encompassing intratumoral poly-ICLC, dendritic-cell vaccination and radiotherapy in advanced cancer patients. *Ann. Oncol.* **2018,** 29, (5), 1312-1319.
[1120] Hafner, A. M.; Corthésy, B.; Merkle, H. P., Particulate formulations for the delivery of poly(I:C) as vaccine adjuvant. *Adv. Drug Delivery Rev.* **2013,** 65, (10), 1386-1399.
[1121] Shir, A.; Ogris, M.; Roedl, W.; Wagner, E.; Levitzki, A., EGFR-Homing dsRNA Activates Cancer-Targeted Immune Response and Eliminates Disseminated EGFR-Overexpressing Tumors in Mice. *Clin. Cancer Res.* **2011,** 17, (5), 1033.
[1122] Abourbeh, G.; Shir, A.; Mishani, E.; Ogris, M.; Rödl, W.; Wagner, E.; Levitzki, A., PolyIC GE11 polyplex inhibits EGFR-overexpressing tumors. *IUBMB Life* **2012,** 64, (4), 324-330.
[1123] Lächelt, U.; Wittmann, V.; Müller, K.; Edinger, D.; Kos, P.; Höhn, M.; Wagner, E., Synthetic polyglutamylation of dual-functional MTX ligands for enhanced combined cytotoxicity of poly(I:C) nanoplexes. *Mol. Pharmaceutics* **2014,** 11, (8), 2631-9.
[1124] Krieg, A. M.; Yi, A. K.; Matson, S.; Waldschmidt, T. J.; Bishop, G. A.; Teasdale, R.; Koretzky, G. A.; Klinman, D. M., CpG motifs in bacterial DNA trigger direct B-cell activation. *Nature* **1995,** 374, (6522), 546-9.
[1125] Hanagata, N., CpG oligodeoxynucleotide nanomedicines for the prophylaxis or treatment of cancers, infectious diseases, and allergies. *Int. J. Nanomed.* **2017,** 12, 515-531.
[1126] Adamus, T.; Kortylewski, M., The revival of CpG oligonucleotide-based cancer immunotherapies. *Contemp. Oncol.* **2018,** 22, (1a), 56-60.
[1127] Krieg, A. M., Development of TLR9 agonists for cancer therapy. *J. Clin. Invest.* **2007,** 117, (5), 1184-1194.
[1128] Zhang, Q.; Hossain, D. M.; Duttagupta, P.; Moreira, D.; Zhao, X.; Won, H.; Buettner, R.; Nechaev, S.; Majka, M.; Zhang, B.; Cai, Q.; Swiderski, P.; Kuo, Y. H.; Forman, S.; Marcucci, G.; Kortylewski, M., Serum-resistant CpG-STAT3 decoy for targeting survival and immune checkpoint signaling in acute myeloid leukemia. *Blood* **2016,** 127, (13), 1687-700.
[1129] Nikitczuk, K. P.; Schloss, R. S.; Yarmush, M. L.; Lattime, E. C., PLGA-polymer encapsulating tumor antigen and CpG DNA administered into the tumor microenvironment elicits a systemic antigen-specific IFN-γ response and enhances survival. *J. Cancer Ther.* **2013,** 4, (1), 280-290.
[1130] Cheng, T.; Miao, J.; Kai, D.; Zhang, H., Polyethylenimine-Mediated CpG Oligodeoxynucleotide Delivery Stimulates Bifurcated Cytokine Induction. *ACS Biomater. Sci. Eng.* **2018,** 4, (3), 1013-1018.
[1131] Kwong, B.; Liu, H.; Irvine, D. J., Induction of potent anti-tumor responses while eliminating systemic side effects via liposome-anchored combinatorial immunotherapy. *Biomaterials* **2011,** 32, (22), 5134-5147.
[1132] Kwon, S.; Kim, D.; Park, B. K.; Wu, G.; Park, M. C.; Ha, Y. W.; Kwon, H. J.; Lee, Y., Induction of immunological memory response by vaccination with TM4SF5 epitope-CpG-DNA-liposome complex in a mouse hepatocellular carcinoma model. *Oncol. Rep.* **2013,** 29, (2), 735-40.
[1133] Kwon, S.; Kim, Y. E.; Park, J. A.; Kim, D. S.; Kwon, H. J.; Lee, Y., Therapeutic effect of a TM4SF5-specific peptide vaccine against colon cancer in a mouse model. *BMB Rep.* **2014,** 47, (4), 215-20.
[1134] Zhao, D.; Alizadeh, D.; Zhang, L.; Liu, W.; Farrukh, O.; Manuel, E.; Diamond, D. J.; Badie, B., Carbon nanotubes enhance CpG uptake and potentiate antiglioma immunity. *Clin. Cancer Res.* **2011,** 17, (4), 771-82.

[1135] Zhou, S.; Hashida, Y.; Kawakami, S.; Mihara, J.; Umeyama, T.; Imahori, H.; Murakami, T.; Yamashita, F.; Hashida, M., Preparation of immunostimulatory single-walled carbon nanotube/CpG DNA complexes and evaluation of their potential in cancer immunotherapy. *Int. J. Pharm.* **2014,** 471, (1-2), 214-23.
[1136] Lee, I. H.; Kwon, H. K.; An, S.; Kim, D.; Kim, S.; Yu, M. K.; Lee, J. H.; Lee, T. S.; Im, S. H.; Jon, S., Imageable antigen-presenting gold nanoparticle vaccines for effective cancer immunotherapy in vivo. *Angew. Chem., Int. Ed. Engl.* **2012,** 51, (35), 8800-5.
[1137] Lin, A. Y.; Almeida, J. P.; Bear, A.; Liu, N.; Luo, L.; Foster, A. E.; Drezek, R. A., Gold nanoparticle delivery of modified CpG stimulates macrophages and inhibits tumor growth for enhanced immunotherapy. *PLoS One* **2013,** 8, (5), e63550.
[1138] Cha, B. G.; Jeong, J. H.; Kim, J., Extra-Large Pore Mesoporous Silica Nanoparticles Enabling Co-Delivery of High Amounts of Protein Antigen and Toll-like Receptor 9 Agonist for Enhanced Cancer Vaccine Efficacy. *ACS Cent. Sci.* **2018,** 4, (4), 484-492.
[1139] Schüller, V. J.; Heidegger, S.; Sandholzer, N.; Nickels, P. C.; Suhartha, N. A.; Endres, S.; Bourquin, C.; Liedl, T., Cellular immunostimulation by CpG-sequence-coated DNA origami structures. *ACS Nano* **2011,** 5, (12), 9696-702.
[1140] Wang, C.; Sun, W.; Wright, G.; Wang, A. Z.; Gu, Z., Inflammation-Triggered Cancer Immunotherapy by Programmed Delivery of CpG and Anti-PD1 Antibody. *Adv. Mater.* **2017,** 29, (15).
[1141] Guo, L.; Yan, D. D.; Yang, D.; Li, Y.; Wang, X.; Zalewski, O.; Yan, B.; Lu, W., Combinatorial Photothermal and Immuno Cancer Therapy Using Chitosan-Coated Hollow Copper Sulfide Nanoparticles. *ACS Nano* **2014,** 8, (6), 5670-5681.
[1142] Tao, Y.; Ju, E.; Ren, J.; Qu, X., Immunostimulatory oligonucleotides-loaded cationic graphene oxide with photothermally enhanced immunogenicity for photothermal/immune cancer therapy. *Biomaterials* **2014,** 35, (37), 9963-9971.
[1143] Tao, Y.; Ju, E.; Liu, Z.; Dong, K.; Ren, J.; Qu, X., Engineered, self-assembled near-infrared photothermal agents for combined tumor immunotherapy and chemo-photothermal therapy. *Biomaterials* **2014,** 35, (24), 6646-56.
[1144] Speiser, D. E.; Schwarz, K.; Baumgaertner, P.; Manolova, V.; Devevre, E.; Sterry, W.; Walden, P.; Zippelius, A.; Conzett, K. B.; Senti, G.; Voelter, V.; Cerottini, J. P.; Guggisberg, D.; Willers, J.; Geldhof, C.; Romero, P.; Kündig, T.; Knuth, A.; Dummer, R.; Trefzer, U.; Bachmann, M. F., Memory and effector CD8 T-cell responses after nanoparticle vaccination of melanoma patients. *J. Immunother.* **2010,** 33, (8), 848-58.
[1145] Cho, H. J.; Takabayashi, K.; Cheng, P. M.; Nguyen, M. D.; Corr, M.; Tuck, S.; Raz, E., Immunostimulatory DNA-based vaccines induce cytotoxic lymphocyte activity by a T-helper cell-independent mechanism. *Nat. Biotechnol.* **2000,** 18, (5), 509-14.
[1146] Gungor, B.; Yagci, F. C.; Tincer, G.; Bayyurt, B.; Alpdundar, E.; Yildiz, S.; Ozcan, M.; Gursel, I.; Gursel, M., CpG ODN nanorings induce IFNα from plasmacytoid dendritic cells and demonstrate potent vaccine adjuvant activity. *Sci. Transl. Med.* **2014,** 6, (235), 235ra61.
[1147] Schmoll, H. J.; Wittig, B.; Arnold, D.; Riera-Knorrenschild, J.; Nitsche, D.; Kroening, H.; Mayer, F.; Andel, J.; Ziebermayr, R.; Scheithauer, W., Maintenance treatment with the immunomodulator MGN1703, a Toll-like receptor 9 (TLR9) agonist, in patients with metastatic colorectal carcinoma and disease control after chemotherapy: a randomised, double-blind, placebo-controlled trial. *J. Cancer Res. Clin. Oncol.* **2014,** 140, (9), 1615-24.
[1148] Weihrauch, M. R.; Richly, H.; von Bergwelt-Baildon, M. S.; Becker, H. J.; Schmidt, M.; Hacker, U. T.; Shimabukuro-Vornhagen, A.; Holtick, U.; Nokay, B.; Schroff, M.; Wittig, B.; Scheulen, M. E., Phase I clinical study of the toll-like receptor 9 agonist MGN1703 in patients with metastatic solid tumours. *Eur. J. Cancer* **2015,** 51, (2), 146-56.
[1149] Wittig, B.; Schmidt, M.; Scheithauer, W.; Schmoll, H. J., MGN1703, an immunomodulator and toll-like receptor 9 (TLR-9) agonist: from bench to bedside. *Crit. Rev. Oncol./Hematol.* **2015,** 94, (1), 31-44.

[1150] Fire, A.; Xu, S.; Montgomery, M. K.; Kostas, S. A.; Driver, S. E.; Mello, C. C., Potent and specific genetic interference by double-stranded RNA in Caenorhabditis elegans. *Nature* **1998,** 391, 806.
[1151] Müller, K.; Wagner, E., RNAi-Based Nano-Oncologicals: Delivery and Clinical Applications. In *Nano-Oncologicals: New Targeting and Delivery Approaches*, Alonso, M. J.; Garcia-Fuentes, M., Eds. Springer International Publishing: Cham, 2014; pp 245-268.
[1152] Allen, K. E.; Weiss, G. J., Resistance may not be futile: microRNA biomarkers for chemoresistance and potential therapeutics. *Mol. Cancer Ther.* **2010,** 9, (12), 3126-36.
[1153] Kong, Y. W.; Ferland-McCollough, D.; Jackson, T. J.; Bushell, M., microRNAs in cancer management. *Lancet Oncol.* **2012,** 13, (6), e249-58.
[1154] Kobayashi, E.; Hornicek, F. J.; Duan, Z., MicroRNA Involvement in Osteosarcoma. *Sarcoma* **2012,** 2012, 359739.
[1155] Iyer, A. K.; Duan, Z.; Amiji, M. M., Nanodelivery Systems for Nucleic Acid Therapeutics in Drug Resistant Tumors. *Mol. Pharmaceutics* **2014,** 11, (8), 2511-2526.
[1156] Croce, C. M., Causes and consequences of microRNA dysregulation in cancer. *Nat. Rev. Genet.* **2009,** 10, (10), 704-714.
[1157] Calin, G. A.; Dumitru, C. D.; Shimizu, M.; Bichi, R.; Zupo, S.; Noch, E.; Aldler, H.; Rattan, S.; Keating, M.; Rai, K.; Rassenti, L.; Kipps, T.; Negrini, M.; Bullrich, F.; Croce, C. M., Frequent deletions and down-regulation of micro- RNA genes miR15 and miR16 at 13q14 in chronic lymphocytic leukemia. *Proc. Natl. Acad. Sci. U.S.A.* **2002,** 99, (24), 15524.
[1158] Awasthi, R.; Rathbone, M. J.; Hansbro, P. M.; Bebawy, M.; Dua, K., Therapeutic prospects of microRNAs in cancer treatment through nanotechnology. *Drug Delivery Transl. Res.* **2018,** 8, (1), 97-110.
[1159] Bader, A. G.; Brown, D.; Winkler, M., The promise of microRNA replacement therapy. *Cancer Res.* **2010,** 70, (18), 7027-30.
[1160] Garzon, R.; Marcucci, G.; Croce, C. M., Targeting microRNAs in cancer: rationale, strategies and challenges. *Nat. Rev. Drug Discovery* **2010,** 9, (10), 775-789.
[1161] Wagner, E., Biomaterials in RNAi therapeutics: quo vadis? *Biomater. Sci.* **2013,** 1, (8), 804-809.
[1162] Krützfeldt, J.; Rajewsky, N.; Braich, R.; Rajeev, K. G.; Tuschl, T.; Manoharan, M.; Stoffel, M., Silencing of microRNAs in vivo with 'antagomirs'. *Nature* **2005,** 438, (7068), 685-689.
[1163] Li, Z.; Rana, T. M., Therapeutic targeting of microRNAs: current status and future challenges. *Nat. Rev. Drug Discovery* **2014,** 13, (8), 622-38.
[1164] Cheng, C. J.; Bahal, R.; Babar, I. A.; Pincus, Z.; Barrera, F.; Liu, C.; Svoronos, A.; Braddock, D. T.; Glazer, P. M.; Engelman, D. M.; Saltzman, W. M.; Slack, F. J., MicroRNA silencing for cancer therapy targeted to the tumour microenvironment. *Nature* **2015,** 518, (7537), 107-10.
[1165] Guilford, P.; Hopkins, J.; Harraway, J.; McLeod, M.; McLeod, N.; Harawira, P.; Taite, H.; Scoular, R.; Miller, A.; Reeve, A. E., E-cadherin germline mutations in familial gastric cancer. *Nature* **1998,** 392, (6674), 402-405.
[1166] Gregory, P. A.; Bert, A. G.; Paterson, E. L.; Barry, S. C.; Tsykin, A.; Farshid, G.; Vadas, M. A.; Khew-Goodall, Y.; Goodall, G. J., The miR-200 family and miR-205 regulate epithelial to mesenchymal transition by targeting ZEB1 and SIP1. *Nat. Cell Biol.* **2008,** 10, (5), 593-601.
[1167] Howe, E. N.; Cochrane, D. R.; Richer, J. K., Targets of miR-200c mediate suppression of cell motility and anoikis resistance. *Breast Cancer Res.* **2011,** 13, (2), R45.
[1168] Kopp, F.; Oak, P. S.; Wagner, E.; Roidl, A., miR-200c sensitizes breast cancer cells to doxorubicin treatment by decreasing TrkB and Bmi1 expression. *PLoS One* **2012,** 7, (11), e50469.
[1169] Kopp, F.; Wagner, E.; Roidl, A., The proto-oncogene KRAS is targeted by miR-200c. *Oncotarget* **2014,** 5, (1), 185-95.
[1170] Mutlu, M.; Raza, U.; Saatci, Ö.; Eyüpoğlu, E.; Yurdusev, E.; Şahin, Ö., miR-200c: a versatile watchdog in cancer progression, EMT, and drug resistance. *J. Mol. Med.* **2016,** 94, (6), 629-644.

[1171] Beg, M. S.; Brenner, A. J.; Sachdev, J.; Borad, M.; Kang, Y. K.; Stoudemire, J.; Smith, S.; Bader, A. G.; Kim, S.; Hong, D. S., Phase I study of MRX34, a liposomal miR-34a mimic, administered twice weekly in patients with advanced solid tumors. *Invest. New Drugs* **2017,** 35, (2), 180-188.
[1172] Hong, D. S.; Kang, Y. K.; Borad, M.; Sachdev, J.; Ejadi, S.; Lim, H. Y.; Brenner, A. J.; Park, K.; Lee, J. L.; Kim, T. Y.; Shin, S.; Becerra, C. R.; Falchook, G.; Stoudemire, J.; Martin, D.; Kelnar, K.; Peltier, H.; Bonato, V.; Bader, A. G.; Smith, S.; Kim, S.; O'Neill, V.; Beg, M. S., Phase 1 study of MRX34, a liposomal miR-34a mimic, in patients with advanced solid tumours. *Br. J. Cancer* **2020,** 122, (11), 1630-1637.
[1173] June, C. H.; O'Connor, R. S.; Kawalekar, O. U.; Ghassemi, S.; Milone, M. C., CAR T cell immunotherapy for human cancer. *Science* **2018,** 359, (6382), 1361.
[1174] Ali, S.; Kjeken, R.; Niederlaender, C.; Markey, G.; Saunders, T. S.; Opsata, M.; Moltu, K.; Bremnes, B.; Grønevik, E.; Muusse, M.; Håkonsen, G. D.; Skibeli, V.; Kalland, M. E.; Wang, I.; Buajordet, I.; Urbaniak, A.; Johnston, J.; Rantell, K.; Kerwash, E.; Schuessler-Lenz, M.; Salmonson, T.; Bergh, J.; Gisselbrecht, C.; Tzogani, K.; Papadouli, I.; Pignatti, F., The European Medicines Agency Review of Kymriah (Tisagenlecleucel) for the Treatment of Acute Lymphoblastic Leukemia and Diffuse Large B-Cell Lymphoma. *Oncologist* **2020,** 25, (2), e321-e327.
[1175] Papadouli, I.; Mueller-Berghaus, J.; Beuneu, C.; Ali, S.; Hofner, B.; Petavy, F.; Tzogani, K.; Miermont, A.; Norga, K.; Kholmanskikh, O.; Leest, T.; Schuessler-Lenz, M.; Salmonson, T.; Gisselbrecht, C.; Garcia, J. L.; Pignatti, F., EMA Review of Axicabtagene Ciloleucel (Yescarta) for the Treatment of Diffuse Large B-Cell Lymphoma. *Oncologist* **2020**.
[1176] Tejeda-Mansir, A.; García-Rendón, A.; Guerrero-Germán, P., Plasmid-DNA lipid and polymeric nanovaccines: a new strategic in vaccines development. *Biotechnol. Genet. Eng. Rev.* **2019,** 35, (1), 46-68.
[1177] Caruso, H. G.; Tanaka, R.; Liang, J.; Ling, X.; Sabbagh, A.; Henry, V. K.; Collier, T. L.; Heimberger, A. B., Shortened ex vivo manufacturing time of EGFRvIII-specific chimeric antigen receptor (CAR) T cells reduces immune exhaustion and enhances antiglioma therapeutic function. *J. Neuro-Oncol.* **2019,** 145, (3), 429-439.
[1178] Iurescia, S.; Fioretti, D.; Rinaldi, M., A blueprint for DNA vaccine design. *Methods Mol. Biol.* **2014,** 1143, 3-10.
[1179] Weiss, T.; Weller, M.; Guckenberger, M.; Sentman, C. L.; Roth, P., NKG2D-Based CAR T Cells and Radiotherapy Exert Synergistic Efficacy in Glioblastoma. *Cancer Res.* **2018,** 78, (4), 1031-1043.
[1180] Di, S.; Zhou, M.; Pan, Z.; Sun, R.; Chen, M.; Jiang, H.; Shi, B.; Luo, H.; Li, Z., Combined Adjuvant of Poly I:C Improves Antitumor Effects of CAR-T Cells. *Front. Oncol.* **2019,** 9, 241.
[1181] Li, Y.; Xiao, F.; Zhang, A.; Zhang, D.; Nie, W.; Xu, T.; Han, B.; Seth, P.; Wang, H.; Yang, Y.; Wang, L., Oncolytic adenovirus targeting TGF-β enhances anti-tumor responses of mesothelin-targeted chimeric antigen receptor T cell therapy against breast cancer. *Cell Immunol.* **2020,** 348, 104041.
[1182] Grunwitz, C.; Kranz, L. M., mRNA Cancer Vaccines-Messages that Prevail. *Curr. Top. Microbiol. Immunol.* **2017,** 405, 145-164.
[1183] Mai, D.; June, C. H.; Sheppard, N. C., In vivo gene immunotherapy for cancer. *Sci. Transl. Med.* **2022,** 14, (670), eabo3603.
[1184] Hernandez, R.; Malek, T. R., Fueling Cancer Vaccines to Improve T Cell-Mediated Antitumor Immunity. *Front. Oncol.* **2022,** 12.
[1185] Banchereau, J.; Steinman, R. M., Dendritic cells and the control of immunity. *Nature* **1998,** 392, (6673), 245-52.
[1186] Edwards, R. A.; Bryan, J., Fascins, a family of actin bundling proteins. *Cell Motil. Cytoskeleton* **1995,** 32, (1), 1-9.
[1187] Mohr, C. F.; Gross, C.; Bros, M.; Reske-Kunz, A. B.; Biesinger, B.; Thoma-Kress, A. K., Regulation of the tumor marker Fascin by the viral oncoprotein Tax of human T-cell leukemia virus

type 1 (HTLV-1) depends on promoter activation and on a promoter-independent mechanism. *Virology* **2015,** 485, 481-91.
[1188] Zeyn, Y.; Harms, G.; Tubbe, I.; Montermann, E.; Röhrig, N.; Hartmann, M.; Grabbe, S.; Bros, M., Inhibitors of the Actin-Bundling Protein Fascin-1 Developed for Tumor Therapy Attenuate the T-Cell Stimulatory Properties of Dendritic Cells. *Cancers* **2022,** 14, (11).
[1189] Medina-Montano, C.; Cacicedo, M. L.; Svensson, M.; Limeres, M. J.; Zeyn, Y.; Chaves-Giraldo, J. E.; Röhrig, N.; Grabbe, S.; Gehring, S.; Bros, M., Enrichment Methods for Murine Liver Non-Parenchymal Cells Differentially Affect Their Immunophenotype and Responsiveness towards Stimulation. *Int. J. Mol. Sci.* **2022,** 23, (12).
[1190] Höhn, Y.; Sudowe, S.; Reske-Kunz, A. B., Dendritic cell-specific biolistic transfection using the fascin gene promoter. *Methods Mol. Biol.* **2013,** 940, 199-213.
[1191] Sudowe, S.; Ludwig-Portugall, I.; Montermann, E.; Ross, R.; Reske-Kunz, A. B., Prophylactic and therapeutic intervention in IgE responses by biolistic DNA vaccination primarily targeting dendritic cells. *J. Allergy Clin. Immunol.* **2006,** 117, (1), 196-203.
[1192] Shen, Z.; Reznikoff, G.; Dranoff, G.; Rock, K. L., Cloned dendritic cells can present exogenous antigens on both MHC class I and class II molecules. *Journal of immunology (Baltimore, Md. : 1950)* **1997,** 158, (6), 2723-30.
[1193] Lin, S.; Taylor, M. D.; Singh, P. K.; Yang, S., How does fascin promote cancer metastasis? *FEBS J.* **2021,** 288, (5), 1434-1446.
[1194] Ujihara, Y.; Ono, D.; Nishitsuji, K.; Ito, M.; Sugita, S.; Nakamura, M., B16 Melanoma Cancer Cells with Higher Metastatic Potential are More Deformable at a Whole-Cell Level. *Cell Mol. Bioeng.* **2021,** 14, (4), 309-320.
[1195] Hashimoto, Y.; Kim, D. J.; Adams, J. C., The roles of fascins in health and disease. *J. Pathol.* **2011,** 224, (3), 289-300.
[1196] Ross, R.; Jonuleit, H.; Bros, M.; Ross, X.-L.; Enk, A. H.; Knop, J.; Reske-Kunz, A. B.; Yamashiro, S.; Matsumura, F., Expression of the Actin-Bundling Protein Fascin in Cultured Human Dendritic Cells Correlates with Dendritic Morphology and Cell Differentiation. *J. Investig. Dermatol.* **2000,** 115, (4), 658-663.
[1197] Chen, H.; Li, P.; Yin, Y.; Cai, X.; Huang, Z.; Chen, J.; Dong, L.; Zhang, J., The promotion of type 1 T helper cell responses to cationic polymers in vivo via toll-like receptor-4 mediated IL-12 secretion. *Biomaterials* **2010,** 31, (32), 8172-8180.
[1198] Cubillos-Ruiz, J. R.; Engle, X.; Scarlett, U. K.; Martinez, D.; Barber, A.; Elgueta, R.; Wang, L.; Nesbeth, Y.; Durant, Y.; Gewirtz, A. T.; Sentman, C. L.; Kedl, R.; Conejo-Garcia, J. R., Polyethylenimine-based siRNA nanocomplexes reprogram tumor-associated dendritic cells via TLR5 to elicit therapeutic antitumor immunity. *J. Clin. Invest.* **2009,** 119, (8), 2231-44.
[1199] Huang, Z.; Yang, Y.; Jiang, Y.; Shao, J.; Sun, X.; Chen, J.; Dong, L.; Zhang, J., Anti-tumor immune responses of tumor-associated macrophages via toll-like receptor 4 triggered by cationic polymers. *Biomaterials* **2013,** 34, (3), 746-755.
[1200] Rothoeft, T.; Balkow, S.; Krummen, M.; Beissert, S.; Varga, G.; Loser, K.; Oberbanscheidt, P.; van den Boom, F.; Grabbe, S., Structure and duration of contact between dendritic cells and T cells are controlled by T cell activation state. *Eur. J. Immunol.* **2006,** 36, (12), 3105-3117.
[1201] Cronin, S. J.; Penninger, J. M., From T-cell activation signals to signaling control of anti-cancer immunity. *Immunol. Rev.* **2007,** 220, 151-68.
[1202] Paudel, Y. N.; Angelopoulou, E.; Piperi, C.; Balasubramaniam, V.; Othman, I.; Shaikh, M. F., Enlightening the role of high mobility group box 1 (HMGB1) in inflammation: Updates on receptor signalling. *Eur. J. Pharmacol.* **2019,** 858, 172487.

10. Publications

10.1 Research and review articles

Zeyn, Y.; Hobernik, D.; Wilk, U.; Pöhmerer, J.; Hieber, C; Medina-Montano, C.; Röhrig, N.; Mohr, C. F.; Thoma-Kress, A. K.; Wagner, E.; Bros, M.*; Berger, S.*, Transcriptional targeting of dendritic cells using an optimized human fascin1 gene promoter. **2023** *to be submitted*

Benli-Hoppe, T.‡; Göl Öztürk, Ş.‡; Öztürk, Ö.; Berger, S.; Wagner, E.*; Yazdi, M.*, Transferrin Receptor Targeted Polyplexes Completely Comprised of Sequence-Defined Components. *Macromol. Rapid Commun.* **2022,** 43, (12), 2100602 – *honored with the Deutsche Gesellschaft für Gentherapie e.V. (DG-GT) "Paper of the Quarter" Award Q4 2021*.

Berger, S.*; Berger, M.; Bantz, C.; Maskos, M.; Wagner, E., Performance of nanoparticles for biomedical applications: The in vitro/in vivo discrepancy. *Biophysics Reviews* **2022,** 3, (1), 011303.

Berger, S.*; Krhač Levačić, A.; Hörterer, E.; Wilk, U.; Benli-Hoppe, T.; Wang, Y.; Öztürk, Ö.; Luo, J.; Wagner, E., Optimizing pDNA Lipo-polyplexes: A Balancing Act between Stability and Cargo Release. *Biomacromolecules* **2021,** 22, (3), 1282-1296.

Krhač Levačić, A.‡; Berger, S.‡; Müller, J.; Wegner, A.; Lächelt, U.; Dohmen, C.; Rudolph, C.; Wagner, E.*, Dynamic mRNA polyplexes benefit from bioreducible cleavage sites for in vitro and in vivo transfer. *J. Controlled Release* **2021,** 339, 27-40.

Spellerberg, R.; Benli-Hoppe, T.; Kitzberger, C.; Berger, S.; Schmohl, K. A.; Schwenk, N.; Yen, H. Y.; Zach, C.; Schilling, F.; Weber, W. A.; Kälin, R. E.; Glass, R.; Nelson, P. J.; Wagner, E.; Spitzweg, C.*, Selective sodium iodide symporter (NIS) gene therapy of glioblastoma mediated by EGFR-targeted lipopolyplexes. *Mol. Ther.-Oncolytics* **2021,** 23, 432-446.

Luo, J.; Schmaus, J.; Cui, M.; Hörterer, E.; Wilk, U.; Höhn, M.; Däther, M.; Berger, S.; Benli-Hoppe, T.; Peng, L.; Wagner, E.*, Hyaluronate siRNA nanoparticles with positive charge display rapid attachment to tumor endothelium and penetration into tumors. *J. Controlled Release* **2021,** 329, 919-933.

Hager, S.*; Fittler, F. J.; Wagner, E.; Bros, M.*, Nucleic Acid-Based Approaches for Tumor Therapy. *Cells* **2020,** 9, (9), 2061.

Ritt, N.; Berger, S.; Wagner, E.; Zentel, R.*, Versatile, Multifunctional Block Copolymers for the Self-Assembly of Well-Defined, Nontoxic pDNA Polyplexes. *ACS Appl. Polym. Mater.* **2020,** 2, (12), 5469-5481.

Hager, S.; Wagner, E.*, Bioresponsive polyplexes - chemically programmed for nucleic acid delivery. *Expert Opin. Drug Delivery* **2018,** 15, (11), 1067-1083.

10.2 Patent application

Berger, S.; Folda, P.; Germer, J.; Grau, M.; Haase, F.; Peng, L.; Thalmayr, S.; Wagner, E.; Weidinger, E.; Yazdi, M., Novel carriers for nucleic acid and/or protein delivery. European patent application (EP22209198.5).

10.3 Talks

Hager, S.; Krhač Levačić, A.; Klein, P.M.; Wagner, E., The Balancing Act between Required Stability and Sufficient Cargo Release: A Systematic Investigation of the Impact of Stabilizing Units within pDNA Lipo-Polyplexes (Abstract #107). American Society of Gene & Cell Therapy (ASGCT), 22nd Annual Meeting in Washington, D.C.; April 29, **2019** – *honored with the Meritorious Abstract Travel Award.*

10.4 Posters

Berger, S.; Wilk, U.; Pöhmerer, J.; Zeyn Y.; Bros, M.; Wagner, E., Transcriptional targeting of pDNA to dendritic cells in vitro and in vivo (Poster #P33). *DG-GT Symposium* **2022** "*Making Gene Therapy a Clinical Reality"*, Hannover, Germany; March 23-25, 2022. – *Oral poster presentation*.

Benli-Hoppe, T. ‡; Yazdi, M. ‡; Folda, P.; Wagner, E.; Berger, S., Optimizing four-armed carriers for pDNA and siRNA delivery: Impact of type and position of hydrophobic amino acids (Poster #P11). *DG-GT Symposium* **2022** "*Making Gene Therapy a Clinical Reality"*, Hannover, Germany; March 23-25, 2022.

Hager, S.; Krhač Levačić, A.; Hörterer, E.; Benli-Hoppe, T.; Wang, Y.; Luo, J.; Wagner, E.*, Optimizing pDNA Lipo-polyplexes: A Balancing Act between Stability and Cargo Release. *CRS-Local Chapter Meeting* **2020**, Ludwig-Maximilians-Universität (LMU), Munich, Germany; February 20-21, 2020.

Hager, S.; Benli-Hoppe, T.; Krhač Levačić, A., Klein, P.M.; Wagner, E.*, Core & Shell Optimization of pDNA Lipo-polyplexes. *CeNS Workshop* **2018**, Venice International University (VIU), San Servolo, Italy; September 24-28, 2018.

‡ Authors contributed equally.
* Corresponding author.

11. Copyright and licenses

The permissions for re-use of published articles in this thesis were requested from the respective journals.

11.1 Hager, S.; Wagner, E.*, Bioresponsive polyplexes - chemically programmed for nucleic acid delivery. *Expert Opin. Drug Delivery* **2018**, 15, (11), 1067-1083.

Taylor & Francis granted permission/license free of charge to the authors of the content for their personal reuse of the full article, charts/graphs/tables or text excerpt in *e.g.,* a thesis/dissertation.

11.2 Berger, S.*; Krhač Levačić, A.; Hörterer, E.; Wilk, U.; Benli-Hoppe, T.; Wang, Y.; Öztürk, Ö.; Luo, J.; Wagner, E., Optimizing pDNA Lipo-polyplexes: A Balancing Act between Stability and Cargo Release. *Biomacromolecules* **2021**, 22, (3), 1282-1296.

American Chemical Society granted permission/license free of charge to the authors of the content for their personal reuse of the full article, charts/graphs/tables or text excerpt in *e.g.,* a thesis/dissertation.

11.3 Berger, S.*; Berger, M.; Bantz, C.; Maskos, M.; Wagner, E., Performance of nanoparticles for biomedical applications: The in vitro/in vivo discrepancy. *Biophysics Reviews* **2022**, 3, (1), 011303.

AIP Publishing LLC does not require authors of the content used to obtain a license for their personal reuse of their own full article, charts/graphs/tables or text excerpt in *e.g.,* a thesis/dissertation.

11.4 Krhač Levačić, A.‡; Berger, S.‡; Müller, J.; Wegner, A.; Lächelt, U.; Dohmen, C.; Rudolph, C.; Wagner, E.*, Dynamic mRNA polyplexes benefit from bioreducible cleavage sites for in vitro and in vivo transfer. *J. Controlled Release* **2021**, 339, 27-40.

Authors of this Elsevier article retain the right to include it in a thesis or dissertation, provided it is not published commercially. Permission is not required.

11.5 Hager, S.*; Fittler, F. J.; Wagner, E.; Bros, M.*, Nucleic Acid-Based Approaches for Tumor Therapy. *Cells* **2020**, 9, (9), 2061.

This MDPI article is an open access article distributed under the terms and conditions of the Creative Commons Attribution (CC BY) license. No special permission is required to reuse all or parts of the article, including figures and tables.

12. Acknowledgements

After an intensive time of more than five years, my PhD studies have finally come to an end. I would like to take the opportunity to thank all the people, who contributed to this thesis, either directly by collaborations and assistance in the lab, or indirectly by support in my private life.

First of all, I would like to thank my supervisor Prof. Dr. Ernst Wagner for giving me the opportunity to work on my thesis in his research group. I am deeply grateful for his support, careful guidance, and scientific input during this time. I very much enjoyed the various fruitful and stimulating discussions, which not unlikely resulted in great new project ideas. I have learned a lot from his expertise and immense knowledge. Furthermore, I really appreciated his encouragement for scientific creativity and development of own ideas.

Next, I would like to thank the various collaboration partners, with whom I have worked on several very interesting projects. Firstly, many thanks to Ethris GmbH (Planegg) for the close collaboration on non-viral mRNA delivery, especially to Prof. Dr. Christian Plank, PD Dr. Carsten Rudolph, Dr. Christian Dohmen, Judith Müller, Andrea Wegner, Dr. Günther Hasenpusch, and Dr. Johannes Geiger. Secondly, many thanks to all the people from the Johannes Gutenberg University (JGU) Mainz for a great collaboration within the SFB1066 “Multi-functional nanoparticulate drug carriers for the immunotherapy of malignant melanoma”. Here, I especially want to thank the people of sub-project B5, namely, Prof. Dr. Rudolf Zentel, and his PhD students Nico Ritt and Silvia Rizzelli, as well as PD Dr. Matthias Bros, Frederic Fittler, and Yanira Zeyn. I very much appreciate that the collaboration on several highly interesting immunological projects with Dr. Bros and co-workers is continued albeit the sub-project B5 stopped in 2021. Moreover, I would like to thank Prof. Dr. Michael Maskos, Christoph Bantz, and Martin Berger, for a nice collaboration on writing a review article. Many thanks also to Prof. Dr. Till Opatz and Matthias Krumb for providing me diverse ligands for mannose receptor targeting, as well as to Prof. Dr. Matthias Barz, Meike Schinnerer, and Christine Seidl for providing me DBCO-functionalized aDEC205 antibody for targeting experiments. Thirdly, many thanks to Prof. Dr. Ivan Huc, Dr. Valentina Corvaglia, Jiaojiao Wu (all LMU Munich), and Dr. Philippe Pourquier (Université de Montpellier, France) for collaborating on the “foldamer project”.

Moreover, I want to thank Ass.-Prof. Dr. Ulrich Lächelt for always having an open ear, answering my many questions, and giving excellent scientific advice. His enthusiasm and motivation in doing science and research are an inspiration for me.

Also, many thanks to our technicians Wolfgang Rödl, Miriam Höhn, Melinda Kiss, Ursula Biebl, and Lorina Bawej for keeping the everyday life in the lab running. Special thanks to Wolfgang for technical support, for repairing almost any broken scientific instrument or computer, for ensuring technical maintenance, and for ordering materials etc., as well as to Miriam for help in cell culture and with microscopy and flow cytometry experiments. Furthermore, many thanks to secretary Olga Brück for her organizational skills and taking care of the administrative things.

A big thank you to all current and former members of the AK Wagner group for the nice atmosphere in the lab and great teamwork during my whole PhD time! I really appreciate to be part of this team. I very much like the conversations and discussions not only about science but also about private matters. And I really enjoyed the team events such as skiing trips to Kühtai, Christmas parties, etc. Special thanks to Dr. Ana Krhač Levačić, who taught me a lot regarding cell culture and biological experiments, and whom I worked very closely together with on several projects, as well as to Dr. Yanfang Wang, who did the siRNA screening of my carrier library. Many thanks to Dr. Philipp Klein and Dr. Sören Reinhard, who introduced me in the work in the chemistry lab in general and in solid-phase peptide synthesis in particular. Also, many thanks to the whole animal team – to Elisa Hörterer, Ulrich Wilk, and Jana Pöhmerer for conducting *in vivo* studies, which are a highly important and relevant part of our research, and to Markus Kovac for taking care of the animals. A huge “thank you” to Sophie Thalmayr, Ricarda Steffens, Paul Folda, Franziska Haase, Victoria Vetter, and Mina Yazdi for the nice teamwork on the diverse projects (mRNA, mannose targeting, 4-arm carriers, LNPs, foldamers etc.), lots of intensive brainstorming, and the many very productive discussions. Moreover, many thanks to the whole “LAF team” for the great team effort, which finally resulted in a patent application and a publication in a high ranking journal, and work on this highly interesting project is still ongoing. Also, many thanks to Teoman Benli-Hoppe for having been not only a good lab-mate and colleague, but for being also a good friend. Thanks to all the students as well, who did their master theses and/or bachelor theses under my

supervision, namely Mara Hageneier, Tobias Burghardt, Elena Corvo, and Nadine Baumeister. Each of them contributed essentially to my own research.

Finally, I want to thank my family and friends for their continuous encouragement, trust, and support during all periods of my life. Thousand thanks to my beloved husband Martin Berger, for his endless love, for enriching my life, and for his patience and dedicated support in good and bad times.